DOCTOR OF PHILOSOPHY

Geophysical evaluation of the geotechnical properties of Quaternary sediments fron the continental margin, northwest of the UK

Finlayson, K.A.

Award date:
1999

Awarding institution:
Bangor University

Geophysical evaluation of the geotechnical properties of Quaternary sediments from the continental margin, northwest of the UK

BY K. A. FINLAYSON

A thesis presented for
the degree of Philosophiae Doctor,
University of Wales

School of Ocean Sciences,
University of Wales, Bangor,
Menai Bridge,
Anglesey,
LL59 5EY,
U.K.

December, 1999

Ysgol Gwyddorau Eigion,
Prifysgol Cymru, Bangor,
Porthaethwy,
Ynys Mon,
LL59 5EY,
D.U.

December, 1999

ABSTRACT

There are a number of inherent problems associated with the interpretation of high resolution seismic data based on seismo-stratigraphic techniques. This is particularly true in complex, glacially influenced depositional environments, and groundtruth data are vital for calibrating the interpretation. Forward modelling, based on data from borehole logging, is one approach which can be used to predict and relate groundtruth data and seismic data in order to understand the seismic character and response. However, during engineering site investigations continuous geophysical logging is not routinely carried out and hence forward modelling is not easily undertaken.

The aim of this project was to investigate inter-relationships between borehole sample derived properties ('Borehole method'), cone penetrometer test results ('CPT method') and the seismo-acoustic response. This investigation aimed to overcome the shortfall in continuous logging data and to understand glacially derived sediments in a seismic facies context. High resolution seismic data in digital form were analysed to calculate seismic attributes to test the relationships between physical properties and the seismo-acoustic response. The ultimate aim of the project was to test the applicability of an integrated approach to high resolution seismic data interpretation.

The global empirical inter-relationship which was adopted in the study to predict acoustic properties for the 'Borehole method' was shown to be applicable for glacially influenced continental slope sediments, and the 'Borehole method' reliably predicted the seismic response. However, it was noted that caution is needed to avoid aliasing as a function of geotechnical sampling frequency. The 'CPT method' was able to produce predictions of major lithologic units through the block-averaging method, and site specific empirical inter-relationships were derived to predict acoustic properties from the CPT results. The geophysical and geotechnical integration was shown to be very useful for determining the depositional environment and for calibrating seismic facies and character analysis. The seismic attribute analysis produced a reliable method of inferring physical properties based on amplitude variations. The results presented in this study have shown that by integrating methods of geotechnical and geophysical interpretation, modelling techniques can be successfully applied to improve calibration within the seismo-stratigraphic interpretation approach to high resolution seismic data.

ACKNOWLEDGEMENTS

I would like to express my thanks to Dr. Angela Davis for her supervision, her patience and for providing me with the opportunity to carry out this project. I am also indebted to Dr. Dei Huws for his encouragement and advice.

Many people have assisted with ideas, input and constructive criticism along the way. Particular thanks to Dr. Tom McGee for providing me with the TENLAYERS program and source signatures. Special thanks to Professor Mike Paul and his group at Heriot-Watt University for the Hebrides data, also to Drs. Jim Bennell and Ron Haynes and to Geraint Williams.

The West Shetland geophysical and geotechnical dataset were provided by B.P. Exploration Ltd. through Fugro-Geoteam Ltd. and Fugro Ltd respectively. I am particularly grateful to Dr. Ian Hamilton who was very helpful during the project and to Fugro-Geoteam Ltd. for allowing me take up office space periodically and for the loan of a DAT recorder. The Liverpool Bay CPT and seismic datasets were provided by BHP Ltd. (formerly Hamilton Oil) and Shell UK Exploration and Production Ltd. provided access to site survey reports from Liverpool Bay.

Sponsorship was provided for the project by Hydrosearch Associates Ltd., and I wish to thank Mick Cook, Peter Andresen and Dr. Phil Williams for the money and the opportunities.

Finally, a special thankyou to my parents and a great big thankyou to all my family and friends who have supported and put up with me over the last few years. Ta to cid for the programming.

LIST OF CONTENTS

CHAPTER 1

INTRODUCTION

CHAPTER 2

FUNDAMENTAL THEORY AND RESEARCH BACKGROUND

CHAPTER 3

THE SYNTHETIC SEISMOGRAM

CHAPTER 4

SEISMIC STRATIGRAPHY

CHAPTER 5

MODELLING FROM BOREHOLE DATA

CHAPTER 6

MODELLING FROM CPT DATA

CHAPTER 7

CASE STUDY - WEST OF SHETLAND SLOPE

LIST OF FIGURES

Chapter 1

Chapter 2

Chapter 3

Chapter 4

Chapter 5

Chapter 6

Chapter 7

LIST OF TABLES

Chapter 4

Chapter 5

Chapter 6

Chapter 7

LIST OF SYMBOLS

a	area
a_r	rate of increase of velocity with depth
c	unit cohesion
c'	unit cohesion with respect to effective stresses
d	resolvable limit of vertical resolution
df	degrees of freedom
e	void ratio
e_L	void ratio at liquid limit
f	frequency
f_s	local side friction or sleeve friction resistance
g(t)	seismic trace
h	depth
h_d	damping factor
h(t)	quadrature trace
k_s	sound attenuation
l	length
n	frequency exponent
pf	pore fluid pressure
q_c	cone resistance
r^2	coefficient of determination/ correlation coefficient
r(t)	reflectivity function
s(t)	source function
s_u	undrained shear strength
t	time
u_d	displacement
u	pore pressure
w	moisture content
x	distance
x(t)	synthetic seismogram
A	amplitude
A_c	projected area of the cone
A_s	sleeve surface area
C_c^*	compression index
D_r	relative density
E	Youngs modulus
E_y	elasticity
F	force
G_s	specific gravity
I_L	liquidity index
I_v	void index
IOI	index of impedance
K	bulk modulus
LL or w_L	liquid limit
M	mass
M_z	mean grain size
Nγ	bearing capacity factor
N_k	cone factor
P	hydrostatic pressure

PI or I_P	plasticity index
PL or w_p	plastic limit
Q	quality factor
Q^{-1}	specific attenuation or dissipation factor
Q_c	total force acting on the cone
Q_f	total frictional resistance acting on a friction sleeve
Q_t	total frictional resistance
R	fresnel zone radius
R_f	friction ratio
R(t)	envelope of the trace
RC	reflection coefficient
S_r	degree of saturation
S(v)	strength/ effective stress ratio
SNR	signal-to-noise ratio
T	period
T_g	geological age in years
TC	transmission coefficient
U	pore-water pressure
V	volume
V_{av}	average velocity
V_{prop}	propagation velocity
V_p	compressional wave velocity
V_s	shear wave velocity
V_{pr}	velocity ratio
VR	variance
W	weight
Z	acoustic impedance

$\theta(t)$	phase
σ	poissons ratio
σ_n	normal stress
σ'	effective stress
σ_{vo}	total vertical stress/ vertical effective stress
μ	shear modulus
τ	shearing stress
τ_f	shear stress at failure
θ	shearing strain
ψ	axial modulus
ψ_i	inferred disturbance
λ	wavelength
λ_L, μ_L	Lame's constants
ρ	density
α	attenuation coefficient
β	bulk compressibility
η	porosity
γ	unit weight
ϕ	grain size
ϕ_i	angle of internal friction
ϕ_s	angle of shearing resistance
ϕ'	effective angle of shearing resistance

CHAPTER 1

INTRODUCTION

Stoker *et al.*, in their 1993b publication on problems associated with seismic facies analysis of Quaternary sediments, concluded that groundtruth calibration is vital when interpreting high resolution seismic data. This is particularly true where a complex depositional environment, such as that affected by glacial activity, could lead to an ambiguous interpretation when based on seismic data alone. Stoker *et al.* (1993b) raised a number of questions which this research aims to investigate.

1.1. Background

Technology associated with seismic reflection data acquisition, processing and interpretation has come a long way forward since the early days of seismic exploration for oil in the 1920s. This has, in recent years, been due to the hydrocarbon industry actively seeking ways both to keep costs to a minimum, and to ensure greater success in discovering recoverable reserves. The vast increase in available computer power allows far quicker manipulation of large and complex data volumes, and with these incentives and technological advances, there is increased demand to extract as much information as possible from seismic data.

Seismic reflection data are used by the oil industry as a means of investigating the subsurface structure and stratigraphy. Exploration depth seismic data are used for reservoir identification, analysis and monitoring. Exploration seismics include both 2D methods, where seismic data are collected along discrete lines, and 3D methods where seismic data are collected and interpreted as an areal package. 3D acquisition tends to cover large areas and in the marine field 3D data can be shot rapidly using multi-streamer acquisition systems. These systems enable up to 12 streamers to be deployed and controlled simultaneously. More recently 4D acquisition has added the dimension of time lapse. In comparison, higher resolution seismo-acoustic 2D data are needed for site investigation, pipeline and platform siting. High resolution seismo-acoustic data, in general, are currently acquired in 2D mode and concentrate on investigating depths of less than 1km below seabed. Resolution of the order of less than a metre can be obtained using very high resolution frequencies (3-30kHz), whereas this level of resolution would be more

difficult to achieve using conventional exploration 3D. This is due to the requirement for lower frequencies to gain greater penetration.

Seismic stratigraphic analysis was developed by the hydrocarbon exploration industry as an advanced method to interpret depositional environments as evidenced in seismic reflection data collected for reservoir analysis. Within this technique seismic facies analysis is used to identify and delineate the facies character produced on the seismic record. Seismic facies analysis makes the assumption that laterally persistent, acoustically homogeneous seismic units are associated with consistent lithologies and geotechnical properties. It is then generally assumed that lateral or vertical changes in seismic character indicate a change of sediment type (Stoker *et al.*, 1993b).

In many cases this assumption is valid, but, the work of Stoker *et al.* (1993b) investigating Quaternary sediments has shown that this is not always true and that fundamental interpretation mistakes are likely to be made using this assumption. An important consideration when using this advanced method of analysis is the inclusion of groundtruth data as control on the interpretation. Prior to Stoker *et al.*'s work, other projects (such as Josenhaus and Fader, 1989, Stewart and Stoker, 1990) that have studied and used the mechanics of seismic facies analysis on high resolution seismic data, have been restricted to qualitative analysis of paper records probably due to the fact that high resolution data were not generally recorded digitally. Clearly, a more in-depth study of the effects of changing sediment physical properties on the high resolution seismo-acoustic response is required.

In order to study its seismo-acoustic response various properties of a sediment are considered and for this project these have been divided into the following classifications. The 'physical' properties include those properties which constitute the structure and composition of the sediment, and combine the material and index properties defined by Bowles (1984). Therefore, physical properties such as particle size and liquid limit are within this classification. The 'acoustic' properties refer to those which relate to the passage of a seismic wave, i.e. compressional wave velocity and acoustic impedance. The 'engineering' properties are those which may be used specifically for stability analysis (Bowles, 1984) or foundation design and include shear strength and consolidation.

Many authors over the last 3 decades have attempted to empirically relate the acoustic and physical properties of a sediment, notably Buchan *et al.* (1972), Hamilton (1970b, 1971b), Hamilton and Bachman (1982) and Richardson and Briggs (1993). In particular, Hamilton (1980) and Hamilton and Bachman (1982) measured sediment physical properties (grain size, porosity, density) and used these to predict the acoustic properties (compressional wave velocity, acoustic impedance, attenuation). Authors such as Bachman (1985) and Richardson and Briggs (1993) have taken this work further and produced the inverse relationships to those of Hamilton and Bachman (1982).

In any site investigation the 'engineering' properties of the sediments, such as shear strength and deformation moduli , as well as the acoustic and physical properties listed above, are crucial for foundation design. Groundtruth used to aid seismic interpretation can take the form of geophysical borehole logging, laboratory tested borehole samples, analysed cores (such as gravity and piston), grab samples and cone penetration test results.

A significant procedure within seismic interpretation is the production and use of forward models in the form of synthetic seismograms. These seismograms are generated from geophysically logged boreholes and wells where continuous sonic and density logs are recorded. These logs enable a seismic trace to be produced and iterated for comparison and initial stratigraphic interpretation of seismic data at the borehole or well location. The synthetic seismogram can be used further to extrapolate away from the initial location in an attempt to quantify lateral changes. However, this type of continuous geophysical logging is not routinely carried out in engineering site investigation and hence forward modelling, which is a routine part of hydrocarbon interpretation, is not easily undertaken. The emphasis is on extracting as much information as possible from all the geotechnical data routinely collected during a site investigation.

A large suite of properties from recovered borehole samples can be measured in the laboratory. Coring and grab samples produce more limited information due to the often limited depth of penetration and sample recovery. Cone penetration testing (CPT) is carried out as part of a marine engineering site investigation programme but does not involve sample recovery. The test measures cone resistance and sleeve friction, with properties such as shear strength derived from

these results. CPT classification charts also exist which classify the sediment type according to the cone resistance and friction ratio (Robertson and Campanella, 1983a, Meigh, 1987), and it is these charts that form the basis of lithological interpretations of CPT measurements. However, until very recently no empirical relationships existed in the literature relating CPT output with acoustic impedance. In this respect the work of Nauroy *et al.* (1998) on carbonate silts represents a key advance with regards to geophysical and geotechnical integration and will be expanded upon in this thesis.

1.2. Research aims and objectives

As previously mentioned, the work of Stoker *et al.* (1993b) identified the need to further investigate the effects of changing physical properties of a sediment on the seismic response. This has been identified as particularly critical in glacigenic environments where the seismic facies are often complex and poorly understood.

The aim of this research project is to attempt to relate the physical properties of a sediment to its seismo-acoustic response, with a view to improving high resolution seismic interpretation of typical glacigenic sediments found on the UK continental slope. This project attempts to advance the existing knowledge by investigating inter-relationships between borehole sample derived properties and the seismo-acoustic response. Through the examination of these inter-relationships the lack of continuous geophysical borehole logging data may be overcome. The CPT is a very useful tool for sediment discrimination and this research attempts to further its use by directly relating the results to the seismic response. In parallel, this research aims to use digital seismic data from an analogue source to calculate seismic attributes with the aim of relating the physical properties to the seismic character. The ultimate aim of the research is to integrate the various methods.

1.3. Approach

To achieve these aims two modelling techniques will be developed and tested using borehole and CPT data. Any seismic response can be studied using forward modelling techniques where the seismic trace is estimated from physical and acoustic properties. The use of forward models in this project allows the iteration of the input variables to understand the nature of the seismic response; in particular,

synthetic seismograms can be produced from acoustic impedance logs (products of density and velocity with depth). However, in the hydrocarbon industry these acoustic impedance logs are typically generated from well logging which ignores the first 100m below seabed. It is though, this missing 100m section that requires thorough investigation for engineering applications, particularly in continental slope environments, where slope stability assessment is critical.

The initial stage of this research project involves a general study of the physical properties of sediments, which can be related to the acoustic properties of a sediment, and their affects on the seismic reflection response. The initial approach concentrates on physical properties from UK continental margin sediments that have been measured from borehole samples. As an essential part of the procedure the sensitivities of the measured physical properties and the empirical relationships used to derive the acoustic properties will be assessed. This initial stage of the research is intended to lead to the development of the first modelling technique, that is the generation of synthetic seismograms from borehole sample testing, henceforth referred to as the 'Borehole method'.

The second modelling technique will use CPT results as a basis for producing forward models. CPTs from the continental shelf, West of Britain, will be used to test the method of automating a published global classification chart to produce a synthetic seismogram. Empirical inter-relationships will be investigated which could relate the CPT results to the acoustic properties of a sediment. These inter-relationships would enhance the interpretation of the CPT results, and would contribute towards fully automating the procedure of interpretation and synthetic seismogram production form a CPT test. This modelling technique is termed the 'CPT method'.

The final stage of the study will be to test these methods on an actual combined geotechnical and geophysical dataset from the West of Shetland slope. This will involve application of the modelling techniques alongside a seismic facies analysis. Seismic attributes will be calculated for the geophysical dataset to assess their viability on high resolution seismo-acoustic data, and also to characterise the physical properties where possible. Figure 1.1 illustrates the research approach schematically.

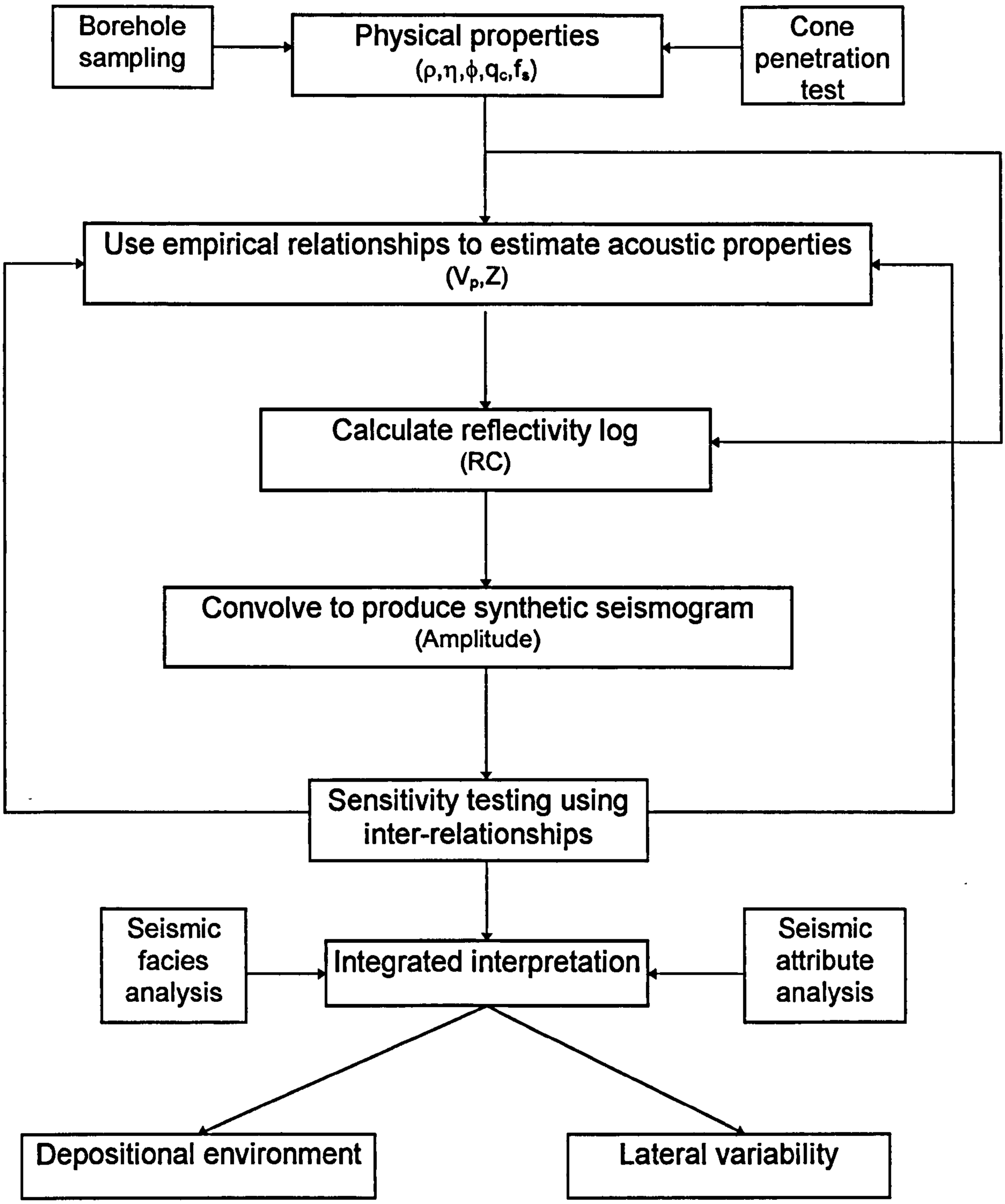

Figure 1.1. Research approach.

1.4. Thesis layout

The preceding sections of this chapter introduced the background to the thesis, the aims and the approach which will be taken in the research. Chapter 2 reviews the geotechnical and geophysical theory and research background that underpins the research. Chapter 3 describes the synthetic seismogram that is the basis of the forward modelling techniques used in this study. Seismic stratigraphic techniques are more recently being used to interpret high resolution seismo-acoustic data, and it is these techniques that are fundamentally being tested in this research. Therefore, Chapter 4 introduces and describes seismic stratigraphy with emphasis on seismic facies analysis and reflection character analysis. Sensitivity analysis of the empirical relationships and the physical properties is detailed in Chapter 5. This chapter also tests the modelling procedure of using borehole sample data from the Hebrides slope to assess the steps in the procedure. Chapter 6 describes the modelling of the seismic response from the CPT data. This begins with the automated classification of the CPT results, using a dataset from Liverpool Bay, and the output of the synthetic seismogram. Chapter 7 is the case study with geophysical and geotechnical data from the West of Shetland slope. This chapter brings all the interpretation methods together and tests the techniques developed in the preceding Chapters 5 and 6. The forward modelling results are compared alongside the two seismo-stratigraphic interpretation methods described in Chapter 4.

The discussion and conclusions generated from the findings in this research are presented in Chapters 8 and 9 respectively.

CHAPTER 2

FUNDAMENTAL THEORY AND RESEARCH BACKGROUND

2.1. Introduction

The main emphasis of this research, as introduced in Chapter 1, is on forward modelling of geophysical high resolution seismic data from a sediment sequences' physical properties. As this involves producing simplified geophysical models to aid interpretation of often complex seismic stratigraphic sequences, all the basic input and environmental variables first require careful consideration.

Basic elastic and seismic wave theory and the seismic reflection method will therefore be reviewed within this early chapter. The sections covering these topics introduce the theories that form the basis of this research project. The basic seismic theory section is followed by a section which will define the physical properties that are referred to within this study. The introduction of the physical properties precedes more specific discussions of theoretically and empirically based studies of geophysical and geotechnical inter-relationships.

2.2. Elastic theory

2.2.1. Stress

Stress is a measure of the intensity of the balanced internal forces which exist when an external force is applied to a body and is defined as force per unit area. The stresses which act on an area of any surface of that body can be divided into components of normal stress and shearing stress. The component of normal stress is where the force is perpendicular to the surface, and the component of shearing stress is where the force is tangential to the plane of the surface.

A body under stress and the three orthogonal planes that can be defined as being acted on by normal stresses, i.e. where there are no shearing stresses, is shown in Figure 2.1. The stresses acting on these planes are called the principal stresses. Each principal stress is seen as a balance of equal magnitude but oppositely directed force components. Compressive and tensile stresses on the body

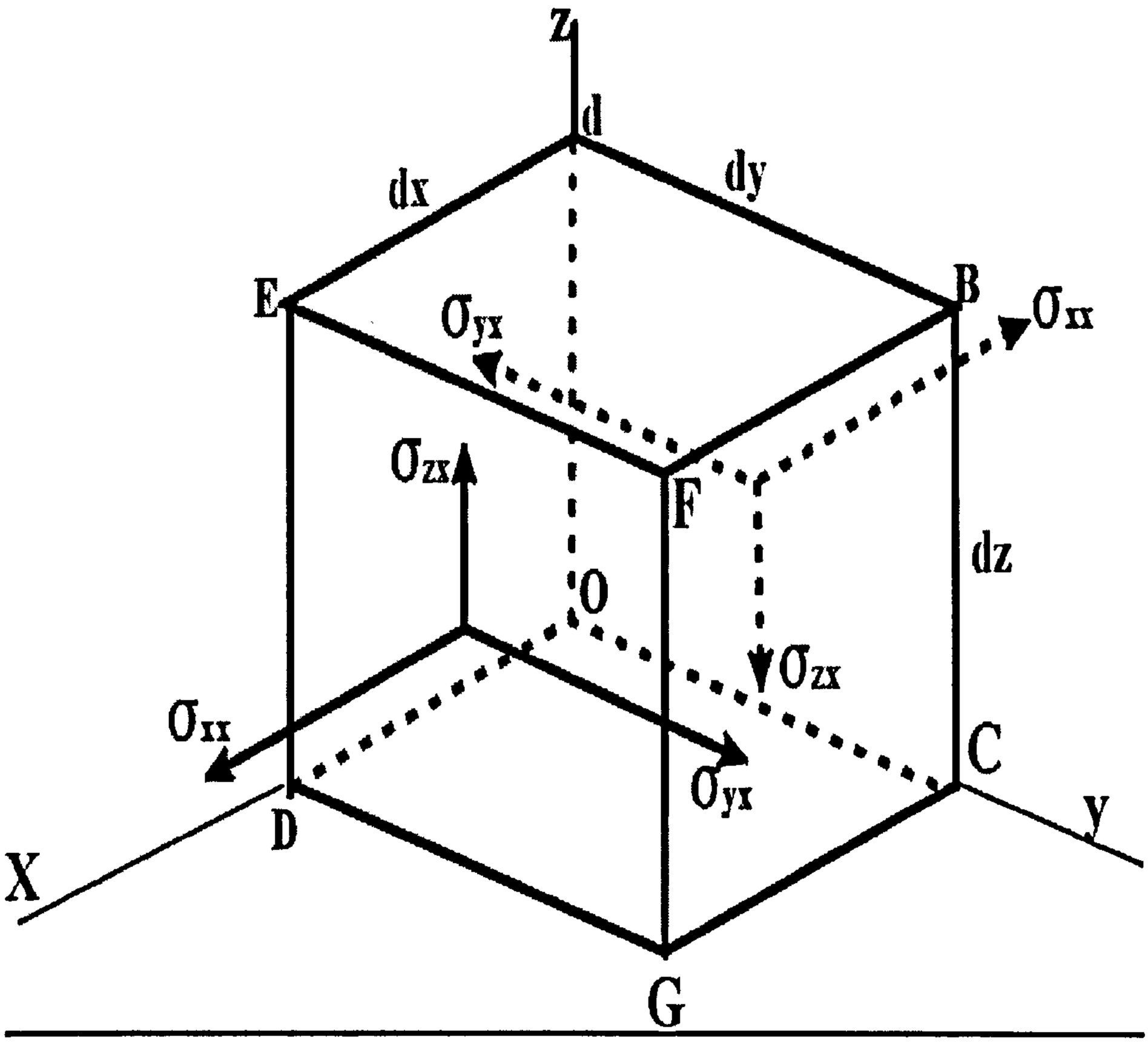

Figure 2.1. Stresses acting on the faces of an element volume inside a stressed body can be broken down into components on the two faces perpendicular to the x-axis. Subscripts indicate the x-, y- and z- axes, σ_{yx} indicates the stress direction (after Sheriff and Geldart, 1995).

represent the situations where the forces are directed towards each other and away from each other respectively. Where the principal stresses become unequal in magnitude then shearing stresses occur along the surfaces of the body (Telford *et al.*, 1976, Kearey and Brooks, 1991, Sheriff and Geldart, 1995).

2.2.2. Strain

When an elastic body is subjected to stress it will undergo changes in shape and dimension known as strain. This is defined as the relative change in a dimension or shape of a body. Strains can be divided into normal and shearing strains depending on the body change.

2.2.3. Hooke's Law

A linear relationship exists between stress and strain and is defined by Hooke's law. This law states that the elastic strain brought about by the applied stress is reversible up to a limiting yield strength or elastic limit of the material, where strains are reasonably small. Above the yield strength the strain due to the stresses becomes non-linear and only partly reversible. This is called plastic strain. Hooke's law generally requires 36 independent elastic constants to describe the behaviour of an anisotropic medium. However, for simplicity isotropy is normally assumed, and this reduces the number of required constants. These can be represented using Lamé's constants, λ_L and μ_L (Schultheiss, 1983). Figure 2.2 shows a typical stress-strain curve defining the limits discussed above.

2.2.4. Elastic moduli

Within the elastic field, shown in Figure 2.2, the linear relationship between stress and strain can be defined for a material by its elastic moduli. These moduli are the ratios of a particular type of stress to the resultant strain. Figure 2.3 illustrates these elastic moduli and the stress-strain relationships.

In the illustration shown on Figure 2.3, a rod of length, l, and area, a, is extended by, Δl, through application of force, F, to the end faces, thereby defining Young's modulus, *E*:

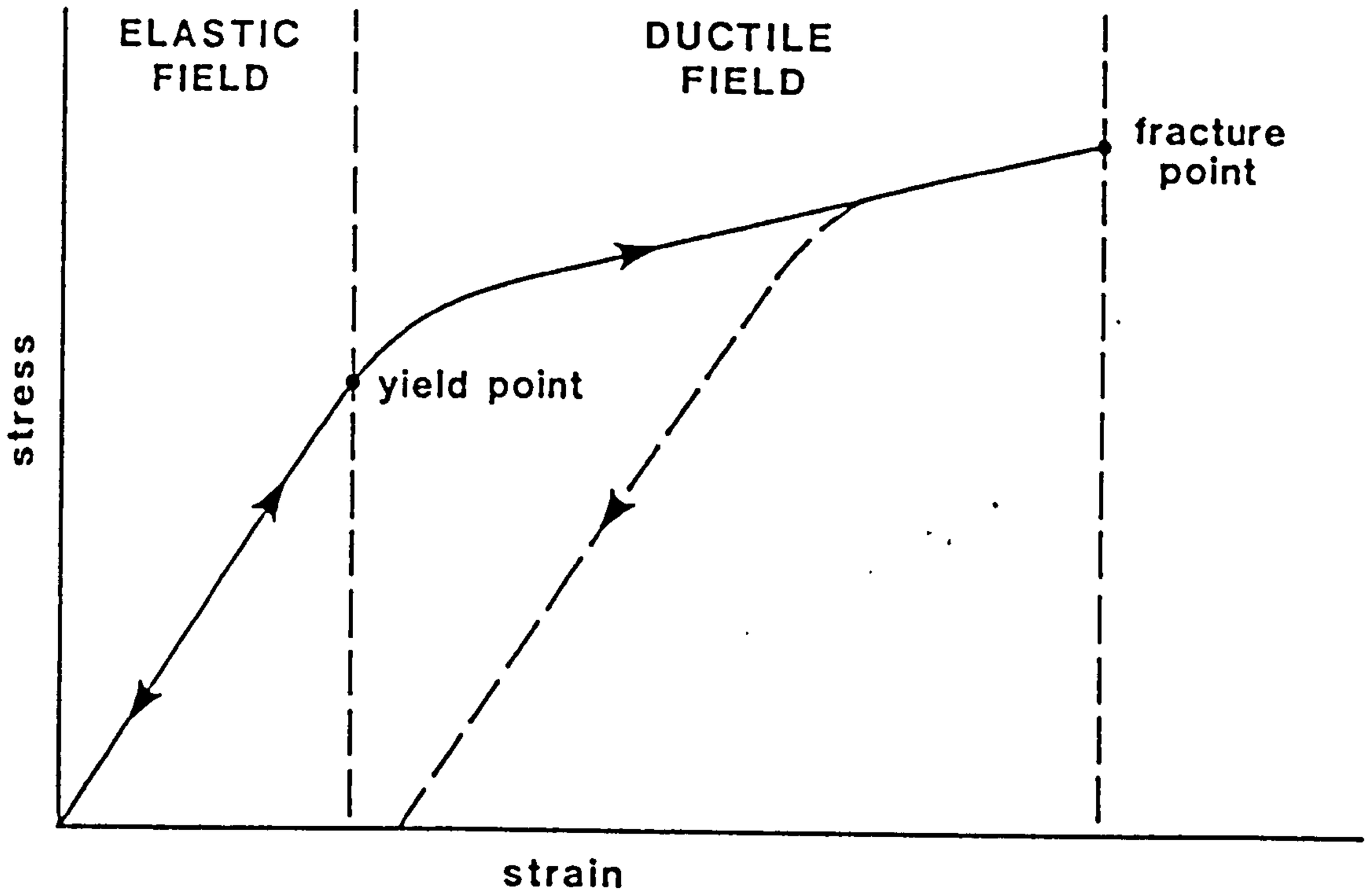

Figure 2.2. A representative stress-strain curve for a solid body (after Kearey and Brooks, 1991).

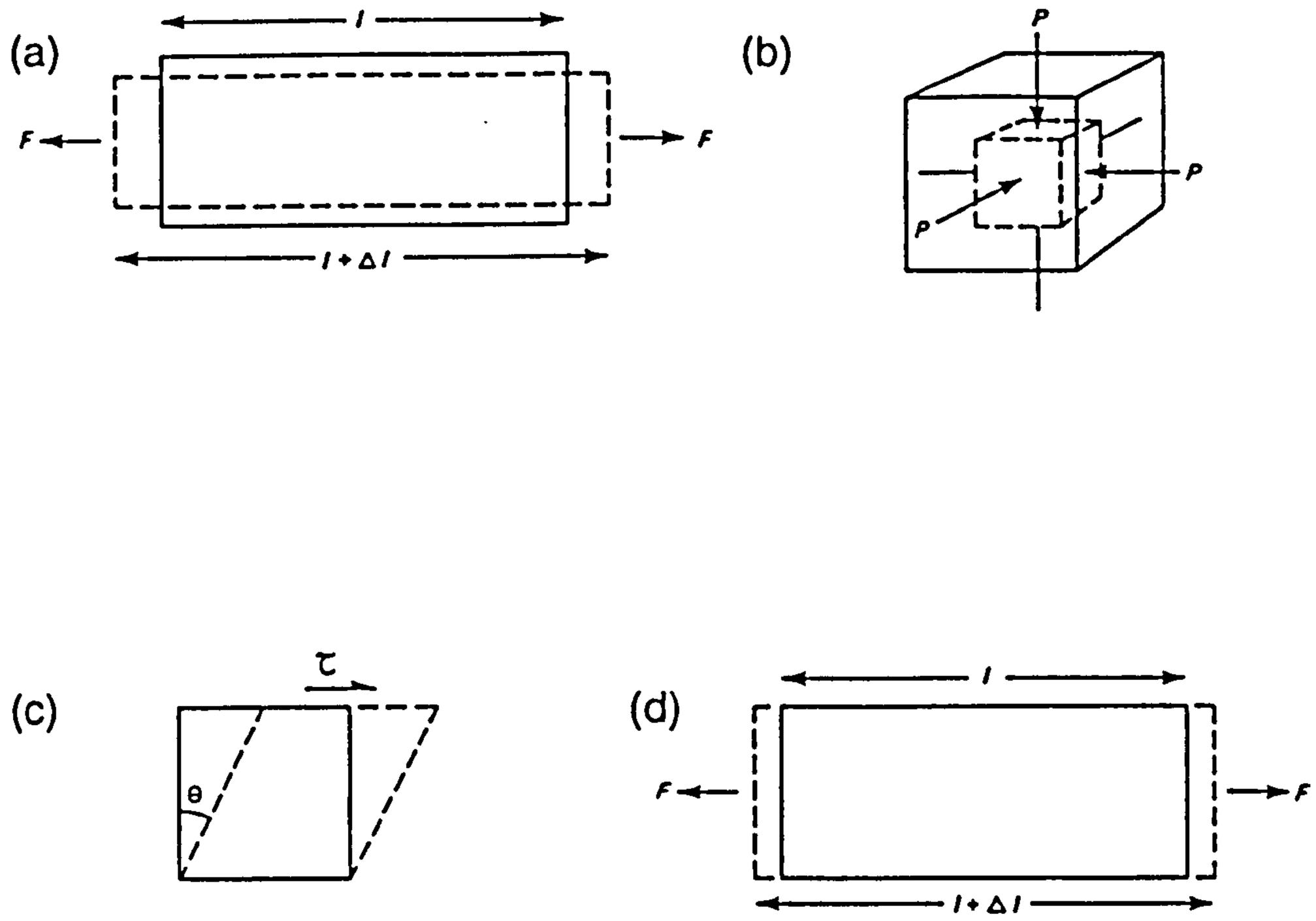

Figure 2.3. The elastic moduli. (a) Young's modulus. (b) Bulk modulus. (c) Shear modulus. (d) Axial modulus (after Kearey and Brooks, 1991).

$$\text{Young's modulus, } E = \frac{\text{Longitudinal stress, F/a}}{\text{Longitudinal strain, } \Delta l/l} \qquad (2.1)$$

As the rod increases in length there is a corresponding reduction in diameter, indicating both lateral and longitudinal strain. The ratio of the lateral to the longitudinal strain is known as Poisson's ratio, σ.

When hydrostatic pressure, P, is applied to a cube, seen in Figure 2.3(b), the strain is a function of a change in volume, ΔV, from the original volume, V. This is described as the stress-strain ratio, bulk modulus, K:

$$\text{Bulk modulus, } K = \frac{\text{Volume stress, P}}{\text{Volume strain, } \Delta V/V} \qquad (2.2)$$

In some cases the inverse, i.e. compressibility, 1/K, is used as an elastic constant rather than the bulk modulus.

The shear modulus, μ, is a measure of the resistance to shearing strain and is often called the modulus of rigidity:

$$\text{Shear modulus, } \mu = \frac{\text{Shearing stress, } \tau}{\text{Shearing strain, } \tan\theta} \qquad (2.3)$$

Where there is no lateral strain, the axial modulus defines the ratio of longitudinal stress to longitudinal strain:

$$\text{Axial modulus, } \psi = \frac{\text{Longitudinal stress, F/a}}{\text{Longitudinal strain, } \Delta l/l} \qquad (2.4)$$

2.3. Seismic waves

2.3.1. Waves

Seismic sources generate seismic waves which are parcels of elastic strain energy. Except in the immediate area close to the source, the strains associated with the passage of the seismic waves are very small and are therefore considered to be

elastic. Seismic waves can be divided into two categories, body waves and surface waves; for the purposes of this study only body waves will be considered.

Body waves can be subdivided into compressional waves (P-waves) and shear waves (S-waves). P-waves propagate by a series of compressions and rarefactions in the direction of wave travel. During the passage of a P-wave, particles oscillate about a fixed point in the direction of wave propagation. S-waves propagate by a pure shear strain perpendicular to the wave direction; individual particles oscillate about a fixed point in a plane perpendicular to the direction of wave travel (Kearey and Brooks, 1991). It is only P-waves which will be considered within this research as it is the measurement of P-waves which forms the basis of marine reflection seismics.

The size of a peak on a wave is the amplitude, A, and the distance between adjacent peaks is the wavelength, λ. The speed at which the wave propagates is the velocity, V_{prop}, and the number of peaks passing one point in a given time is the frequency, f. In general, the velocities and wavelengths increase with depth below the free surface, whereas the frequencies decrease. These characteristics can be related by:

$$\text{velocity} = \text{wavelength} \times \text{frequency} \qquad (2.5)$$

2.3.2. The wave equation

A generalised wave equation can be developed using the basic assumption of small strain to describe the wave propagating elastically through a medium. This wave equation is formulated for a body wave travelling through a homogeneous, uniform, linear, isotropic medium. It is a partial differential equation and describes the motion of waves within a medium that have been generated by a wave source (McQuillin *et al.*, 1986).

A wave propagating in the x_1 direction through a cube is shown in Figure 2.4. One face of the cube is initially in the plane of P (x_1, x_2, x_3), and the opposite face initially in the plane Q ($x_1 + \Delta x_1$, x_2, x_3). Due to the passage of the wave the cube has been subjected to an elastic strain, and P and Q are displaced to P' ($x_1 + u_1$, x_2, x_3) and Q' ($x_1 + u_1 + \Delta x_1 + \Delta u_1$, x_2, x_3). Newton's second law of motion states that the

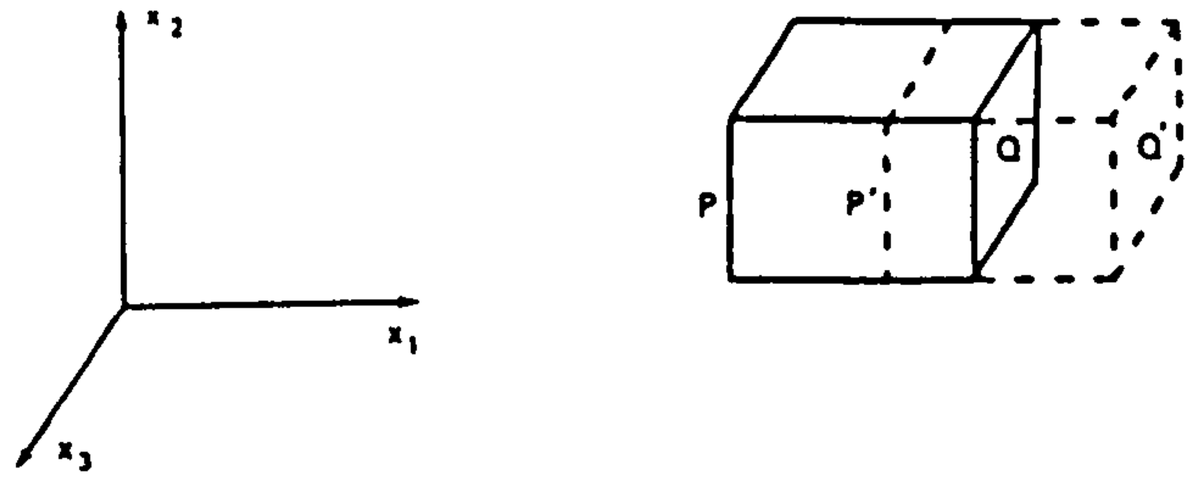

Figure 2.4. Compressional wave propagation (after McQuillin *et al.*, 1986).

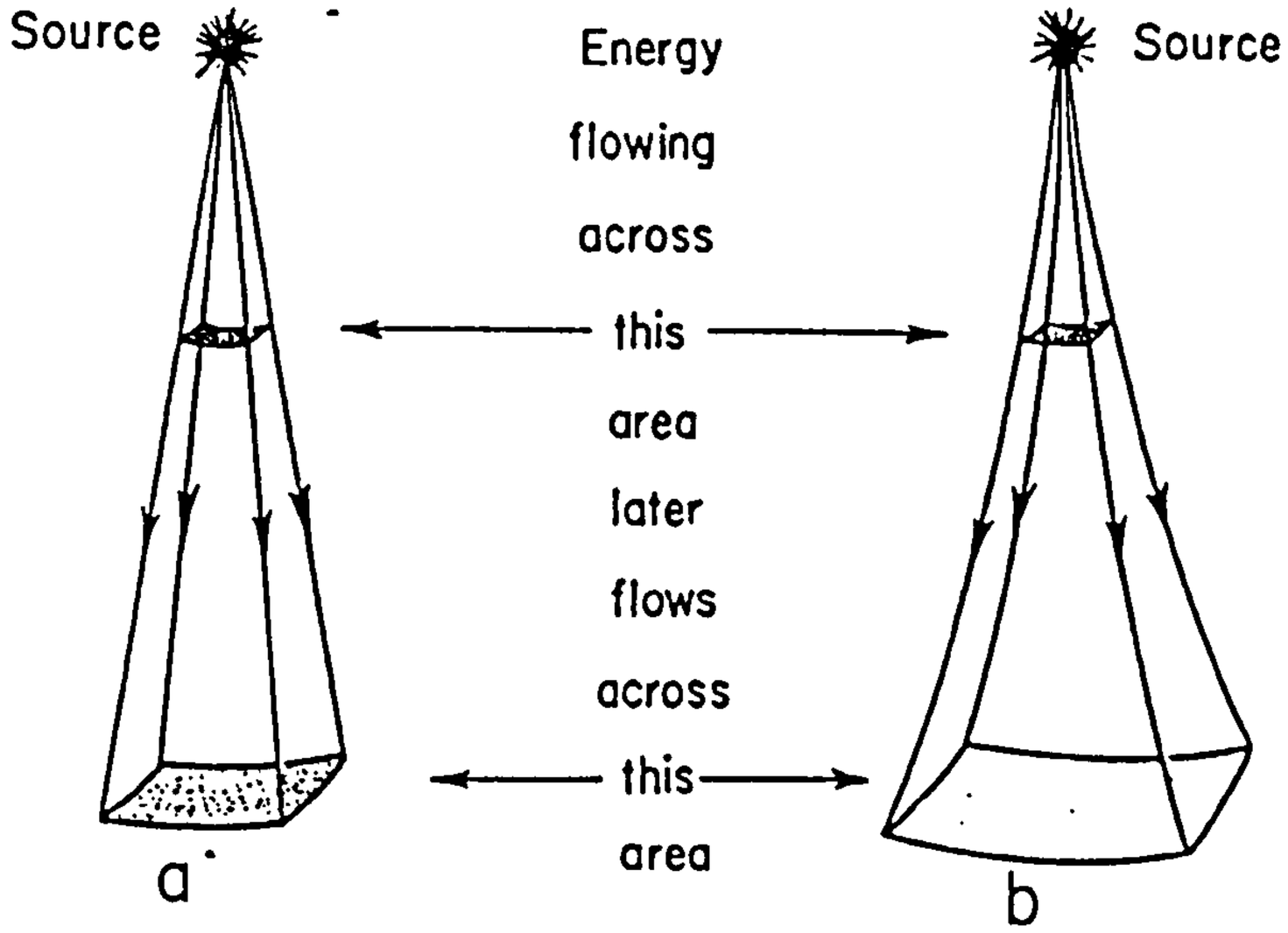

Figure 2.5. Amplitude decay due to spherical divergence. (a) Decay in a uniform medium. (b) Decay in a medium where there is an increase in velocity with depth (after O'Doherty and Anstey, 1971).

unbalanced force equals the product of mass and acceleration; therefore an equation of motion can be defined for the cube having considered the force acting on it due to the strain on the x_1-axis. Using Hooke's law the strains can be expressed as displacements and allowance made for boundary conditions, i.e. the wave travelling through the earth. The one-dimensional wave equation becomes :

$$\rho \frac{\partial^2 u_d^1}{\partial t^2} = (\lambda_L + 2\mu_L) \frac{\partial^2 u_d^1}{\partial x_1^2} \qquad (2.6)$$

where ρ is the density of the material, u_d is the displacement and λ_L and μ_L are Lamé's elastic constants. The general solution to this is :

$$u_d^1 = f (x_1 - V_{prop}t) + g (x_1 + V_{prop}t) \qquad (2.7)$$

where f and g are arbitrary functions and

$$V_{prop} = \left(\frac{\lambda_L + 2\mu_L}{\rho} \right)^{1/2} \qquad (2.8)$$

The solutions show disturbances propagating in the positive and negative x_1 direction with a propagation velocity V_{prop}.

The solutions of the wave equation for the body waves, compressional (V_p) and shear (V_s), can be written as :

$$V_p = \left(\frac{(\lambda_L + 2\mu_L)}{\rho} \right)^{1/2} \qquad (2.9)$$

$$V_s = \left(\frac{\mu_L}{\rho} \right)^{1/2} \qquad (2.10)$$

where λ_L and μ_L are Lamé's constants and by assuming Hookean behaviour then μ can be defined as the shear modulus (McQuillin *et al.*, 1986).

2.3.3. Huygen's principle

Huygen's principle for wave propagation is applied when estimating successive positions of wavefronts. The principle states that each point on a wavefront can be regarded as a new source point creating diverging spherical wavefronts. When a particle moves from its equilibrium position the same way each time, it thereby alters the elastic forces of nearby particles. There is a change of force associated with this movement along the wavefront, and this change produces the motion to form the next wavefront (Sheriff and Geldart, 1995).

2.4. Seismic compressional wave velocity

In order to assess the velocities at which the seismic waves propagate through a medium, various authors, e.g. Sheriff and Geldart (1995) have shown that the seismic wave velocities are a function of the elastic moduli and the density of the material through which they pass. The velocity of propagation of any body wave through a material is defined by, amongst others, Anstey (1991) as:

$$\text{Velocity} = \left(\frac{\text{Elasticity}}{\text{Density}}\right)^{1/2} \tag{2.11}$$

The solutions of the wave equation for the propagation of body waves were introduced in Section 2.3.2. These solutions can be rewritten in terms of measurable elastic constants. For shear waves, the one component to the elasticity is rigidity:

$$V_s = \left(\frac{\text{Rigidity}}{\text{Density}}\right)^{1/2} = \left(\frac{\mu}{\rho}\right)^{1/2} \tag{2.12}$$

For compressional waves, the elastic components are rigidity (resistance to change of shape) and bulk modulus (resistance to change of volume), and for the case where the wave travels through a perfectly elastic, isotropic and homogeneous medium:

$$V_p = \left(\frac{\text{Bulk modulus + 4/3 Rigidity}}{\text{Density}}\right)^{1/2} = \left(\frac{K+4/3\mu}{\rho}\right)^{1/2} \quad (2.13)$$

Compressional waves, unlike shear waves, propagate through water (where $\mu = 0$), so in water:

$$V_p = \left(\frac{K}{\rho}\right)^{1/2} = \left(\frac{1}{\beta\rho}\right)^{1/2} \quad (2.14)$$

where β is the bulk compressibility (1/K).

Early work on the velocity of sound in unconsolidated sediments was presented by Wood (1955). A series of equations were produced for a two phase ideal mixture, i.e. a suspension of solid particles in liquid, resulting in the velocity equation:

$$V_p = \left(\frac{E_y}{\rho}\right)^{1/2} = \left(\frac{E_{y_1}\, E_{y_2}}{\{\chi E_{y_2}+(1-\chi)E_{y_1}\}\{\chi\rho_2+(1-\chi)\rho_1\}}\right)^{1/2} \quad (2.15)$$

where ρ_1, E_{y1} and ρ_2, E_{y2} are the density and elasticity of the two phase components, χ is the proportion of the first constituent by volume, and $(1-\chi)$ is the proportion of the second constituent by volume. This is Wood's emulsion equation.
Urick (1947) applied Wood's equation to measurements of the speed of sound within a pure suspension, i.e. having no sediment frame. By replacing each particle of fluid by a sediment particle of the same volume then the following equations were obtained (Buchan *et al.*, 1972),

$$\rho = \eta\rho_w + (1-\eta)\rho_s \quad (2.16)$$

$$\beta = \eta\beta_w + (1-\eta)\beta_s \quad (2.17)$$

where η is the porosity and subscripts w and s are the water and solid components respectively. Substituting ρ and β into Wood's equation:

$$V_p = \left(\frac{1}{[\eta\rho_w + (1-\eta)\rho_s][\eta\beta_w + (1-\eta)\beta_s]} \right)^{1/2} \quad (2.18)$$

Buchan *et al.* (1972) following other authors (e.g. Hamilton, 1971a), confirmed that Wood's emulsion equation puts a lower limit on the magnitude of a sediment's velocity even though a marine sediment is generally regarded as a two-phase medium, i.e. sediment particles and seawater in the pores. In reality the frame structure within a seafloor sediment arises due to the interaction of the mineral particles. This is through frictional contact in coarse sediments and by electrochemical forces in finer grained sediments. As a result of this structural frame, the bulk modulus of the system increases (via frame compressibility) and the rigidity modulus is no longer zero.

Several authors (e.g. Gassmann, 1951, Nafe and Drake, 1957, and Buchan *et al.*, 1972) have made empirical modifications to Wood's equation to help provide a fit to their data. These adjustments show that variations of sound velocity in saturated sediments are dependent to a major extent on grain-size distribution, porosity and bulk density.

Gassmann (1951), in particular, states that the rigidity modulus of a seafloor sediment is not negligible. Gassmann (1951) concludes that by accounting for the sediment frame in consolidated sediments higher velocities are predicted.

2.4.1. Factors influencing compressional wave velocity

Equation (2.11) shows velocity in a homogeneous medium to be simply dependent on density and elasticity. Sheriff and Geldart (1995) state that, in fact, the situation is not as straightforward. This is due to the inter-relationship of elasticity and density and each depending on other factors, such as lithology, porosity, pressure, depth and degree of compaction. Schreiber (1968) states that as sediments are porous and contain fluid filled spaces, then porosity is possibly the single most important factor governing the velocity of a material.

Anstey (1991) argued that the link between compressional wave velocity and porosity is incidental rather than causal and that the velocity is determined to a large extent by the grain fabric of the material. Other variables which affect velocity

and which were discussed by Anstey (1991) were grain shape and sorting, overburden pressure and cementation.

2.4.2. Variation of velocity with depth

Velocity is generally assumed to increase with depth, therefore producing positive sound velocity gradients. These positive gradients are of invaluable use in the understanding of subseafloor structure. Nafe and Drake (1957) were among the early authors to study and quantify velocity gradients following the work of Hill (1952), who first discovered the existence of these gradients. Hamilton (1979) calculated that in sands the velocity gradient is about $4ms^{-1}/m$ for depths between 1 and 20m and that for silt clays the range is from 0.6-1.9 ms^{-1}/m. The major factors which contribute to sound velocity gradients in silt clays include pressure-induced porosities and effects on the sediment frame, temperature increases due to heat flow, pore-water pressure increases and increases in rigidity caused by diagenesis.

2.5. Attenuation

As a seismic wave propagates through the ocean and the seafloor, its phase and amplitude characteristics are altered by a variety of causes including, significantly, spherical divergence and absorption. As a separate value absorption is very difficult to estimate, therefore it is total attenuation which is generally referred to with no differentiation of the causes (Kibblewhite, 1989).

2.5.1. Spherical divergence

As a wave moves away from the source the energy spreads out thereby leading to a decrease in strength at any point; in a homogeneous medium this amplitude decrease would be inversely proportional to distance (Sheriff and Geldart, 1995). The intensity diminishes as the inverse square of the radius of the wavefront (O'Doherty and Anstey, 1971), as illustrated in Figure 2.5.

2.5.2. Absorption

Absorption is defined as the process where elastic energy associated with wave motion is gradually absorbed by the medium and ultimately converted to heat. This

energy loss is due to the earth's anelasticity in its response to the passage of the seismic wave.

The decrease in amplitude due to absorption is shown to be exponential with distance for elastic waves and can be represented by

$$A_x = A_0 e^{-\alpha x} \qquad (2.19)$$

where A_x and A_0 are values of amplitude of a plane wavefront at two points x distance apart, and α is the attenuation coefficient.

Absorption can also be expressed in terms of a decrease in amplitude with time, and assuming a cyclic waveform the quality factor, Q, can be defined as:

$$Q = \frac{2\pi}{\text{(fraction of energy lost per cycle } (E/\Delta E)} \qquad (2.20)$$

During one period, a wave travels one wavelength. If the loss of energy is due to absorption only, then $h_d T = \alpha\lambda$ where h_d is the damping factor and T is period, therefore:

$$Q = \frac{\pi}{\alpha\lambda} \qquad (2.21)$$

(Toksoz *et al.*, 1979, Jannssen *et al.*, 1985)

2.5.3. A review of sediment attenuation

Attenuation is dependent on frequency (Attewell and Ramana, 1966), with the high frequency components of a wave attenuating faster than the low frequency components. In the sediment column, Kibblewhite (1989) and Buckingham (1997) refer to intrinsic and effective attenuation. Intrinsic attenuation is the energy loss due to the fundamental structure of the material affecting the sound propagation. Effective attenuation is defined as the sum of all loss mechanisms.

Stoll (1977), based on work by Biot (1956a, 1956b), proposes two fundamentally different mechanisms to explain wave propagation through a saturated medium and the loss of energy incurred. The first mechanism involves losses brought about by the grain contacts within the skeletal frame. In finer grained sediments where fluid mobility is low, energy loss is nearly independent of frequency. In coarser sediments, fluid losses become greater than frame losses and the losses are thought to be a frictional phenomenon, whereas in finer grained sediments there are a variety of processes determining the loss, including friction and other inelastic effects.

The second loss mechanism proposed by Stoll (1977) results from the motion of the pore-water relative to the sediment frame. The instantaneous pressure varies from place to place during the propagation of the wave and the subsequent pressure gradients move the fluids within the connected pore spaces (Sheriff, 1975).

Hamilton (1972) defines frequency dependent attenuation as:

$$\alpha = kf^n \qquad (2.22)$$

where α is attenuation coefficient (dB/m), k is a constant, f is frequency (kHz) and n is a frequency exponent which is assumed to be one where the attenuation is in the frequency range, f^1.

Q^{-1}, the dissipation factor or specific attenuation factor, is often measured alongside Q (Hamilton, 1972) as defined above. Hamilton (1972) states that both Q and Q^{-1} are approximately independent of frequency in the range 10^1-10^6 Hz and that inter-grain friction is the dominant mechanism for attenuation in marine sediments. Attewell and Ramana (1966) presented the case of liquids where Q^{-1} is proportional to frequency as did McCann and McCann (1969) who discussed the frequency dependence of Q^{-1} in unconsolidated sediments. McCann and McCann (1985) explained the variation of compressional wave attenuation (at all frequencies) in unconsolidated sediments by a viscous dissipation mechanism provided a distribution of pore spaces is incorporated into the theory. This is in agreement with Biot's (1956a, 1956b) theory which accounts for attenuation as a function of viscous interaction between the solid particles and pore fluid.

In order to estimate attenuation in a marine sediment, Hamilton (1972) identifies porosity, grain size, shape and distribution as important variables defining the attenuation coefficient in coarse grained sediments, and electro-chemical effects as dominant in finer grained sediments. Toksoz *et al.* (1979) state that attenuation varies much more than seismic velocity in relation to physical changes of the material through which the wave is passing. However, determination of attenuation is much more difficult than that of velocity.

More recently, Buckingham (1997, 1998) has developed further theories on sound propagation in saturated marine sediments. Buckingham's theory introduces a dissipation factor accounting for loss due to interparticle contact and states that hysteresis associated with this mechanism defines the acoustic properties of a sediment.

2.6. Seismic reflection method

The field seismic method central to this study is high resolution seismic reflection. Within reflection surveying travel times are measured from arrivals reflected from subsurface boundaries. These reflecting surfaces are generated between two layers with differing acoustic impedances (Z). Acoustic impedance is defined as the product of the P-wave velocity and density for an individual layer.

2.6.1. Reflection and transmission coefficients.

The reflection coefficient, RC, is defined as the ratio of the reflected amplitude, A_r, to the amplitude of the incident wave, A_i. For normal incidence, i.e. the angle of incidence is 0° at a boundary in an elastic medium:

$$RC = \frac{A_r}{A_i} = \frac{\rho_2 V_{prop2} - \rho_1 V_{prop1}}{\rho_2 V_{prop2} + \rho_1 V_{prop1}} = \frac{Z_2 - Z_1}{Z_2 + Z_1} \qquad (2.23)$$

Subscripts 1 and 2 refer to the layers above and below the reflecting boundary respectively.

The transmission coefficient, TC, is the ratio of the amplitude of the transmitted wave, A_t, to the amplitude of the incident wave, A_i. The second part of the equation is a solution of Zoeppritz's equation for a normal incidence wave.

$$TC = \frac{A_t}{A_i} = \frac{2 Z_1}{Z_2 + Z_1} \qquad (2.24)$$

The transmission coefficient is generally described as (1 - RC). The two-way transmission coefficient at the boundary will therefore be
(1 - RC) (1 + RC) = 1 - RC^2. A seismic reflection is the product of its own reflection coefficient with the product of all the two-way transmission coefficients of the surfaces above it (O'Doherty and Anstey, 1971).

Reflection coefficients between natural sediment layers are typically less than ± 0.2. The sea surface is an almost perfect reflector of seismic waves incident from below, i.e. the water column, and the reflection coefficient approaches -1. The negative sign indicates a 180° phase reversal.

2.6.2. Multiples

The primary reflections which return to the surface after a single reflection at an interface have been discussed above. However, many more reflections can be recorded at the receiver. These are termed reverberations or multiples with the most prominent on marine seismic data involving reflection from the sea surface.

Multiples can be classified into two categories, either short path or long path which distinguishes between multiple reflections that arrive soon after the primary reflection or at a longer travel time respectively. For seabed and subsurface multiples to be distinguished as separate events they will have been generated from a reflector with a high reflection coefficient as the multiple amplitude is proportional to the reflection coefficient of the boundary. However, the multiple amplitude may be lower due to energy dissipation from multiple boundary reflections, Figure 2.6 illustrates the types of multiples likely to be produced during reflection surveying.

In marine surveying, ghost multiples are generated when energy initially travels upwards from the source and is reflected back from the sea surface. The sea

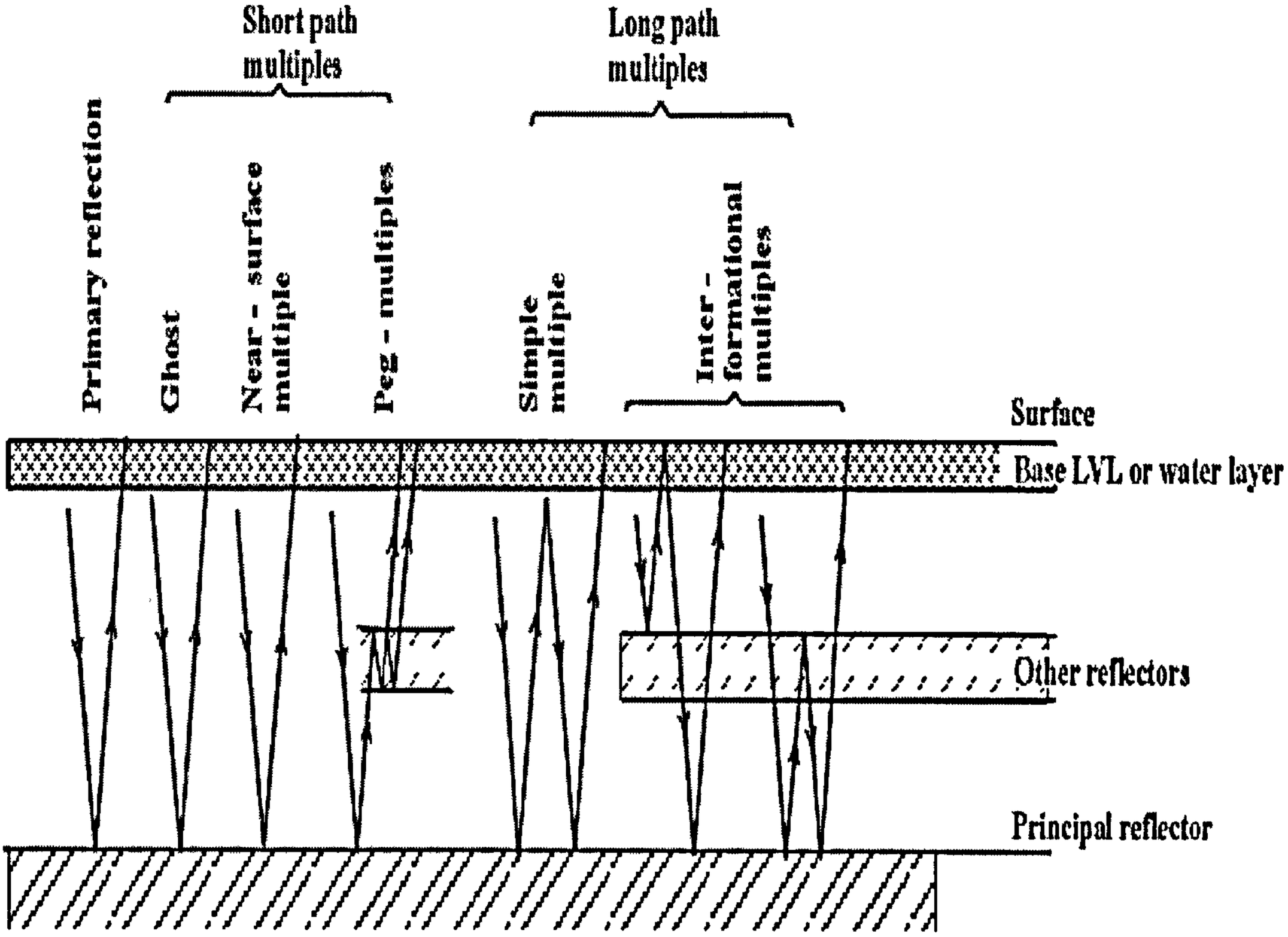

Figure 2.6. Types of multiples (after Sheriff and Geldart, 1995).

surface is an almost perfect reflector (depending on the sea state) therefore the ghost multiple will be strong, but it will also undergo a 180° phase shift, i.e. reversed polarity. Ringing is an effect which can be caused by multiple reflections in the water column. Because of the high reflection coefficient of both the sea surface and seabed these reflections are very strong and can affect the frequency content of the final recorded data (Trabant, 1984).

Peg-leg multiples tend to be produced where several, often thin layers, are present and the energy reverberates within these layers, usually on its way to or from the main reflecting surface (Sheriff and Geldart, 1995).

2.6.3. Resolution

Resolution is the minimum distinguishable distance between two reflecting points on a seismic profile. Resolution needs to be considered in both the vertical and horizontal planes.

2.6.3.1. Vertical resolution

Vertical resolution is the minimum distance between two reflectors to allow them to be separated vertically on the seismic profile. The limit to vertical resolution is defined by the fact that the reflections from two adjacent reflectors will interfere with each other, and by the pulse length. Sheriff (1980) defines the resolvable limit, d, as:

$$d \approx \frac{\lambda}{4} \approx \frac{V_{prop}}{4f} \qquad (2.25)$$

Widess (1973) states that there are various factors involved when attempting to define the threshold of resolution. These include the dominant frequency, and signal-to-noise ratio. Widess (1973) defines a thin bed's resolvable limit as thickness less than $\lambda_b / 8$, where λ_b is the predominant wavelength calculated using the velocity of the bed. Beds which are thinner than the resolution will also generate a seismic response. To estimate thickness, the amplitude of the reflection, where a reference amplitude is known, is linearly proportional to the thickness of the bed.

Generally, in order to increase resolution higher frequencies need to be recorded and the signal-to-noise ratio improved.

2.6.3.2. Horizontal resolution

Horizontal resolution is defined by how far apart features have to be from each other laterally to be distinguishable as separate features, This distance can be defined by the Fresnel Zone on unmigrated data, i.e. unmigrated data are referenced to an observational subsurface reflection point half way between the source and receiver as opposed to the actual reflecting point. The area of a reflecting surface (illustrated in Figure 2.7) from which reflected energy has been received within half a wavelength of reflection onset is defined as the Fresnel Zone. The size of the Fresnel Zone can be calculated from :

$$R = \frac{V_{av}}{2}\left(\frac{t}{f}\right)^{1/2} \qquad (2.26)$$

where R is the radius of the Fresnel Zone, V_{av} is the average velocity, t is the two way time to the reflector and f is the dominant frequency at the reflector (Sheriff and Geldart, 1995).

2.7. Physical Properties

In order to develop the theory of the effects of various physical properties on a sediment's compressional wave velocity, the properties themselves need first to be defined. The physical properties defined in the following section have been measured and used by several authors (e.g. Hamilton *et al.*, 1956, Hamilton, 1970a, 1970b, 1978, 1980, Hamilton and Bachman, 1982, and Richardson and Briggs, 1993) to develop empirical inter-relationships involving compressional wave velocity. These relationships will be critically reviewed in Section 2.9.

2.7.1. Grain size and cohesion

The grain size distribution of a sediment refers to the diameters of the particles making up the sediment mass. Particle size ranges from clay particles smaller than 0.002mm through silts, sands, gravels and cobbles up to boulders in excess of

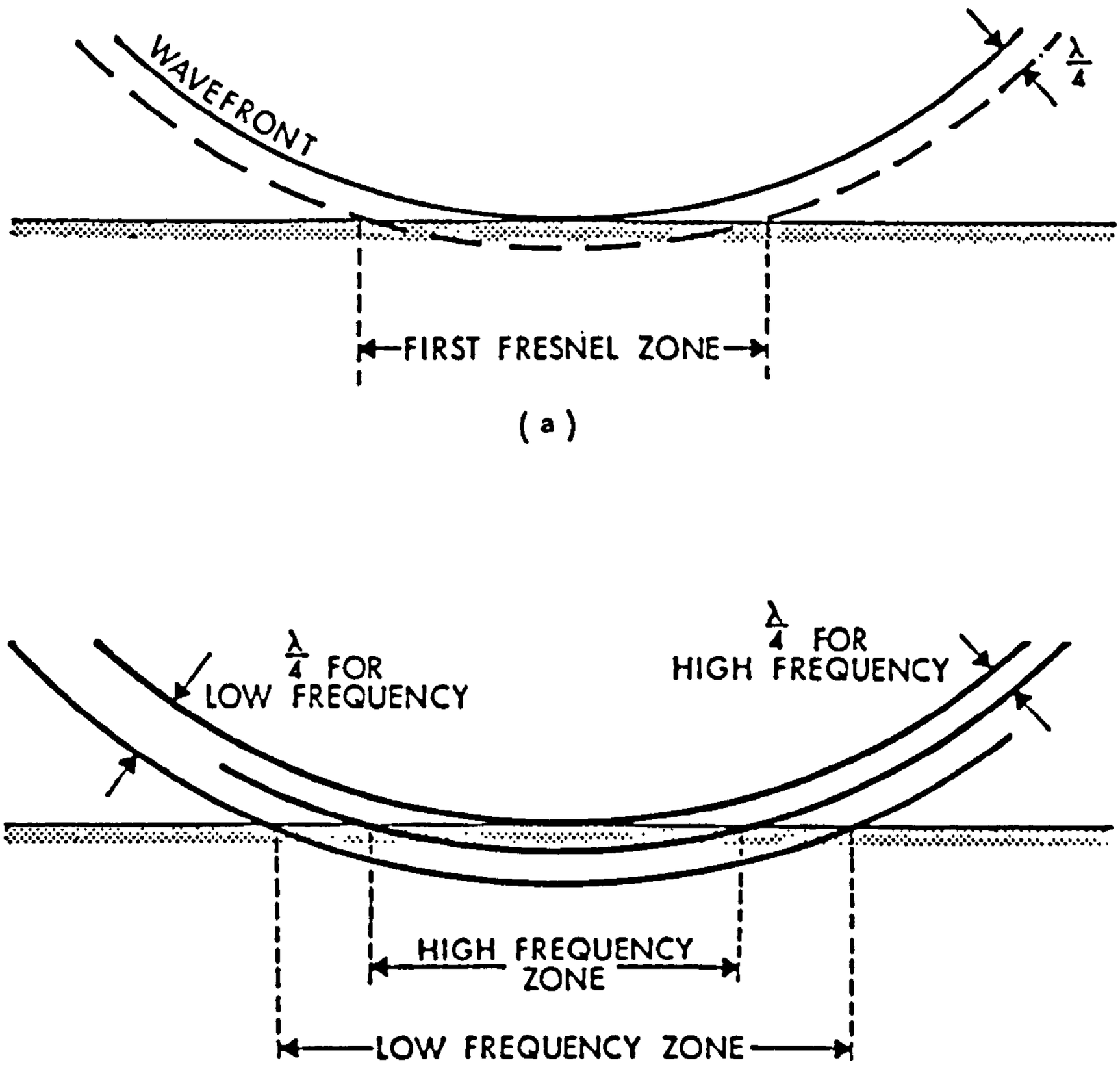

Figure 2.7. (a) The fresnel zone. (b) The fresnel zone for low frequency components is larger than for higher frequencies (after Sheriff, 1977).

200mm (Atkinson, 1993). The results may be quoted in mm and/or phi units,ϕ, where $\phi = \log_2 d$, and d is grain diameter.

Sediments may be referred to as cohesive or non-cohesive. Cohesion can be described as a function of surface particle and self weight forces. The magnitude of interparticle force is proportional to particle surface area and the self-weight force is proportional to the volume of the particles. Their relative importance can be defined by the specific surface which is the total surface area of all grains in unit mass. In coarse-grained sediments particle surface forces are minor compared to self weight therefore these sediments can be referred to as non-cohesive. When fine-grained sediments are densely packed the amount of contacts in unit volume increases producing a small cohesive strength (Atkinson, 1993). Atkinson (1993) states, however, that true cohesion is negligible unless the particles are cemented by other materials.

2.7.2. Moisture content (w)

Moisture content is a measure of the ratio of the amount of water to the amount of dry sediment and is expressed as a percentage:

$$w = \frac{\text{Weight of water}}{\text{Weight of solids}} = \frac{W_w}{W_s} \text{ or } w = \frac{\text{Mass of water}}{\text{Mass of solids}} = \frac{M_w}{M_s} \qquad (2.27)$$

2.7.3. Atterberg limits

These limits determine the changes in sediment strength behaviour in relation to moisture content. In a non-cohesive sediment a change in moisture content has only a slight affect on its strength. However, in a cohesive sediment changes in moisture content have a very noticeable affect on sediment strength. Therefore Atterberg limits only apply to fine-grained sediments.

The liquid limit (LL or w_L) is the boundary moisture content at which a sediment stops acting as a liquid and becomes a plastic solid. As the sediment becomes drier then it is able to resist greater shearing stresses, and eventually it becomes a brittle solid where it fractures. The moisture content at the fracture point is the plastic limit

(PL or w_P). The plasticity index (PI) is the range of water contents between the liquid and plastic limits.

Plasticity index = liquid limit - plastic limit

$$PI = LL - PI$$

$$I_P = w_L - w_P \qquad (2.28)$$

The liquidity index (I_L) provides a means of comparing a sediment's plasticity with its natural moisture content (w), i.e. defining the sediment behaviour in the context of its liquid and plastic limits, as illustrated in Figure 2.8:

$$I_L = \frac{w - PL}{PI} \qquad (2.29)$$

If $I_L = 1$, the sediment is at its liquid limit; if $I_L = 0$, the sediment is at its plastic limit.

2.7.4. Porosity (n) and void ratio (e)

As discussed above, porosity is quoted as being one of the most important properties governing sediment compressional wave velocity (Schreiber, 1968, Sheriff and Geldart, 1995, Esker *et al.*, 1996). Porosity is defined as the ratio of the volume of the voids to the total sample volume and in natural sediments porosity tends to range between about 35% and 90% (Hamilton and Bachman, 1982).

$$\eta = \frac{\text{volume of voids}}{\text{total volume}} = \frac{V_v}{V} \qquad (2.30)$$

Porosity can also be measured from void ratio, which describes pore space distribution and is defined as:

$$e = \frac{\text{volume of voids}}{\text{volume of solids}} = \frac{V_v}{V} \qquad (2.31)$$

The relationship between porosity and void ratio is:

$$n = \frac{V_v}{V} = \frac{V_v}{V_v + V_s} = \frac{e}{1 + e} \qquad (2.32)$$

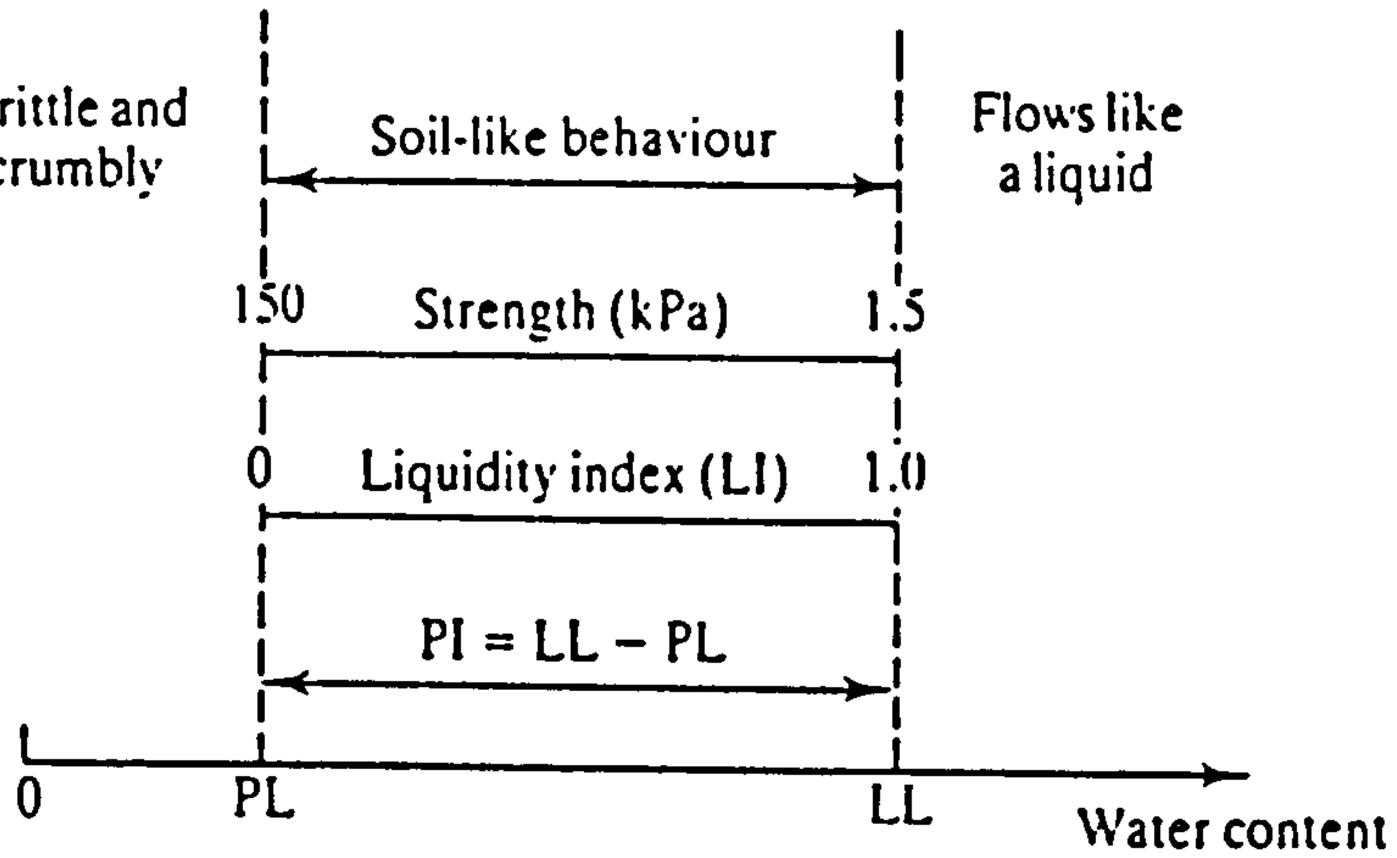

(a) Fine-grained soils

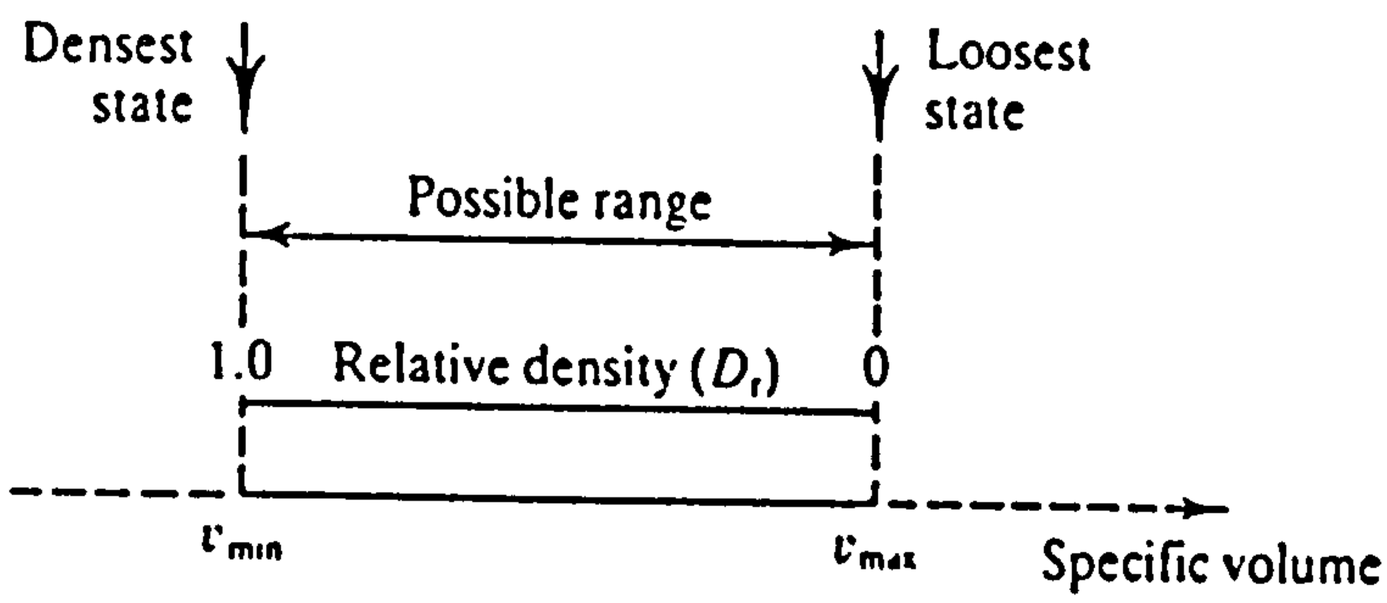

(b) Coarse-grained soils

Figure 2.8. Atterberg limits. (a) Fine-grained sediment limits. (b) Coarse-grained sediment limits (after Atkinson, 1993).

2.7.5. Degree of Saturation (S_r)

The pore spaces of a sediment can be either filled with fluid, gas or both, depending on environmental factors, and a sediment is described as saturated, dry or partially saturated respectively.

$$S_r = \frac{\text{volume of fluid}}{\text{volume of voids}} = \frac{V_w}{V_v} \text{ expressed as a percentage} \qquad (2.33)$$

2.7.6. Particle specific gravity (G_s)

The specific gravity of a material is the ratio of the weight or mass of a volume of material to the weight or mass of an equal volume of water.

$$G_s = \frac{M_s}{V_s \rho_w} = \frac{W_s}{V_s \gamma_w} \qquad (2.34)$$

where M_s is mass of the solids, V_s is volume of the solids, ρ_w is the density of the water, W_s is weight of the solids and γ_w is unit weight of water. As sediments contain a range of particles the G_s is an average value. As a guide, sands have an average value of 2.65 and clays 2.75.

Specific gravity and moisture content (w) can be related to void ratio by:

$$e = wG_s \qquad (2.35)$$

2.7.7. Unit weight (γ) and density (ρ)

For a given volume, the amount of sediment in that volume can be expressed in terms of its quantity of mass, M, or weight, W, in the volume:

$$\gamma = \frac{\text{weight}}{\text{volume}} = \frac{W}{V} \qquad (2.36)$$

$$\rho = \frac{\text{mass}}{\text{volume}} = \frac{M}{V} \qquad (2.37)$$

Unit weights can be defined as follows:

$$\text{Bulk unit weight, } \gamma = \frac{\text{Total weight}}{\text{Total volume}} = \frac{W}{V} = \frac{W_s + W_w}{V_s + V_v}$$

$$= \frac{G_s V_s \gamma_w + V_v \gamma_w S_r}{V_s + V_v} = \gamma_w \frac{(G_s + eS_r)}{1 + e} \qquad (2.38)$$

$$\text{Saturated unit weight, } \gamma_{sat} = \frac{\text{Saturated weight}}{\text{Total volume}}$$

$$= \gamma_w \frac{G_s + e}{1 + e} \quad S_r = 100\% \qquad (2.39)$$

$$\text{Dry unit weight, } \gamma_d = \frac{\text{Dry weight}}{\text{Total volume}} = \frac{\gamma_w G_s}{1 + e} \quad S_r = 0 \qquad (2.40)$$

Buoyant unit weight, γ', is the effective *in situ* weight of the sediment, where part of its weight is balanced by the buoyant effect of the water. This can also be referred to as submerged unit weight.

Buoyant unit weight = saturated unit weight - unit weight of water.

$$= \gamma_w \frac{G_s - 1}{1 + e} \qquad (2.41)$$

Similar expressions can be derived for the various densities:

$$\text{Bulk density, } \rho = \rho_w \frac{(G_s + eS_r)}{1 + e} \qquad (2.42)$$

$$\text{Saturated density, } \rho_{sat} = \rho_w \frac{(G_s + e)}{1 + e} \qquad (2.43)$$

$$\text{Dry density, } \rho_d = \rho_w \frac{G_s}{1 + e} \qquad (2.44)$$

$$\text{Buoyant density, } \rho' = \rho_w \frac{G_s - 1}{1 + e} \qquad (2.45)$$

Relative density (D_r)

A non-cohesive sediment can have a large range of void ratios dependent on packing. Maximum and minimum values can be calculated in the laboratory and related to the *in situ* void ratio. The relationship between maximum and minimum void ratios is expressed as relative density:

$$D_r = \frac{e_{max} - e}{e_{max} - e_{min}} \qquad (2.46)$$

For coarse-grained sediments it is the minimum and maximum densities which define the moisture content limits for sediment behaviour. As discussed in Section 2.7.3, it is the Atterberg limit tests which describe moisture content limits for fine-grained sediments. For example the minimum density of a sand is equivalent to the liquid limit of a clay and the maximum density, the plastic limit of the clay (Atkinson, 1993).

2.7.8. Shear strength

The shear strength (shear resistance) of a sediment can be defined as the maximum shear stress the sediment can withstand before failure results. The shear strength is a result of a combination of the frictional forces and cohesion which act together. Failure is resisted either by rupture along a slip surface, or by plastic deformation due to application of external stresses (Smith, 1990).

Frictional resistance varies with the value of the normal stress acting on the slip surface. This is as opposed to cohesive resistance which is independent of applied stress and is a constant value for a particular sediment. With this knowledge, Coulomb developed an equation in 1766 to describe the strength envelope of a sediment.

$$\tau_f = c + \sigma_n \tan \phi_i \qquad (2.47)$$

where τ_f = shear stress at failure on the slip surface,

c = unit cohesion (interparticle attraction effect),

σ_n = total normal stress on slip surface,

ϕ_i = angle of internal friction (angle of shearing resistance).

However, a further consideration for marine sediments is that the pore-water between the grains may be under pressure. When a load is applied to a saturated sediment, this load can be carried either by the sediment frame (grain to grain contact stresses), by the pore-water (causing an increase in pressure), or by a combination of both. This leads to the definition of effective stress σ':

$$\sigma' = \sigma_n - U \qquad (2.48)$$

where σ is total applied normal stress and U is pore-water pressure.

Coulomb's equation can be modified to account for effective stress instead of the total stress.

$$\tau_f = c' + \sigma' \tan \phi' \qquad (2.49)$$

where c' = unit cohesion, with respect to effective stresses,

σ' = effective normal stress acting on failure plane,

ϕ_i' = angle of shearing resistance, with respect to effective stresses.

Sediment shear strength will be further discussed in Chapter 6 with reference to cone penetrometer testing.

2.7.9. Sediment state

The following definitions are also used in descriptions of the state of a sediment (Smith, 1990):

Overburden - The overburden pressure at a point in a sediment is the weight per unit area of the material above it. The effective overburden is the pressure from this material less the pore water pressure due to height of water above the point.

Normally consolidated - This refers to a sediment which at no time in its history has been subjected to greater pressures than its current overburden pressure.

Underconsolidated - A sediment is considered to be underconsolidated when it has not been subjected to the pressures expected for the depth of burial (Davis, pers. comm., 1999).

Overconsolidated - An overconsoliated sediment is one which during its history has been subjected to greater pressures than its current overburden pressure.

Preconsolidation pressure - This is the maximum pressure of the overconsolidated sediment before removal of the pressure.

Overconsolidation ratio - This refers to the ratio of the effective preconsolidation pressure to the current effective overburden pressure.

2.7.10. Void index (I_v)

The void index profile represents a measure of the structural state of a sediment (Burland, 1990). This index is essentially a normalised void ratio which relates the *in situ* void ratio to that expected from the fully remoulded sediment at the same effective stress. It is therefore, considered to be a measure of the 'intrinsic' compactness of a sediment (Burland, 1990).

All remoulded sediments obey a common relationship which plots as the intrinsic compression line (ICL). Natural intact sediments tend to have a more open structure and consequently a higher void index and fall around another empirical curve called the sediment compression line (SCL). Figure 2.9 is a plot of void index versus effective stress which plots the ICL and the SCL.

The void index is defined as:

$$I_v = \frac{e_0 - e_{100}^*}{C_c^*} \qquad (2.50)$$

where e_0 = in situ void ratio

e_{100}^* = void ratio at 100kPa

C_c^* = compression index

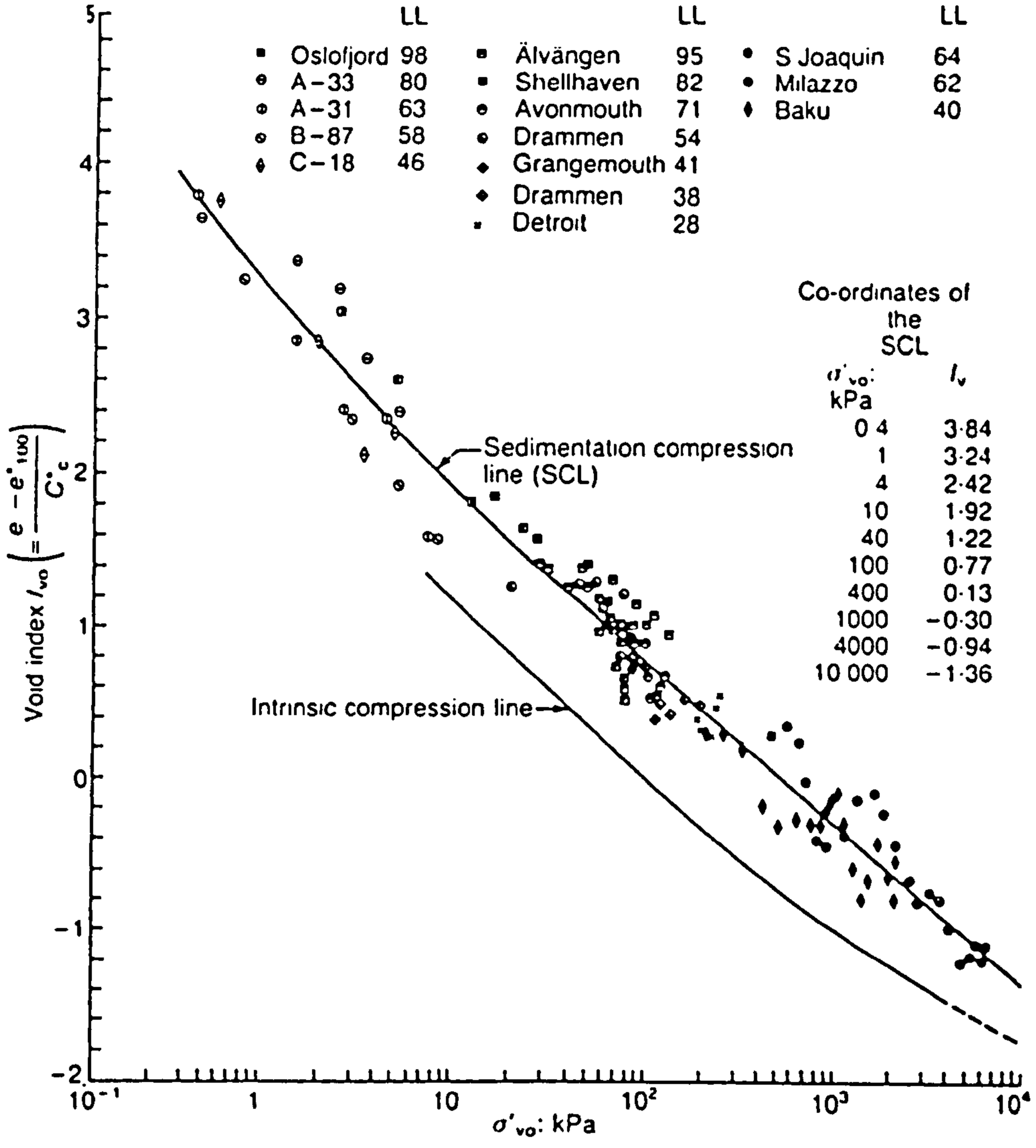

Figure 2.9. The general relationship between void index and effective stress for a range of normally consolidated clays (after Burland, 1990).

Burland (1990) presents a method for calculating the compression index and the 100kPa void ratio from the liquid limit:

$$e_{100}^* = 0.109 + 0.679e_L - 0.089e_L^2 + 0.016e_L^3 \quad (2.51)$$

$$C_c^* = 0.256e_L - 0.04 \quad (2.52)$$

where e_L is the void ratio at the liquid limit.

2.8. Theoretical studies of inter-relationships between physical and acoustic properties of marine sediments

Empirically-based measurements and models attempt to relate measurable properties. The relationships and models referred to in this section (2.8) are those developed purely theoretically and have no empirical basis.

2.8.1. Inter-relationships

As introduced in Section 2.4, Wood (1955) produced one of the first theoretical inter-relationships in unconsolidated sediments. Gassmann (1951) and several other authors used the basic Wood's emulsion equation as a basis for their work. In the case of Gassmann (1951) an equation for consolidated sediments which relates to low frequencies was developed.

2.8.2. Theoretical models

The theoretical model which is most often referred to is that of Biot (1956a, 1956b) who devised a general theory for elastic wave propagation in a fluid saturated porous medium.

Essentially Biot's theory predicts that, in the absence of boundaries, three kinds of body waves can propagate in a fluid-saturated, porous medium. Two of these waves are dilatational and subdivided into the "first kind" and the "second kind", and the other is a rotational wave, similar to a shear wave found in an elastic medium. In the "first kind" of dilatational wave the motions of the skeletal frame and the interstitial pore fluid are virtually in phase, and the attenuation due to viscous losses

is relatively small. Waves of the "first kind" are of principal interest in geophysical work in water-saturated sediments. The "second kind" of dilatational wave is highly attenuated, with the frame and interstitial fluid moving largely out of phase and is of most importance in acoustical problems involving compressible fluids such as air.

The Biot theory is for an isotropic, porous medium and is based on three constitutive equations which describe the coupled motion of the fluid and the solid frame. Biot (1962) added the effects of anisotropy, visco-elasticity and solid dissipation to the model.

In order to use the equations of Biot's general theory it is necessary to decide on realistic values for approximately 13 different parameters. Stoll (1989) divides the necessary physical parameters into three groups. The first group are frequency-independent operators, e.g. mass, density and compressibility of the sediment grains and the pore fluid; these can be extracted from standard references reasonably easily. The second group includes variables that affect the global fluid motion, e.g. permeability and viscosity of the pore fluid. The third group includes variables controlling the frequency-dependent response of the skeletal frame, i.e. shear and bulk moduli.

Stoll (1989) postulates that in many situations the permeability of the sediment and the frequencies of interest are low enough that the increasing fluid content is negligibly small for Biot's equations of motion to be simplified, thus becoming equivalent to those of Gassmann (1951). Indeed, in very soft sediments or suspensions, Wood's equation for the compressibility of a water sediment mixture can be deduced. Therefore Biot's theory is deemed to be a natural extension of earlier work by Wood (1955) and Gassmann (1951).

As the theory becomes better understood and more comprehensive, the necessary number of input parameters has increased to produce a more accurate model. Therefore the purpose now served by the general theory is to define the most meaningful input parameters for more simplified models (Stoll, 1989). In view of this, Badiey *et al.* (1998) have attempted to produce a simplified model on the basis of Biot-Stoll theory. An empirical process has been proposed in which existing empirical relationships have been reviewed and the data have been used in the simplified model to evaluate sound velocity and attenuation. Breitzke *et al.* (1996)

have used the Biot-Stoll model to produce full waveform ultrasonic transmission seismograms with a view to determining physical parameters of cores. Muthukrishniah *et al.* (1995) tested permeability predicted from the Biot-Stoll . method with measured values and found that the Biot-Stoll model generally underestimated the coefficient of permeability. However, they concluded that considering the variability of clay permeability the underestimation was relatively small.

2.9. Empirical studies of inter-relationships between physical and acoustic properties of a marine sediment

Throughout the literature a large number of empirical inter-relationships exist between the physical and acoustic properties of marine sediments. Hamilton (1970b) emphasises the great practical use in predicting physical and acoustic properties. However, Hamilton (1970b) also states that "compressional wave velocity is an elastic property of the sediment and is transmitted because of the sediment elasticity. Expressions such as 'the dependence of velocity on porosity' are not literally true in a physical sense. The 'non-elastic' properties affect velocity only in the effect they have on the sediment elasticity."

2.9.1. Inter-relationships

Faust (1951) realised that velocity tends to increase with depth (as discussed in Section 2.4) and produced an empirical relationship which relates velocity to burial depth and geological age:

$$V_p = 125.3\,(hT_g)^{1/6} \qquad (2.53)$$

Where V_p is in ft/s, h is in ft and T_g is geological age in years.

Wyllie *et al.* (1956) reviewed the variation of seismic velocity with porosity by conducting experiments to determine the affect of porosity on velocity in synthetic and natural porous media. They developed the following empirical relationship or time-average equation:

$$\frac{1}{V_p} = \frac{\eta}{V_{p(w)}} + \frac{1 - \eta}{V_{p(m)}} \qquad (2.54)$$

where η is porosity and $V_{p(w)}$ and $V_{p(m)}$ are the P-wave velocities through fluid and the solid matrix respectively. This time-average equation for a water saturated porous medium is based on the assumption that the porous medium can be replaced by alternating series of solid and liquid layers. Geertsma and Smit (1961) point out that the use of this relationship is reasonably acceptable, but the relationship does not take into account the bulk properties which are pressure-dependent.

Gardner *et al.* (1974) examined the relationship between velocity and density for rocks and the factors which influence reflection coefficients. A relationship was established between density and velocity, i.e. from a cross-plot of velocity and density which most rock types could fit empirically:

$$\rho = 0.23\, V_p^{1/4} \qquad (2.55)$$

where V_p is in ft/s. Gardner *et al.* (1974) summarised the effects and referred to Gassmann's theory (1951) to conclude that particle frame, microcracks and effective pressure (depth) are amongst the factors which will ultimately determine the reflection response.

Various authors concentrated on sediments and further developed relationships between acoustic and physical properties of a sediment to include attenuation, and to extend the interacting physical properties to take into account factors such as grain size and permeability.

Stoll (1986) postulated that the most important parameters which control the acoustic response of a marine sediment are:

- Porosity
- Density
- Overburden stress
- Degree and type of lithification
- Grain size and distribution

- Dynamic strain amplitude
- Material property of grains
- Sediment structure

Haynes *et al.* (1993b) summarised the relationships between the three main acoustic parameters (impedance, velocity and attenuation) and related physical properties of most interest to geotechnical engineers. Their summary is based on literature examples (e.g. Buchan *et al.*, 1972, Hamilton and Bachman, 1982, Richardson and Briggs, 1993). Figure 2.10 is a modified version of the relationships related to P-wave velocity.

Buchan *et al.* (1972) developed multiple regression relationships which allowed more than one variable to be used in the prediction. The variables used were essentially independent of each other. This approach meant that other variables, such as grain size distribution and specific gravity could be taken into account when developing empirical inter-relationships.

Inter-relationships developed and published by Hamilton and Bachman (1982) have been produced for specific geographical areas; the majority of the relationships apply to the upper 30cm of seafloor. An important feature of this work involved dividing the results into three general environments: continental shelf and slope, continental rise and abyssal plain. Regression analyses were performed on all of the physical and acoustic measurements and the definitive equations are listed in Figure 2.11. The regression equations for the continental shelf and slope were derived from the plots shown in Figure 2.12.

Many of the more recent studies of empirical inter-relationships refer back to the work of Hamilton (1980) and Hamilton and Bachman (1982). Orsi and Dunn (1991) examined glacial sediments from the seabed of the Barents Sea and produced a series of empirical relationships between geophysical and physical properties. They found that their relationships and errors were in agreement with those of Hamilton and Bachman (1982). Any differences found were attributed to the variations in clay mineralogy, and Orsi and Dunn (1991) concluded statistically that percent clay and mean grain size were the most important indices when calculating sound velocity.

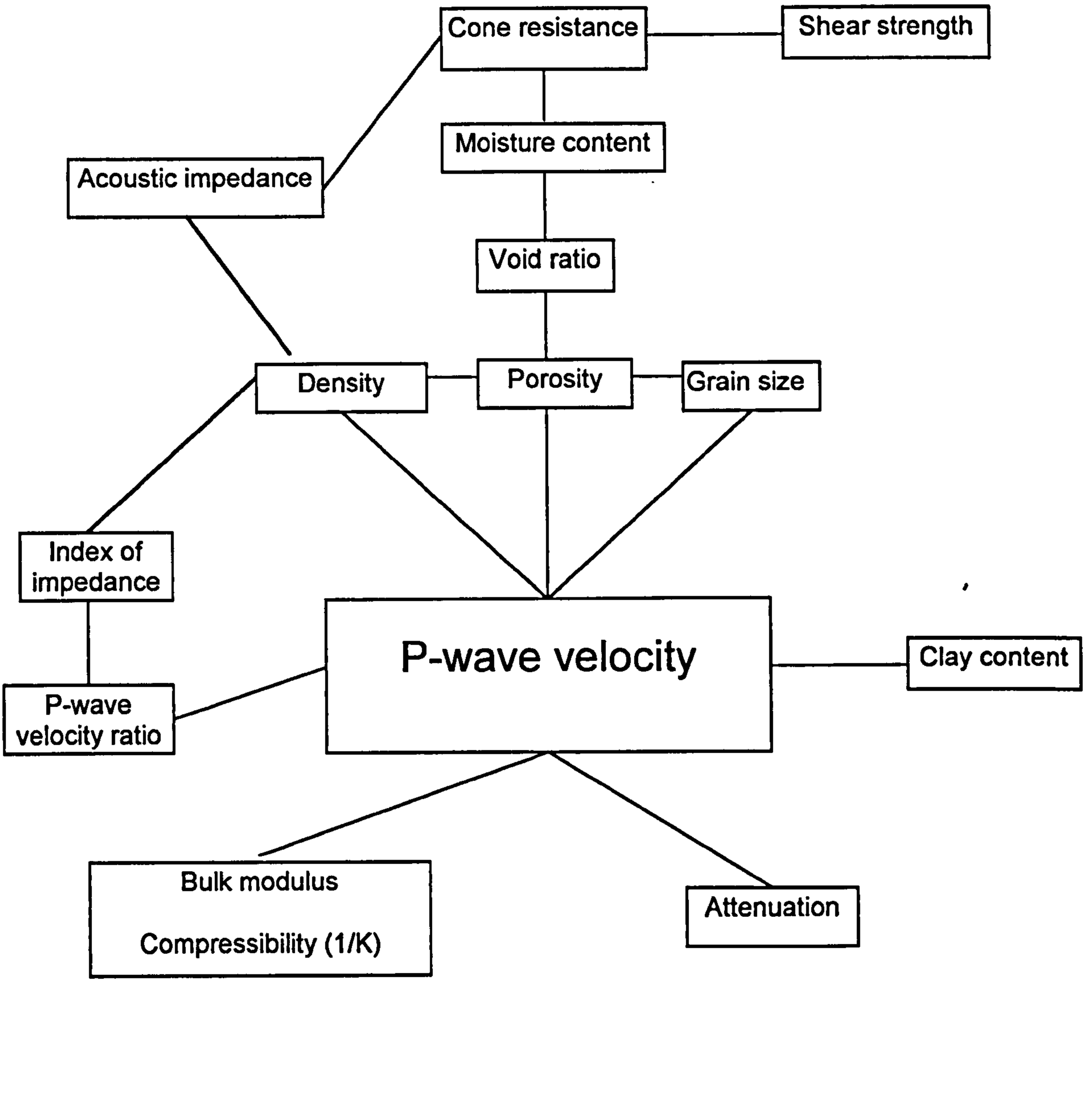

Figure 2.10. Empirical inter-relationships between the physical properties of a marine sediment and P-wave velocity.

Regression variables	Regression equations	Std. error of estimate
η (%) vs. ϕ	$\eta = 22.01 + 9.24\phi - 0.365\phi^2$	6.5
ρ (g/cm^3) vs. ϕ	$\rho = 2.374 - 0.175\phi + 0.008\phi^2$	0.11
V_p (m/s) vs. ϕ	$V_p = 1952.5 - 86.26\phi + 4.14\phi^2$	29
V_p (m/s) vs. η (%)	$V_p = 2502.0 - 23.45\eta + 0.14\eta^2$	31
V_p (m/s) vs. ρ (g/cm^3)	$V_p = 2330.4 - 1257.0\rho + 487.7\rho^2$	33

Figure 2.11. Empirical inter-relationships between physical and acoustic properties and calculated statistics (after Hamilton and Bachman, 1982).

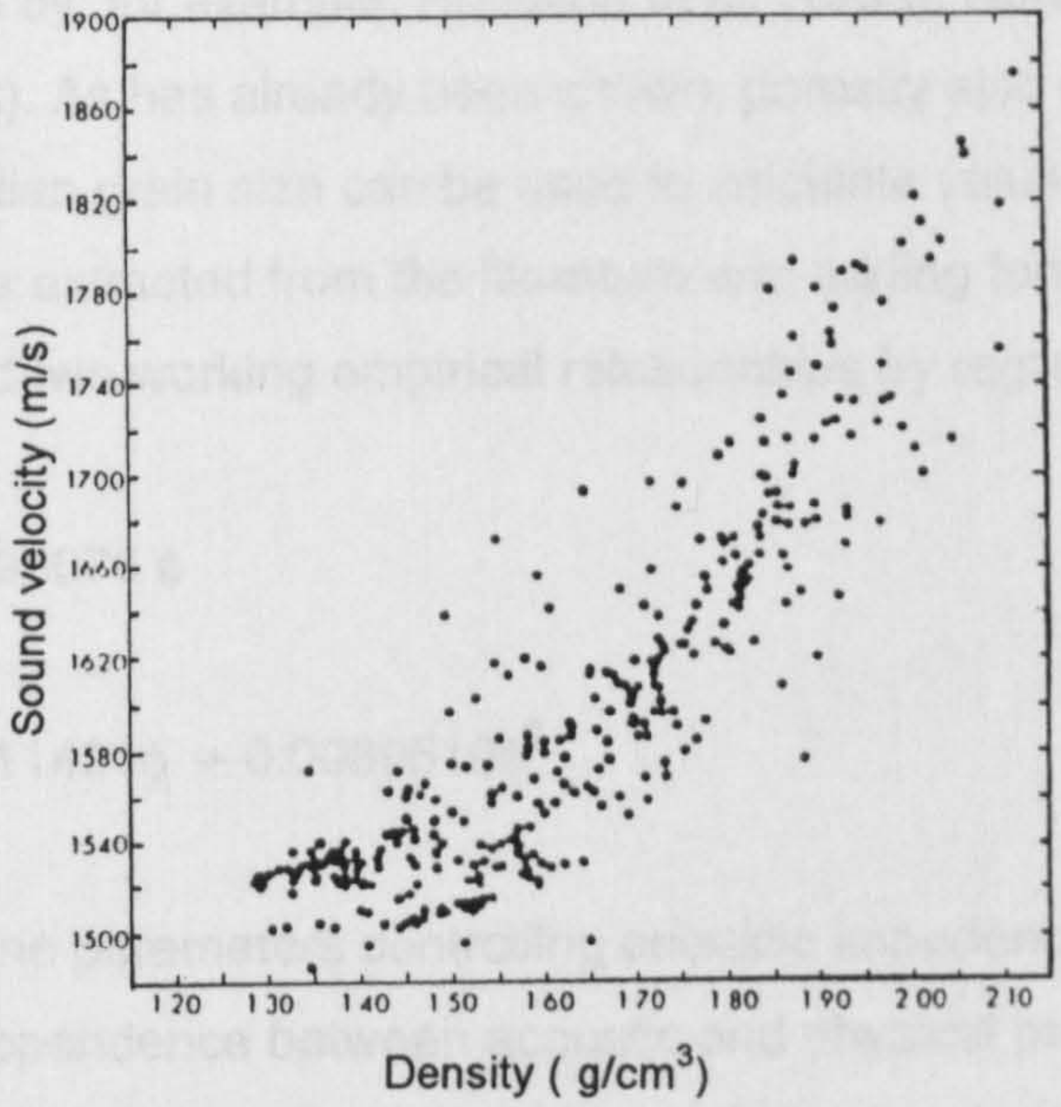

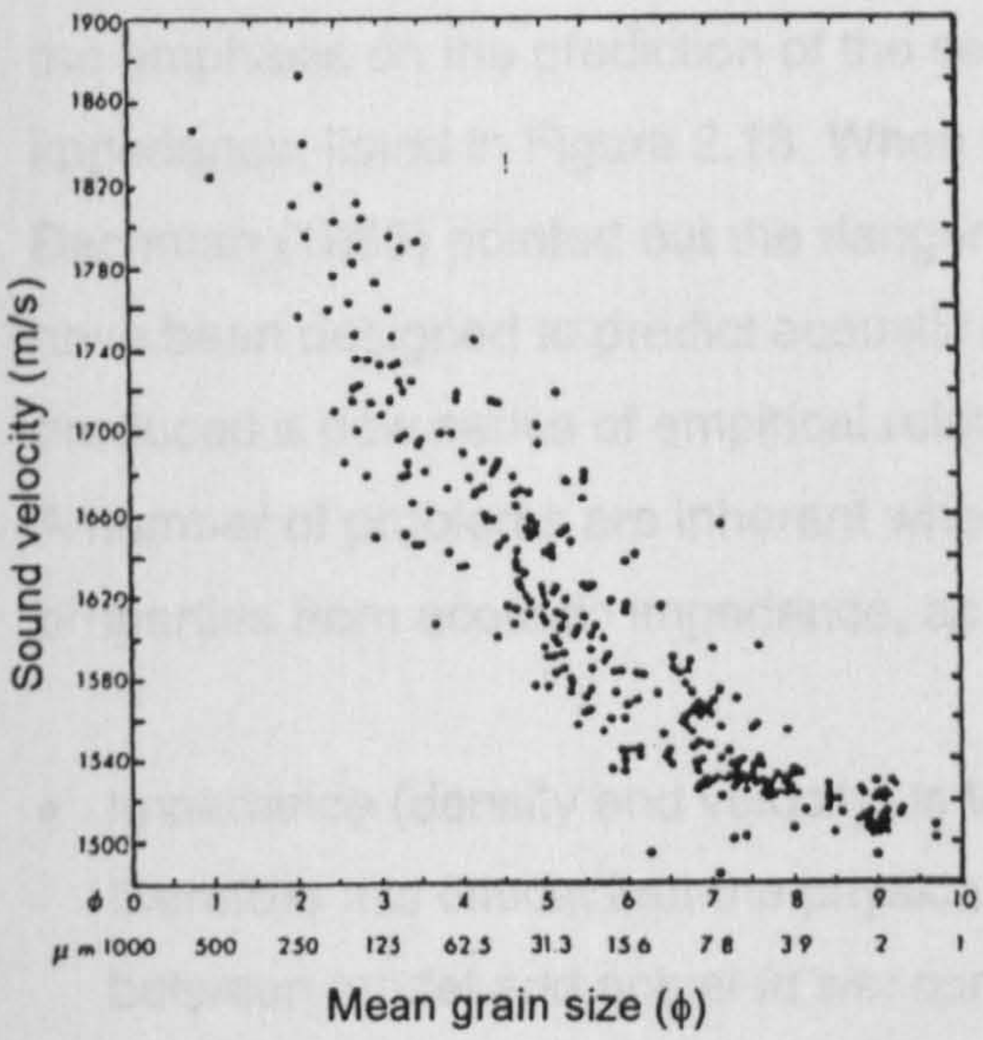

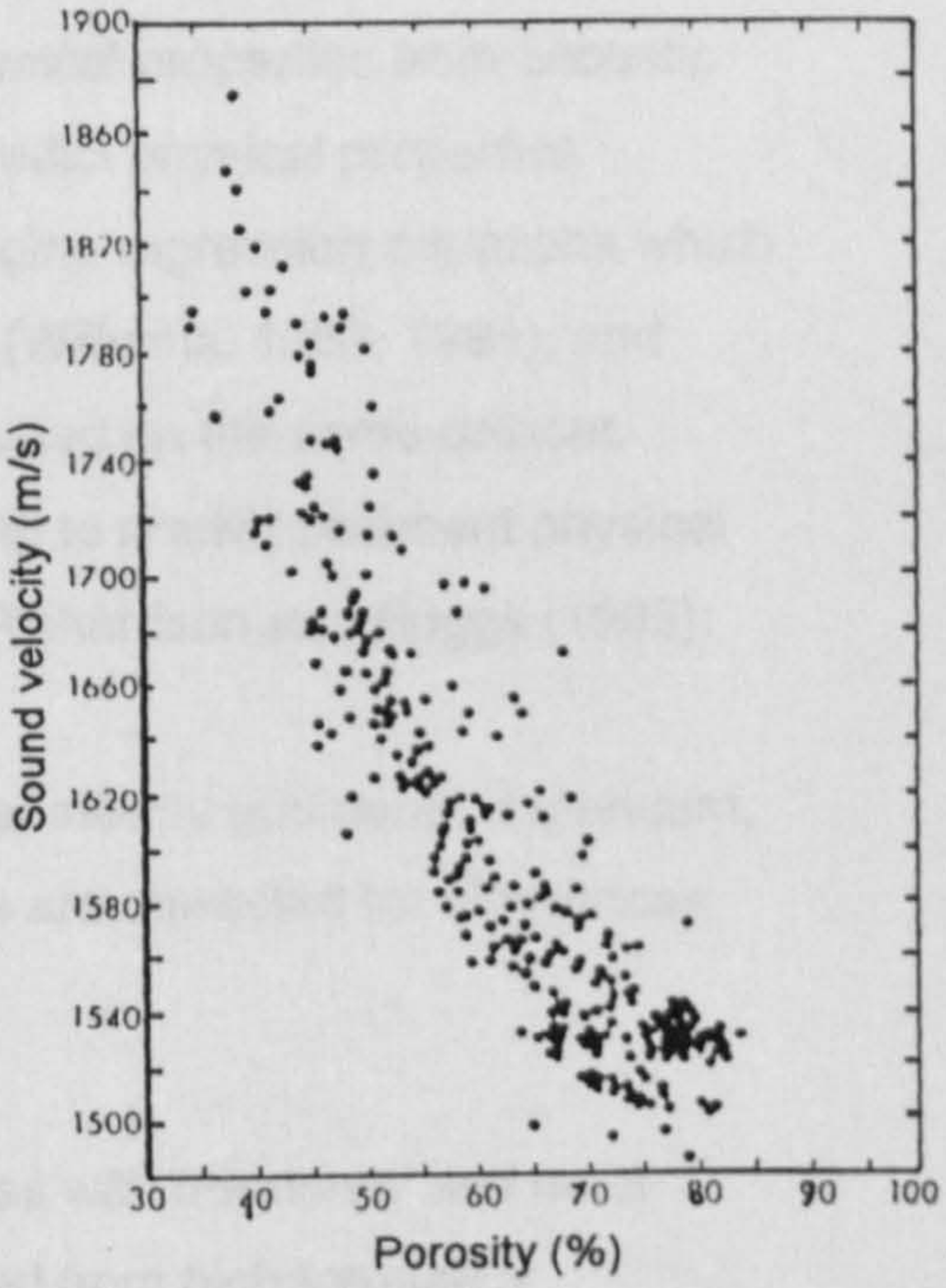

Figure 2.12. Relationships between physical and acoustic properties (after Hamilton and Bachman, 1982).

Esker *et al.* (1996) referred to porosity and median grain size as being the primary controls on density and velocity for siliciclastic sediment. Similar observations had already been made by, for example, Hamilton *et al.* (1956), Nafe and Drake (1957) and Almagor (1978). As has already been shown, porosity also depends on grain size, therefore median grain size can be used to calculate values of density and velocity. Using data extracted from the literature and adding further points, Esker *et al.* (1996) produced two working empirical relationships by regression:

$$\rho = 2.1539 - 0.098076\,\phi \qquad (2.56)$$

$$V_p = 1.9050 - 0.11401\phi + 0.0080510\phi^2 \qquad (2.57)$$

Referring back to the parameters controlling acoustic impedance given by Stoll (1986), the inter-dependence between acoustic and physical properties should clearly allow the extraction of physical property information from seismo-acoustic reflection data (Haynes *et al.*, 1993b). This is effectively the inverse to the approach used by, for example, Hamilton and Bachman (1982) who derived acoustic properties from physical property measurements. Bachman (1985) reviewed the empirical relationships previously derived by Hamilton and Bachman (1982) but with the emphasis on the prediction of the sediment physical properties from acoustic impedance, listed in Figure 2.13. When trying to predict physical properties Bachman (1985) pointed out the danger of rearranging regression equations which have been designed to predict acoustic properties (Williams, 1983, 1984), and produced a new series of empirical relationships based on the same dataset.
A number of problems are inherent when attempting to predict sediment physical properties from acoustic impedance, as noted by Richardson and Briggs (1993):

- Impedance (density and velocity) is temperature, salinity and depth dependent, therefore it is critical that the physical properties are corrected for differences between model and actual *in situ* conditions.

- The velocity and attenuation of a sediment varies with frequency and most published empirical relationships are constructed from high frequency measurements (100-400 kHz). However, most *in situ* seismic reflection systems operate at much lower frequencies (1-30 kHz) therefore frequency dispersion may be a critical consideration.

Regression variables	Regression equations
Z (kg/m^2/s) vs. ϕ	$Z = 4.5 \times 10^6 - 4.51 \times 10^5 \phi + 2.027 \times 10^4 \phi^2$
Z (kg/m^2/s) vs. ρ (kg/m^3)	$Z = 2.14 \times 10^6 - 1.63 \times 10^3 \rho + 1.163 \rho^2$
Z (kg/m^2/s) vs. η (%)	$Z = 6.06 \times 10^6 - 7.33 \times 10^4 \eta + 2.90 \times 10^2 \eta^2$
Z (kg/m^2/s) vs. V_p (m/s)	$Z = -1.607 \times 10^7 + 1.774 \times 10^4 V_p - 3.775 V_p^2$

Figure 2.13. Empirical inter-relationships between physical and acoustic properties (after Bachman, 1985).

- Most acoustic and physical property measurements and correlations are produced from measurements on laboratory core samples. Cores are often disturbed during handling, collection and analysis, resulting in laboratory measurements differing from the *in situ* state measurements.

- Empirical relationships developed from data relating to surficial sediments will differ from those relating to sediments from deeper within the sediment column.

- Physical property variability does occur on various spatial scales which may distort the interpretation of data where the same acoustic classification systems are used globally (Panda *et al.*, 1994, Sawyer *et al.*, 1997).

Following the work of Buchan *et al.* (1972) and Hamilton and Bachman (1982), Richardson and Briggs (1993) produced a new series of empirical relationships based on geoacoustic and physical properties measured on 211 cores from 11 worldwide sites. The properties measured were normalised sound speed, V_{pr} (ratio of sediment speed to speed of overlying water in the core), sound attenuation, k_s, porosity, bulk density, mean grain size, M_z, impedance, Z, and the index of impedance, IOI (the product of sediment velocity ratio and the sediment density). Figure 2.14 show the regression equations and the coefficients of determination (r^2) which were constructed for the properties discussed above.

Richardson and Briggs (1993) agreed with Anstey (1991) in that empirical relationships are correlative rather than causal and common in marine sediments. The relationships developed by Richardson and Briggs (1993) proved to be similar to those given by Bachman (1985) for continental terrace sediments.

2.9.2. Empirical models

Hamilton (1980) defined an empirical, geoacoustic model as 'a model of the real sea floor with emphasis on measured, extrapolated and predicted values of those properties important in underwater acoustics, and those aspects of geophysics involving sound transmission'.

Regression variables	Regression equations	r^2
V_p ratio vs. ϕ	$V_p = 1.180 - 0.034\phi + 0.0013\phi^2$	0.820
V_p ratio vs. η (%)	$V_p = 1.574 - 0.015\eta + 0.0001\eta^2$	0.954
V_p ratio vs. ρ (g/cm^3)	$V_p = 1.623 - 0.936\rho + 0.3417\rho^2$	0.944
V_p ratio vs. Z x 10^5 (g/cm^3/s)	$V_p = 1.174 - 0.207Z - 0.0560Z^2$	0.972
ϕ vs. IOI	$\phi = 20.23 - 9.48IOI + 0.667IOI^2$	0.828
η (%) vs. IOI	$\eta = 202.14 - 120.70IOI + 21.598IOI^2$	0.996
ρ (g/cm^3) vs. IOI	$\rho = -0.502 + 1.802IOI - 0.3050IOI^2$	0.966
V_p ratio vs. IOI	$V_p = 1.173 - 0.315IOI + 0.1296IOI^2$	0.972
ϕ vs. η (%)	$\phi = -4.55 + 0.169\eta$	0.805
ϕ vs. ρ (g/cm^3)	$\phi = 22.85 - 10.275\rho$	0.809

Figure 2.14. Empirical inter-relationships between physical and acoustic properties with calculated statistics (after Richardson and Briggs, 1993).

Hamilton (1980) considered that for a full geoacoustic model for any type of geophysical/geological study or investigation then the following fundamental parameters are required:

- Geological interpretation over the depth of interest
- True thickness measurements and major boundary identification
- Compressional and shear wave velocities and attenuation estimates
- Density
- Elastic properties

A significant part of geoacoustic model construction is the measurement and calculation of the input parameters. By using various inter-relationships from the literature, parameters which are deemed unmeasureable can be estimated. This enables a fuller picture to be produced and therefore greater available parameter selection.

One of the ultimate aims of creating explicit models, such as those produced by Huws (1993), is to make seismo-geotechnical data, particularly location specific data, available to a range of users who may not be familiar with this type of information.

2.9.3. Correlation between properties

Figures 2.11, 2.13 and 2.14 illustrate the empirical relationships described above together with the associated statistical correlations. It is these statistics which are used to determine the degree of correlation between properties.

2.9.3.1. Porosity

As shown previously, porosity is a measure of the amount of pore space in a sediment and is a result of complex, interrelated factors such as grain size, shape, distribution, packing and mineralogy. In general, a decrease in porosity corresponds with an increase in grain size.

Porosity is an easily measured parameter and produces a predictable relationship with compressional wave velocity. Hamilton (1970b) attributes this to the

compressional wave velocity being determined largely by the effects of the compressibility of the pore fluid as opposed to the compressibility of the mineral grains in an elastic system.

Nobes (1989) constructed a set of equations which relate velocity to porosity using a modification of the time average model developed by Wyllie *et al.* (1956), (reviewed in Section 2.9.1) and Wood's equations, (Wood, 1955). Measurements were made on both consolidated and unconsolidated sediments and a good correlation was found between these measurements and the models.

2.9.3.2. Grain size

Hamilton (1970b) discovered that the most easily recognisable attribute of a sediment is its predominating particle size, and showed that an increase in mean grain size brought about an increase in velocity. Horn *et al.* (1968) concluded that mean grain size is a better index of the other properties than median grain size as it is a more effective measure of size distribution.

Hamilton and Bachman (1982) and Schreiber (1968) identified a large amount of scatter in the relationship between mean grain size and porosity and attributed this to a number of interrelated factors, the most significant being grain size, sorting, shape, packing and mineralogy. However, as grain size decreases into the silt/clay range, then it is the intermolecular forces between the mineral grains which become important and the sediment assumes a highly porous structure (honeycomb structure).

A further importance of this relationship is that size analyses can be conducted on dried samples whereas, in order to be valid, the other physical measurements need to be made on fully saturated samples.

2.9.3.3. Density

The relationship between density and sound velocity is similar to that of porosity and sound velocity due to the linear relationship between density and porosity. Hamilton (1970b) quotes environmental differentiation as a major factor in any deviation from the general trend of this relationship.

2.9.3.4. Index of impedance

Richardson and Briggs (1993) identified the index of impedance, IOI (the product of sediment velocity ratio and the sediment density) as a very good predictor of bulk density, porosity, mean grain size and sound speed and suggested that it could be used with confidence to predict sediment type.

2.10. Summary

Research into the inter-relationships between acoustic and physical properties has been carried out over many decades. This published research has illustrated the large number of correlations possible between physical and acoustic parameters. The literature also shows the large variety of data required for empirical inter-relationship studies when considering all the types of depositional environments.

A fundamental element of the research presented in this thesis involves understanding the physical/geotechnical environment, with the emphasis on being able to relate this to, and better understand, seismo-acoustic responses. The chapter has introduced the complexities involved in the passage of a seismic wave and the influences of the physical environment on these acoustic properties. This emphasises the difficulties encountered when attempting to model the resultant seismic trace.

Forward modelling for comparison with seismic data requires access to impedance logs; these however are generally not available for the sediments close to seabed. This project therefore, attempts to make use of empirical inter-relationships to derive the acoustic properties from physical parameters of a sediment in order to allow forward models to be produced for improving the interpretation of seismo-acoustic data.

The published inter-relationships referred to in this chapter are for measurements made on Quaternary seabed, and close to seabed, sediments. Within this project these relationships will be extrapolated to the deeper subsurface Quaternary sediments. This will therefore be a significant test of their applicability beyond the zone of initial measurement. The main case study used to test the validity of the

method revolves around a deep-water, glacially influenced environment for which no empirical inter-relationships currently exist.

CHAPTER 3

THE SYNTHETIC SEISMOGRAM

3.1. Introduction

A very effective and powerful method of predicting and understanding the seismic response of a layered subsurface is by forward modelling. This can be achieved through the production of synthetic seismograms. Synthetic seismograms are widely used as a method of identifying and modelling stratigraphic features which have produced reflections on multi-channel common depth point (CDP) seismic reflection sections.

Chapter 2 introduced the concepts of physico-acoustic empirical relationships and the physical properties which provide the basis for these inter-relationships. In this research project synthetic seismograms are generated to predict and evaluate the seismic response. The synthetic seismograms in this project will be modelling single channel, normal incidence high resolution seismic data from CPT results and borehole sampling test data. High resolution seismic data may often still be collected in analogue format only and will have had a gain function added to compensate for signal attenuation. Therefore a synthetic seismogram, which accounts for transmission losses and multiples, is used in this project as a basis from which to model the seismic data. The rationale behind beginning with a simple method is that it is hoped that, in the first instance, the geological environment can be better understood by starting from basics. A 1-D, simple synthetic seismogram also allows evaluation of the forward modelling method developed in this project using CPT results and borehole sampling test data to produce impedance logs. Chapter 2 also discussed the affects of spherical divergence and attenuation on seismic data and these factors will be further evaluated and discussed in Chapter 5.

The theory behind the generation of a synthetic seismogram, which forms the basis of the forward model developed in this project, is presented in this chapter.

3.2. Basic principles

The simplest synthetic seismogram is one-dimensional and assumes horizontal subsurface layering and normal incidence vertical raypaths. This basic synthetic seismogram, x(t), is a convolution of a source function, s(t), with a reflectivity function, r(t):

$$x(t) = s(t) * r(t) \qquad (3.1)$$

Convolution is a mathematical calculation which determines the effect of a filter on a signal, in this case the filter is the water column and the sediment layers. The reflectivity function is built from the assumption that a wavelet, reflected from and transmitted through an acoustic impedance change, has the same waveshape as the incident wave. Therefore the seismic record is built up of a series of these wavelets generated from reflections back from the acoustic impedance discontinuities and is represented by the reflectivity function. As described in Section 2.6, acoustic impedance of a specific layer is calculated by multiplying velocity and density; Section 2.6.1 explained the calculation of the reflection coefficient from impedance changes and Figure 3.1 illustrates the procedure for the generation of a synthetic seismogram both in terms of time and depth.

3.3. Development of the synthetic seismogram method

The first synthetic seismograms were developed in the 1950s and have become more mathematically complex, but their basic use still remains, i.e. to aid in the identification and mapping of interfaces and beds of interest. For instance, seismic sections may have time and phase shifts of unknown magnitude which can be estimated by modelling using synthetics.

Peterson *et al.* (1955) used velocity logs to simulate acoustic impedance variations and produce synthetic reflection records. The synthetic depth records were then converted to reflectivity records in time. By convolution of the reflectivity function with an assumed source wavelet, the first synthetic seismograms were produced.

Wuenschel (1960) developed synthetic seismograms which included multiples and transmission coefficients at normal incidence in the time domain. Treitel and

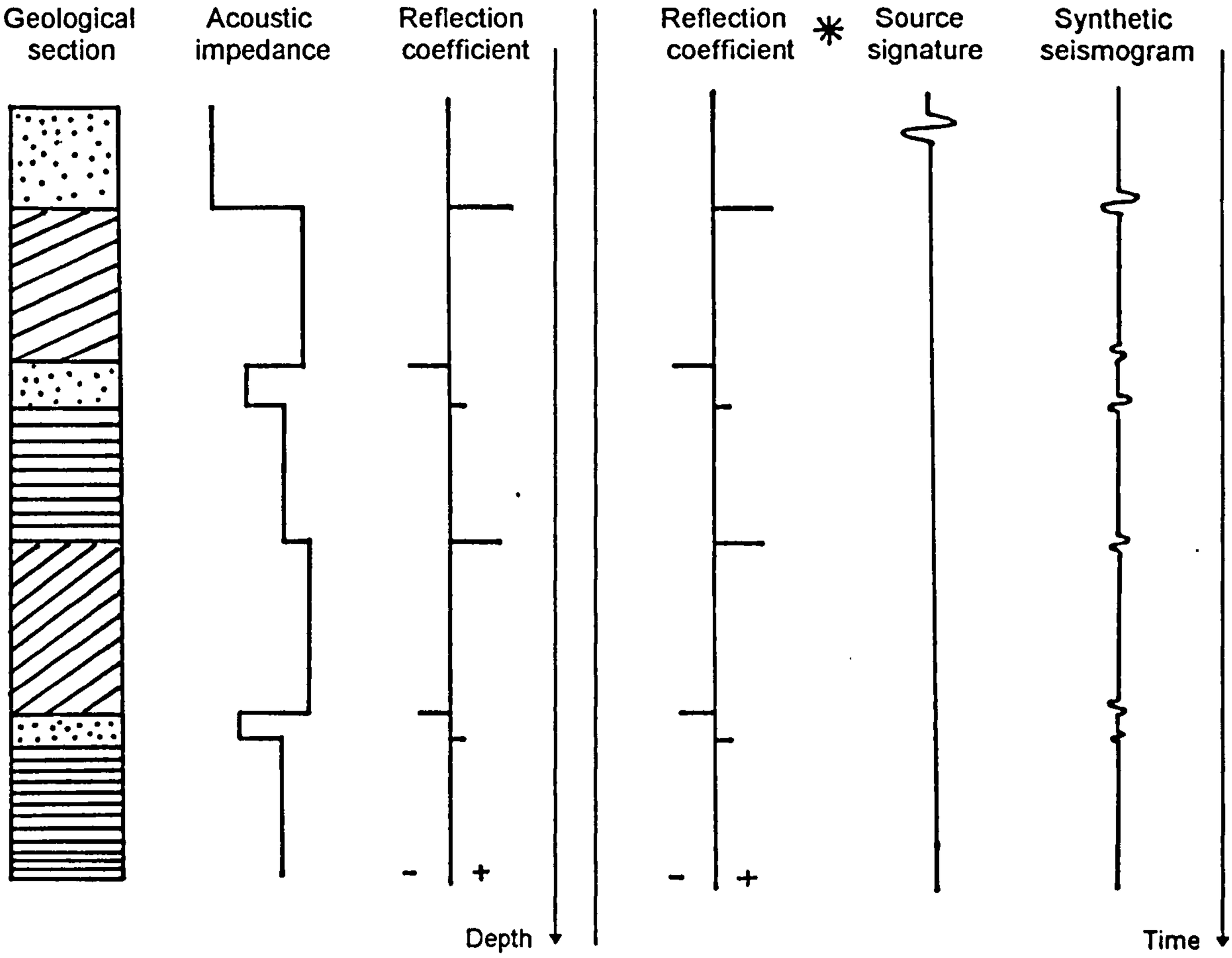

Figure 3.1. Synthetic seismogram process in the depth and time domains.

Robinson (1966) and Claerbout (1968) produced the impulse response of a horizontally layered earth assuming plane waves at normal incidence generated by a source at the surface.

Fuchs and Muller (1971) made comparisons between the ray theory method introduced by Peterson *et al.* (1955) and performed in the time domain, and the reflectivity method, which Treitel and Robinson (1966) performed in the frequency domain. The ray theoretical method essentially traces rays from a source, i.e. summing of the seismograms corresponding to the primary and multiple rays from the source to the point of observation or receiver. This method tends to be used for more general situations to give an overall picture of the subsurface and is less detailed.

The reflectivity method is a numerical integration of the reflection coefficient of a layered medium and is carried out in the horizontal wavenumber or angle of incidence domain. The reflectivity method is more likely to incorporate multiples and converted waves in the reflecting zone and is therefore used for more accurate studies of particular features (Fuchs and Muller, 1971). Thybo (1989) points out the problems of using frequency domain methods, i.e. the method implies uniformly digitised spectra therefore the resulting time series are periodic. Late arrivals are wrapped around showing false arrival on the synthetic seismograms. Thybo (1989) has developed a method of removing this wrap-around effect which allows frequency domain methods to be used in any horizontal stratification as opposed to time domain methods which need equal traveltime pseudolayering. Time domain methods are by far the most popular (Thybo, 1989).

Trorey (1962) included dispersion, while Ganley (1981) and more recently Turgot and Yamamoto (1988) developed one dimensional synthetic seismograms for normal incidence waves in a horizontally layered poroelastic medium which includes the effects of dispersion and attenuation. These effects are predicted from Biot's theory and were developed specifically for vertical seismic profiling (VSP). When calculating the reflection and transmission coefficients, Turgot and Yamamoto (1988) included mode conversion which occurs when fast and slow compressional waves are excited. This effect was the energy-loss mechanism associated with conversion to slow compressional waves in the resulting synthetic seismograms. Turgot and Yamamoto (1988) also postulated a spectral ratio method of extracting

porosity and permeability from the synthetic seismograms once the phase velocity and attenuation have been accurately determined by waveform inversion.

3.4. Use of synthetic seismograms

In general in the production of synthetic seismograms the acoustic impedance information is taken from borehole logs, i.e. sonic and density. Where only sonic logs are available density can be assumed to be constant or it can be related to velocity using Gardner's rule (Sheriff and Geldart, 1995) which applies generally to the major sedimentary lithologies:

$$\rho = a_r V^{1/4} \qquad (3.2)$$

where $a_r = 0.31$ when V is in m/s. In practice the logs tend to be sampled at a regular traveltime interval and where small variations occur then an average value is assumed.

When matching the synthetic seismogram with actual seismic data many differences often become apparent, particularly when the match is not very good. The methods of acquisition and processing will critically affect the results, such as inaccurate logging and positioning. The data used to construct the seismograms are an obvious area where discrepancies may occur. Walden and White (1984) postulate that the most accurate synthetic seismogram will have the best estimate of noise on the traces.

Velocity mismatches are a very common problem, particularly in a geologically complex area, and the use of velocities from sonic logs, compared with velocities derived during processing, may cause discrepancies where they do not agree (Schnack-Friedricksen, 1997). The use of single point well logs highlights the issue of comparing a model of vertical raypaths in horizontal bedding with common depth point sections.

Knowledge of the wavelet shape being used is of great importance to understanding the synthetic output; use of a reliable extracted wavelet will aid in the interpretation. However, Ziolowski (1991), in the context of deconvolution, is critical of wavelet estimation methods and stresses the importance of source signature

measurements (Hron and Covey, 1983). The inclusion of transmission losses and multiples may have an effect on the seismic energy and therefore the velocity. Initial synthetic seismograms may contain primary reflections only, and multiples and transmission losses may be added during successive iterations to build up the picture and to understand the seismic data. Anstey (1960) puts forward criteria for making the decision on how complicated a synthetic seismogram should be for comparison with seismic traces. The main criteria is the quality of the field data to which the synthetic seismogram will ultimately be compared.

High resolution seismic reflection data tend to be more difficult to model using synthetic seismograms due to the general lack of well logging data, i.e. the continuous sonic and density logs generally available in hydrocarbon exploration. The top 100m tends not to be rigorously logged therefore velocity and density information is often not available, and geophysical logging is not normally performed as a part of a shallow site investigation. This in turn leaves more reliance on the seismic data alone and coarse sampling methods which may not give adequate depth information.

3.5. Seismic data inversion

As a compliment to forward modelling many researchers are also working on extracting impedance from the reflection record with a view to deriving physical properties from seismic data. Research is well advanced on the extraction of impedance, such as presented by Berteussen and Ursin (1983), Carrion and Patton (1983), Oldenburg *et al.* (1983). More recently, using high resolution seismo-acoustic data, Haynes *et al.* (1993a and 1993b) and Haynes (1996) have attempted to extract impedance values from seismic reflection data. Empirical inter-relationships can then be used to calculate physical properties for calibration of seismo-acoustic data for sediment classification (Richardson and Briggs, 1993). Panda *et al.* (1994) produced a sediment classification scheme using impedance inversion of wideband sonar data with estimates of attenuation. The impedance values were then used to predict physical and acoustic properties.

Nauroy *et al.* (1998) used inversion techniques to integrate very high resolution (VHR) site investigation seismic and geotechnical data offshore Monaco in stiff carbonate silts. Borehole profiling by vertical seismic profiling (VSP) using a seismic

cone produced V_p velocities which could be directly related to CPT test data at the same location. Impedance logs were generated from the VSP measurements and correlated with cone resistance measurements, these correlations were then applied to the inversion of VHR seismic data. Nauroy *et al.* (1998) were then able to transform derived impedance versus time to cone resistance versus depth and to invoke empirical inter-relationships between cone resistance, velocity and impedance. However, through testing they concluded that the inter-relationships were highly site specific and were not applicable for global use.

3.6. Summary

Synthetic seismograms range from very simple to very complex and the choice of synthetic algorithm is dependent upon the end purpose. The synthetic seismogram to be used in the forward modelling for the purpose of this study needs to be simple. This necessary simplicity is to enable all the potential variables which affect the seismic response to be assessed. Only once this has been adequately achieved should any complexity be added.

Synthetic seismograms have been successfully used for forward modelling based on physical properties (Esker *et al.*, 1996). In Esker *et al.*'s study median grain size was measured from 4-6m vibrocores and plotted alongside published empirical sample data from water depths of less than 200m. Two empirical inter-relationships (Equations 2.56 and 2.57) were calculated which could predict density and velocity with which to generate synthetic seismograms. This research project aims to go beyond the work of Esker *et al.* (1996) by using borehole sampled groundtruth data, as opposed to vibrocore samples for physical properties, in the 'Borehole method' which would have been subjected to less sample disturbance than the samples recovered by vibrocoring. The 'CPT method' attempts to automate the test interpretation process and relate the seismic response directly to the CPT test. A further dimension of this research is to use the published empirical inter-relationships which relate to sediments close to seabed and test their applicability to sediments deeper within the sediment column.

The synthetic seismograms will also be used in this study to consider the influences of the indirect properties, such as mean grain size, on the seismic response. Chapter 5 will evaluate the affects on the seismic amplitudes of noise, spherical

divergence and absorption and assess the applicability of including these effects on a synthetic seismogram.

CHAPTER 4

SEISMIC STRATIGRAPHY

4.1. Introduction

Forward modelling and prediction of the seismic response can be particularly crucial aspects of seismic interpretation. It is the rigorous integration of geotechnical and geophysical data which will provide an optimum interpretation.

For interpretation of seismic data which goes beyond a pure structural analysis, the hydrocarbon industry employs seismic stratigraphic techniques. The justification for the widespread use of this approach in hydrocarbon exploration is highlighted by Sheriff (1980) who postulates that "better data quality, improved understanding of the geological significance of waveshape, and the need for standardised analysis procedures, has meant that the use of seismic stratigraphy is clearly feasible".

Seismo-stratigraphic techniques were developed for the interpretation of exploration 2D/3D seismic data. However, these techniques are now increasingly being applied to interpretation of high resolution seismo-acoustic data but without, as yet, a full understanding of the complex process interactions controlling the seismo-acoustic response. This project concentrates specifically on Quaternary sequences where seismo-stratigraphic methods are not routinely applied. The additional complexities with Quaternary sequence investigation is the general lack of physical and acoustic data for groundtruthing and forward modelling. This lack of data is particularly critical where the depositional environment is glacially influenced as is the case with the data chosen for this research.

4.2. Sequence stratigraphy

The concept of sequence stratigraphy is concerned with the effects of relative sea level changes on sedimentation.

Sheriff and Geldart (1995) define the four factors controlling sediment deposition which they postulate as being the underlying concepts of sequence stratigraphy:

- Accommodation or space available to receive sediments created because of subsidence of the crust due to tectonics (and/or thermal expansion) and/or isostasy (the tendency of the earth's crust to maintain a state of near equilibrium).

- Sediment inflow, i.e. sediment infilling the accommodation space.

- Eustasy, i.e. rises and falls of absolute sea level. It is the combination of subsidence and eustasy which ultimately determines relative sea level which in turn dictates the amount of accommodation available.

- Climate, which will determine the nature of the sediments being deposited.

It is the interaction of these factors, in particular the sediment inflow and eustasy, which determines depositional patterns. Thus it can also be concluded that seismic reflections indicate the surface of the solid earth at the time of sediment deposition.

4.3. Seismic stratigraphy

Seismic stratigraphy is the subdivision of the seismic record into sequences of reflections (units) that are interpreted as being genetically related sedimentary sequences. This effectively makes it possible to attempt to work out the depositional environment of these units from their 2D/3D shape and internal configuration.

The fundamental principle of seismic stratigraphy is that within the resolution of the seismic method, seismic reflections follow gross bedding surfaces and as such they approximate time lines. A seismic sequence therefore, is defined as the representation on a seismic record of a depositional sequence, i.e. it is a group of concordant or near-concordant reflection events that terminate against the discordant reflections of adjacent seismic sequences (Bertram, 1995).
The approach to seismic stratigraphy was first subdivided by Mitchum and Vail (1977) into:

- *Seismic sequence analysis* - dividing the seismic record into time-depositional units.

- *Seismic facies analysis* - determining depositional environment from reflection characteristics, an extension of seismic sequence analysis.

- *Sea level analysis* - analysis of relative changes of sea level for comparison with global data based on a regional scale.

Sheriff (1980) postulated a working approach as being (1) seismic sequence analysis, (2) seismic facies analysis and (3) reflection character analysis which is the study of the lateral variation of individual and groups of reflection events.

The approach of Mitchum and Vail (1977) was further refined by Vail (1987) into seven steps, (1) seismic sequence analysis, (2) well-log analysis, (3) well-to-seismic synthetic tie analysis, (4) seismic facies analysis, (5) interpretation of depositional environment and lithofacies, (6) forward modelling and (7) the final integrated interpretation.

Within seismic stratigraphy there are two scales of interpretation: seismic sequence and seismic facies analyses which are carried out on a regional level, and reflection character analysis which examines individual reflections looking for the specific stratigraphic changes (McQuillin *et al.*, 1986). This project will concentrate on seismic sequence analysis, seismic facies analysis and reflection character analysis and these will be introduced in this chapter. Chapter 3 has introduced forward modelling and the integrated interpretation approach is tested in Chapter 7.

4.4. Seismic sequence analysis

This type of analysis involves separating time-stratigraphic units and is based on detecting unconformities or changes in the seismic pattern. Sheriff (1980) defines a time-stratigraphic unit as a "three-dimensional set of facies deposited contemporaneously as parts of the same system, linked genetically by depositional processes and environments". These units are often referred to as depositional units, and facies is defined as the sum total of features such as sedimentary structure and bedding which characterises a sediment as having been deposited in a particular environment (Whitten and Brooks, 1972).

A critical concept in seismic sequence analysis is that seismic reflections are depositional time surfaces rather than seismic facies surfaces. This constant time (isochronous) surface at some time was the surface of the solid earth, as re-iterated from above. Sheriff (1980) explains this apparent paradox by the fact that geological events tend to be episodic, in that a short-term event such as a major storm or flood will re-distribute sediments over a large area. Therefore the long-term steady deposition of sediments will not tend to leave any record as this sediment will ultimately be re-arranged by a short-term major event. Hence a succession of these type of events which are widespread will mark constant time and produce nearly parallel minor but widespread markers; that is to say that stratal surfaces follow time surfaces.

It has also been the case that individual stratal unit thicknesses tend to be smaller than the seismic resolution available therefore these units will only potentially produce minor composite reflections. However, interference of these widespread, generally parallel surfaces produces coherent reflection events. Facies boundaries may also be irregular or gradational and therefore significant coherent reflections may not be generated (Sheriff, 1980).

4.4.1. Mapping and Interpreting seismic sequences

Reflections will tend to indicate either time surfaces, as discussed above, or unconformities which represent a depositional hiatus (or non-deposition) during which conditions will have changed. Lithology may therefore be different above and below an unconformity (Sheriff, 1980). These unconformities are associated with some degree of angularity and Sheriff and Geldart (1995) quote the principal evidence of seismic stratigraphy as being the angularities between reflections where one of them terminates. The sequence boundaries can be picked out and followed laterally to the point where they become conformable. At this point seismic facies analysis is then carried out to understand the nature and structure of reflections within the sequences.

The major depositional patterns which are identified can often be correlated over large areas and can be interpreted as being associated with major sea level changes, Figure 4.1 shows the patterns expected for a rise and fall in sea level. A model has been developed of global cycles of major sea level change and

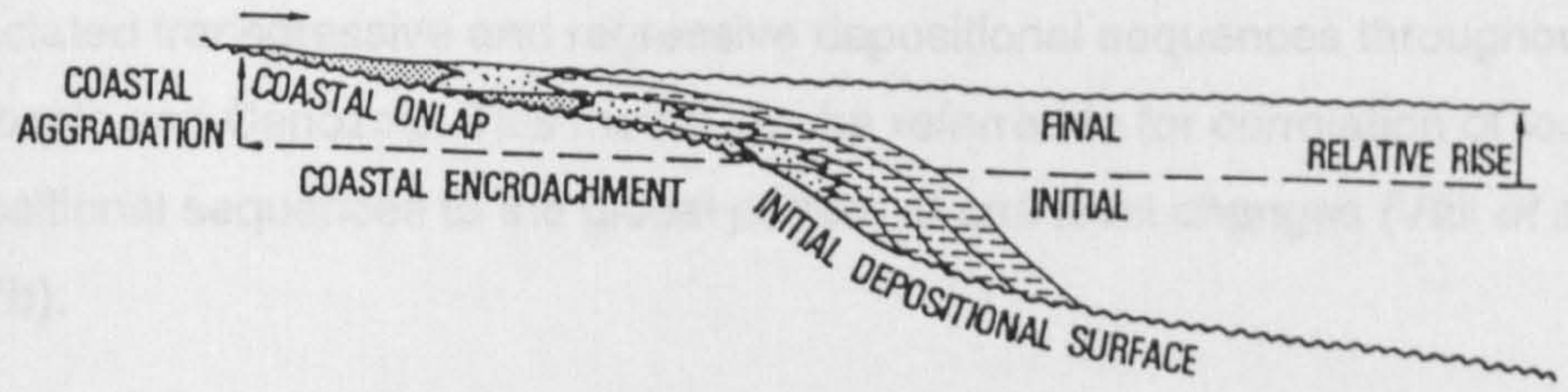

Figure 4.1. Patterns associated with sea-level changes. (a) A transgression is due to a sea-level rise where there is low terrigenous input. (b) A regression occurs where there is a sea-level rise and large terrigenous input. (c) Slow sea-level fall causes top erosion. (d) Rapid sea-level fall causes a seaward shift of onlap (after Vail *et al.*, 1977b).

associated transgressive and regressive depositional sequences throughout the Mesozoic and Cenozoic. This model can be referred to for correlation of localised depositional sequences to the global pattern of sea level changes (Vail *et al.*, 1977b).

A predictive sequence stratigraphic model has been developed, called the Exxon Model; Figure 4.2 shows the Exxon Model surfaces. The model attempts to explain and put into context all the stratigraphic relationships and is based on the concept of the effects of relative sea level changes on sedimentation (Bertram, 1995). Using the bounding surfaces, system tracts can be defined which are contemporaneously linked depositional systems, identified by the nature of their bounding surfaces and by their internal stratigraphy. These system tracts model the effects of eustatic change on the depositional patterns. Figure 4.3 shows schematics of system tracts on a passive margin and identifies the three most common tracts, i.e. highstand, transgressive and lowstand.

4.5. Seismic facies analysis

Mitchum *et al.* (1977) defines seismic facies analysis as the description and geological interpretation of seismic reflection parameters, including configuration, continuity, amplitude, frequency and interval velocity, and attempts to provide an interpretation of the depositional environment.

A seismic facies unit is a mappable three-dimensional unit of reflections; the characteristics of the unit differ from adjacent units. An important distinction needs to be made between a seismic stratigraphic unit and a seismic facies unit. The former is a package of reflections from sediments within a time-stratigraphic depositional unit, i.e. a particular age interval. The latter unit has characteristics resulting from the depositional environment, e.g. marine or non-marine (Sheriff, 1980). Figure 4.4 illustrates the various types of angularities which can occur at the tops and bottoms of reflection packages.

Various analysis and classification schemes exist to categorise and interpret the seismic facies seen on seismic records. The classifications may be based on reflection terminations, reflection characteristics, e.g. amplitude, abundance,

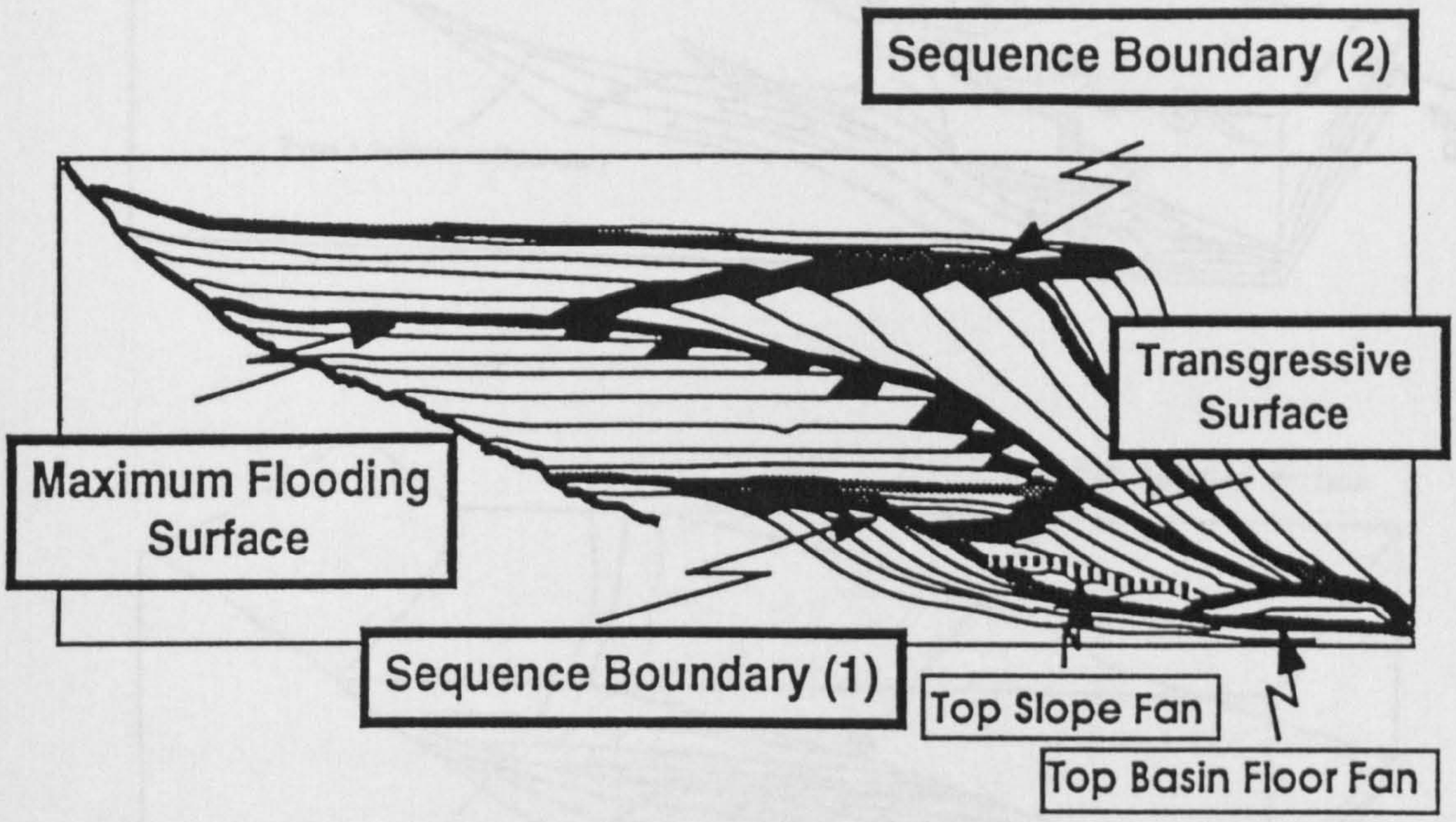

Figure 4.2. The Exxon model (after Bertram, 1995).

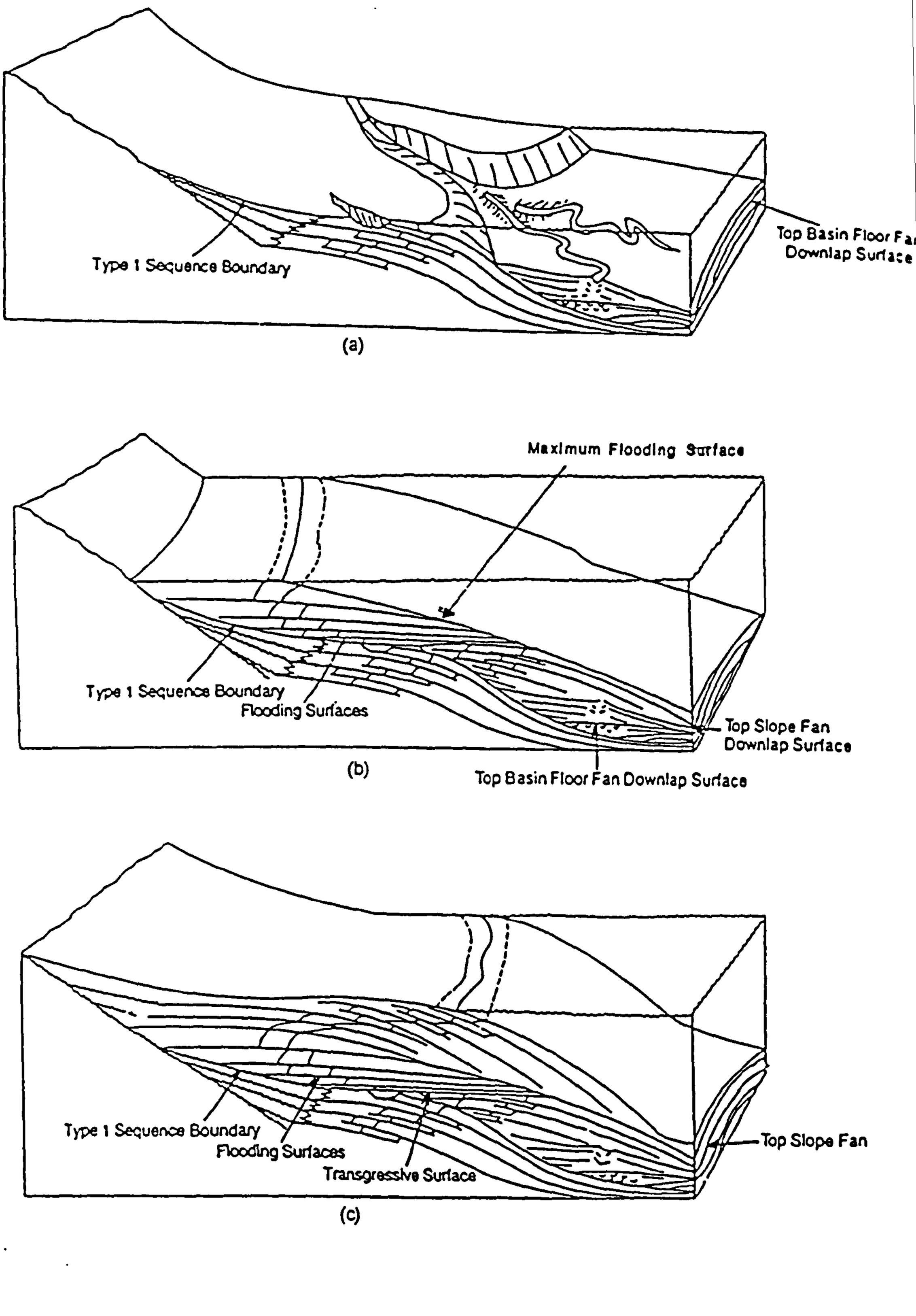

Figure 4.3. Systems tracts on a passive margin. (a) Sea-level lowstand. (b) Transgressive tract. (c) Sea-level highstand (after Posamentier *et al.*, 1988).

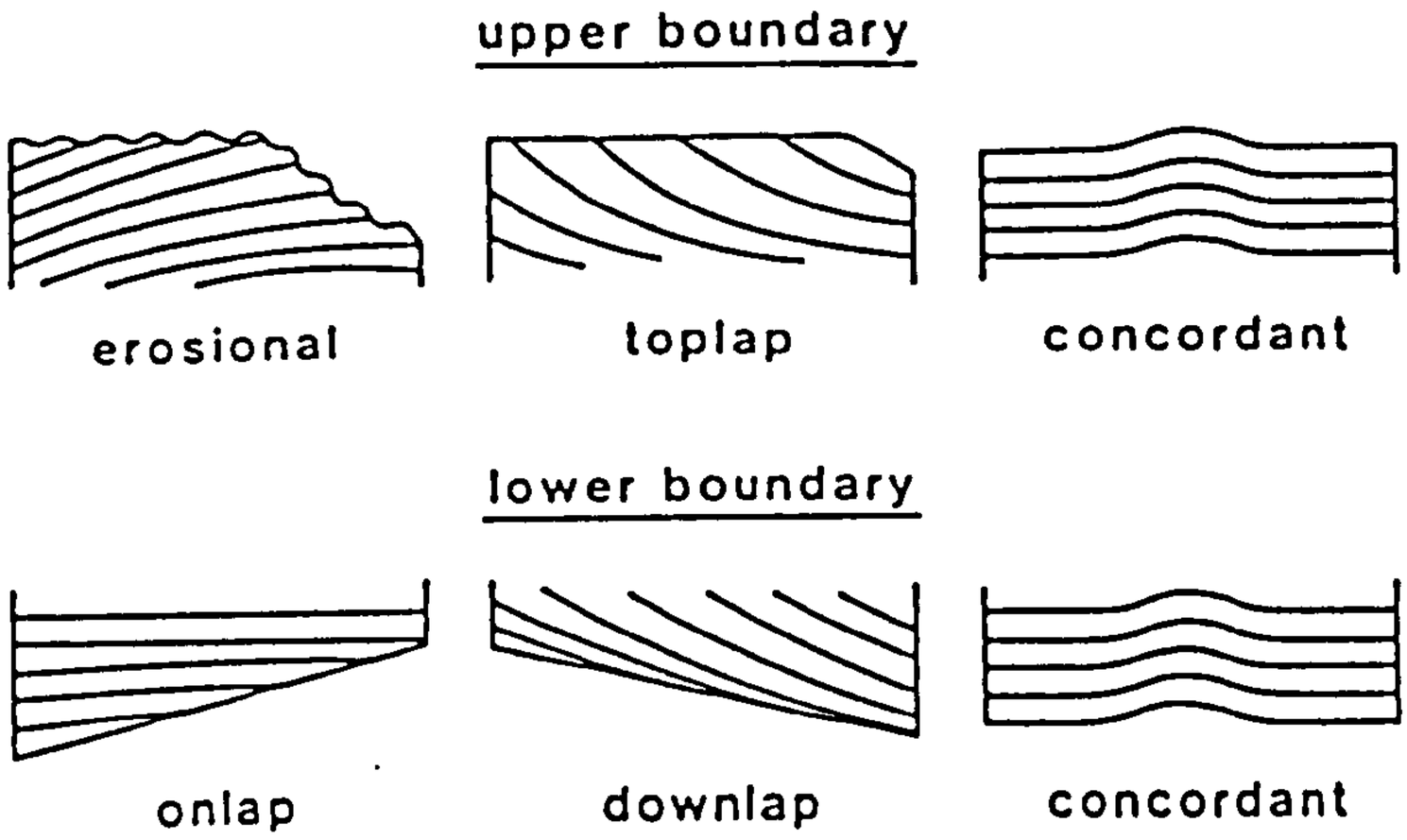

Figure 4.4. Relationships of the sequence reflections to the sequence boundaries which the reflections terminate against. The termination style generally indicates geometry but depositional limit may also be deduced (after Sheriff, 1980).

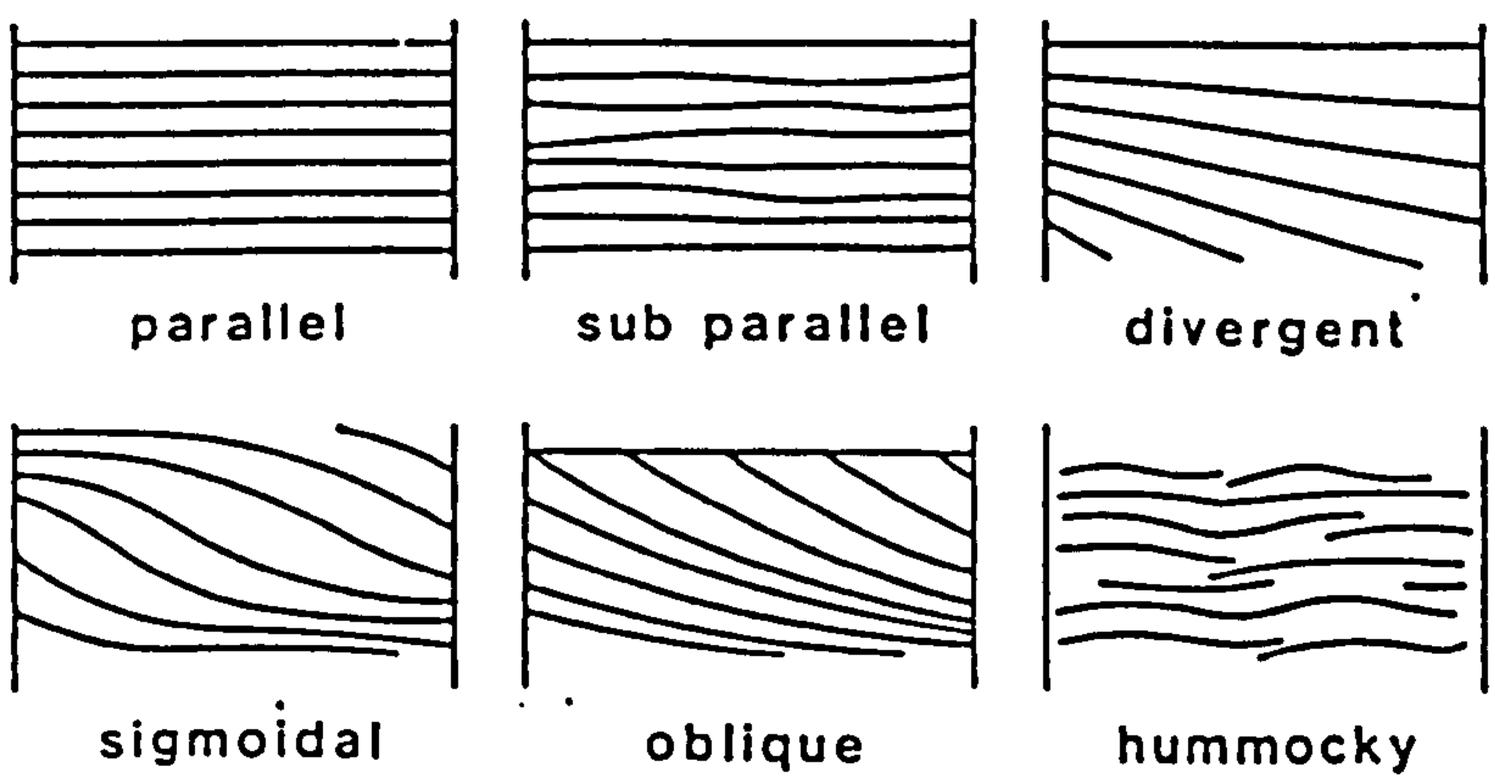

Figure 4.5. Internal bedforms within a prograding basin-margin clinoform on a seismic section (after Sheriff, 1980).

continuity and smoothness, stratal patterns or the external shapes of sequences (Sheriff and Geldart, 1995).

By studying the seismic record and the nature of the reflectors, qualitative stratigraphical information can be extracted, as shown in Table 4.1. Sangree and Widmier (1979) identify amplitude, frequency and continuity as being most useful for interpreting environments. Reflection amplitude yields information on velocity and density at each surface and the amount of inter-bedding. Frequency can aid in interpreting the spacing of reflectors and lateral changes in velocity. Continuity of reflections is closely related to the continuity of the bedding.

Seismic facies parameters	Geological interpretation
Reflection configuration	• Stratification patterns • Depositional processes • Erosion
Reflection continuity	• Bedding continuity • Depositional processes
Reflection amplitude	• Velocity-density contrast • Bed spacing • Fluid content
Reflection frequency	• Bed spacing • Fluid content
External form and areal association	• Gross depositional environment • Sediment source • Geological setting

Table 4.1. Geological interpretation of seismic parameters (after Sangree and Widmier, 1979).

A further underlying basic concept is that seismic reflections tend to parallel bedding surfaces within the resolution of a seismic cycle (Sangree and Widmier, 1979, Vail *et al.*, 1977a). This is defined from the fact that stratified sediments lithologically exhibit strong lateral continuity and in turn physical property surfaces are parallel to depositional surfaces.

4.5.1. Reflection patterns

Understanding reflection patterns within the facies units involves interpreting both the nature of the terminations and the reflection configurations. Sangree and Widmier (1979) divide the configurations found into three principal types:

- Reflection-free: areas where there are very few reflecting surfaces. This type of pattern is indicative of a uniform, single lithology.

- Chaotic: reflections are discontinuous, often mounded and there may be a lot of diffractions. These reflectors imply a high energy environment and variable deposition or disruption after deposition.

- Stratified: parallel or divergent reflectors which are relatively continuous. This suggests uniformity in layering and lithology and stable depositional conditions. The stratified pattern can be subdivided into simple or complex configurations.

  Simple stratified: parallel arrangements of cycles are indicative of uniform deposition on a stable or overall subsiding surface.

  Simple stratified: divergent arrangements suggest areal variations in the rate of deposition and/or progressive tilting of the surface.

Complex stratified configurations are typically sigmoid and oblique, both of which form by the progressive development of depositional surfaces that slope from a gently dipping, relatively shallow-water area into deeper water. Figure 4.5 identifies the configurations in zones, i.e. upper (topset), middle (foreset) and lower (bottomset).

Complex stratified; 'sigmoid' - this is a simultaneous out- and up-building of the upper (topset) beds during a rise in sea level or subsidence of underlying beds, generally in deep water.

Complex stratified; 'oblique' - an out-building of the middle (foreset) beds during a time of sea level stability.

As a way of summarising this potentially large section on seismic facies analysis, Figure 4.6 provides a regional framework devised by Sangree and Widmier (1979). This classifies seismic facies units potentially found on the shelf, shelf margin, prograded slope, basin slope and basin floor and describes classic sediment facies types.

4.6. Reflection character analysis

Amongst other authors, Sheriff and Geldart (1995) define reflection character analysis as the study of trace-to-trace changes in the waveshape of one or more reflections associated with a reflectivity change. The objective of this type of analysis is to locate and determine the nature of changes in the stratigraphy or fluid in the pore spaces. These changes are most often in amplitude, waveshape, frequency, velocity or interval thickness (Sheriff, 1980).

Reflection character can be studied more easily by the use of particular displays which illustrate changes more clearly. In the method of this study, seismic attribute displays such as amplitude, phase and frequency will be generated. White (1991) defines the use of attributes in seismic interpretation as understanding and inferring the components of the seismic response. Frequency displays may be able to characterise interference patterns from closely spaced reflectors, and phase displays aid in evaluating lateral discontinuities and discriminating weak coherent events.

4.6.1. Seismic attribute analysis

Complex trace analysis allows the extraction of attributes from seismic data and the evaluation of amplitude and phase independently. Analysis of a seismic trace as a component of an analytic signal allows the measurement of attributes and the description of the seismic character. The amplitude attribute is also called "reflection strength" and the phase is an attribute in its own right. Other attributes such as instantaneous frequency can be derived from these (Taner *et al.*, 1979), and it is these instantaneous attributes which are used to describe waveform shape (White, 1991).

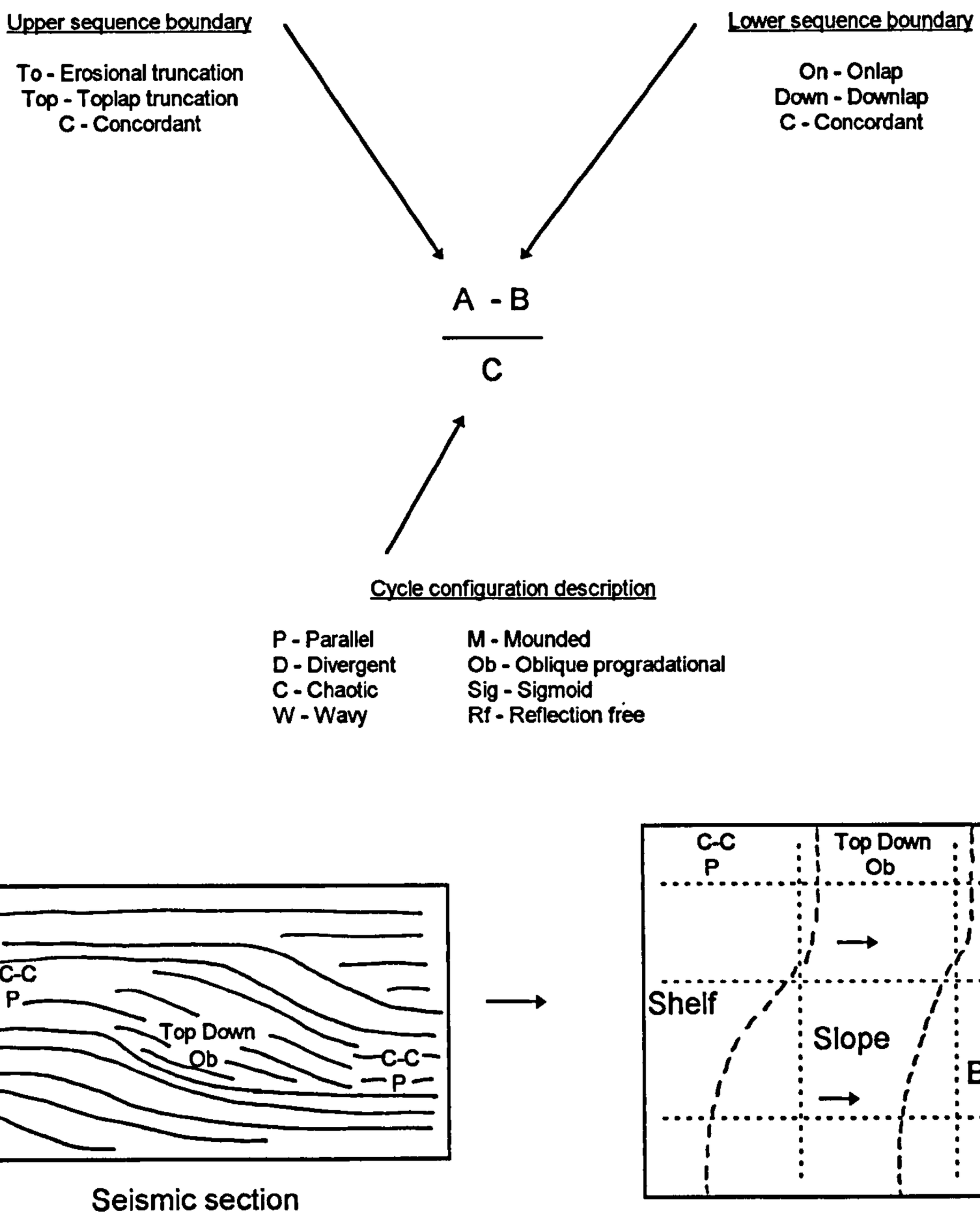

Figure 4.6. System for mapping of the reflection character (after Sangree and Widmier, 1979).

Seismic waves can be represented in both real and imaginary parts although it is only the real part which is detected and displayed. This can also be expressed as a time-dependent phasor with the seismic trace defined as:

$$g(t) = R(t) \cos \theta(t) \qquad (4.1)$$

where g(t) is the seismic trace, R(t) is the envelope of the trace and θ(t) is the phase. Figure 4.7 shows a vector perpendicular to the time axis and its length varies as a function of time as does the vector rotating about the time axis. Taner and Sheriff (1977) explain that the projection of the head of the rotating vector on the real plane gives the seismic trace. The head of the vector can also be projected on to the imaginary plane to give the quadrature trace h(t) :

$$h(t) = R(t) \sin \theta(t) \qquad (4.2)$$

This technique, i.e. the Hilbert transform, allows both parts of the complex trace to be analysed by mathematical manipulation. Figure 4.8 illustrates the attributes from a segment of a seismic trace and White (1991) defines the attributes of Figure 4.8 as follows:

- The peaks and troughs of the quadrature trace correspond to zero crossings on the original trace, i.e. a phase shift of 90°.
- The instantaneous amplitude defines the seismic envelope.
- Instantaneous phase is plotted between ± 180° giving a sawtooth picture.
- Instantaneous frequency dips below zero at the inflection point of the original trace.

4.6.1.1. Reflection strength

Referring to the discussion above, the amplitude envelope or reflection strength R(t) can be defined in terms of the seismic and quadrature trace at every sample point, i.e. reflection strength is amplitude independent of phase.

$$R(t) = [\, g(t)^2 + h(t)^2 \,]^{1/2} \qquad (4.3)$$

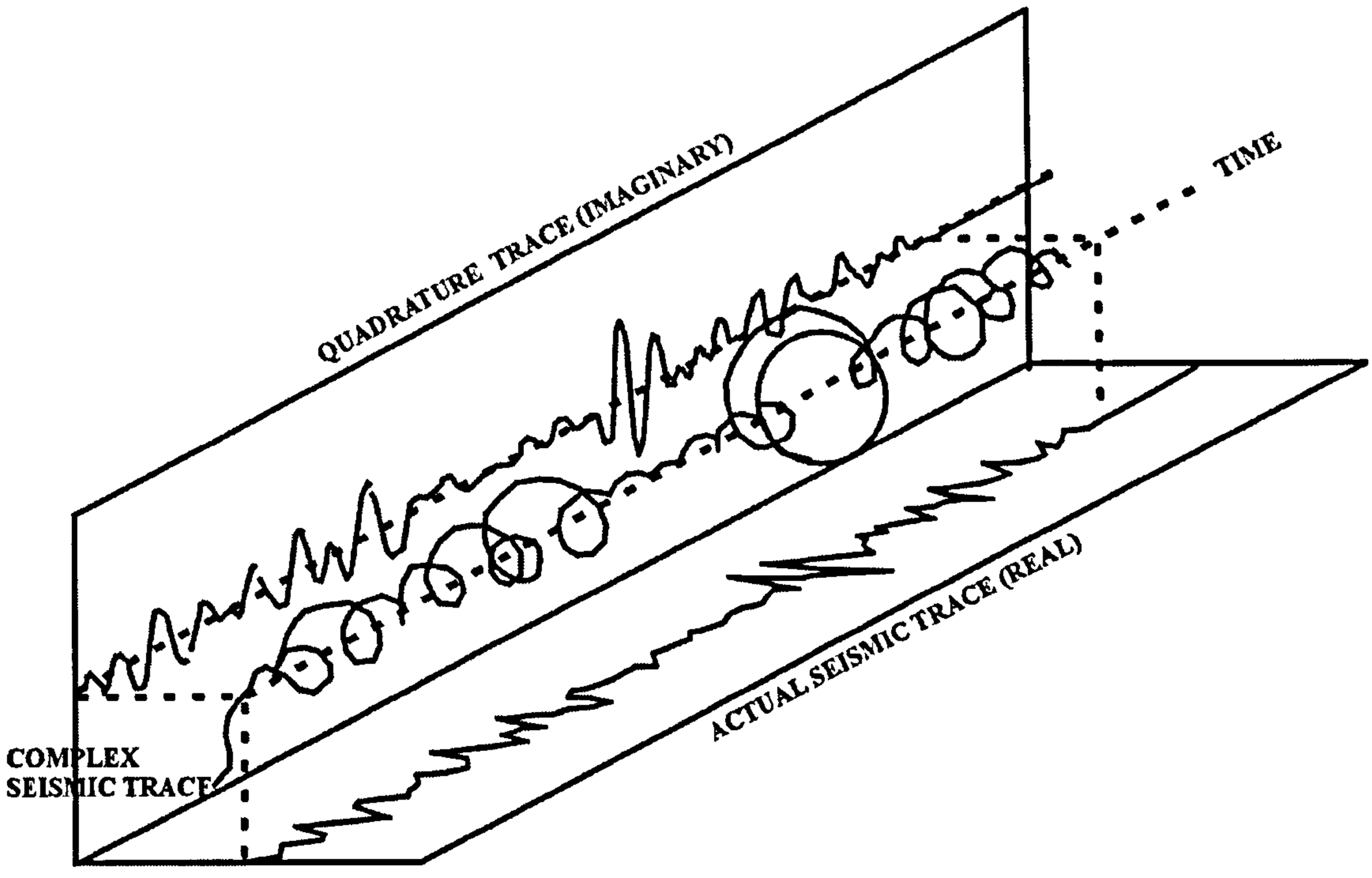

Figure 4.7. The complex seismic trace generated by a vector with a time-dependent length and rotation (after Taner and Sheriff, 1977).

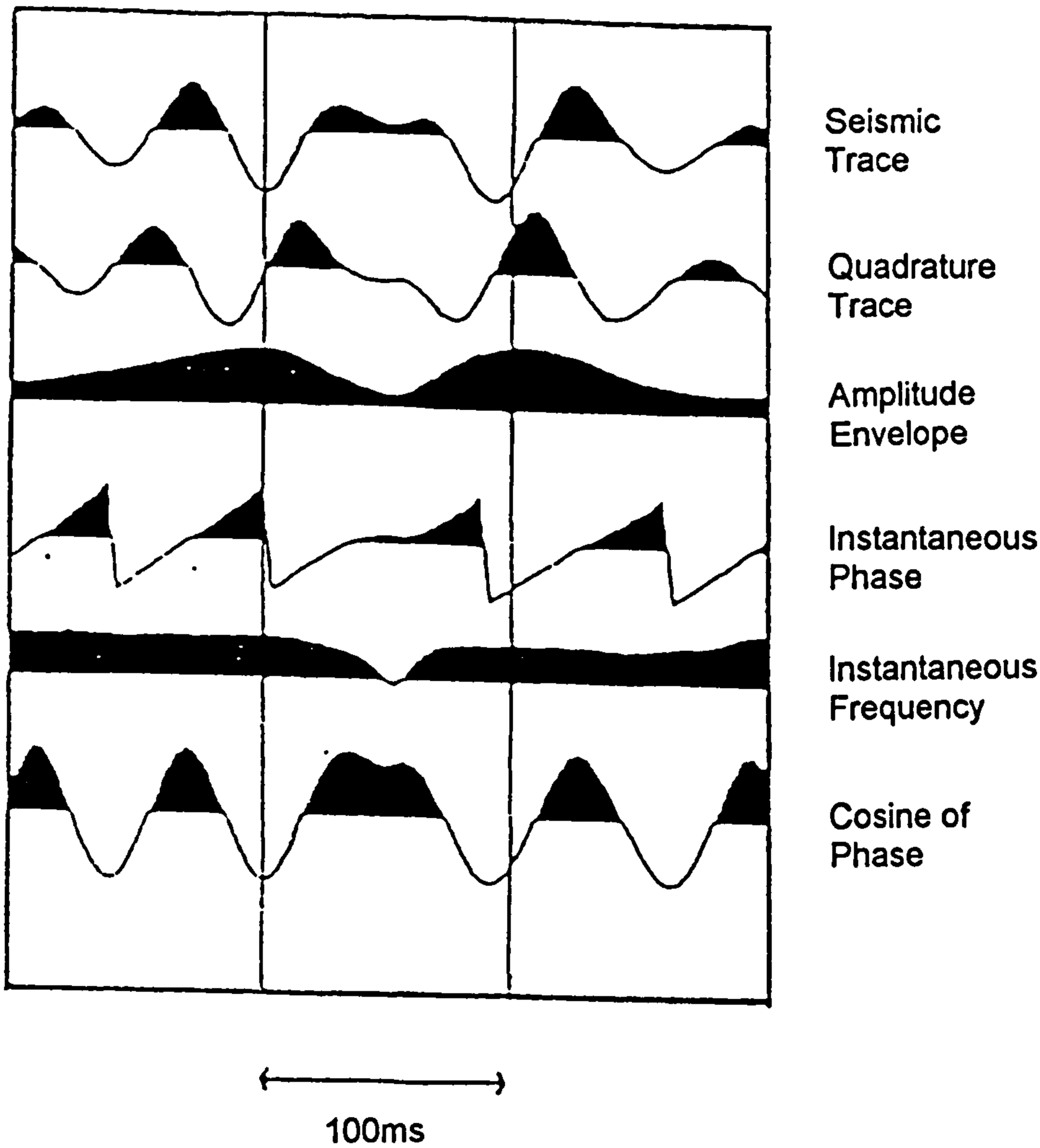

Figure 4.8. Instantaneous seismic attributes which describe the seismic trace segment (after White, 1991).

Reflected energy first increases then decreases representing a reflection as an increase in reflection strength. The polarity of the event will depend upon the reflection coefficient being negative or positive as well as further interference on the reflected and transmitted energy and the acquisition parameters. It is an important point that the reflection strength may have a maximum at phase points other than peaks or troughs when the returning reflection is a composite of minor subreflections, i.e. differentiating between amplitude and reflection strength (Taner and Sheriff, 1977). Reflection strength may aid in identifying gas accumulations, faulting and lateral variation of bed thickness (Taner *et al.*, 1979).

4.6.1.2. Instantaneous phase

Instantaneous phase is also an attribute which can be measured directly using the terms of the seismic and quadrature trace, i.e. it is the angle between the trace and its Hilbert transform at a given time (Robertson and Nogami, 1984).

$$\theta(t) = \tan^{-1}\left[\frac{h(t)}{g(t)}\right] \qquad (4.4)$$

The phase displays are used for assessing the continuity of events and to detect the presence of gas.

4.6.1.3. Instantaneous frequency

Instantaneous frequency is the time derivative of instantaneous phase and likewise is measured at a particular point and is not an interval average. This has the advantage of not masking change which will occur during averaging, but has the disadvantage of potentially producing incomprehensible changes. Frequency can be smoothed by weighting to enhance interpretation (Taner and Sheriff, 1977). Instantaneous frequency is used for identifying the presence of, for example, gas sands and for correlating beds characterised by composite reflections.

4.7. Problems identified with seismic stratigraphy

Pitfalls when applying the principles of sequence stratigraphy are well documented. One of the major drawbacks is the lack of good borehole and biostratigraphic

control. Myers and Milton (1996) also highlight the problems of complex geology and of correlating surfaces where there are features such as incised valleys.

There are a number of 'implicit assumptions' behind the methodology of sequence stratigraphy enabling its use as a predictive interpretation scheme (Thorne, 1992). Thorne (1992) grouped these assumptions into four categories: seismic stratal geometry identification, the depositional sequence model, the inverse model for seismic data interpretation and the global correlation model used to construct the Exxon model. Thorne (1992) analysed the 24 implicit assumptions involved in the Vail (1987) hypothesis and concluded that the sensitivity of the predictions is not well known. Thorne (1992) advised awareness to the lack of sensitivity and suggested that numerical stratigraphic modelling could go some way towards assessing the assumption sensitivity for greater interpretation confidence.

Work done exclusively on Quaternary sediments of the UK continental margin has highlighted problems associated with the use of seismic facies analysis. Stewart and Stoker (1990) quoted an example where subglacial till had been interpreted on the seismic data using the seismic stratigraphic approach, and a depositional model constructed. The borehole results however logged the presence of a glaciomarine facies. Stewart and Stoker (1990) concluded that, although acoustic character may imply a particular lithofacies, it should not be used as a predictive genetic indicator of a specific depositional process.

Stoker *et al.* (1993b) reviewed borehole and shallow core data from the UK continental margin and discovered inconsistencies between predictive depositional models and lithology. Assumptions in seismic stratigraphy are made such that laterally persistent, acoustically homogeneous seismic units can be associated with consistent lithologies and physical properties. Assumptions are also made that lateral or vertical changes in seismic character indicate a concurrent change in sediment type and properties. Consequently Stoker *et al.* (1993b) found that these assumptions were valid at some locations but were by no means infallible.

Alternative approaches to seismic stratigraphy have been developed, in particular in areas where there are Quaternary and pre-Quaternary glacial sequences (e.g. Syvitski, 1991). Eyles *et al.* (1983, 1985) developed a scheme, based on the visual appraisal of field sequences and drill cores, for the description and interpretation of

glacial diamict and diamictite sequences. Although their approach is essentially not seismo-stratigraphic, it is an important scheme to bear in mind when trying to apply seismic facies analysis to distinguish glacial and glaciomarine facies, due to the complexity of the glacial system.

4.8. Summary

As introduced in Chapter 1, Stoker *et al.* (1993b) identified a critical factor for the successful interpretation of high resolution seismic data: groundtruth calibration is vital to geophysical interpretation. This is particularly valid where a complex depositional environment could lead to ambiguous interpretations. These conclusions have led to a number of issues which this research aims to address.

The early studies which highlighted these issues (Stoker *et al.*, 1993b) were carried out based on analogue data alone. However, more recently Butcher (1997) made use of digital data although this was mainly to test seismic stratigraphic analysis in the broadest of senses, and concentrated on shallow water Quaternary sediments. Butcher (1997) concluded that this method of analysis was valid for Quaternary sediments occurring in the shallow water around the UK.

At the commencement of the current research project questions remained as to the affects of the physical properties on the seismic response for continental slope Quaternary sediments and how ambiguity in interpretations could be avoided. This research project specifically attempts to relate physical properties to the seismic response with a view to improving high resolution seismic interpretation of glacigenic, UK continental slope sediments. The project aims to proceed towards this end goal by developing models based on physical and engineering properties derived from a limited number of borehole samples and cone penetration test records, i.e. the required groundtruthing. This validity of the modelling methods will be tested by applying the approach to an existing geotechnical/geophysical dataset acquired in the UK frontier area. Further efforts to improve the analysis will be attempted through attribute analysis and integration.

CHAPTER 5

MODELLING FROM BOREHOLE DATA

5.1. Introduction

Seismic facies analysis has until recently been the preserve of hydrocarbon, reservoir level studies, with well defined depositional models in place as a result of the vast databank of well log information. However, seismic facies analysis techniques are increasingly being applied to the interpretation of high resolution seismic reflection data, and more particularly to Quaternary sediment investigation (Butcher, 1997).

As previously mentioned, Stoker *et al.* (1993b) and Stewart and Stoker (1990) identified the fallibility of the assumptions of seismic facies analysis when applied to Quaternary sediments, i.e. assumptions that laterally continuous acoustically homogeneous seismic units have consistent geotechnical properties and character. Equally, they questioned the assumptions that any lateral or vertical change in seismic character indicates lithological change. The work which challenged these assumptions was essentially qualitative and based on analogue paper records, thus an opening was left for a more detailed quantitative study into the effects of physical property control on the acoustic response. The aims of this chapter are to go some way towards testing and providing an understanding of why these assumptions are apparently not valid in every situation, and to attempt to better understand the relationship between physical properties and the high resolution acoustic responses. This research uses forward modelling techniques in an attempt to model the acoustic response on the basis of input physical properties. Within the modelling, established empirical relationships published in the literature are tested and are used to relate the acoustic parameters to the physical properties.

Forward modelling is a routine part of hydrocarbon seismic interpretation, whereas forward modelling of high resolution seismic data is not as straightforward because geophysical borehole logging, which produces the data required to derive impedance logs, is not routinely carried out in engineering site investigations. This lack of logging information is generally due to the inability of the logging tools to make measurements when the upper section of the borehole has been cased.

Other *in situ* logging tools exist, such as a gamma logger, which can provide subsurface density information which, even through the casing could be used in the forward modelling process. This project aims to overcome this shortfall in available data by using CPT and borehole sample data to derive the equivalent logs.

This chapter will present a method in the form of a predictive model which allows the production of synthetic seismograms from the physical properties of a sequence of sediments. The work in this chapter relates specifically to borehole sample data and emphasises the general shortfall in information available with which to model high resolution seismic data due to the lack of geophysical logging. In the case of borehole samples it may be rare for both density and velocity measurements to be made. Empirical inter-relationships are used to predict the missing parameter(s) for the production of impedance logs in the method developed in this chapter. The background to the production of synthetic seismograms has been introduced in Chapter 3 and the particular method used in this study will be discussed in detail as the model is built up.

Once the modelling process has been completed, the analysis section will review the specific empirical inter-relationships and the use of these relationships in estimating the physical and acoustic properties which are input into the forward model. Errors will be considered, as well as the sensitivities, of the empirical relationships and the parameters used in the regression equations. Statistics will be applied to the relationships developed by several authors to assess the significance and variance of the output of the series of relationships.

On completion of the quantitative analysis of the inter-relationships, a descriptive analysis will be undertaken. The empirical relationships link the physical properties to acoustic impedance. From impedance a reflectivity log will be constructed and convolved with an example wavelet en route to producing a synthetic output. This approach is, on a very basic level, purely for descriptive purposes to assess the impact and sensitivity of the relationships used in the forward modelling. Limitations and uses of the synthetic method will be assessed.

A dataset from the Hebrides slope is used to test the applicability of the empirical relationships and acts as a case study for testing the borehole method.

By the end of the chapter it is intended that a system will have been put in place which will model acoustic properties from geotechnical borehole investigations. This system will produce synthetic output to be interpreted alongside actual seismo-acoustic data.

5.2. Geotechnical borehole

Once geophysical high resolution seismic data have been collected it is essential that the data are calibrated. The use of groundtruth data will aid in understanding the seismic character and the geological context for interpretation. Ideally, calibration data from a geotechnical borehole would be used for this purpose, particularly where samples have been recovered and laboratory tested.

5.2.1. Borehole data acquisition

Figure 5.1 is an illustration of a purpose-built drill ship which can perform heave-compensated rotary soil borings (Power and Aldridge, 1997, Fugro-Geoteam Ltd., 1997). Dynamic positioning is used to control the ship's thrusters in order to maintain an exact position over the borehole location.

Drilling in up to 800m of water is performed by a standard 5" steel drillpipe. Downhole sampling and testing tools such as the hydraulic push sampler can then be deployed on conventional electro-hydraulic umbilical cables. Water and/or mud is injected downhole to ease the removal of the cuttings and samples (Cernica, 1995).

Various field tests will usually be carried out before the recovered samples begin to lose their *in situ* state, that is, loss of moisture content and structure. Commonly, hand penetrometer tests are carried out to determine relative density and strength, and vane shear tests to determine *in situ* shear strength.

5.2.2. Borehole data

Borehole logs, such as the example in Figure 5.2, detail all the information relating to the samples together with any other information relevant to their future use. The borehole log contains a lithological description and may also contain some of the

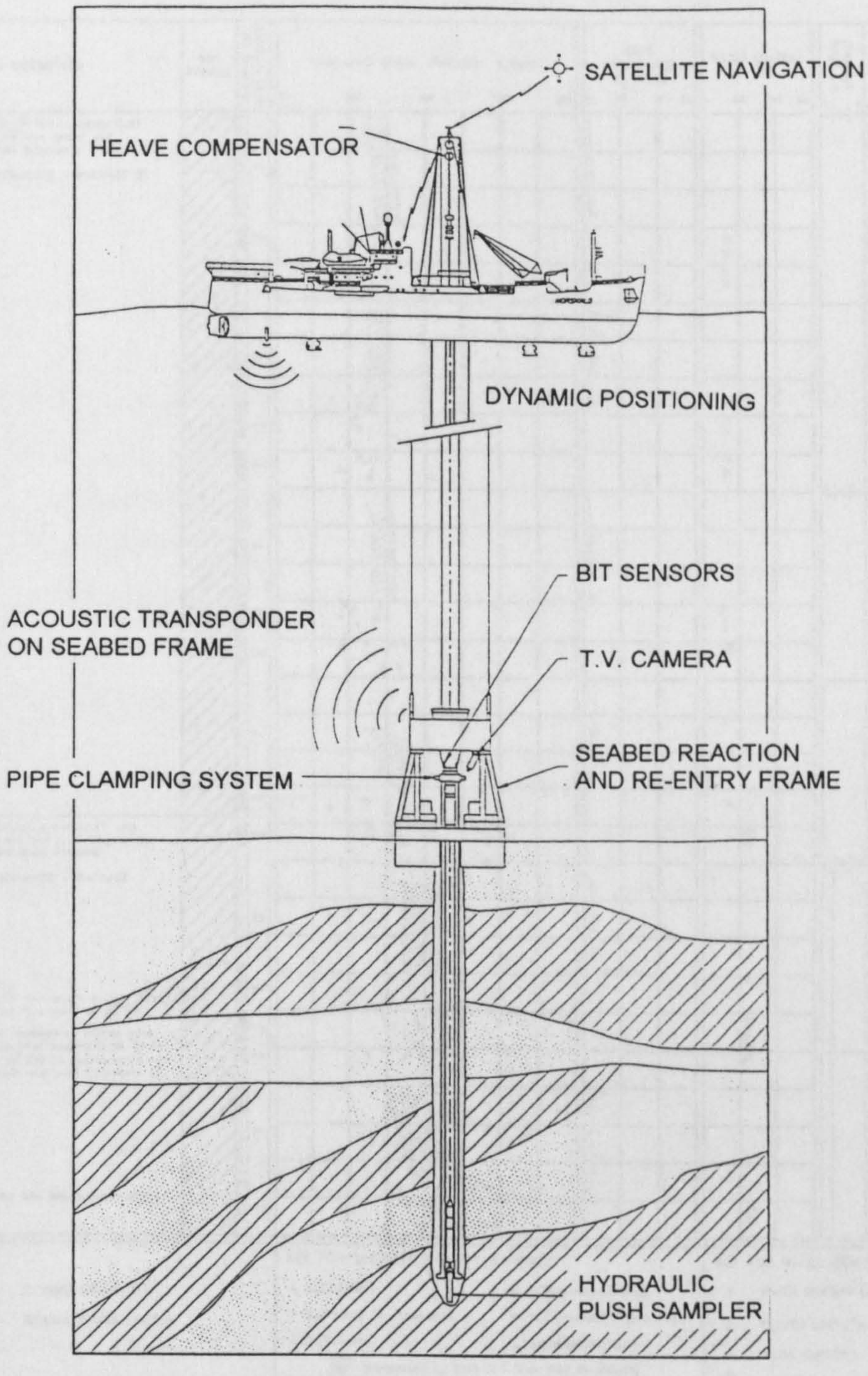

Figure 5.1. Drillship in borehole drilling mode (after Hampson and Power, 1996).

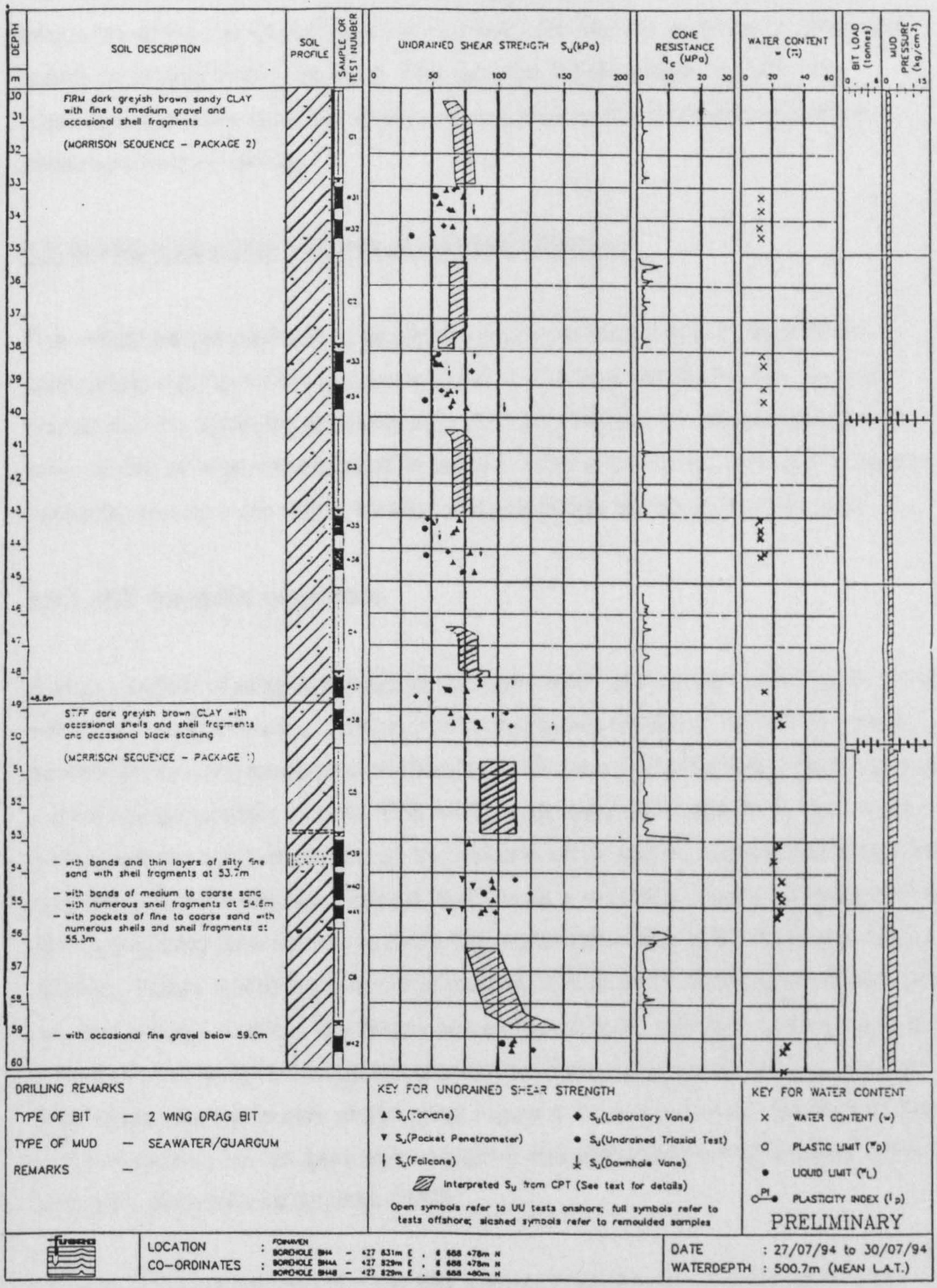

DRILLING REMARKS

TYPE OF BIT — 2 WING DRAG BIT

TYPE OF MUD — SEAWATER/GUARGUM

REMARKS —

KEY FOR UNDRAINED SHEAR STRENGTH

▲ S_u(Torvane) ◆ S_u(Laboratory Vane)

▼ S_u(Pocket Penetrometer) ● S_u(Undrained Triaxial Test)

╎ S_u(Falcone) ⸸ S_u(Downhole Vane)

Interpreted S_u from CPT (See text for details)

Open symbols refer to UU tests onshore; full symbols refer to tests offshore; slashed symbols refer to remoulded samples

KEY FOR WATER CONTENT

× WATER CONTENT (w)

○ PLASTIC LIMIT (w_P)

● LIQUID LIMIT (w_L)

PI ○—● PLASTICITY INDEX (I_P)

PRELIMINARY

LOCATION : FORMAVEN

CO-ORDINATES : BOREHOLE BH4 - 427 831m E , 6 688 478m N
BOREHOLE BH4A - 427 829m E , 6 688 478m N
BOREHOLE BH4B - 427 829m E , 6 688 480m N

DATE : 27/07/94 to 30/07/94

WATERDEPTH : 500.7m (MEAN L.A.T.)

Figure 5.2. Example of a borehole log (after Fugro, 1994).

sample testing results, particularly those which are measured directly following recovery such as moisture content, Atterberg limits and shear strength. The frequency of recovered borehole sample tests will depend upon the quantity and quality of sample that is retrieved. The samples will be further tested in the laboratory and may be re-sampled to assess factors such as loss of moisture, settlement and sensitivity.

5.3. Model production - choice of synthetic method

The critical part of the forward model production in this work is to choose the appropriate synthetic seismogram method. It was essential within this research project that the synthetic seismogram algorithm provided an interpretable result which could be logically analysed. A simple model showing the effects of property variability can be more easily iterated and complexity added only where valid.

5.3.1. ISX synthetic generation

A large number of programs exist for the generation of synthetic seismograms and within this study several programs were considered. UWB has its own in-house seismic processing system, SierraSeis/ISX (Western Geophysical), which contains a synthetic generation module. This module can generate a synthetic zero trace onto which various processes can be added such as spikes, random noise and long and short period multiples. Figure 5.3(a) shows a reflectivity series generated using ISX by inputting time/amplitude pairs. On closer inspection of the trace after spike addition, Figure 5.3(b) illustrates that the output is in fact a zero phase, Ricker type wavelet and not a spike. The Ricker wavelet is the most common wavelet used in the production of synthetic seismograms for a homogeneous and isotropic earth. The Ricker wavelet is zero phase, (see Figure 5.4) i.e. symmetric about time zero, and non-causal, i.e. not zero when negative and extends to infinity on both sides of time-zero (Sinvhal and Sinvhal, 1992).

Therefore, it was decided that the ISX approach would not be followed. For the work in this study different sources will be considered, i.e. boomers and sparkers, therefore, the ability to input different wavelets into the synthetic seismogram process for convolution is essential.

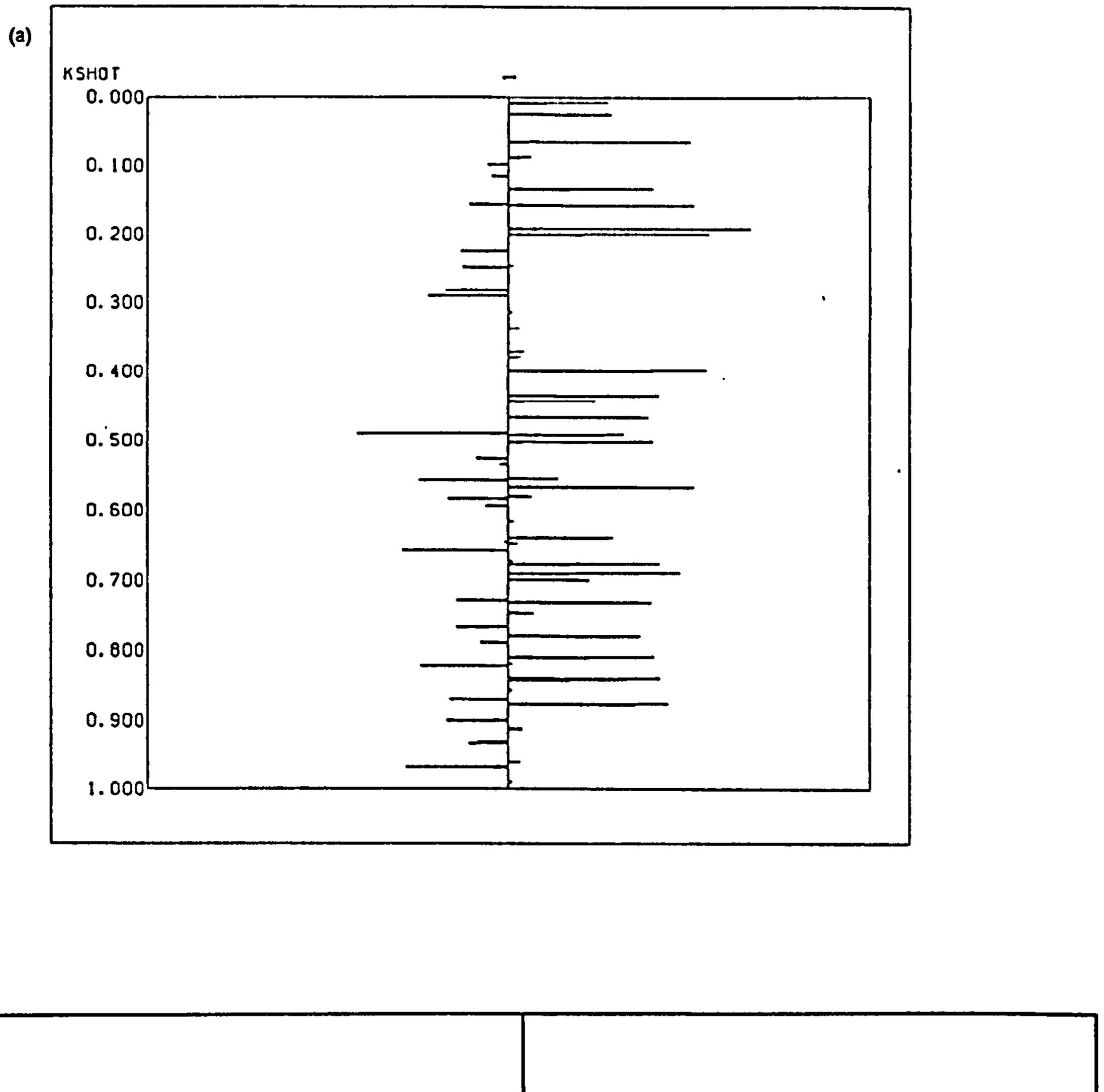

Figure 5.3. An example of ISX synthetic output. (a) Reflection series. (b) A Ricker wavelet is generated where there should ideally be a spike.

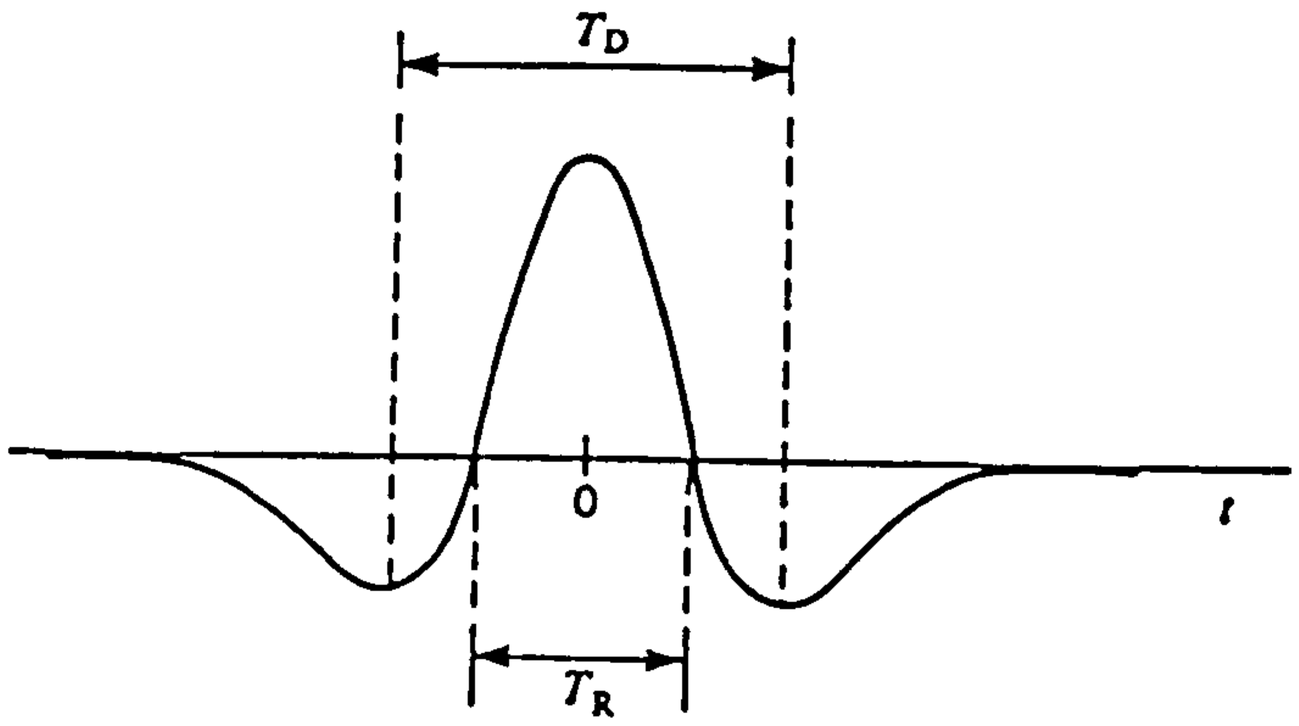

(a)

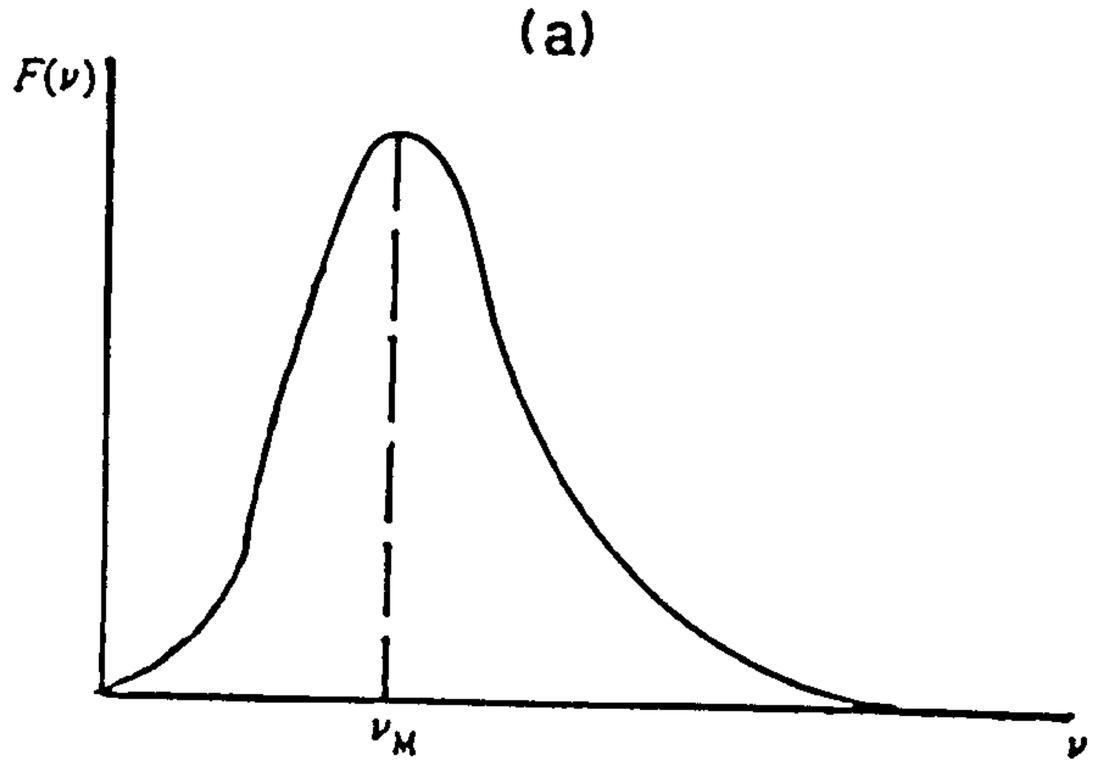

(b)

Figure 5.4. Ricker wavelet. (a) Time domain. (b) Frequency domain, where t= time, T_D = distance between side lobes, T_R = peak width, ν = frequency and F(ν) = frequency domain filter (after Sheriff and Geldart, 1995).

5.3.2. TENLAYERS synthetic generation

McGee (1991) developed a one-dimensional impulse response generation program for investigation of reverberatory sequences which occur in a system of horizontally layered blocks between two half-spaces. The inputs to the program are layer thickness and reflection coefficient and the output is an impulse response which accounts for transmission losses and multiples. The separate impulse response program allows a convolution process to be added and gives the flexibility of changing source signatures depending on the type of seismic data which are to be modelled.

Following McGee (1991), the first block or layer below the halfspace is the water column and possibly the uppermost layer of the sea floor sediment if the seabed is a weak reflector. The top of this block (the zero-th interface) is the air/water interface which is an almost perfect reflector. Therefore RC = -1 is a reasonable approximation. The reference point (pseudo-source position) within the program is in the first layer immediately beyond the zero-th interface. A positive reflection coefficient implies an acoustic impedance increase in the direction of propagation. Figure 5.5 illustrates the raypaths and calculations for the impulse response and Figure 5.6 is an example of an impulse response function generated before convolution.

The impulse response is then convolved in the time domain with a source wavelet within the program and output to a file. Appendix A contains the FORTRAN code of the TENLAYERS program with adaptations written within this study. The output from the TENLAYERS program is then imported into a plotting package, in this case Microsoft Excel.

The impulse response from the TENLAYERS program was compared with, and found to be consistent alongside, an impulse response generated from the FORTRAN code supplied in Claerbout (1968). Sinvhal and Sinvhal (1992) also refer to Claerbout's program as the basis of their synthetic seismogram. Therefore the TENLAYERS program was chosen as being the optimum tool for this research due to it being a basic 1-D process and having the flexibility to have further modules, such as convolution, various source signatures and corrections for noise, spherical divergence and absorption, added.

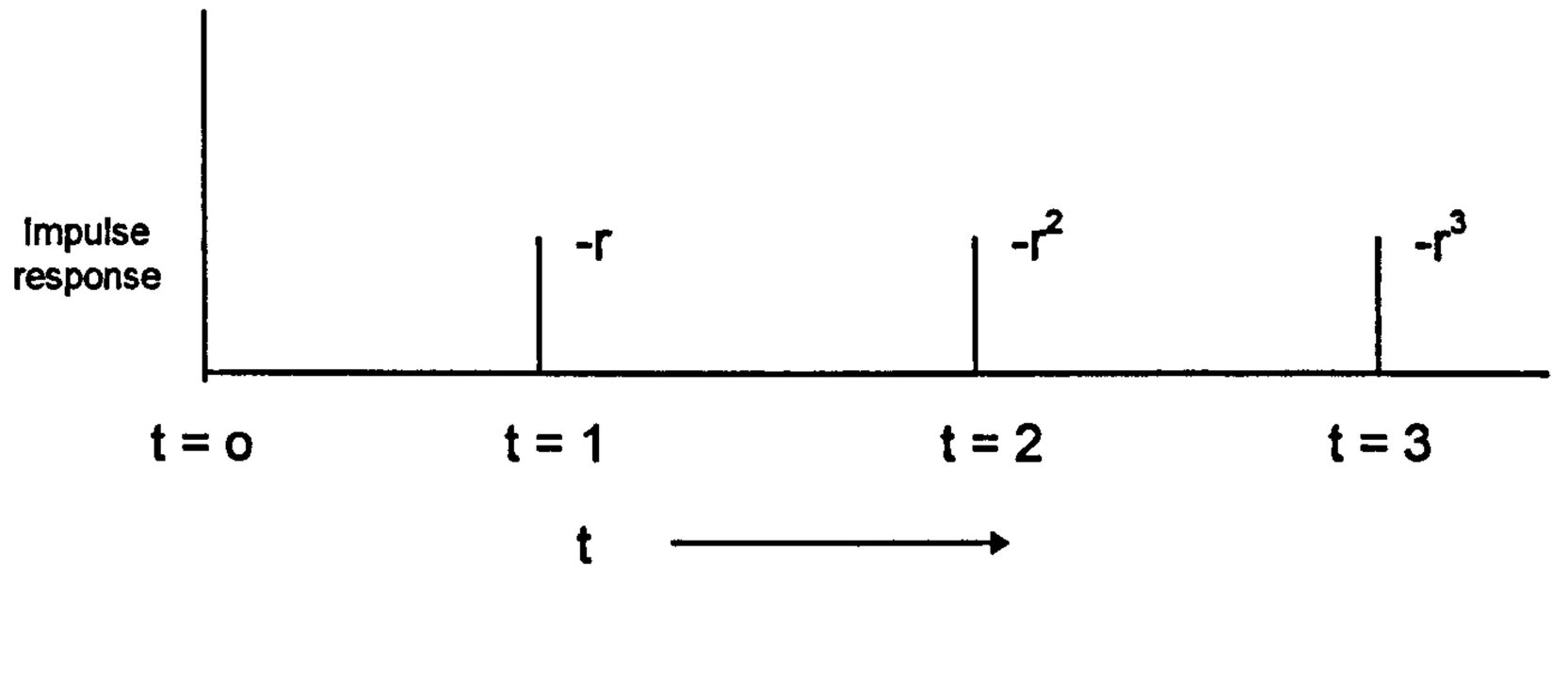

Figure 5.5. Impulse response raypaths where the source and receiver positions are separated for clarity and explanation, the project is based on single channel, normal incidence (after Sinvhal and Sinvhal, 1992).

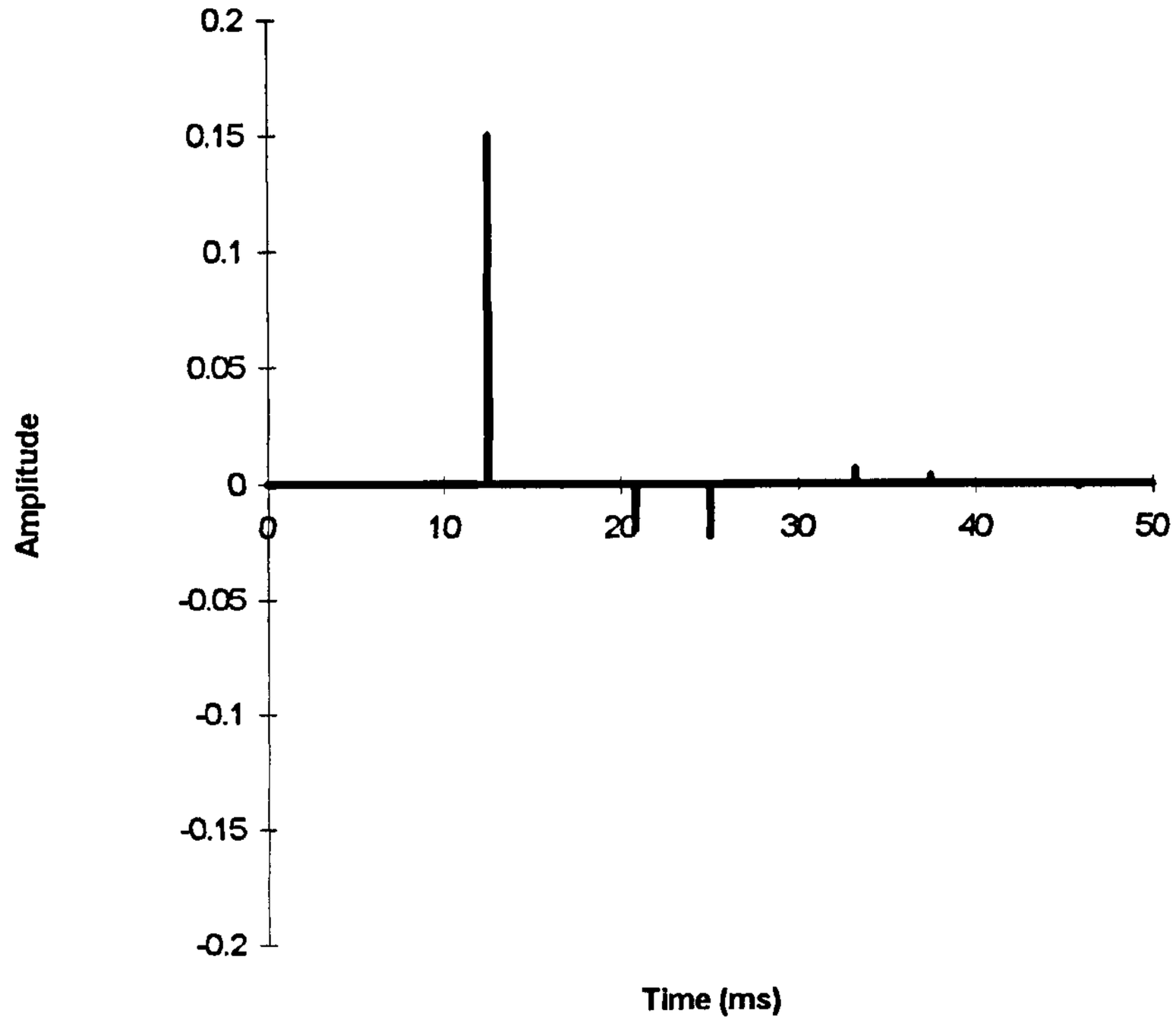

Figure 5.6. Impulse response function using arbitrary inputs.

5.4. Model production - source wavelet

When data are recorded on paper only, i.e. in analogue format, only a general understanding of the source signature is necessary for interpretation (Verbeek and McGee, 1995). However, when working with digitally recorded data, detailed knowledge is required of the source pulse in order to choose representative sampling rates. A well defined source signature is necessary for processing and for modelling, such as generating synthetic seismograms and inversion.

The most common wavelet used in the production of synthetic seismograms is the Ricker wavelet for a homogeneous and isotropic earth. An alternative approach is to use the embedded source waveshape from the digitally recorded data; this can be extracted from the actual dataset by wavelet processing.

5.4.1. Geopulse source signatures

Two O.R.E. "Geopulse" 5810B boomer signatures, one at a power of 105J and the other at 175J, were used for the testing phase of the synthetic seismogram (Verbeek and McGee, 1995) and the production of models. These signatures were chosen as the boomer is widely used for offshore site investigation.

The boomer is an impulsive source which releases energy in sudden bursts. Essentially a boomer consists of an induction coil mounted against an aluminium plate using a system of springs. A bank of capacitors produce electrical discharges through the coil at regular intervals and at each discharge, the currents induced in the conductive plate cause it to move violently away from the coil. It is this initial movement of the plate which triggers the acoustic pulse.

The receiver is a pressure sensitive hydrophone which is separate to the source and towed behind. The hydrophone consists of an array of piezo-electric crystals, which produce a voltage when subjected to deformation. Within the seismic survey this deformation is due to the passage of a pressure wave and noise. The received signal tends to be very weak so it is usually passed through frequency filters and amplified before being recorded. The propagating signal decays as a function of travel time due to spherical spreading and absorption. By using a time varying gain (TVG) a gain ramp can be applied which increases the amplitude with respect to

record time. Alternatively the overall gain can be altered using an automatic gain control (AGC) (McGee, 1995, Trabant, 1984).

A graphic recorder is generally used to provide an analogue record and this produces a display of reflection time against distance by the sweep of a stylus. Adjustments can be made to the recorder, for example, sweep rates and delay can be altered to optimise the display. However, in recent years raw analogue signals have also been recorded digitally to allow further processing and interpretation (Butcher, 1997). These systems allow output of the converted signal in various formats, in particular SEG-Y, which enables loading onto conventional industry-standard processing and interpretation systems.

Impulse source signals are characterised by their frequency bandwidth, wavelet generation and repeatability of the wavelet shape. The boomer's principal advantages over other types of high resolution seismic sources are its ability to produce broad bandwidths and the well-defined, repeatable signal (Verbeek and McGee, 1995).

Figure 5.7(a) and (c) show the Geopulse wavelets as supplied where they have been digitised at a rate of 203 846 times/second in the time domain and Figure 5.7(b) and (d) are the spectral analysis plots of these wavelets following Fourier transformation. The 105J wavelet has a central frequency of around 10kHz and the higher power 175J wavelet has a central frequency of approximately 7kHz. The boomer source will be discussed in greater depth in Chapter 7.

5.4.2. Detectable limit

Stoker *et al.* (1993b) postulate that an understanding of the bounds of vertical and lateral resolution are crucial to avoid oversimplistic interpretation of depositional environments. A test was carried out in this study to assess the minimum separation of wavelets to maintain the defined shape of the source pulse, i.e. a test of resolution. Widess (1973) defined the detectable limit equating to thickness less than $\lambda/8$ which, in this example, would produce a detectable limit of approximately 0.13m, assuming a velocity of 1600m/s, i.e. a typical velocity for Quaternary sediments and a dominant frequency of 1.5kHz. However, the maximum arbitrary two-way thickness which allows for approximately no change in shape for both

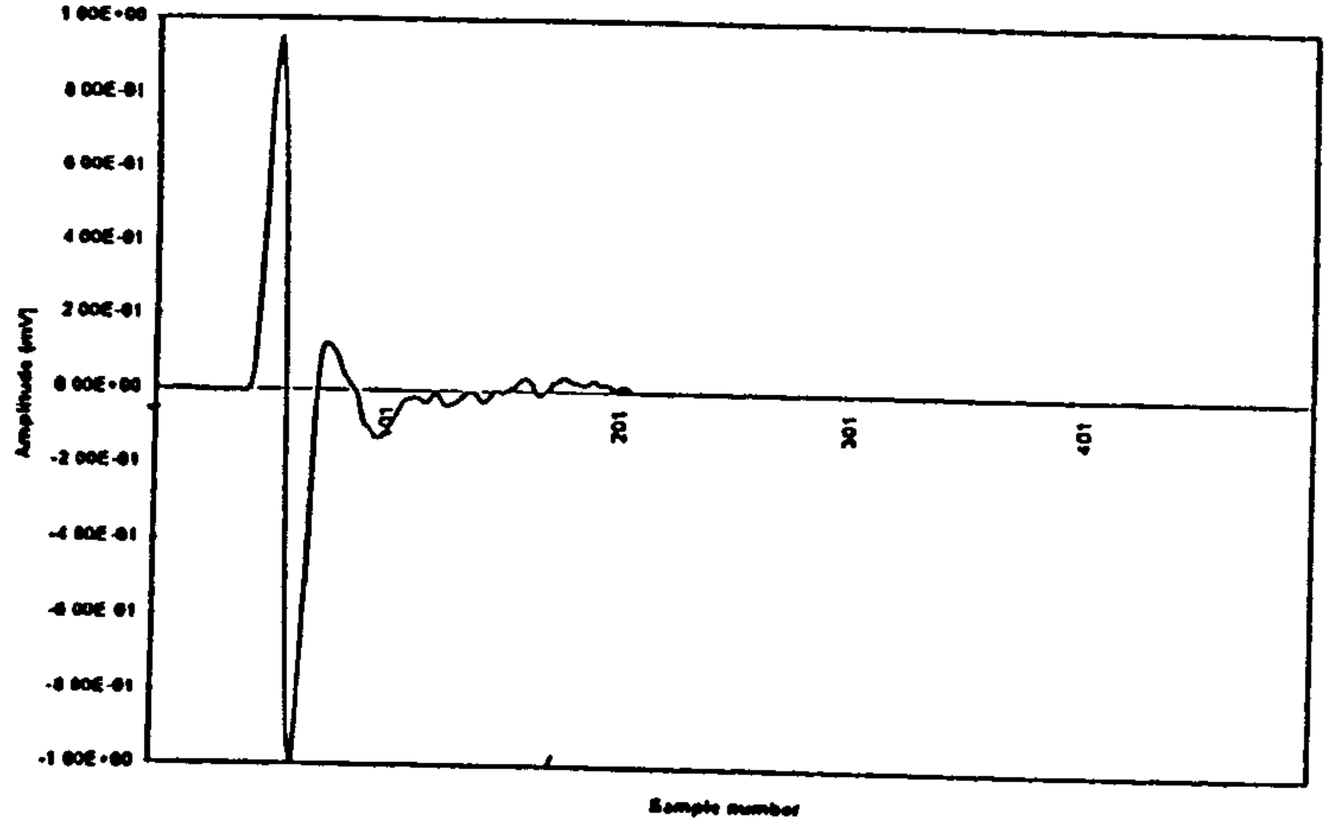

(a)

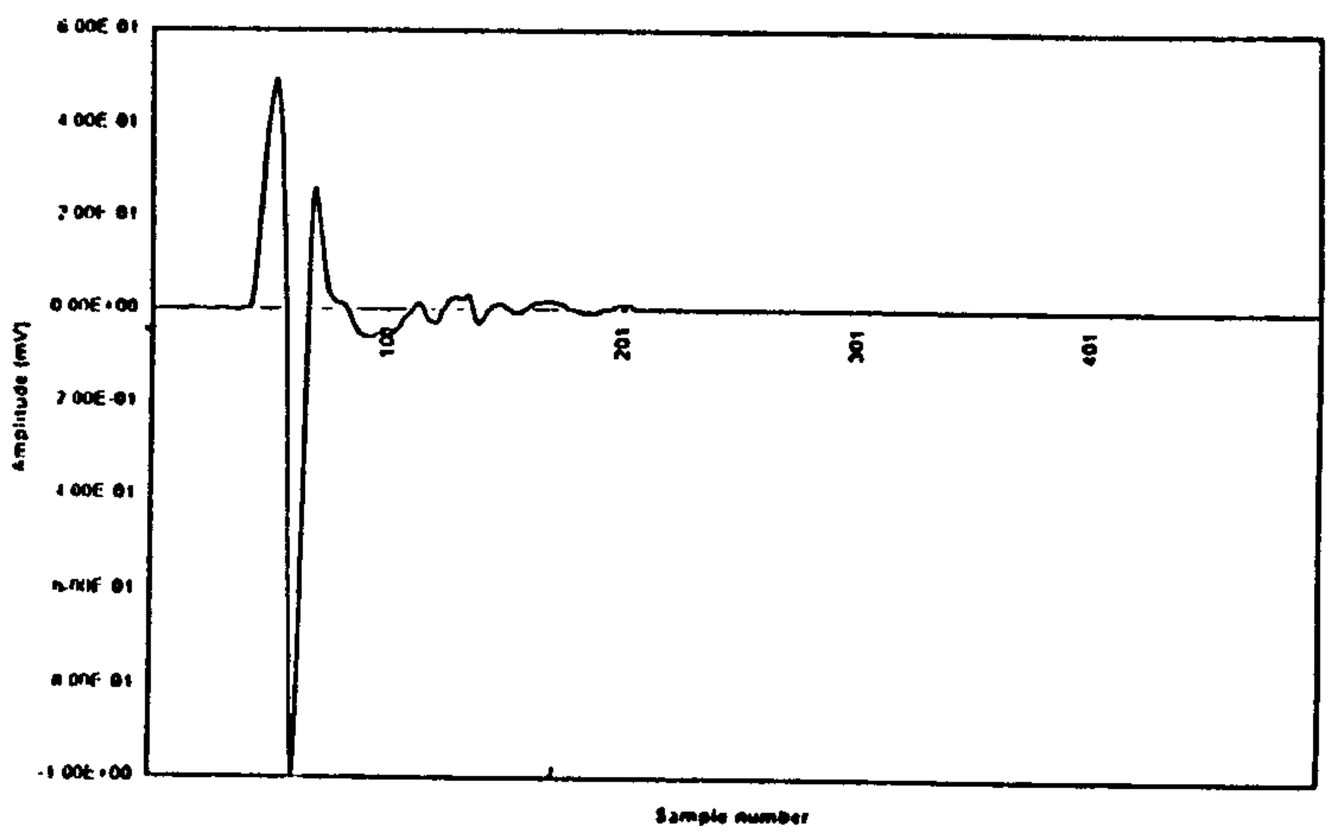

(c)

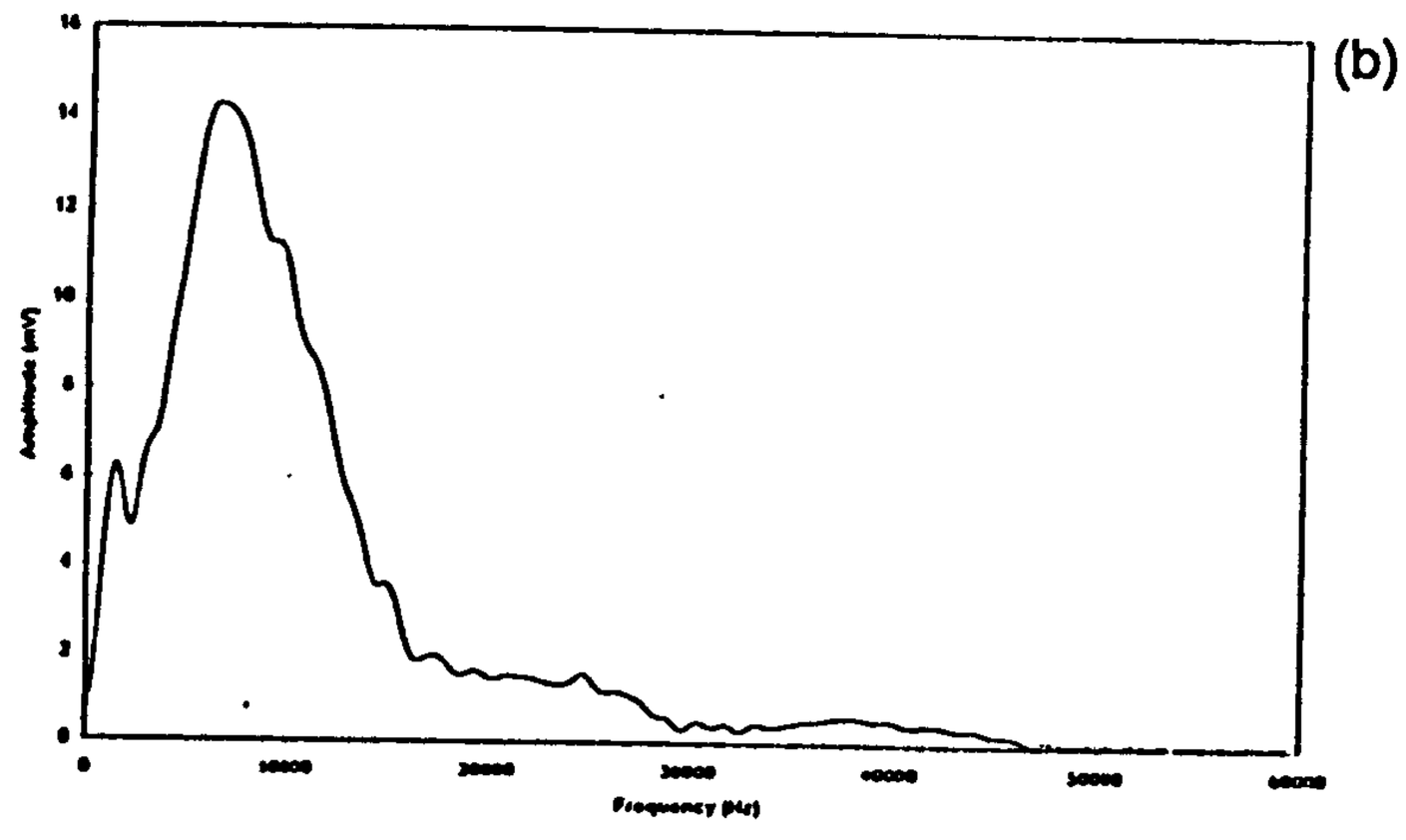

(b)

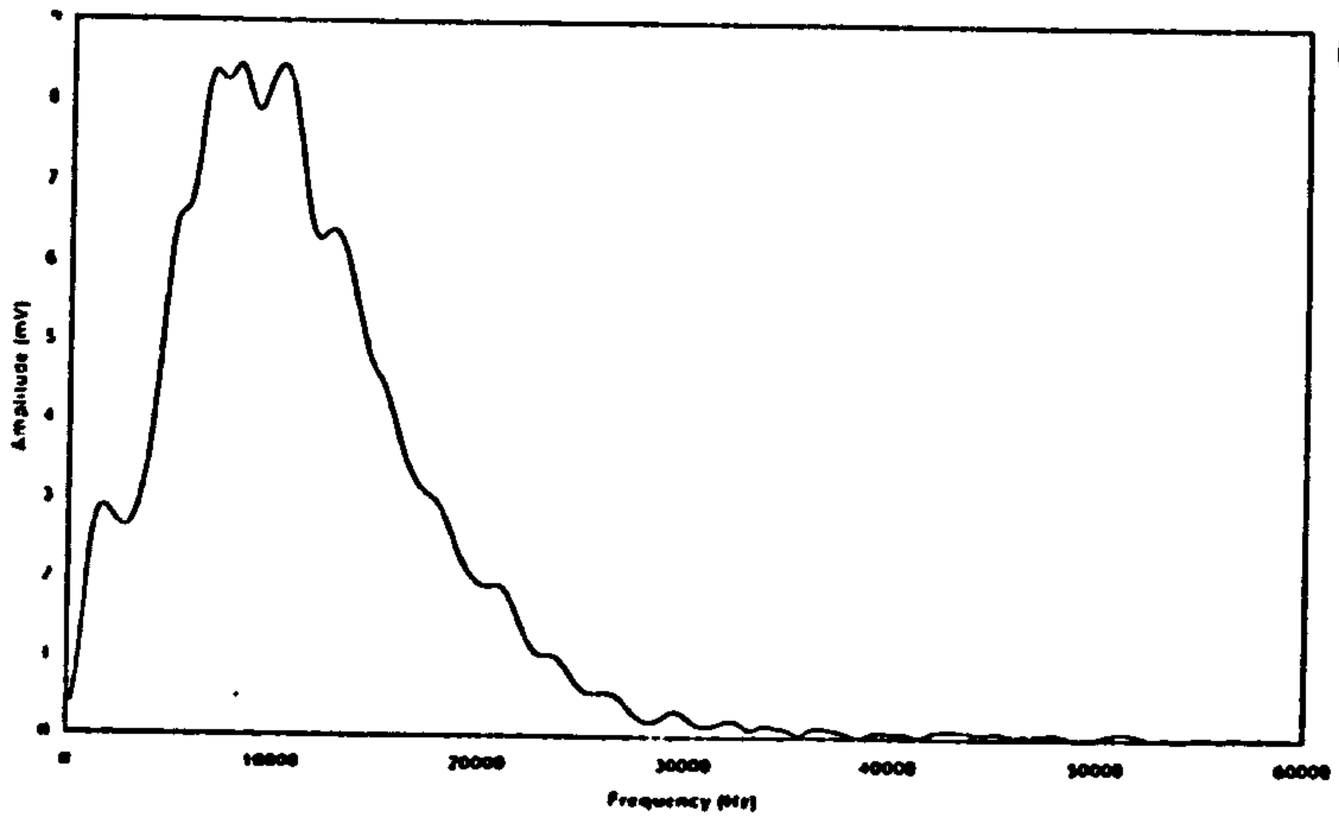

(d)

Figure 5.7. Geopulse boomer source signatures. (a) 175J in the time domain. (b) 175J in the frequency domain. (c) 105J in the time domain. (d) 105J in the frequency domain.

boomer sources is 4. For a sampling rate of 20kHz this equates to 0.15ms, and assuming a velocity of 1600m/s, then the distance is approximately 0.25m which is consistent with commonly quoted limits for this type of source (such as those listed in Trabant, 1984 or UKOOA, 1996).

5.5. Synthetic seismogram variables

The synthetic seismogram program (TENLAYERS) was tested in order to relate changes seen to the specific inputs. The first part of the program involved generating an impulse response or reflectivity function (as shown in Figure 5.5). Initially the program was used to look at a single layer and the convolution process tested with the boomer signatures described in Section 5.4.1. Figure 5.8 shows the convolved single layer model using an arbitrary thickness and reflection coefficient.

The synthetic program has deliberately been kept simple except for compensation for transmission losses and multiples, however, there is no inherent correction for absorption losses or spherical divergence. This initial simplification is considered necessary as a first estimate for producing a modelling technique to enable identification of any subtle changes of waveshape and amplitude due to physical property changes. Other than the obvious variability associated with the impulse response and the source wavelet, there are several variables which need to be considered before moving on to assess the inter-relationships between the physical properties and the seismo-acoustic response.

However, whether or not a synthetic seismogram is corrected for certain effects, such as absorption or noise added, will be determined by the seismic data which is being modelled. In the case of analogue data collected on paper only, compensation will have been made during recording for attenuating signals with depth and for divergence. Overall gain such as automatic gain control is often added to aid display. A time varying gain may also improve relative amplitude recovery. The time window which is being considered is also important to assess the impact and major cause of signal loss.

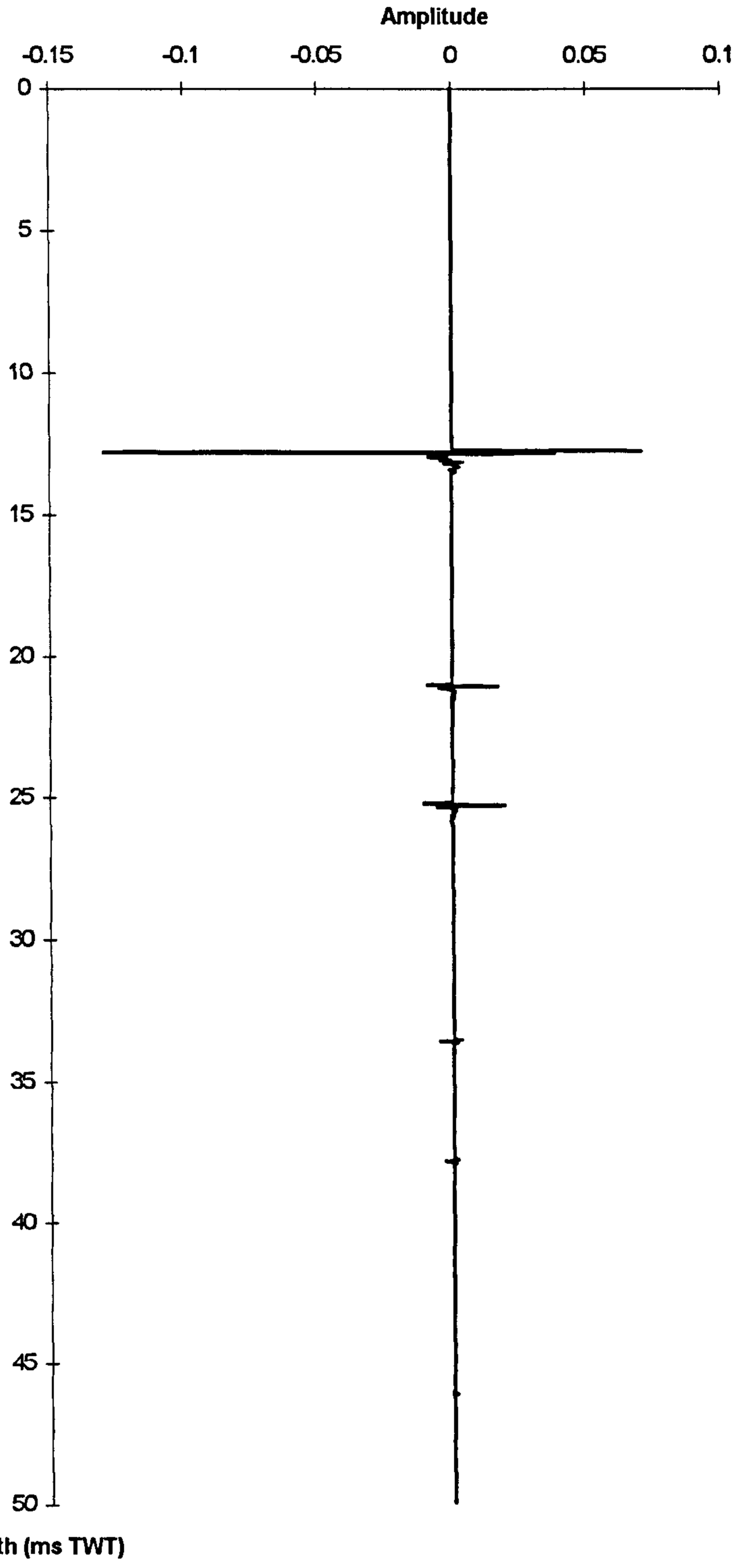

Figure 5.8. Convolution of a single layer.

5.5.1. Spherical divergence and absorption

Hron and Covey (1983) stated that "for maximum benefits to be obtained from the use of synthetic seismograms, the computational method must incorporate realistic approximations of the seismic source, the subsurface media, and the total wavefield". The TENLAYERS program used in this study accounts for transmission losses and multiples. The other two major factors for a 1-D normal incidence synthetic seismogram are spherical divergence (Section 2.5.1) and absorption (Section 2.5.2).

In order to assess the effects on the amplitude of the seismic response, losses due to absorption and spherical spreading were calculated and the change of amplitude estimated using a reference amplitude of 1. The assumptions for the calculations were: velocity = 1500m/s, frequency = 800Hz, wavelength = 1.9m and the loss coefficient = 0.15dB/λ. The estimation of spherical divergence was calculated on depth only and did not account for any change in velocity.

Depth (m)	Spreading factor	dB loss	Absorption factor	Amplitude
1	1	1	1	1
2	0.5	0.08	0.99	0.50
3	0.33	0.15	0.98	0.33
4	0.25	0.23	0.97	0.24
5	0.20	0.30	0.97	0.19
6	0.17	0.38	0.96	0.16
7	0.14	0.45	0.95	0.14
8	0.13	0.53	0.94	0.12
9	0.11	0.60	0.93	0.10
10	0.10	0.68	0.93	0.09
15	0.07	1.05	0.89	0.06
20	0.05	1.43	0.85	0.04
25	0.04	1.80	0.81	0.03
30	0.03	2.18	0.78	0.03
40	0.03	2.93	0.71	0.02
50	0.02	3.68	0.66	0.01
60	0.02	4.43	0.60	0.01

70	0.01	5.18	0.55	0.01
80	0.01	5.93	0.51	0.01
90	0.01	6.68	0.46	0.01
100	0.01	7.43	0.43	0.00

Table 5.1. Change in amplitude due to spherical divergence and absorption

When the loss multiplication factors were plotted together (Figure 5.9(a)), the spherical divergence curve showed a sharp drop in the first 20m, whereas the absorption curve shows a more linear decrease. The relative amplitude curve (Figure 5.9(b)) resembles the spherical divergence multiplication factor curve with the biggest drop in amplitude occurring in the first 20m, the affect of absorption appears to be negligible. For the frequencies and depths investigated in this project the dominant loss factor is considered to be spherical divergence.

This assessment of absorption and spherical divergence is meant simply as a guide. The absorption coefficient used was a constant with depth. This will not be the case in the real situation and may vary. Buchan *et al.* (1972) show attenuation coefficients ranging from 1 to 20dB/m with sediment mean diameter. McQuillan *et al.* (1986) quote absorption for rocks varying between 0.1 and 3dB/λ.

5.5.2. Noise

A major cause of distortion on seismic records is uncorrelated or random noise and therefore random noise has been added to the synthetic to assess the effect on the resulting trace. The subroutine used to add noise to the synthetic seismogram was modified from the subroutine NOISE from Sinvhal and Sinvhal (1992).

The subroutine calculates the variance of the synthetic seismogram, VR_s, and of a series of random numbers generated in the range -0.2 to 0.2, VR_n, i.e. the amplitude range of the signal. The signal to noise ratio, SNR, assuming 10% noise is computed by:

$$\text{SNR (10\%)} = \sqrt{\frac{VR_s / VR_n}{10}} \qquad (5.1)$$

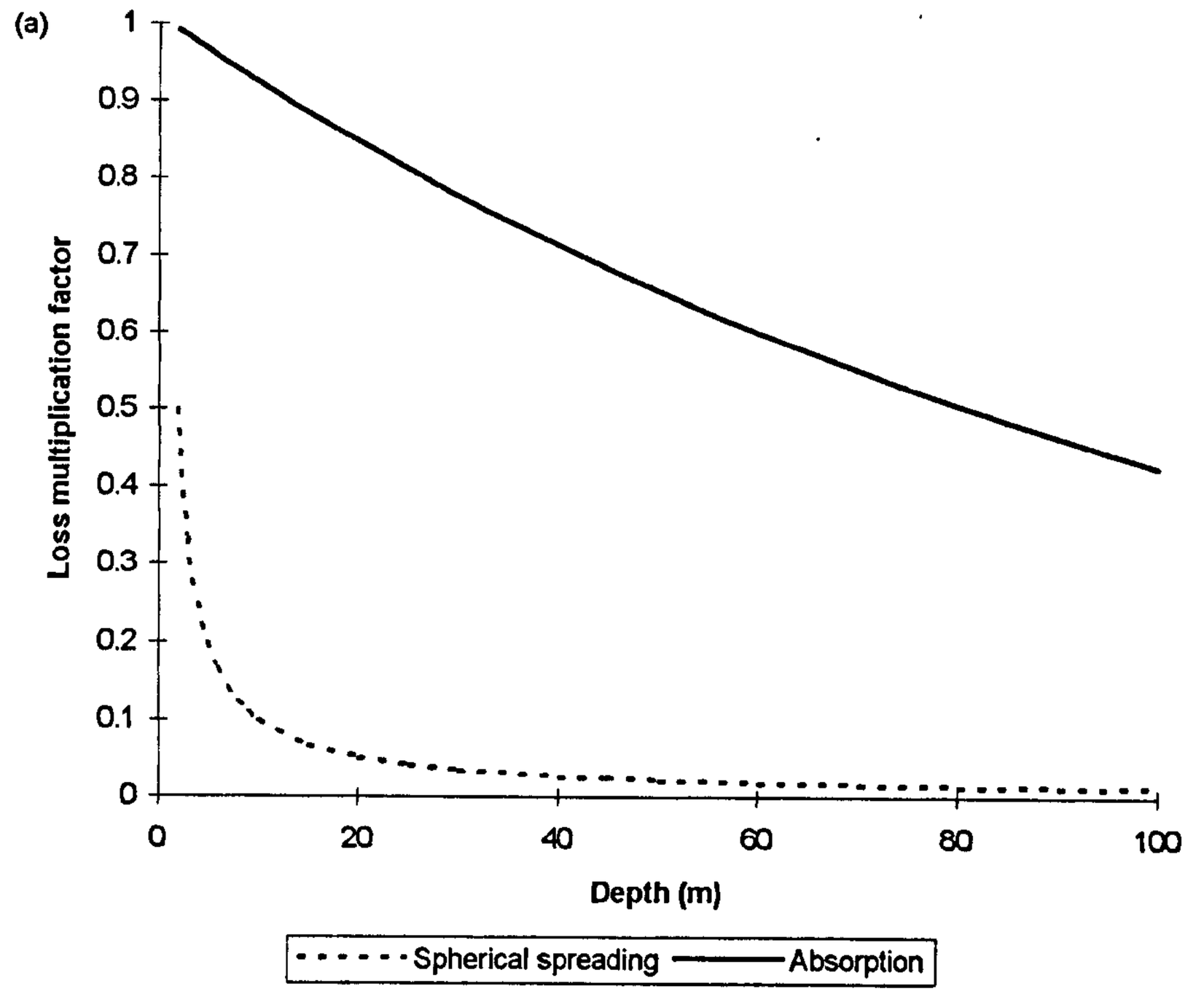

Figure 5.9. (a) Loss multiplication factors due to spherical divergence and absorption. (b) Effects of losses on amplitude.

The required amount of random numbers are then multiplied by the SNR to give the noise signal. This noise signal is then added to the original synthetic seismogram signal to produce a synthetic seismogram which has been corrupted with noise. Figure 5.10(a) shows the synthetic seismogram before and 5.10(b) after the addition of random; 10% noise shows little effect on the seismogram. During processing, noise is removed as far as possible whilst still maintaining a good signal.

5.5.3. Sampling frequency

The TENLAYERS program was designed to handle the very high sampling rates needed when investigating reverberatory sequences in shallow sediments with very high resolution geophysical techniques. The most significant frequency when sampling is the Nyquist frequency which is defined as the bandwidth of a signal, and is the frequency of half the sampling frequency. The boomer signatures which were supplied (see Section 5.4.1) were sampled at a rate of approximately 204kHz. The signatures were subsequently re-sampled and a digitisation rate of 20kHz was chosen for the data analysis which saved memory and computing time. Using 20kHz also meant that digitising source signatures from paper was more straightforward, as source signatures may not be routinely digitally recorded. The effect of resampling is illustrated in Figure 5.11, the shift observed in Figure 5.11 is a function of the re-sampling and plotting. A sampling frequency of 20kHz is adequate for the 175J source which has the peak frequency lower than 10kHz (Figure 5.7(b)). The 105J source peak frequency is around 10kHz (Figure 5.7(d)) and this may lead to changes in the frequency content of the re-sampled signal. When choosing a sampling frequency it is essential that the rate is fast enough to retain resolution and does not produce aliasing, which may account for the shift seen in the source signatures. Although the higher sampling frequency gives a better signal definition, the lower sample rate provides a good representation of the wavelet.

5.5.4. Significant figures and smoothing

The number of significant figures to which reflection coefficients are quoted can have a noticeable effect on the amplitude when reliance on amplitude changes is considered important. Figure 5.12(a) illustrates the influence of the number of

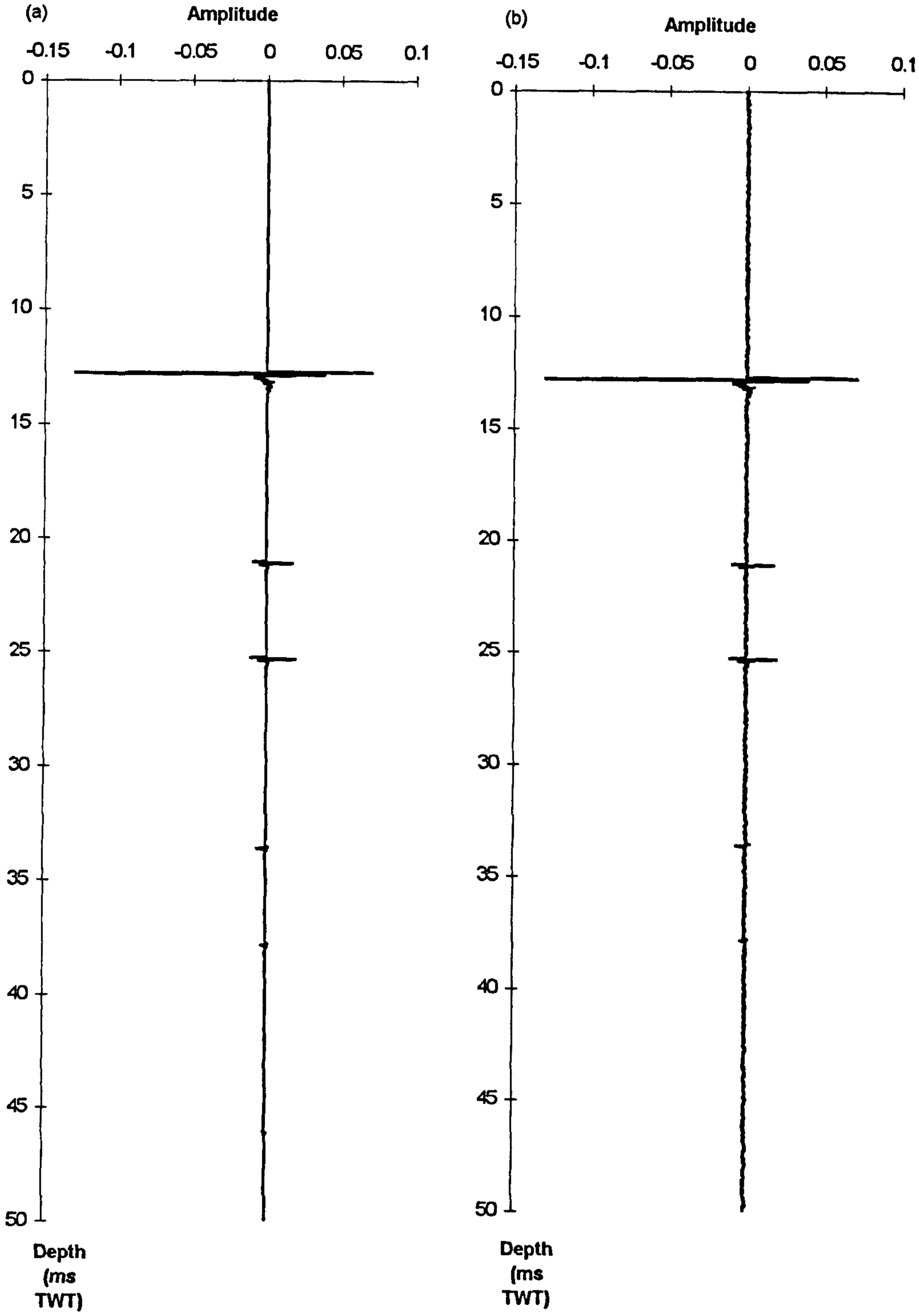

Figure 5.10. Effect of noise on the system. (a) No noise. (b) 10% noise.

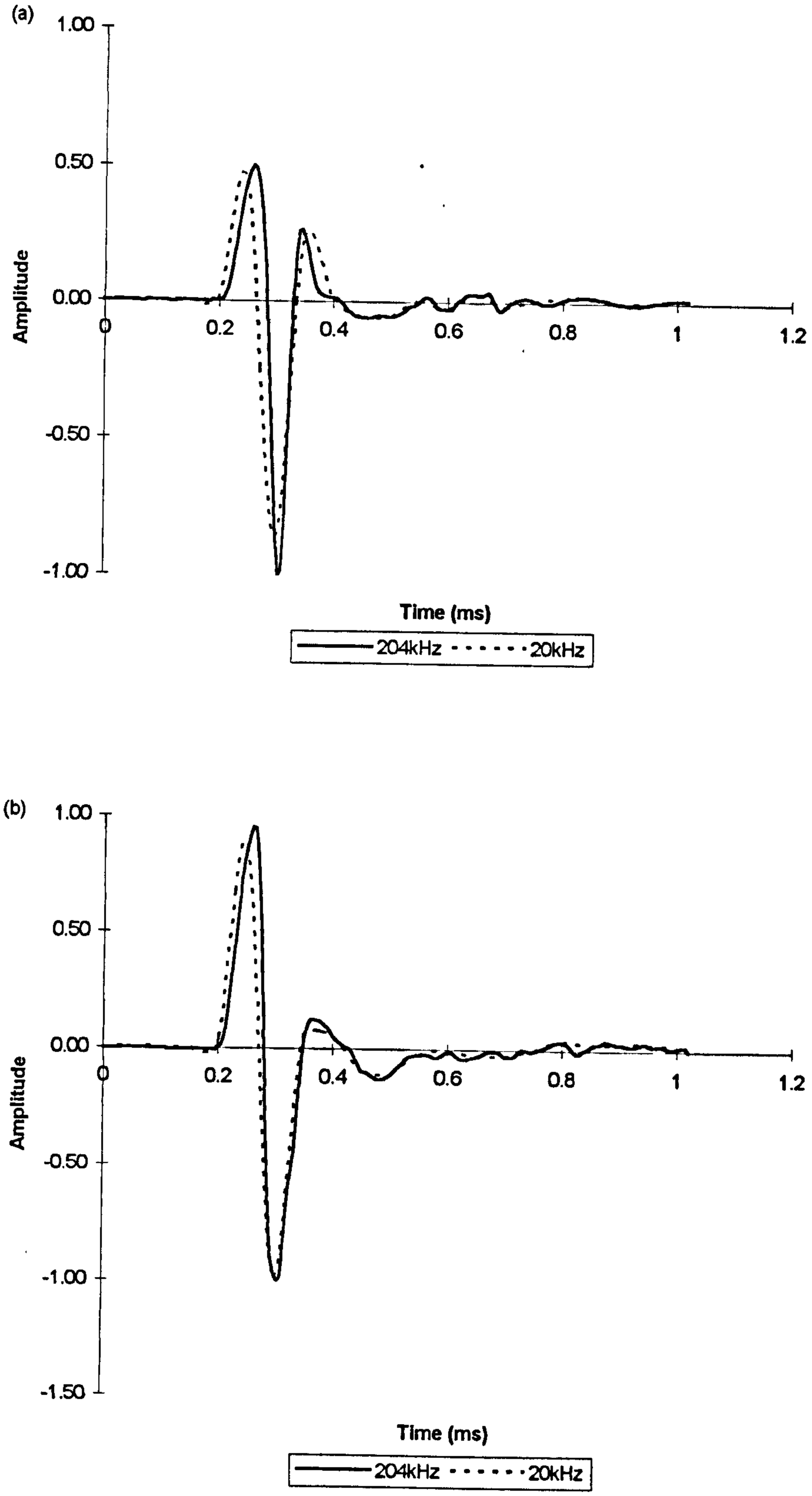

Figure 5.11. Variation of sampling frequency for boomer sources. (a) 105J. (b) 175J.

(a)

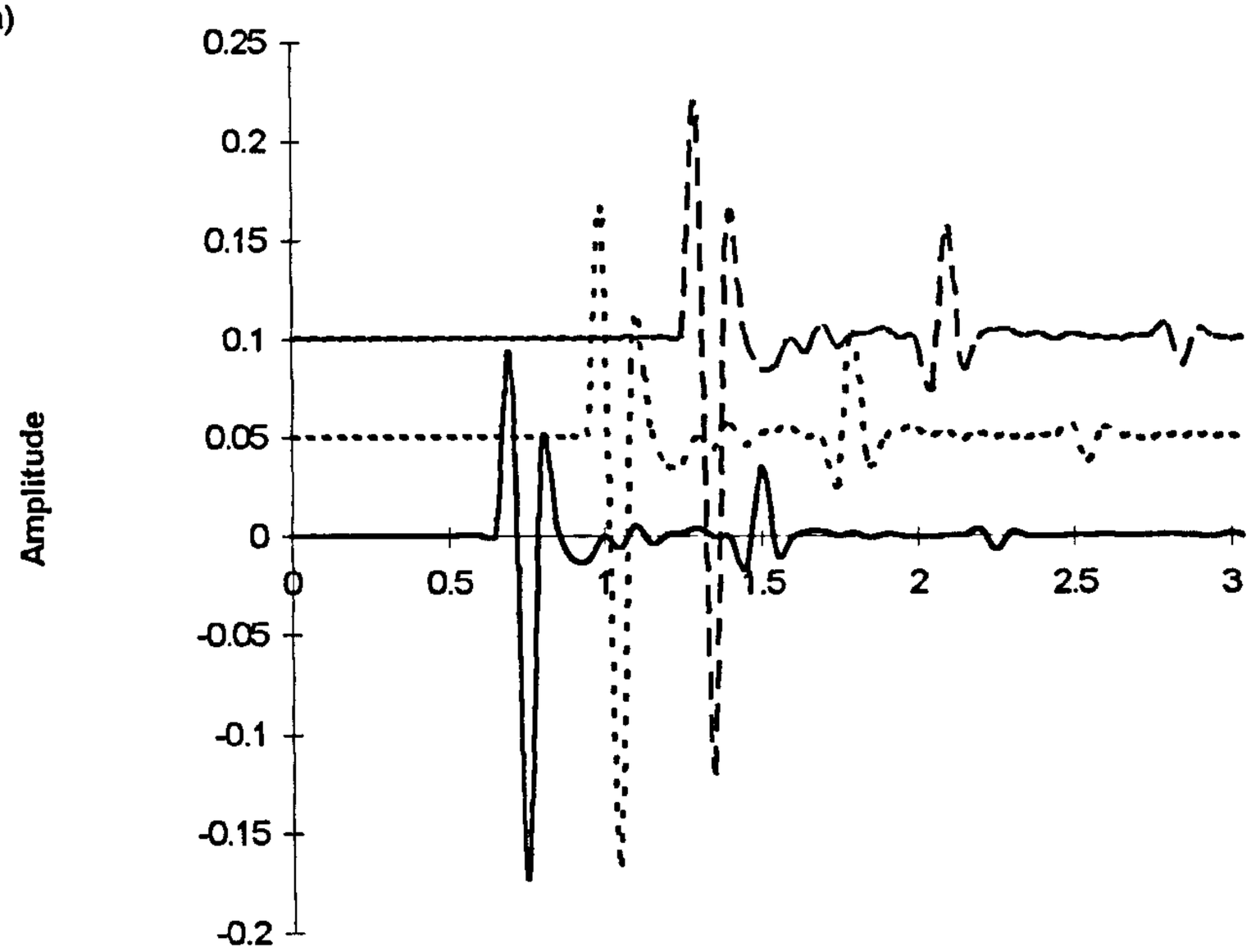

(b)

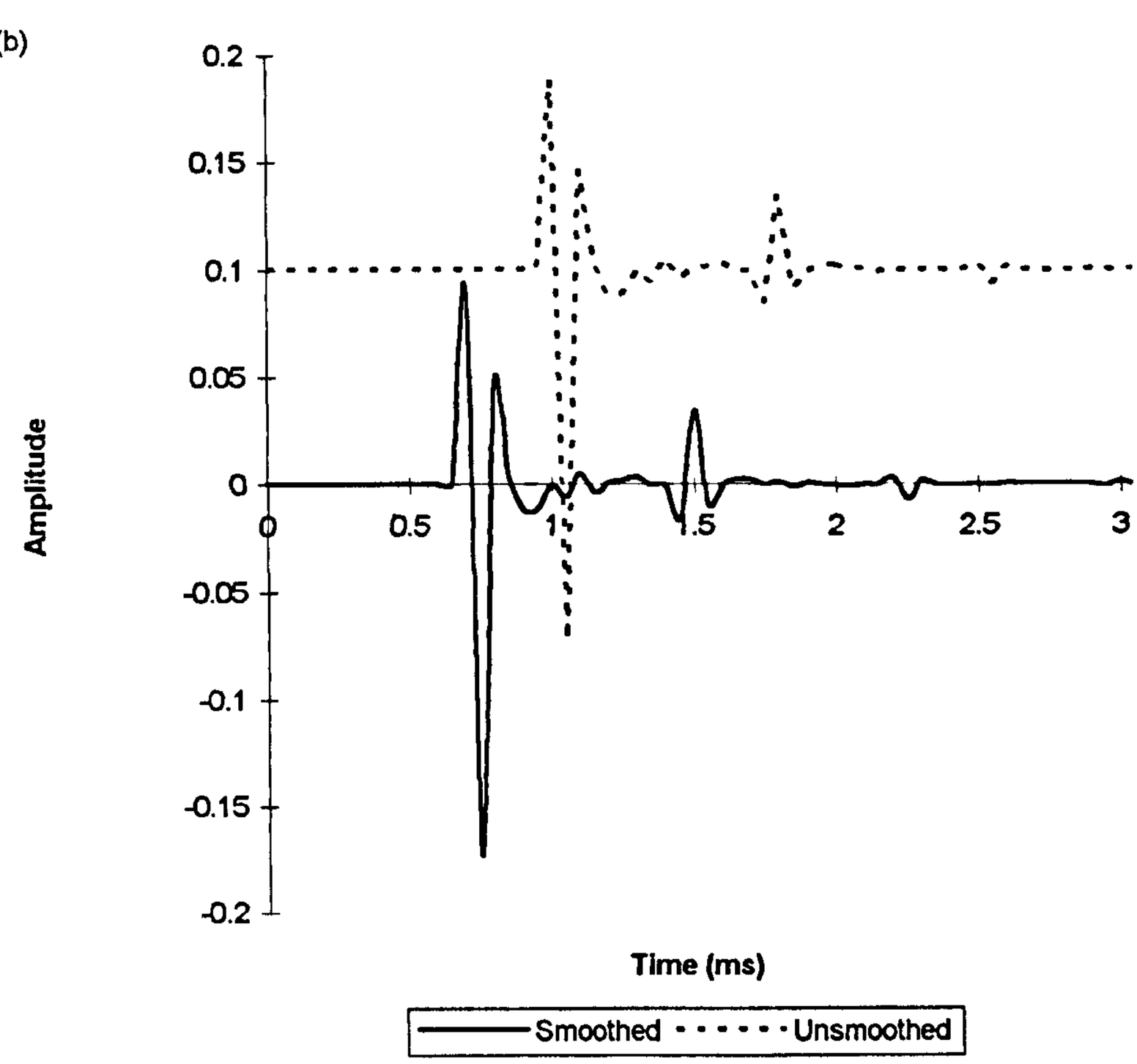

Figure 5.12. 175J source. (a) Variation of significant figures. (b) Effects of smoothing.

significant figures in the synthetic return. There is a relative increase in relative amplitude of 0.08 corresponding to an increase of the reflection coefficient by 0.05.

When plotting any synthetic seismogram a degree of smoothing is involved which may or may not be quantified. Within the ISX program discussed above the smoothing factor was unknown. However, when plotting through Microsoft Excel the smoothing function can be turned on and off as shown in Figure 5.12(b). Smoothing is not considered to be significant for this study.

5.6. Analysis of empirical relationships in the model

The method of the basic modelling production technique and the output expected, i.e. the synthetic seismogram, has been presented. The next stage is to assess the inputs to the model and their effects on the output model. The process of achieving this has been through sensitivity analysis. The first part is to study the main input parameters to the seismogram, i.e. density and velocity. Acoustic impedance is calculated, and then a reflection coefficient which quantifies the acoustic impedance change across the layers.

5.6.1. Sensitivity analysis of synthetic input parameters

5.6.1.1. Impulse response

The first step in this analysis was to test the sensitivity of density and velocity. In order to assess the sensitivity, errors on the original measurements need to be considered to establish limits.

In relation to bulk density measurements, Paul and Jobson (1987) discuss the density error resulting from volume measurements (Section 2.7.7 gives the parameters and definitions involved in the measurement of bulk density). Paul and Jobson (1987) identify the distribution of the variations in saturation as being due partly to error and partly to natural variation. It is assumed that any measurements in weight are going to be as exact as any measurement could be, and is based on the accuracy of the balance, therefore the error must be in the measurement of volume.

Velocity measurements in the laboratory are generally taken by measuring the transmit time of an ultrasonic pulse across the diameter of a core. There are two potential sources of error in this method, incorrect knowledge of the core diameter, and thickness variations in the core liner (Paul and Jobson, 1987). However, these errors can be removed by making calibrating the core liner by making measurements using distilled water at a known temperature. Velocity measurements will also be affected by sampling disturbance on recovery, sample size, settlement, loss of moisture as well as possible errors in measuring the onset time.

Obviously, by altering the density by a known amount against a fixed velocity will alter the impedance by a fixed amount and vice versa. Figure 5.13(a) illustrates the effect on the reflection coefficient when a constant velocity is assumed and the density changed, and Figure 5.13(b) has a constant density and a varying velocity.

The next stage is to vary the reflection coefficient and relate this to amplitude by convolving the impulse response with the boomer source wavelet. Figure 5.14 illustrates the variation of reflection coefficient in 0.05 steps in a single layer model. The changes in reflection coefficient are plotted as a smoothed and an unsmoothed curve. These curves show that for a 0.05 change in reflection coefficient the corresponding change in amplitude of the first peak is 0.07; this change is a function of the convolution process. The smoothing factor in the plotting package appears to have a negligible effect on the amplitude output. Therefore the synthetic output and the resulting amplitudes are directly related to changes in reflection coefficient and the source wavelet with no other influences.

5.6.1.2. Source wavelet

For this study, the two sources wavelets described in Section 5.4.1 will be used to which allow a comparison of factors affecting the acoustic response such as bandwidth and power. Figure 5.15 shows the difference in amplitude produced for each source in a single layer convolved model. The 105J boomer source has a maximum peak amplitude of 0.09, whereas, the 175J peak amplitude is 0.18.

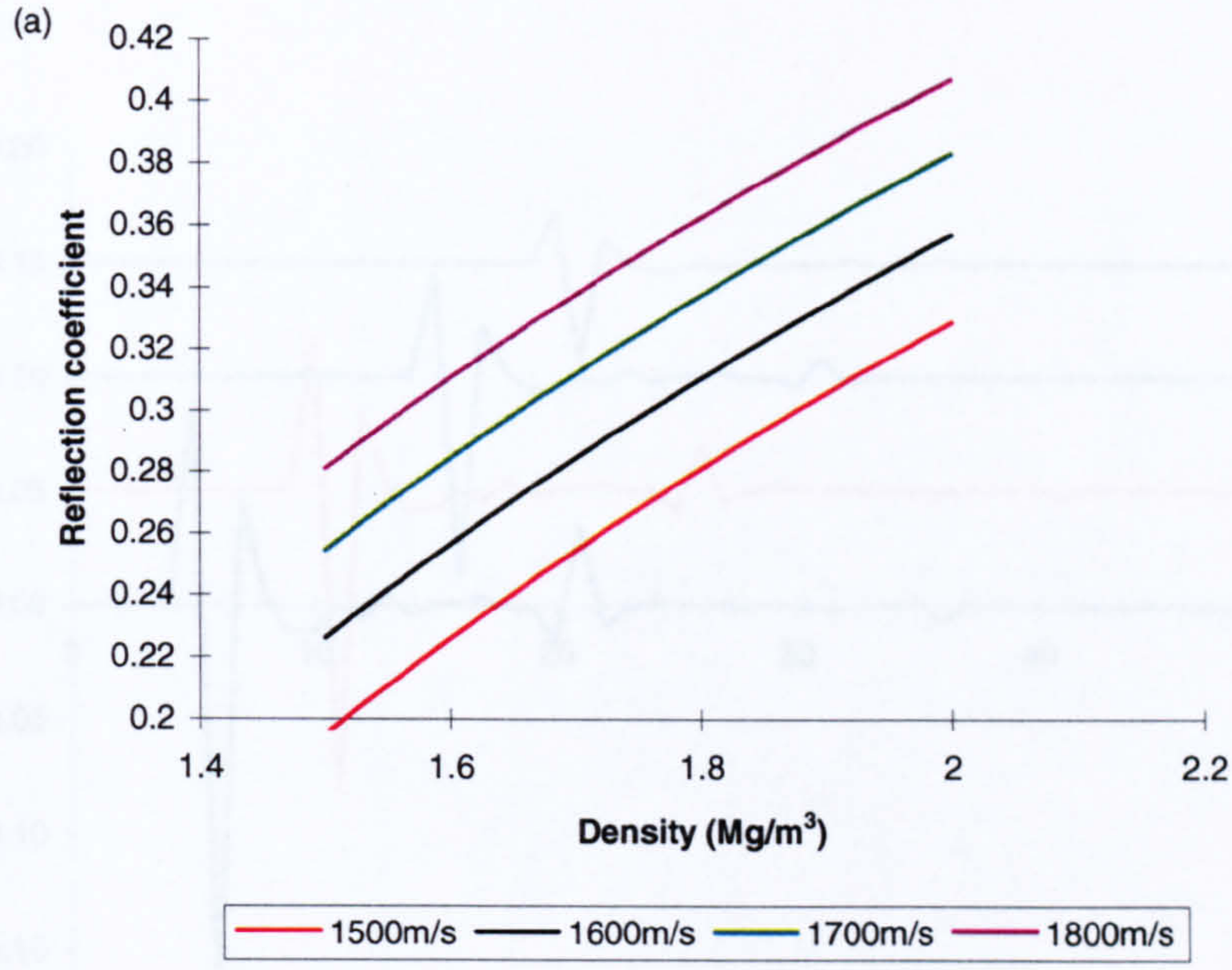

Figure 5.13. Effect on reflection coefficient due to variations of density and velocity. (a) Constant density. (b) Constant velocity.

(a)

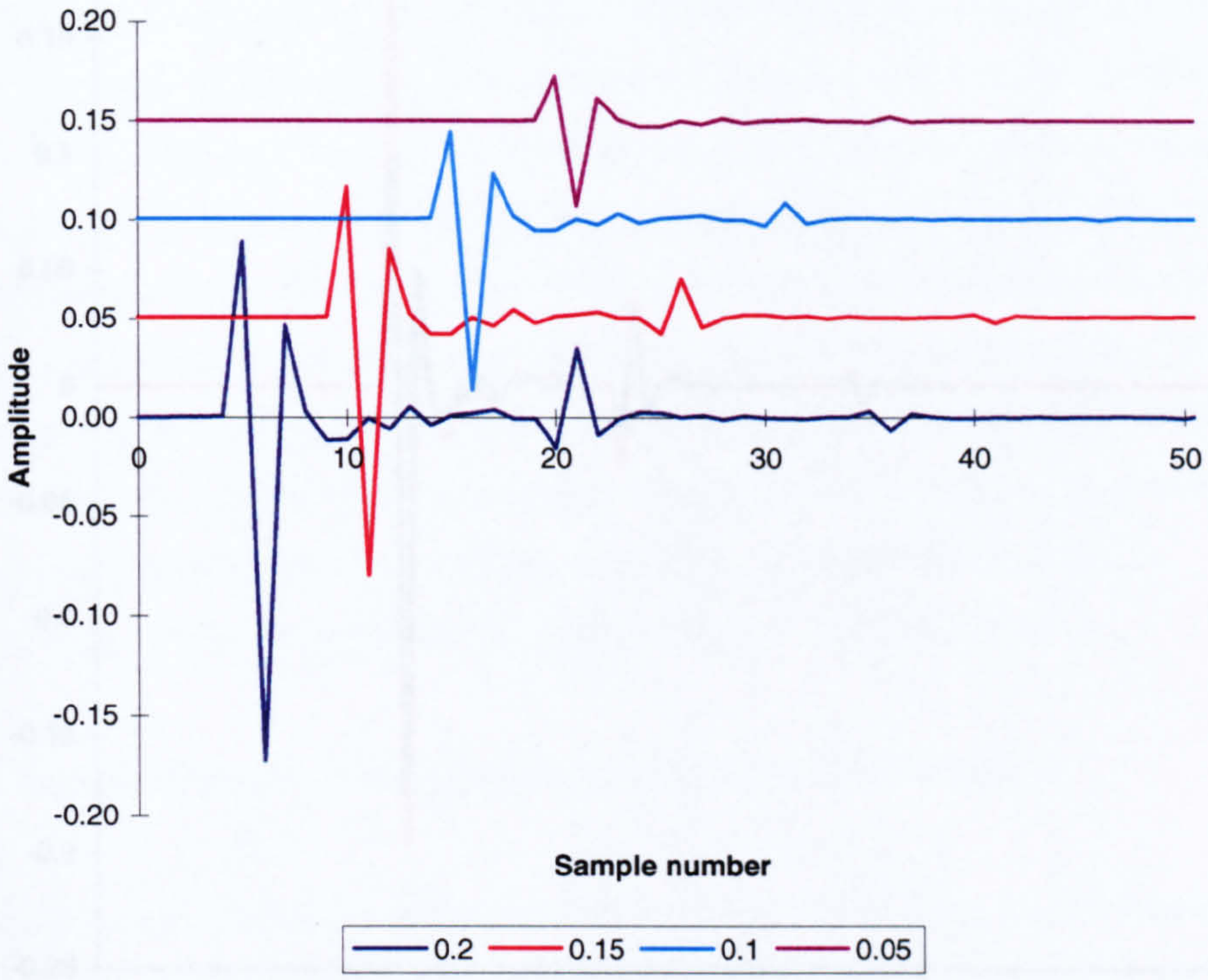

(b)

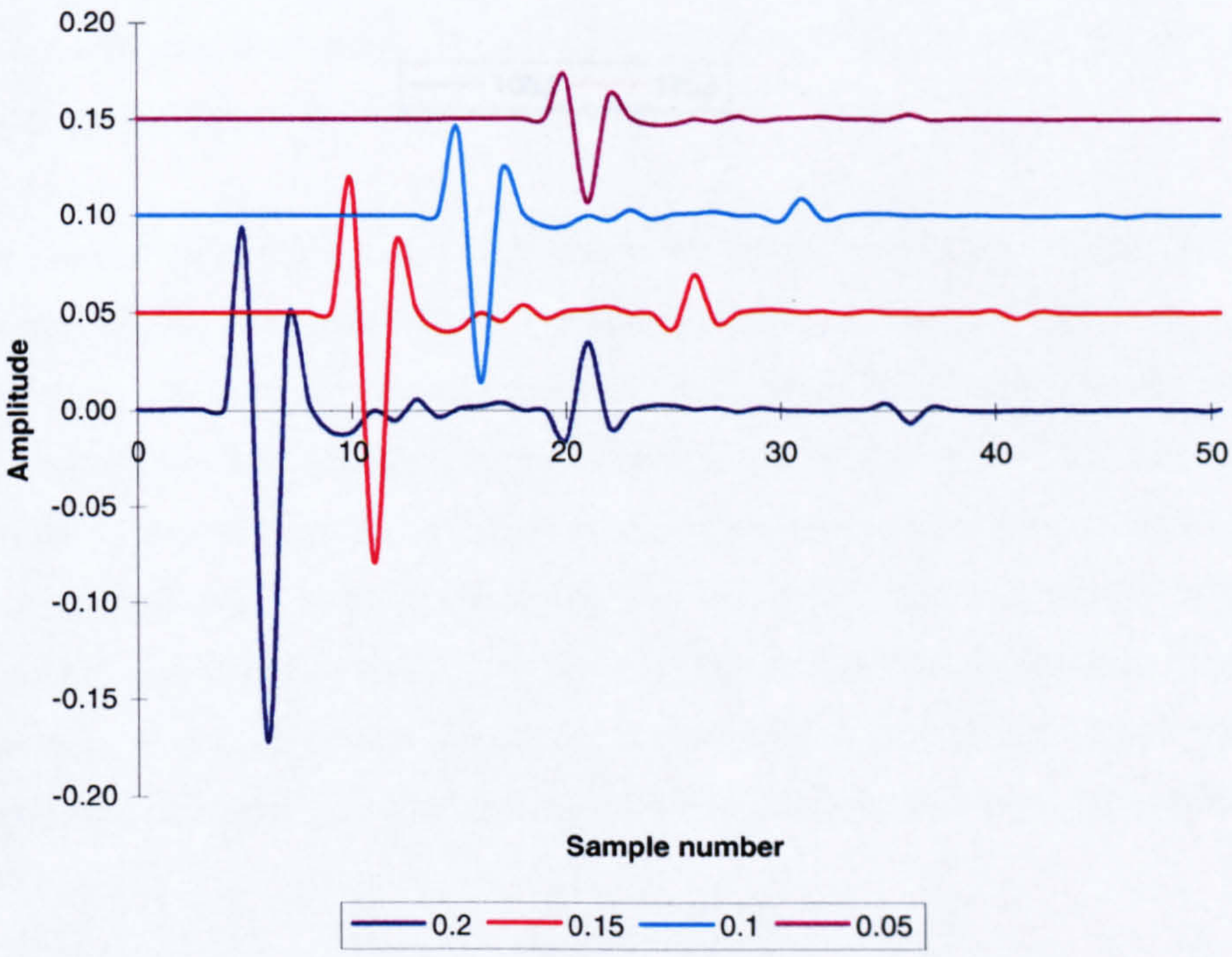

Figure 5.14. Variation of reflection coefficient. (a) Unsmoothed. (b) Smoothed.

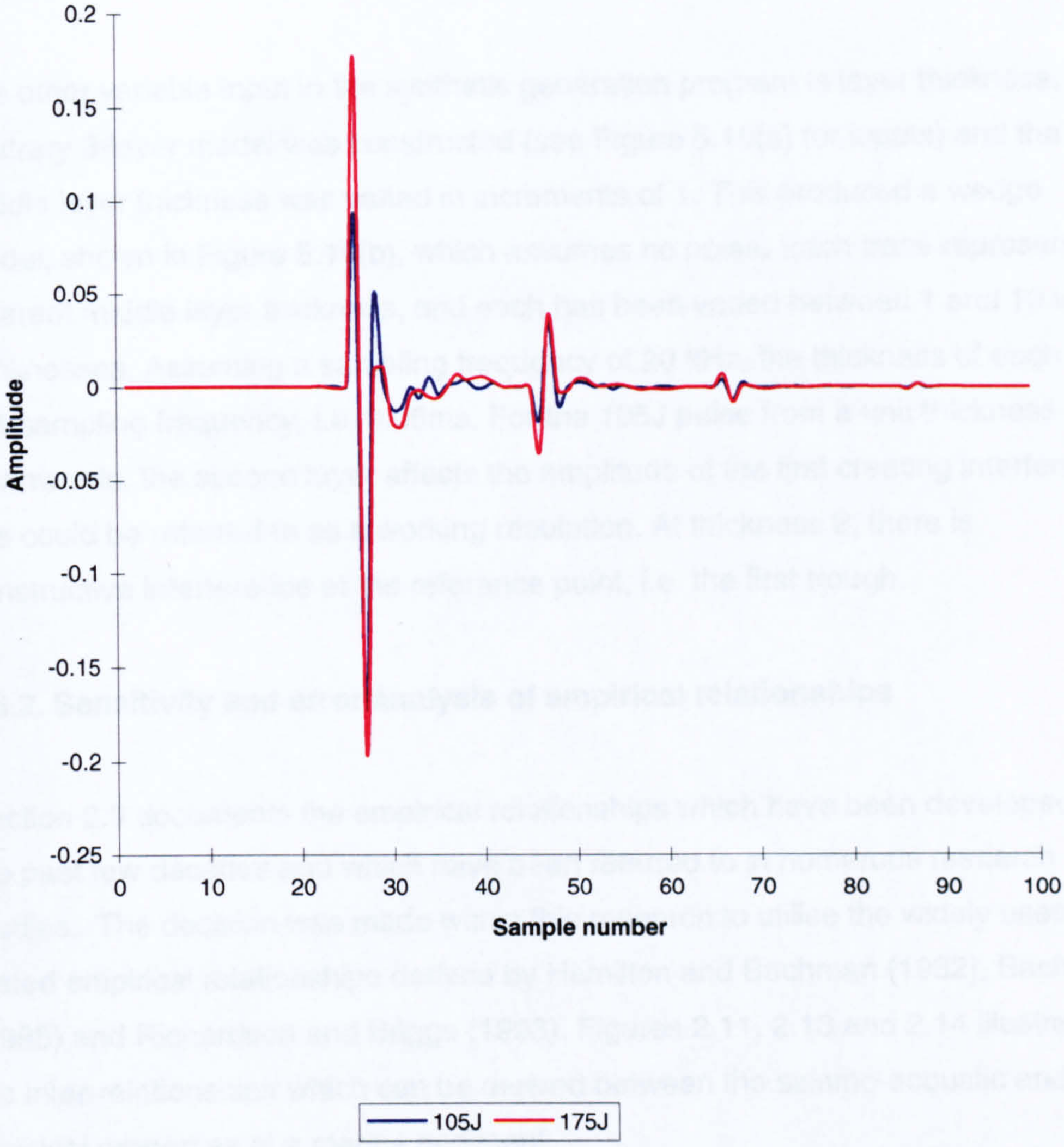

Figure 5.15. Difference in amplitude due to source power.

5.6.1.3. Thickness of sediment units

The other variable input in the synthetic generation program is layer thickness. An arbitrary 3-layer model was constructed (see Figure 5.16(a) for inputs) and the middle layer thickness was varied in increments of 1. This produced a wedge model, shown in Figure 5.16(b), which assumes no noise. Each trace represents a different middle layer thickness, and each has been varied between 1 and 10 unit thicknesses. Assuming a sampling frequency of 20 kHz, the thickness of each unit is 1/sampling frequency, i.e. 0.05ms. For the 105J pulse from a unit thickness of 8 downwards, the second layer affects the amplitude of the first creating interference; this could be referred to as a working resolution. At thickness 2, there is constructive interference at the reference point, i.e. the first trough.

5.6.2. Sensitivity and error analysis of empirical relationships

Section 2.9 documents the empirical relationships which have been developed over the past few decades and which have been referred to in numerous research studies. The decision was made within this research to utilise the widely used and tested empirical relationships derived by Hamilton and Bachman (1982), Bachman (1985) and Richardson and Briggs (1993). Figures 2.11, 2.13 and 2.14 illustrated the inter-relationships which can be derived between the seismo-acoustic and physical properties of a marine sediment.

In the context of this study the regression equations produced by Hamilton and Bachman (1982) and reviewed in Bachman (1985), which predict the acoustic parameters, i.e. velocity, impedance and attenuation from the physical properties, are better suited to the techniques of forward modelling. In contrast the correlations of Richardson and Briggs (1993), which predict the physical properties from the acoustic parameters, are indirectly valid for this method as this study concentrates on using physical properties to predict acoustic properties. Reference is also made to Esker *et al.* (1996) where similar forward modelling techniques have been developed based on geotechnical measurements from amongst others Hamilton *et al.* (1956).

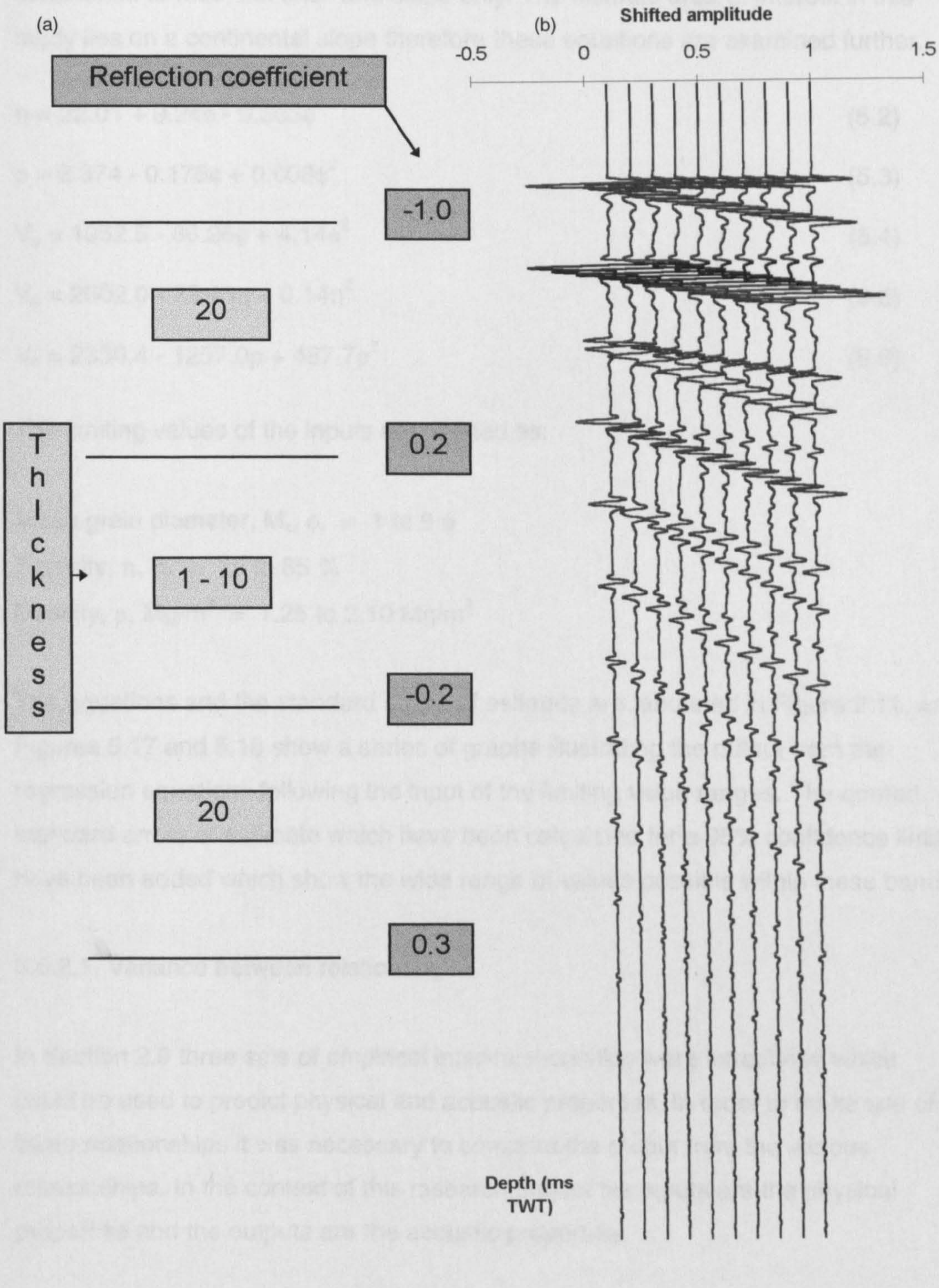

Figure 5.16. (a) Wedge model input. (b) 105J wedge model.

The set of equations listed below from Hamilton and Bachman (1982) refer to the continental terrace, i.e. shelf and slope only. The ultimate area of interest in this study lies on a continental slope therefore these equations are examined further.

$$\eta = 22.01 + 9.24\phi - 0.365\phi^2 \quad (5.2)$$

$$\rho = 2.374 - 0.175\phi + 0.008\phi^2 \quad (5.3)$$

$$V_p = 1952.5 - 86.26\phi + 4.14\phi^2 \quad (5.4)$$

$$V_p = 2502.0 - 23.45\eta + 0.14\eta^2 \quad (5.5)$$

$$V_p = 2330.4 - 1257.0\rho + 487.7\rho^2 \quad (5.6)$$

The limiting values of the inputs are defined as:

Mean grain diameter, M_z, ϕ, = 1 to 9 ϕ

Porosity, η, % = 35 to 85 %

Density, ρ, Mg/m^3 = 1.25 to 2.10 Mg/m^3

The equations and the standard errors of estimate are tabulated in Figure 2.11, and Figures 5.17 and 5.18 show a series of graphs illustrating the output from the regression equations following the input of the limiting value ranges. The quoted standard errors of estimate which have been calculated for a 95% confidence limit have been added which show the wide range of values possible within these bands.

5.6.2.1. Variance between relationships

In Section 2.9 three sets of empirical inter-relationships were introduced which could be used to predict physical and acoustic properties. In order to make use of these relationships it was necessary to compare the output from the various relationships. In the context of this research project the inputs are the physical properties and the outputs are the acoustic properties.

A two-way analysis of variance (ANOVA) for single observations (after Fowler and Cohen, 1990) was run between the inter-relationship outputs of velocity of Hamilton and Bachman (1982) and Richardson and Briggs (1993).

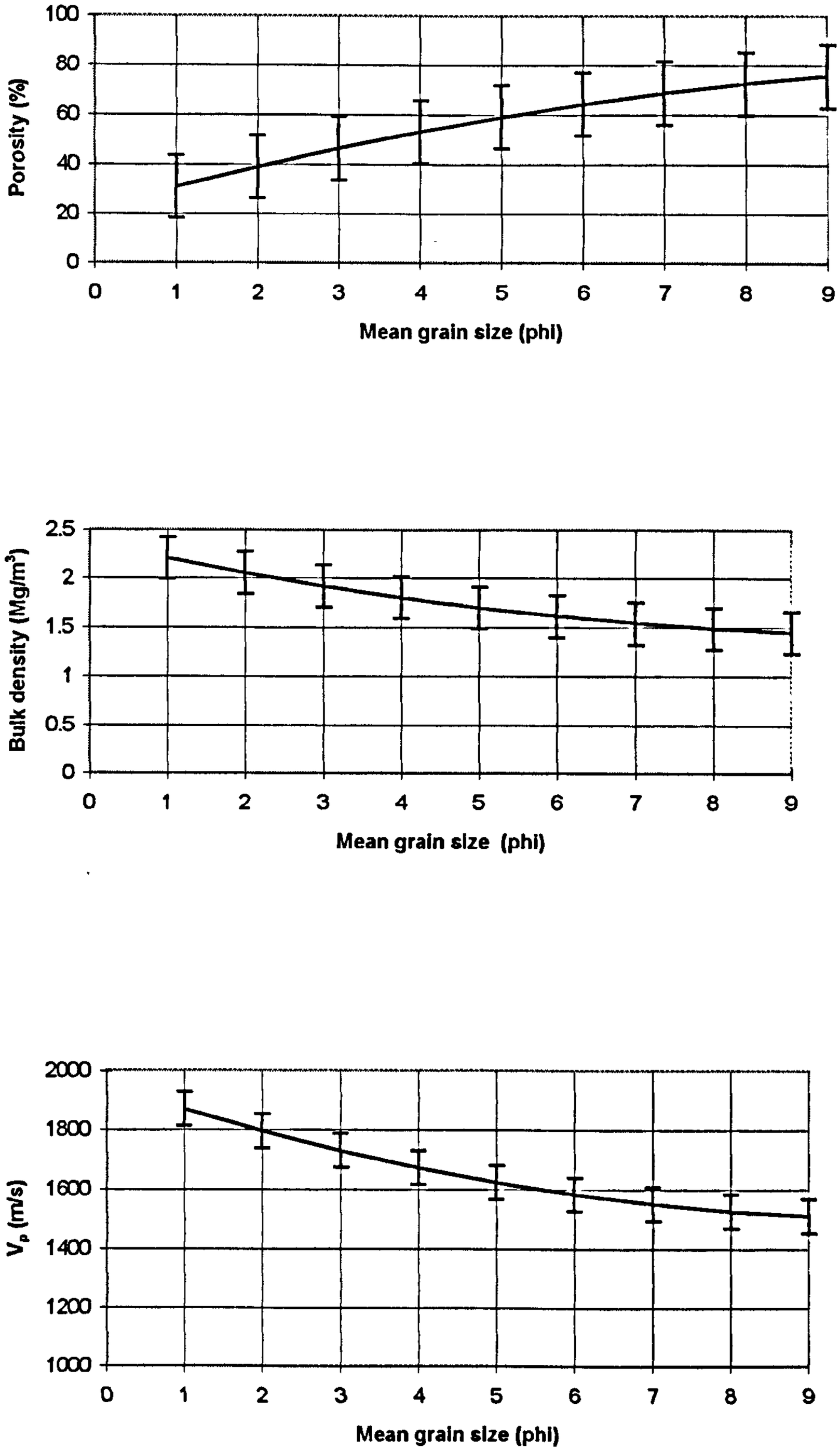

Figure 5.17. Graphical representation of the empirical relationships of Hamilton and Bachman (1982).

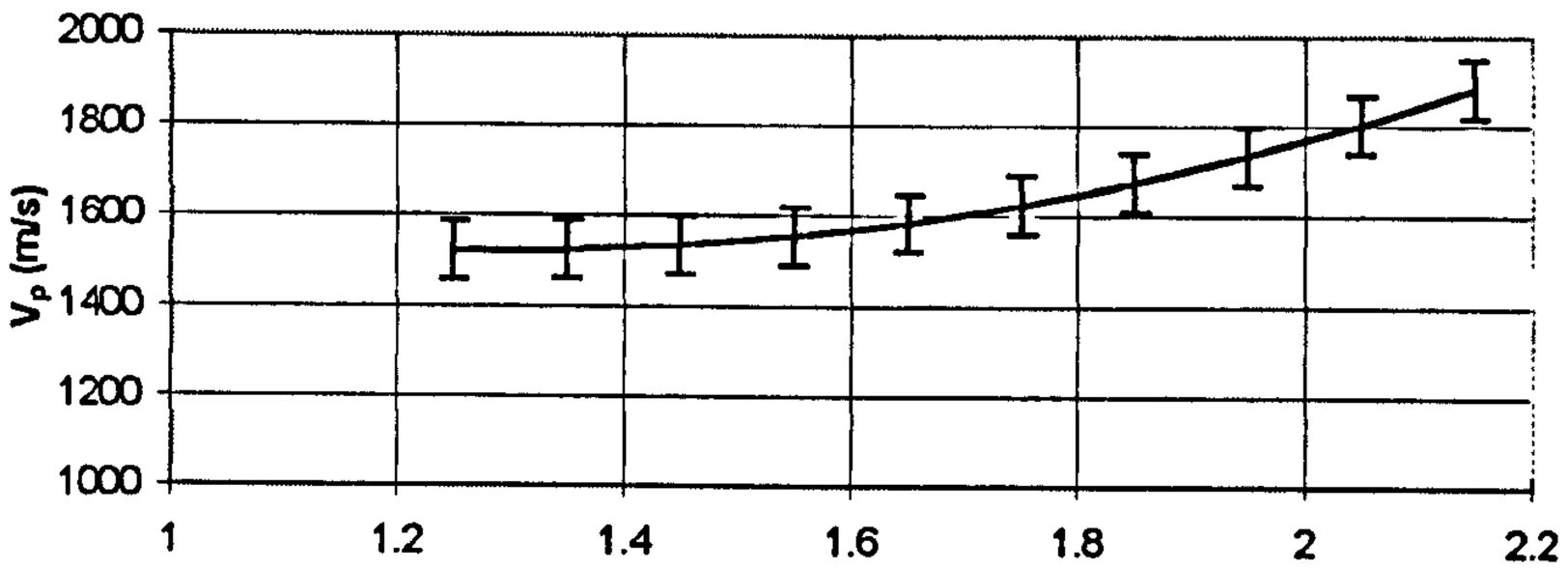

Figure 5.18. Graphical representation of the empirical relationships of Hamilton and Bachman (1982).

A depth model from the Devil's Hole area of the North Sea was created as a test model (Fyfe, 1985), and the inputs are shown in Table 5.2.

Description	Thickness (m)	Reflection coefficient
Water column	-	-
Post glacial, shallow marine sands	6	0.42
Late glacial, low energy soft marine clays	28	-0.17
Interglacial, shallow marine, interlaminated stiff clay and sand	73	0.16
Glaciomarine hard clay	-	0.3

Table 5.2. Devils Hole geological model.

V_p values were used directly from BGS information and were calculated from porosity and density information through the empirical inter-relationships of Hamilton and Bachman (1982). Table 5.3 lists the ANOVA results which confirm that there is no significant difference between the method used to calculate V_p, but that there are significant differences between the depth interval as would be expected.

Source of variation	Sum of squares	df	variance	F-value
Variable A - input parameter	859.74	3	286.58	0.33
Variable B - depth interval	116271.10	3	38757.04	45.01
Within	7750.20	9	861.13	
Total	124881.00	15	8325.40	

Table 5.3. - ANOVA results from BGS data and inputs into empirical inter-relationships from Hamilton and Bachman (1982).

The method was repeated on the same depth model using the empirical inter-relationships of Richardson and Briggs (1993) to produce V_p ratios. Table 5.4 lists the ANOVA results and the outcome is similar to the previous ANOVA test, i.e. whichever method of calculating the V_p ratio is used will produce a similar result yet there are significant differences between the depth intervals.

Source of variation	Sum of squares	df	variance	F-value
Variable A - input parameter	0.011722	3	0.003907	6.51
Variable B - depth interval	0.054974	3	0.018325	30.53
Within	0.005402	9	0.0006	
Total	0.072098	15	0.004807	

Table 5.4. - ANOVA results from the prediction of V_p ratio using the empirical inter-relationships from Richardson and Briggs (1993).

It can be assumed that if each input parameter was assessed similar ANOVA results would be produced. This test has been carried out to confirm that the use of the empirical relationships from Hamilton and Bachman (1982) is valid when compared alongside other commonly used empirical relationships documented in the literature.

5.6.3. Sensitivity analysis of amplitude

The empirical relationships discussed above relate the output to a single property which creates an extra step towards producing the synthetic response. Bachman (1985) recast the data used to produce the empirical relationships in Hamilton and Bachman (1982). This enabled physical properties to be predicted confidently from acoustic parameters. Simple re-arrangement of regression equations has been shown to be invalid by Williams (1983).

Bachman's (1985) empirical relationships (listed in Figure 2.13) relate physical properties to acoustic impedance. Accompanying each coefficient in each equation is the 95% confidence limit. The sensitivity of Bachman's relationships were tested as there were no means of assessing errors of the regression equations presented by Hamilton and Bachman (1982).

Bachman (1985) also quoted the standard error of the estimate of the response variable expressed as a percent of the mean of the observations. Due to lack of information on the number of observations and the methods of calculation, the 95% confidence limits were used to obtain a range. A cross check was done using the standard error and only a minor difference was found depending on the critical value used in the calculation.

Each impedance value was then related to standard water column values of velocity and density and a reflection coefficient obtained. The reflection coefficient was convolved with the 105J boomer pulse and a synthetic profile produced. The first peak was chosen as the reference point for measurements of amplitude. The amplitude at each peak for each parameter input was obtained and plotted.

Figure 5.19(a) is a graph of mean grain size against impedance. The shape of the curves corresponds to the trend observed on the plot of the actual measurements on Figure 5.17 as would be expected. At mean grain sizes 1-2 ϕ, i.e. coarser sediments, the scatter is small, whereas at 7-9 ϕ, the scatter is much greater. The graph of mean grain size against amplitude in Figure 5.20(a) has a similar shape to Figure 5.19(a). This reflects the contrast expected when the sound wave encounters a hard seabed surface producing a high amplitude reflector, whereas a softer seabed will produce a lower amplitude response.

Figure 5.19(b) is a plot of density against impedance which shows the relationship between a higher density and higher impedance. This would be expected as there is a similar trend between P-wave velocity and impedance in Figure 5.19(c). Porosity against impedance in Figure 5.19(d) has very little scatter, which follows the same trend as the density plot. This similarity of response is expected due to the linear relationship between density and porosity. Hamilton and Bachman (1982) and Bachman (1985) has shown that laboratory measurements of density and porosity can be used as *in situ* values. When applying these measurements to *in situ* measurements from the first tens of metres below seabed there is negligible difference. The scatter observed at higher velocities in the velocity/impedance and velocity/amplitude plots may be a function of a lack of sample points on the original data.

The graphs of amplitude described above relate to the contrast between an assumed water column impedance (Z1) and the first layer impedance (Z2) defined by the regression equation outputs. Figure 5.21 shows the same plots as Figure 5.20(a) to (d), but with additional dashed lines, these lines are the result of the contrast between two imaginary layers. The upper layer has a density of 1.7 Mg/m^3 and a velocity of 1620 m/s, i.e. silty clay (Z1) (Hamilton and Bachman, 1982) and the lower layer impedance (Z2) is defined above. The forms of the curves are the

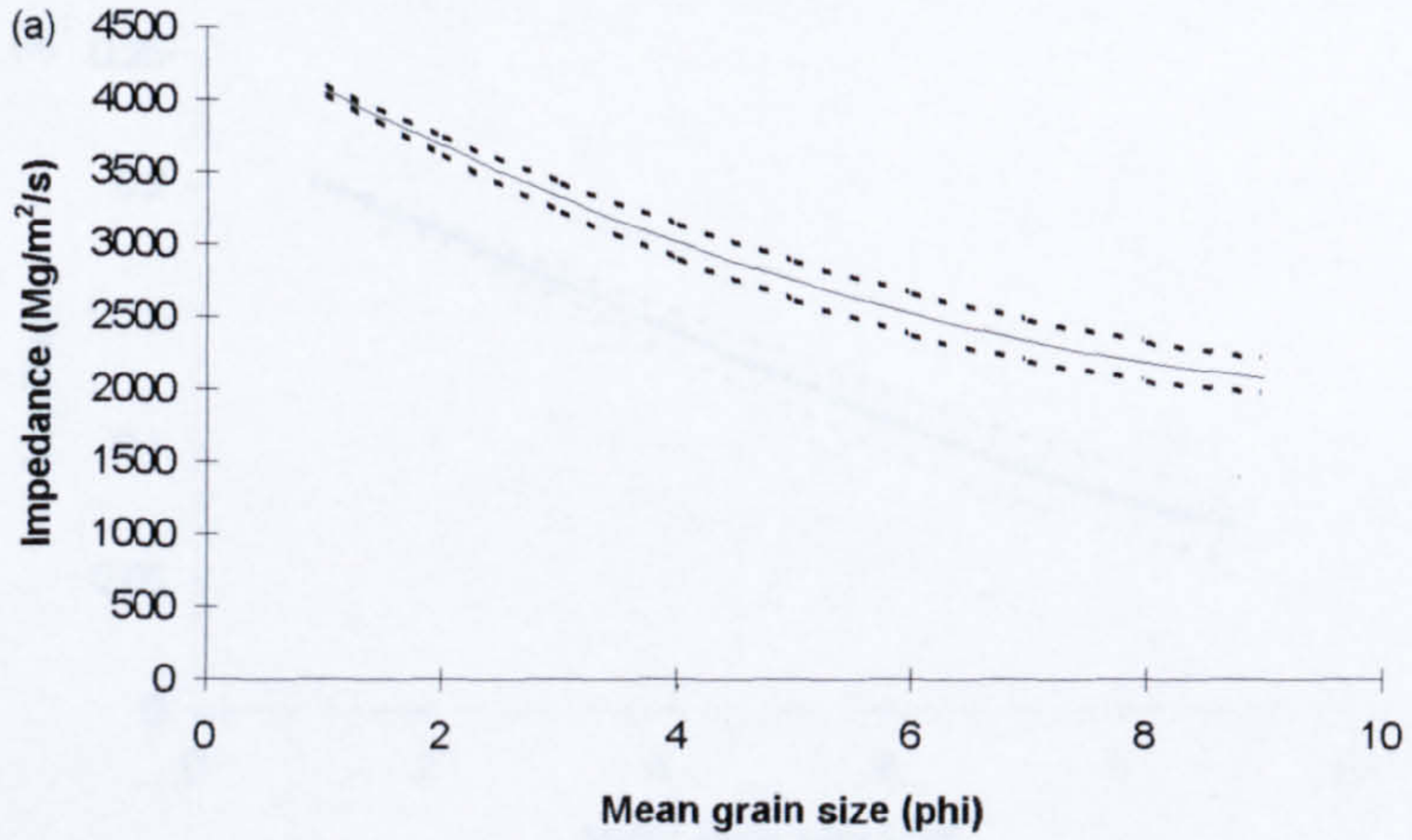

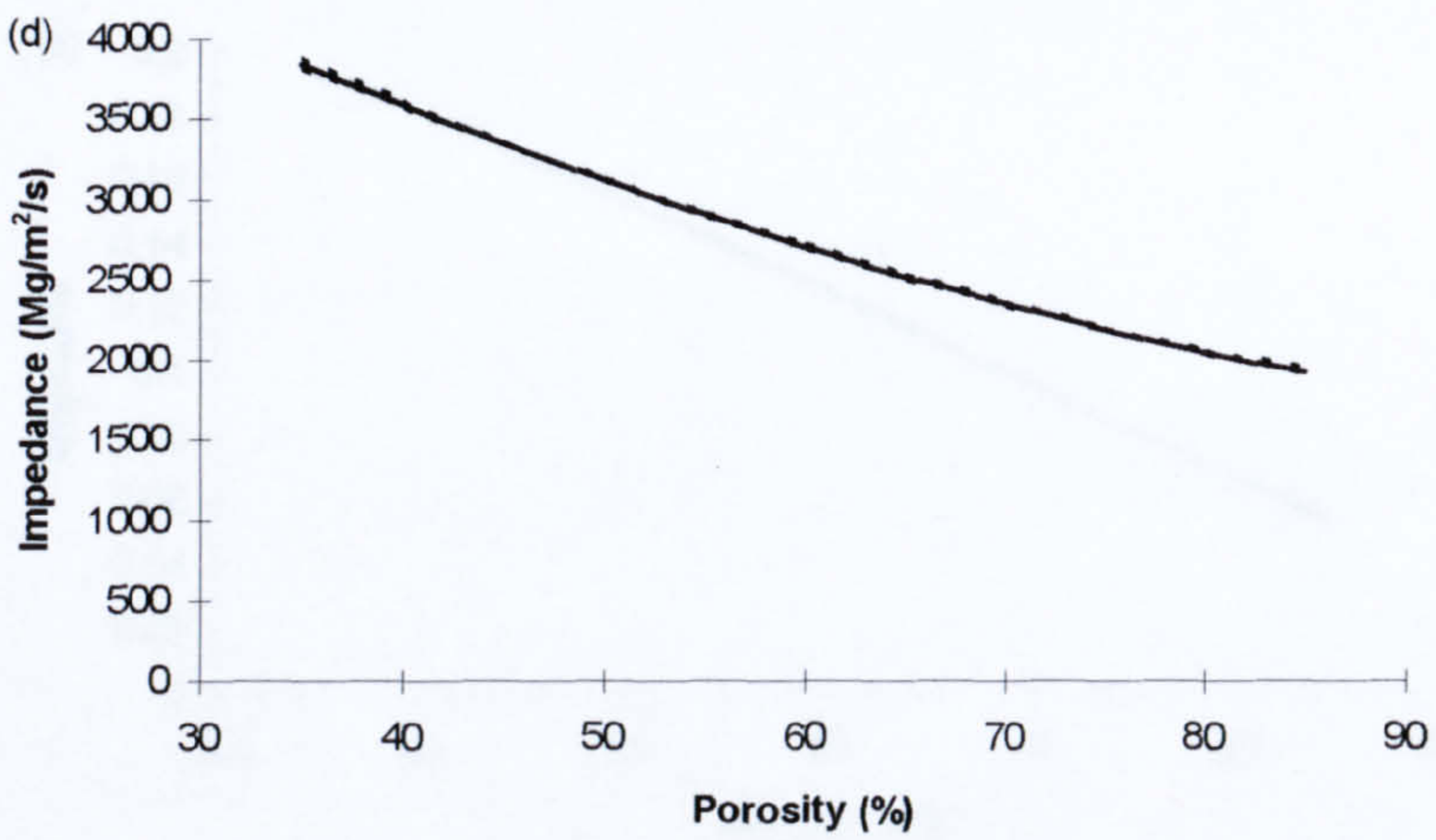

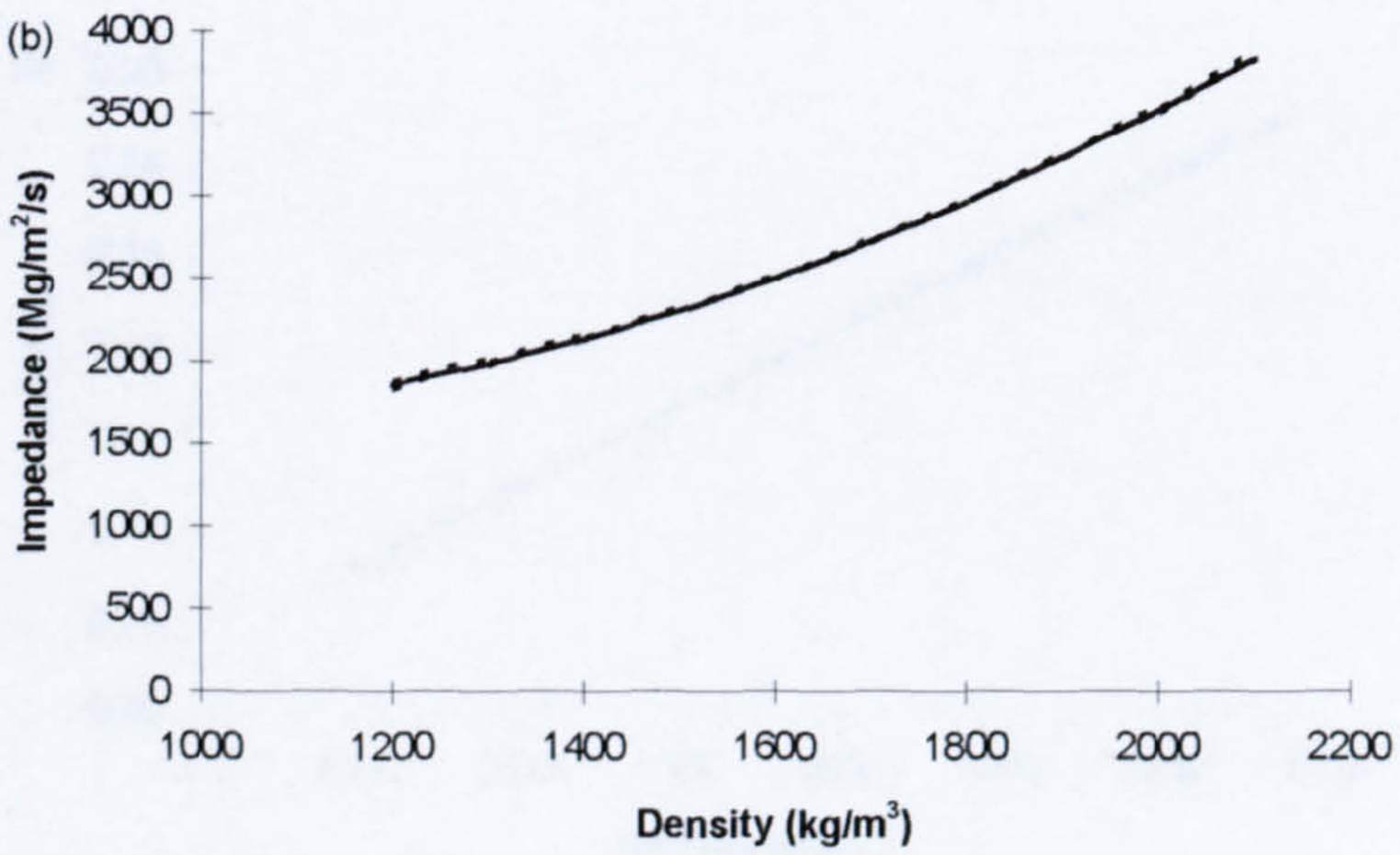

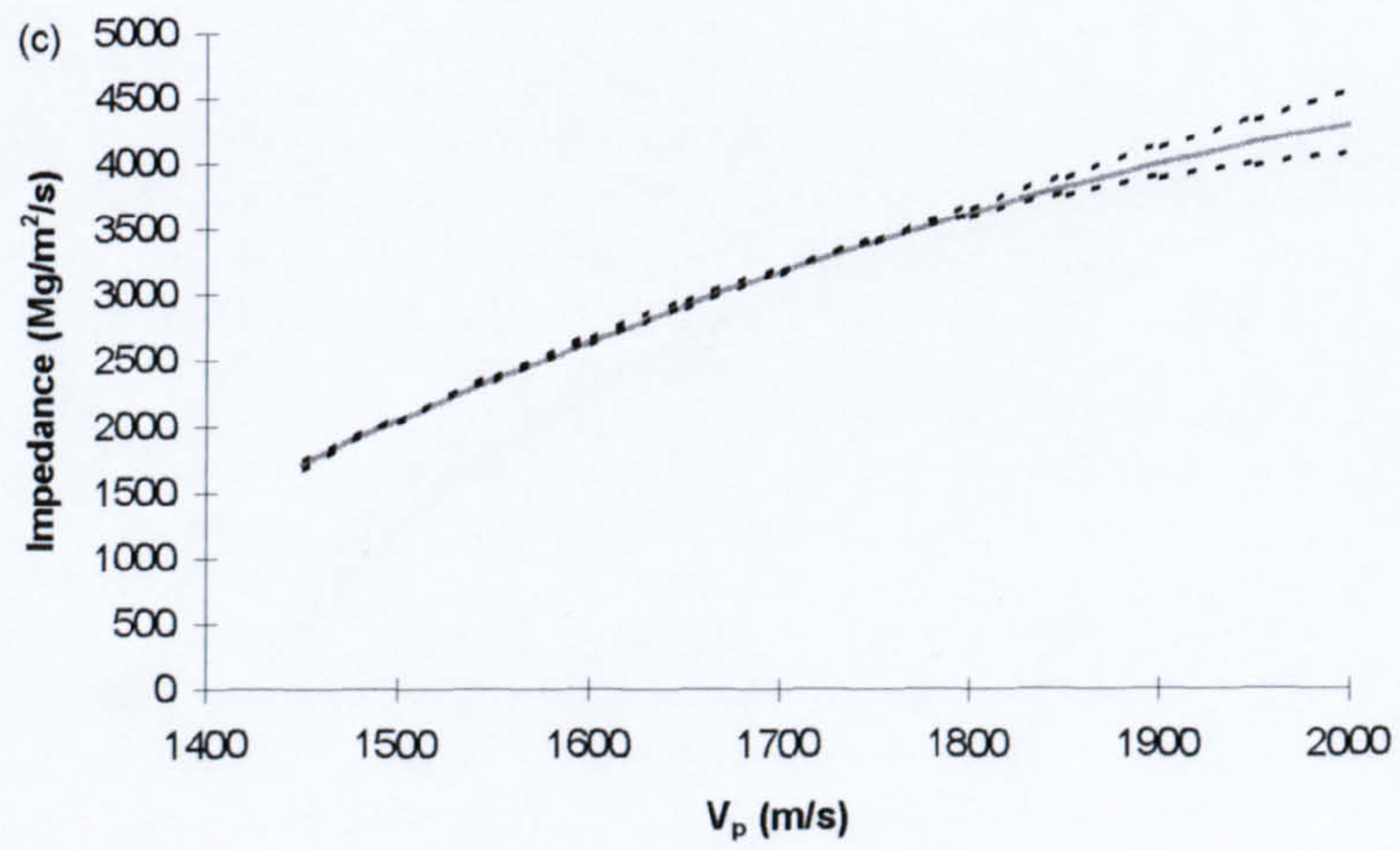

Figure 5.19. Impedance as a function of physical and acoustic properties.

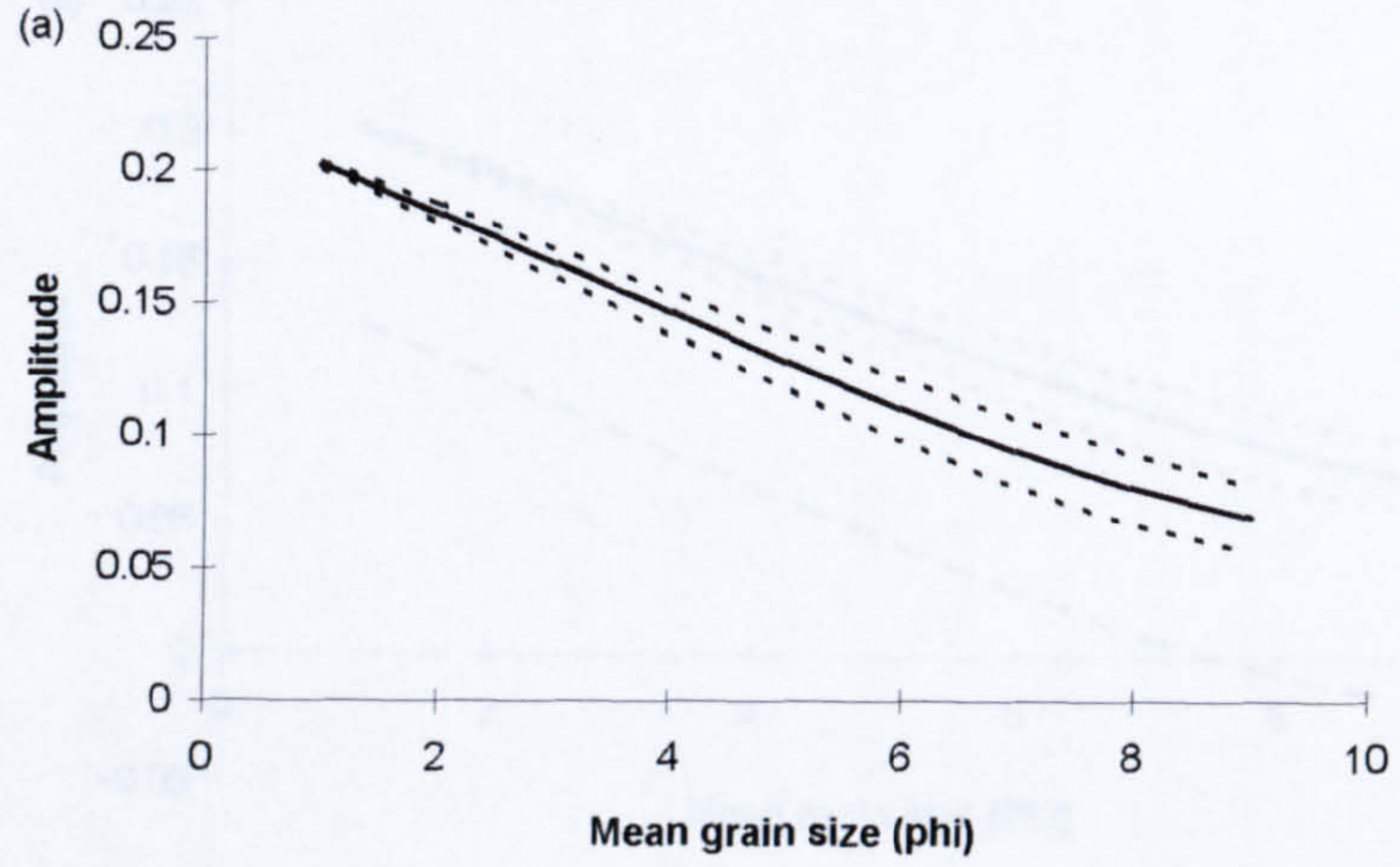

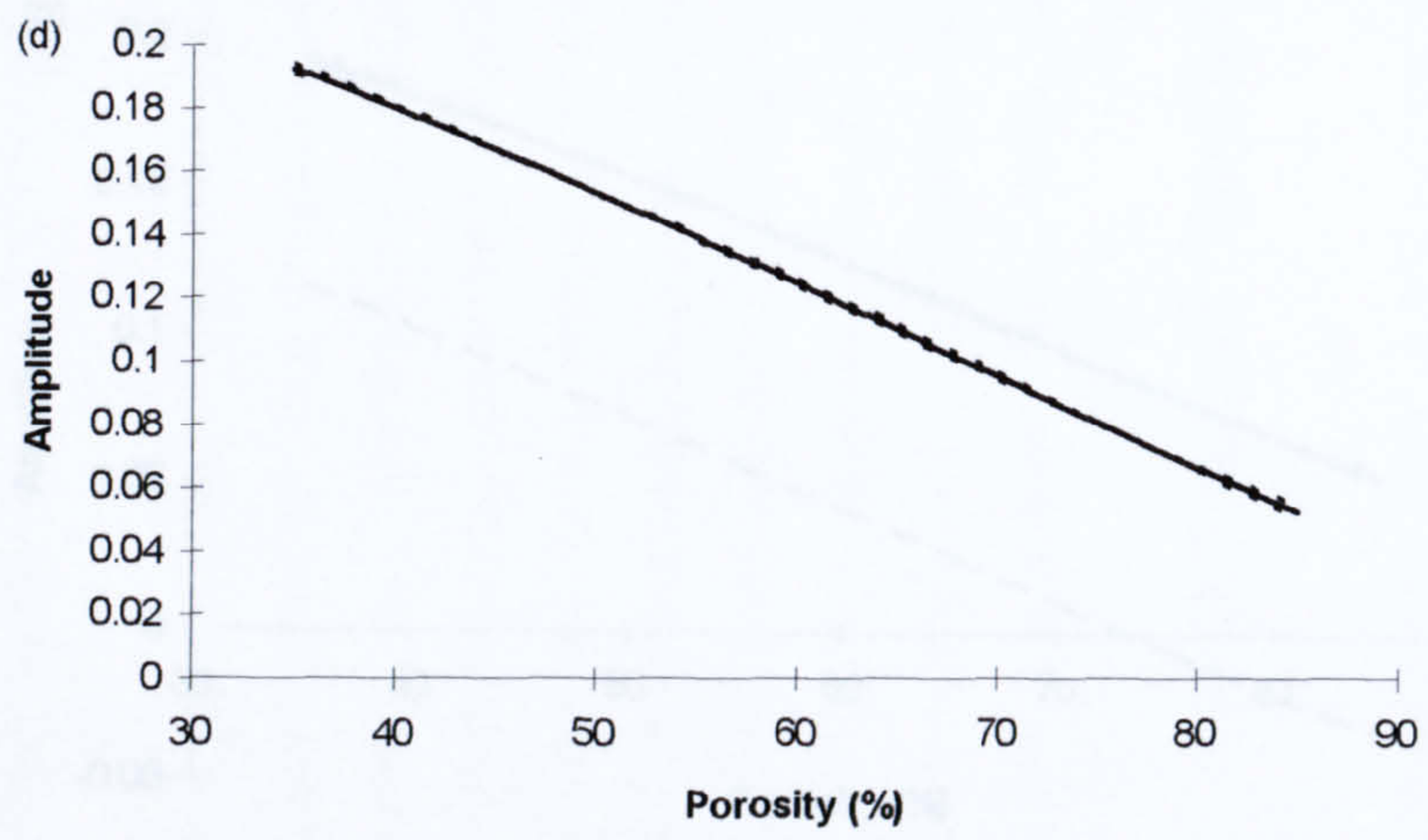

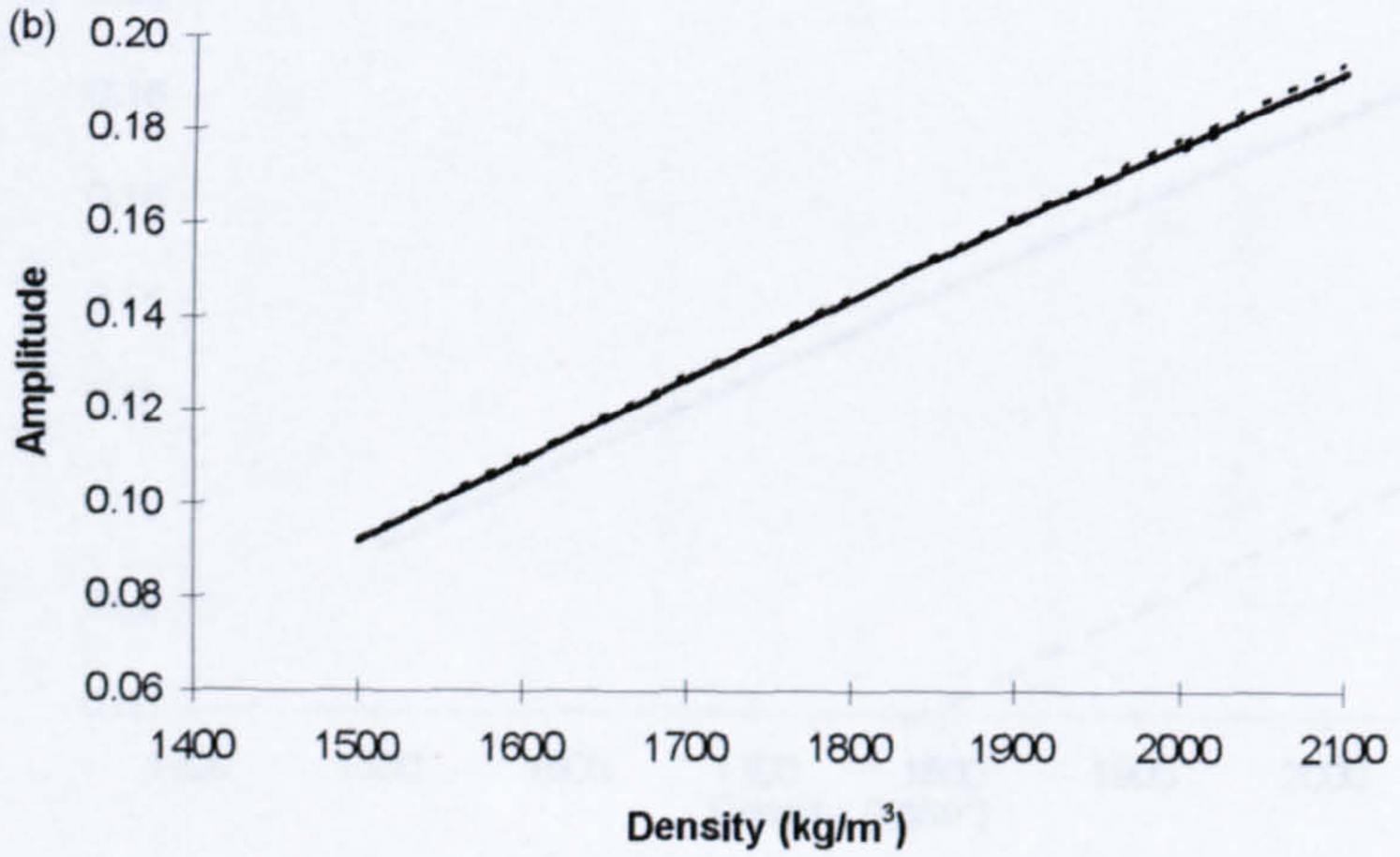

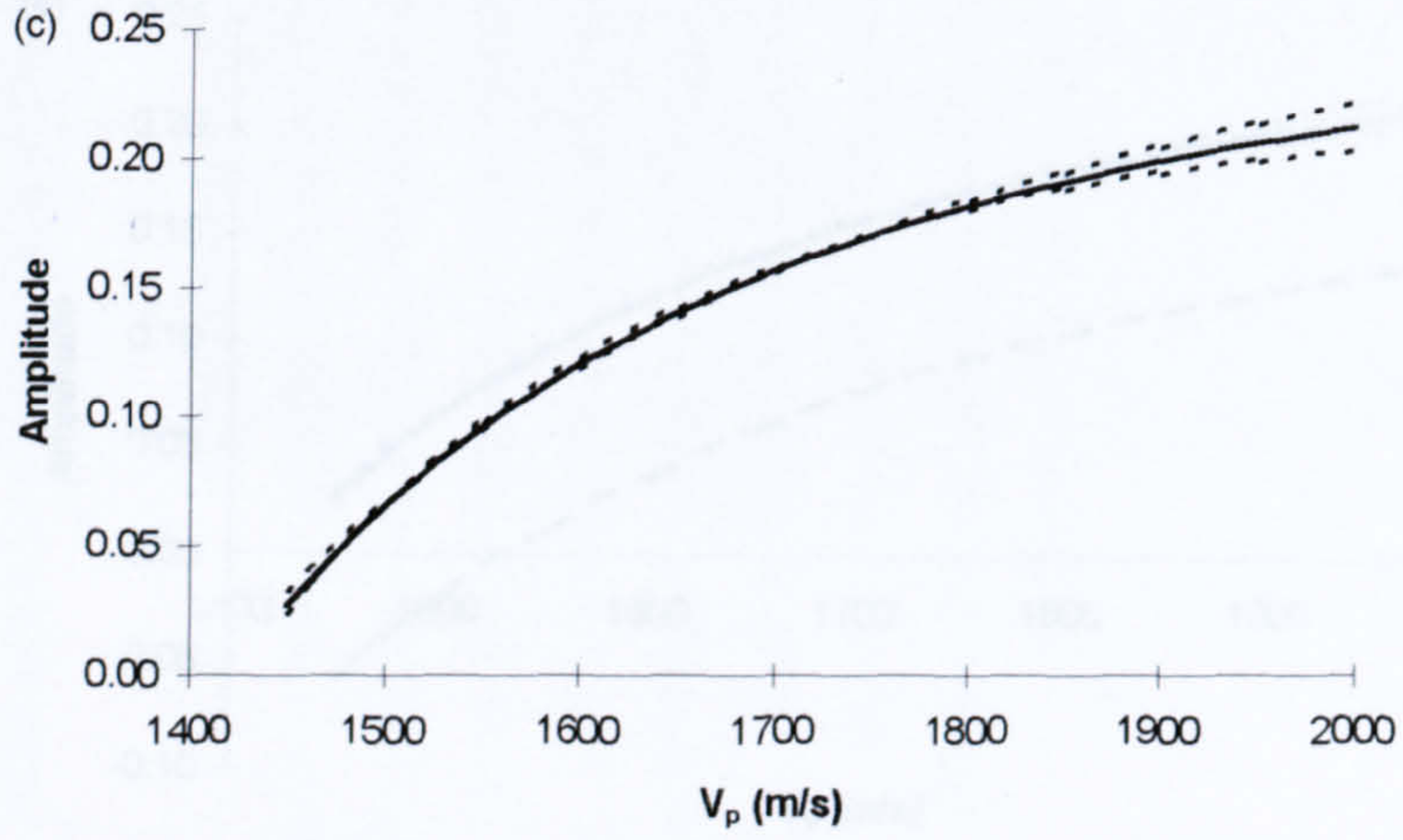

Figure 5.20. Amplitude as a function of physical and acoustic property inputs using the first amplitude peak point of measurement for a seabed interface.

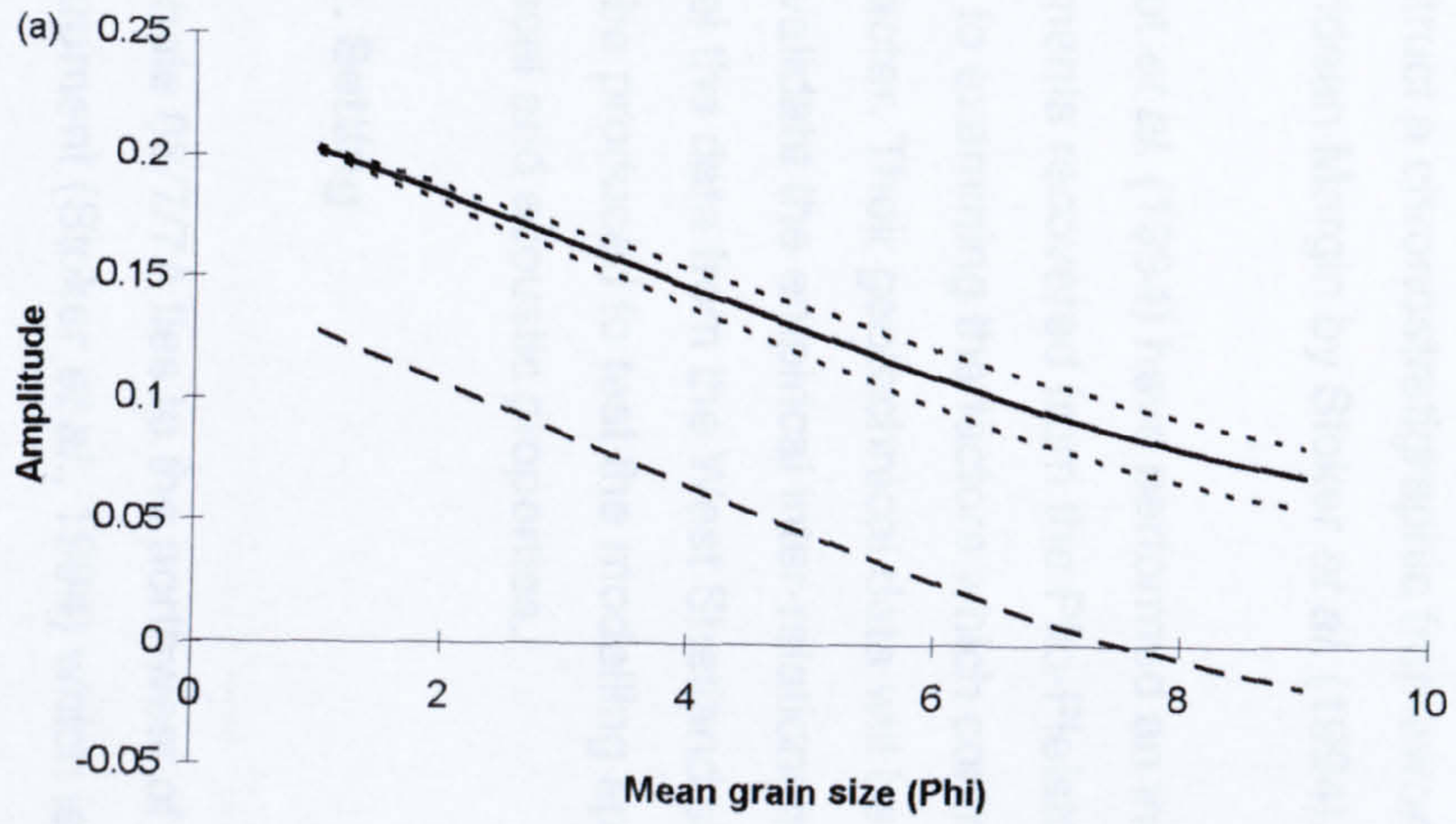

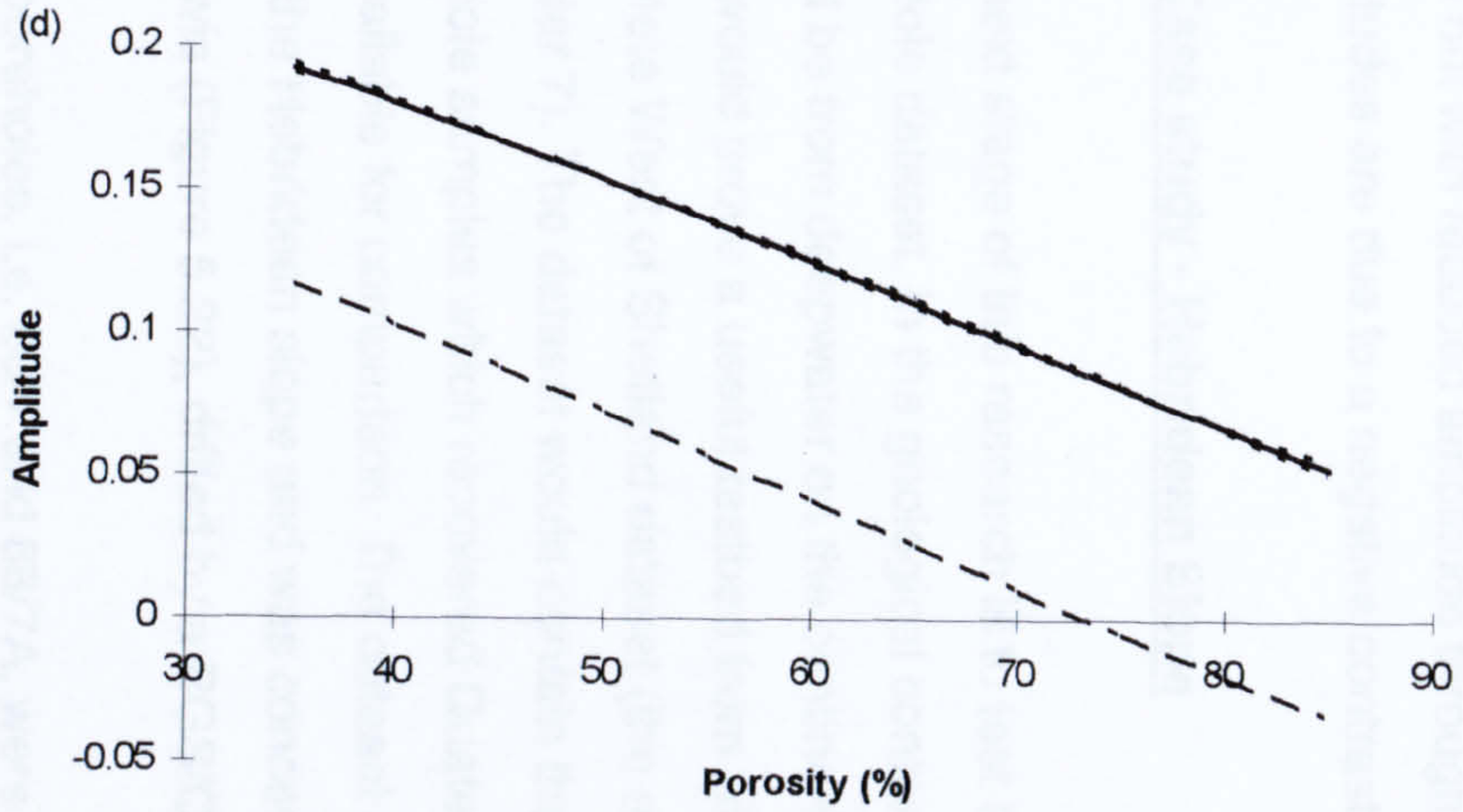

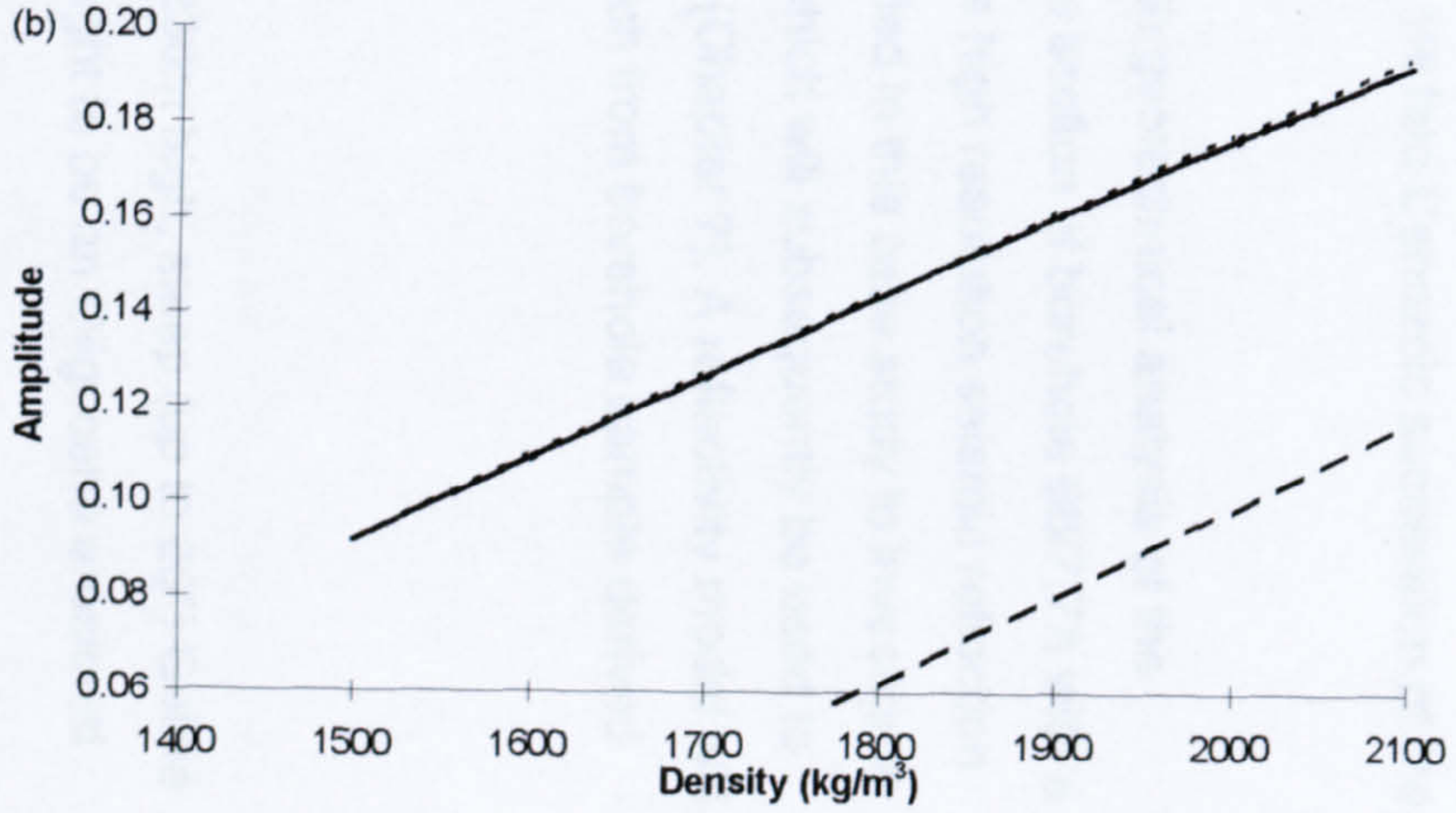

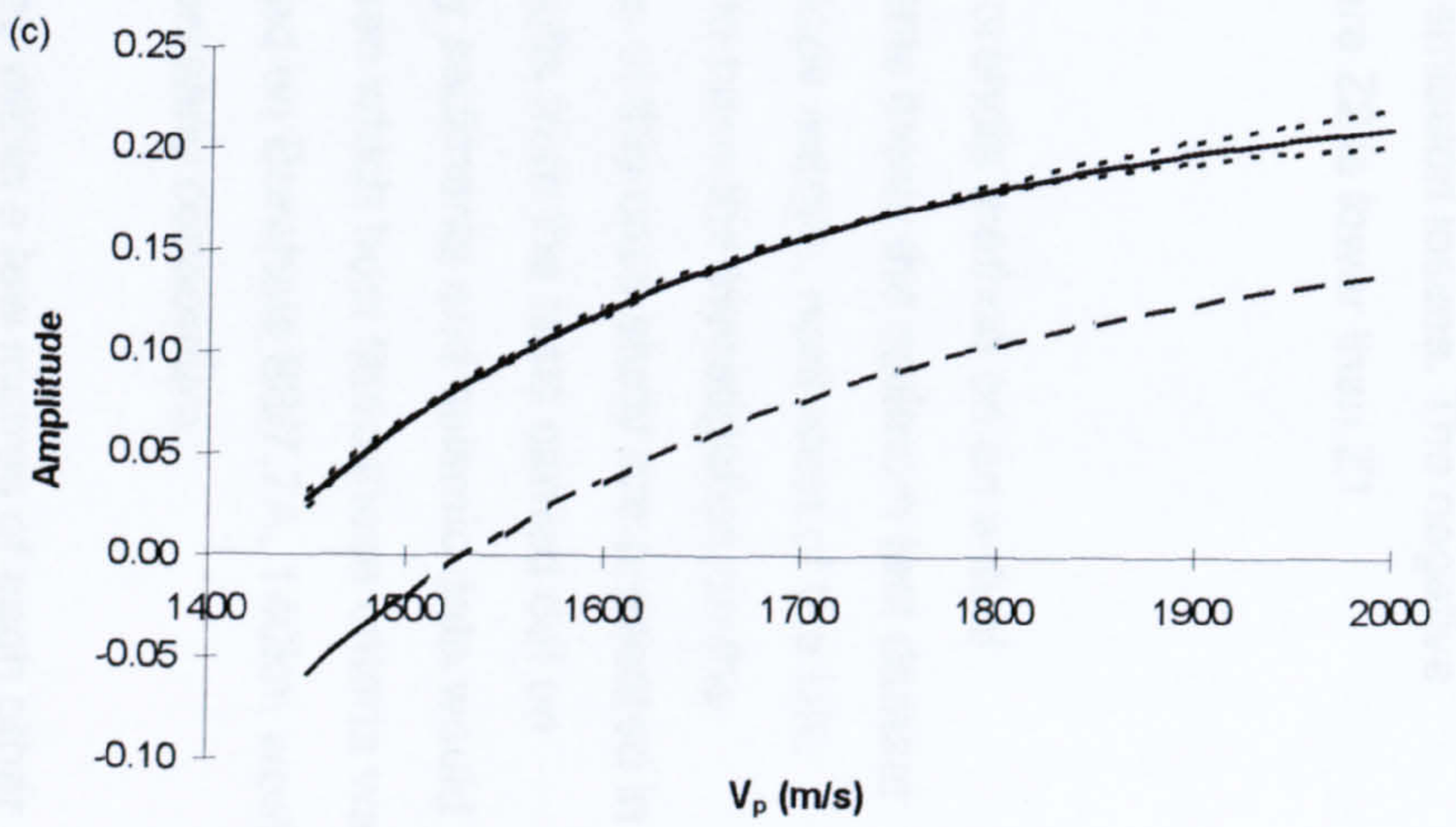

Figure 5.21. Amplitude as a function of physical and acoustic property inputs using the first amplitude peak as the point of measurement for a two layer system.

same but with reduced amplitude through transmission losses. The negative amplitudes are due to a negative contrast where Z2 is lower than Z1.

5.7. Case study - Hebridean Slope

The next stage of this research is to test the borehole method on an actual borehole dataset. In the geological context of this thesis the optimum test dataset would be from deepwater on the continental slope margin, northwest of the UK. This would prove a useful testbed from which to base the investigation on the complete West of Shetland dataset (the results of this case study are presented in Chapter 7). The dataset would contain the results from the tests carried out on borehole samples which recovered Quaternary sediments and seismic data would be available for comparison. The dataset chosen which best fitted these criteria was from the Hebridean slope and was concentrated on Borehole 88/7,7A, 140km west of Lewis (Figure 5.22), drilled by a BGS/Oil Company consortium.

Two boreholes, i.e. 88/7 and 88/7A, were drilled within a few metres of each other to maximise recovery, however, they will be referred to as composite borehole 88/7,7A (Stoker *et al.*, 1994). Borehole 88/7, 7A (Figure 5.22) was drilled in 565m of water to a depth of 103.3m below seabed. The borehole was drilled in order to construct a chronostratigraphic framework for the late Cenozoic succession of the Hebridean Margin by Stoker *et al.* (1994).

Talbot *et al.* (1994) have performed an in-depth geotechnical analysis of the sediments recovered from the Plio-Pleistocene section of borehole 88/7,7A with a view to examining the factors which control the high resolution seismic reflection character. Their geotechnical data will be applied in this case study to investigate and validate the empirical inter-relationships which will subsequently be used to model the data from the West Shetland slope (Chapter 7). A reflectivity model will also be produced to test the modelling approach from borehole sample derived physical and acoustic properties.

5.7.1. Setting

Borehole 88/7/7A lies to the northwest of the 230m high, steep (up to 28°) Geikie Escarpment (Stoker *et al.*, 1994) which is thought to be an Oligocene erosional

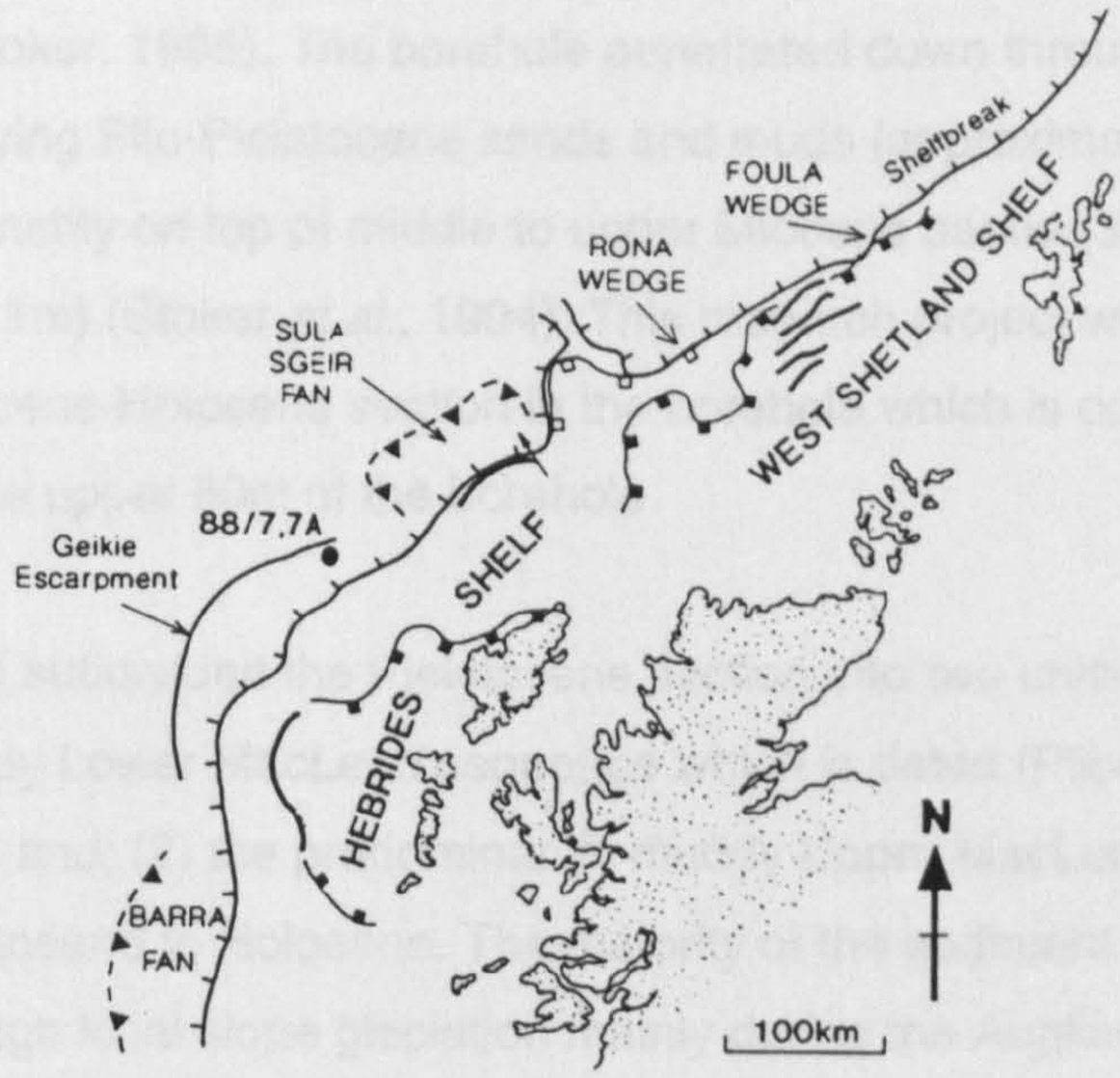

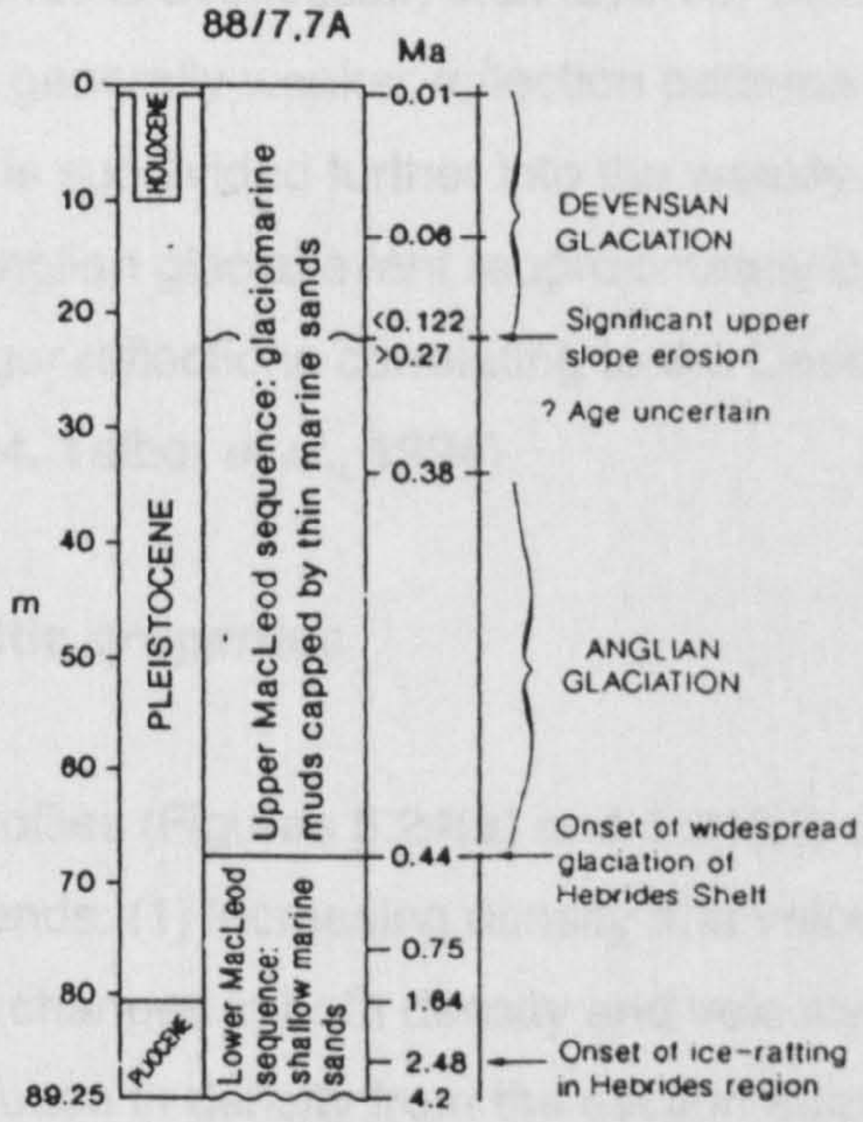

Figure 5.22. Location map and stratigraphy of borehole 88/7,7A (after Stoker, 1995).

structure formed by bottom currents during a period of lower sea level (Miller and Tucholke, 1983, Stoker, 1995). The borehole penetrated down through a Holocene seabed layer overlying Plio-Pleistocene sands and muds (approximately 89m) which lie unconformably on top of middle to upper Miocene sands (3m) and upper Oligocene muds (11m) (Stoker *et al.*, 1994). This research project will concentrate only on the Pleistocene-Holocene section in the borehole which is contained approximately in the upper 80m of the borehole.

Stoker *et al.* (1994) subdivided the Pleistocene section into two units: (1) the predominantly sandy Lower MacLeod sequence which is dated (Pliocene to) lower middle Pleistocene and; (2) the predominantly muddy Upper MacLeod sequence, dated middle Pleistocene to Holocene. The majority of the sediment accumulation in this area is through local slope glaciation mainly during the Anglian and Devensian stages and by bottom current re-distribution (Stoker, 1995, Talbot *et al.*, 1994).

5.7.2. Seismic characteristics

The Lower MacLeod sequence is acoustically well-layered, whereas the Upper MacLeod sequence shows generally weaker reflection patterns (Figure 5.23). The Lower MacLeod sequence is subdivided further into the weakly reflective section which correlates with the Anglian glacial event (approximately 0.44-0.35 Ma) and a younger section with stronger reflections correlating to the Devensian stage (0.12-0.01Ma) (Stoker *et al.*, 1994, Talbot *et al.*, 1994).

5.7.3. Physical and acoustic properties

The density and velocity profiles (Figures 5.24(a) and 5.24(b)) can be divided approximately into three trends: (1) increasing density and velocity (approximately 7-30m), (2) relatively small changes in both density and velocity (approximately 30-70m), and (3) an initial increase in density from the section above which then decreases to the values of the sections above, and an increase in velocity which is maintained through this third section (approximately 70-80m).

These trends can be seen clearly on the impedance profile (Figure 5.25). With reference to the stratigraphy (Figure 5.23), the top section of increasing density and

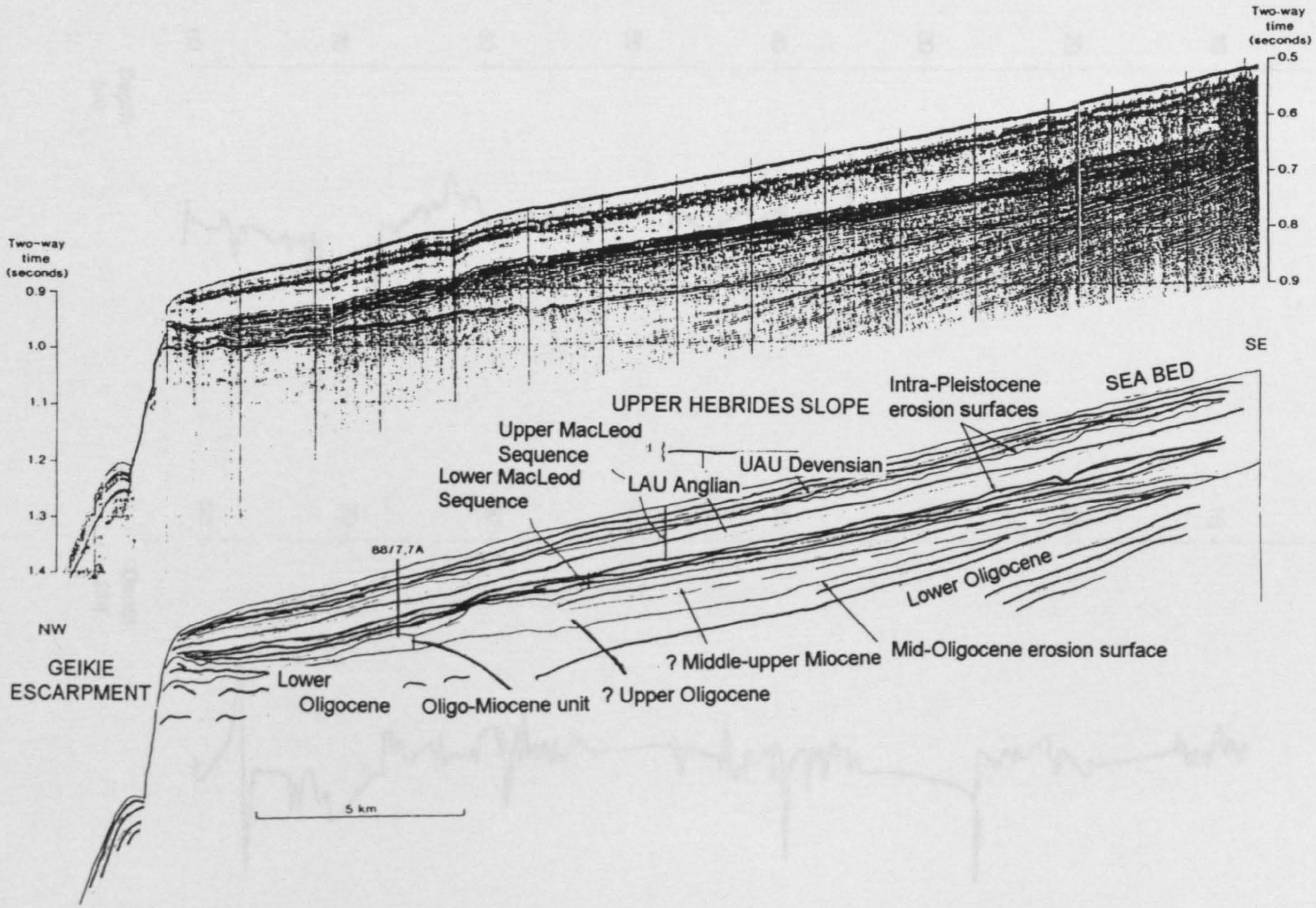

Figure 5.23. Interpretation of the Upper Hebrides slope based on borehole 88/7,7A location (after Stoker *et al.*, 1994).

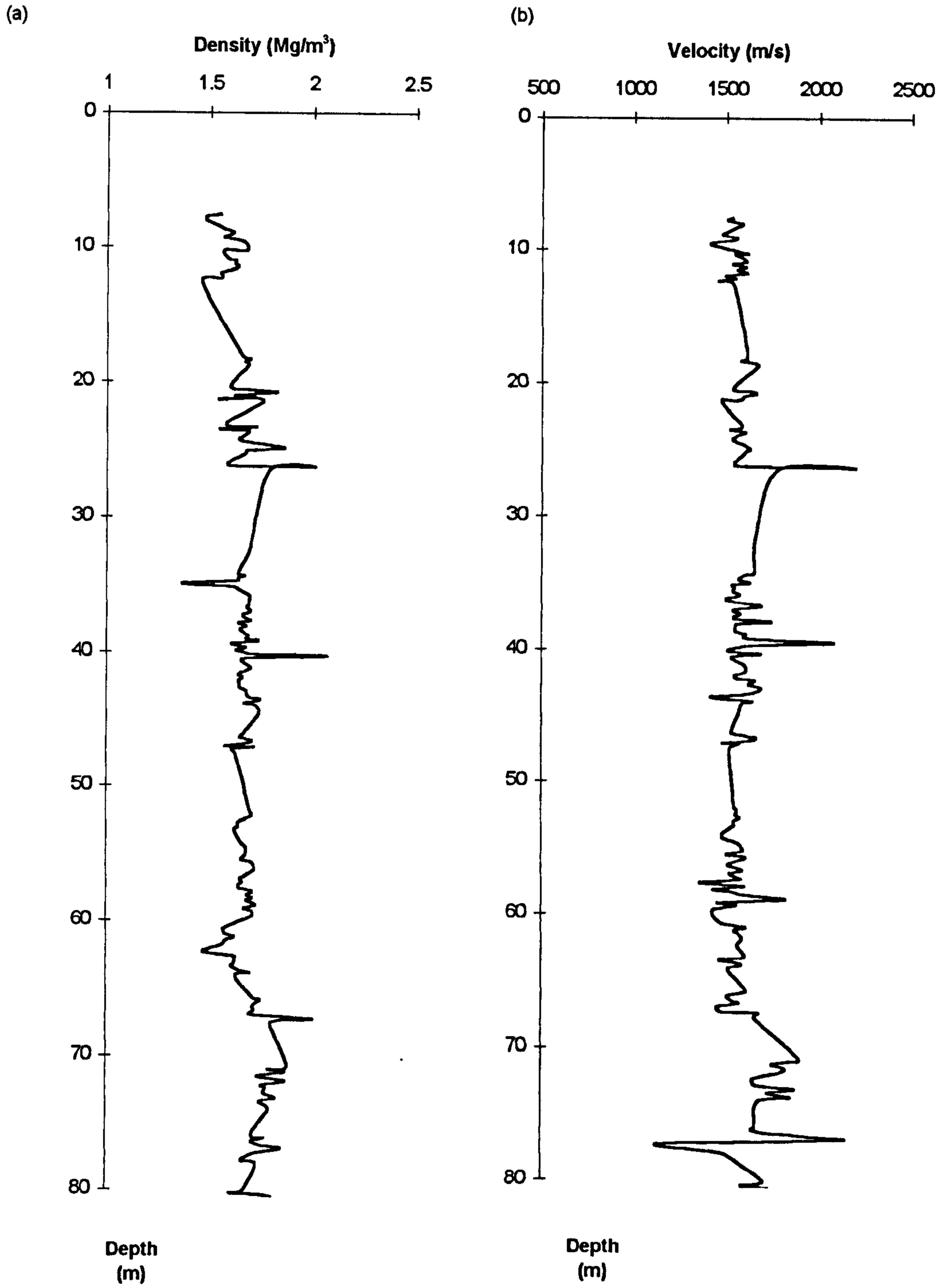

Figure 5.24. Measured physical properties from borehole 88/7,7A. (a) Density (b) Velocity.

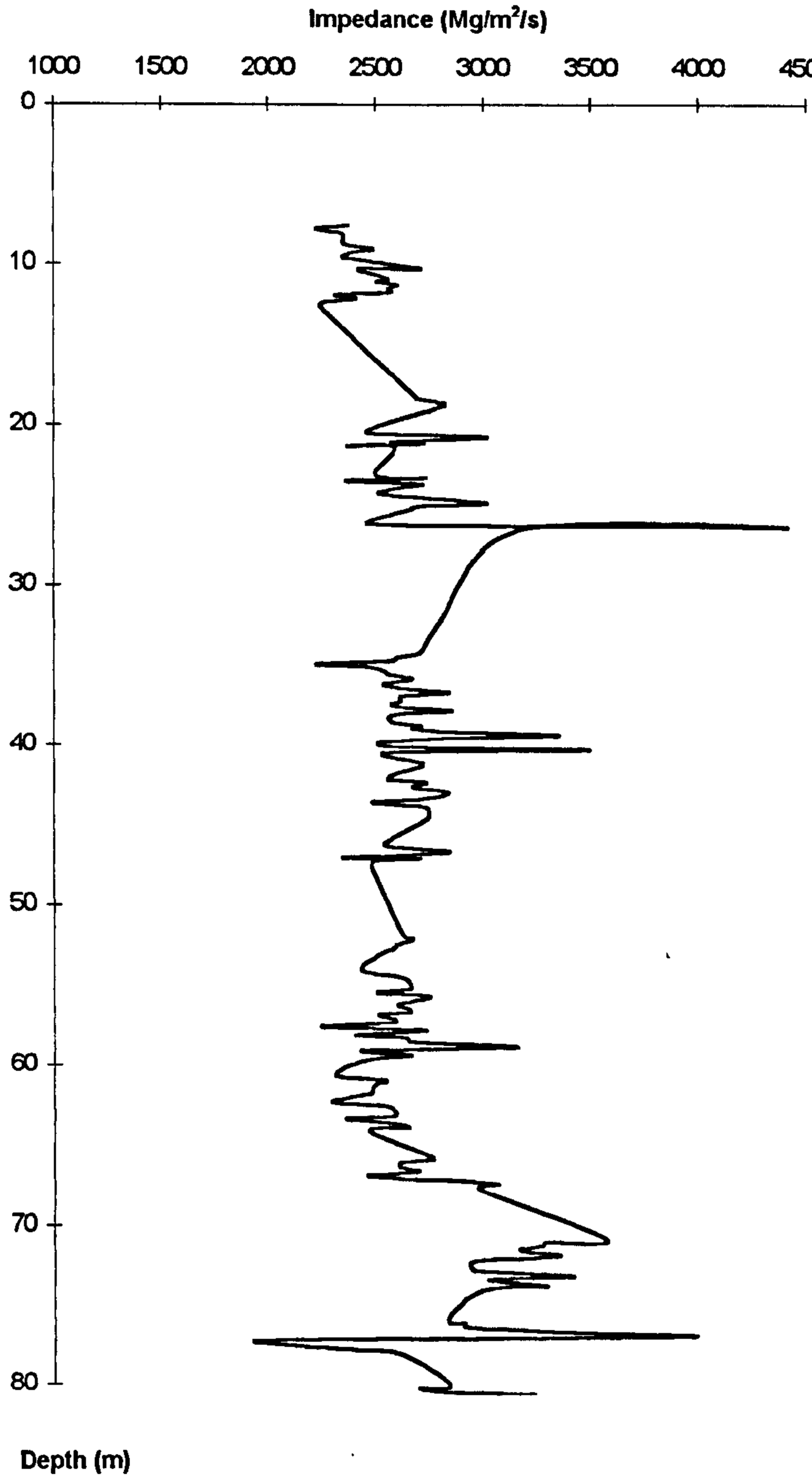

Figure 5.25. Impedance profile for borehole 88/7,7A.

velocity relates to well-layered upper acoustic unit of the Upper MacLeod sequence. The middle section with no significant change in density and velocity appears to correlate with the weakly reflective lower acoustic unit of the Upper MacLeod sequence. The third section within the Pleistocene-Holocene succession where there is a decrease in density and only velocity variation relates to the acoustically well layered Lower MacLeod sequence.

5.7.4. Validation of empirical inter-relationships between physical and acoustic properties

The most significant aspect of the 'Borehole method' is the ability to relate the results of the borehole sample testing to the seismic response, as mentioned previously, due to the lack of geophysical logging data available for the shallow section. Section 2.9 introduced the existence of various published empirical inter-relationships such as those by Hamilton and Bachman (1982) which enable the physical property data to be related to acoustic properties and subsequently modelled.

In order to make use of the inter-relationships their validity for the area of interest should be tested. This is particularly true where the application is in the assessment of complex glacigenic sediments and sequences. From the assessment of the inter-relationships in Section 5.6 the empirical relationships produced by Hamilton and Bachman (1985) were principally chosen for use in this study, however one of the inter-relationships from Bachman (1985) is tested for comparison purposes.

The physical and acoustic properties from borehole 88/7,7A were plotted and the data were then re-cast using the relationships from Hamilton and Bachman (1982) and Bachman (1985) and the results plotted against the 88/7,7A data.

The density-velocity plot (Figure 5.26(a)) is tightly clustered between densities of 1.6 and 1.75Mg/m^3 and velocities of 1500 and 1600m/s. When the velocity is re-calculated from density through the regression equation of Hamilton and Bachman (1982) and plotted (also Figure 5.26(a)), the data fall within the range of the original data.

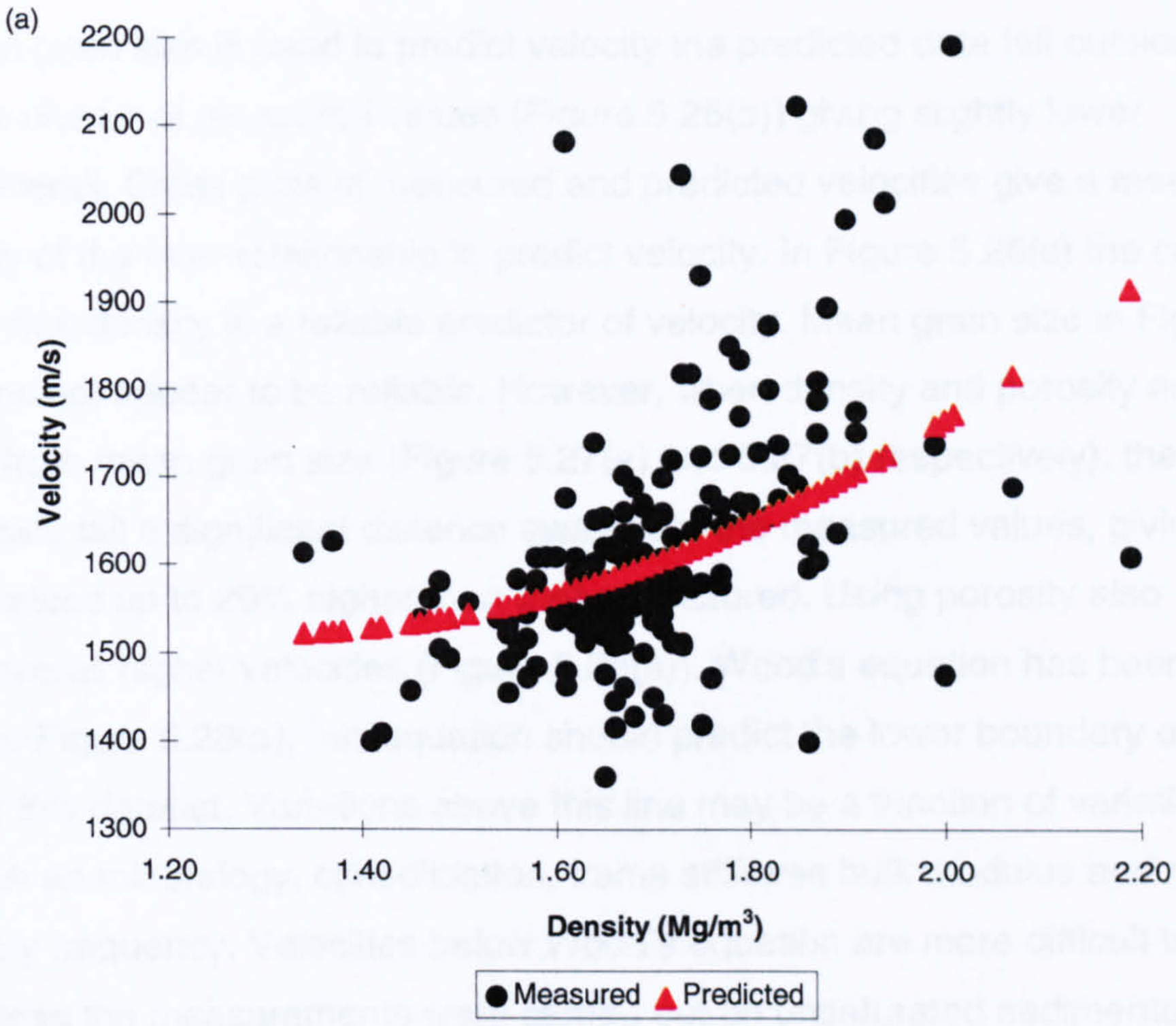

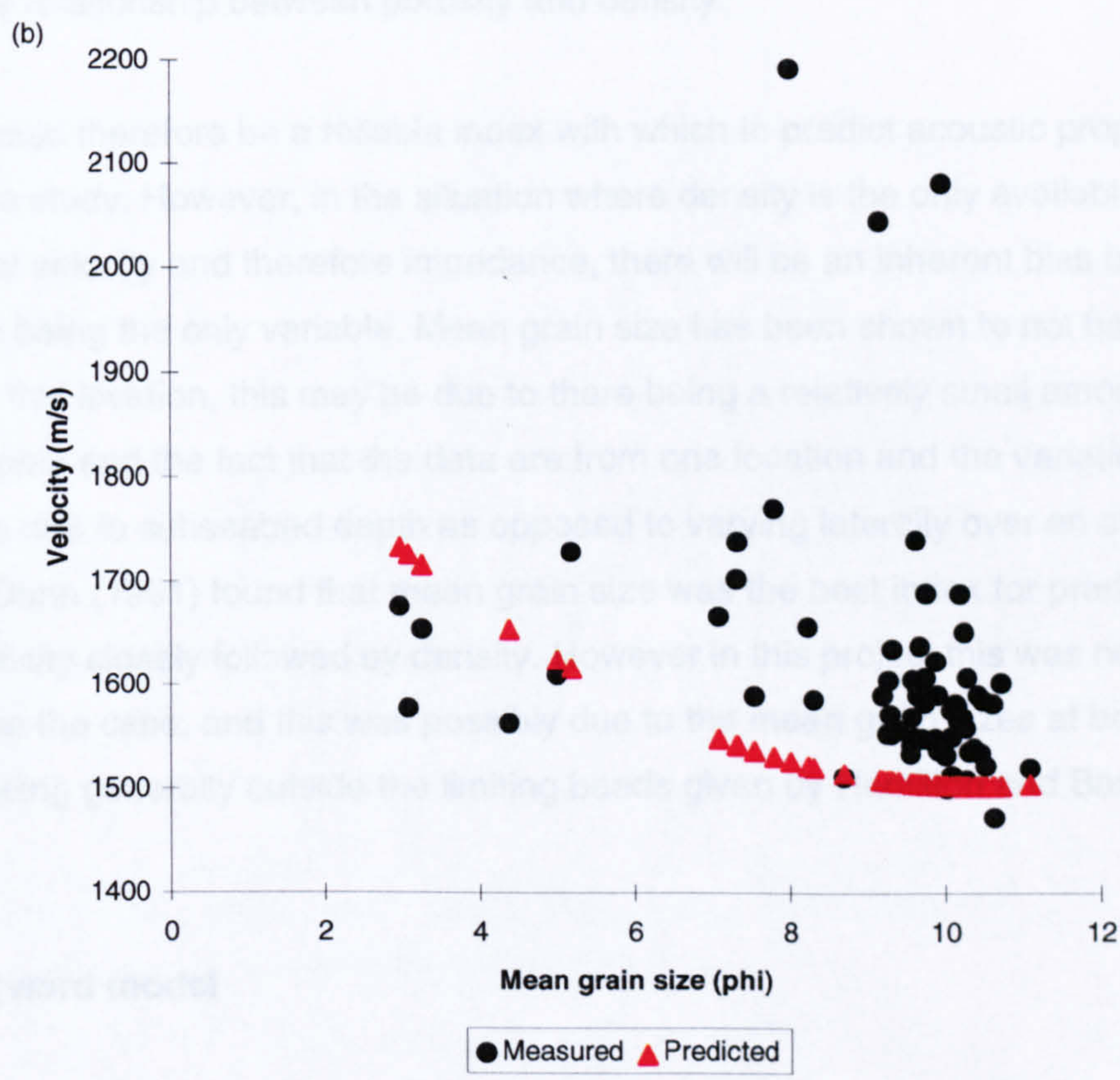

Figure 5.26. Measured and predicted properties for inter-relationship validation. (a) Density-velocity. (b) Mean grain size-velocity.

When mean grain size is used to predict velocity the predicted data fall outside but close to the cluster of measured values (Figure 5.26(b)) giving slightly lower velocities overall. Cross plots of measured and predicted velocities give a measure of the ability of the inter-relationship to predict velocity. In Figure 5.26(c) the cross plot shows that density is a reliable predictor of velocity. Mean grain size in Figure 5.26(d) does not appear to be reliable. However, when density and porosity are calculated from mean grain size (Figure 5.27(a) and 5.27(b) respectively), the predicted data fall a significant distance away from the measured values, giving predicted values up to 20% higher than those measured. Using porosity also produces overall higher velocities (Figure 5.28(a)). Wood's equation has been plotted onto Figure 5.28(a), this equation should predict the lower boundary of velocity for this dataset. Variations above this line may be a function of variations of factors such as mineralogy, consolidation, frame stiffness bulk modulus and rigidity and possibly frequency. Velocities below Wood's equation are more difficult to explain unless the measurements were carried out on unsaturated sediments. The cross plot in Figure 5.28(d) also appears to be a reliable predictor of velocity which reflects the relationship between porosity and density.

Density would therefore be a reliable index with which to predict acoustic properties in this case study. However, in the situation where density is the only available predictor of velocity and therefore impedance, there will be an inherent bias based on density being the only variable. Mean grain size has been shown to not be reliable at this location, this may be due to there being a relatively small amount of data available and the fact that the data are from one location and the variation of results are due to subseabed depth as opposed to varying laterally over an area. Orsi and Dunn (1991) found that mean grain size was the best index for predicting sound velocity closely followed by density. However in this project this was not found to be the case, and this was possibly due to the mean grain sizes at borehole 88/7,7A being generally outside the limiting bands given by Hamilton and Bachman (1982).

5.7.5. Forward model

The impedance profile (Figure 5.25) for the borehole strongly reflects the trend of the density profile in Figure 5.24(a) as the velocity profile in Figure 5.24(b) has shown the velocity gradient to be relatively small and the velocity constant down

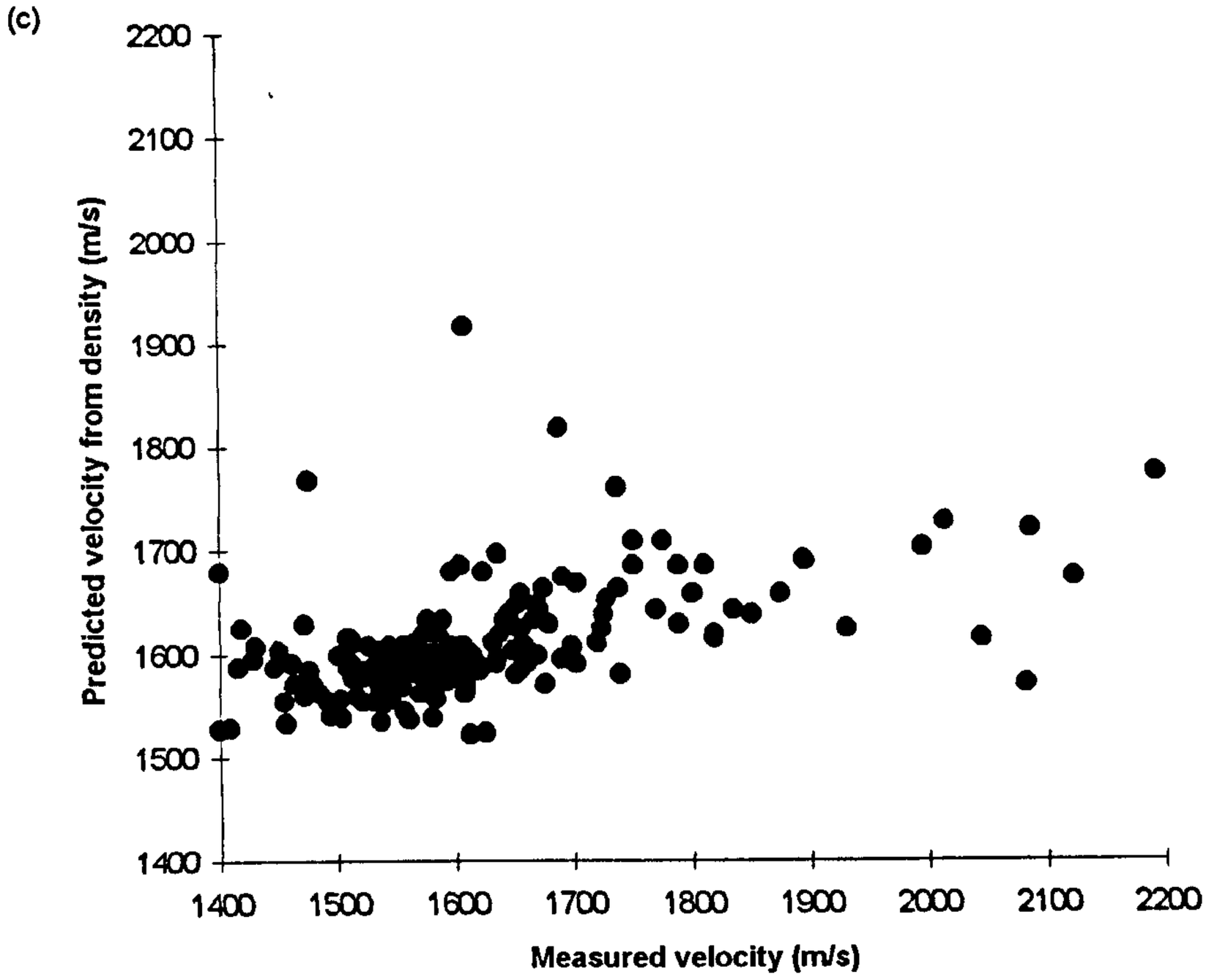

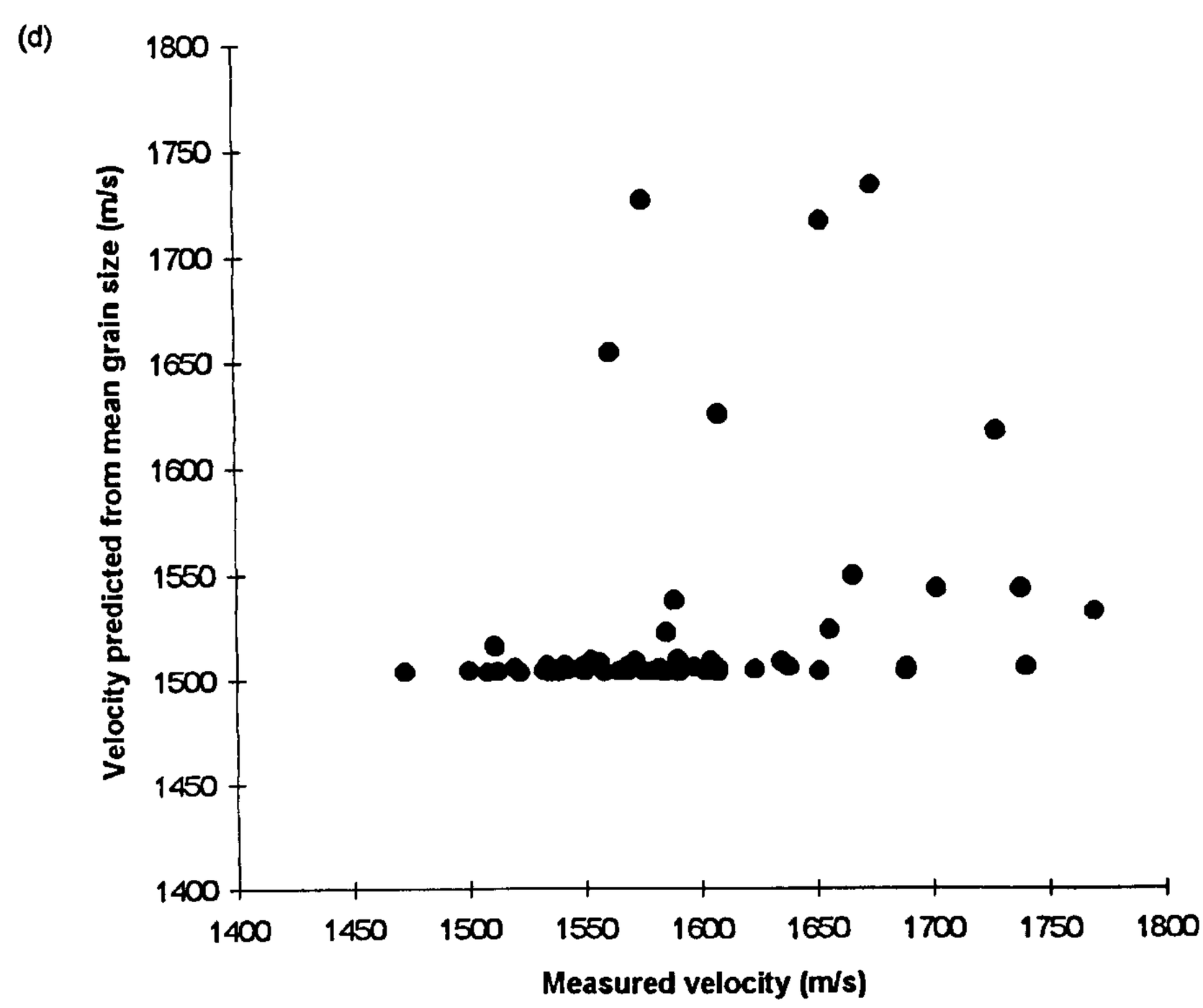

Figure 5.26. Measured and predicted properties for inter-relationship validation. (c) Cross plot of measured velocity against velocity predicted from density, (d) Cross plot of measured velocity against velocity predicted from mean grain size.

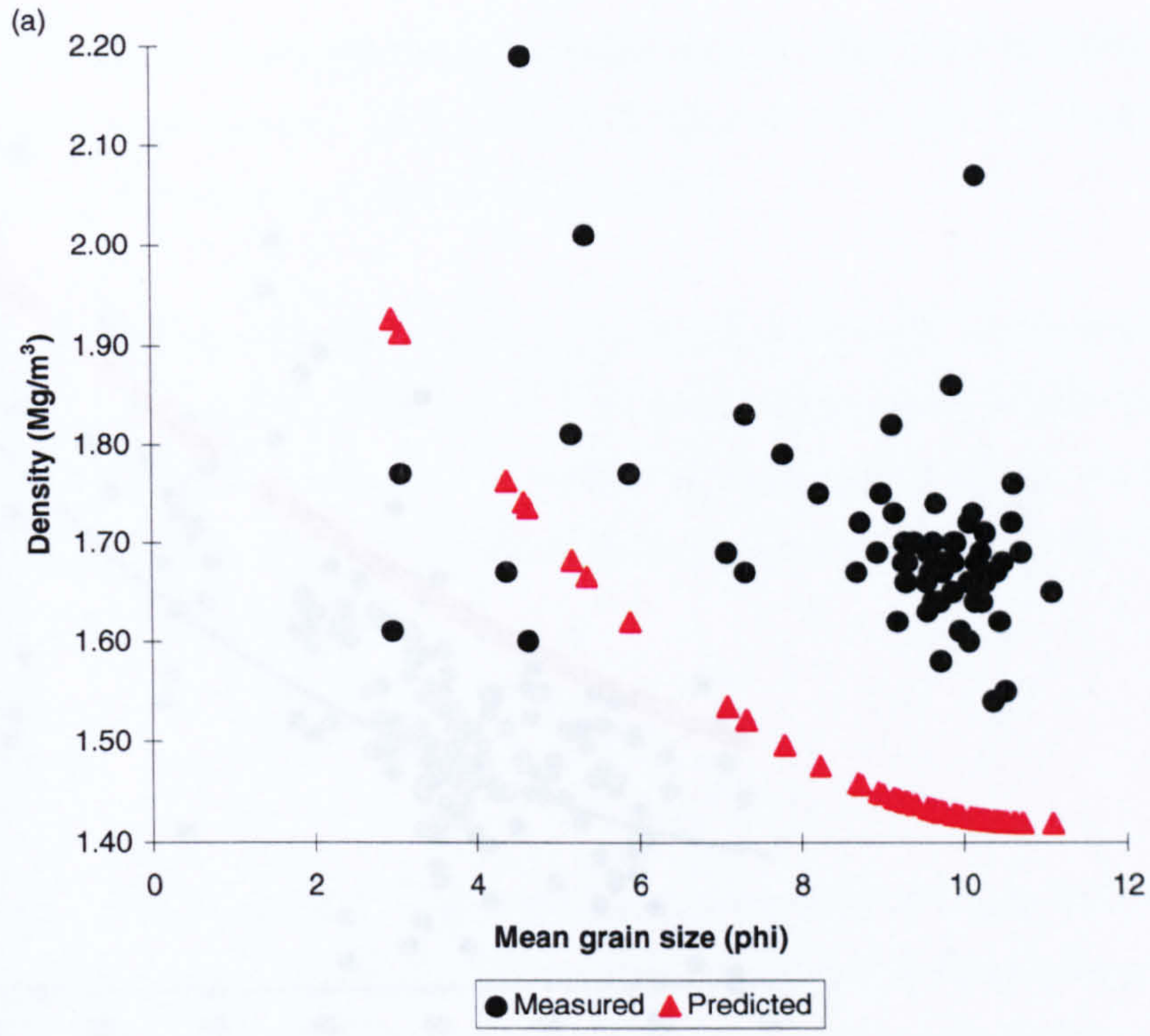

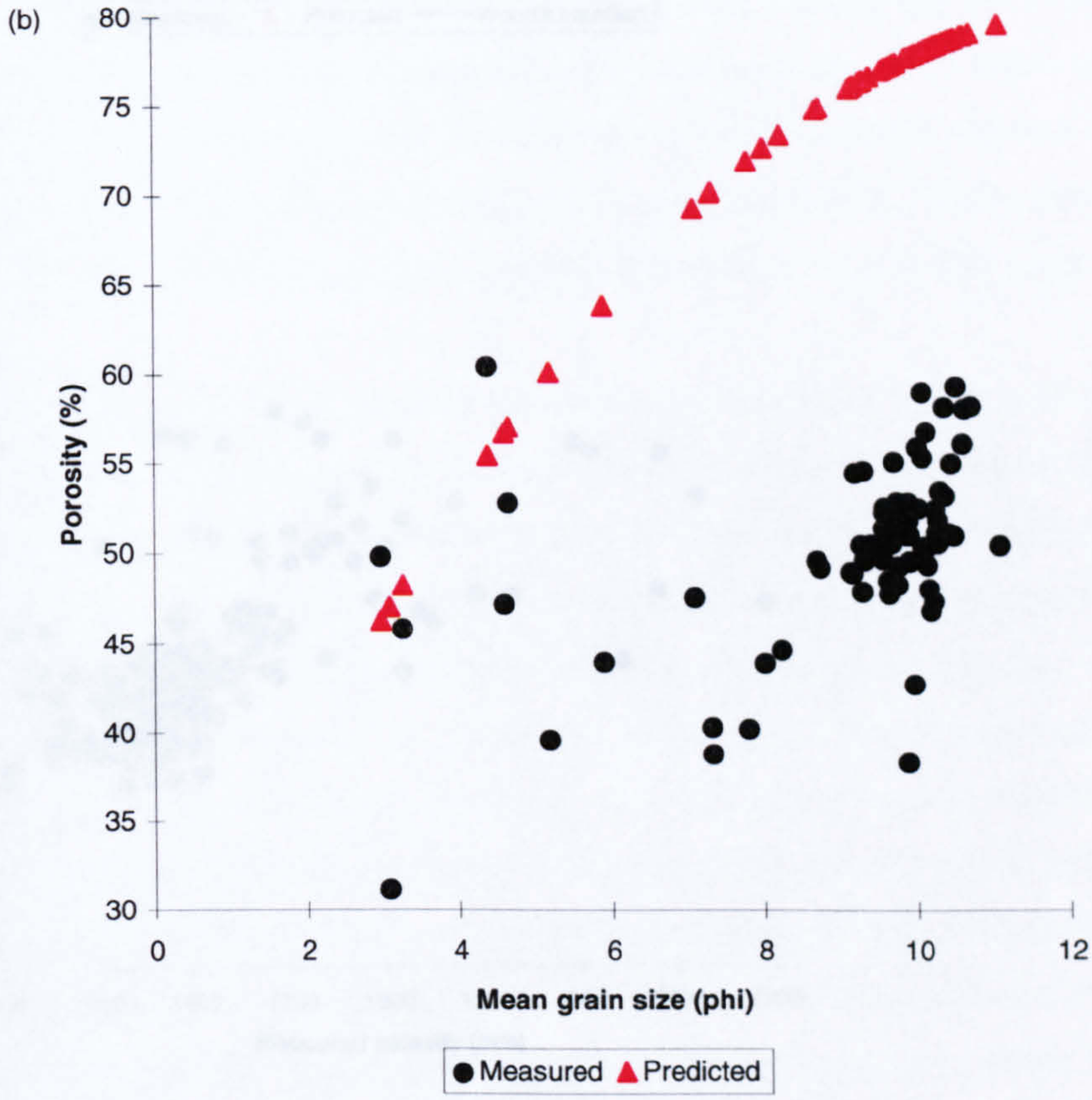

Figure 5.27. Measured and predicted properties for inter-relationship validation. (a) Mean grain size-density. (b) Mean grain size-porosity.

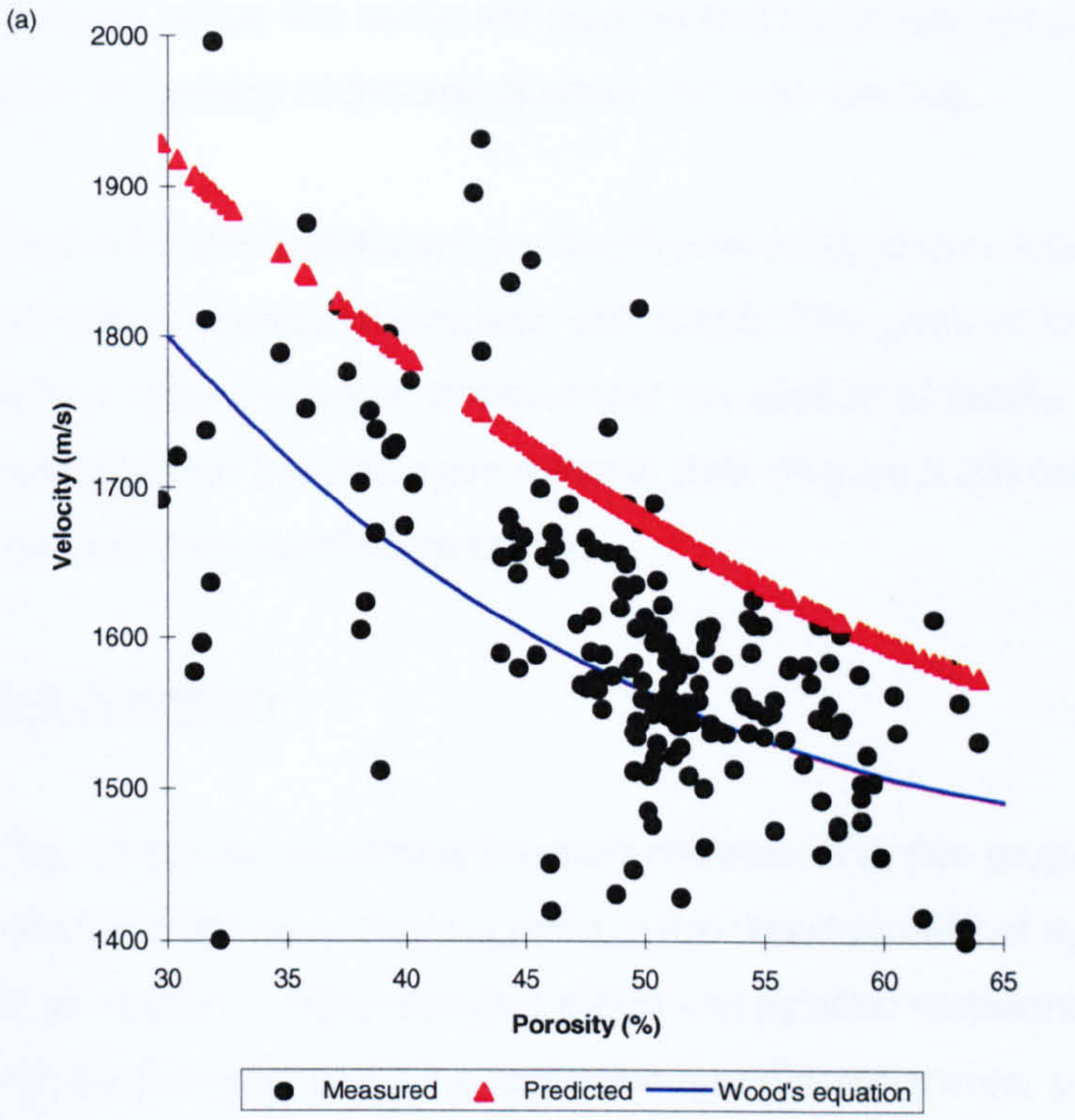

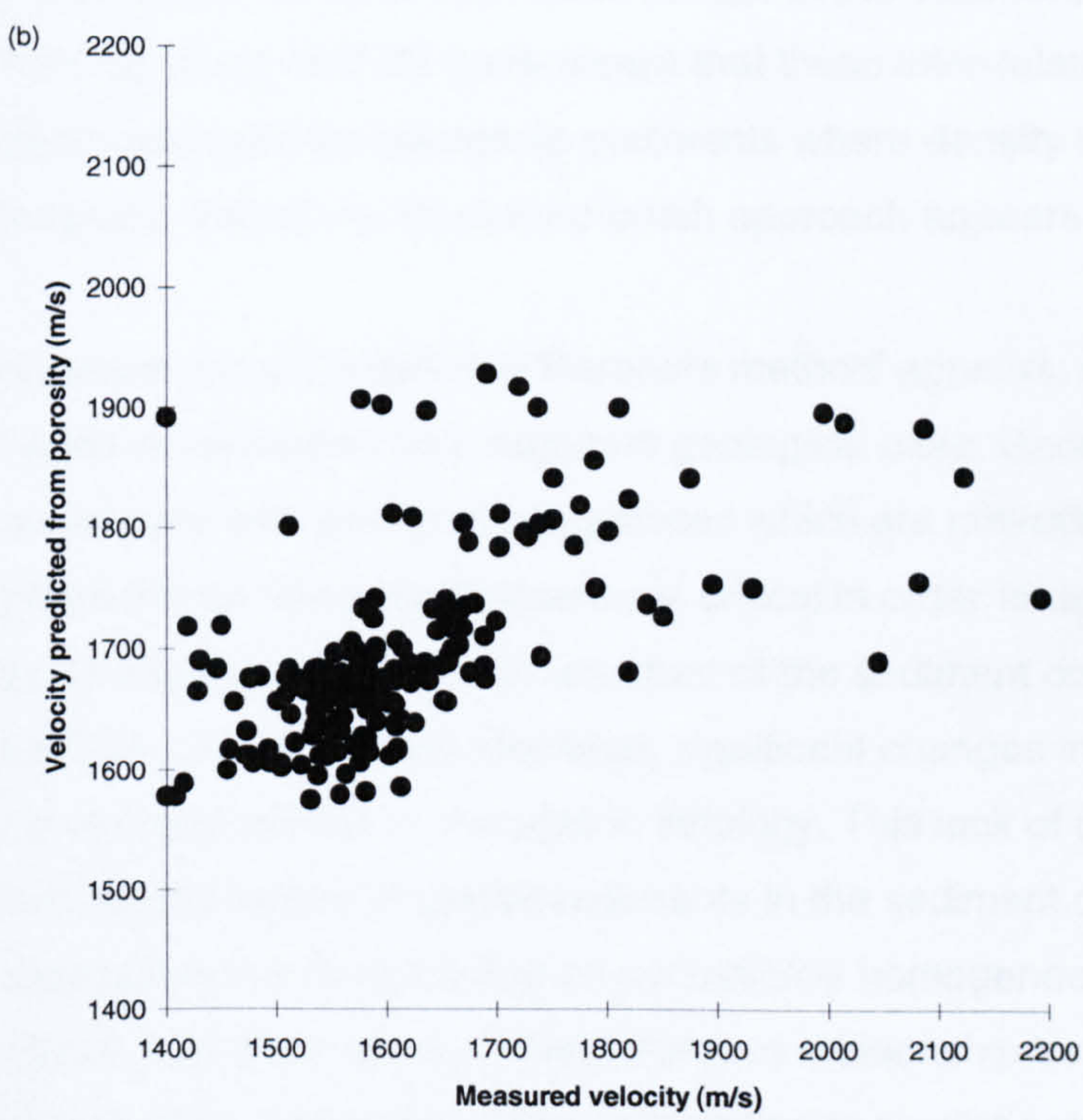

Figure 5.28. (a) Measured and predicted properties for inter-relationship validation, porosity-velocity, (b) cross plot of measured velocity and predicted velocity from porosity.

through the borehole. The variations in density may be due to the degrees of packing within the sediment column and could also be a function of changes in the specific gravity of the solids which will alter density.

The reflection coefficient profile (Figure 5.29) shows a positive, slowly increasing reflection coefficient gradient with depth. The gaps on the profile are where there are no data available. Interestingly the section of profile which shows weak reflectors on the analogue seismic data (Figure 5.23) cannot be clearly identified on the reflection coefficient profile.

5.8. Summary

The 'borehole modelling' method developed in this project attempts to use empirical relationships as a starting point in the development of synthetic seismograms. This is en route to understanding the *in situ* seismic response. Inevitably though, there will be many inherent inaccuracies and discrepancies, particularly when applying these relationships to sediments deeper in the sediment column. However, the data from borehole 88/7,7A have shown that these inter-relationships are valid with depth and valid for glacigenic sediments where density is used as the predictor property. Therefore, this broad brush approach appears valid in this case.

However 'broad brush' this 'Borehole method' appears, each location of study needs to be treated as a separate geological case. Geologically this project deals specifically with glacigenic sequences which are potentially very complex, therefore geotechnical sampling frequency is critical in order to detect all the potential small scale changes in fabric and structure of the sediment column. However, as the 88/7,7A case study has identified, significant changes in seismic character are not necessarily related to changes in lithology. This lack of correlation may be due to the chaotic nature of glacial sediments in the sediment column which create destructive interference and an acoustically homogeneous unit. The dataset has shown that there is not a straightforward relationship between seismic character and physical properties. When attempting to predict acoustic properties such as velocity, there are a range of variables other than density affecting the lithology, such as grain size, porosity, specific gravity and consolidation. Therefore, when basing a regression, and therefore prediction, on a bivariate approach these other factors need to be considered.

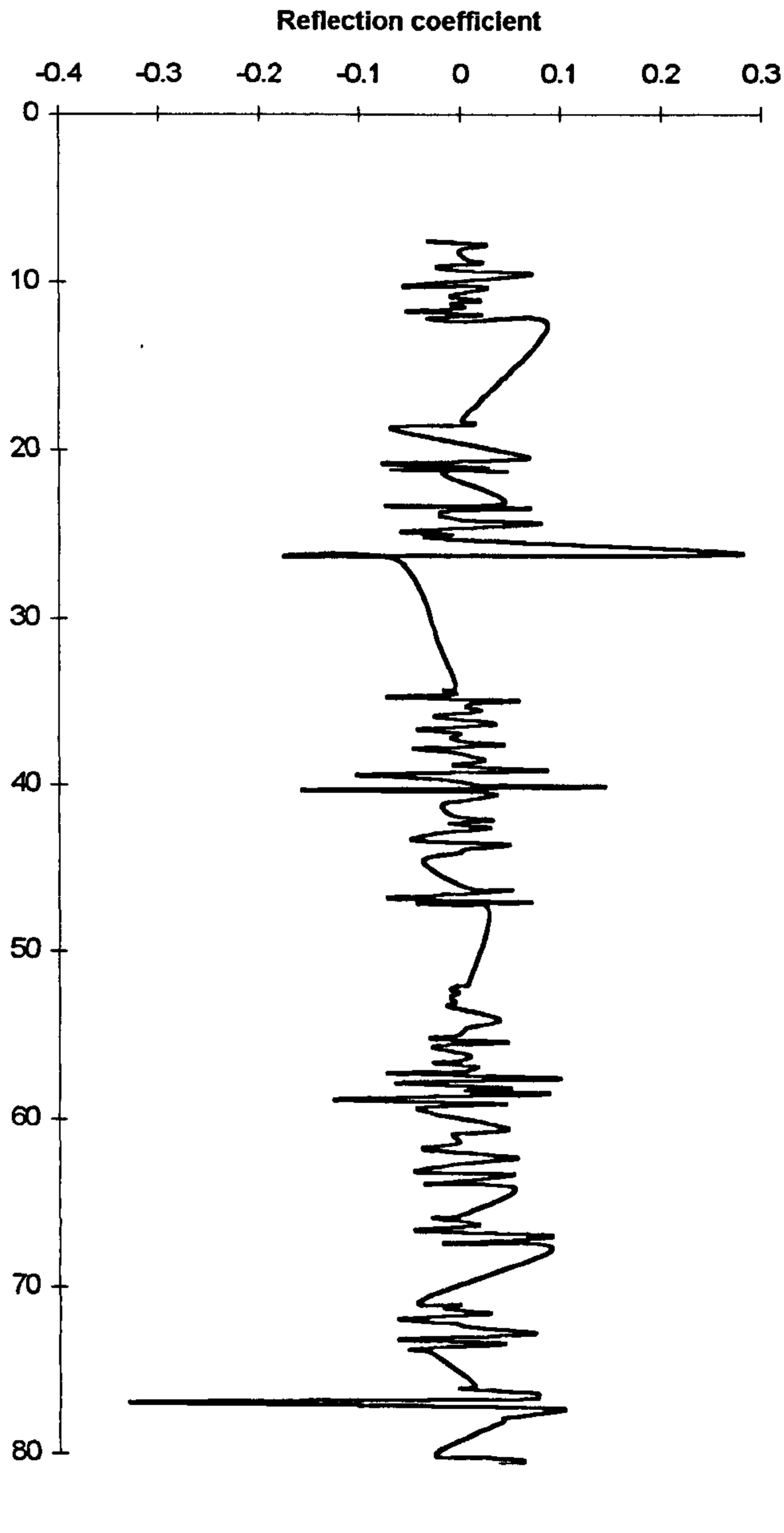

Figure 5.29. Reflectivity profile for borehole 88/7,7A.

This modelling approach does not include any discussion of gassy sediments. Any attempt to produce a model could be complicated by the lack of any confident physical property information from a gassified sediment at a given site. Sampling of gassy sediments may be difficult due to dissipation on recovery. Wilkens and Richardson (1998) have shown that, at those frequencies commonly used in site investigation, velocities are much lower than those found in bubble-free sediments, and scattering from impedance contrasts are the dominant influences on attenuation.

CHAPTER 6

MODELLING FROM CPT DATA

6.1. Introduction

Chapter 5 was concerned with modelling the seismic response from physical properties measured from samples recovered from boreholes. The empirical inter-relationships which enabled prediction of the acoustic properties were assessed and validated for a deepwater, glacially influenced slope environment. In many areas, geotechnically logged boreholes which provide detailed information on the sediment sequence and aid seismic interpretation, may not be available within the immediate vicinity of interest. Other methods of extracting groundtruth for seismic interpretation would therefore have to be relied on for the measurement of physical properties, such as analysis of recovered core and grab samples. However, there are inherent problems when relying on these methods, including undefined sample disturbance, shallow penetration and poor recovery of non-cohesive sediments. As an alternative, cone penetration provides a method of continuous *in situ* measurement of physical properties and does not involve sample recovery. It is generally considered that penetrometers are strong enough tools to not be adversely affected by continuous use in environments where sediments may be stiff or dense (Moran *et al.*, 1989), i.e. in a glacially influenced setting. This chapter presents a method for forward modelling high resolution seismo-acoustic reflection responses from the results of a cone penetration test.

Lithological interpretation of CPT test results makes use of published CPT classification charts. Currently though there appear to be no commercially available automated CPT classification programs to speed up the interpretation of very large files of results. The University of Victoria have developed CPTINT, and Fugro Ltd. use an in-house program. This part of the research presented in this thesis aims to produce an automated procedure which will use the CPT measurements of cone resistance and sleeve friction as inputs to output a synthetic seismogram. The study also tests the validity of global classification charts for general use. The intention in developing this method is to compliment, not replace, existing interpretation methods, by making as much use as possible of available geotechnical test data to estimate lithology, and where possible, physical properties.

The cone penetration test will be described at the beginning of the chapter and the subsequent sections will present the results of the CPT modelling on data from Liverpool Bay.

6.2. Cone Penetration Testing (CPT)

Alongside borehole sampling, the other main *in situ* investigation method used offshore for geotechnical site investigation is the standard cone penetrometer test. Performing these tests is generally far more cost-effective than drilling boreholes. Various classification schemes have been published for interpretation of the results. The review of the CPT presented here includes a discussion of the basic test and its results, and will provide a background to the work carried out on the CPT results presented later in this chapter and used as part of the integrated study in Chapter 7.

The background to CPTs presented in this chapter comes primarily from two reports presented by Schmertmann (1978) and Meigh (1987). The description included in the following section relates primarily to the piezocone CPT (PCPT).

6.2.1. Introduction

The cone penetration test (CPT) provides a method of soil classification and produces data which can be analysed to provide information on indices of soil strength. Its major advantage is that it is able to provide continuous measurement of soil properties. Meigh (1987) lists the three main applications of the CPT as:

1. Determination of the soil profile and soil identification.
2. Interpolation of ground conditions between control boreholes.
3. Investigation of engineering parameters.

The standard equipment is remotely controlled and lowered to the seabed on heavy lift cables (Power and Aldridge, 1997), as shown in Figure 6.1. The test involves pushing a standard cone supported on the end of a series of rods into the ground at a constant rate and making measurements of the resistance of the ground to the penetration. Measurements can be made of the combined resistance to penetration

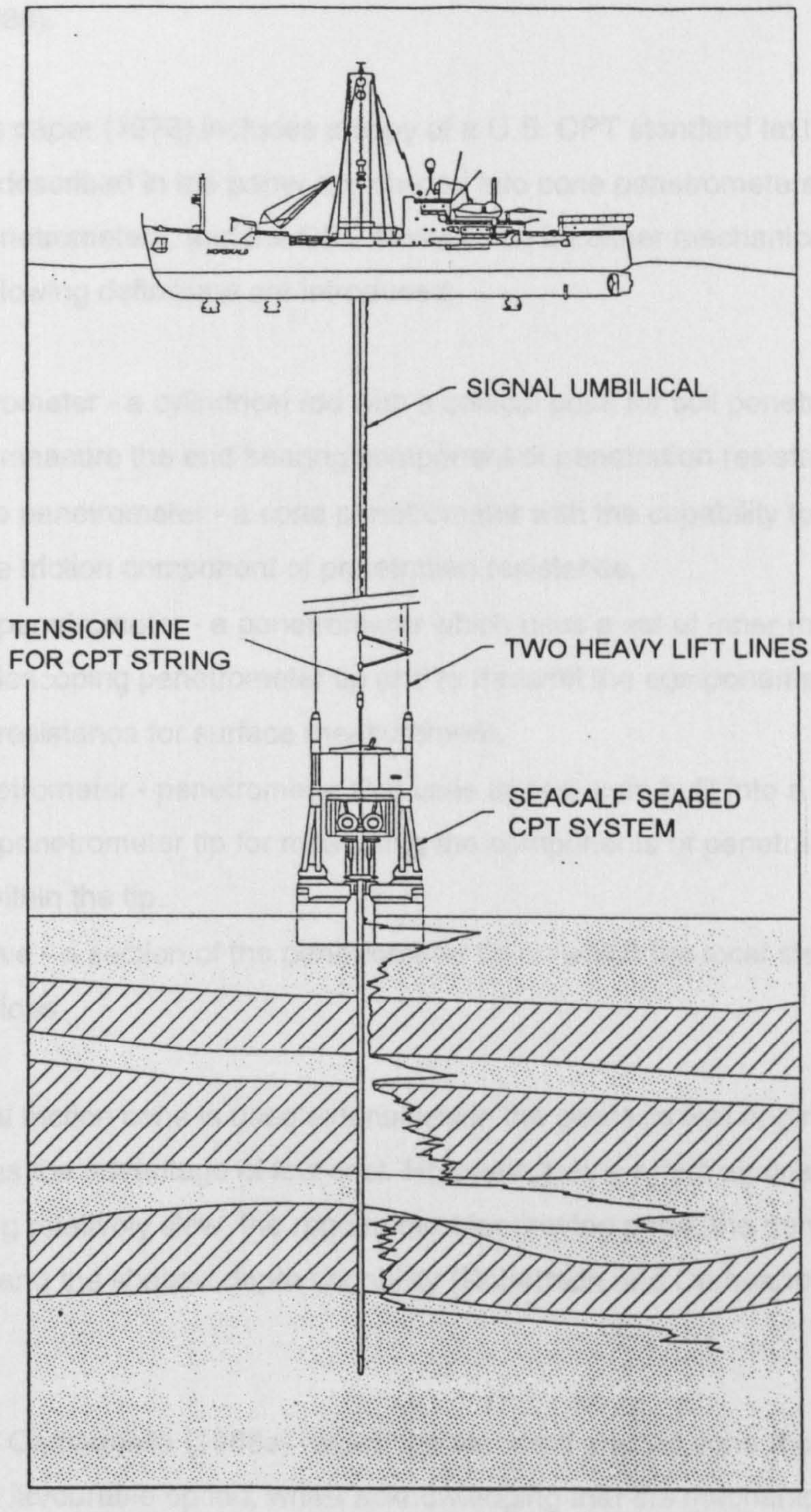

Figure 6.1. Drillship in CPT mode (after Hampson and Power, 1996).

of the cone and the local side friction, illustrated in Figure 6.2 (Meigh, 1987, Olsen and Malone, 1988).

Schmertmann's paper (1978) includes a copy of a U.S. CPT standard text. The penetrometers described in the paper are divided into cone penetrometers and friction cone penetrometers, and the CPT method can be either mechanical or electric. The following definitions are introduced:

- Cone penetrometer - a cylindrical rod with a conical point for soil penetration designed to measure the end bearing component of penetration resistance.
- Friction-cone penetrometer - a cone penetrometer with the capability to measure the local side friction component of penetration resistance.
- Mechanical penetrometer - a penetrometer which uses a set of inner rods to operate a telescoping penetrometer tip and to transmit the components of penetration resistance for surface measurement.
- Electric penetrometer - penetrometer that uses transducers built into a non-telescoping penetrometer tip for measuring the components of penetration resistance within the tip.
- Friction sleeve - a section of the penetrometer tip on which the local sleeve friction develops.

The mechanical friction cone is used extensively in the geotechnical engineering industry and has the advantage of low cost. However, this is offset against the procedure being relatively slow, the requirement for moving parts, the generally poor accuracy and the shallow depth capability (Robertson and Campanella, 1983a).

Robertson and Campanella (1983a) regard the standard electric cone method as a generally more favourable option, whilst acknowledging that the mechanical cones are useful for their lower cost and simple operation. An invaluable addition to the electric cone procedure is the capability of measuring pore pressure which enhances its use as a stratigraphic interpretation tool. The cost of this equipment is higher but the advantages include a more rapid procedure, continuous recording, higher accuracy and repeatability.

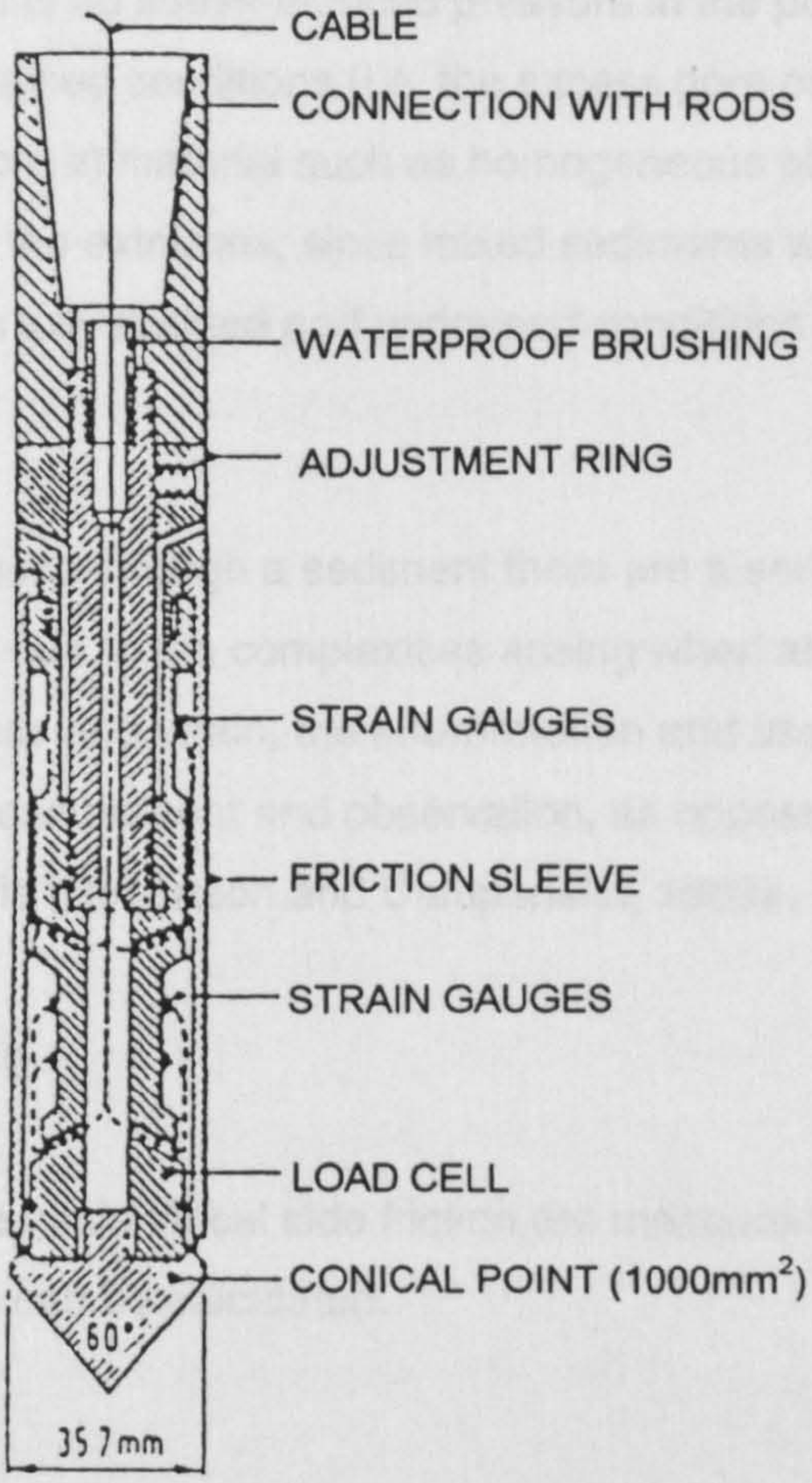

Figure 6.2. CPT tools (after Meigh, 1987).

CPT methods can provide useful information in most soil types but have proved most useful in coarser more permeable sediments such as sand. In reasonably permeable sediments such as fine and coarser sands, pore pressure effects during penetration may have a negligible influence. Therefore, the CPT is measuring fully drained behaviour, i.e. there is no stress-induced pressure in the pore water. The CPT will measure fully undrained conditions (i.e. the excess pore pressure is at its initial value before dissipation) in material such as homogeneous plastic clays. These conditions represent the extremes, since mixed sediments will generally produce behaviour between fully drained and undrained conditions (Schmertmann, 1978).

As the penetrometer tip passes through a sediment there are a series of changes in stress and strain. However, due to the complexities arising when attempting to quantify the changes in stress and strain, the interpretation and use of CPT data is empirically based, i.e. by measurement and observation, as opposed to being based on theoretical analysis (Robertson and Campanella, 1983a, Meigh, 1987).

6.2.2. Penetrometer testing

Cone resistance and sleeve friction/local side friction are measured during the test and from these friction ratio can be calculated.

6.2.2.1. Cone resistance, q_c

Cone resistance is a measure of end bearing stress, i.e the total force acting on the cone, Q_c, divided by the projected area of the cone, A_c, which importantly, through laboratory testing, has been shown to vary with vertical effective stress. Knowledge of the variables which influence cone resistance enable interpretations of CPT data to be made in various sediment types. Cone resistance measurements are used to identify changes in density and consistency, e.g. dense sand and overconsolidated clay have higher cone resistance values (Moran *et al.*, 1989).

Schmertmann (1978) postulates various factors which influence cone resistance. The net result of the passage of the cone penetrometer on a soil element is a radial expansion of the element to the radius of the penetrometer tip. Therefore, this *in situ* radial effective stress will have a significant effect on cone resistance, as shown

by laboratory chamber testing. Cone resistance responds to sediment changes within 5 to 10 tip diameters above and below the cone; this distance increases with increasing sediment stiffness. Changes in sediment properties may not be accurately located, particularly where there are thin layers. Meigh (1987) states that in a sand/clay sequence a sand layer less than 100mm thick will not be distinguished from the surrounding clay. Similarly, a clay layer less than 150 to 200mm thick will not be detected as a separate layer from the surrounding sand.

Compressibility has the effect of altering cone resistance, i.e. a cone pushing through the sediment will either displace or increase the particle packing. If the compressibility of a sediment is changed then there is a change in relative density which will bring about a change in cone resistance. Relative density will be discussed in Section 6.2.3.1. in relation to non-cohesive sediments. Cementation and particle size are variables which will also have an affect on the measurement of cone resistance.

Figure 6.3 provides a series of cone resistance profiles with possible interpretations. Generally clays have a significantly lower cone resistance than sands due to a lower effective angle of shearing resistance, and due to pore pressure effects as illustrated in Figure 6.3(a) and 6.3(b). Parts (c) and (d) of the same (Figure (6.3)) show one of the fundamental uncertainties when interpreting cone resistance profiles: increased stress and density produce similar effects.

6.2.2.2. Sleeve friction, f_s

Sleeve friction or local side friction is a localised large-strain index of shear strength and is described as the total frictional resistance acting on the friction sleeve, Q_f divided by its surface area, A_s. Sleeve friction, as with cone resistance, should be corrected, in theory, for pore pressure effects. However, Meigh (1987) points out that in published data these corrections are generally not made.

6.2.2.3. Friction ratio, R_f

Friction ratio is the ratio of the local side friction to the cone resistance expressed as a percentage and is an indicator of grain size or texture (Moran *et al.*, 1989). Interpretation of cone resistance data allows broad identification of a sediment

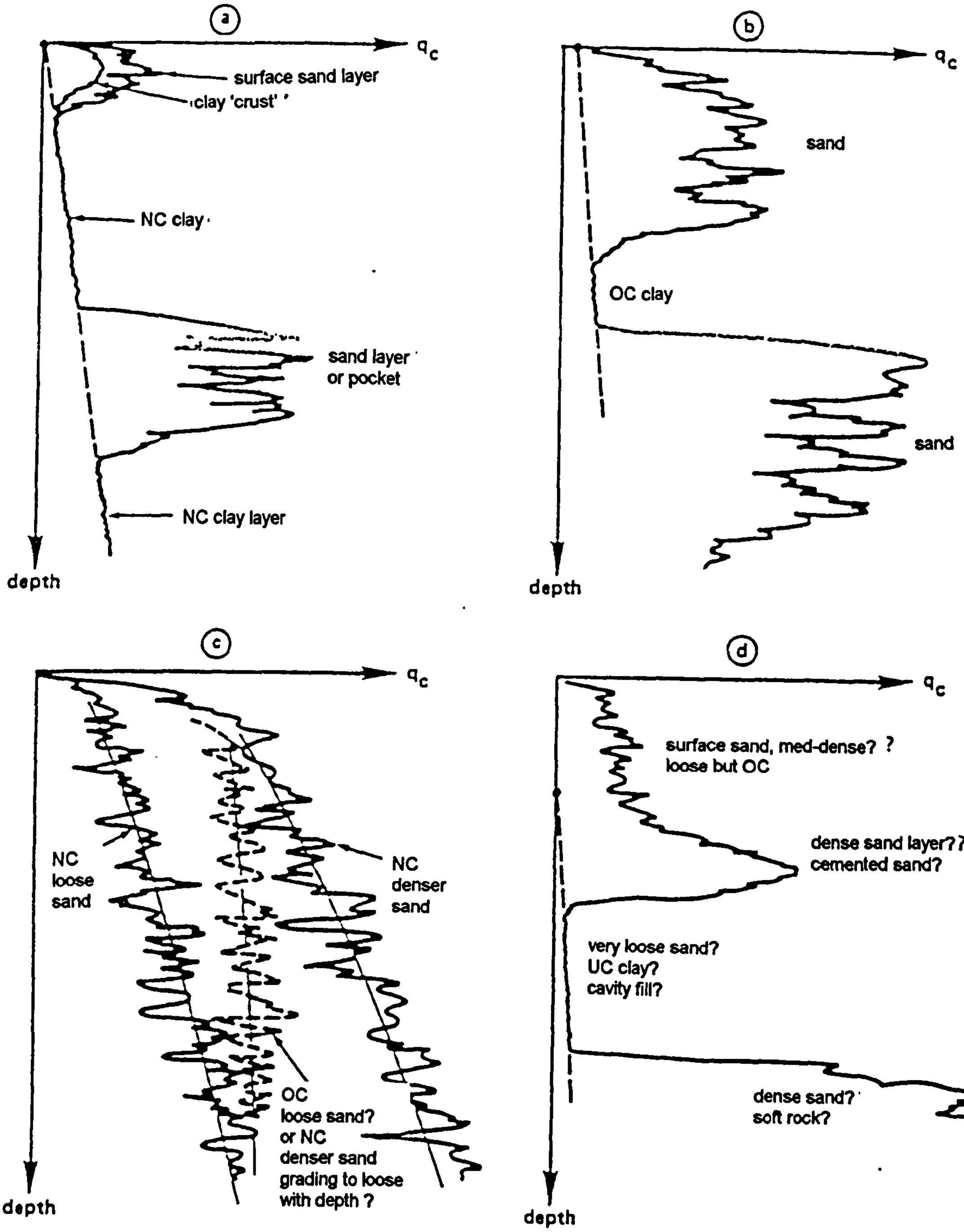

Figure 6.3. Cone resistance profiles with possible interpretations (after Schmertmann, 1978).

profile but simultaneous knowledge of friction ratio is considered to improve interpretation in terms of grain size and consistency (Robertson and Campanella, 1983a).

6.2.3. Derivations of engineering parameters using CPT data - non-cohesive sediments.

Meigh (1987) divides the CPT engineering parameters into those used for the investigation of non-cohesive sediments and those used for cohesive sediments. The same format will be followed in this thesis.

Sampling methods such as coring in non-cohesive sediments can produce problems with sample recovery, e.g. disturbance and loss of structure. The CPT therefore, has a very significant role in the investigation of non-cohesive sediments. By using the cone resistance measured during the test, relative density, shear strength and modulus values can be empirically derived.

6.2.3.1. Relative density

In normally consolidated sands the relationship between cone resistance and relative density is highly dependent on compressibility. Due to the complexity of the stress-strain and strength behaviour in non-cohesive soils, the correlation should only be used as a guide. Difficulties have also been recognised in the determination of the maximum, minimum and *in situ* densities. The correlation could be improved if the compressibility of the sand could be measured from the grain properties.

6.2.3.2. Drained shear strength

The peak effective angle of shearing resistance, ϕ', can be estimated using relative density as an intermediate parameter. Schmertmann (1978) produced a graph of the relationship between peak angle of shearing resistance and relative density, by using the relationship between cone resistance and relative density.

Meigh (1987) refers to a correlation between Terzaghi's bearing capacity factor for general shear, N_γ, and cone resistance, $N_\gamma = 12.5\ q_c$. Again N_γ can be used as an intermediate parameter, but there is a great deal more uncertainty in this indirect

approach than using a direct method. The direct correlation between cone resistance and ϕ' has been derived from bearing capacity theory and ignores soil compressibility.

6.2.3.3. Moduli

Depending on the specific problem, one of three moduli can be evaluated: the shear modulus, the constrained modulus or the Young's modulus. Stress-strain curves for sands are non-linear, therefore a stress range for the modulus has to be defined. Robertson and Campanella (1983a) review the various correlations of the moduli with cone resistance and conclude that when interpreting CPT data in sands, more reliance can be put on friction angle than density or moduli. This is due to variations of the small strain measurements of density and moduli with grain characteristics. In contrast the cone resistance and the peak friction angle are large strain measurements and therefore the influence of the grain characteristics on their values are not as significant.

6.2.4. Derivations of engineering parameters using CPT data - non-cohesive sediments.

CPT measurements are often considered to be of less importance for cohesive sediments due to the widely available established methods of geotechnical evaluation, such as *in situ* vane tests. However, as discussed above, the CPT is a cost-effective, relatively fast, robust method of continuous measurement of the sub-surface. Therefore, where CPT data have been the only geotechnical data collected for a site investigation, it is essential to be able to extract engineering properties for both cohesive and non-cohesive sediments.

6.2.4.1. Shear strength

Robertson and Campanella (1983b) show that the undrained shear strength of a clay is dependent on the type of test, the rate of strain and the orientation of the failure planes.

Meigh (1987) presents a the relationship between cone resistance and the undrained shear strength of a cohesive sediment as:

$$q_c = N_k s_u + \sigma_{vo} \quad (6.1)$$

where N_k is the cone factor (unitless), s_u is the undrained shear strength and σ_{vo} is the total vertical stress (this may also be interpreted as the *in situ* horizontal stress or the *in situ* octahedral stress). Robertson and Campanella (1983b) quote an average N_k of 15, with a range of 11 to 19 in normally consolidated clays obtained using a standard type electric cone at a standard rate of penetration of 2 cm/s. The cone resistance in clays is highly dependent on the rate of penetration and Meigh (1987) quotes an acceptable tolerance of ± 0.5 mm/s on the standard of 2 cm/s.

In overconsolidated clays it is more difficult to correlate cone resistance with shear strength due to the effects of fabric, fissures and other discontinuities on the response of the clay, and the marked effect on the cone factor. Quoted values for N_k in stiff marine clays are 27 ± 3 and 18 ± 4 for glacial clays (Meigh, 1987).

6.2.4.2. Overconsolidation ratio

Baltzer *et al.* (1994) use information on the consolidation state as a further means of interpreting the geological environment. Schmertmann (1987) produced a method of estimating the overconsolidation ratio. This has been modified by Robertson and Campanella (1983b) :

1. Estimate s_u from q_c.
2. Estimate the vertical effective stress, σ_{vo}'
3. Calculate the strength/effective stress ratio

$$S(v) = s_u/\sigma_{vo}'. \quad (6.2)$$

4. Baltzer *et al.* (1994) quote S(v) = 0.31 (Schmertmann (1978) suggests S(v) = 0.33) for normally consolidated sediment, for overconsolidated sediment, S(v) > 0.40 and for under-consolidated sediment, S(v) < 0.20.
5. Estimate the average S(v).

Baltzer *et al.* (1994) compared the overburden stress value, as found by the method above, with the present overburden stress (by summing bulk densities). Differences were calculated between the real and theoretical sediment thicknesses by:

$$= \frac{\left[\frac{\gamma' \times h - Su}{(0.11 + 0.0037 \times I_p)}\right]}{\gamma'} \qquad (6.3)$$

where $\gamma' \times h$ is the effective overburden pressure measured from the submerged unit weight and burial depth. Positive values correspond to underconsolidated sediments and negative values to overconsolidated sediments.

6.2.4.3. Moduli

As with non-cohesive sediments, the stress range needs to be known when making correlations with the moduli. For a more in depth description of the calculations reference should be made to the work of authors such as Robertson and Campanella (1983b) who review methods of estimating the constrained modulus and Young's modulus.

6.2.5. The piezocone

The CPT is a major offshore site investigation tool, but, in recent years it is piezocone penetration testing (PCPT), with the measurement of excess pore pressure alongside cone resistance and sleeve friction, which have been widely performed. Moran *et al.* (1989) state that "in general, neither coring nor drilling can presently obtain such data as completely and continuously as the piezocone penetrometer".

The first pore-water pressure measurements were made in the early 1970s in Sweden. Subsequent developments resulted in the PCPT which simultaneously measures pore water pressure, cone resistance and sleeve friction. Since 1985 the PCPT has largely superceded the CPT and, "become the most important tool for offshore use", (Lunne and Powell, 1993). Meigh (1987) divides the applications of the piezocone into two categories: profiling, which gives more accuracy than the CPT, and assessment of engineering parameters. An example of the assessment of engineering parameters is where the pore pressure values are used as an aid to the interpretation of cone resistance and sleeve friction for material type and behaviour (Moran *et al.*, 1989).

The basic design of a 10cm^2 PCPT showing the filter placed in the face of the cone is illustrated in Figure 6.4. The process of measurement is the same as has been described in Section 6.2.1 except that pore-pressure dissipation testing is also carried out alongside measurements of cone resistance and sleeve friction.

The cone and friction sleeve are made of high-quality steel and the filter is ceramic. The cone and sleeve friction sensors are load-cell type measuring transducers arranged in series. Improved *in situ* accuracy compared to the CPT comes from a stiffer penetrometer design due to this arrangement of sensors (Fugro-Geoteam Ltd., 1997).

6.2.6. Interpretation and soil parameters from the piezocone

Current sediment classification charts exist, such as that by Robertson and Campanella (1983a), which use cone resistance and friction ratio to classify sediment type in the upper 30m of the sediment column. Meigh (1987) proposes a tentative correlation of the change in pore pressure and the net cone resistance (shown in Figure 6.5). This correlation can be used where the filter is placed above the base of the cone (Meigh, 1987). However, Lunne and Powell (1993) state that a large amount of research is currently taking place to increase the reliability of soil parameters from the PCPT. For sediments at significantly greater depths than 30m it has been recognised that sediments change their apparent classification with increasing depth (Robertson, 1990). Robertson (1990) has produced a sediment classification using cone resistance, friction ratio and pore pressure which involves normalising the PCPT data to consider the influence of overburden stress.
Meigh (1987) comprehensively discusses the possibilities of the use of piezocone results. Naturally occurring, *in situ* sediment pore pressures may be equal to or higher than hydrostatic pressure and will produce no or positive excess pore pressures. In addition the action of the cone penetrometer alters pore pressures; these changes in pore pressures are a result of stress history, permeability, density and plasticity (Moran *et al.*, 1989). One of the major advantages of the PCPT is the ability to detect thin layers down to 3-5 mm thick which may not be picked up solely from measurements of cone resistance or sleeve friction. Therefore, it is the excess pore pressure which is able to delineate thin lithological units and the unit characteristics are interpreted using all the measurements discussed above, i.e.

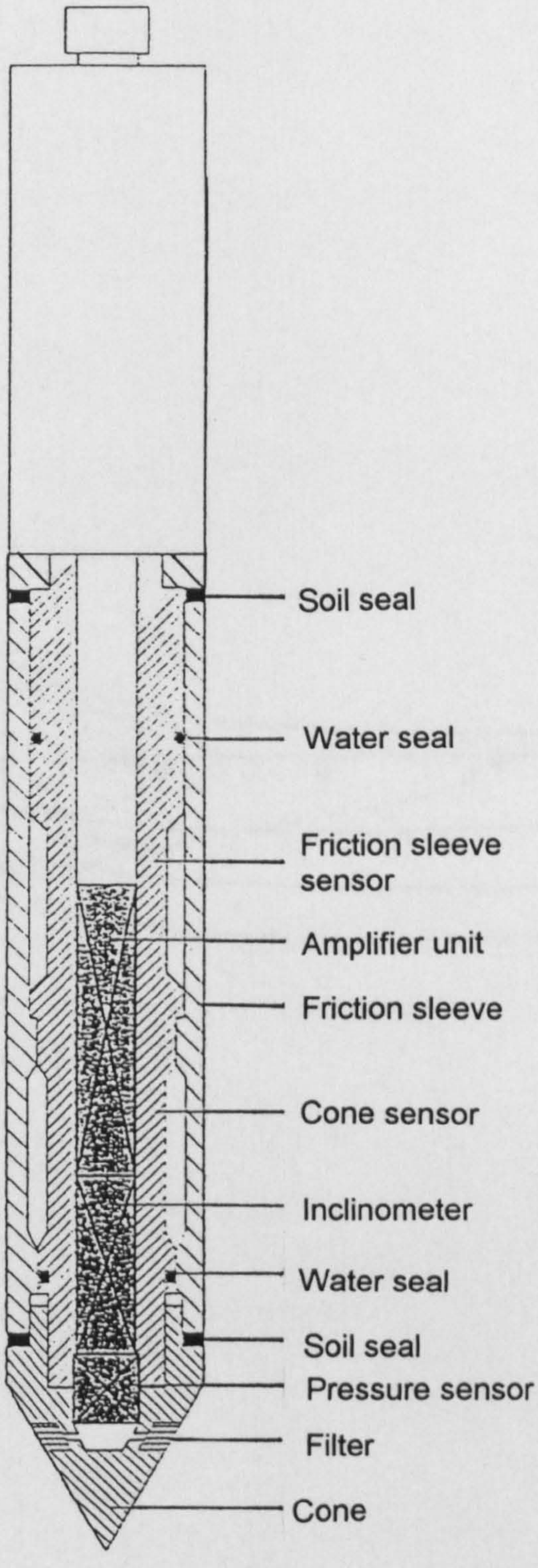

Figure 6.4. PCPT tool (after Fugro, 1994).

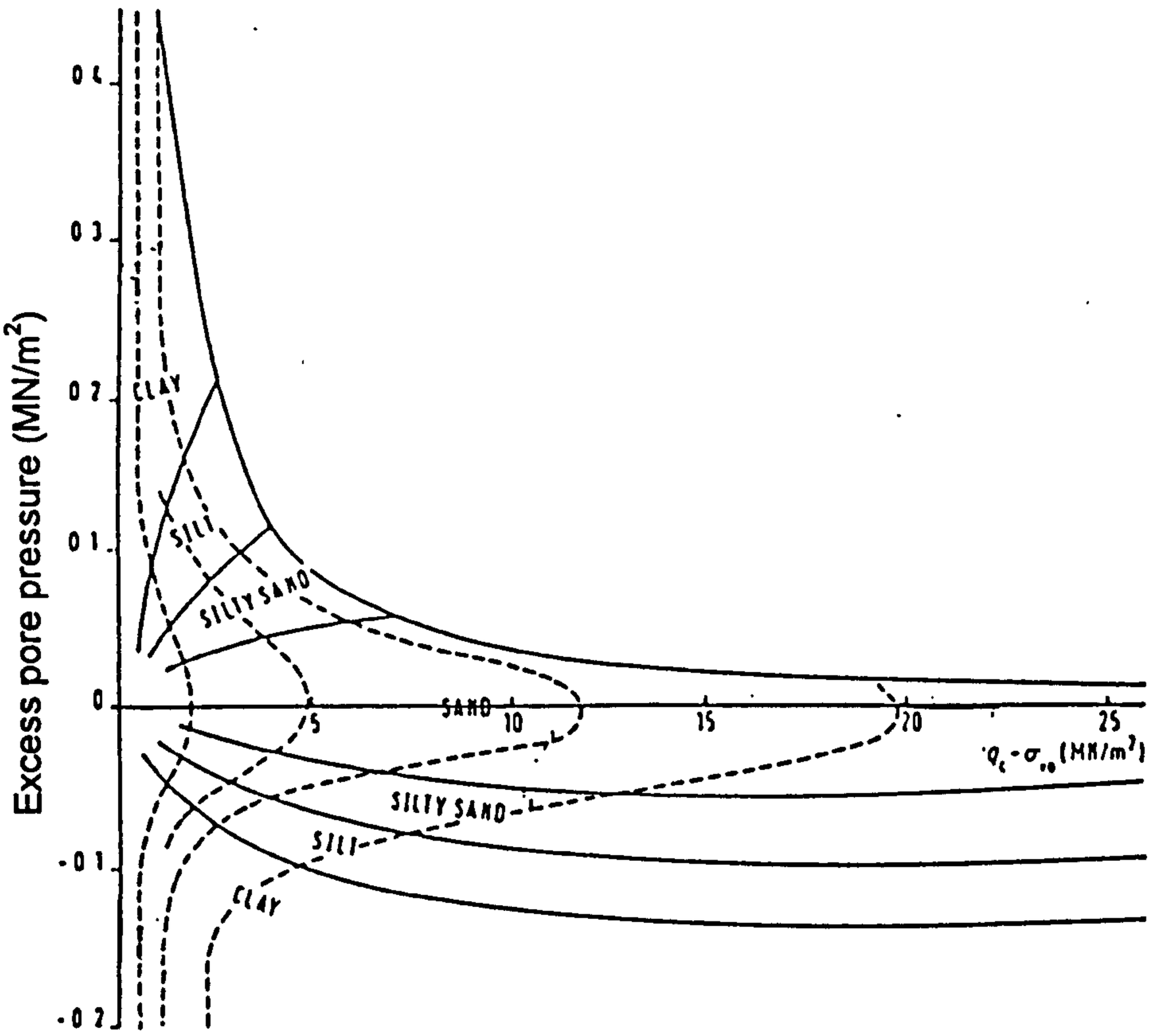

Figure 6.5. Tentative pore pressure and cone resistance correlation diagram (after Meigh, 1987).

cone resistance, sleeve friction, friction ratio and excess pore pressure (Moran *et al.*, 1989).

The engineering parameters which can be derived from PCPT results will be described only briefly with reference to Meigh (1987).

6.2.6.1. Undrained shear strength

An empirical relationship between pore pressure and shear strength is given by Meigh (1987) as:

$$\Delta_u = N_{\Delta u} \cdot s_u \qquad (6.4)$$

where $N_{\Delta u}$ is a correlation factor and $N_{\Delta u} = \Delta_{u/su}$

For some Canadian clays $N_{\Delta u} = 7.9 \pm 0.7$, for $0.8 < I_L < 2.0$

$N_{\Delta u} = 11.7 \pm 2.0$, for $I_L > 2.0$

However this may be complicated by the fact that Δ_u/q_c varies depending upon the overconsolidation ratio (OCR).

6.2.6.2. Effective stress shear strength

There is no reliable method of determining this parameter, but it may be possible to detect soft, normally consolidated clays from the negative intercept on a plot of net cone resistance against effective overburden pressure.

6.3. Modelling from CPT data

In the situation where CPT results are the only available means of groundtruthing seismic data, it is necessary to make as much use of these data as possible. This includes correlations not only with engineering properties but with acoustic properties such as acoustic impedance. The PCPT results which are generally supplied for groundtruthing seismic data are profiles of cone resistance, sleeve friction and pore pressure.

Interpretation of CPT data often tends to be qualitative rather than quantitative to gain an overview of soil types. The use of cone resistance is widespread for this purpose, as previously shown by Schmertmann (1978), (see Figure 6.3).

As mentioned previously, various soil classifications exist for interpretation of CPT results, for example the chart presented by Robertson and Campanella (1983a). Measurements of parameters such as cone resistance and sleeve friction can be applied to these charts and a soil type estimated.

Zhang and Tumay (1996) have reviewed these charts and attempted to simplify the classifications. They have based this work on simplifying the current charts which have two tendencies, i.e. soil type changing in one direction and *in situ* soil state changing in another. They postulate that these tendencies relate to soil composition and environment. By taking all these factors into account these two dimensions have been simplified into a one-dimensional classification system by linear conformal mapping.

6.4. CPT classification

The initial stage of this research was to make use of an existing classification chart to categorise the sediment types. The classification chart of Robertson and Campanella (1983a) (also documented in Robertson (1990)) which has been modified for British soils by Fugro Ltd. was used as the basis for the method, and therefore cone resistance and sleeve friction are the two parameters required. Pore pressure results are also used but are discussed directly and not through any classification or interpretation scheme. This chart appears to be the most representative of general soil conditions from the literature, (shown in Figure 6.6) and for the purposes of this project. The chart was automated by assigning a classification number to each sediment type, as shown in Table 6.1.

Classification number	Sediment type
1	Coarse grained sand
2	Sand
3	Silty sand
4	Sandy clay

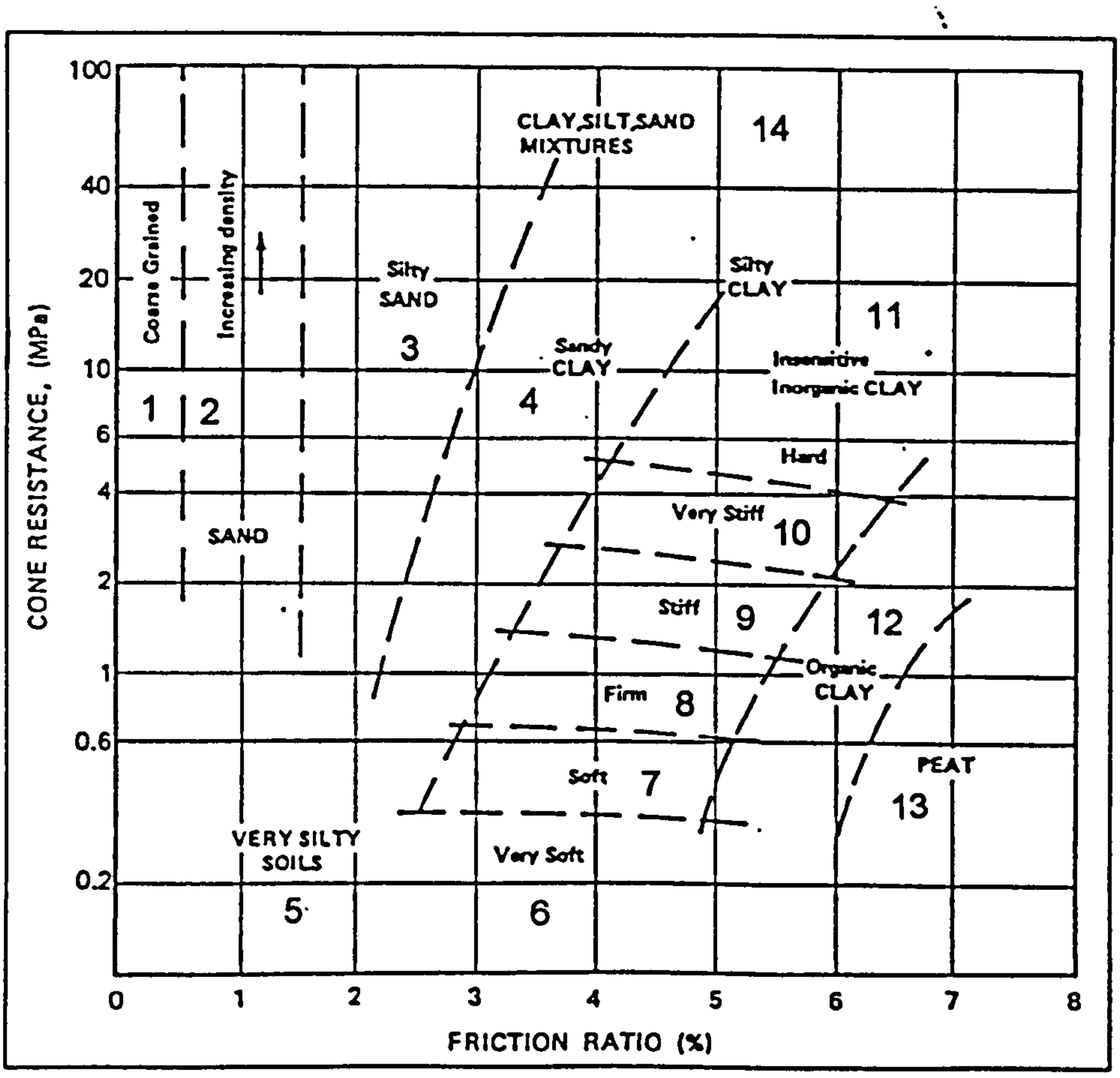

Figure 6.6. Sediment classification chart (modified from Robertson and Campanella, 1983a).

5	Very silty sediment
6	Very soft clay
7	Soft clay
8	Firm clay
9	Stiff clay
10	Very stiff clay
11	Hard clay
12	Organic clay
13	Peat
14	Clay, sand, silt mix

Table 6.1. Sediment type classification scheme.

The next stage of the method was to assign a density and velocity (and impedance) to each of the sediment types in the classification scheme. This needs to be done on a site by site basis and requires knowledge of the geotechnical environment. Ideally a local borehole or series of boreholes could provide this information; additionally, BGS charts often contain general geotechnical information. However, depending on the site location assigning accurate geotechnical values may not be straightforward if the required data do not exist. The sensitivity of changes in density, velocity and impedance have already been investigated in Chapter 5. As the acoustic values are assigned based on lithology it is not possible in this case to accurately test the sensitivity of the cone resistance and sleeve friction values. More detailed studies would need to be carried out on the specific lithologies where acoustic measurements are made alongside CPT tests to establish empirical inter-relationships between the physical properties (cone resistance and sleeve friction) and the acoustic properties, in the manner of Hepton (1989). These studies would also need to be carried out for a variety of locations in an attempt to establish whether these types of inter-relationships could feasibly have a 'global' applicability. This method is intended to be a best estimate, broadbrush approach to CPT interpretation by producing forward models based on CPT results to aid seismic interpretation. The intention is not to produce a detailed CPT interpretation for detailed geotechnical design.

The middle stage of the process was automation of the interpretation procedure to allow large amounts of data to be processed quickly. The CPT input is in the digital

form of depth, cone resistance and sleeve friction. The program then outputs depth, friction ratio, classification number and the corresponding impedance value.

The final stage of the process is where the results are interpreted and divided into litholgical blocks to produce the input for the synthetic seismogram. From the blocked impedance log a reflectivity log is constructed and, by convolution with a source wavelet, a synthetic seismogram is generated in the same process as introduced in Chapter 5. Appendix B contains the C++ code used for the automation process.

6.5. Case study - Liverpool Bay

Liverpool Bay, which is shallow water compared to the two main sites considered in this study, was chosen for study to allow access to the range of short CPTs and high resolution boomer data. Butcher (1997) has shown that this area is a good testbed for the integration of CPT and high resolution seismic data. Four CPTs, which penetrated Quaternary sediments of glacial and post glacial origin, were selected from the Liverpool Bay area (Figure 6.7). The CPTs were collected as part of commercial exploration in Liverpool Bay by BHP Ltd. (formerly Hamilton Oil Ltd.) in 1993. Boomer data were shot over the CPT locations and will be used to assess the synthetic seismograms.

6.5.1. Setting

Liverpool Bay is situated in the south-east corner of the East Irish Sea Basin which is one of the largest and deepest post-Carboniferous depocentres west of the UK. The Basin consists of Carboniferous rocks overlain by rocks of Permian-Triassic age which are, in turn, overlain by more recent Quaternary sediments (Jackson *et al.*, 1995).

Quaternary sediment thicknesses in the Irish Sea are up to 300m, however, no areas of continuous deposition have been found in the geological record due to periods of uplift and erosion (Jackson *et al.*, 1995). Borehole evidence has shown that the Quaternary sediments are unlithified and range from soft to very stiff or hard.

Figure 6.7. Liverpool Bay location map.

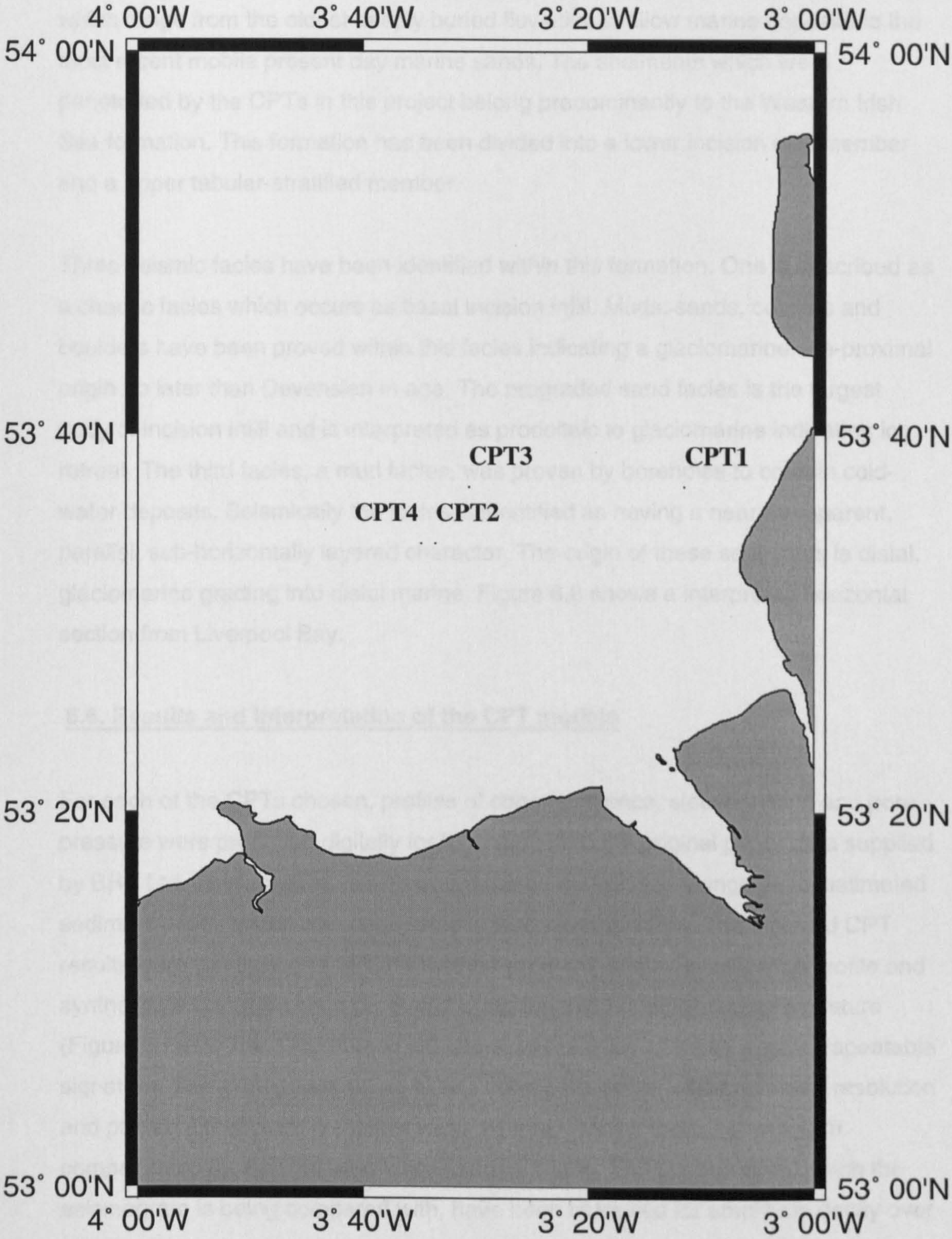
4° 00'W
3° 40'W
3° 20'W
3° 00'W
54° 00'N
53° 40'N
53° 20'N
53° 00'N
CPT3
CPT1
CPT4
CPT2

6.5.2. Seismic characteristics

Jackson *et al.* (1995) divided the Irish Sea Quaternary sediments into six formations which range from the oldest deeply buried fluviatile, shallow marine deposits to the most recent mobile present day marine sands. The sediments which were penetrated by the CPTs in this project belong predominantly to the Western Irish Sea formation. This formation has been divided into a lower incision infill member and a upper tabular-stratified member.

Three seismic facies have been identified within this formation. One is described as a chaotic facies which occurs as basal incision infill. Muds, sands, cobbles and boulders have been proved within this facies indicating a glaciomarine, ice-proximal origin no later than Devensian in age. The prograded sand facies is the largest body of incision infill and is interpreted as prodeltaic to glaciomarine indicating ice retreat. The third facies, a mud facies, was proven by boreholes to contain cold-water deposits. Seismically the facies is identified as having a near-transparent, parallel, sub-horizontally layered character. The origin of these sediments is distal, glaciomarine grading into distal marine. Figure 6.8 shows a interpreted horizontal section from Liverpool Bay.

6.6. Results and interpretation of the CPT models

For each of the CPTs chosen, profiles of cone resistance, sleeve friction and pore pressure were produced digitally for this study from the original paper data supplied by BHP Ltd. These profiles were hand digitised and plotted alongside an estimated sediment profile which was originally supplied with the CPTs. The digitised CPT results were run through the 'CPT method program' and a classification profile and synthetic seismogram were produced using the 175J boomer source signature (Figure 5.7(a)). The 175J source signature was chosen as it has a clear, repeatable signature. The 175J power rating allows good penetration whilst retaining resolution and proved effective as a shallow water source. The synthetic seismogram compensated for transmission losses and multiples. The boomer data, which the seismogram is being compared with, have been corrected for amplitude decay over time by the application of gain functions therefore any further correction of the synthetic seismogram was considered unnecessary. The synthetic seismogram was

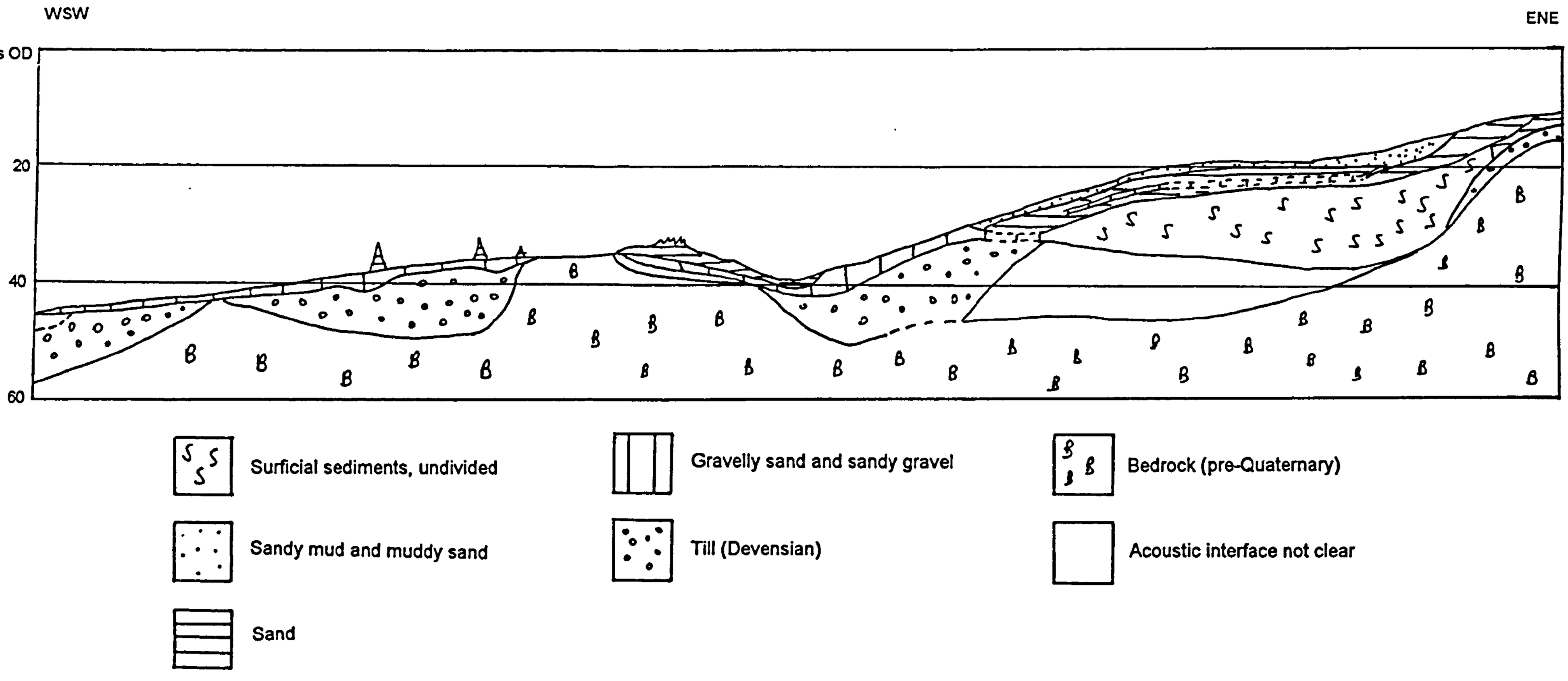

Figure 6.8. Liverpool Bay stratigraphic interpretation (after Wingfield, 1984).

plotted alongside the boomer data which crossed the CPT location, and all the profiles were subsequently integrated in the interpretation of each CPT.

6.6.1. CPT1 (2 LEN)

CPT 1 was the easternmost CPT and was collected in the shallowest water of the four CPTs in this case study, at 12.4m. The estimated sediment types show a sequence of sands and clay (Figure 6.9(a)). The loose sand section is characterised by a low cone resistance and sleeve friction (Figure 6.9(b) and 6.9(c) respectively). There is a large peak of 11MPa of width extending from 0.5-1.2m below seabed and which has been identified as dense sand. The upper boundary of the soft clay can be identified by a large drop in cone resistance to less than 1MPa and a positive pore pressure. The pore pressure profile (Figure 6.9(d)) relates well to the cone resistance profile and it fluctuates between negative (indicating coarser material) and positive values (indicating finer material); values close to zero may indicate well-drained conditions. Where the density of sand in the upper sand layer produces an increase in cone resistance, up to 10MPa, there is a corresponding relatively sharp drop in pore pressure. The positive pore pressures generally relate to the finer sands and soft clays and as the cone resistances increase the pore pressures become negative. It is more difficult to separate the lower layers in the profile on the cone resistance and sleeve friction profiles, however the pore pressure shows a better layer definition with the silty layers producing negative pressures (Figure 6.9(d)).

The classification profile (Figure 6.10(a)) is successful in delineating the estimated sediment types. Within the upper section the classification chart identifies silt which has not been previously interpreted on the estimated sediment profile supplied with the CPT. However, this interpretation may be a function of the difficulties encountered when applying upper and lower limits to the sediment types on the classification chart which was used to produce the CPT program. Loose sands will fall close to the silt boundary according to the chart from Robertson and Campanella (1983a).

Following the output from the classification program the profile can be blocked, i.e. layers are interpreted for calculating reflection coefficients for input into the synthetic seismogram program.

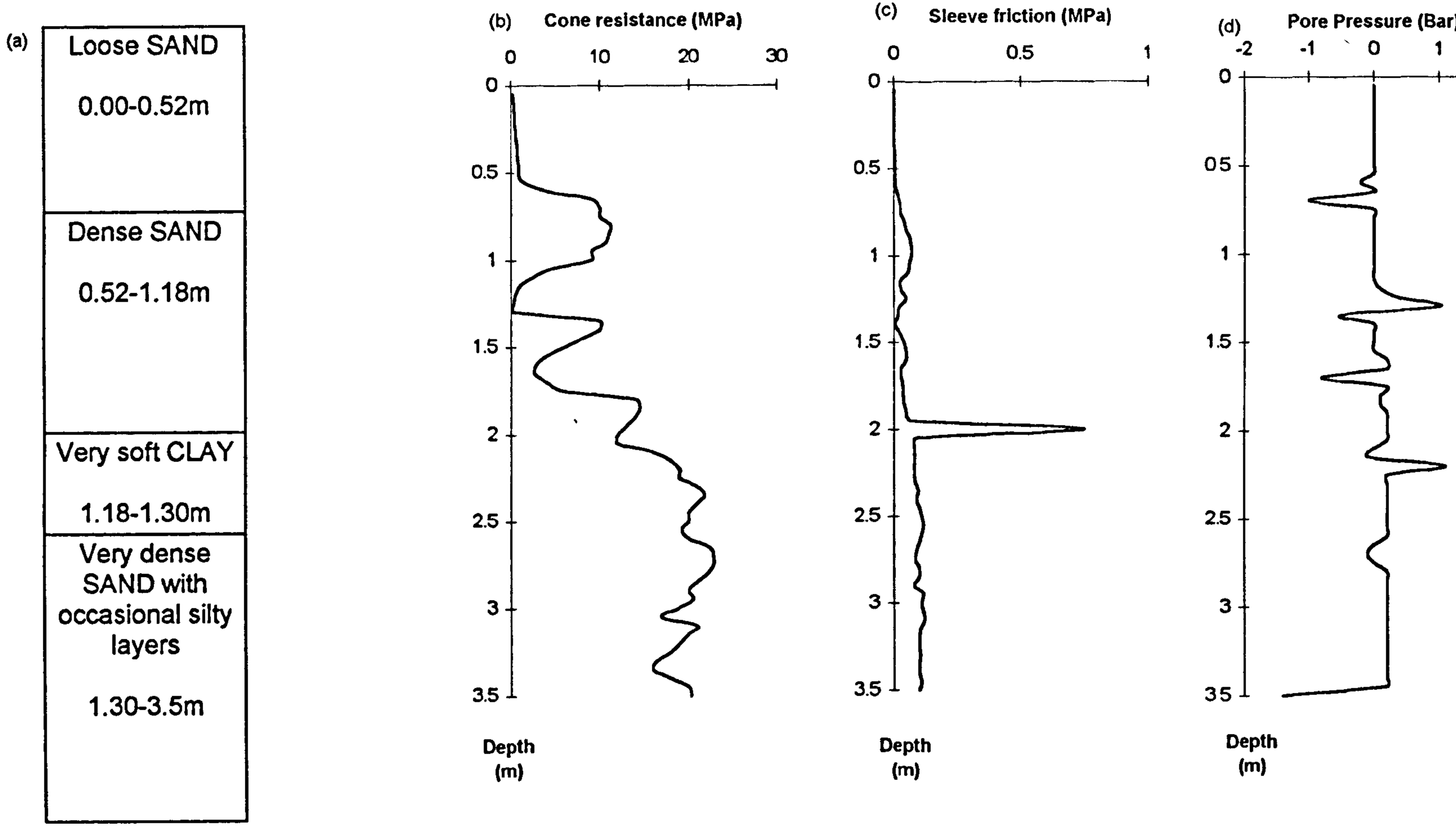

Figure 6.9. CPT1 profiles. (a) Estimated sediment type. (b) Cone resistance. (c) Sleeve friction. (d) Pore pressure.

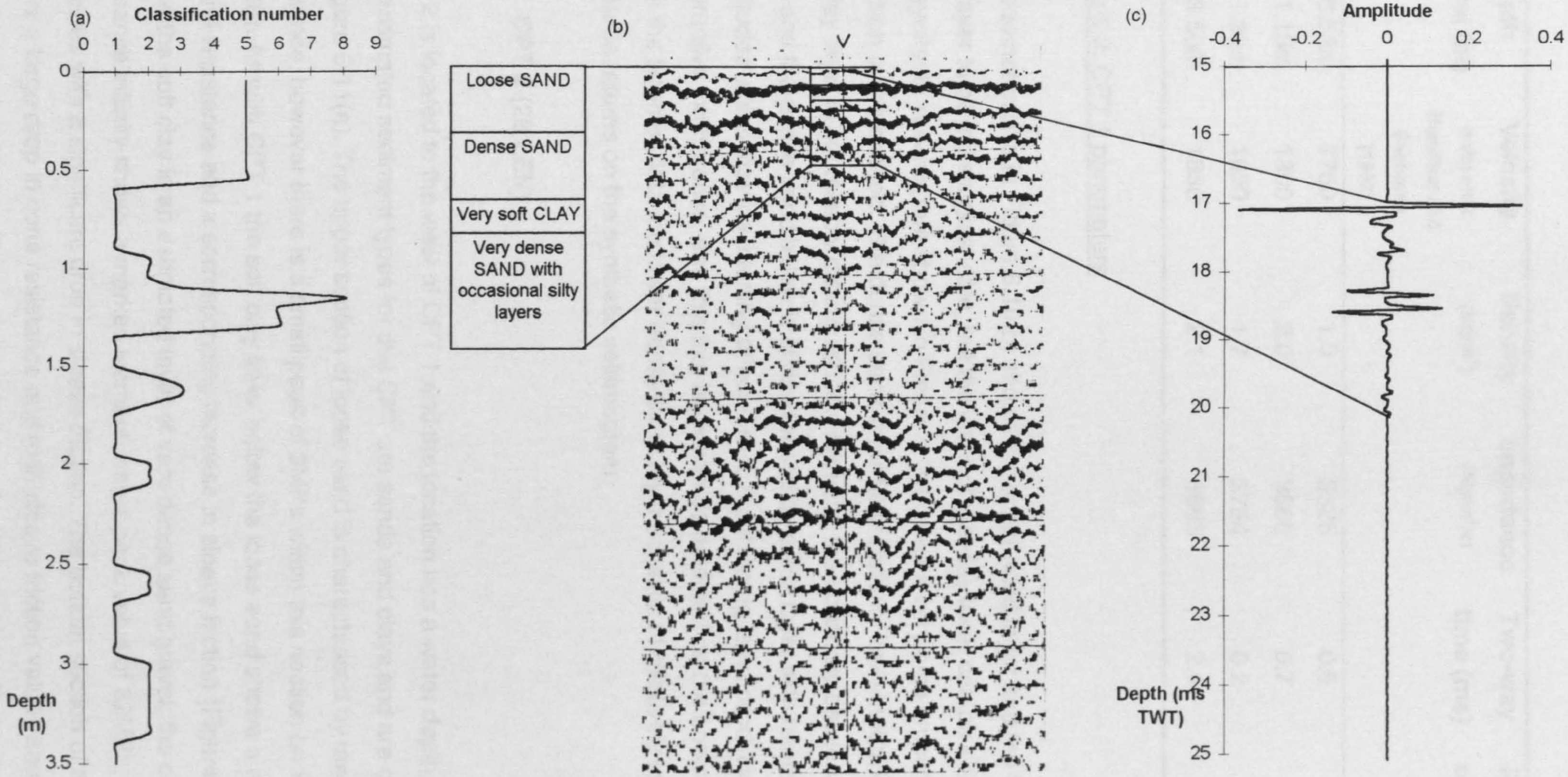

Figure 6.10. CPT1 profiles. (a) Sediment classification. (b) Boomer profile, vertical scale; 1cm = 2.6ms TWT. (c) Synthetic seismogram.

Depth interval (m)	Velocity (m/s) after Hamilton and Bachman (1982)	Density (Mg/m^3)	Impedance ($Mg/m^2/s$)	Two-way time (ms)	Reflection coefficient
0.00-0.52m	1750	1.9	3325	0.6	0.37
0.52-1.18m	1800	2.0	3600	0.7	0.04
1.18-1.30m	1620	1.7	2754	0.2	-0.13
1.30-3.50m	1850	2.1	3885	2.4	0.16

Table 6.2. CPT 1 parameters

The boomer profile in Figure 6.10(b) shows the upper sand layer and the top of the clay layer to be indistinguishable, but the base of the clay layer can be identified. The synthetic seismogram shown in Figure 6.10(c) has a very high amplitude reflection at the seabed. The dense sand layer has relatively low amplitudes and the clay layer is not reliably distinguished. However, the boundary between the clay layer and the dense sand below is characterised by a thin layer with relatively high amplitudes which may be a tuning effect due to the thinning layer producing constructive interference, and this thin layer can be detected on the boomer data. As on the boomer data the lower dense sand layer consists of relatively lower amplitude returns on the synthetic seismogram.

6.6.2. CPT 2 (28 LEN)

CPT 2 is located to the west of CPT 1 and the location has a water depth of 26m. The estimated sediment types for this CPT are sands and clays and are displayed in Figure 6.11(a). The upper section of loose sand is characterised by low cone resistance, however there is a small peak of 3MPa within this section on Figure 6.11(b). As with CPT 1 the soft clay layer below the loose sand shows a decrease in cone resistance and a corresponding increase in sleeve friction (Figure 6.11(c)). Below the soft clay in an estimated layer of very dense sand/gravel, the cone resistance initially shows a marked increase with a peak value of 32MPa; this peak coincides with a significant drop in sleeve friction. The bottom section of the CPT shows a large drop in cone resistance and high sleeve friction values and is interpreted as hard clay. The pore pressure profile (Figure 6.11(d)) shows a

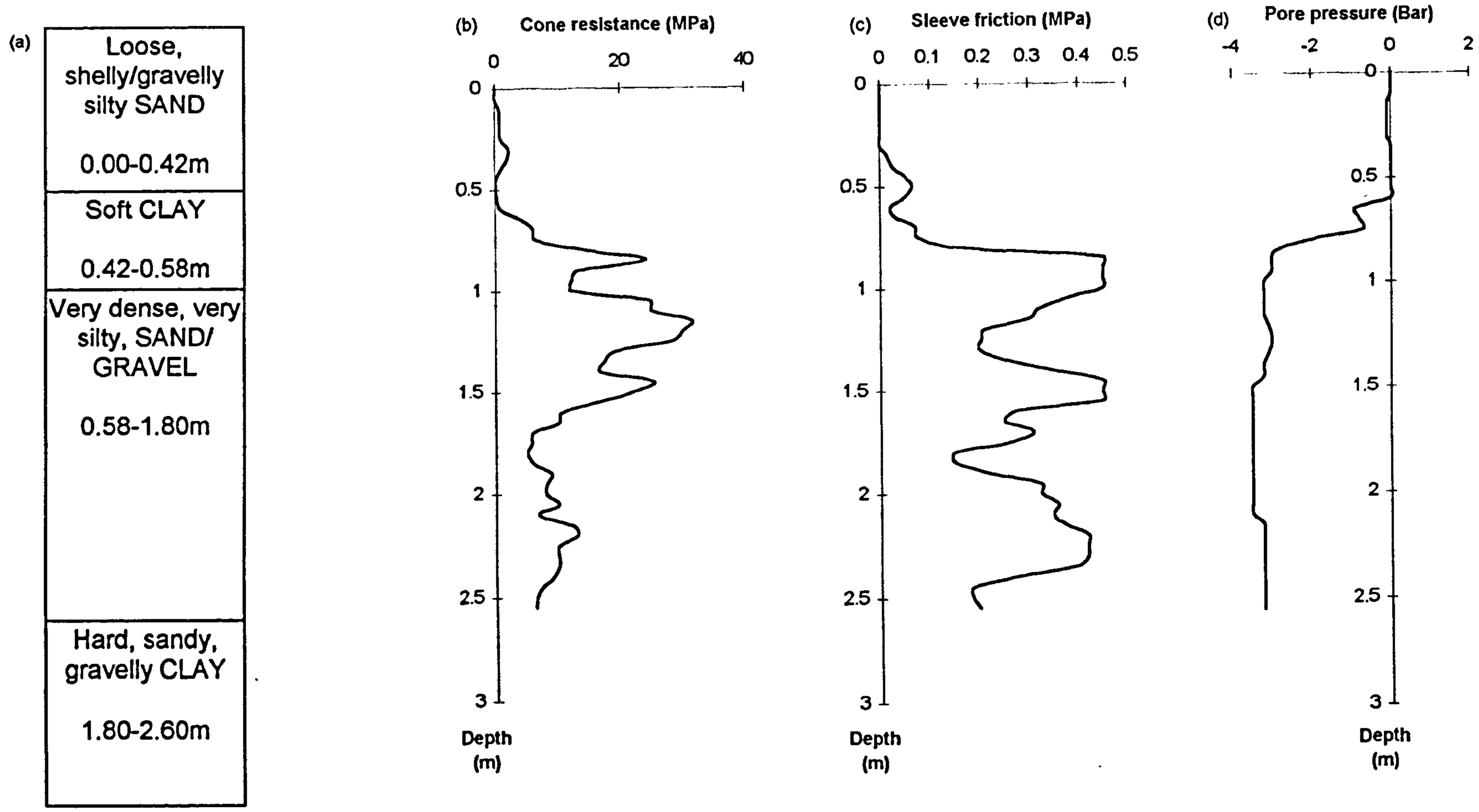

Figure 6.11. CPT2 profiles. (a) Estimated sediment type. (b) Cone resistance. (c) Sleeve friction. (d) Pore pressure.

significant change, from positive pressures close to zero to large negative pressures which coincide with the increase in both cone resistance and sleeve friction. These negative pressures are maintained throughout the very dense sand/gravel and the hard clay at approximately -3Bar, indicating the coarser sediment beds.

The classification plot (Figure 6.12(a)) identifies the overall trend of the CPT and the lithological boundaries can be identified. However the lower section of the very dense sand/gravel grades into the hard clay as opposed to a definitive boundary.

Depth interval (m)	Velocity (m/s) after Hamilton and Bachman (1982)	Density (Mg/m^3)	Impedance ($Mg/m^2/s$)	Two-way time (ms)	Reflection coefficient
0.00-0.42m	1750	1.9	3325	0.5	0.37
0.42-0.58m	1650	1.8	2970	0.2	-0.06
0.58-1.80m	1850	2.1	3885	1.3	0.13
1.80-2.60m	1925	2.2	4235	0.8	0.04

Table 6.3. CPT 2 parameters

The loose sand and clay layers are difficult to distinguish from the seabed return (0.5ms) on the boomer profile for CPT2 shown in Figure 6.12(b). The profile also identifies the top of the hard clay which is a high amplitude broken reflector; the seismic character is chaotic and penetration appears to be limited. The synthetic seismogram shows the high amplitude seabed return and also a high amplitude more complex return which indicates the top of the very dense sand. At the scale of the boomer record these layers are very difficult to distinguish. This inability to separate the layers on the boomer record strengthens the case for recording analogue data digitally which would allow more manipulation of the seismic data.

6.6.3. CPT 3 (4 HNO)

CPT 3 is located approximately 500m north of the other 3 CPTs discussed in this chapter and consists of sands overlying gravel and hard clay as shown in Figure 6.13(a). The upper loose and soft clayey sand sections of the CPT are

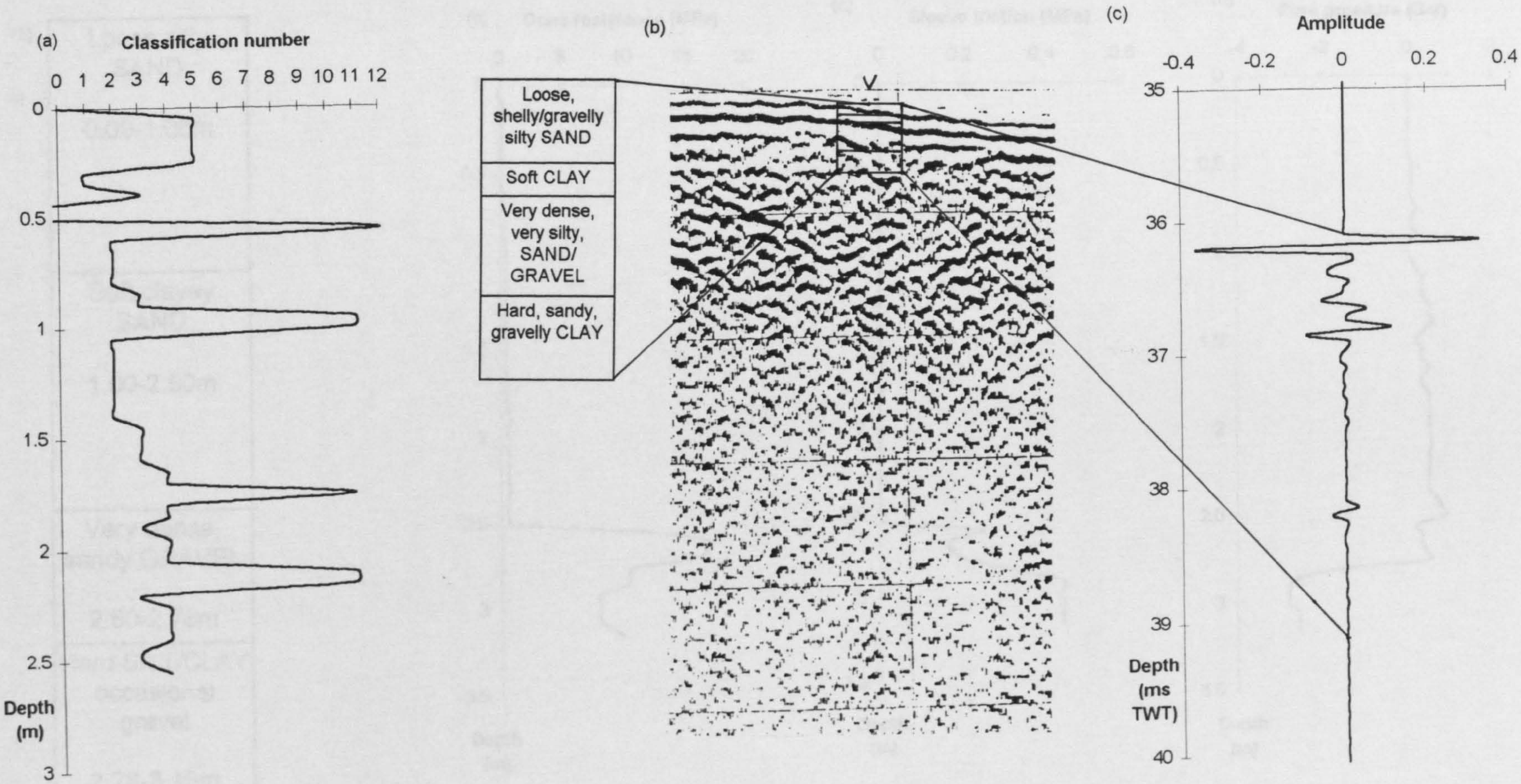

Figure 6.12. CPT2 profiles. (a) Sediment classification. (b) Boomer profile, vertical scale; 1cm = 2.6ms TWT. (c) Synthetic seismogram.

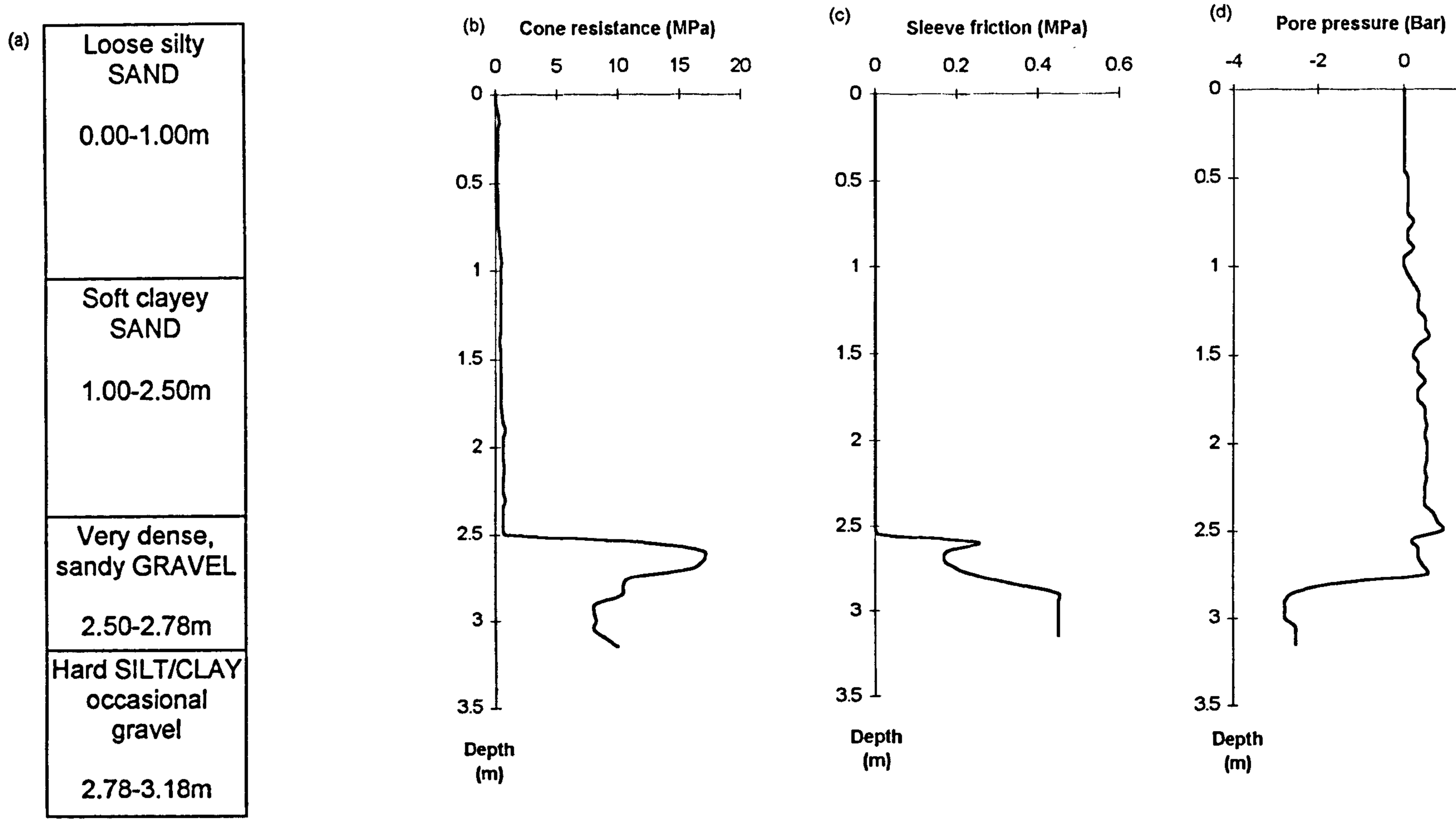

Figure 6.13. CPT3 profiles. (a) Estimated sediment. (b) Cone resistance. (c) Sleeve friction. (d) Pore pressure.

characterised by cone resistance values of less than 1MPa (Figure 6.13(b)), and low sleeve friction values of less than 0.01MPa (Figure 6.13(c)). The cone resistances peak at 17.5MPa within the very dense gravel layer, and in the hard clay the cone resistance values fall between 8 and 10MPa. The pore pressure profile in Figure 6.13(d) fluctuates around and above zero in the sands where there is finer material. Within the hard clay the pore pressure reduces sharply to -3Bar with a corresponding increases in cone resistance and sleeve friction, this evidence may relate to deposits of coarser sediments.

The classification profile does not distinguish between the loose silty sand and the soft clayey sand in Figure 6.14(a).

Depth interval (m)	Velocity (m/s) after Hamilton and Bachman (1982)	Density (Mg/m^3)	Impedance ($Mg/m^2/s$)	Two-way time (ms)	Reflection coefficient
0.00-2.50m	1650	1.8	2970	3	0.32
2.50-2.78m	1850	2.1	3885	0.3	0.13
2.78-3.16m	1925	2.2	4235	0.4	0.04

Table 6.4. CPT 3 parameters

The boomer profile displayed in Figure 6.14(b) does not distinguish clearly between the upper units of loose silty sand and soft clayey sand. The dense gravel and hard silt/clay layers are delineated by a high amplitude reflector below which the seismic character is more disordered. The synthetic seismogram in Figure 6.14(c) shows two reflecting surfaces, the seabed and the top of the very dense gravel 3ms below seabed. These two boundaries are clearly seen on the boomer profile.

6.6.4. CPT 4 (13 OLU)

CPT 4 lies in the deepest water (35m) and is the westernmost test location. The estimated succession through the CPT is from loose sand to dense gravel overlying stiff clay (Figure 6.15(a)). The cone resistance profile shown in Figure 6.15(b) identifies a peak of 14MPa in the dense gravel and a second peak of 10MPa in the stiff, shelly silt/clay. Also within this silt/clay layer is a peak in sleeve friction (Figure

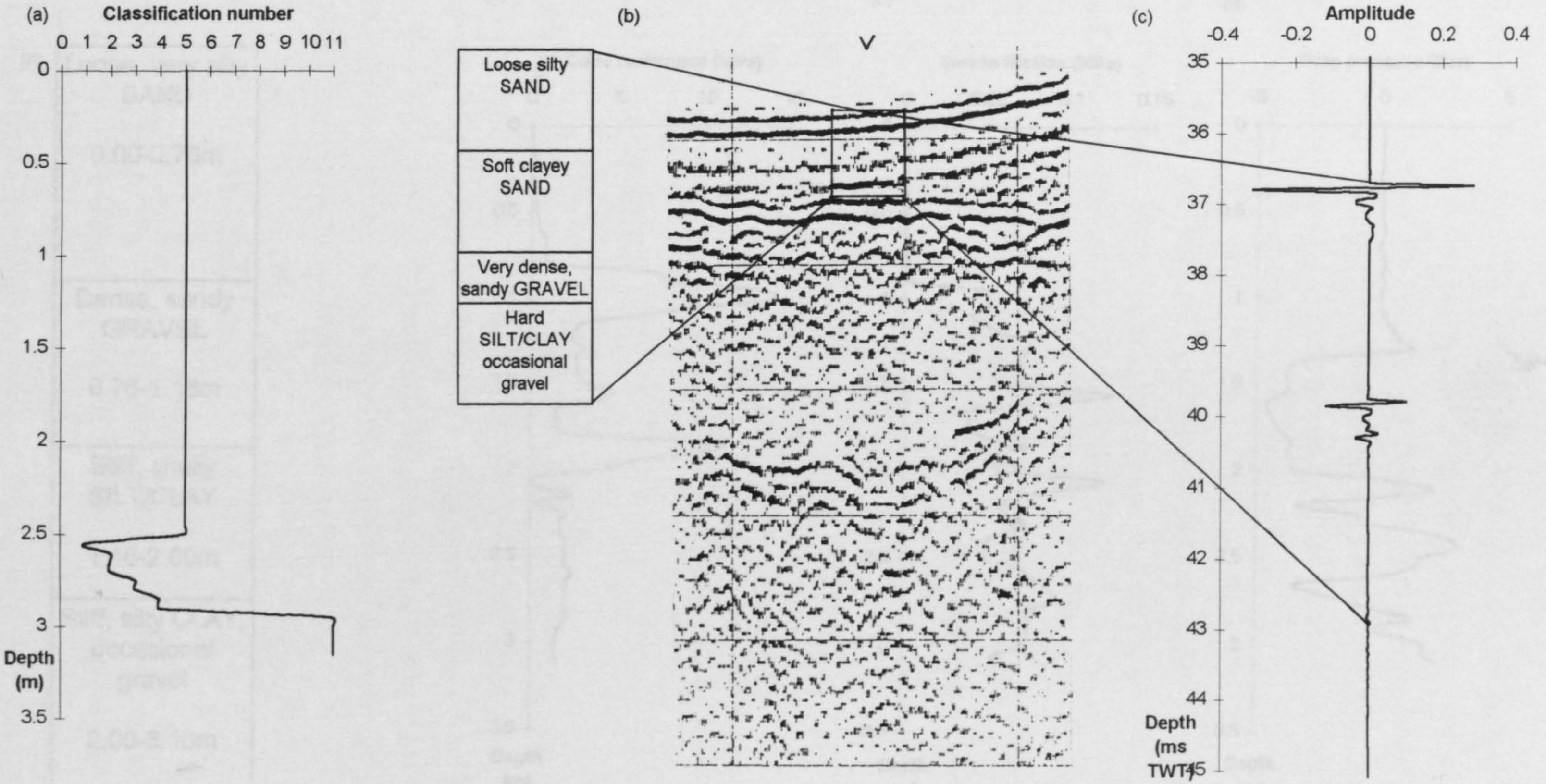

Figure 6.14. CPT3 profiles. (a) Sediment classification. (b) Boomer profile, vertical scale; 1cm = 2.6ms TWT. (c) Synthetic seismogram.

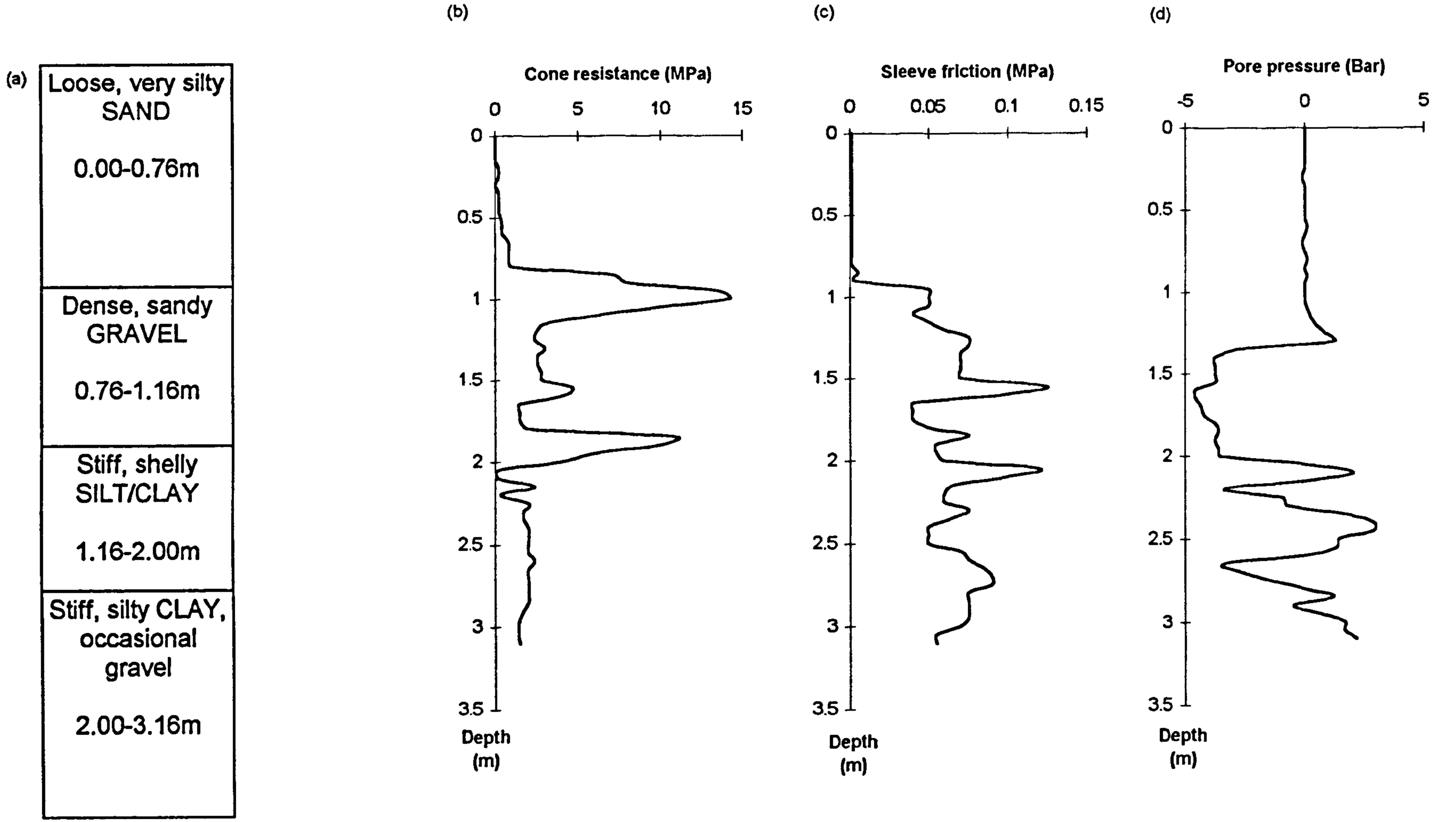

Figure 6.15. CPT4 profiles. (a) Estimated sediment. (b) Cone resistance. (c) Sleeve friction. (d) Pore pressure.

6.15(c)) which corresponds to the trough of cone resistance in the silt/clay layer. The pore pressure profile in Figure 6.15(d) in this CPT also shows very low pore pressures close to zero within the sand and gravel units indicating well drained sands and gravels. The stiff clay exhibits pore pressures down to -4Bar and the positive peaks may indicate gravel; the peaks occur at a rate of two cycles in 0.5m, therefore the gravel thickness may be around 25cm.

The classification output (Figure 6.16(a)) shows a good correlation between the lithological boundaries and the classification estimates. The silty sediments can be delineated from the stiffer clays.

Depth interval (m)	Velocity (m/s) after Hamilton and Bachman (1982)	Density (Mg/m^3)	Impedance ($Mg/m^2/s$)	Two-way time (ms)	Reflection coefficient
0.00-0.76m	1750	1.9	3325	0.9	0.37
0.76-1.16m	1800	2.0	3600	0.4	0.04
1.16m-3.16m	1850	2.1	3885	2.2	0.04

Table 6.5. CPT 4 parameters

The base of the upper layer of sand can be identified on the boomer record in Figure 6.16(b) close to the seabed. The dense gravel and stiff clay can be identified by a strong continuous reflector and the lack of reflector continuity below. The stiff clay layers are characterised by more broken reflectors, this may be due to the coarse gravel. The synthetic seismogram in Figure 6.16(c) also shows a high amplitude seabed return and identifies the corresponding layers.

6.7. Empirical inter-relationships

Hepton (1989) used measurements of shear wave velocity, cone resistance and pore pressure made on the same sediment sample to investigate the relationships between shear wave velocity and cone resistance. Hepton (1989) assigned a single value of shear wave velocity and cone resistance for every 1m of penetration and produced several relationships.

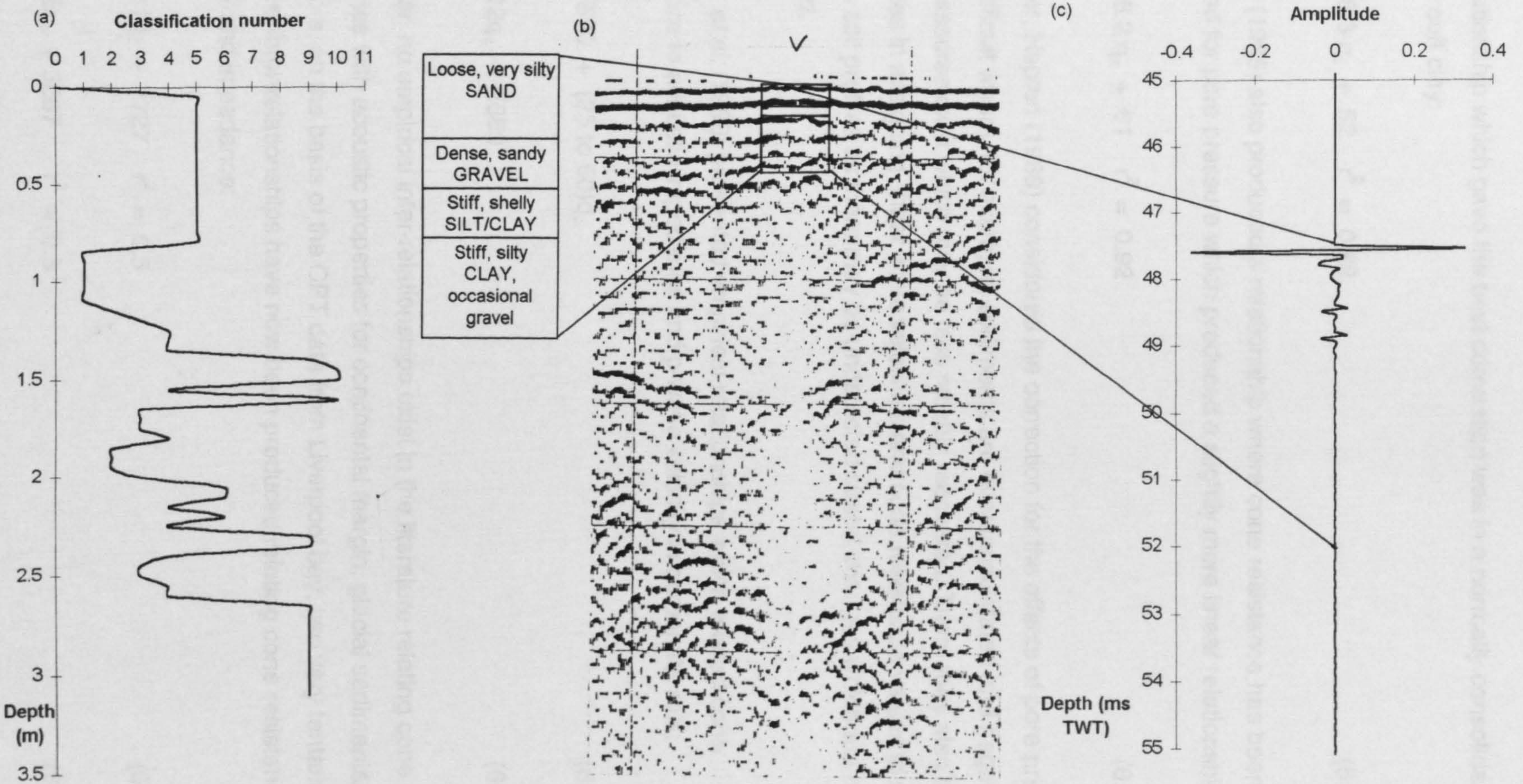

Figure 6.16. CPT4 profiles. (a) Sediment classification. (b) Boomer profile, vertical scale; 1cm = 2.6ms TWT. (c) Synthetic seismogram.

The relationship which gave the best correlation was in a normally consolidated uniform soft clay:

$$V_s = 96.3\, q_c + 52 \quad r^2 = 0.89 \qquad (6.5)$$

Hepton (1989) also produced a relationship where cone resistance has been corrected for pore pressure which produced a slightly more linear relationship:

$$V_s = 96.2\, q_c + 61 \quad r^2 = 0.92 \qquad (6.6)$$

However, Hepton (1989) considered the correction for the effects of pore pressure to be difficult where, for example, sediments are overconsolidated and negative pore pressures exist which may be less reliably recovered. There may also be difficulties in assigning shear wave velocities and cone resistance values in non-uniform soil profiles as there may be undetected stratal changes which are not included.

Nauroy *et al.* (1998) presented empirical relationships which related cone resistance to acoustic impedance and p-wave velocity in carbonate silts:

$$V_p = 1500 + (25 \text{ to } 60)q_c \qquad (6.7)$$

$$Z = 112q_c + 2689 \qquad (6.8)$$

However, no empirical inter-relationships exist in the literature relating cone resistance with acoustic properties for continental margin, glacial sediments. Therefore, on the basis of the CPT data from Liverpool bay, two very tentative empirical inter-relationships have now been produced relating cone resistance to velocity and impedance:

$$V_p = 11q_c + 1727 \quad r^2 = 0.5 \qquad (6.9)$$

$$Z = 55q_c + 3267 \quad r^2 = 0.5 \qquad (6.10)$$

All the cone resistance, velocity and impedance data were collated for CPTs 1 to 4 and plotted on two graphs, Figures 6.17(a) and 6.17(b) respectively. The linear

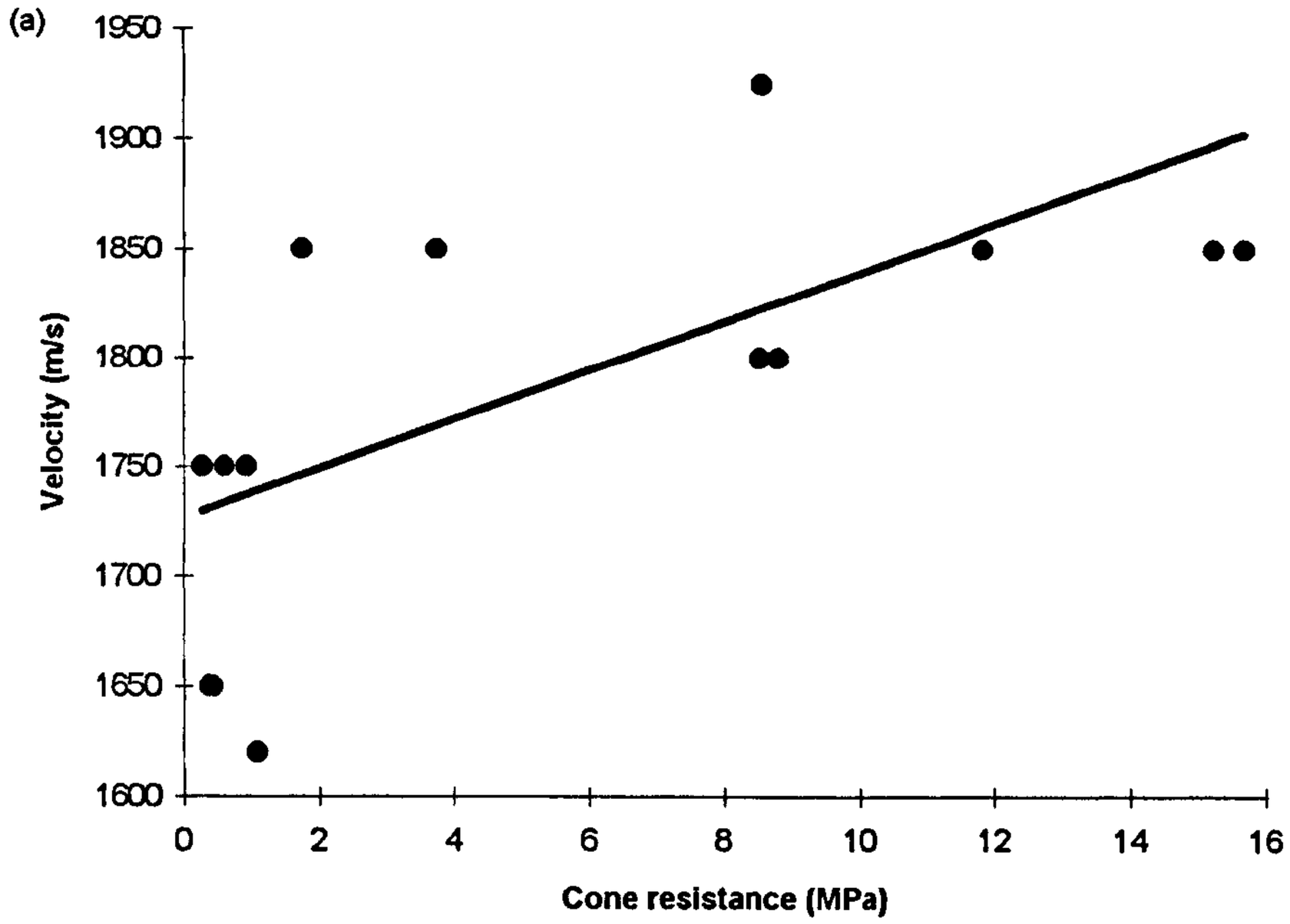

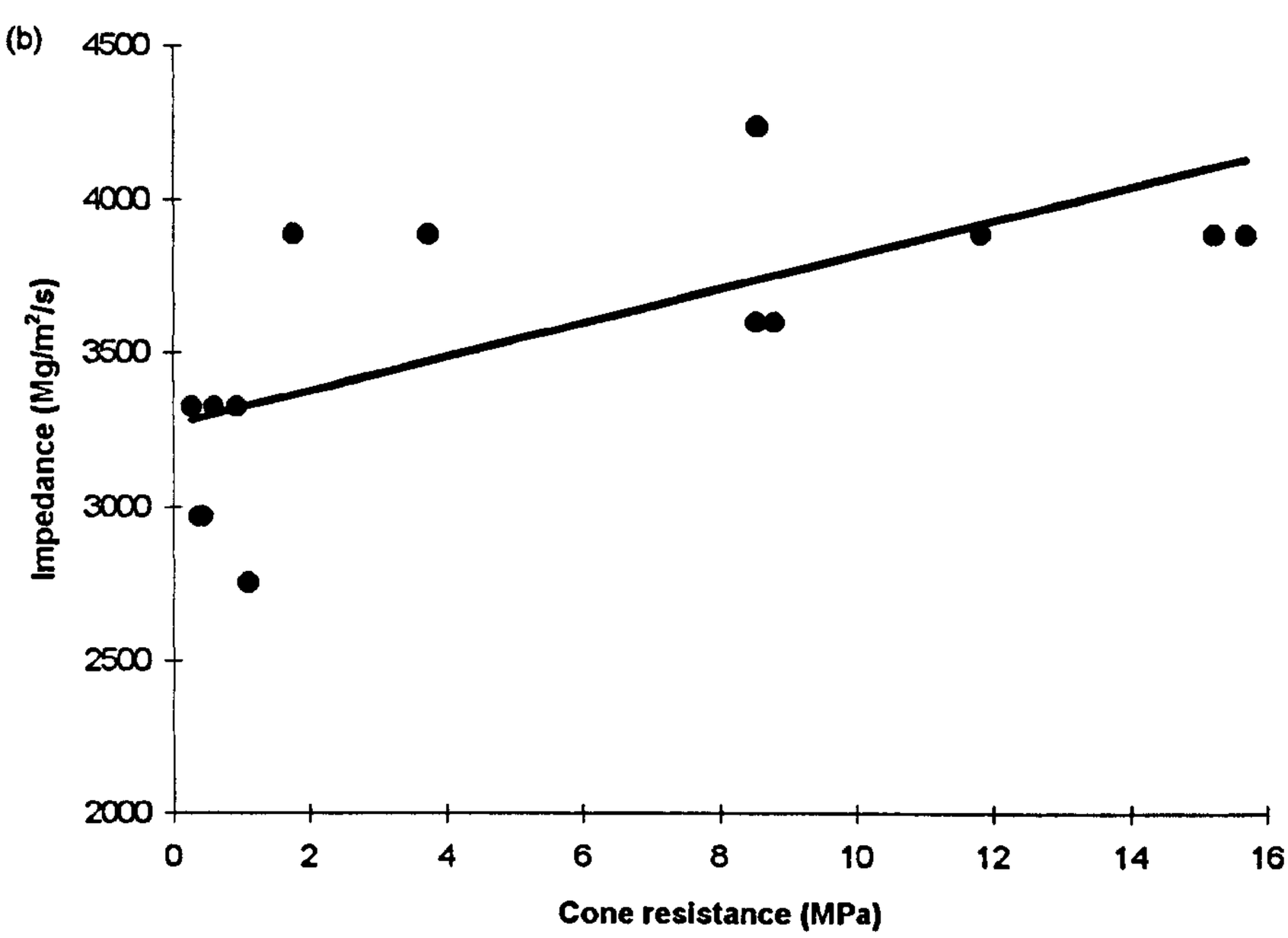

Figure 6.17. Prediction of empirical inter-relationships. (a) Cone resistance-velocity. (b) Cone resistance-impedance.

trend was plotted and equations 6.9 and 6.10 were produced. The correlation coefficients predict a tentative relationship does exist, however for optimum results the dataset would need to consist of concurrent measurements of cone resistance, velocity and density. The results from PCPT11 in Chapter 7 will be applied to the inter-relationships above to test their viability and applicability.

6.8. Summary

In this chapter it has been shown that by using a coarse classification system CPT data files can be interpreted quickly and a sediment type estimated. The data have further shown that a useful and realistic image of the seismic response can be generated for comparison with seismic data. This indicates that CPT data could be applied to forward modelling of high resolution seismic data in the 0-100m subseabed zone. It is this zone that is often inadequately sampled during well logging but it is this section that is critical in terms of engineering investigations.

The synthetic seismograms for each CPT proved the method to be useful, particularly when dealing with an analogue seismic record where it is difficult to distinguish the layers. Any testing of sensitivity, in the manner of Chapter 5, was difficult as there were no concrete inter-relationships with which to confidently relate the cone resistance, sleeve friction and friction ratio to the seismic response. The block-averaging process was used in the CPT to produce the synthetic seismogram. This process involved dividing the CPT profile into blocks based on major lithology, therefore only the gross lithological boundaries are delineated. This process is useful for producing an overall picture of the major subsurface lithology without the complications of the finer layering which may be generated from finer scale changes of lithology within a unit or by composites of reflectors or smaller scale peg-leg multiples.

The synthetic seismograms were also able to provide amplitude information on the lithology at seabed which is very difficult to discern on the analogue boomer record. As the synthetic seismograms were based on cone resistance and sleeve friction, the finer detail seen on the pore pressure profiles is not seen. It would be difficult, however, to attempt to relate pore pressure directly to the acoustic properties due to the amount of potential unreliability involved in the measurement of excess pore pressure.

The inter-relationships which have been produced in this study are a first attempt at trying to relate the cone resistance directly to the seismic response. No attempt has been made to make any serious comment on their applicability due to their tentative nature. The aim in producing the relationships was to assess the general correlation of cone resistance and velocity in the sediments of Liverpool Bay.

CHAPTER 7

CASE STUDY - WEST OF SHETLAND

7.1. Introduction

Chapters 5 and 6 have proposed and presented integrated methods of interpreting data collected within a marine geotechnical/geophysical investigation. The methods for modelling seismic data have been applied to aid integration of physical property groundtruth data into the seismic interpretation. This chapter aims to test these interpretation techniques on a commercial dataset where both relevant geotechnical and high resolution seismic reflection data have been acquired. An attempt will be made to validate seismic facies analysis through the use of forward models. This will be supplemented by the production and interpretation of seismic attributes to attempt to characterise physical properties seismically. The dataset chosen for this part of the study is from the West Shetland slope. The dataset was chosen to take advantage of the large geotechnical and geophysical dataset collected from a deepwater, glacially influenced environment.

The initial part of this chapter presents background information on the site and contains a detailed description of the geological history of the area and an in-depth review of the Tertiary-Quaternary succession. This level of detail is necessary to act as an aid to understanding and interpreting the geophysical and geotechnical data. Within the interpretation part (Section 7.4) of this chapter the results from each method of investigation will be presented and a description of the integrated datasets will be presented (Section 7.6). The purpose of this integration is to assess the use and application of physical properties in the interpretation of high resolution seismic data. In particular this part of the research aims to assess the methods tested in Chapters 5 and 6 and to assess the use of seismic facies analysis for high resolution seismo-acoustic data interpretation. The role of complex seismic attributes in association with physical property discrimination is also tested within the integration.

7.2. Site background

Exploration in the North Sea has slowed significantly in recent years. However, with the advance of technologies such as directional drilling, previously uneconomical reservoirs are able to be developed and drilled from the existing infrastructure.

The search for reserves though has now extended out onto the continental slope and into deeper water and harsher environments. One such area is on the UK Atlantic margin to the west of the Shetland Islands. This area has, in recent years become a focus of attention for the oil industry and is designated as a "Frontier Area". This research project concentrates on two subareas (fields) within the Frontier Area on the West Shetland Slope. These are called Foinaven and Schiehallion, both approximately 150km west of Shetland, as shown on Figure 7.1(a), Figure 7.1(b) shows the bathymetry of the study area. As previously mentioned, the aim of choosing two areas close together at this location was to make it possible to take advantage of the large volume of available geophysical, and more particularly geotechnical, information.

Speculative surveys using state of the art deep seismic methods have revealed potentially large oil reserves on the West Shetland continental margin. However, in exploitation terms the environment is significantly different to that of the North Sea, the most obvious differences being water depth and the open Atlantic exposure. Previous developments in the area have been concentrated in the east, in the Clair Field (BP), which is situated on the Rona Ridge in water depths of around 200m. The Foinaven and Schiehallion areas which are being investigated in this study lie in water depths of between 400m and 600m.

Adding to the challenge of this environment, the geology and geophysics of the area, particularly the Quaternary and late Tertiary succession, have not previously been well documented. However, in recent years with the advent of more concentrated hydrocarbon exploration, this situation is rapidly changing. Early work in the area was carried out by the British Geological Survey and others investigating the deeper geology. More recent work on the Tertiary-Quaternary stratigraphy has been published by various authors notably Damuth and Olsen (1993), Stoker *et al.* (1993a) and Paul *et al.* (1993) all of which seek to improve the understanding of the geological and geotechnical environment of the area.

Figure 7.1(a). West of Shetland location map.

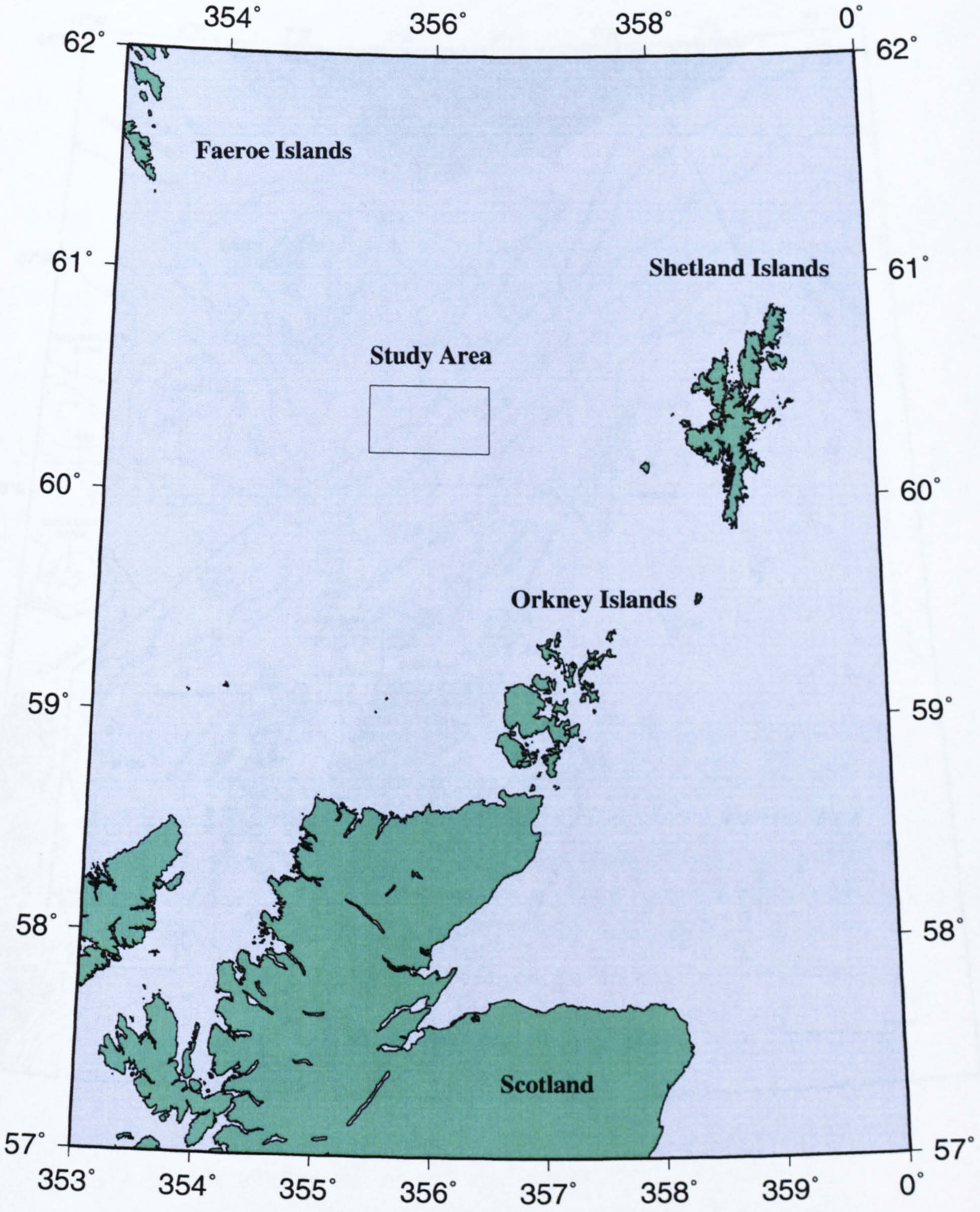
354°
356°
358°
0°
62°
62°
Faeroe Islands
61°
61°
Shetland Islands
Study Area
60°
60°
Orkney Islands
59°
59°
58°
58°
Scotland
57°
57°
353°
354°
355°
356°
357°
358°
359°
0°

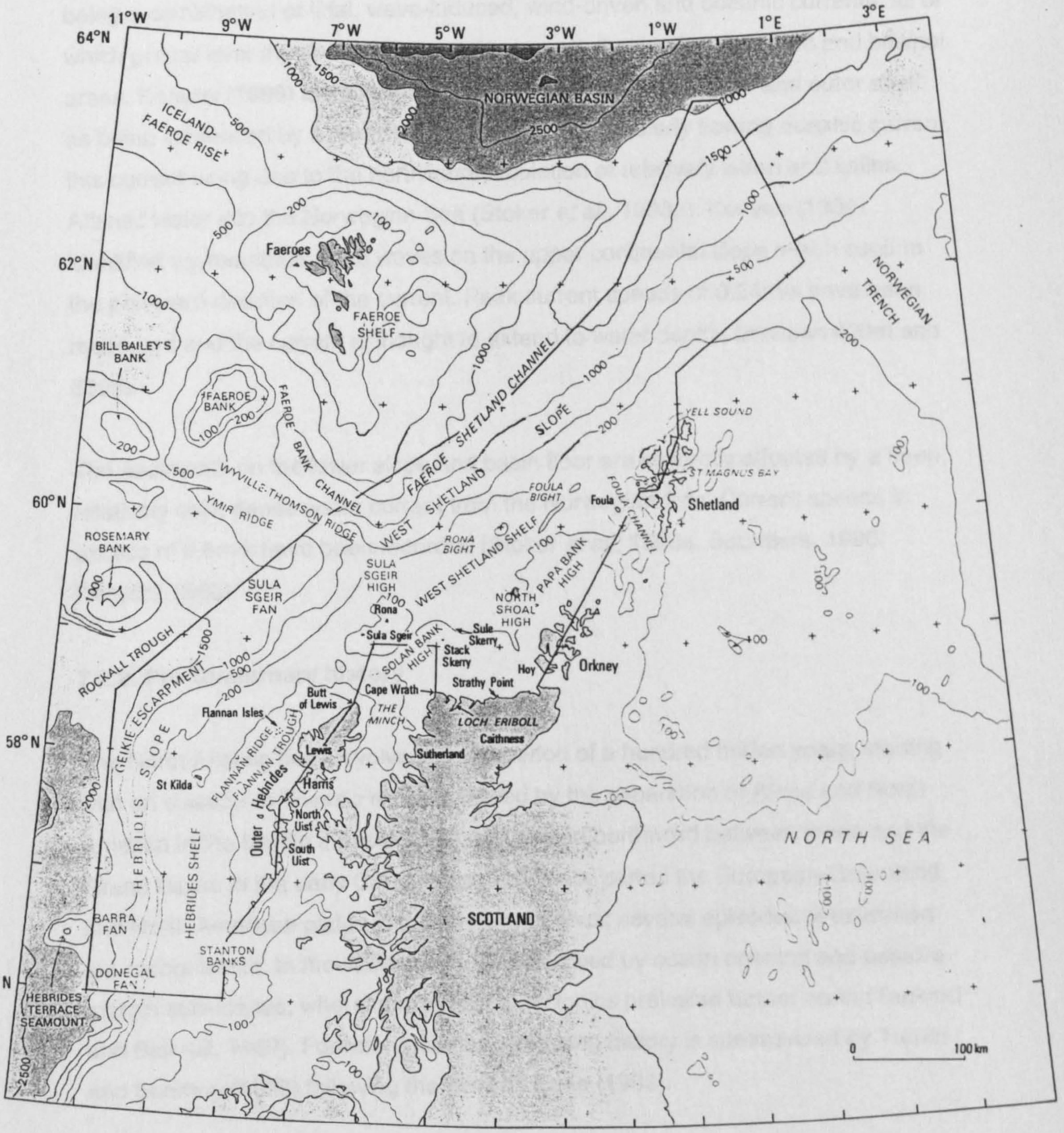

Figure 7.1(b). Bathymetry map for the continental margin, north-west of the UK (after Stoker *et al.*, 1993).

7.2.1. Oceanographic regime

Stoker *et al.* (1993a) identify primary oceanographic influences on sedimentation as being a combination of tidal, wave-induced, wind-driven and oceanic currents, all of which prevail over the shelf, with oceanic currents dominating the slope and basinal areas. Kenyon (1986) identifies the sediments on the upper slope and outer shelf as being influenced by a persistent, northerly/north-easterly flowing oceanic current, this current being due to the northward circulation of relatively warm and saline Atlantic water into the Norwegian Sea (Stoker *et al.*, 1993a). Kenyon (1986) identified asymmetrical sand waves on the upper continental slope which confirm the poleward direction of the current. Peak current speeds of 0.84m/s have been measured and the current is thought to extend to water depths between 400m and 600m.

The sediments on the lower slope and basin floor are indirectly affected by a deep, relatively cold, dense water current from the Norwegian Sea. Current speeds in excess of 0.6m/s have been recorded (Stoker *et al.*, 1993a, Saunders, 1990, Kenyon, 1986).

7.2.2. Pre-Quaternary history

The North Atlantic basin evolved over a period of a hundred million years, starting with an episode of Triassic rifting, followed by the separation of Africa and North America in the Middle Jurassic. The tear spread northward between Iberia and the Grand Banks in the early Cretaceous, and finally parted the European-Greenland and North American plates in the late Cretaceous; several episodes of extension are recognisable. In the south, rifting was followed by ocean opening and passive margin subsidence, whereas extensional tectonics prevailed further north (Tankard and Balkwill, 1989). For reference, the stretching history is summarised by Turner and Scrutton (1993) following the work by Earle (1989).

Margins such as those along the United States and Nova Scotia underwent much postrift or thermal subsidence that resulted in the deposition of a seaward thickening terrace wedge, which in places is more than 10km thick. These thick cover sediments effectively mask much of the underlying structure of the extensional basins. Margins with such deeply buried structure became known as

Atlantic type margins and were considered typical of this tectonic process. Elsewhere, the postrift cover is comparatively thin, permitting reconstruction of the extensional architecture and revealing a wide variety of styles (Tankard and Balkwill, 1988).

The predominantly rifted continental margin of NW Europe stretches over 3000km from Ireland to the Barents Sea and comprises sectors off Ireland (800km), off the UK and the Faeroe Islands (1000km), and off Norway (1200km). These Atlantic margins lie in waters as deep as 2500m, and in total area the margins cover 1.5 x 10^6 km^2 (Spencer and Eldholm, 1993).

The development of the United Kingdom continental margin is well understood apart from the origin of the Rockall Trough and Faeroe-Shetland Channel. In the Permo-Triassic, graben systems developed following the closure of the Hercynian Ocean and Haszeldine (1984) put forward a seafloor spreading hypothesis to explain the deep channels. Scrutton (1986) argues that the evidence for late Palaeozoic seafloor spreading is even more tenuous than that used to argue for younger oceanic crust. Furthermore, as a general rule for passive continental margins, seafloor spreading follows the youngest identified rifting event, and this is of Upper Jurassic-Lower Cretaceous age around the Rockall Trough. Nevertheless, it was probably at about late Palaeozoic time that the Rockall Trough and Faeroe-Shetland Channel were formed (Scrutton, 1986). Figure 7.2 is a structural map which identifies the structure on the northwest margin of the UK, the map shows the Rockall Trough and the Faeroe-Shetland Channel.

Continental rift basin development in the North Atlantic region continued intermittently throughout Jurassic and Lower Cretaceous time (see geological timescale in Figure 7.3). Scrutton (1986) maintains that from the geometry of spreading and plate movements the most satisfactory time for the Rockall Trough and Faeroe-Shetland Channel to have grown to their present width is between 105 Ma and 85 Ma. This growth probably involved some seafloor spreading in both areas (Scrutton, 1986).

Seafloor spreading started in the Labrador Sea 85 Ma. This moved the focus of the crustal separation away from the Rockall Trough. Rapid subsidence is then thought to have occurred in the Rockall Trough and Faeroe-Shetland Channel. The Tertiary

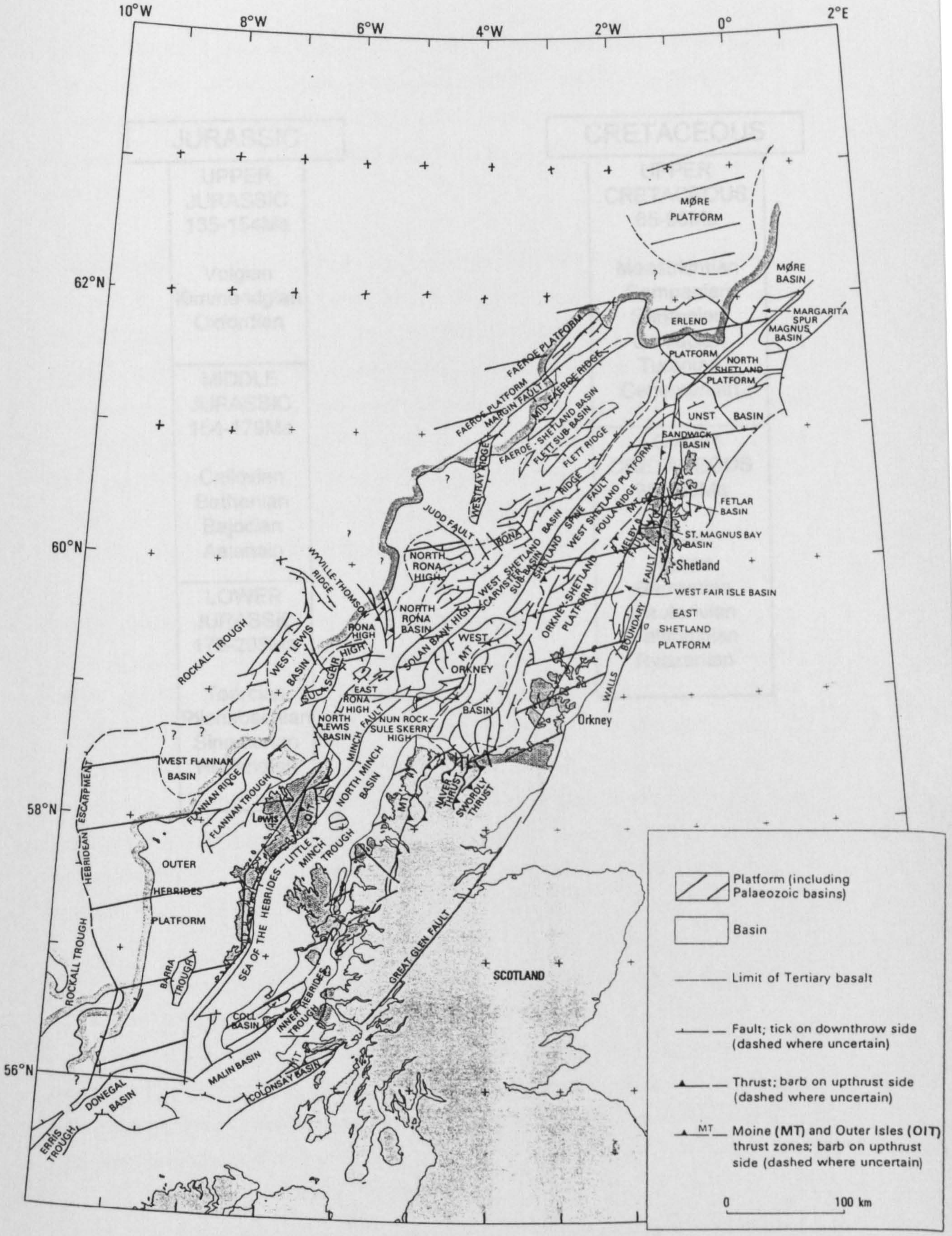

Figure 7.2. Structural map for the continental margin, north-west of the UK (after Stoker *et al.*, 1993).

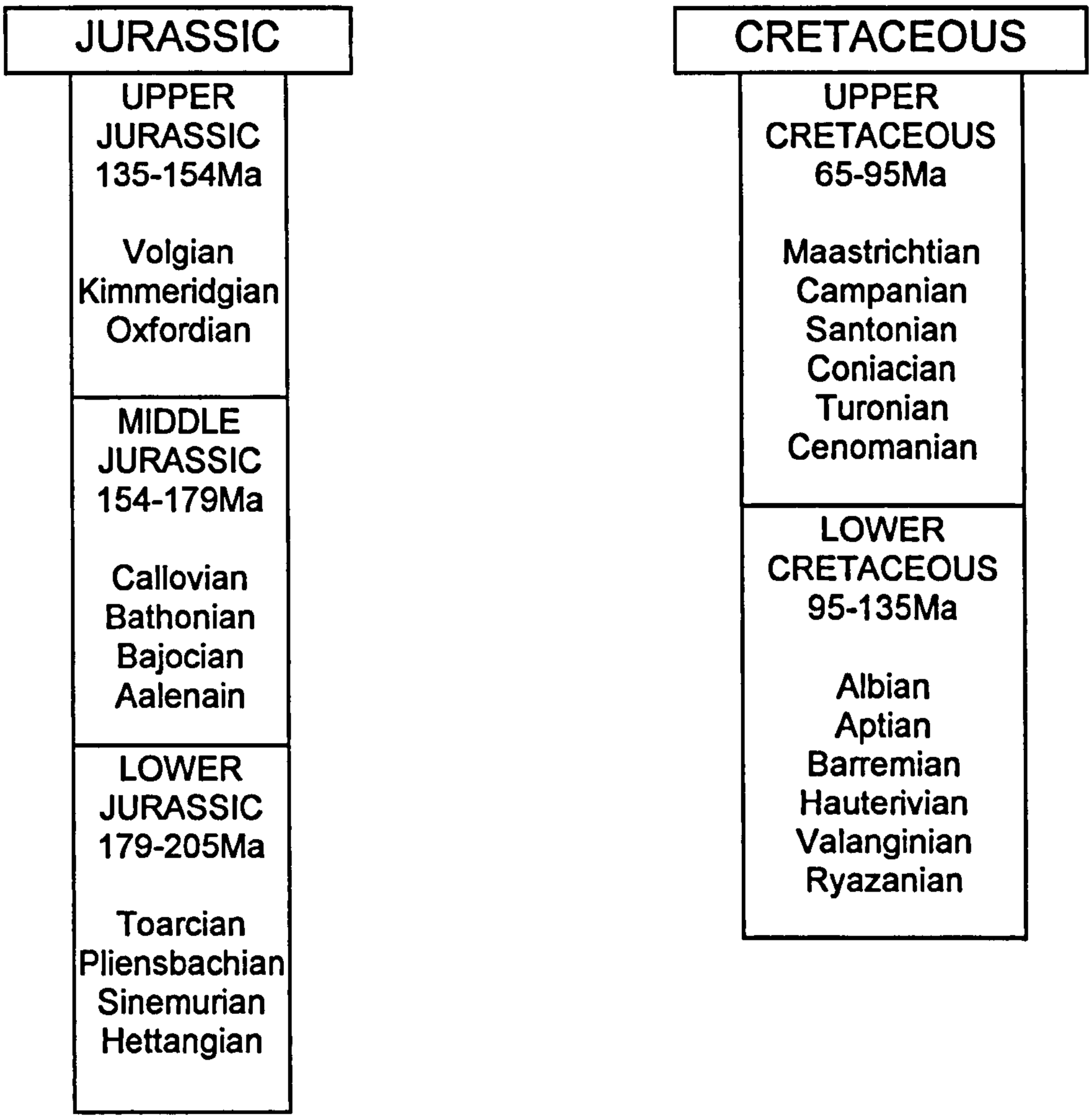

Figure 7.3. Jurassic - Cretaceous periods with series and stage geological timescales, Ma is millions of years.

episode was at its peak around 55-60 Ma and it was then that seafloor spreading moved from the Labrador Sea to the Reykjanes Ridge between the Rockall-Faeroes block and Greenland. Volcanic output during the Palaeocene and early Eocene covers much of the northern part of the Rockall Trough/Faeroe-Shetland area (Roberts *et al.*, 1983).

The Faeroe-Shetland Basin is an important area regarding Palaeocene deposition. Towards the end of the Palaeocene, the north-west margin of the Faeroe-Shetland Basin was inundated by lavas of the Faeroes Lower Series and to the north-east the Erlend and West Erlend volcanoes were erupting. The axis of the Faeroe-Shetland Basin has shifted north-west and the present major downwarp, elongate basin of post-Paleogene sediments overlain by Early Tertiary volcanics, is referred to as the Faeroe-Shetland Channel (Meadows *et al.*, 1987, Damuth and Olsen, 1993). The development of the slope aprons has been locally modified by intermittent failure of the slope (Stoker *et al.*, 1993a).

Tertiary sediments appear to form a seaward thickening wedge of subhorizontally bedded sediments which extend westwards from the outer shelf into the adjacent deep-water basins (Figure 7.4 is a Tertiary to Quaternary timescale for reference). However, Tertiary sediments are absent from the inner shelf. Within the basins the Palaeocene strata lie directly on top of the Cretaceous, but towards the eastern edge Tertiary strata oversteps onto Mesozoic, Permo-Triassic or older rocks. The inner shelf has remained a broad platform with the landward limit being erosional and partially controlled by faulting or flexure along the zone of crustal thinning (Stoker *et al.*, 1993a).

The Neogene succession appears to unconformably overlie the Paleogene, thickening westward on the outer shelf and upper slope, but with a variable thickness on the lower slope and in deep water. In the Faeroe-Shetland Channel, strong bottom currents have eroded and/or severely restricted the distribution of Neogene deposits, particularly at the southwestern end of the channel, where Paleogene rocks crop out locally.

A very prominent regional unconformity is observed throughout the region and represents a major sequence boundary that can be consistently traced from beneath the West Shetland Shelf downslope to the axis of the Faeroe-Shetland

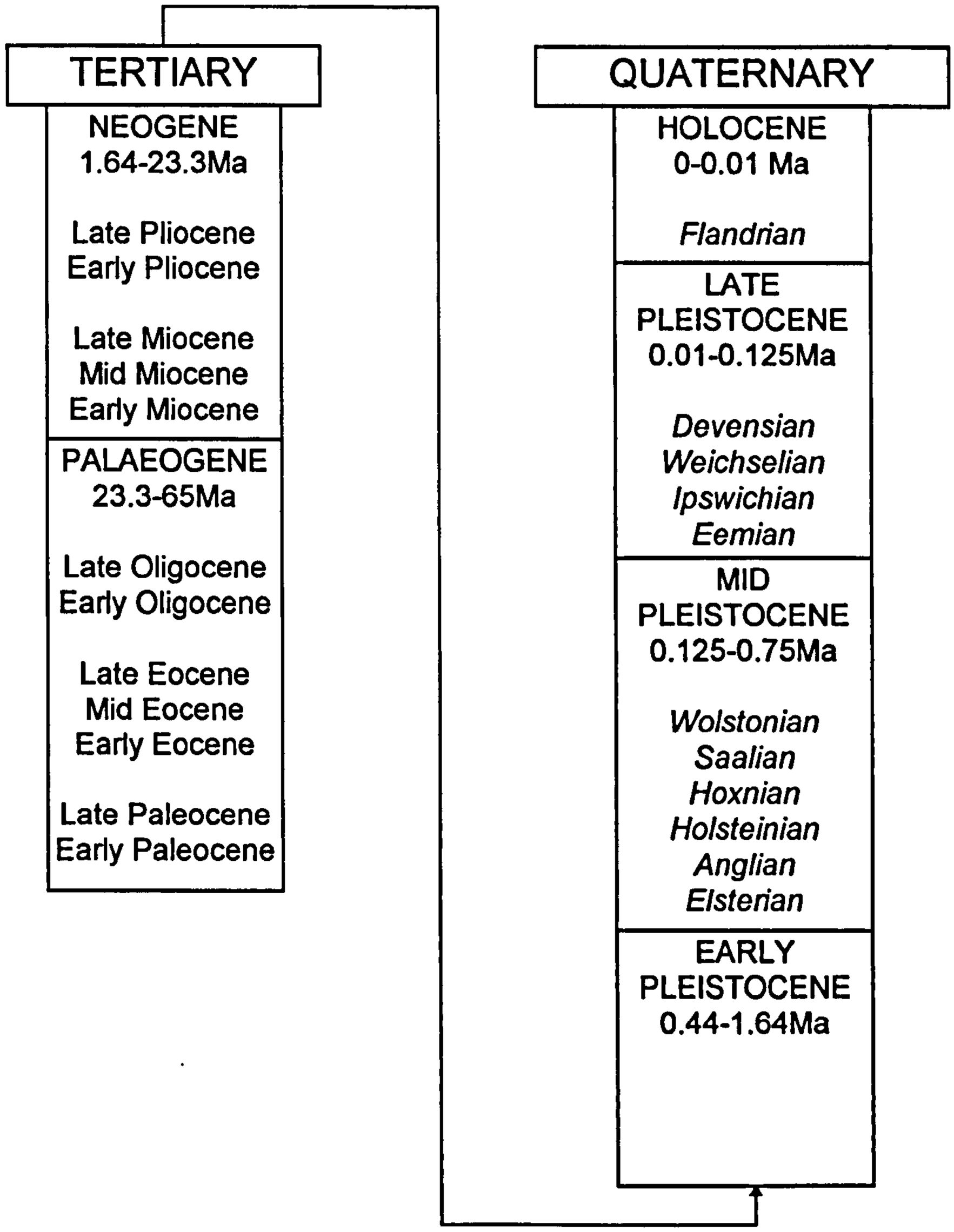

Figure 7.4. Tertiary - Quaternary epoch geological timescales, the stratigraphic ages in the Quaternary are in italics and Ma is millions of years.

Channel. This unconformity represents a major erosional surface at most locations, especially in the southwestern end of the channel. The unconformity is overlain by a clastic wedge of Miocene to Holocene sediments, which ranges in thickness from less than 60m beneath the channel floor to more than 400m beneath the upper continental slope.

The section above this unconformity generally shows highly reflective parallel, acoustically well stratified deposits that thin upslope beneath the middle of the continental slope (Damuth and Olsen, 1993). In contrast, the section below the unconformity is generally non-reflective to semi-transparent, and acoustic penetration is usually very limited. At many locations, groups of dipping reflectors with various orientations appear to represent steeply dipping sets of clinoforms, whereas at other locations the reflections show evidence of extensive faulting and deformation (Damuth and Olsen, 1993).

Damuth and Olsen (1993) attempted to explain the development of this unconformity, following lines of evidence from Stoker (1990a) and Stoker *et al.* (1991). They suggested that the unconformity may have formed in response to the initiation of intense bottom water flow from the Arctic to the North Atlantic. This was thought to have occurred after the separation of Greenland and Svalbard during the late Eocene to early Oligocene. The precise age of the unconformity is difficult to determine but a probable age is during the latest Oligocene or early to middle Miocene.

The Neogene-Quaternary clastic wedge above the prominent regional unconformity, is thickest beneath the present day upper slope, but rapidly thins basinward beneath the lower slope and Faeroe-Shetland Channel axis (Damuth and Olsen, 1993).

7.2.3. Quaternary and glacial history

Quaternary sedimentation has mainly been controlled by bottom current activity and the Quaternary glacial processes were important factors in deposition and erosion. These processes eroded shelf areas and deposited substantial prograding slope-front sequences which were subsequently modified by a variety of deep-water depositional processes, both downslope and parallel-to-slope.

Quaternary strata are widespread over the area with the thickest accumulations preserved on the upper to mid-slope. The overall geometry of the succession displays a marked shelf to basin asymmetry; a thin to locally absent and extensively eroded sediment cover on the inner shelf thickens to over 800m on the outer shelf to mid-slope. It is a relatively condensed sequence, generally <100m thick, on the floors of the deep water basins. This asymmetry reflects a seaward progradation of the shelf by up to 50km during the Pliocene-Pleistocene, although the shelf break has been locally eroded in the post-Anglian interval (Stoker *et al.*, 1993a).

During the Late Pliocene and Early Pleistocene, a lowered eustatic sea level may have controlled the development of a laterally extensive, prograding, lowstand wedge of deltaic and shallow-marine sediments along the outer shelf. Sediment was probably derived from the Scottish Highlands and Islands through intense weathering and erosion under warm, humid temperate, climatic conditions. These sediments may have been fluvially transported to the shelf edge (Hall, 1991, Stoker *et al.*, 1993a).

The climate deteriorated in a fluctuating manner during the Early Pleistocene (Boulton *et al.*, 1991), when glacial activity remained distal in character, as represented by ice-rafted debris. These climatic conditions persisted into the Mid-Pleistocene, until about 0.44Ma when major ice sheet activity first affected the area. The glaciated shelves display evidence of extensive erosion and deposition. At their maximum extent, the ice sheets extended, at least locally, out to the shelf edge, and delivered ice-marginal sediments directly to the slope (Stoker, 1990a). Debris flows and turbidites occasionally travelled the entire width of the slope, dumping substantial amounts of shelf-derived material on to the floor of the Faeroe-Shetland Channel (Stoker *et al.*, 1991).

Stoker and Holmes (1991) postulate that there is only direct evidence for two glaciations over North West of Britain, although the ages for these are unknown. However at least three episodes of widespread glacial activity are known to have occurred in this area (Stoker *et al.*, 1993a). Early Pleistocene evidence for distal glacial activity is in the form of ice-rafted debris at a time when the climate was becoming fluctuatingly colder. The first major episode of glaciation during the Mid Pleistocene has been correlated with the Anglian stage and the ice sheet may have reached the edge of the northern Hebrides Shelf and on to the Wyville-Thomson

Ridge (Stoker, 1988). The West Shetland Shelf appears to have been most affected by subsequent glaciations during the Devensian (Stoker *et al.*, 1993a, Stoker and Holmes, 1991, Bowen *et al.*, 1986).

Glacio-eustatic falls in sea level will have ultimately brought grounded ice to the shelf edge (Stoker *et al.*, 1991) depositing material straight onto the slope. Concurrently, icebergs periodically broke away from the ice front and melted, depositing glacially eroded sediment onto the deeper seabed. This is in contrast to the interglacial periods of higher sea level with hemipelagic sedimentation locally modified by bottom current activity.

The upper part of the West Shetland slope (200-800m) is dominated by mass-transport deposits, predominantly debris flows with some slumps and slides, that were apparently deposited during glacial cycles when sea level was low and an ice sheet extended to the shelf edge and supplied large quantities of terrigeneous sediment to the upper slope (Stoker, 1990a). In contrast to the upper slope, the middle to lower slope (800-1200m) seems to be dominated by glacial marine and hemipelagic sediments along with possible significant deposition by turbidity currents and related gravity-controlled flows. Particularly on the lower slope these deposits apparently incurred major reworking by contour-current activity.

7.2.4. Stratigraphic divisions

Three stratigraphic units, identified by BGS, are referred to within this area which require elucidation. These descriptions have been adapted from Stoker *et al.* (1993a) and from Holmes *et al.* (1991) and Stoker (1990a). Pre-Anglian, Morrison sequence (unit 1) has been identified which forms an outer-shelf to upper-slope prograding sediment wedge which thins downslope. Seismically the sequence consists of transparent and structureless to chaotic packages which are bounded by high-amplitude, laterally continuous reflectors. It is postulated that the sequence consists of mass-flow deposits.

During the Anglian to middle Devensian, the Morrison sequence (unit 2) has been described which also forms an outer shelf to slope prograding wedge up to 100m thick. The base of this sequence is erosive on the shelf and locally on the slope, and on the upper slope it has been disturbed and eroded by icebergs.

Seismically on the slope, lensoid packages have been identified which are bounded by moderate-to-high-amplitude, laterally continuous reflectors. Akhurst (1989) found that the lensoid packages are debris flow diamictons which are re-sedimented glacigenic material, and that the layered deposits comprise current-reworked, distal-glaciomarine sediments.

In the upper Devensian, Morrison sequence (unit 2) may be found due to evidence of the late Devensian ice sheet locally reaching the shelf edge sending mass flow deposits down the slope. The upper unit expected in the study area is of the MacAulay sequence deposited at the end of the Pleistocene and into the Holocene. This is an ice-distal slope-front to basin-plain covering which overlies the debris flows of the Morrison sequence (unit 2) discussed above. The unit consists of glaciomarine muds with scattered shells and dropstones and seismically the sequence is well-layered. Figure 7.5 is geological cross-sections which defines the West of Shetland slope.

7.3. Data acquisition

The geophysical data, in whose collection the author was involved, and the geotechnical data presented in this project were collected by Fugro-Geoteam Ltd. and Fugro Ltd. respectively on behalf of BP Exploration. This acquisition was part of the Atlantic Frontier Project (AFP) on the United Kingdom Continental Shelf (UKCS) Quadrants 204 and 205.

7.3.1. Geophysical data

The geophysical data were collected as part of a blanket survey which covered an area of approximately 950 km^2 (Hamilton, 1996). Four separate 'sensors' were used to collect information during the survey: swathe bathymetry, side scan sonar, deep tow boomer and mini-airgun. This project makes extensive use of the deep tow boomer seismic records and makes reference to the mini-airgun seismic data.

7.3.1.1. Deep tow boomer

A Huntec deep tow boomer (Figure 7.6) was used throughout the survey with the following specifications:

a.

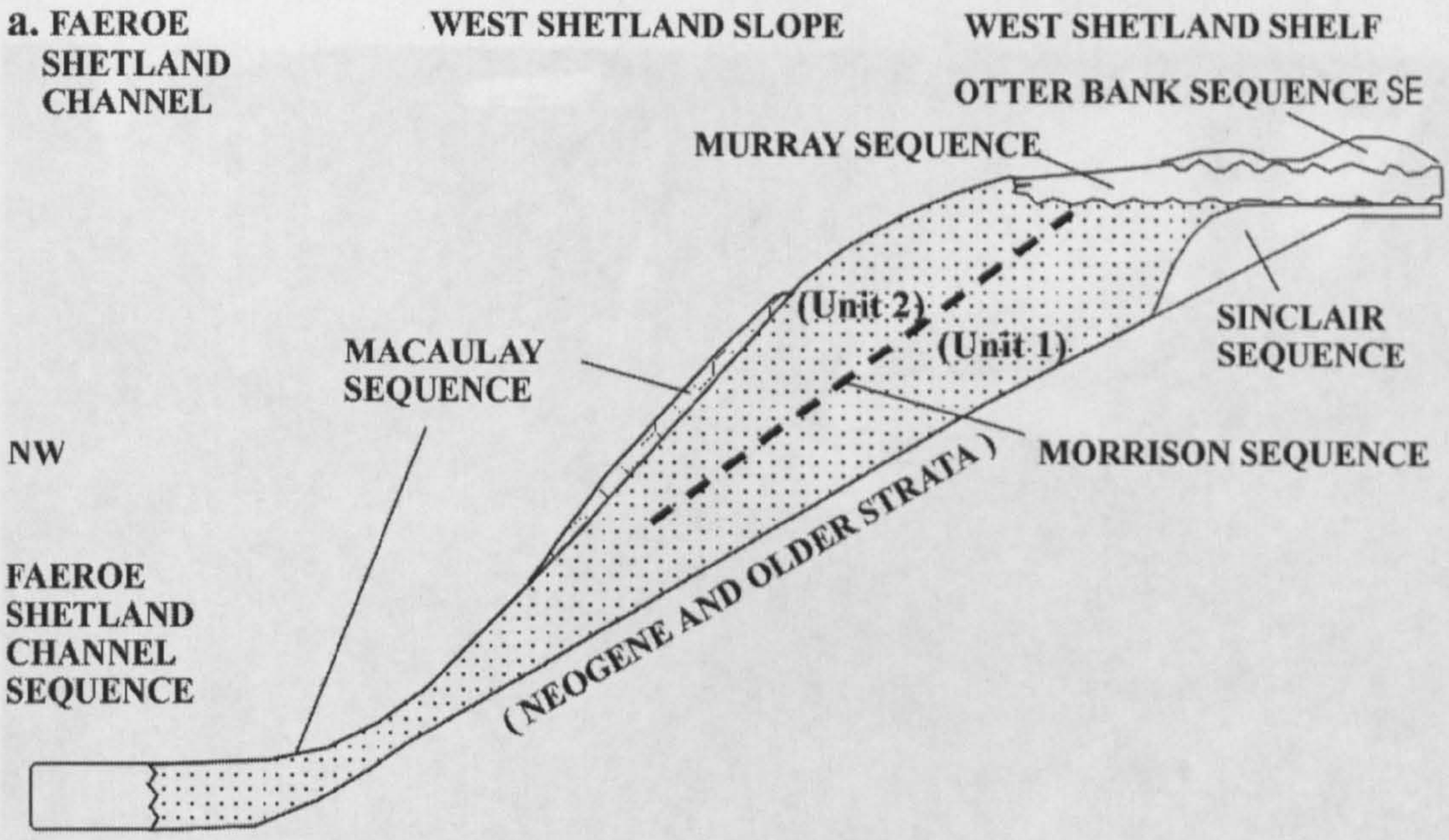

b

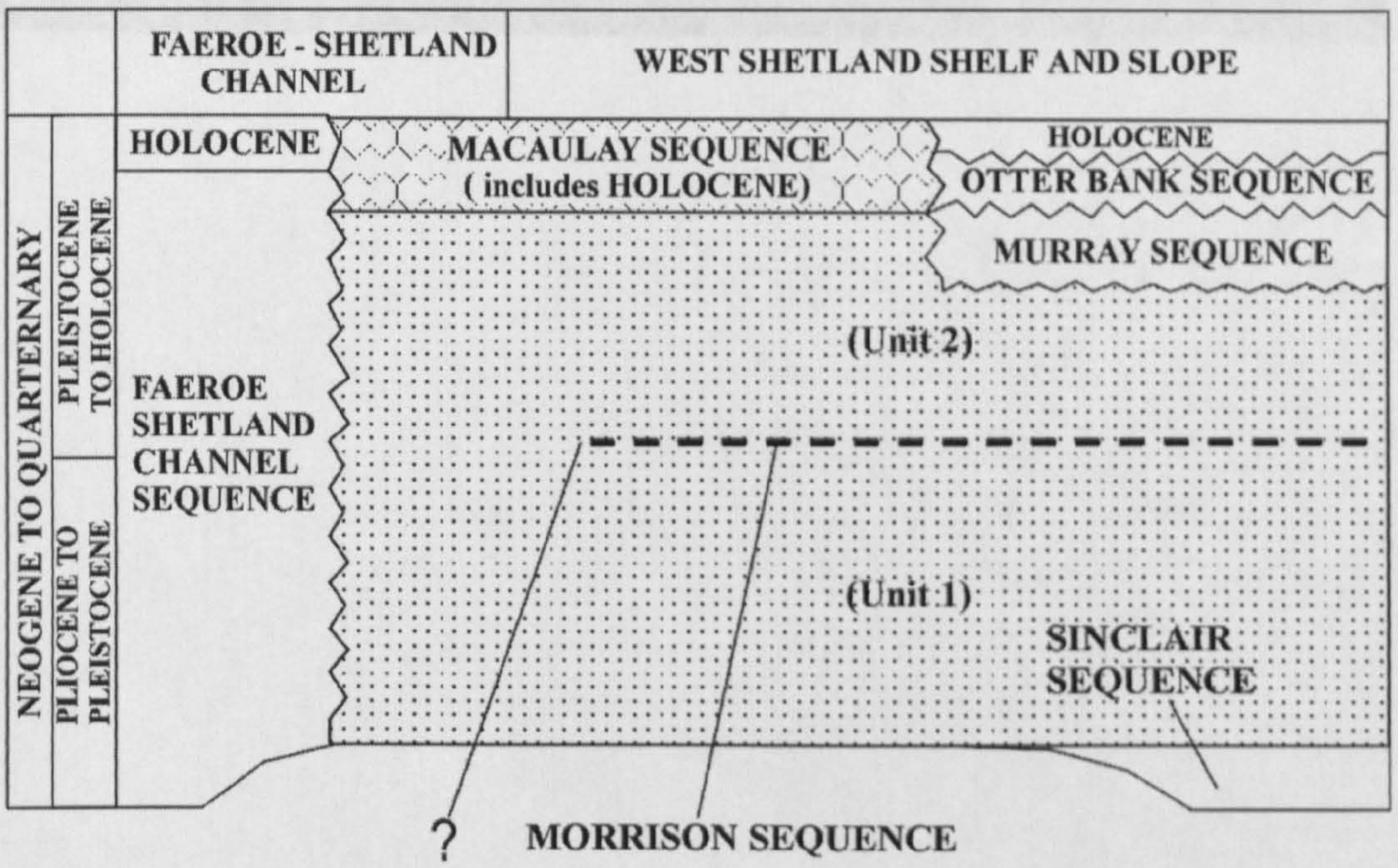

Figure 7.5. Stratigraphy of the upper Neogene to Quaternary succession on the West Shetland slope. (a) Seismic stratigraphy. (b) Relative age relationships of the seismic sequences (after Stoker *et al.*, 1991).

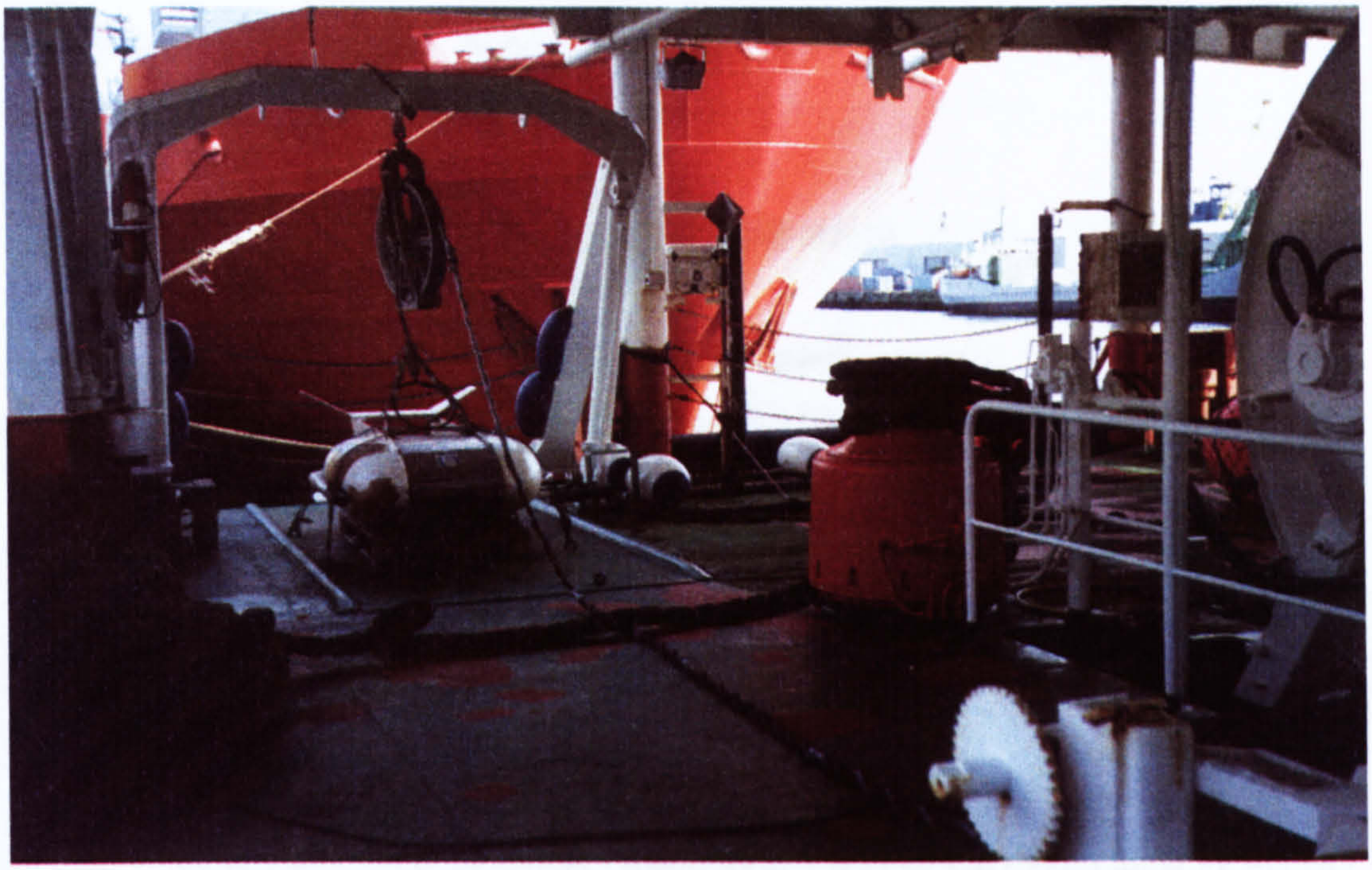

Figure 7.6. Huntec deep tow boomer.

Power	:	540 Joules
Pulse length	:	Approx. 0.5 ms
Hydrophone	:	LC10/32 internal
Fire rate	:	0.9 - 1.0 s
Bandwidth	:	0.2 - 5.5 kHz (-10dB down)
Filter	:	Low cut - 0.7 kHz
Layback	:	Water depth dependent
Towing depth	:	Up to 250 m below sea level

Recording:

Graphic display	:	Dowty Waverley 3710
Sweep	:	62.5 ms

The raw boomer signal was recorded onto a multi-channel DAT tape on a TEAC RD 130T PCM Data Recorder and onto a G-LOG digital acquisition system. Selected data from the DAT tapes were replayed through an Elics Delph 2 system at UWB, with a sampling rate of 20kHz. This sampling rate was chosen as it gave the optimum representation of the data. No digital source signature was available for the 540J pulse, and therefore, in order to reproduce the source for the forward models, the paper copy of the signature supplied by Fugro-Geoteam Ltd. was digitised. An automatic delay was applied to compensate for the water depth and to decrease the amount of processing time needed. The trigger signal from the DAT recorder was put through an external amplifier and pulse generator during playback. The digitised data were output in SEG-Y format.

The SEG-Y files were loaded and imported into the SierraSeis processing software at UWB. As the boomer data were single channel, only a limited number of standard processes such as filtering or gain control could be applied. The boomer was being used at its limits during the survey, due to the large water depths and long survey line length. Testing of various processes indicated that it was preferable to preserve as much of the original signal as possible.

7.3.1.2. Mini-airgun

The mini-airgun system was to enable deeper penetration to depths below seabed of up to 100m. However, this resulted in loss of resolution.

Energy	:	30 cu in
Pulse length	:	5 ms
Fire	:	Approx. 1.8 s
Bandwidth	:	30 - 800 Hz (-10dB down)
Filter	:	Variable Time Varying Filter (TVF)
Streamer	:	GECO programmable
Channels	:	5
Group interval	:	12.5 m
Shot interval	:	3.125 m
Layback	:	Approx. 32 m from back of ship to rear of first group

The airgun signal was also recorded onto DAT tape and onto the G-LOG system. Processing was carried out on the digitally collected airgun data by Fugro-Geoteam Ltd. Details of the processing can be found in Conway and Hill (1994); output of the processed data was in the form of Sierra SEG-Y.

The specifications listed above were in accordance with those recommended by UKOOA (1996) for rig site investigations.

7.3.2. Geotechnical characteristics from borehole data

Within the Foinaven field, six borehole locations were drilled and sampled with downhole piezocone penetration tests (PCPT) and borehole samples were recovered. A series of 'Wheeldrive Seacalf' PCPTs and boxcores were also collected. The locations of the geotechnical sampling points are shown in Figure 7.7.

In the Schiehallion field, five borehole locations were drilled as at Foinaven, and a further series of PCPTs, seabed vane and boxcore locations were sampled. Figure 7.7 shows the sample locations in the Schiehallion field (Hampson and Power, 1996).

Figure 7.7. Geophysical and geotechnical locations map.

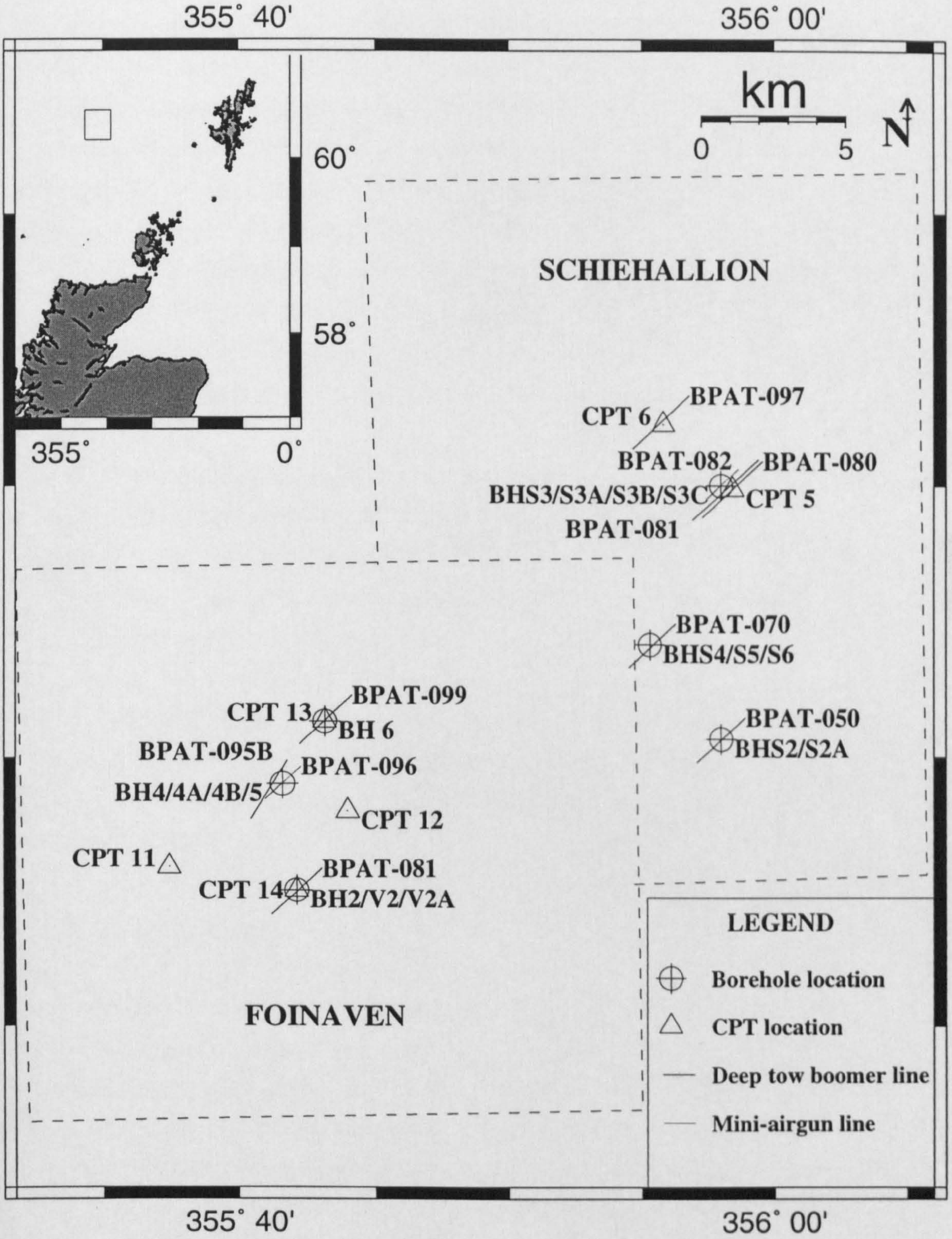
355° 40'
356° 00'
km
0
5
N
60°
58°
355°
0°
60° 30
60° 25
60° 20
60° 15
SCHIEHALLION
BPAT-097
CPT 6
BPAT-082
BPAT-080
BHS3/S3A/S3B/S3C
CPT 5
BPAT-081
BPAT-070
BHS4/S5/S6
BPAT-050
BHS2/S2A
BPAT-099
CPT 13
BH 6
BPAT-095B
BPAT-096
BH4/4A/4B/5
CPT 12
CPT 11
BPAT-081
CPT 14
BH2/V2/V2A
FOINAVEN
LEGEND
Borehole location
CPT location
Deep tow boomer line
Mini-airgun line
355° 40'
356° 00'

The following descriptions of the geotechnical testing equipment have been adapted from literature provided by Fugro Engineers B.V. and with reference to Hampson and Power (1996) and Power and Barwise (1996).

The borehole drilling phase used the SEACLAM system which consists of a frame resting on the seabed which acts as a re-entry base allowing better horizontal and vertical control over the drillstring. Figure 5.1 illustrates the SEACLAM system in operational mode. In drilling mode, samples are obtained using wireline push sampling equipment such as the WIPSAMPLER used as part of this survey. This sampler is a downhole jacking unit to which 1m long thin walled sample tubes of varying diameter are attached. The unit is then lowered down the inside of the drillstring attached to an umbilical cable. At the drill-bit the unit latches on to the assembly and the sample tube is forced into the sediment at a constant rate of penetration by means of an internal hydraulic piston.

The WISON cone penetration test system was used during the downhole testing, where the downhole jacking unit is lowered to the drill-bit and seated. The cone penetrometer is then hydraulically pushed through the sediment at the standard rate of 20 mm/s. Measurements using the PCPT are made of cone tip resistance, sleeve friction and pore pressure.

For the PCPTs collected *in situ* away from the boreholes, the SEACLAM system was converted to a 'Wheeldrive' Seacalf Casing System. This allowed cone penetration tests to be carried out from the mudline and Figure 6.1 illustrates this system.

7.4. Data Interpretation

The datasets utilised for this study were not collected with the intention of any further work other than for interpretation within the bounds of a conventional, standard site survey investigation. As a result the data may not be ideal, mainly in terms of sampling frequency, both geophysically and geotechnically, for the purposes to which they are being applied in this project. However, it was hoped that by attempting to treat this type of conventional dataset in this context, all engineering site survey interpretations might become the ultimate beneficiaries.

The Foinaven and Schiehallion areas were both used in this project due to the density of geotechnical information available, proximity of locations and profile variability. The uniqueness of applying these interpretation/integration methods to this area of the slope is in the use of high resolution seismic reflection techniques in a deep water frontier environment where there is an increasing need for high resolution site investigation. This study also adds the dimension of attempting to model physical properties derived from glacigenic and non-glacigenic sediments from both laboratory tested samples and *in situ* testing.

Figures 7.7 is the location map showing the positions of the boreholes and PCPTs; each location was analysed and representative geotechnical and geophysical sections are presented.

7.4.1. Geotechnical interpretation

A series of geotechnical test results were plotted for each borehole; where possible further physical and acoustic properties were calculated at each borehole location to give a full geotechnical description. The geotechnical data were not supplied with any estimate of error functions. The intention was to interpret the plots in order to build up a geotechnical profile for integration (in Section 7.6) with the seismic facies identified in 7.4.2. Subsequently the aim was to combine the datasets and put the results into a geological context (Section 7.6). In Figures 7.9 to 7.12, 7.14 to 7.17, 7.19 to 7.22 and 7.24 to 7.25 the circular symbols on the geotechnical property profiles indicate that the specific measurement was carried out offshore and the triangular symbols indicate that the measurement was made in an onshore laboratory. The geotechnical descriptions cover the full length of each borehole; this was included for completeness although the deep tow boomer profile penetration does not generally exceed 20 to 30m below seabed.

7.4.1.1. Schiehallion - BHS3/S3A/S3B/S3C

The upper 10.9m of this borehole, shown in Figure 7.8, consists of very soft clay with varying amounts of sand as well as a layer of fine to coarse sand. The initial moisture content, plotted in Figure 7.9(a), is 76%. The moisture content decreases rapidly with depth in this upper section which would be expected due to self weight compression (Talbot *et al.*, 1994). Within this upper layer the natural moisture

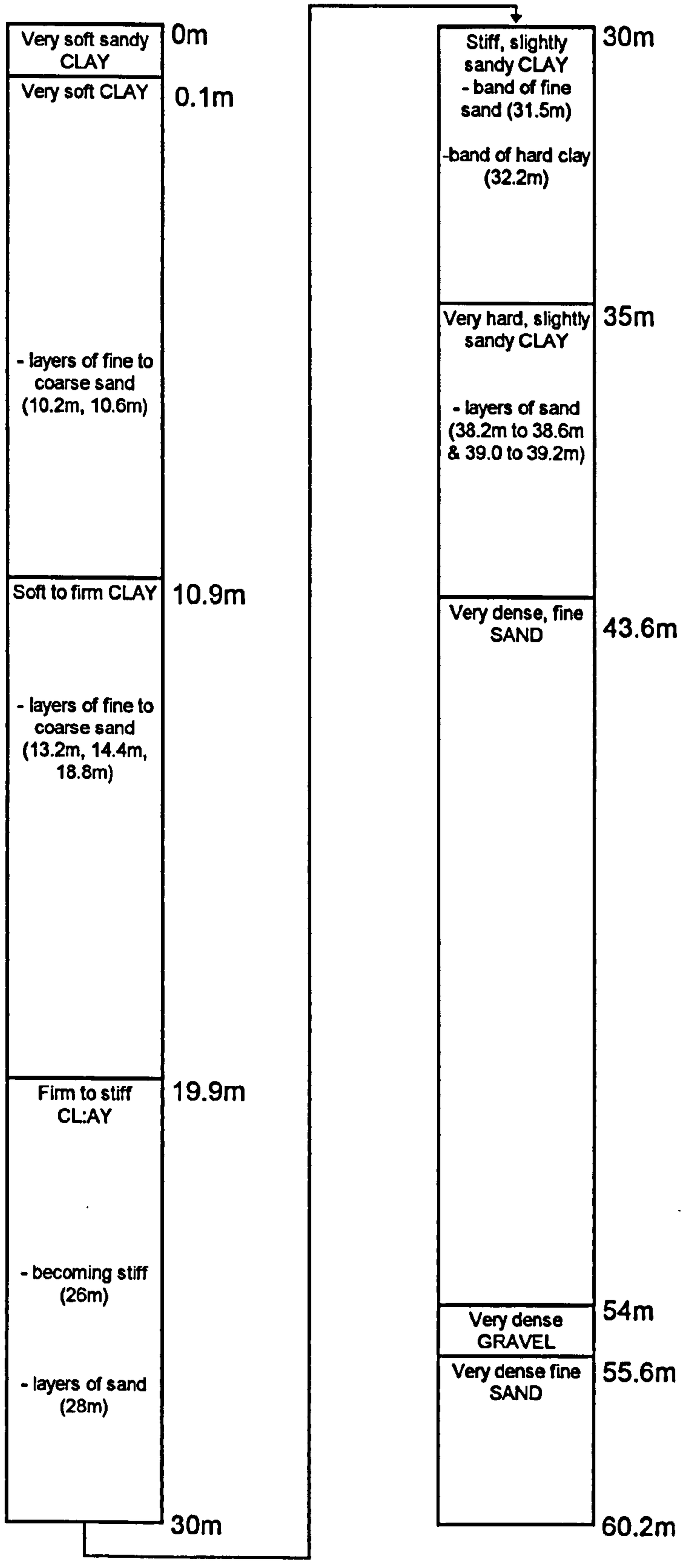

Figure 7.8. BHS3/S3A/S3B/S3C borehole log.

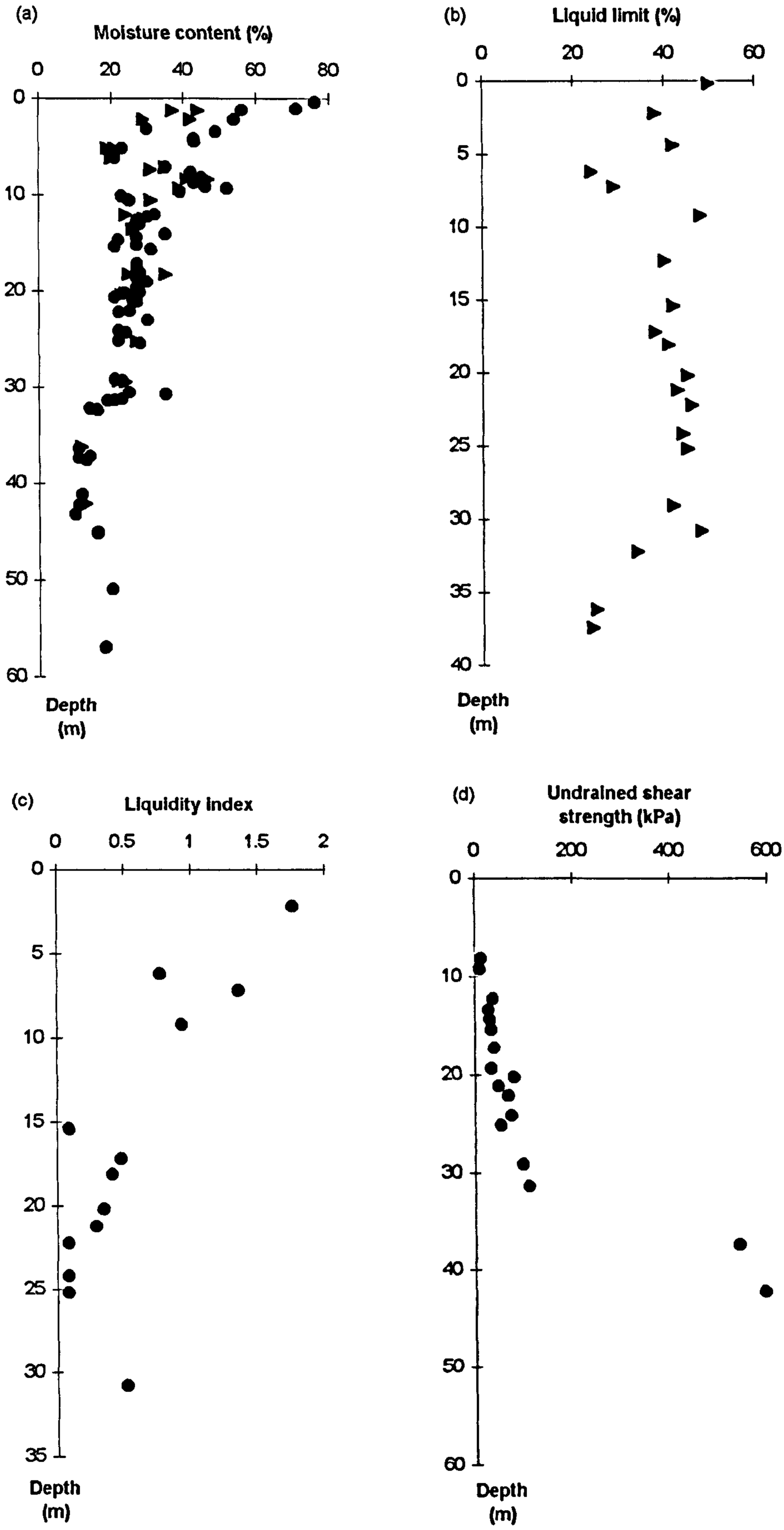

Figure 7.9. BHS3/S3A/S3B/S3C physical property profiles. (a) Moisture content. (b) Liquid limit. (c) Liquidity index. (d) Undrained shear strength.

content is closer to the liquid limit, shown in Figure 7.9(b). The liquidity index in Figure 7.9(c) is high, coming close to 2 near the top of the borehole. Respectively the undrained shear strength values, shown in Figure 7.9(d) are reasonably low reflecting the higher moisture content values.

The effective stress profile in Figure 7.10(a) follows a linear pattern and values of less than 100 kPa can be derived from the upper section of the borehole. The void index profile in Figure 7.10(b) shows higher values within the upper section illustrating the more open structure of the natural sediment. Talbot *et al.* (1994) note from their study on the Hebrides slope that as void index is calculated from the water content and index limits then there is the possibility of underestimation in void index value caused by incomplete saturation of the sediment following storage.

The bulk density profile within the upper section shown on Figure 7.11(a) ranges from 1.78 Mg/m^3 to 2.03 Mg/m^3; this physical property trend is reflected in the velocity and impedance profiles (Figure 7.11(b) and (c) respectively) which have been produced from the bulk density values. Velocity values in Figure 7.11(b) range from around 1680m/s near the seabed to 2000m/s at about 40m and then they fall deeper down the section with values of 1685m/s at the bottom of the borehole. Below the 10m borehole depth, the geotechnical profiles experience a change in character. The water content and liquid limit profiles exhibit less scatter, however this may also be a function of the sampling frequency.

The void index profile shows decreasing values with increasing depth with the points lying to the left of the intrinsic compression line indicating overconsolidation. Following the method of Paul *et al.* (1993), the plot of liquid limit against plasticity index shows the samples lying close to the till line in Figure 7.12; this shows that the sediment probably has a glacial origin. This may also indicate the clay content as Boulton and Paul (1976) found that percentage clay in a sample increased along the till line from left to right due to sorting processes determining the grain-size distribution.

The bulk density profile shows values around 2.0 Mg/m^3 until a depth of about 44m where there is a drop to 1.9 Mg/m^3 which corresponds to an increase in water content and distinct change in material type. This material is described in the borehole log as very dense fine sand.

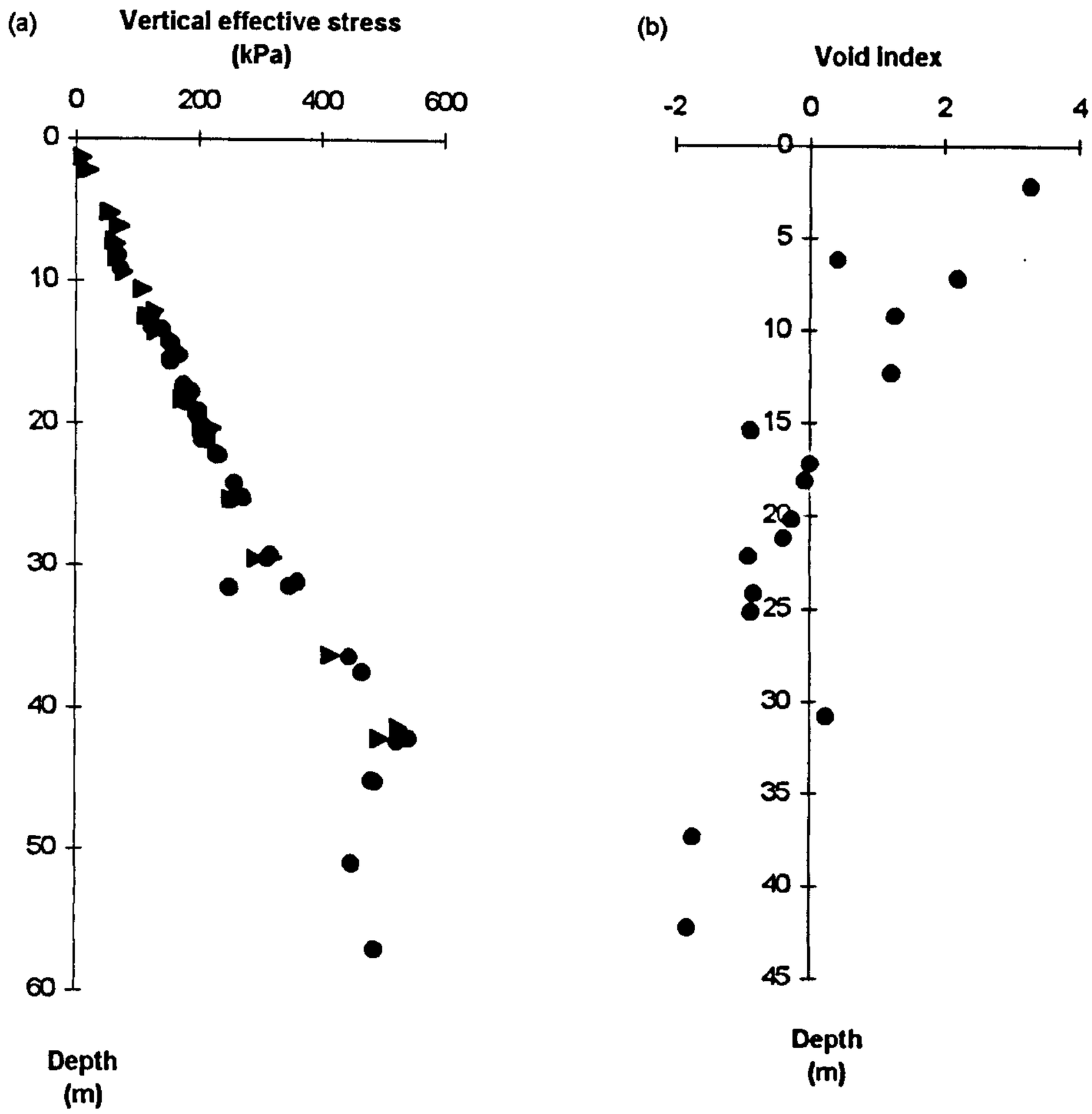

Figure 7.10. BHS3/S3A/S3B/S3C physical property profiles. (a) Vertical effective stress. (b) Void index.

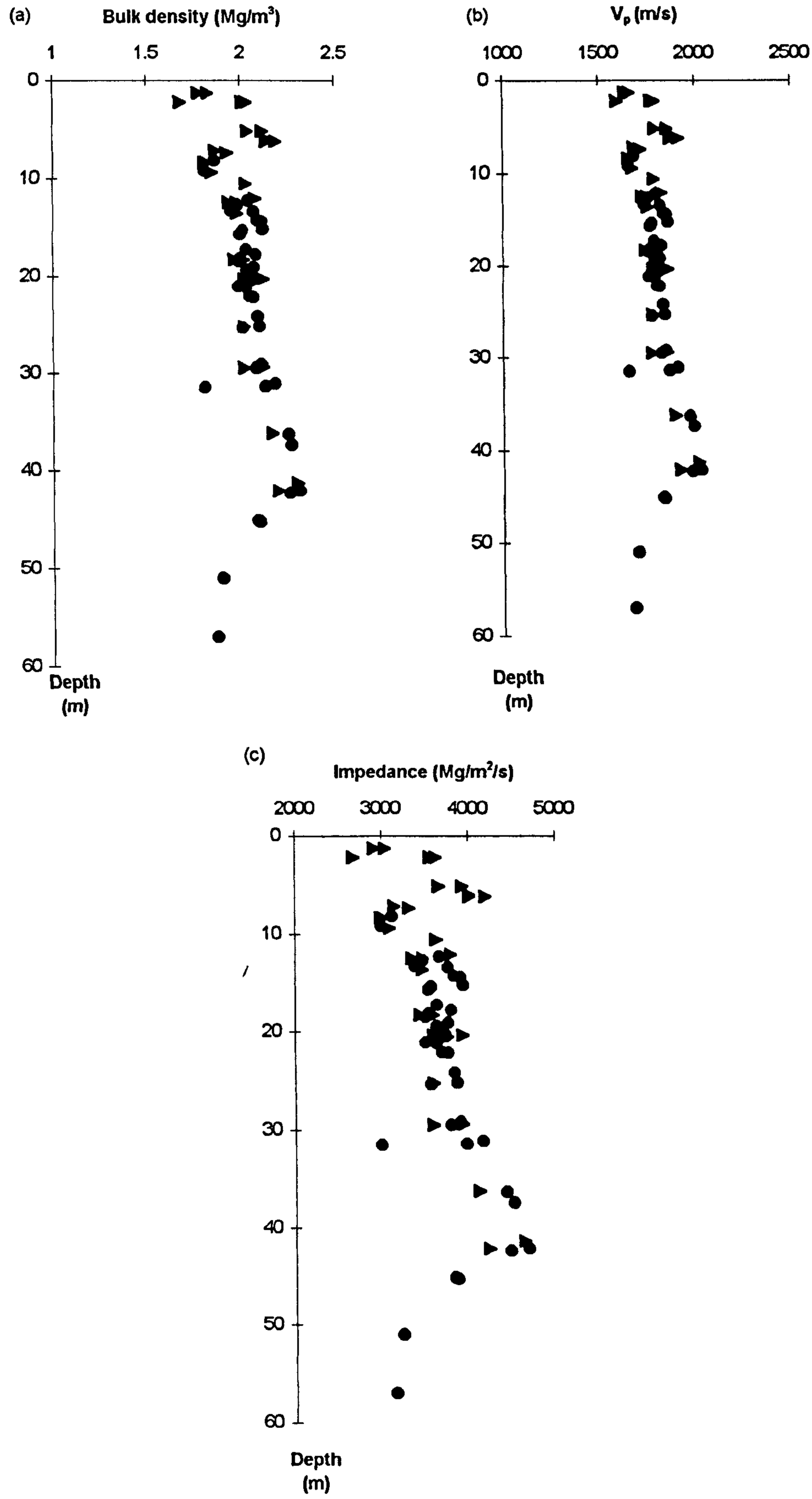

Figure 7.11. BHS3/S3A/S3B/S3C acoustic property profiles. (a) Bulk density. (b) Velocity. (c) Impedance.

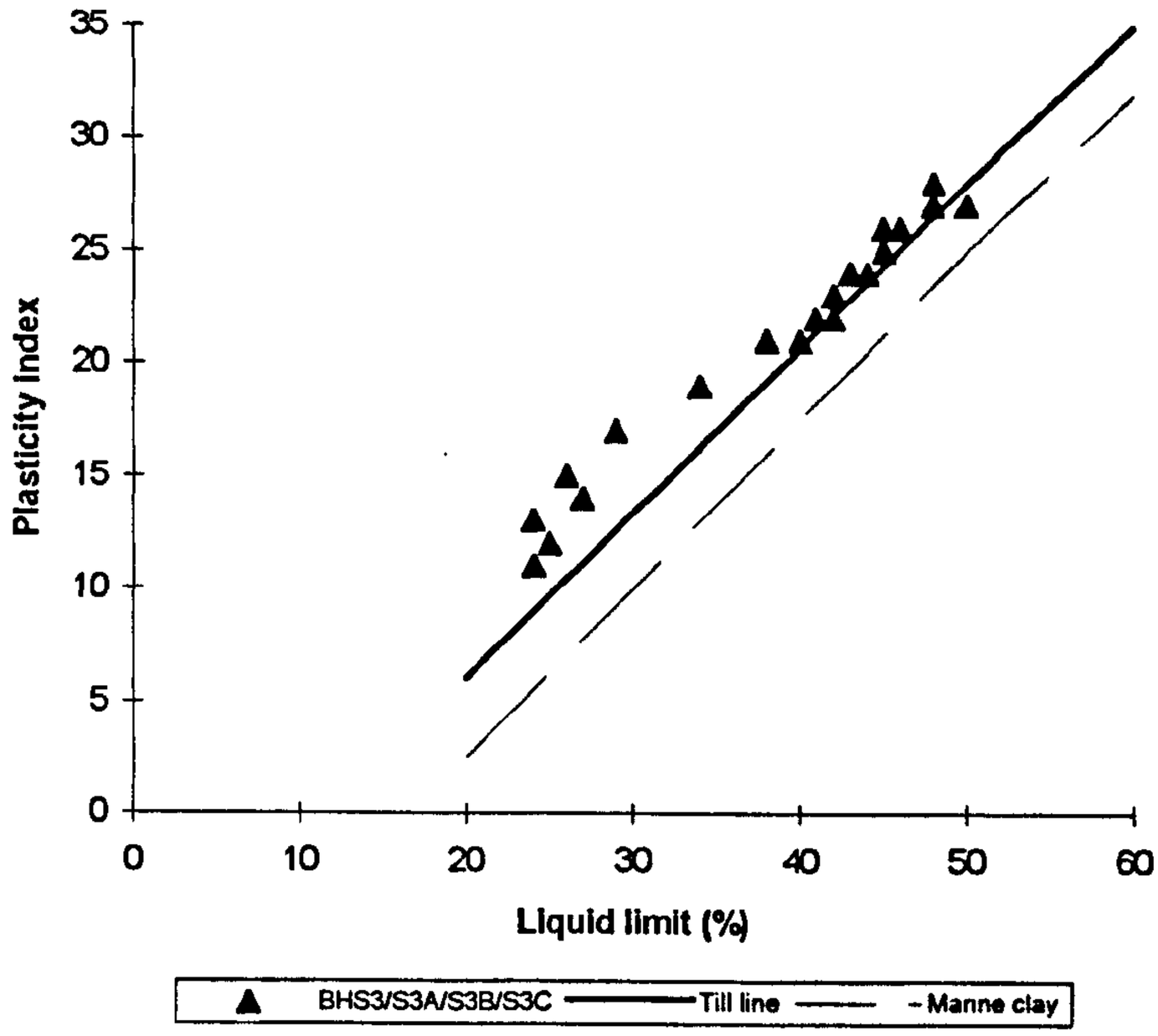

Figure 7.12. BHS3/S3A/S3B/S3C plasticity index profile.

7.4.1.2. Schiehallion - BHS4/S5/S6

The upper part of the description for BHS4/S5/S6 obtained from the borehole log shown in Figure 7.13 comes from S4/S5 and the lower section is S6, the boreholes are 10m apart.

The upper 5m of the borehole has high moisture contents as shown in Figure 7.14(a), with a maximum of 65% which decreases to approximately 27% around 5m. These values are reasonably close to the liquid limit in Figure 7.14(b) indicating normally consolidated very soft clay. The liquidity index in the upper 5m as shown in Figure 7.14(c), exceeds 2 but rapidly falls to around 0.6 at 5m. The void index values in this upper 5m, shown in Figure 7.14(d), are positive, lying to the right of the SCL.

Bulk densities plotted in Figure 7.15(a) in the upper 5m are relatively low at 1.7 Mg/m^3 but quickly rise to around 2.0 Mg/m^3. This variation in density is reflected in the velocity and impedance profiles in Figures 7.15(b) and 7.15(c) respectively, with velocities averaging around 1800m/s but reaching 1900m/s at 5m depth.

Following the significant drop in moisture content at 5m, the values show little variation down the borehole. This consistency of values is illustrated through the rest of the borehole in all the profiles presented. The shear strength profile increases with depth (in Figure 7.16(a)) as the clay increases in strength. This strength trend is reflected in Figure 7.16(b). The liquid limit against plasticity index plot in Figure 7.17 illustrates the samples lying close to the till-line of Boulton and Paul (1976).

7.4.1.3. Foinaven - BH4/4A/4B

The upper 4-5m of this borehole, illustrated in Figure 7.18, contains very soft clay with natural moisture contents in excess of 60% decreasing rapidly and becoming closer to 20% at 5m (see Figure 7.19(a)). These moisture content values are close to the liquid limit values and the liquid limit profile exhibits a similar trend as shown in Figure 7.19(b). The liquidity index in Figure 7.19(c), however, varies approximately between 1.4 and -0.8. The void index values in this upper 5m, shown in Figure 7.19(d), are around 2 indicating an open fabric structure.

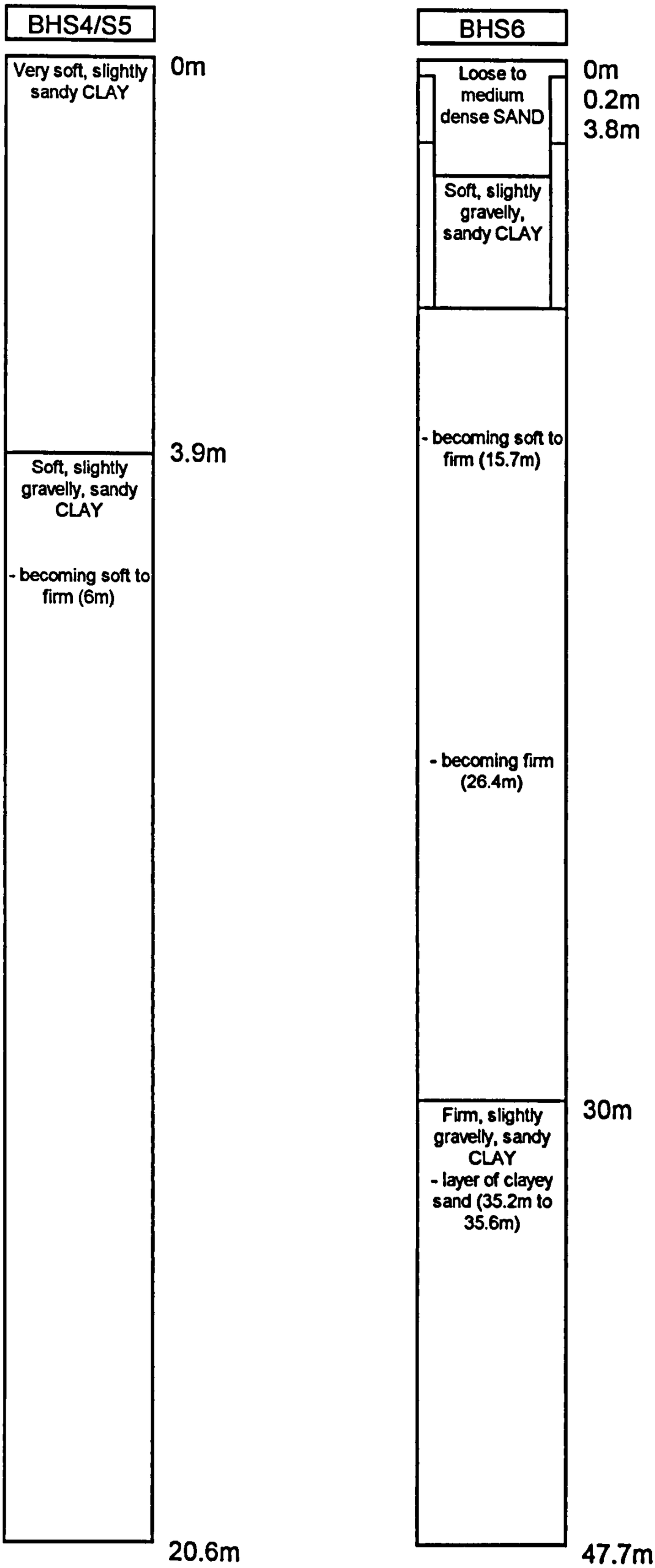

Figure 7.13. BHS4/S5/S6 borehole log.

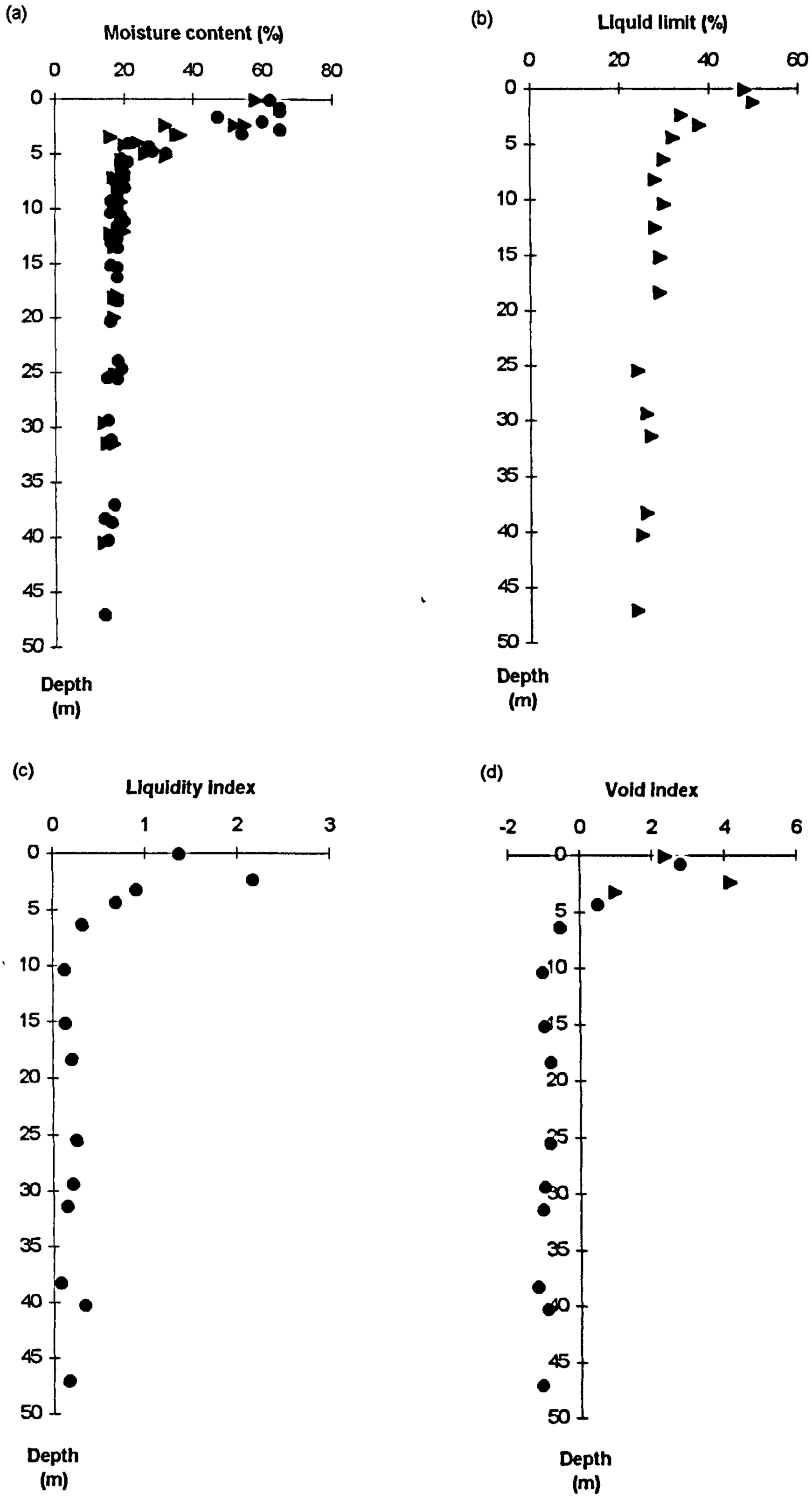

Figure 7.14. BHS4/S5/S6 physical property profiles. (a) Moisture content. (b) Liquid limit. (c) Liquidity index. (d) Void index.

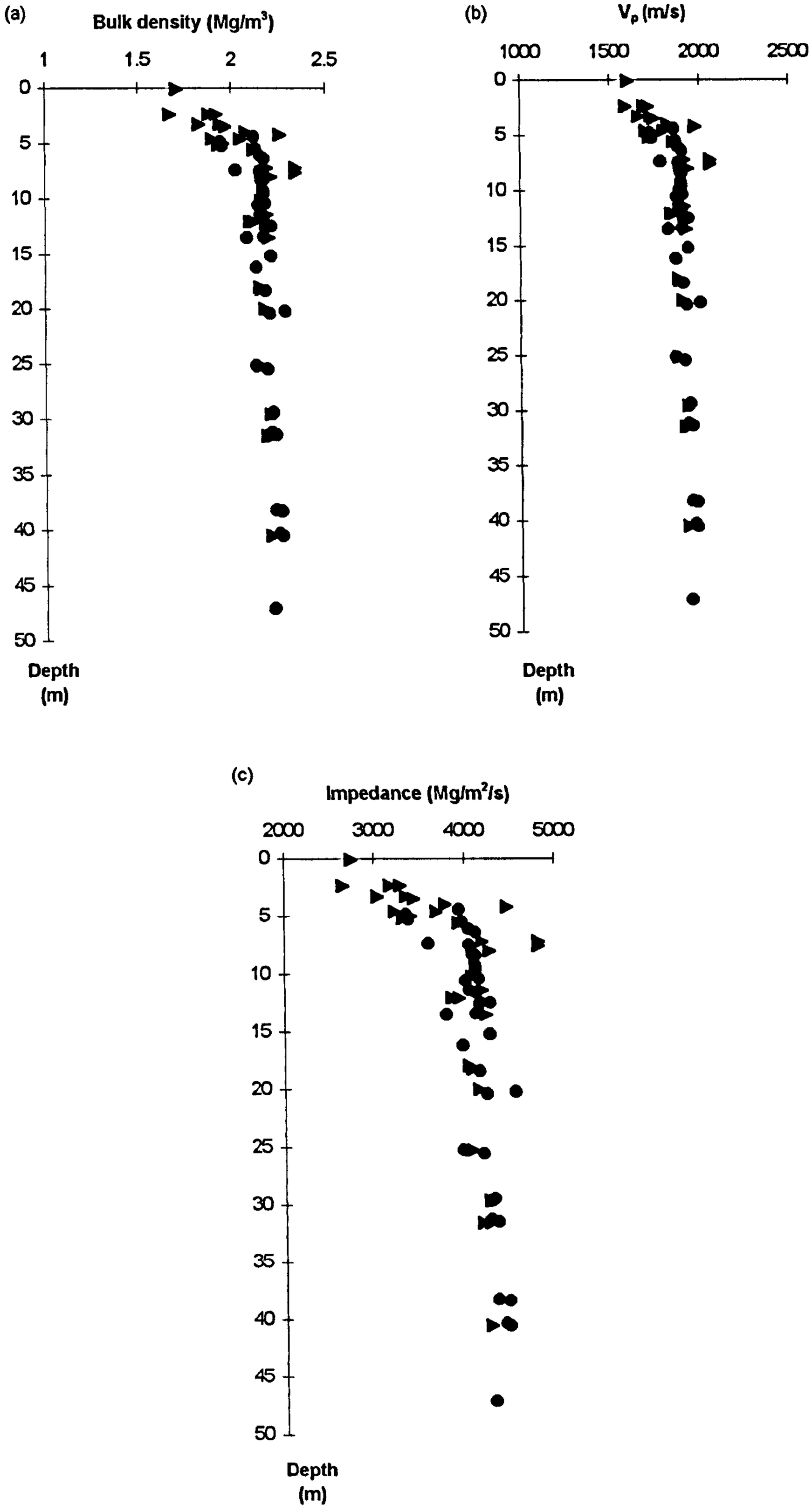

Figure 7.15. BHS4/S5/S6 acoustic property profiles. (a) Bulk density. (b) Velocity. (c) Impedance.

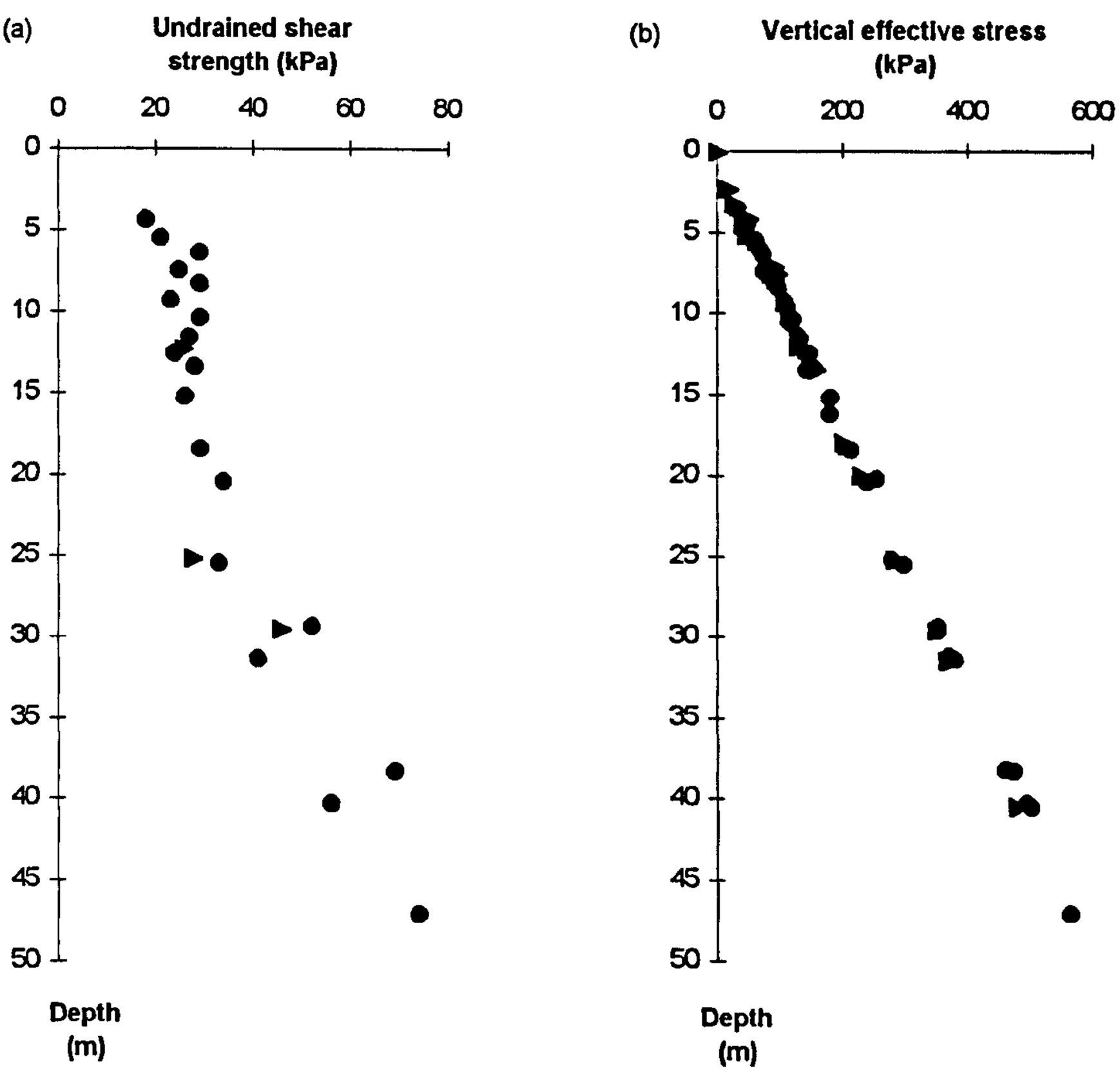

Figure 7.16. BHS4/S5/S6 physical property profiles. (a) Undrained shear strength. (b) Vertical effective stress.

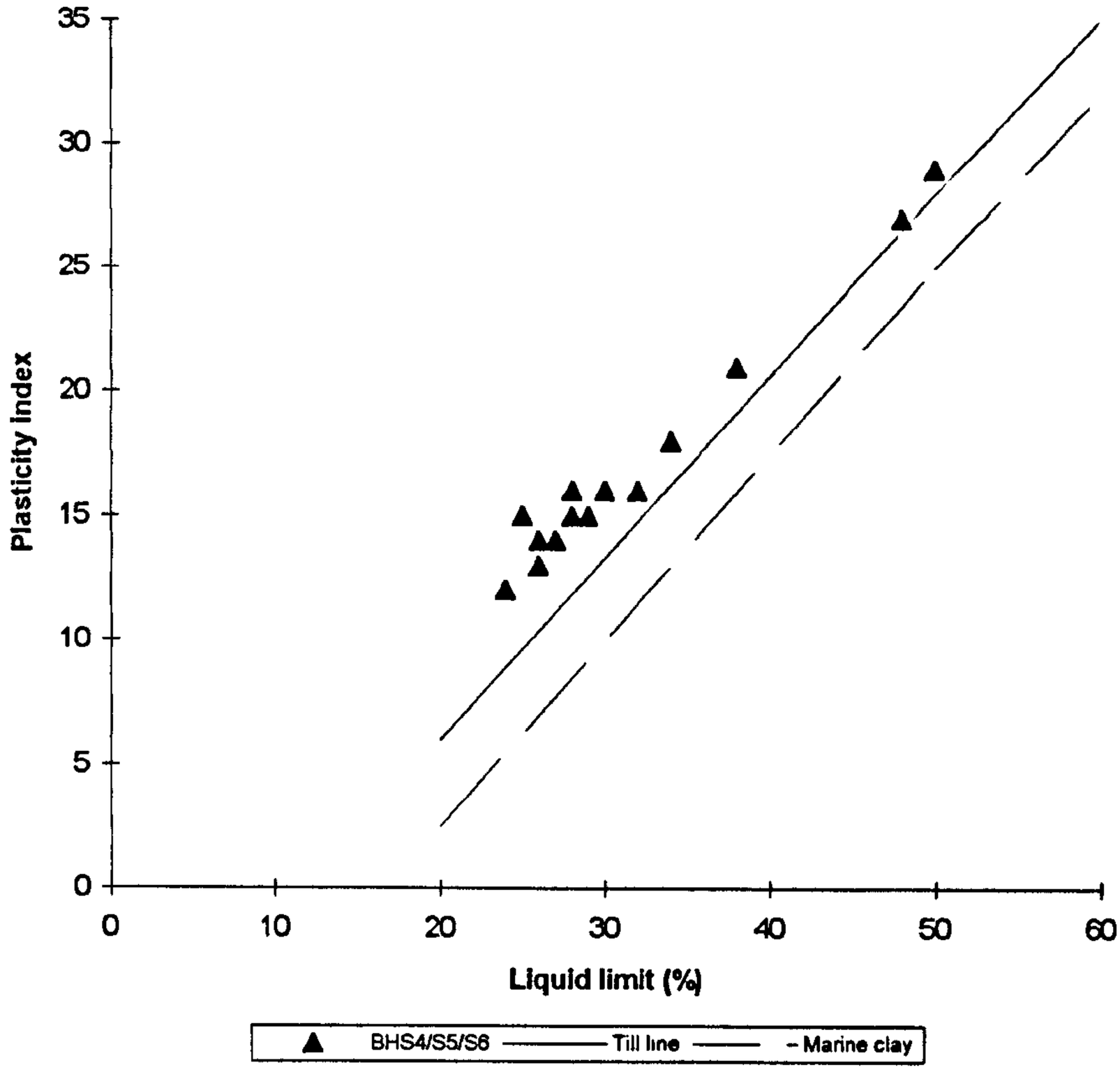

Figure 7.17. BHS4/S5/S6 plasticity index profile.

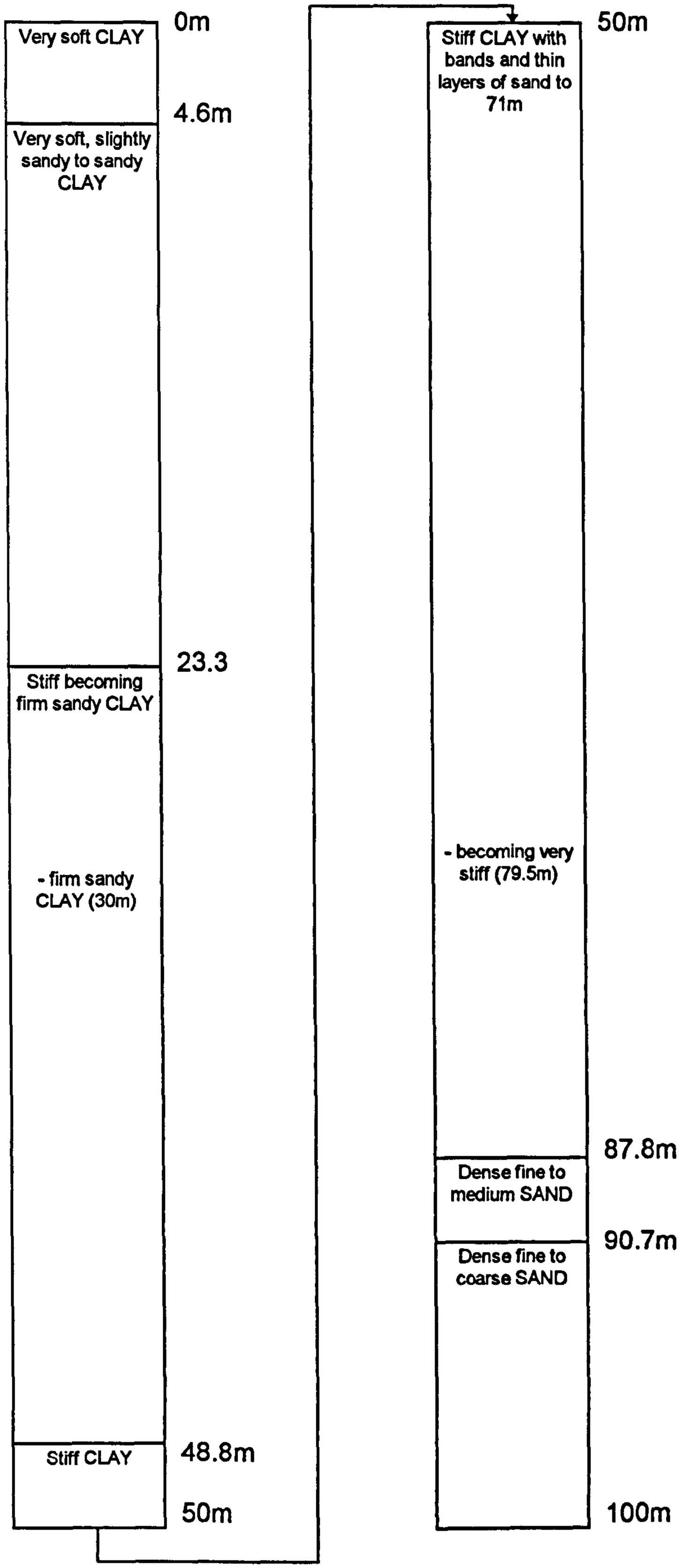

Figure 7.18. BH4/4A/4B borehole log.

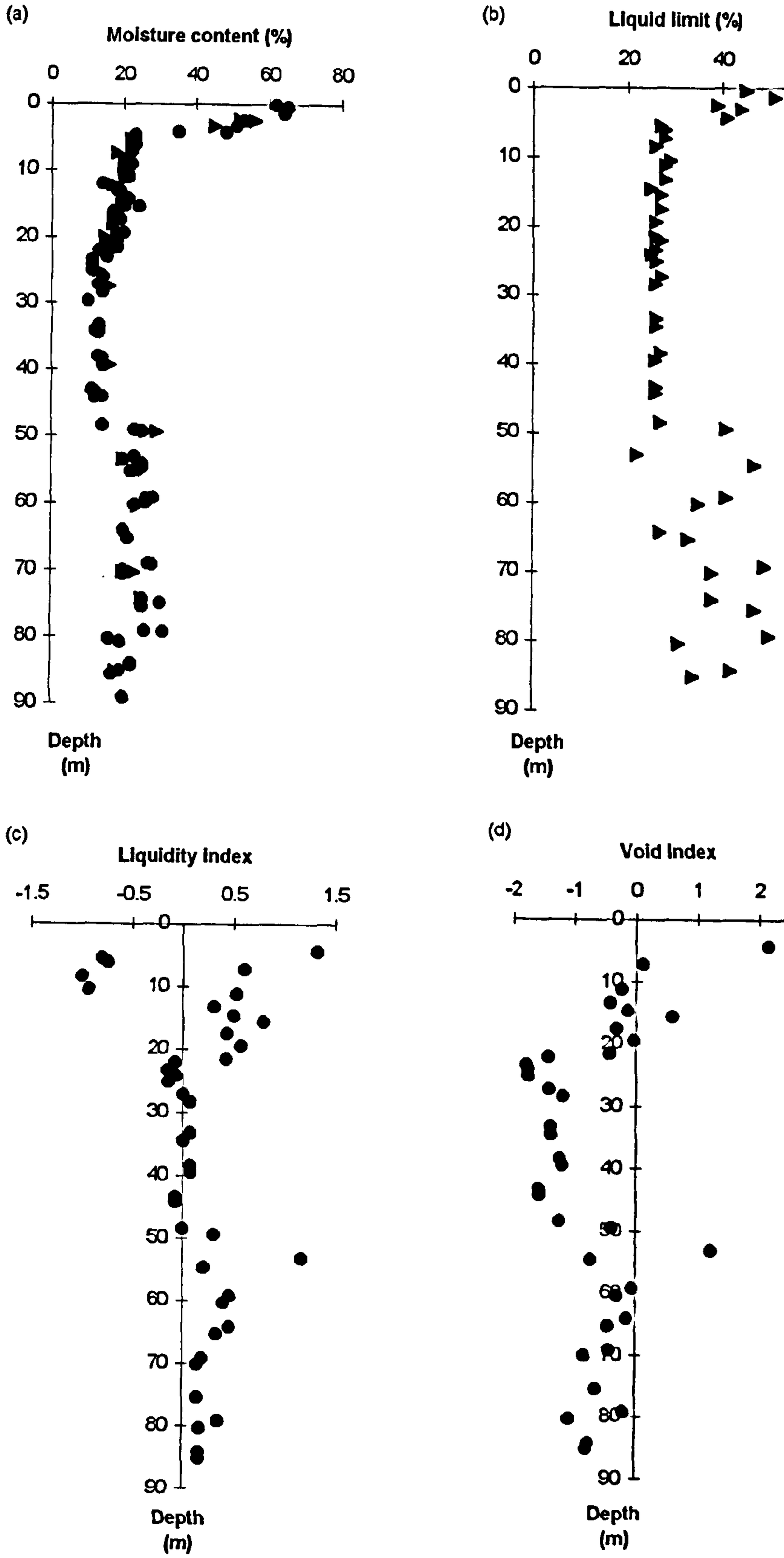

Figure 7.19. BH4/4A/4B physical property profiles. (a) Moisture content. (b) Liquid limit. (c) Liquidity index. (d) Void index.

Bulk densities in the upper section shown in Figure 7.20(a) average around 1.85 Mg/m^3 resulting in calculated velocities of around 1700m/s, as shown in Figure 7.20(b). There is a subsequent low impedance in this upper section (Figure 7.20(c)). Also around the 50m mark there is a slight decrease in bulk density which results in a decrease of velocity below the previous values of around just under 2000m/s.

Down through the borehole there is only a small decrease in moisture content, this decrease continues to around 50m where there is a corresponding increase of around 10%. The liquid limit profile shows large scatter from this point on and there is a corresponding increase in the liquidity index. The void index values appear to gather around zero from this point down through the borehole succession reaching -1 between the 5m and 50m levels. Shear strength shows a marked increase in Figure 7.21(a) from around 50m and there is more scatter from this point on. This scatter is reflected on the effective stress profile shown in Figure 7.21(b). However, the crucial consideration of sampling frequency again has to be re-iterated. The plasticity chart for this borehole in Figure 7.22 also shows the samples lying on the till line with the exception of one sample which lies on the marine clay line. Paul *et al.* (1993) postulate that the restricted scatter of the points on a plasticity plot indicates a lack of grading within the borehole and that the left to right trend of the sample points could be a result of changing clay content; however the clay content data are not available for verification.

7.4.1.4. Foinaven - BH6

The borehole log for BH6 is illustrated in Figure 7.23, and the geotechnical profiles presented in Figures 7.24 and 7.25. The geotechnical profiles show a similar pattern to BH4. The water content and liquid limit values in the upper 3-4m are high as shown in Figures 7.24(a) and 7.24(b) respectively. Below this depth and down the rest of the borehole the illustrated geotechnical properties show little variation with the sediment being described as very soft clay becoming firm to stiff sandy clay with depth.

Bulk densities displayed in Figure 7.25(a) range from 1.8Mg/m^3 close to the seabed then averaging approximately 2.0Mg/m^3 to the base of the borehole. These correspond to velocities of around 1900 m/s to 2000m/s, (shown in Figure 7.25(b))

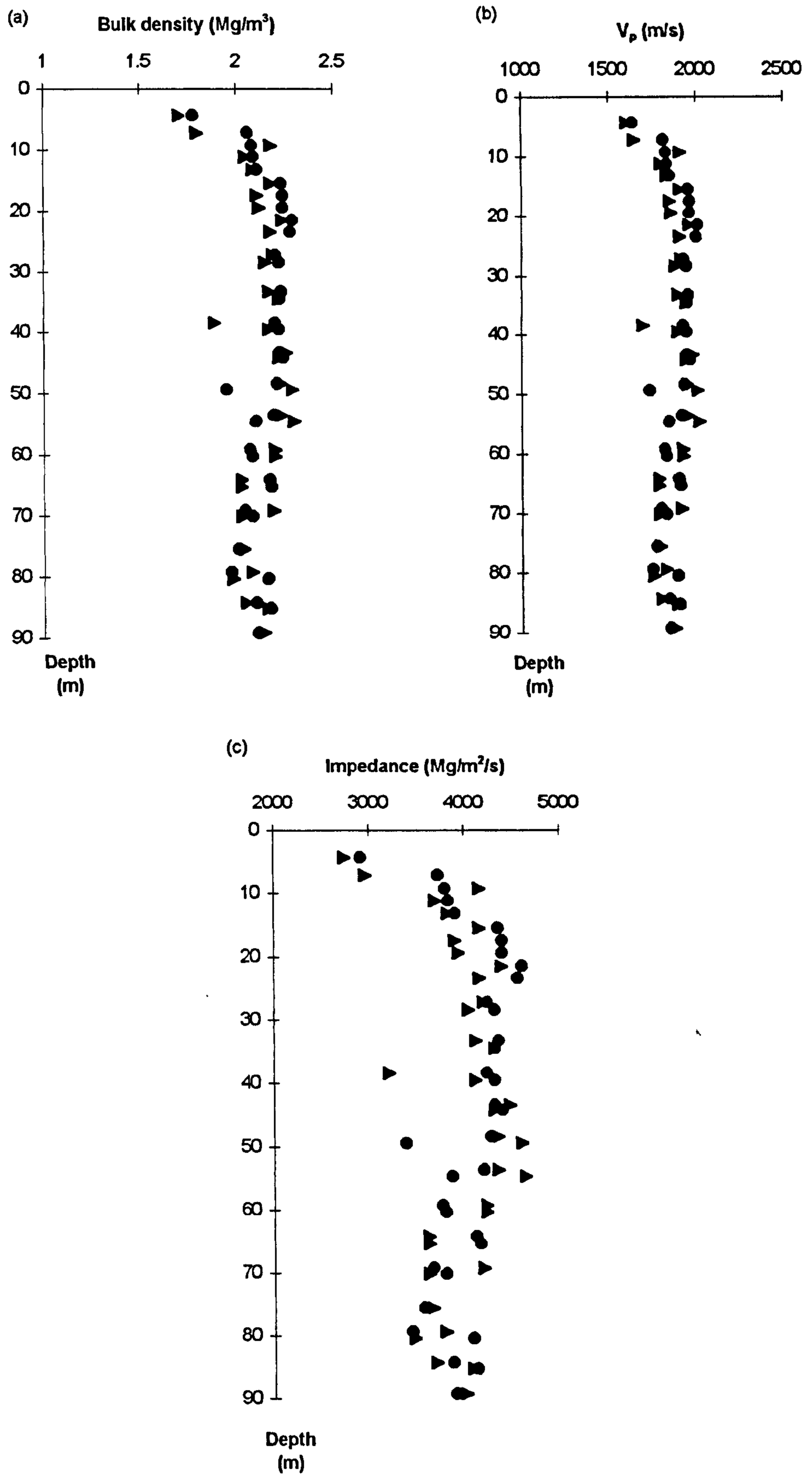

Figure 7.20. BH4/4A/4B acoustic property profiles. (a) Bulk density. (b) Velocity. (c) Impedance.

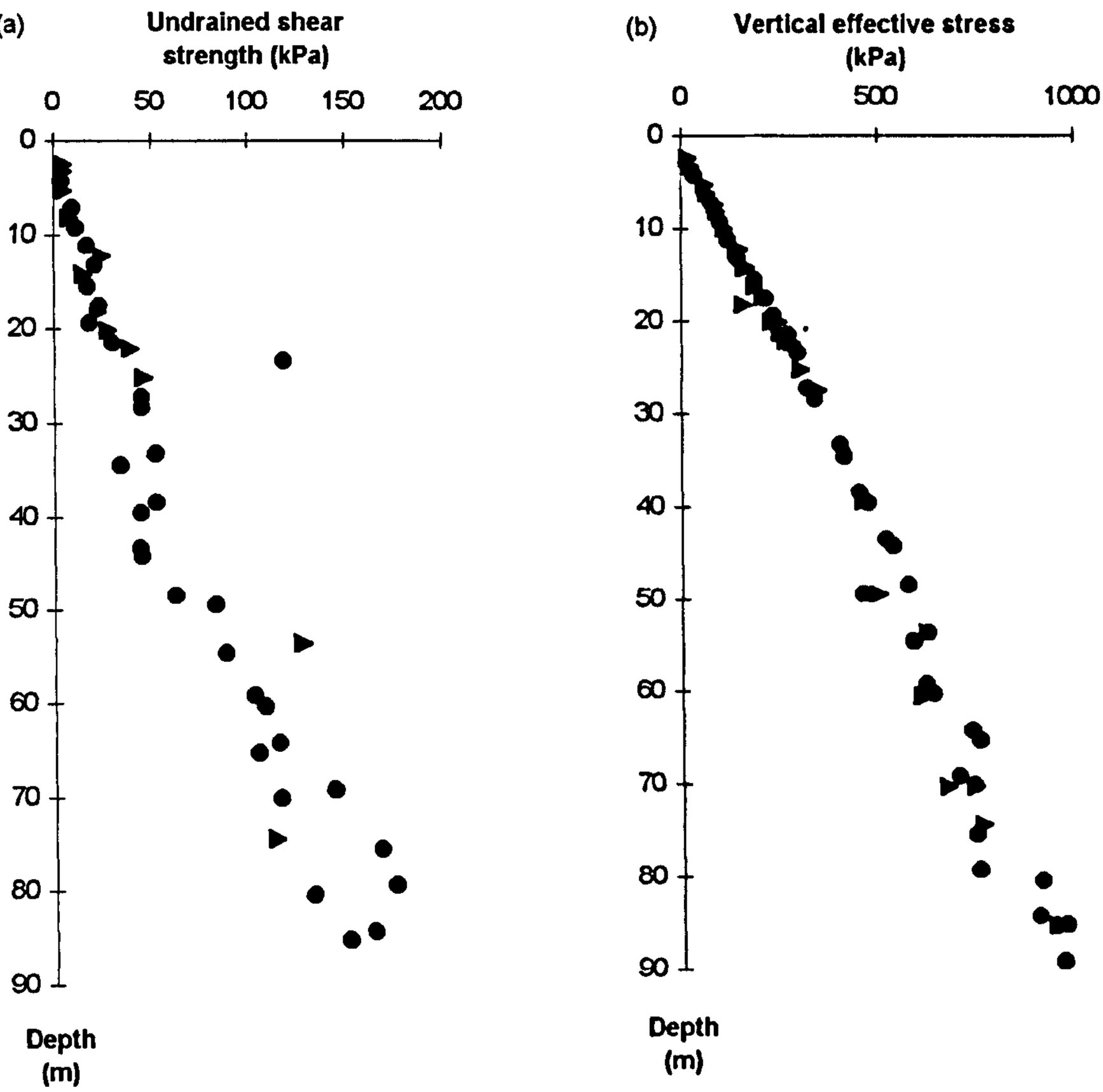

Figure 7.21. BH4/4A/4B physical property profiles. (a) Undrained shear strength. (b) Vertical effective stress.

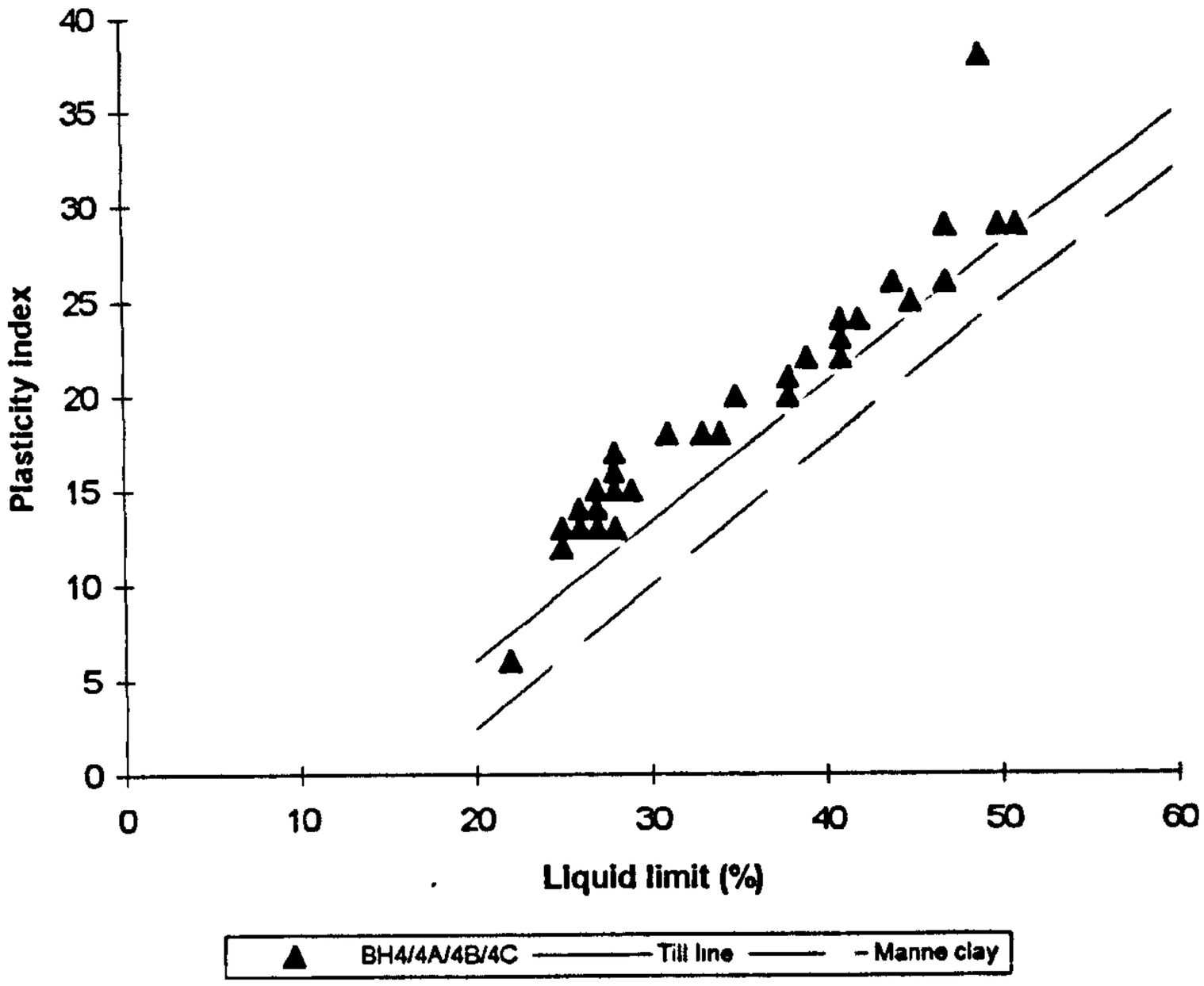

Figure 7.22. BH4/4A/4B plasticity index profile.

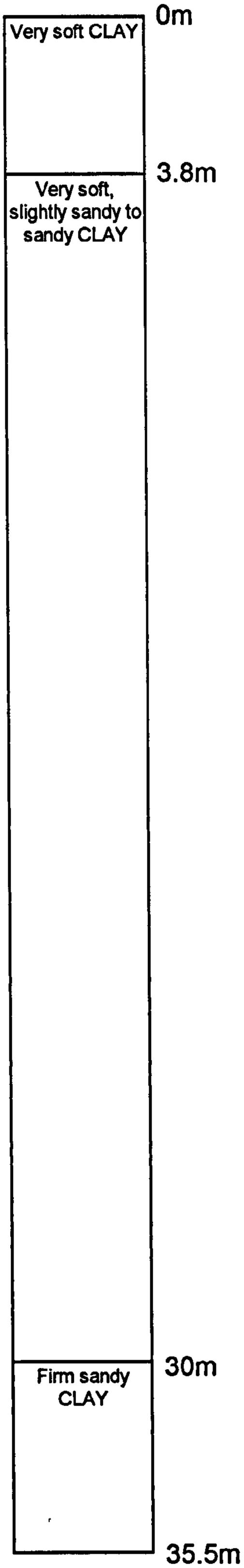

Figure 7.23. BH6 borehole log.

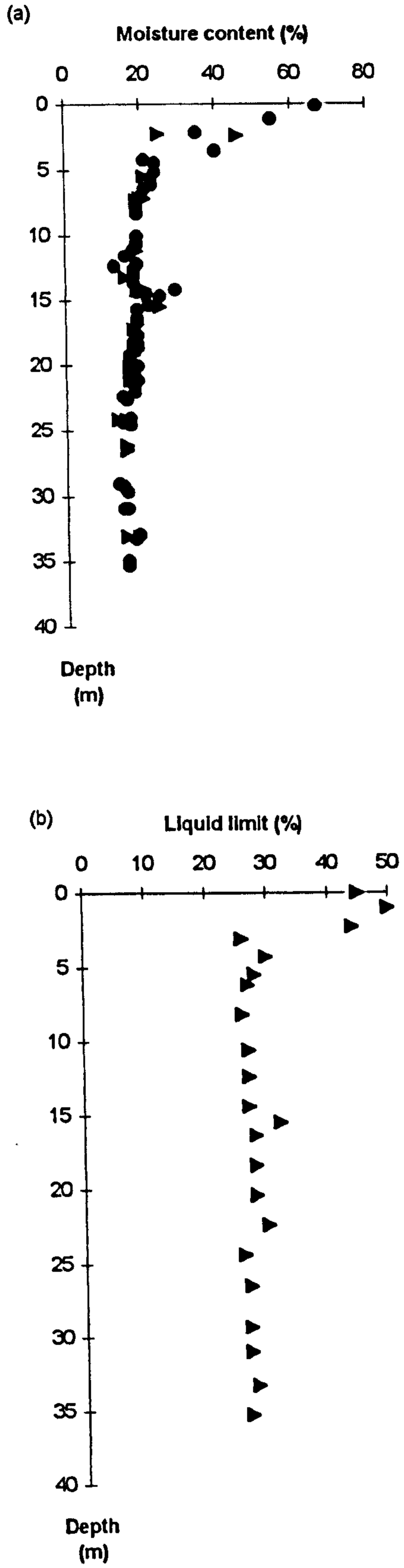

Figure 7.24. BH6 physical property profiles. (a) Moisture content. (b) Liquid limit.

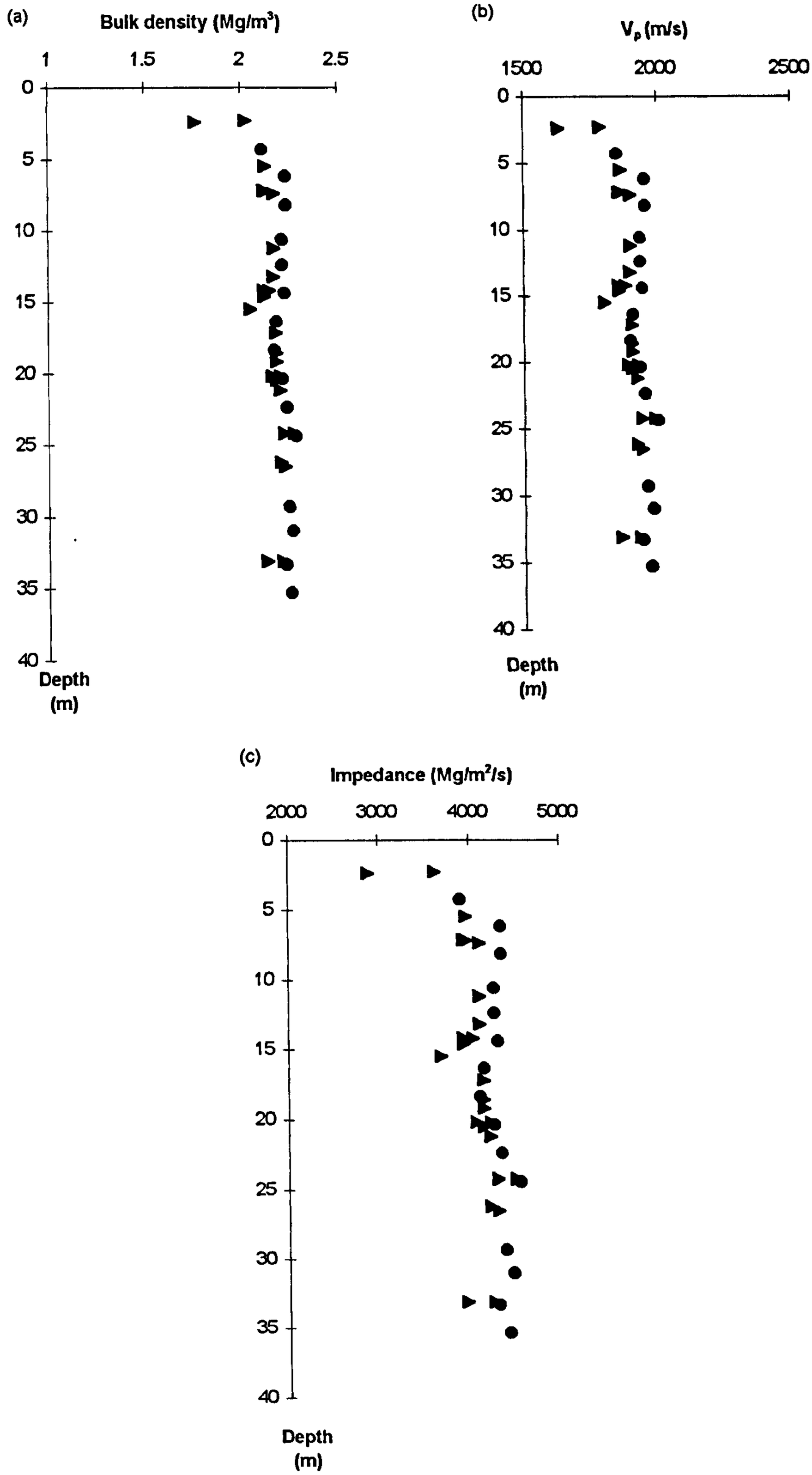

Figure 7.25. BH6 acoustic property profiles. (a) Bulk density. (b) Velocity. (c) Impedance.

and impedances from less than 3000 Mg/m^2/s to approximately 4000 Mg/m^2/s (Figure 7.25(c)).

7.4.2. Geophysical interpretation - deep tow boomer

Figure 7.7 shows the locations of the geotechnical sampling points, i.e. boreholes and CPTs and the closest seismic line available on both paper and tape.

7.4.2.1. Schiehallion - BHS3/S3A/S3B/S3C

There are three seismic facies types recognisable on the section shown in Figure 7.26 corresponding to the BHS3/S3A/S3B/S3C borehole. The upper unit (A) extends to 2.5ms below seabed and is well-layered and appears to be draped over the underlying topography. This draping indicates low-energy deposition (Sangree and Widmier, 1977) and from the geotechnical response is consistent with an ice-distal environment (Syvitski, 1991). The base of this facies unit is not very well-defined but the layering gives way to a more acoustically chaotic/transparent unit (B) which has the form of lense/clinoform type geometry. Below these lensoid packages there is once again more of a layered response but with less closely spaced layering. Below these layers, at around 20ms, no obvious structure is evident and the response is more chaotic once again (see Figure 7.26).

The upper seismically well-layered unit can be correlated with the laying down of a soft to very soft clay sequence seen in the upper section of the borehole. The layering may be a result of composite reflectors where there are small scale changes in properties not detected through coarse geotechnical sampling. The amplitude of these layers in the upper unit are relatively low which may be due to uniform lithology with varying density producing the layering. The transition between this well-layered unit and the acoustically chaotic/transparent zone is less well defined from the borehole data. The significant change in physical properties in the borehole is at 12.2ms below seabed on the deep tow boomer section. At this level there appears to be a transition from the acoustically chaotic/transparent section into a more layered facies.

Given the evidence from the borehole of the scatter in this upper 12.2ms and the chaotic boomer section it is possible that this middle facies is a mass flow unit.

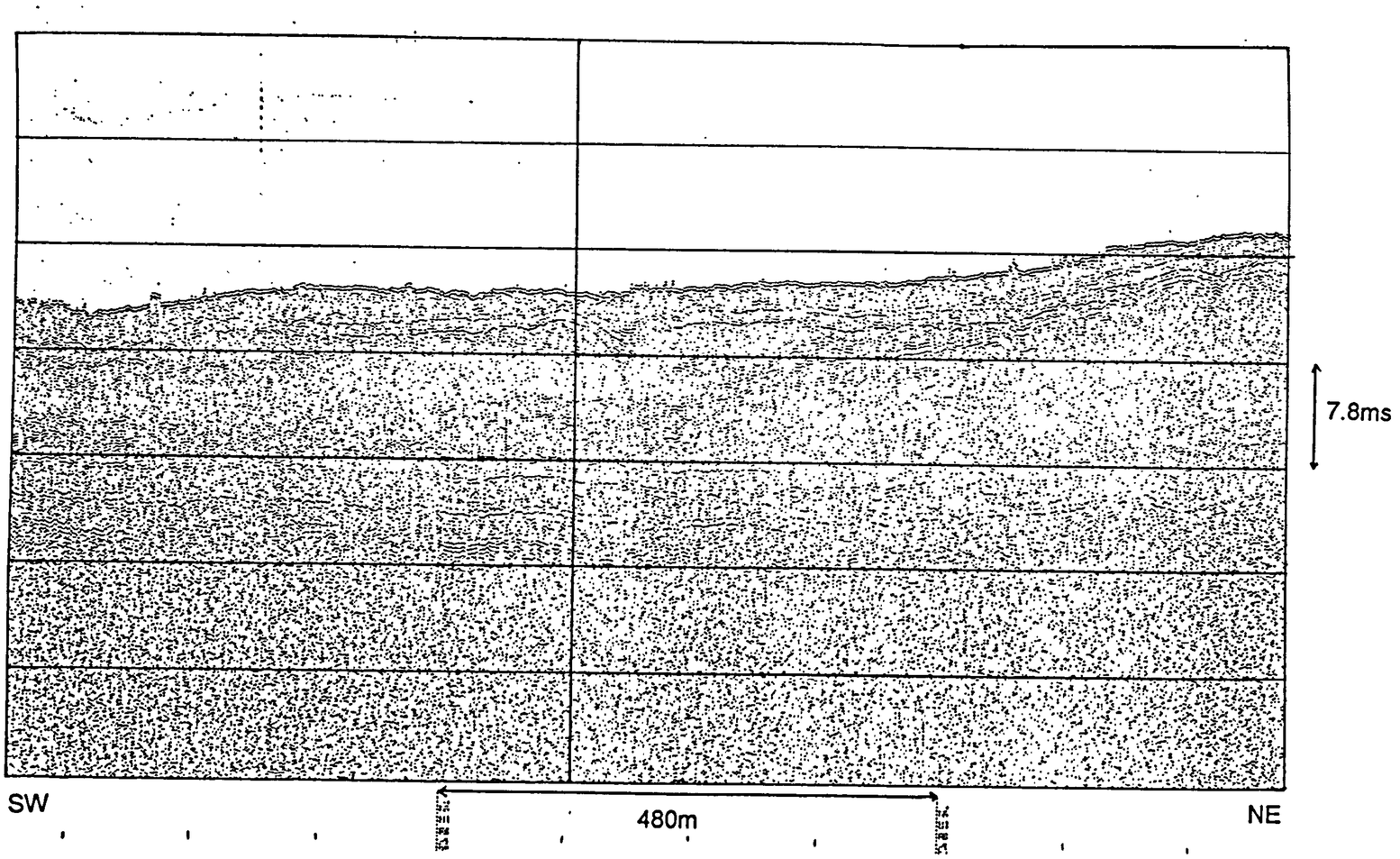

Figure 7.26. BHS3/S3A/S3B/S3C deep tow boomer location profile; BPAT-081. Horizontal scale, 1cm = 59m. Vertical scale, 1cm = 5ms TWT.

Figure 7.26

7.4.2.2. Schiehallion - BHS4/S5/S6

BPAT-070 lies approximately 80m north of the borehole and two possible facies types may be visible at this location, as shown in Figure 7.27. The upper unit (B) which is well-defined has a strong basal reflector with some internal layering, but in places this layer is very thin. There then appears to be a second layered unit which grades into a more unstructured chaotic facies. Again the upper unit appears draped over the lower unit. The upper layered unit has an average thickness of around 3ms, but the whole lower unit has no defined limits. The boomer section however, may be misleading due to sideswipe. This may be due to spurious reflections being generated off the line of the section by, for example, a dipping reflection feature caused by iceberg action. Some features therefore, may not be a true representation of the stratigraphy. To confirm this sideswipe interpretation, it would necessary to re-run the line in a different orientation.

All the borehole sample test results show a change in physical properties occurring at approximately 3m below seabed. Within the 0-3m section of the borehole there is a more subtle change occurring around 2m below seabed. This change correlates with the base reflector of the upper unit seen at 3ms below seabed on the deep tow boomer section. The slight discrepancies in depths below seabed may be due to a difference between the actual velocity and the velocity chosen for the depth conversion.

7.4.2.3. Foinaven - BH4/4A/4B

BPAT-096A is 20m south of the borehole and Figure 7.28 is the seismic section closest to the borehole. The upper unit (A) is subhorizontally well-layered with a fairly well defined base at approximately 5ms below seabed. This seismic unit correlates with the upper section of the borehole which has a very high moisture content, 65% at seabed, dropping significantly to 20% at approximately 5ms below seabed. This seismic unit is also characterised by a relatively low bulk density and velocity. However within this upper unit there may be a further division of seismic character which cannot be correlated with any change in physical properties. The upper 2ms of this unit is less well-layered than the section between 2ms-5ms below seabed.

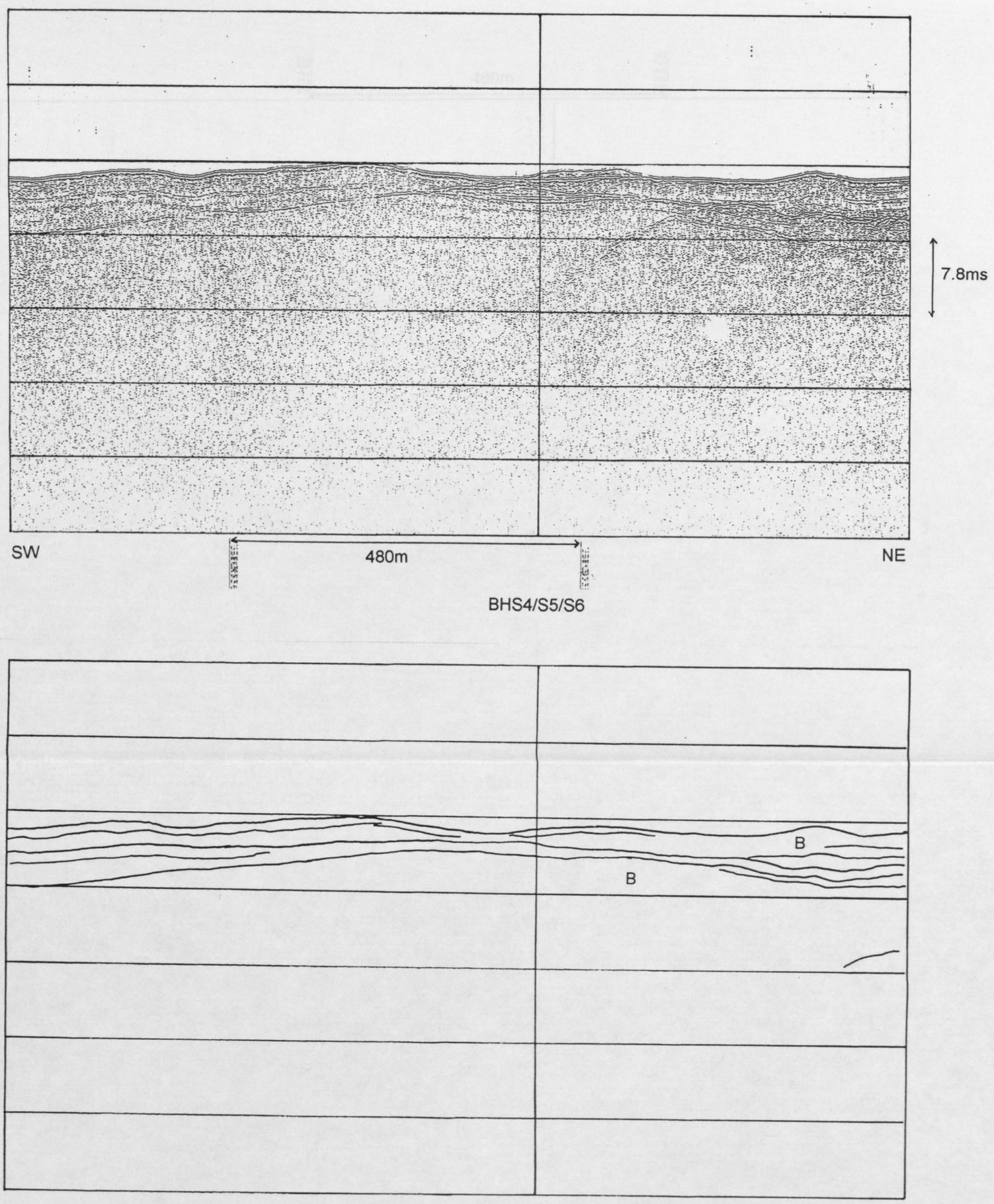

Figure 7.27. BHS4/S5/S6 deep tow boomer location profile; BPAT-070. Horizontal scale, 1cm = 59m. Vertical scale, 1cm = 5ms TWT.

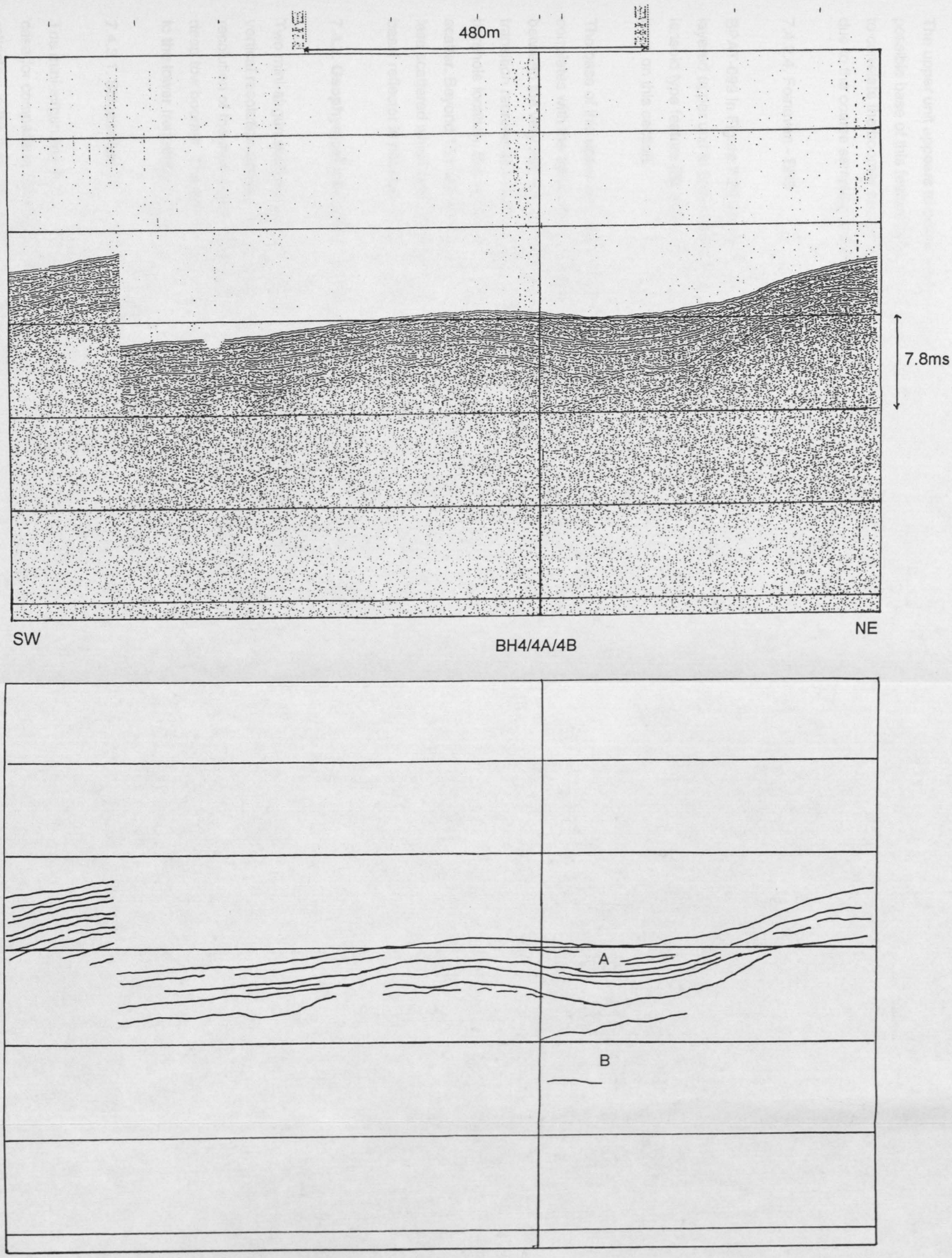

Figure 7.28. BH4/4A/4B deep tow boomer location profile; BPAT-096A. Horizontal scale, 1cm = 59m. Vertical scale, 1cm = 5ms TWT.

The upper unit appears to drape over a lensoid/mass flow type feature (B). The possible base of this feature is faintly seen at 10ms below the seabed. It is difficult to correlate the boomer section any further with the borehole sample test results due to the coarse sampling at the borehole.

7.4.2.4. Foinaven - BH6

BPAT-099 in Figure 7.29 is 100m south of the BH6. The boomer section has a layered upper unit to 5ms below seabed (A) and this unit appears to drape over a lensoid type feature (B). However, this feature does not appear to have a definitive base on this section.

The base of this upper unit lies approximately 5ms below seabed and this correlates with the transition seen in the borehole lithological log (see Figure 7.23) between the very soft clay and the very soft, slightly sandy clay to sandy clay. This transition represents the most significant change in physical properties seen at this borehole location. Below this level the physical property measurements show some scatter. Beyond 15m subseabed at the borehole the physical properties become less scattered which could signify the base of a mass flow sequence. However, this basal reflector is not seen on the deep tow boomer profile.

7.4.3. Geophysical interpretation - mini-airgun

Two mini-airgun sections were reviewed at two borehole locations to compare the vertical resolution between the two systems, i.e. airgun and boomer. The vertical resolution of the mini-airgun is approximately 1.5m as opposed to 25cm for the deep tow boomer. The advantage of the mini-airgun is the deeper penetration due to the lower frequency.

7.4.3.1. Schiehallion

The mini-airgun line through BHS3/S3A/S3B/S3C was used as an example in this case for comparison. The wiggly trace section on Figure 7.30 shows two major reflectors in the first 20ms below seabed. These reflectors correspond to the top and base of the package/mass flow unit seen on the deep tow boomer in Figure 7.26. The mini-airgun section only shows the major reflectors and the finer layering

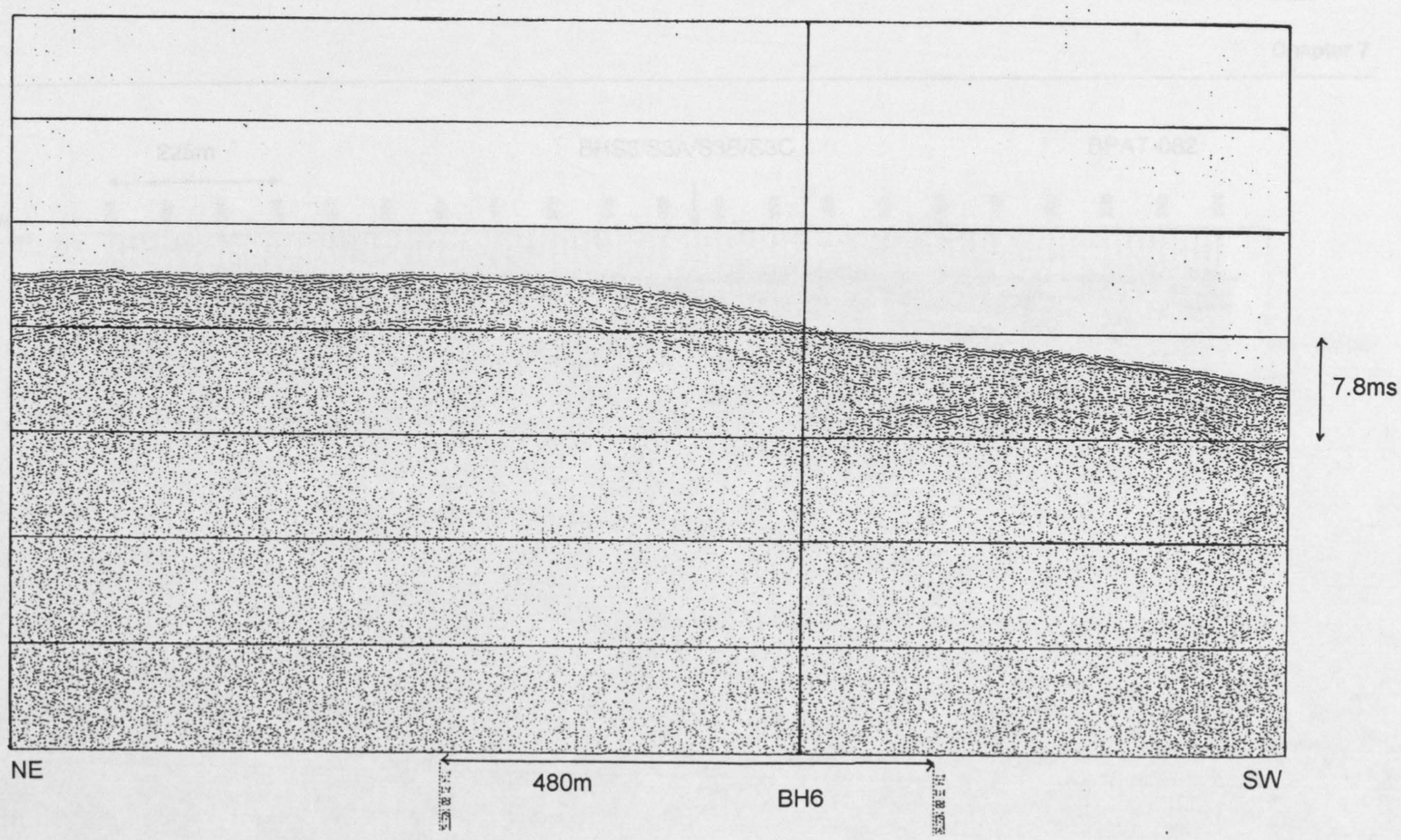

Figure 7.29. BH6 deep tow boomer location profile; BPAT-099. Horizontal scale, 1cm = 59m. Vertical scale, 1cm = 5ms TWT.

Figure 7.29

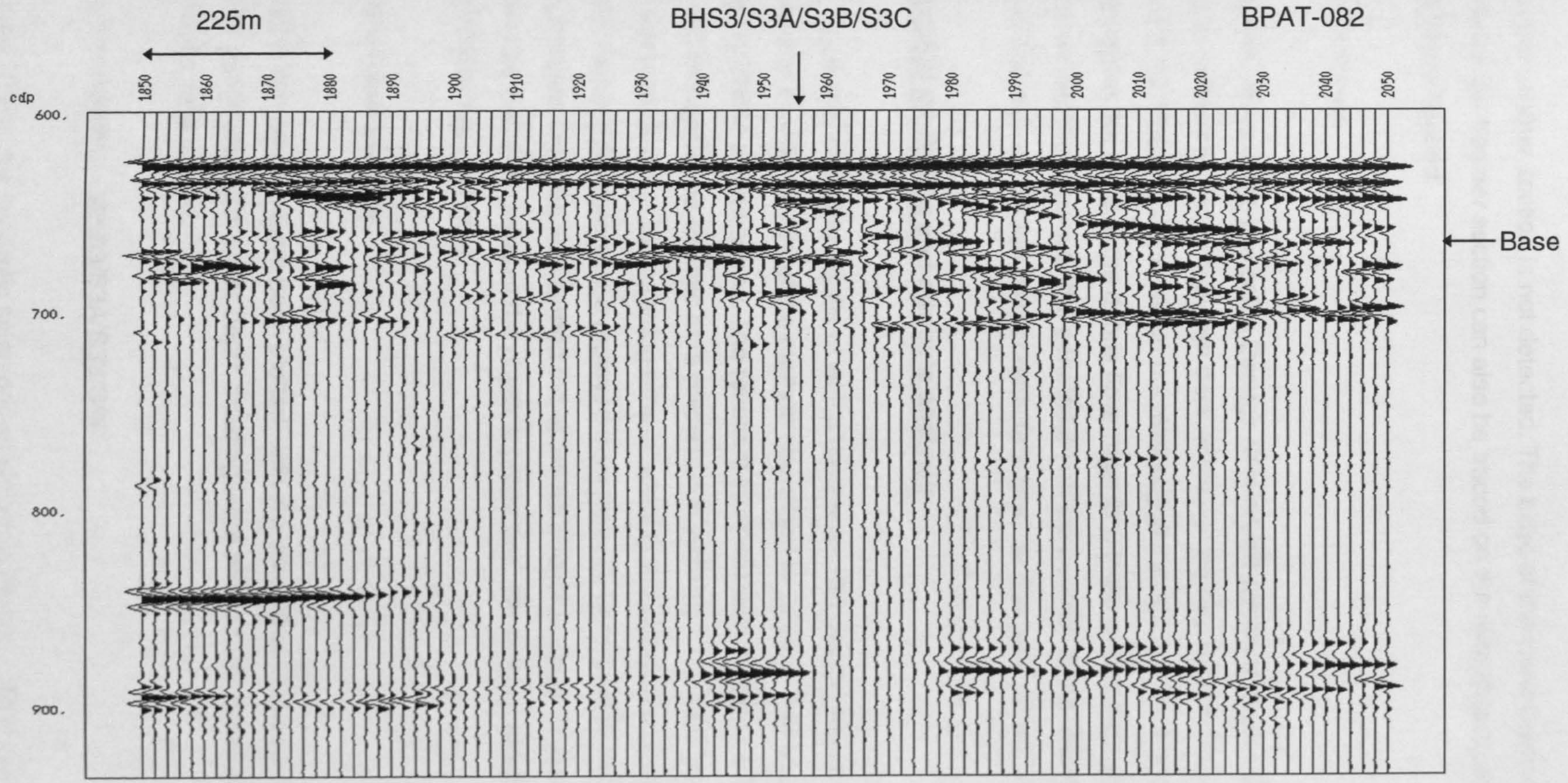

Figure 7.30. BHS3/S3A/S3B/S3C mini-airgun profile.

seen on the boomer section is not detected. The base of the lower layered package on the deep tow boomer section can also be traced on the mini-airgun section at 26.2ms below seabed.

7.4.3.2. Foinaven

In the upper 30ms of the line going through BH4/4A/4B shown in Figure 7.31 some layering is defined on the mini-airgun data which can be seen on the boomer data in Figure 7.28. The reflector seen on the mini-airgun section at 9.3ms below seabed corresponds to the base of the debris flow/mass flow feature identified on the deep tow boomer section. However the penetration on the boomer is not sufficient to pick up any of the high amplitude deeper reflectors seen on the mini-airgun section.

7.5. Forward modelling and attribute analysis

The geotechnical data, the results of which have been discussed in Section 7.4.1, were used to enable the 'Borehole method' described in Chapter 5 to be used to produce synthetic seismograms. The resultant synthetic seismograms will be compared alongside the seismic data presented in Section 7.4.2, and an attempt will be made to describe the seismograms in terms of the physical properties. The analogue seismic data were also replayed from tape, as described in Section 7.3, and an attribute analysis was carried out at the borehole locations to try and establish any patterns between the physical properties, the seismic response and the instantaneous attributes.

7.5.1. Borehole models

Synthetic seismograms have been plotted, with the seabed at 0ms due to the problems associated with water depth creating large amounts of effectively insignificant data points.

7.5.1.1. Schiehallion - BHS3/S3A/S3B/S3C

The upper 7ms of the synthetic seismogram shown in Figure 7.32(a) contains very low amplitude responses with one major reflector close to the seabed. Below the 7ms level there is a closely spaced series of reflecting surfaces, extending to 35ms;

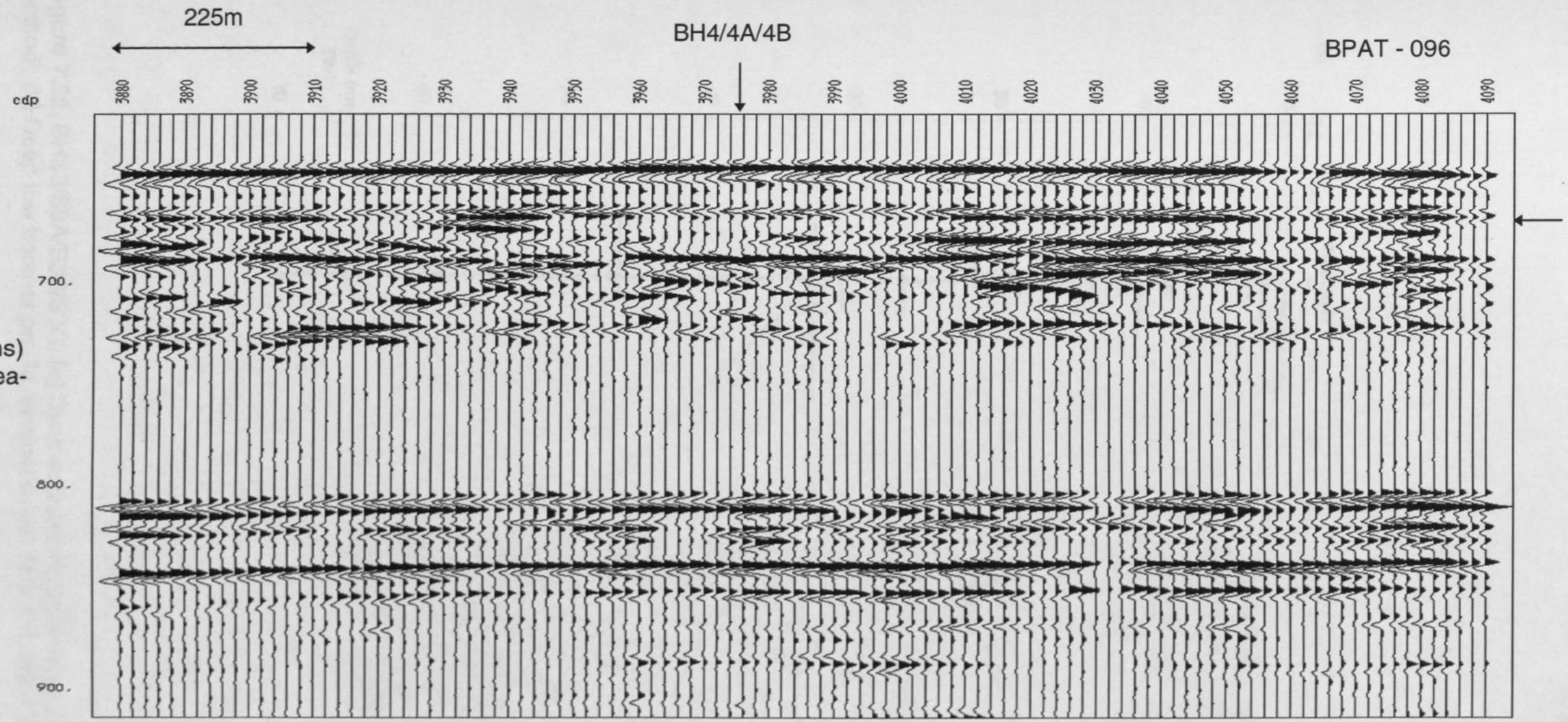

Figure 7.31. BH4/4A/4B mini-airgun profile.

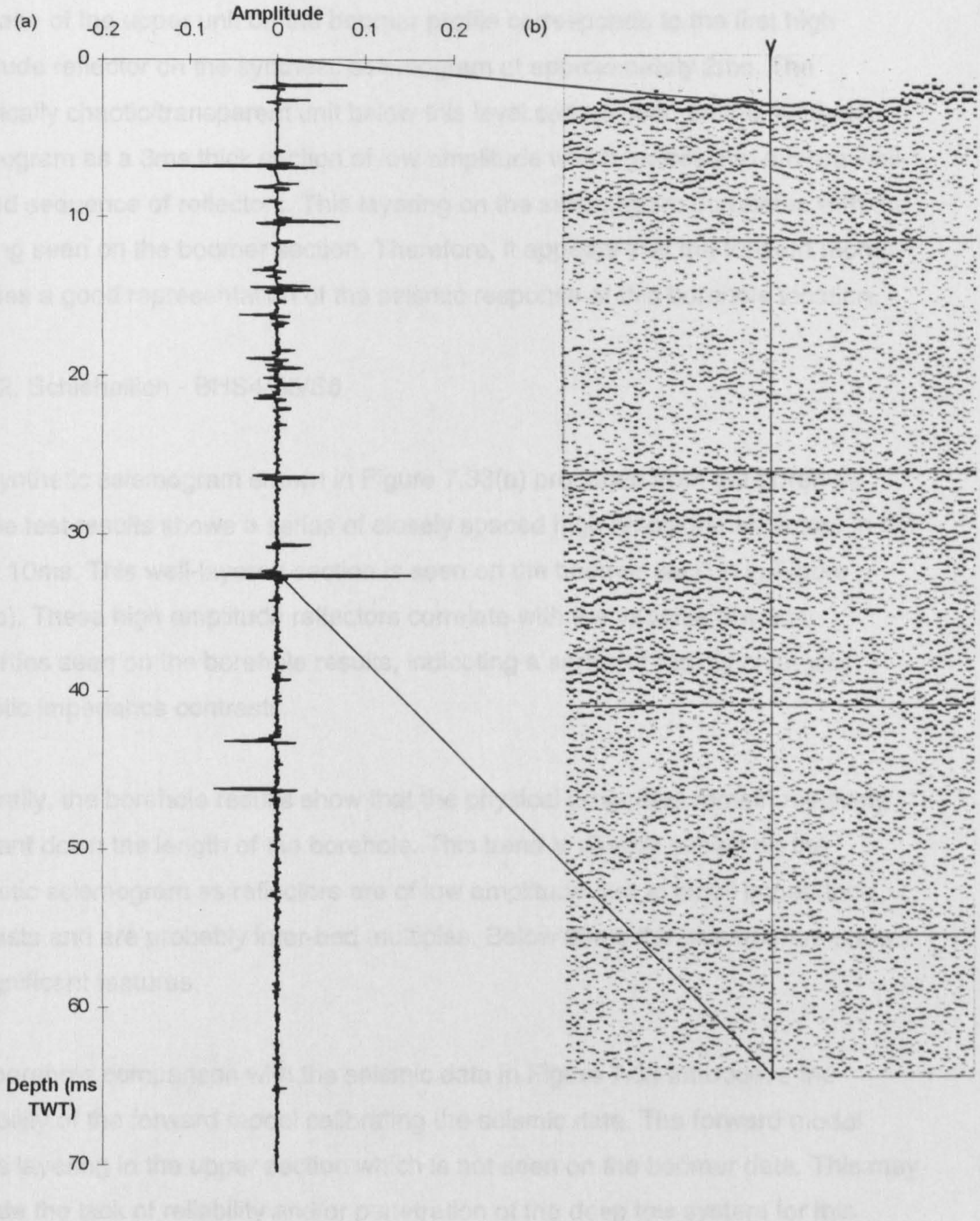

Figure 7.32. BHS3/S3A/S3B/S3C. (a) Synthetic seismogram using the 'Borehole method'. (b) Deep tow boomer profile, vertical scale; 1cm = 2.3ms TWT.

from this point to the base of the seismogram there are less higher amplitude reflectors compared to the section between 7ms and 35ms.

These reflectors can be correlated with the boomer section (see Figure 7.32(b)). The base of the upper unit on the boomer profile corresponds to the first high amplitude reflector on the synthetic seismogram at approximately 2ms. The seismically chaotic/transparent unit below this level can be seen on the synthetic seismogram as a 3ms thick section of low amplitude which grades into a more well-layered sequence of reflectors. This layering on the seismogram correlates with the layering seen on the boomer section. Therefore, it appears that the forward model provides a good representation of the seismic response at this borehole location.

7.5.1.2. Schiehallion - BHS4/S5/S6

The synthetic seismogram shown in Figure 7.33(a) produced from the borehole sample test results shows a series of closely spaced high amplitude reflectors in the upper 10ms. This well-layered section is seen on the boomer section in Figure 7.33(b). These high amplitude reflectors correlate with the variable physical properties seen on the borehole results, indicating a series of rapidly changing acoustic impedance contrasts.

Generally, the borehole results show that the physical properties remain relatively constant down the length of the borehole. This trend is directly shown on the synthetic seismogram as reflectors are of low amplitude due to small impedance contrasts and are probably inter-bed multiples. Below 20ms the seismogram shows no significant features.

This borehole comparison with the seismic data in Figure 7.33 introduces the possibility of the forward model calibrating the seismic data. The forward model shows layering in the upper section which is not seen on the boomer data. This may indicate the lack of reliability and/or penetration of the deep tow system for this environment. However, this forward model may also be biased by the geotechnical sampling frequency, since the layering shown in the upper part of the seismic section is not present in the early part of the synthetic seismogram. In this instance the layering present in the seismic data may in part be due to out of plane reflections or side swipe.

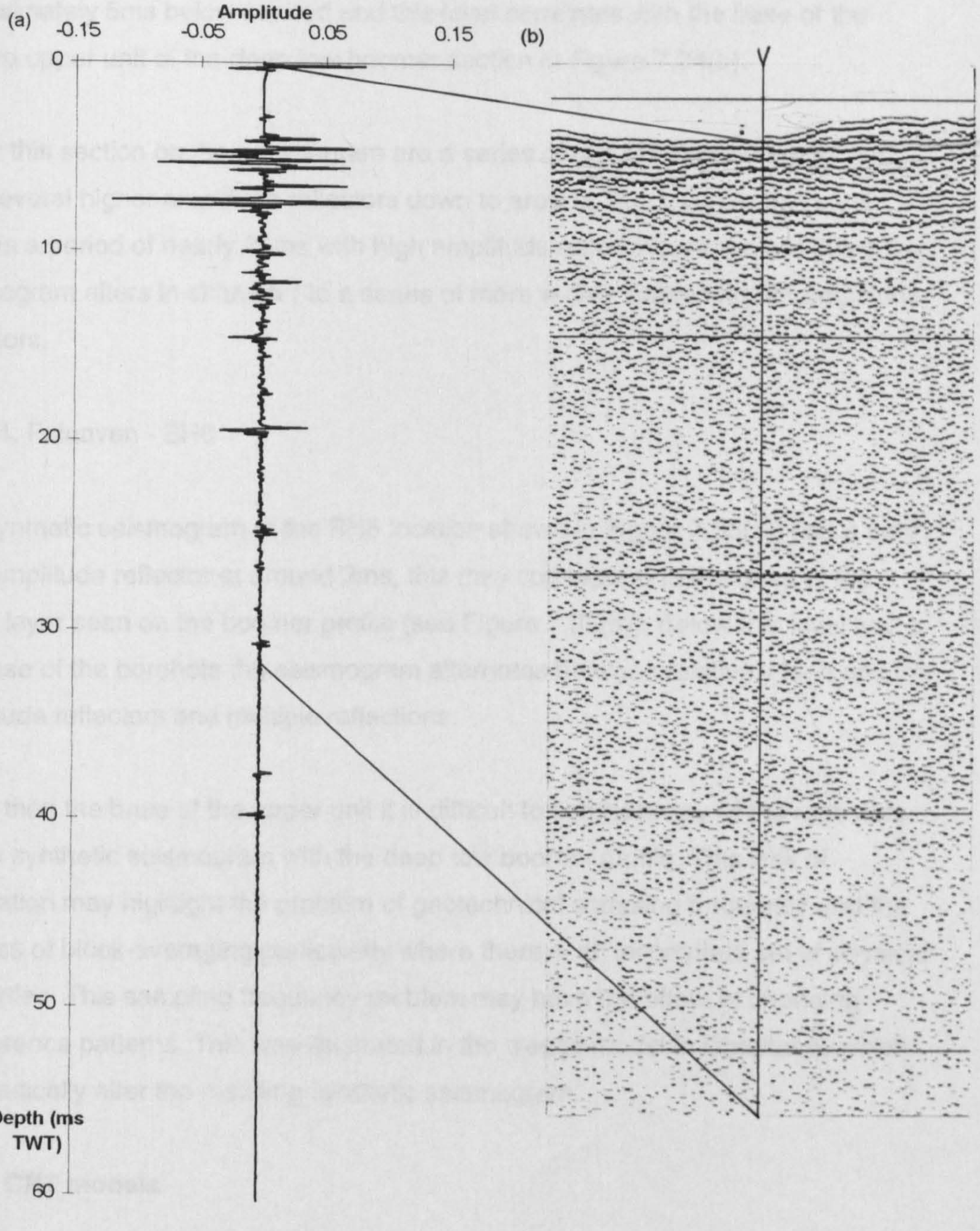

Figure 7.33. BHS4/S5/S6. (a) Synthetic seismogram using the 'Borehole method'. (b) Deep tow boomer profile, vertical scale; 1cm = 2.3ms TWT.

7.5.1.3. Foinaven - BH4/4A/4B

The synthetic seismogram in Figure 7.34(a) shows an upper section with no apparent reflectors to about 2.5ms below seabed. There is a high amplitude peak at approximately 5ms below seabed and this level correlates with the base of the layered upper unit of the deep tow boomer section in Figure 7.34(b).

Below this section on the seismogram are a series of regularly spaced reflectors with several higher amplitude reflectors down to around 28ms. Below this level there is a period of nearly 20ms with high amplitude reflectors. At around 50ms the seismogram alters in character to a series of more widely spaced higher amplitude reflectors.

7.5.1.4. Foinaven - BH6

The synthetic seismogram at the BH6 location shown in Figure 7.35(a), has a very high amplitude reflector at around 3ms, this may correspond to the base of the upper layer seen on the boomer profile (see Figure 7.35(b)). Below this level and to the base of the borehole the seismogram alternates between relatively high and low amplitude reflectors and multiple reflections.

Other than the base of the upper unit it is difficult to correlate any of the reflectors on the synthetic seismogram with the deep tow boomer profile. This lack of correlation may highlight the problem of geotechnical sampling frequency and the process of block-averaging particularly where there is an incomplete set of physical properties. This sampling frequency problem may have the effect of changing interference patterns. This was illustrated in the wedge model in Chapter 5, which may radically alter the resulting synthetic seismogram.

7.5.2. CPT models

Following the 'CPT method' presented in Chapter 6, downhole PCPT results, where available, were analysed, classified for sediment type and then used to produce synthetics.

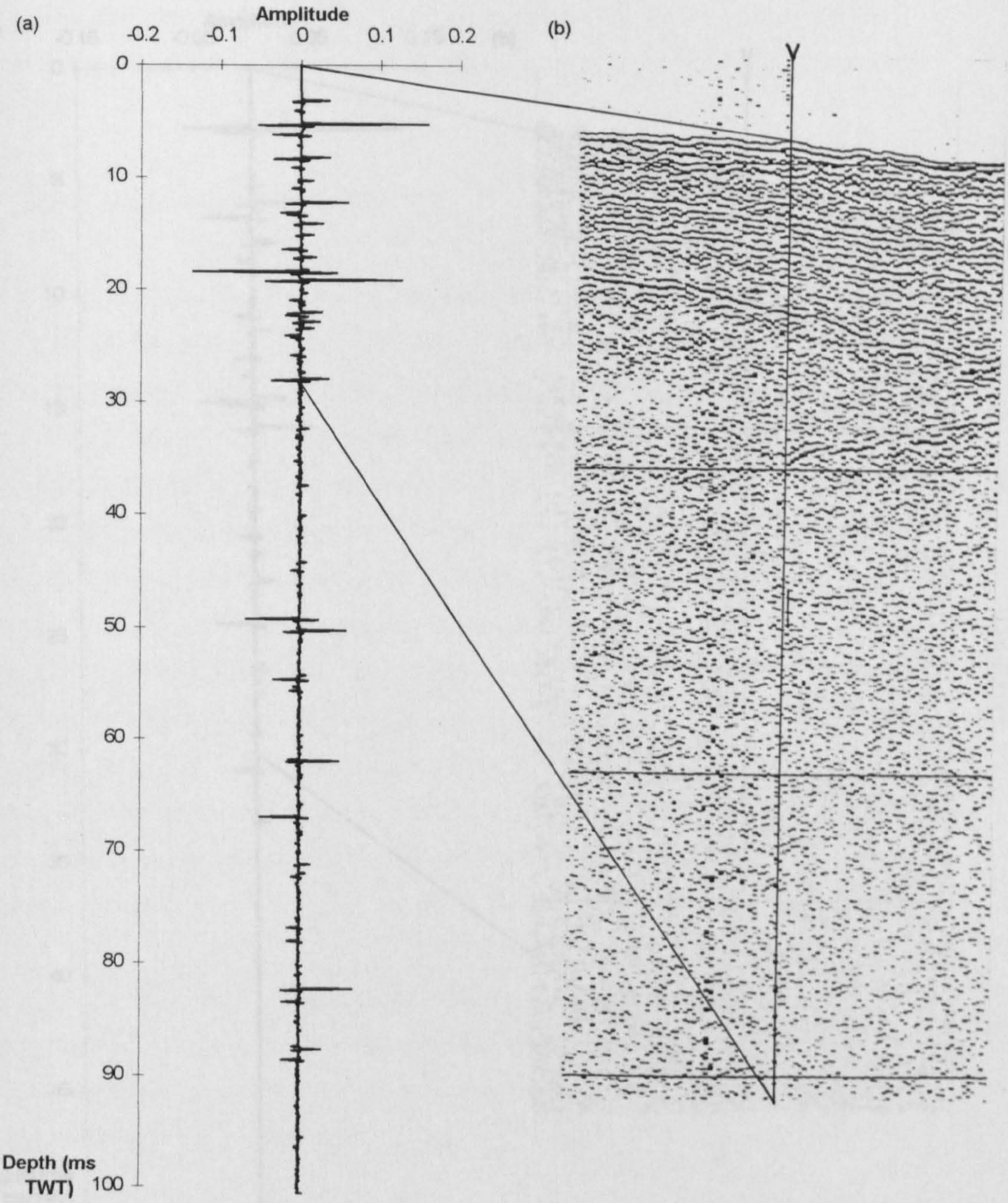

Figure 7.34. BH4/4A/4B (a) synthetic seismogram using the 'Borehole method'. (b) Deep tow boomer profile, vertical scale; 1cm = 1.8ms TWT.

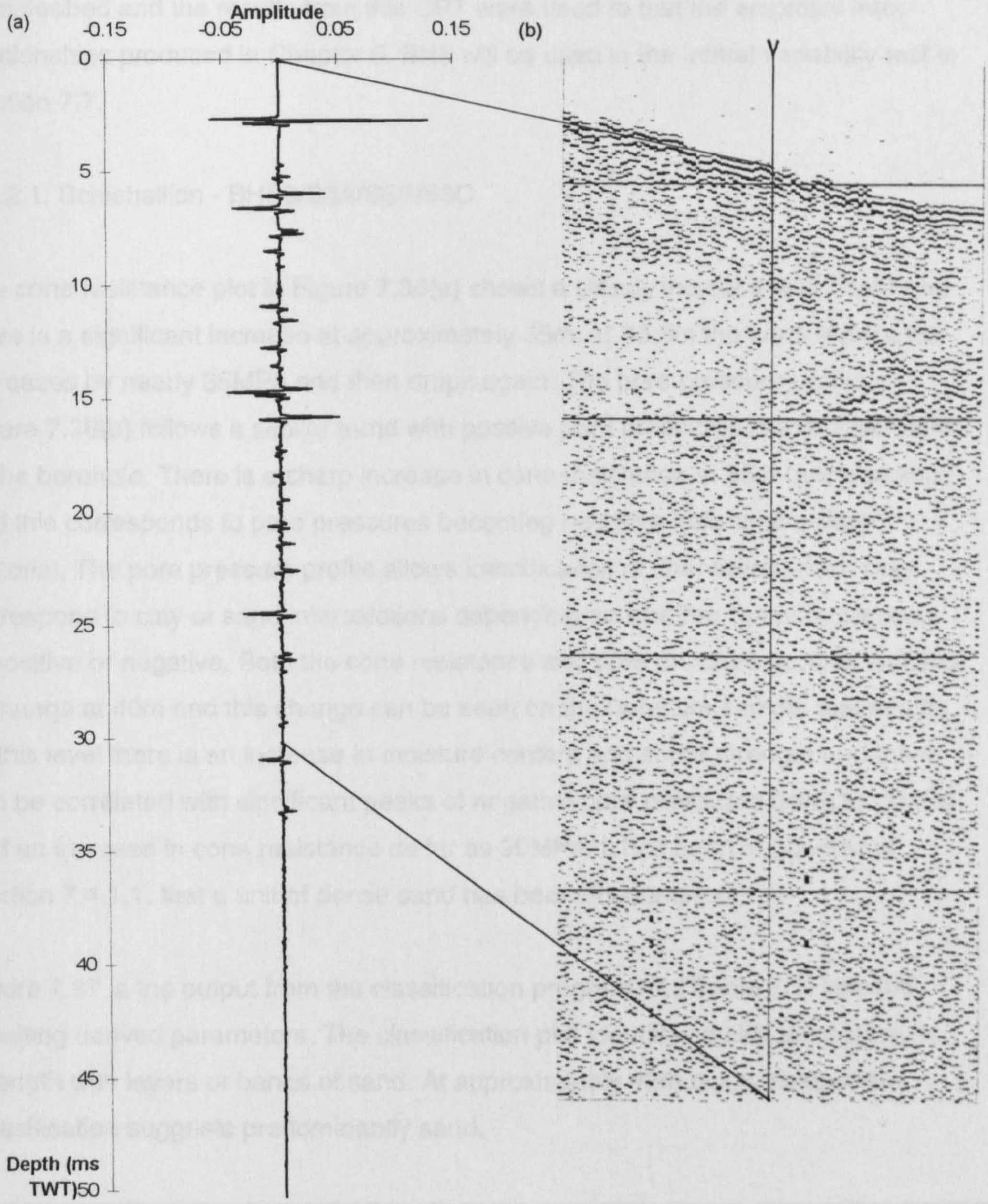

Figure 7.35. BH6. (a) Synthetic seismogram using the 'Borehole method'. (b) Deep tow boomer profile, vertical scale; 1cm = 2.3ms TWT.

In the Schiehallion area BHS6 was logged by PCPT from the seabed enabling direct comparison with the deep tow boomer sections and BHS3/S3A/S3B/S3C was analysed for completeness. In the Foinaven area the results from BH4/4A/4B have been included for illustration. PCPT11 from the Foinaven area was also analysed from seabed and the results from this CPT were used to test the empirical inter-relationships produced in Chapter 6. BH6 will be used in the lateral variability test in Section 7.7.

7.5.2.1. Schiehallion - BHS3/S3A/S3B/S3C

The cone resistance plot in Figure 7.36(a) shows a steady increase with depth and there is a significant increase at approximately 35m; at 38.5m the cone resistance increases by nearly 35MPa and then drops again. The pore pressure profile in Figure 7.36(b) follows a similar trend with positive pore pressures in the upper 35m of the borehole. There is a sharp increase in cone resistance at 36m below seabed and this corresponds to pore pressures becoming negative indicating denser material. The pore pressure profile allows identification of finer detail which may correspond to clay or sand intercalations depending on whether the pore pressure is positive or negative. Both the cone resistance and pore pressure profiles indicate a change at 40m and this change can be seen on the borehole sample test results. At this level there is an increase in moisture content and shear strength and these can be correlated with significant peaks of negative pore pressures down to -5MPa and an increase in cone resistance as far as 90MPa. It has been suggested in Section 7.4.1.1. that a unit of dense sand has been encountered.

Figure 7.37 is the output from the classification program and Table 7.1. lists the resulting derived parameters. The classification plot identifies a clay increasing in strength with layers or bands of sand. At approximately 43m below seabed the classification suggests predominantly sand.

Depth interval (m)	Velocity (m/s) after Hamilton and Bachman (1982)	Density (Mg/m^3)	Impedance ($Mg/m^2/s$)	Time (ms) TWT	Reflection coefficient
26-29	1849	2.11	3902	3.2	0.10
29-35	1908	2.18	4159	6.3	0.03
35-38	1981	2.26	4476	3.0	0.04

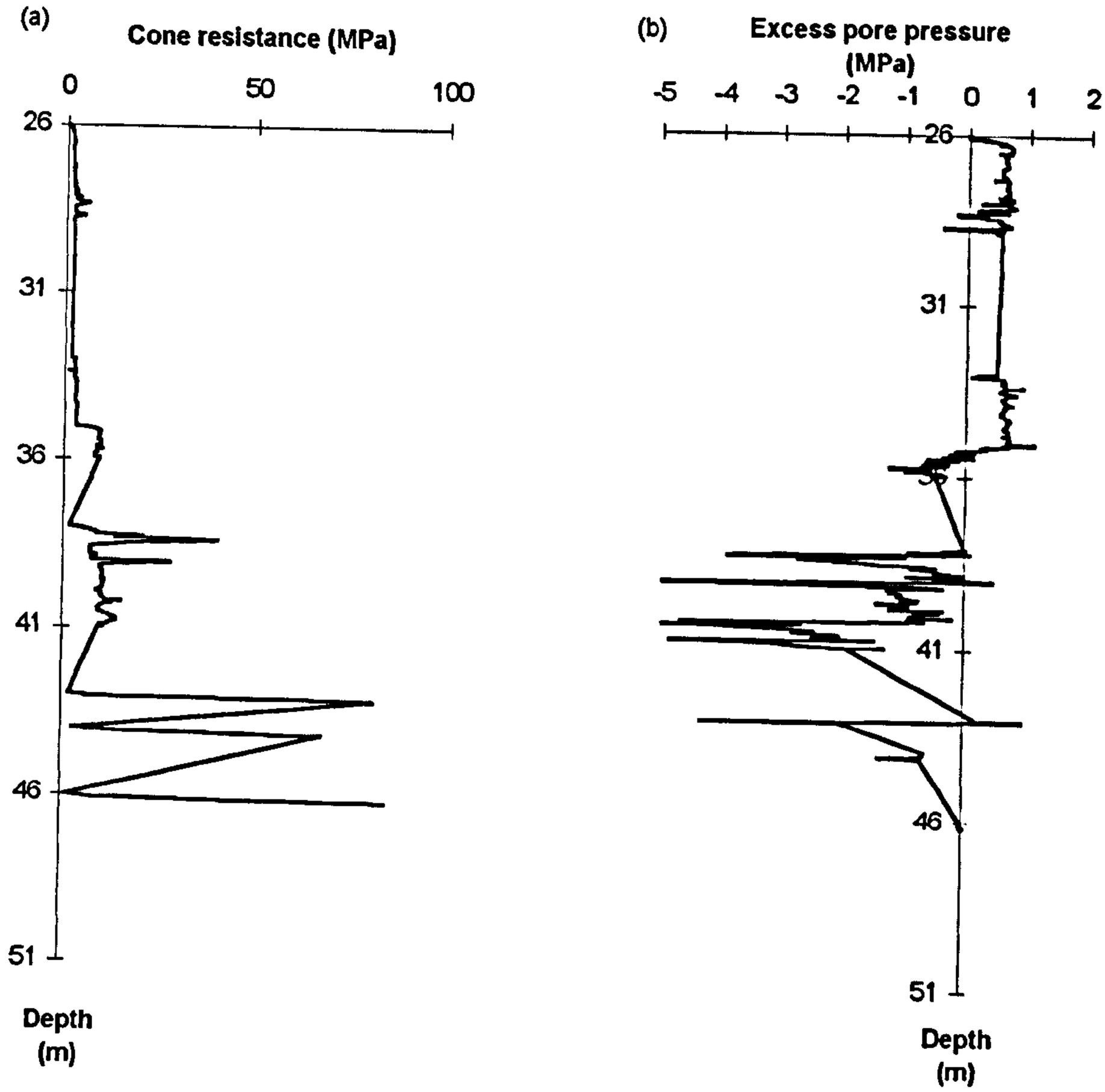

Figure 7.36. BHS3/S3A/S3B/S3C profiles. (a) Cone resistance. (b) Pore pressure.

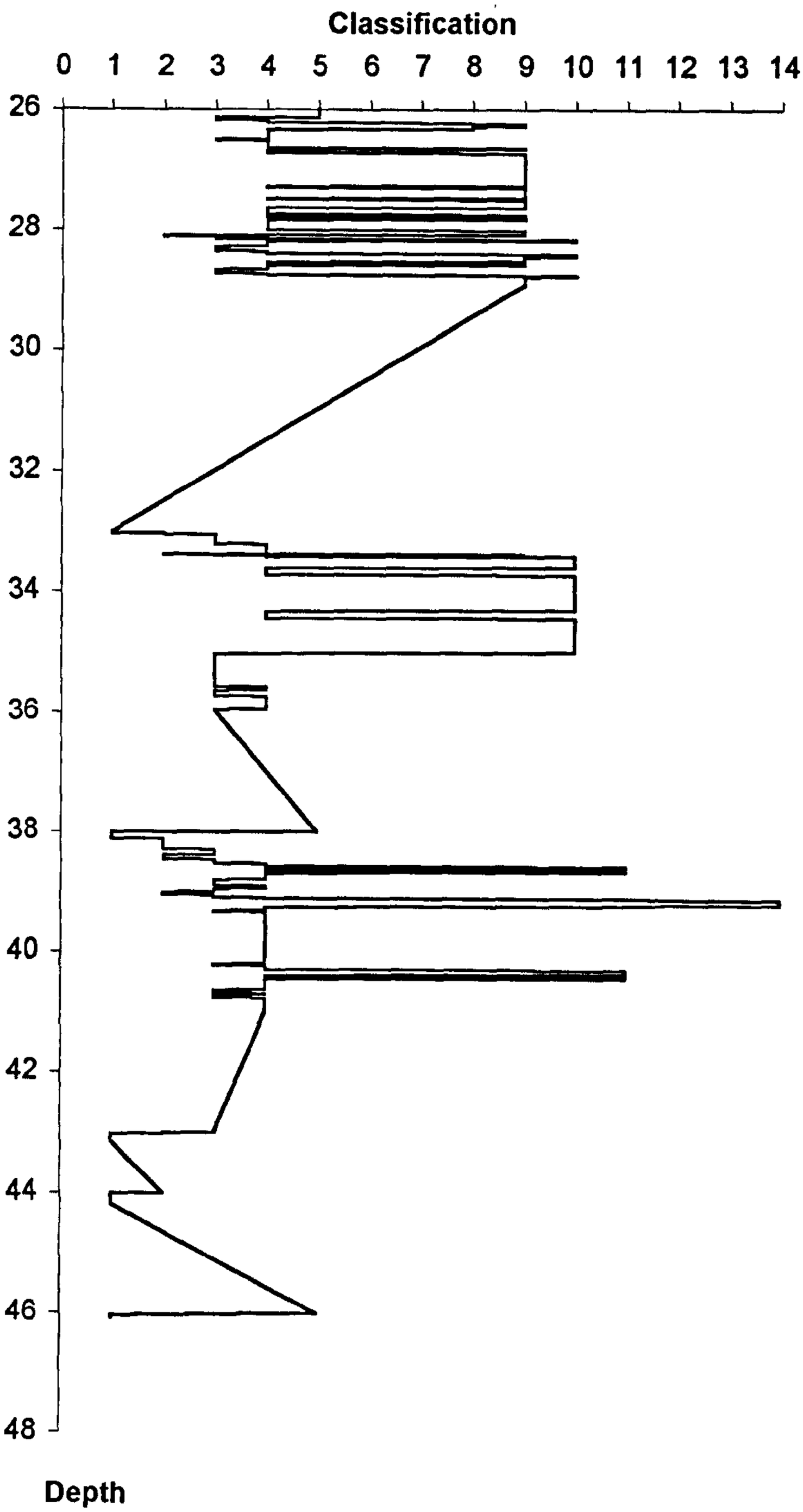

Figure 7.37. BHS3/S3A/S3B/S3C sediment classification.

38-43	2000	2.28	4559	5.0	0.01
43-46	1842	2.10	3867	3.3	-0.08
46-46.5	1685	1.87	3151	0.6	-0.10

Table 7.1. BHS3/S3A/S3B/S3C parameters

The synthetic seismogram produced in Figure 7.38(a) identifies these boundaries and the associated multiples. The reflectors on the 'CPT method' synthetic seismogram can be confidently correlated with the reflectors on the 'Borehole method' seismogram in Figure 7.38(b), despite the lack of data from the seabed to 26m below seabed.

7.5.2.2. Schiehallion - BHS4/S5/S6

Cone resistance and pore pressure versus depth are plotted in Figure 7.39(a) and 7.39(b) respectively. The cone resistance increases steadily over the first 20m with a sharp peak at 3.5m and 15m. The pore pressures are increasingly positive over the first 3m which could indicate a normally consolidated clay. The pore pressure trend over this interval shows a more frequent pattern of layers than can be seen in Figure 7.39(a). The peak in cone resistance at 15m below seabed corresponds to a negative pore pressure of approximately 0.5MPa. Below 20m the cone resistance and pore pressure values are more variable (the smooth lines indicate areas of no data). The section below 40m shows large peaks in cone resistance and sharp drops in positive pore pressure. The layers encountered within the borehole appear to be of sufficient thickness to be identified both on the cone resistance and pore pressure profiles.

From 33m below seabed to the end of the borehole both plots show a much more variable sequence of both cone resistance and pore pressure values. It is difficult to identify the point at which this begins due to gaps in the acquisition. Generally the cone resistance and pore pressure profiles correlate with the borehole sample test results which indicate a relatively linear trend of increase with depth.

Figure 7.40 gives the results from the classification program and the parameters derived are listed in Table 7.2. The plot shows a very variable trend and the upper 4m from seabed consists of very soft clay. The general inferred trend is a clay

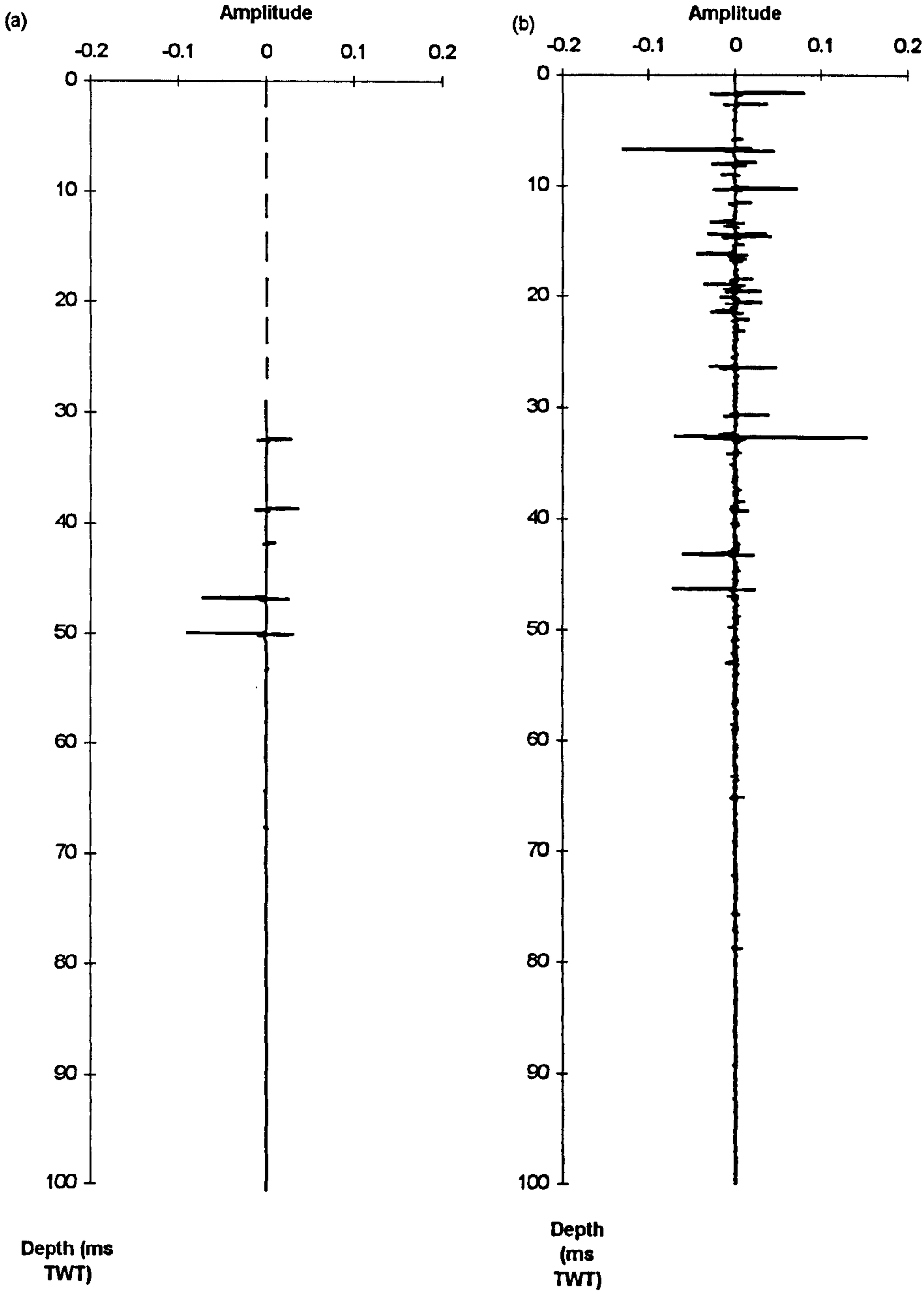

Figure 7.38. BHS3/S3A/S3B/S3C. (a) Synthetic seismogram using the 'CPT method'. (b) Synthetic seismogram using the 'Borehole method'.

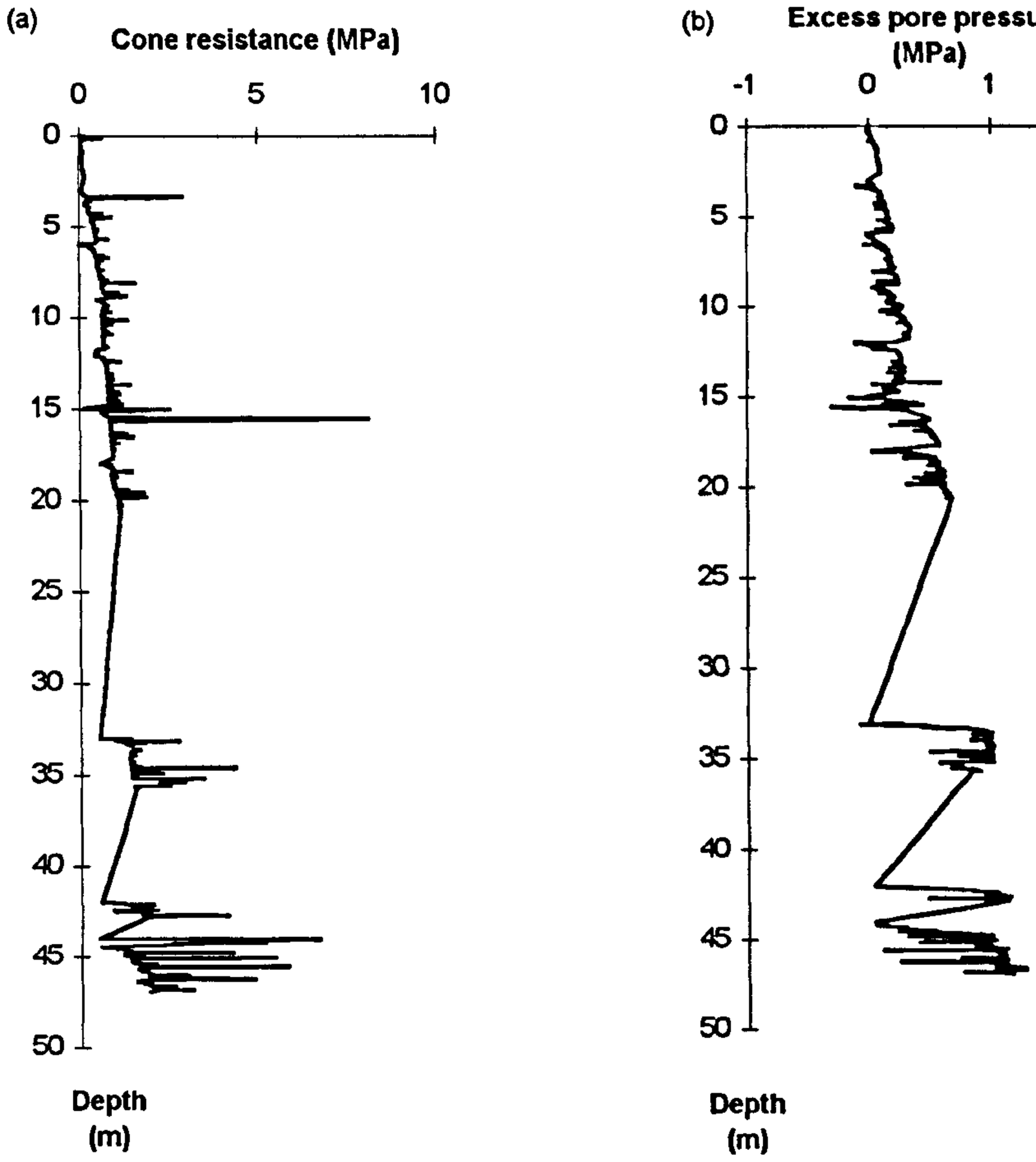

Figure 7.39. BHS4/S5/S6 profiles. (a) Cone resistance. (b) Pore pressure.

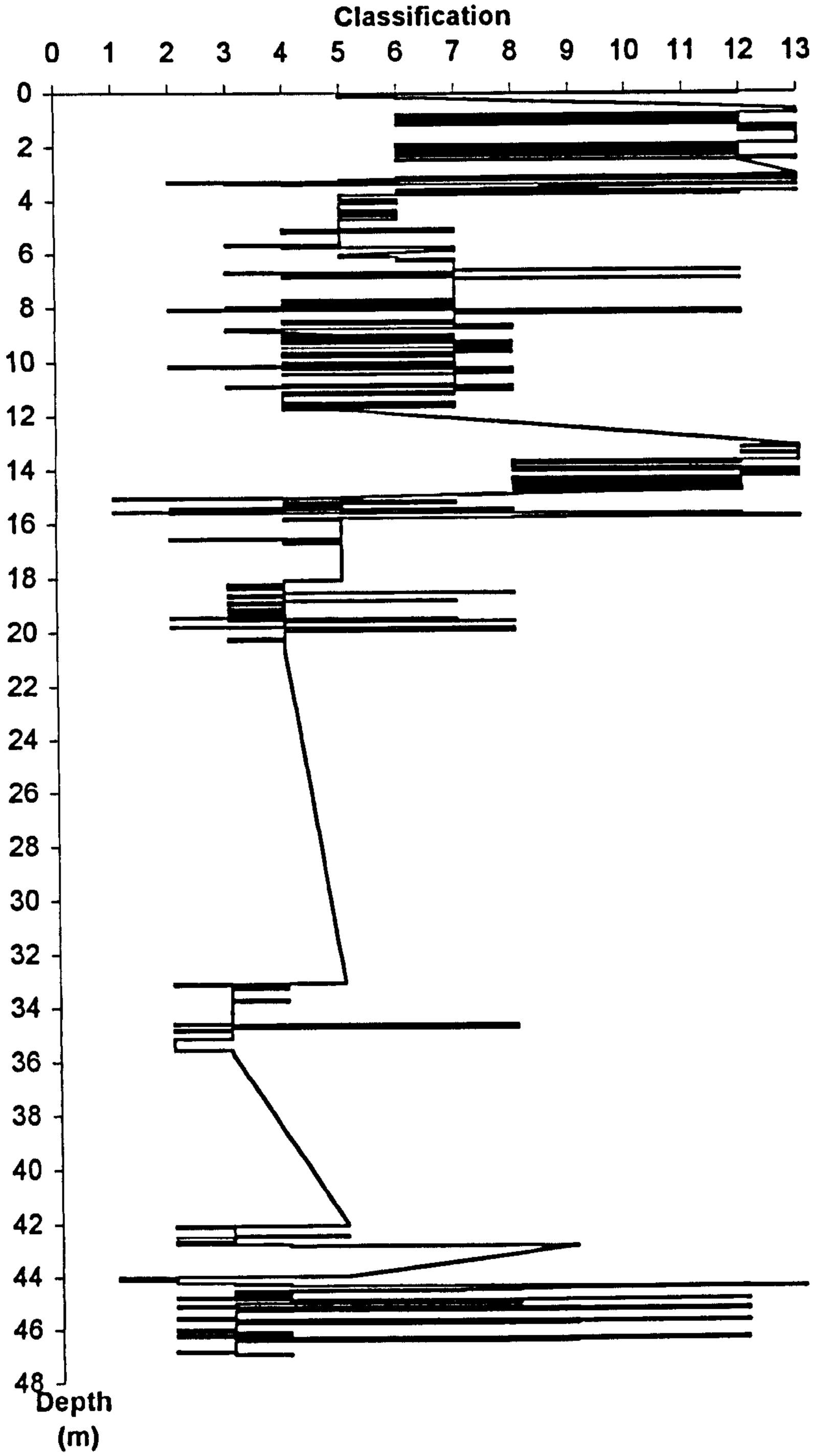

Figure 7.40. BHS4/S5/S6 sediment classification.

increasing in strength with layers and bands of sand and stiffer clay, perhaps gravels and shells also present.

Depth interval (m)	Velocity (m/s) after Hamilton and Bachman (1982)	Density (Mg/m^3)	Impedance ($Mg/m^2/s$)	Time (ms) TWT	Reflection coefficient
0-5	1721	1.93	3322	5.8	0.37
5-11.8	1767	2.00	3534	7.7	0.03
11.8-15	1882	2.15	4047	3.4	0.07
15-21	1891	2.16	4084	6.4	0
21-36	1908	2.18	4159	15.7	0.01
36-46	1934	2.21	4275	10.3	0.01

Table 7.2. BHS6 parameters

The synthetic seismogram in Figure 7.41(a) shows a particularly high amplitude at 14ms below seabed indicating the significant change identified on the classification chart. However, the seismic characters defined on the boomer section in Figure 7.27 and 7.41(b) are less clearly identified.

The general trend of the synthetic seismograms from the 'Borehole and CPT methods', Figures 7.41(a) and 7.41(c) are similar, particularly the peak amplitudes at approximately 6ms. However, fewer reflection coefficient points in the 'CPT method' reflect the inherent difficulties in the blocking processes depending on the data which is available.

7.5.2.3. Foinaven - BH4/4A/4B

Figure 7.42(a) is a plot of cone resistance with depth and Figure 7.42(b) is excess pore pressure versus depth. The cone resistance plot shows a steady increase with depth until 90m below seabed. The cone resistance at this level becomes erratic with a sharp increase which then decreases markedly before another sharp increase at the bottom of the profile. The cone resistance spike at approximately 88m below seabed can be recognised on the pore pressure profile however no more measurements were made below this level.

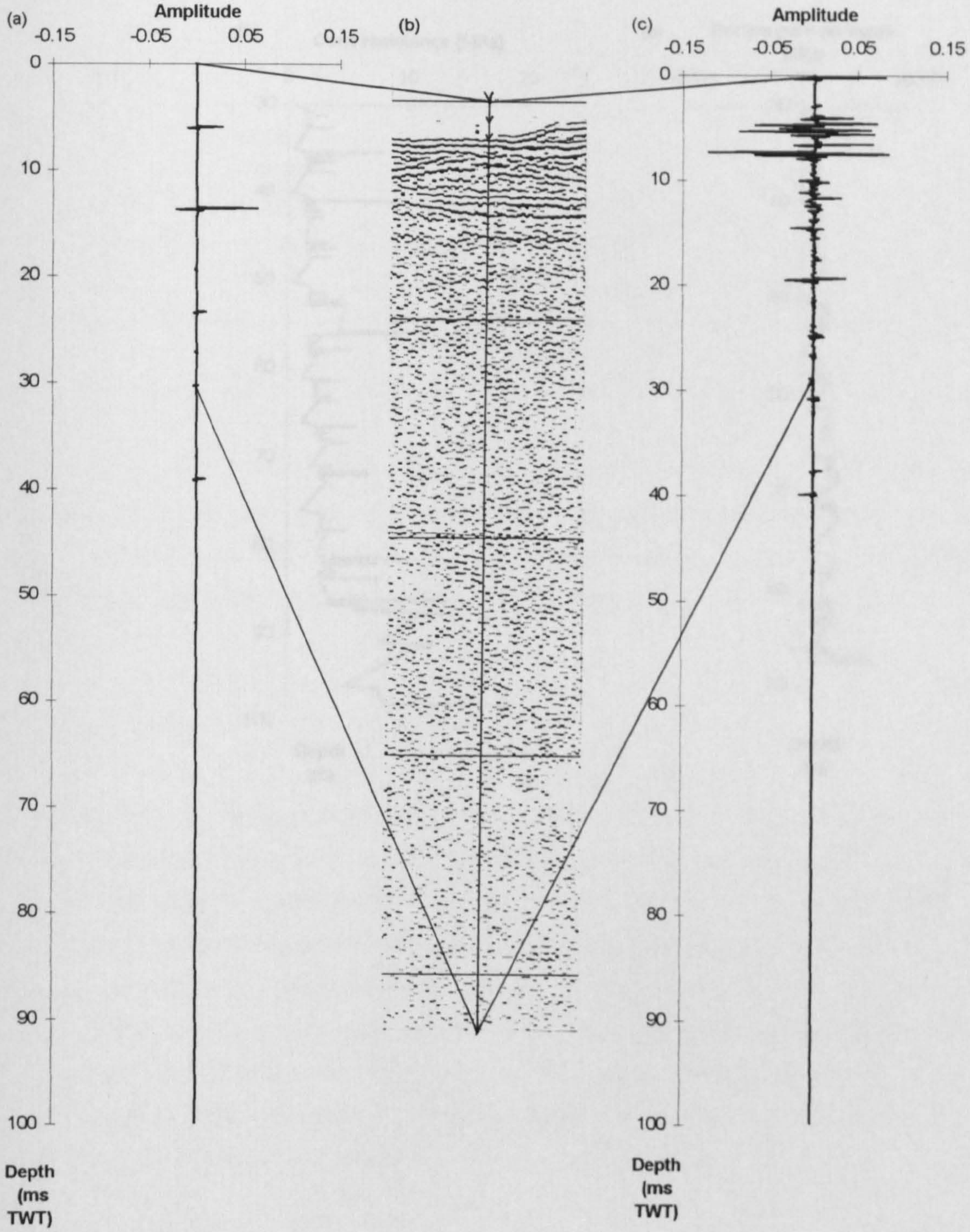

Figure 7.41. BHS4/S5/S6. (a) Synthetic seismogram using the 'CPT method'. (b) Deep tow boomer profile, vertical scale; 1cm = 2.3ms TWT. (c) Synthetic seismogram using the 'Borehole method'.

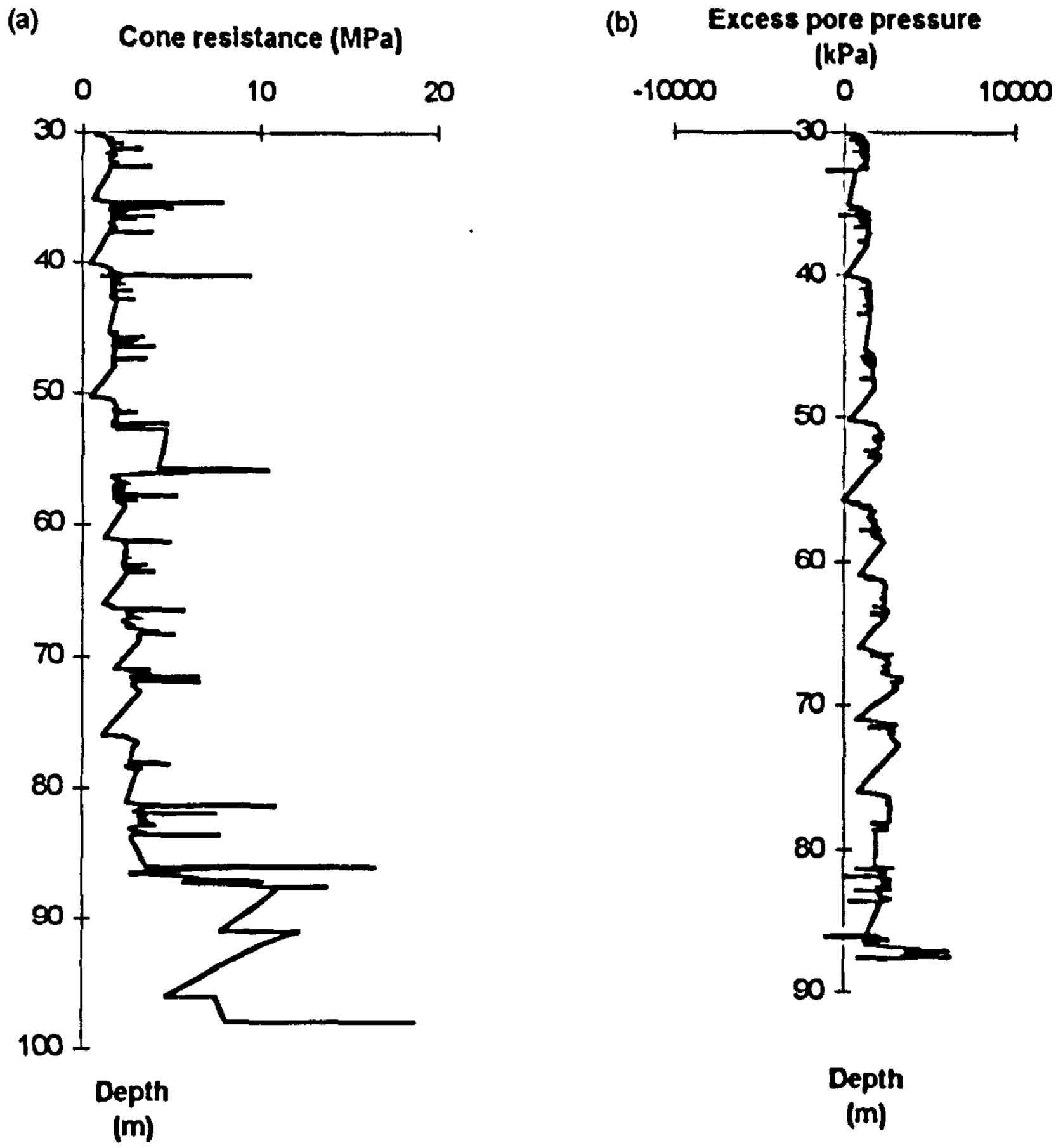

Figure 7.42. BH4/4A/4B profiles. (a) Cone resistance. (b) Pore pressure.

The cone resistance and sleeve friction measurements were run through the classification program and Figure 7.43 is the plot of the output. The character of the classification profile mirrors the trend of Figures 7.42(a) and 7.42(b) which is a function of the acquisition.

Depth interval (m)	Velocity (m/s) after Hamilton and Bachman (1982)	Density (Mg/m^3)	Impedance ($Mg/m^2/s$)	Time (ms) TWT	Reflection coefficient
30-35	1948	2.23	4334	5.1	-0.05
35-83	1858	2.12	3938	51.7	-0.05
83-91	1845	2.11	3885	8.7	-0.01

Table 7.3. BH4/4A/4B parameters

The parameters listed in Table 7.3 reflect the synthetic response in Figure 7.44(a) which has one main reflector at approximately 5ms and the second at the 83ms boundary. Due to the CPT data quality it is difficult to relate the results to either the physical properties or the 'Borehole method' synthetic seismogram in Figure 7.44(b).

7.5.2.4. PCPT11

The cone resistance plot (Figure 7.45(a)) shows a clay increasing in strength with a peak at around 10m below seabed where the cone resistance increases significantly over approximately 2m. The general trend of the pore pressure plot (Figure 7.45(b)) shows the positive pore pressures increasing with depth. The section to around 7m shows a smooth trend; however the section from 7m to 15m contains some thin layers with negative pore pressures which may be the result of sand. The interval between approximately 15m and 20m has a smoother trend. From 20m to the end of the PCPT there is more stratification with a large drop in pore pressure at 23m probably due to a change in the strength of the clay.

As a further test of extracting and integrating physical properties from CPT results, undrained shear strength was calculated using cone resistance. Equation 6.1 relates cone resistance to shear strength and overburden pressure. This equation

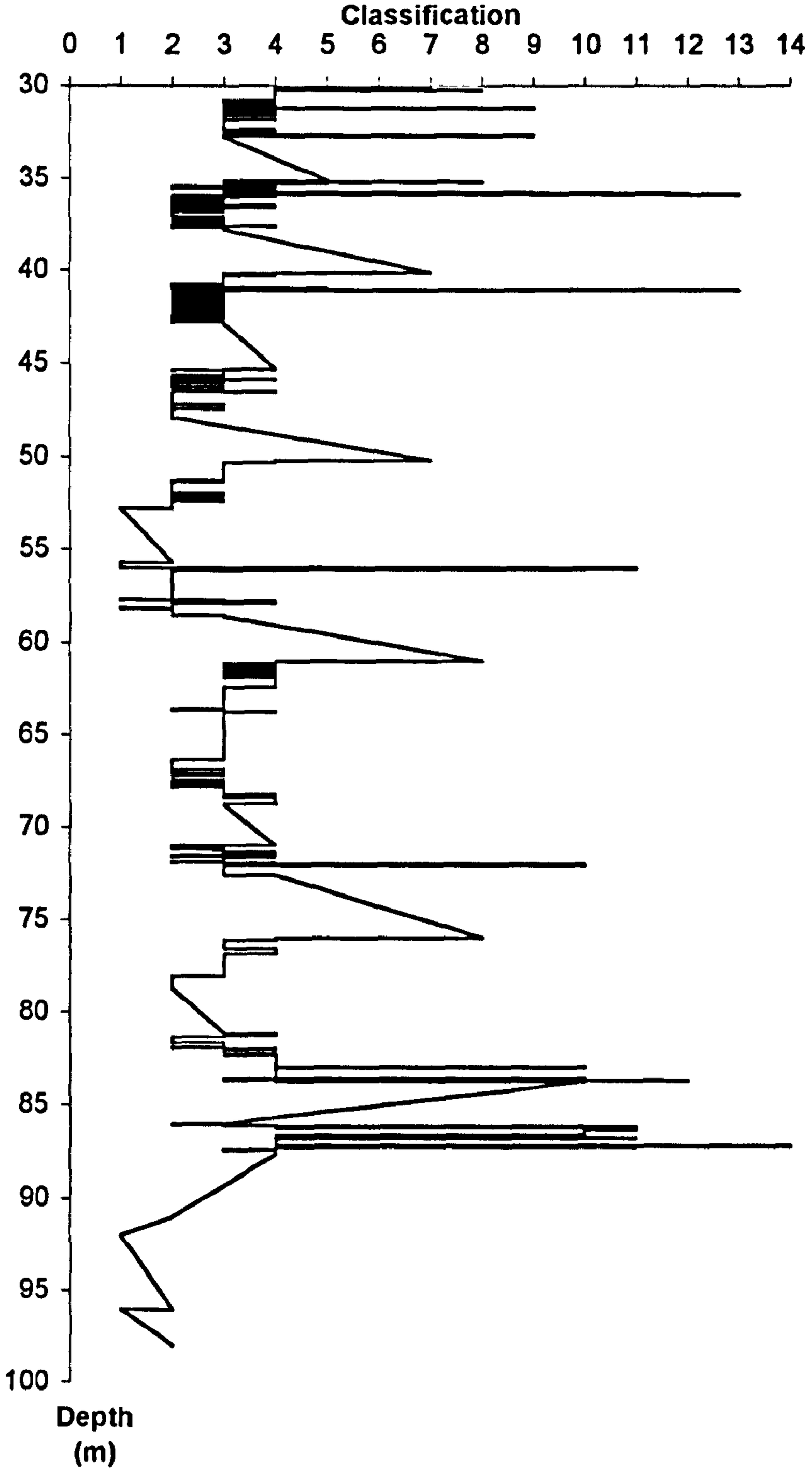

Figure 7.43. BH4/4A/4B sediment classification.

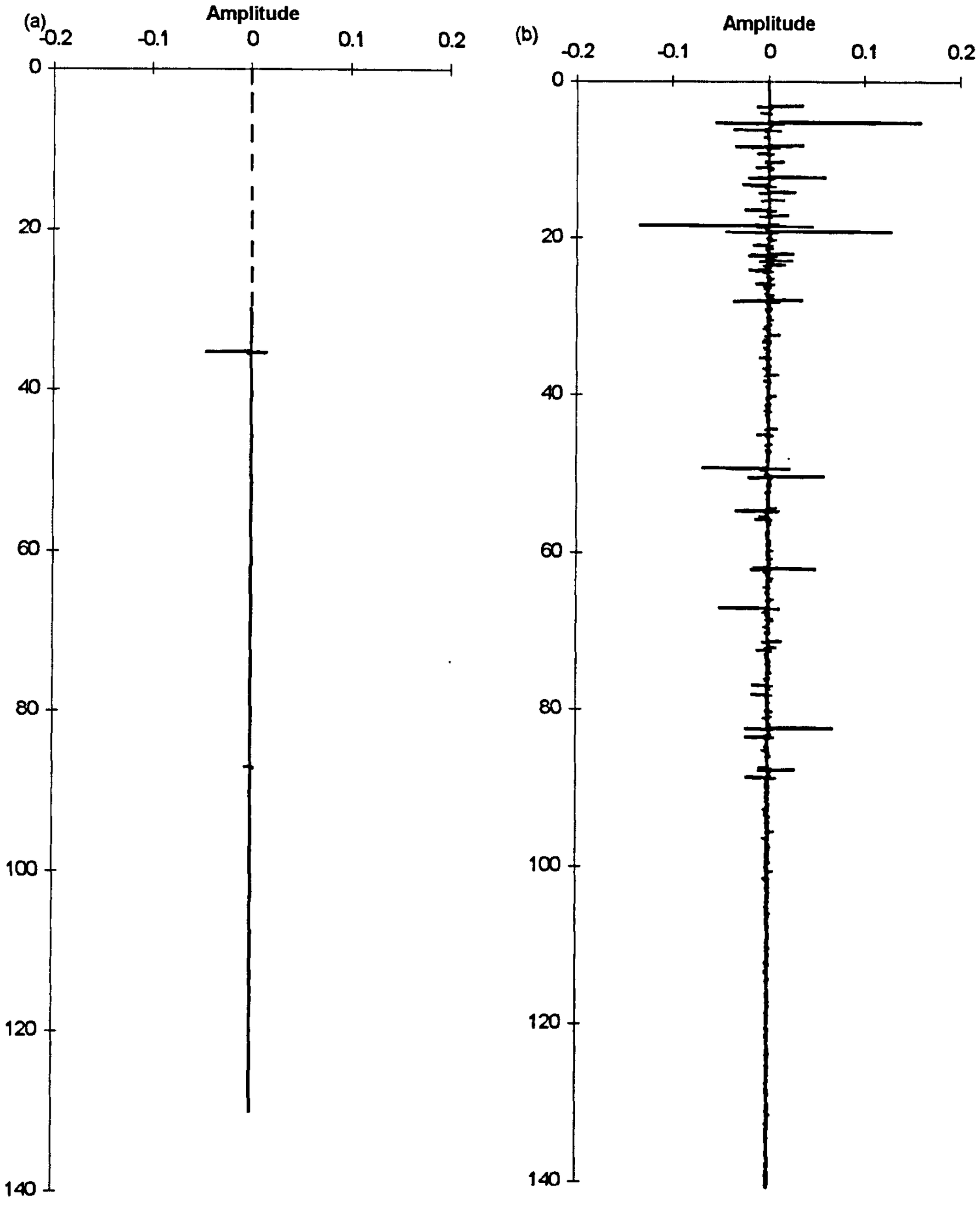

Figure 7.44. BH4/4A/4B. (a) Synthetic seismogram using the 'CPT method'. (b) Synthetic seismogram using the 'Borehole method'.

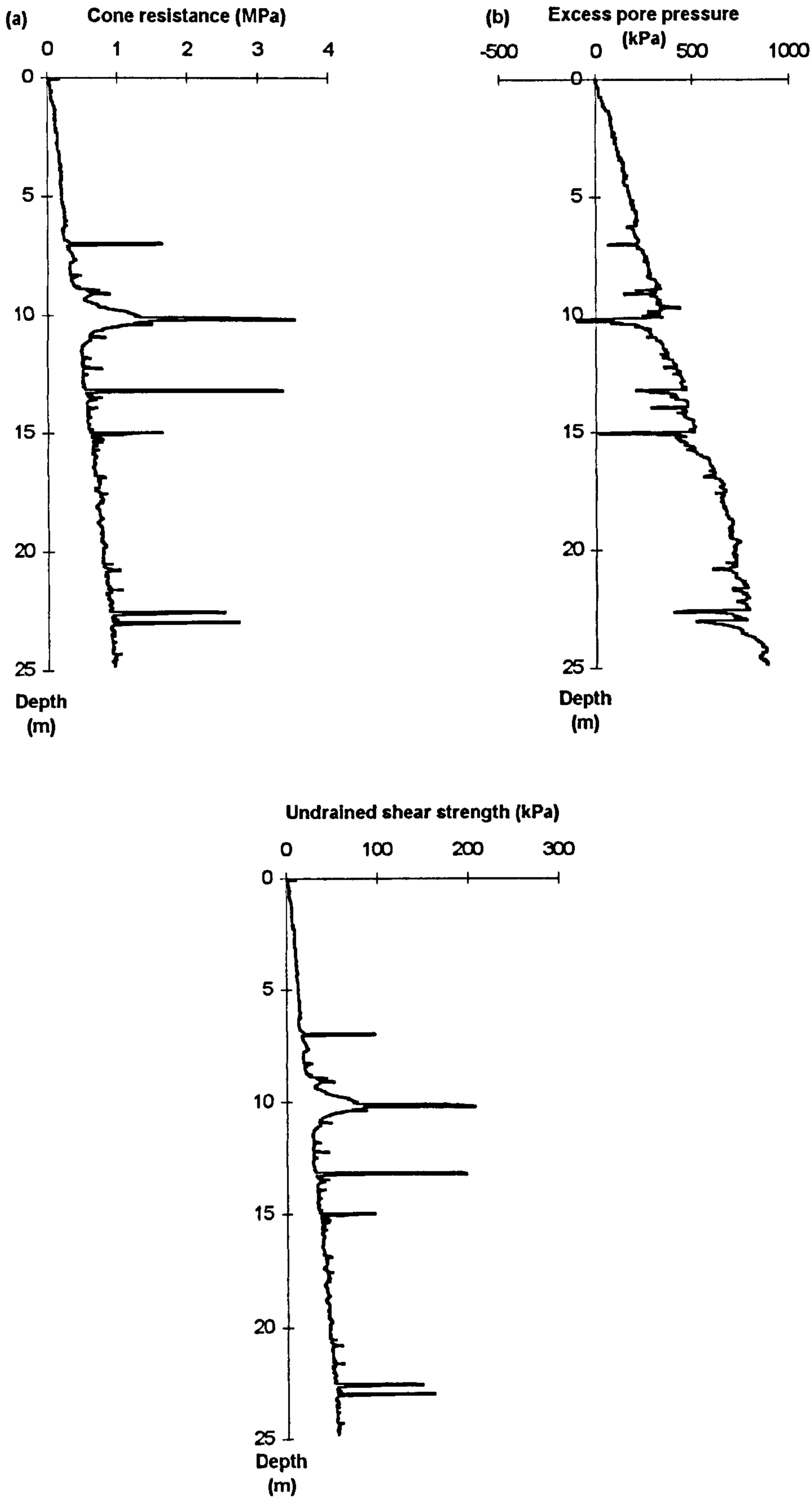

Figure 7.45. PCPT11 profiles. (a) Cone resistance. (b) Pore pressure. (c) Undrained shear strength.

can be modified to allow the overburden pressure to be included in the unitless cone factor to give:

$$q_c = s_u N'_k \qquad (7.1)$$

Various studies, such as Robertson and Campanella (1983b), quote average values of N_k. However, it is obviously preferable to determine the cone factor empirically or by correlation from previous work on the clay in question.

Figure 7.45(c) is a plot of undrained shear strength against depth. Equation 7.1 was used to calculate undrained shear strength and a cone factor of 17 was estimated from the results of Fugro Ltd. (1994). Comparison of the undrained shear strength profile against the pore pressure plot shows that the changes on the pore pressure curve can be correlated with high amplitude peaks on the shear strength curve indicating possible interbedded lenses of harder clay or dense sand.

The classification program output for PCPT11 (Figure 7.46) identifies a relatively simple sequence, i.e. a clay increasing in strength with depth. The interpretation of the output is that there is very soft clay close to seabed grading to a firm clay at approximately 20m below seabed. There is some scatter on the plot although the major trends can generally be easily identified.

The parameters which calculated from the results of PCPT11 and which form the input to the synthetic seismogram program are listed in Table 7.4.

Depth interval (m)	Velocity (m/s) after Hamilton and Bachman (1982)	Density (Mg/m^3)	Impedance ($Mg/m^2/s$)	Time (ms)	Reflection coefficient
0-10.62	1638	1.78	2916	12.97	0.32
10.62-14.82	1781	2.02	3598	4.72	0.10
14.82-20.54	1843	2.09	3852	6.20	0.03
20.54-22.74	1882	2.15	4047	2.34	0.02

Table 7.4. PCPT11 parameters

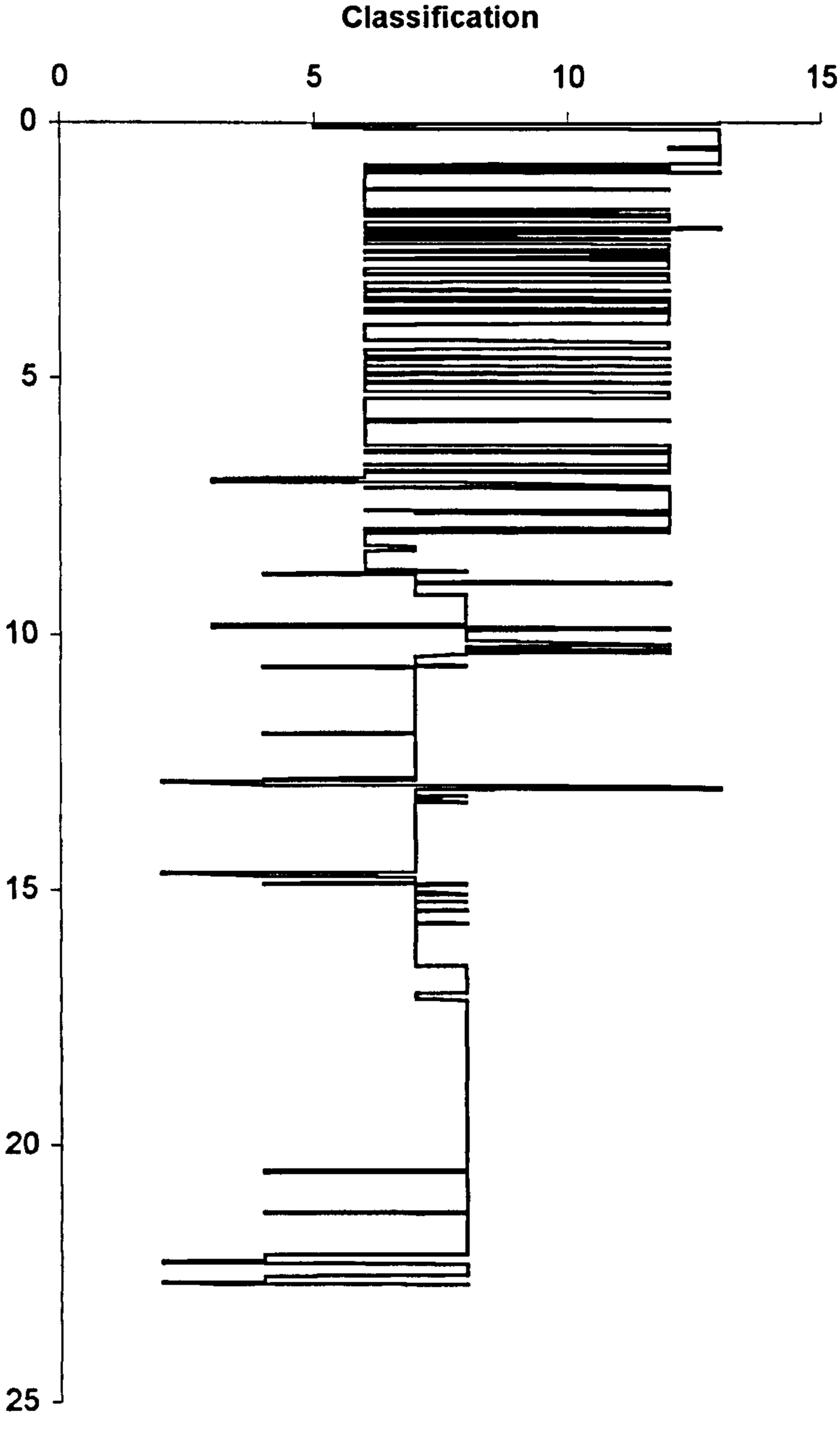

Figure 7.46. PCPT11 sediment classification.

The synthetic seismogram produced from PCPT11, is shown in Figure 7.47(a). The major boundary identified on the cone resistance plot at approximately 10m is the highest amplitude signal at 13ms below seabed and this can be identified as the change between the very soft clay to the soft clay which has a significant change in density as noted in Table 7.4.

The impedance changes between the soft clay to the soft to firm clay and from soft to firm clay to firm clay are not seen as evidently on the cone resistance plots. However these density changes and corresponding impedance changes are far more subtle.

7.5.2.5. Empirical inter-relationships

Two empirical inter-relationships were produced from the CPT data in Chapter 6 and related cone resistance to velocity and acoustic impedance. The relationships are very tentative based on the assumptions of the acoustic properties involved but they may be of use during an interpretation where limited data are available. In order to assess the generality of the inter-relationships they need to be tested using a dataset from, at the very least, one other area.

To address this question this was attempted using the results from PCPT11 from the West Shetland slope were used and Table 7.5 summarises the parameters used for the calculations.

Depth interval (m)	Velocity (m/s)	Impedance ($Mg/m^2/s$)	Cone resistance (MPa)
0 - 10.62	1638	2915.9	0.34
	(1698)	(3187)	
10.62 - 14.82	1781	3598.2	0.61
	(1701)	(3202)	
14.82 - 20.54	1843	3852.2	0.74
	(1702)	(3209)	
20.54 - 22.74	1882.2	4046.8	0.92
	(1704)	(3219)	

Table 7.5. PCPT11 inter-relationship parameters

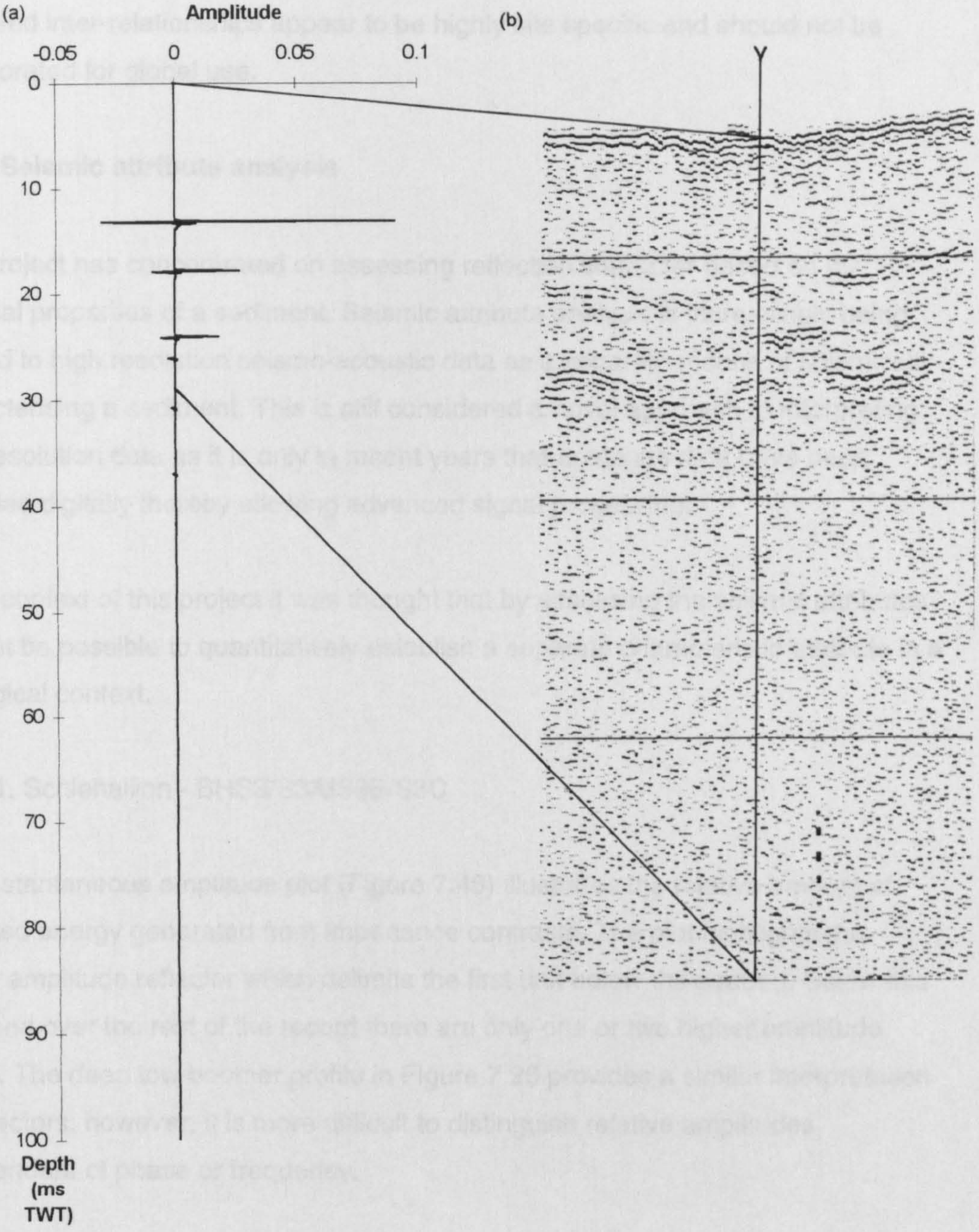

Figure 7.47. PCPT11. (a) Synthetic seismogram using the 'CPT method'. (b) Deep tow boomer profile, vertical scale; 1cm = 2.3ms TWT.

The values in brackets in Table 7.5 are those estimated using the empirical inter-relationships. The results show that the inter-relationships predict very small changes in velocity and impedance whereas the actual values, predicted on the basis of lithology, at PCPT11 show much greater variation. Therefore, these proposed inter-relationships appear to be highly site specific and should not be incorporated for global use.

7.5.3. Seismic attribute analysis

This project has concentrated on assessing reflection character based on the physical properties of a sediment. Seismic attribute analysis is increasingly being applied to high resolution seismo-acoustic data as a separate means of seismically characterising a sediment. This is still considered a novel approach to interpreting high resolution data as it is only in recent years that analogue data have been recorded digitally thereby allowing advanced signal processing.

In the context of this project it was thought that by assessing the seismic attributes it might be possible to quantitatively establish a separate characteristic attribute in a geological context.

7.5.3.1. Schiehallion - BHS3/S3A/S3B/S3C

The instantaneous amplitude plot (Figure 7.48) illustrates the relative amount of reflected energy generated from impedance contrasts. The plot highlights the higher amplitude reflector which delimits the first unit below the seabed. Below this level and over the rest of the record there are only one or two higher amplitude points. The deep tow boomer profile in Figure 7.26 provides a similar interpretation of reflectors, however, it is more difficult to distinguish relative amplitudes independent of phase or frequency.

The colour scale of the instantaneous phase plot (Figure 7.49) cycles to give the same colour for +180° and -180° as these have the same phase angle. This display shows the continuity of the major reflector close to the seabed and identifies a small channel like feature at shot point 730. Below this major reflector, however, there is very little continuity. This may confirm the chaotic nature of a mass flow sediment origin.

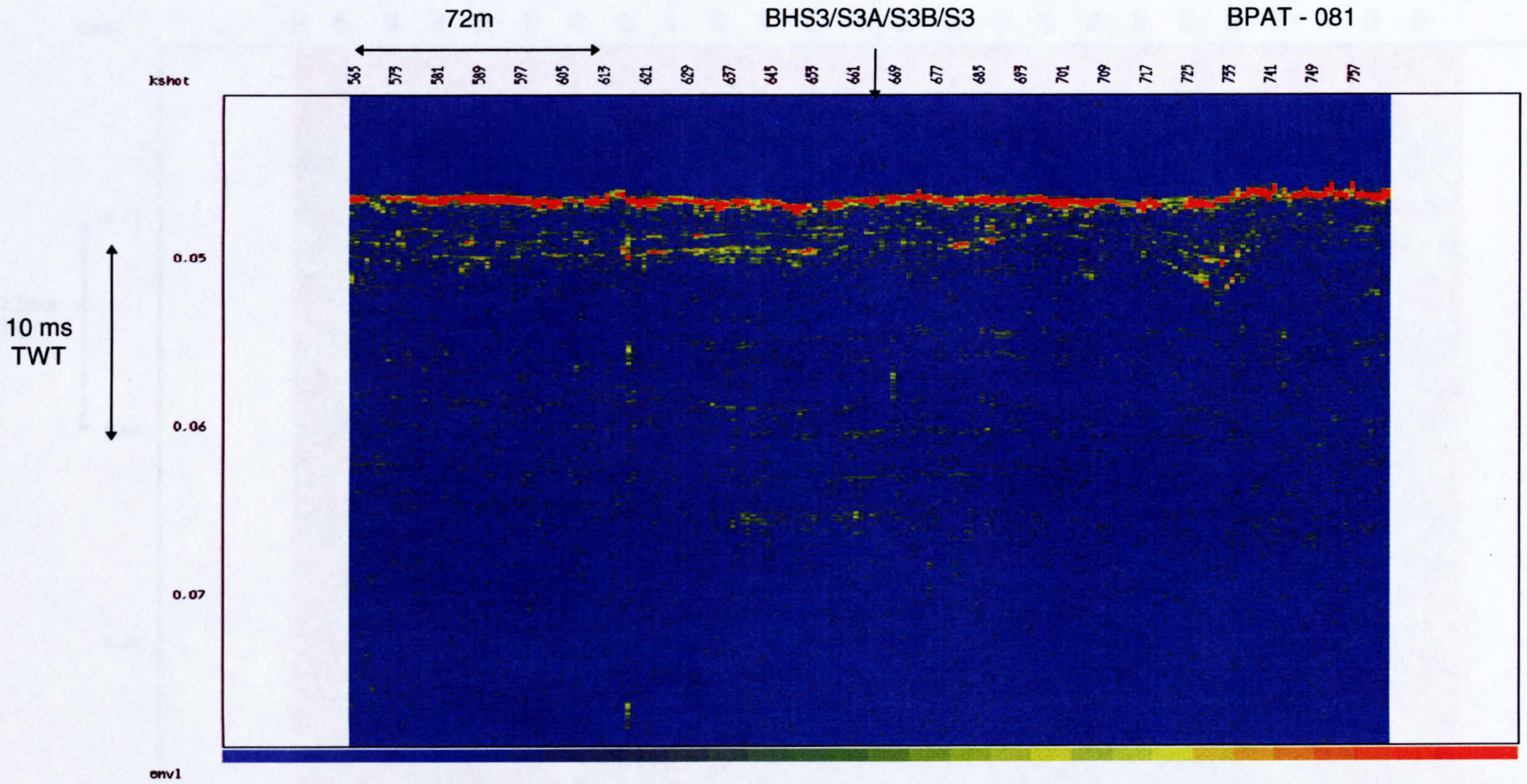

Figure 7.48. BHS3/S3A/S3B/S3C instantaneous amplitude display.

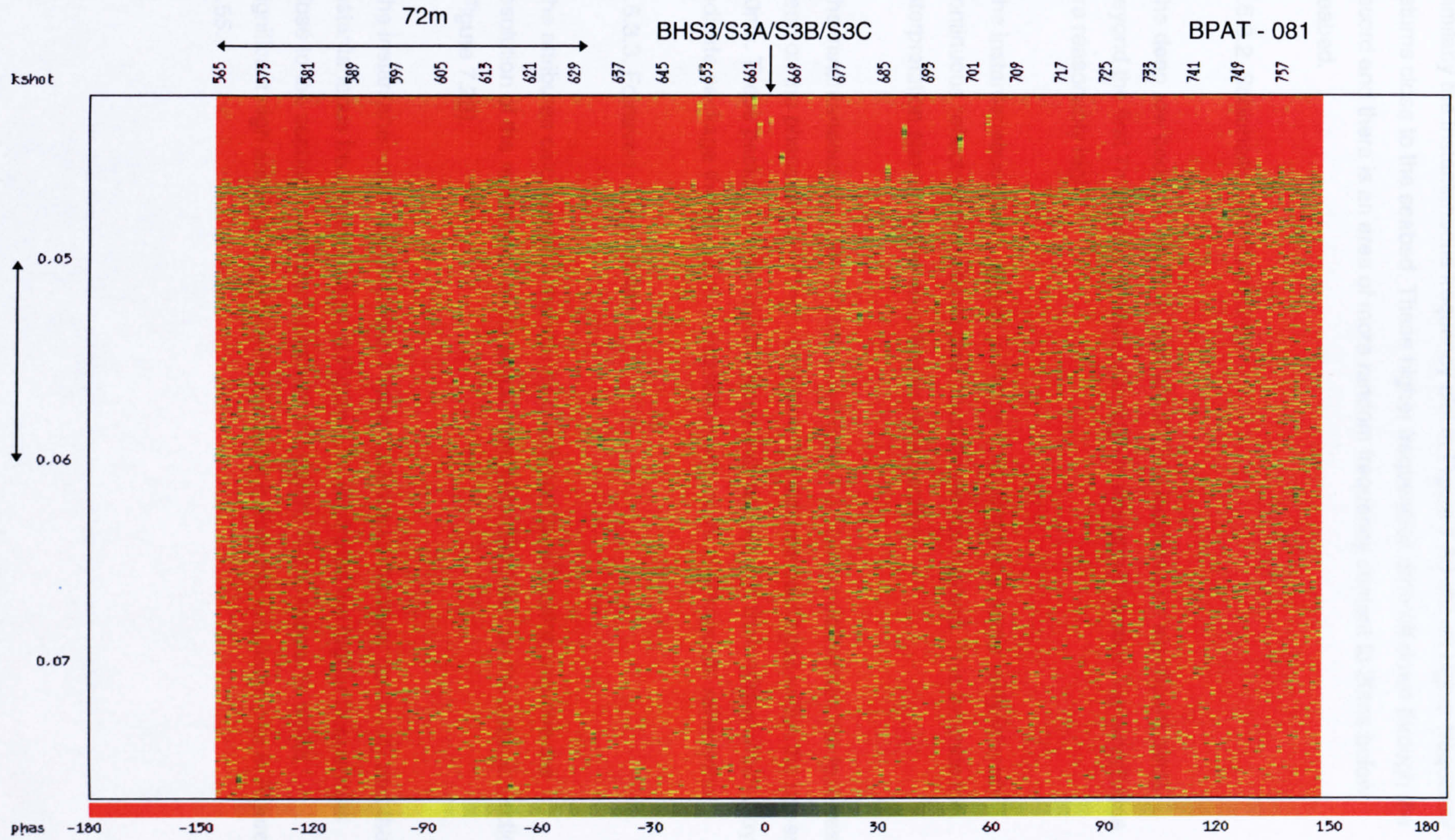

Figure 7.49. BHS3/S3A/S3B/S3C instantaneous phase display.

Similarly the instantaneous frequency plot in Figure 7.50 shows higher frequency returns close to the seabed. These higher frequencies drop off down through the record and there is an area of more random frequency content to 20ms below seabed.

7.5.3.2. Schiehallion - BHS4/S5/S6

The deep tow boomer record in Figure 7.27 has indicated no significant detail beyond the first 7ms below seabed, although in this upper section the amplitudes are reasonably high.

The instantaneous phase display in Figure 7.51 brings out some fairly laterally continuous reflectors down to around 10ms below the seabed. This extends the interpretation shown on the deep tow boomer section.

The instantaneous frequency display in Figure 7.52 further delineates the features seen on the phase display. There appear to be discrete packages within the upper 10ms. These packages have distinct frequency changes at their edges which may indicate package thinning with increased interference of composite reflections.

7.5.3.3. Foinaven - BH4/4A/4B

The attributes calculated for the vicinity of this borehole location improve the resolution of the reflector patterns which have been identified on the seismic section (Figure 7.28).

The instantaneous phase display in Figure 7.53 shows the layer continuity and the instantaneous frequency section in Figure 7.54 illustrates the higher frequencies close to the seabed which decrease with the depth. There appear to be no significant high amplitudes evident on the section from the amplitude plot in Figure 7.55.

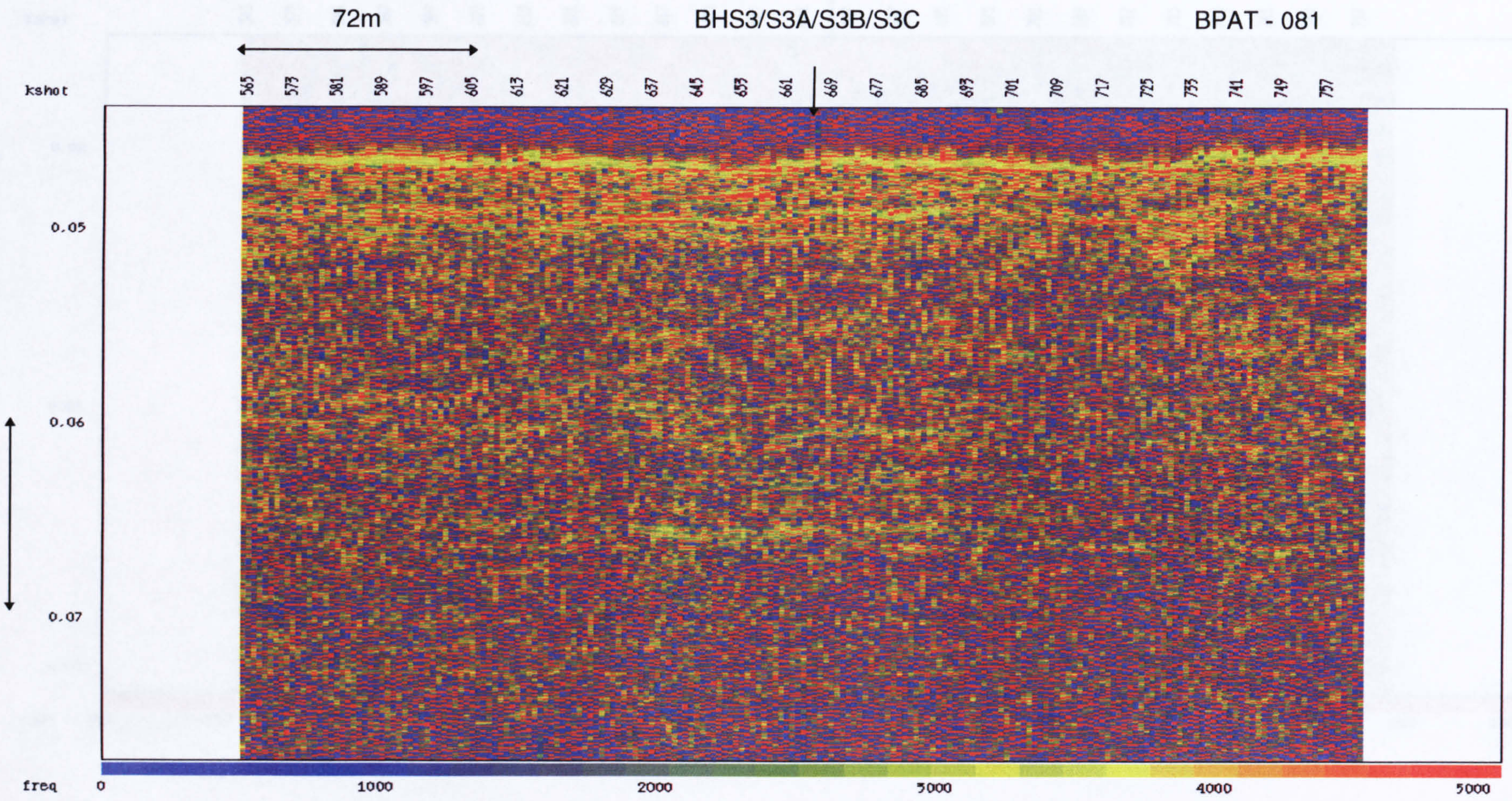

Figure 7.50. BHS3/S3A/S3B/S3C instantaneous frequency display

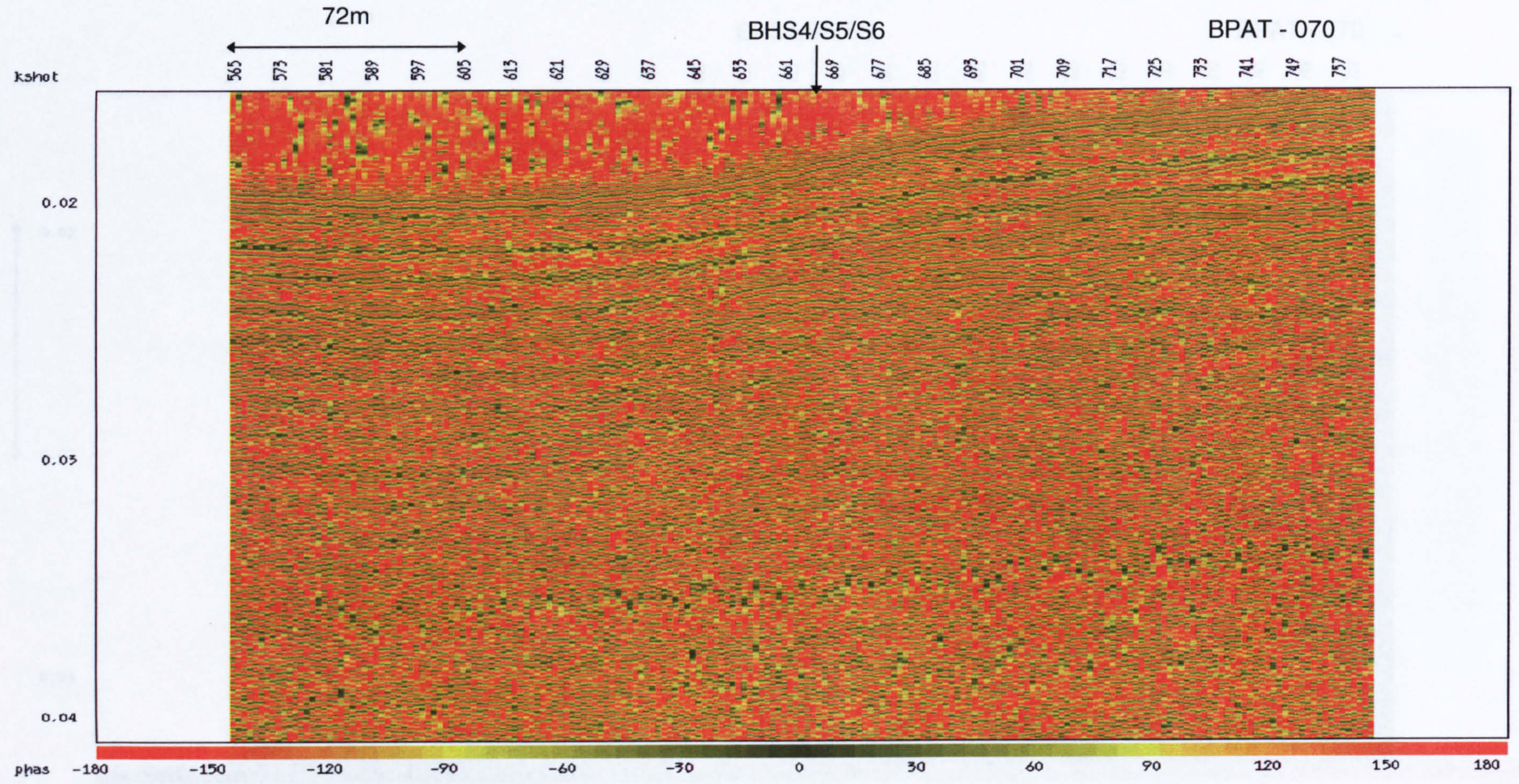

Figure 7.51. BHS4/S5/S6 instantaneous phase display.

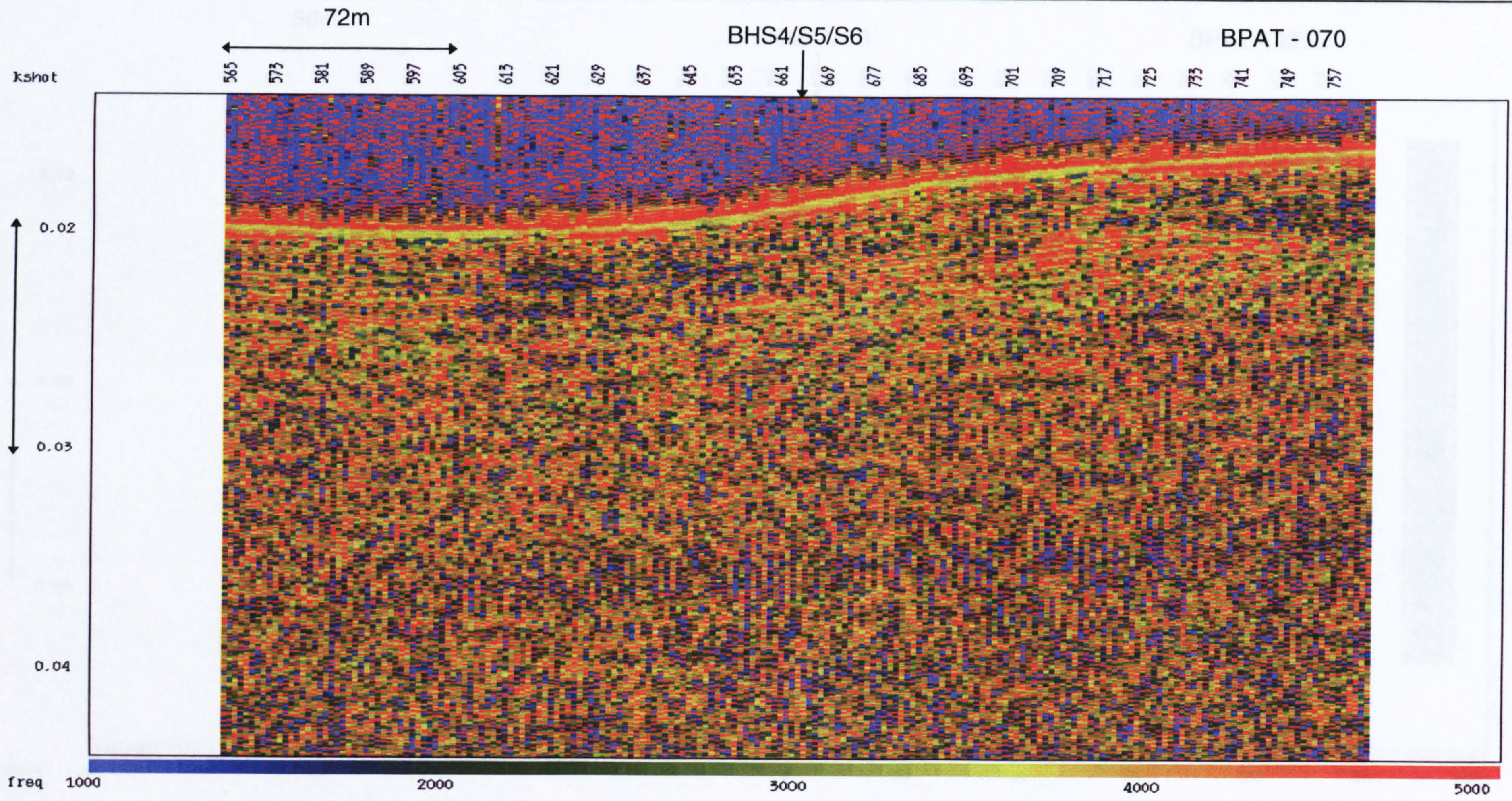

Figure 7.52. BHS4/S5/S6 instantaneous frequency display.

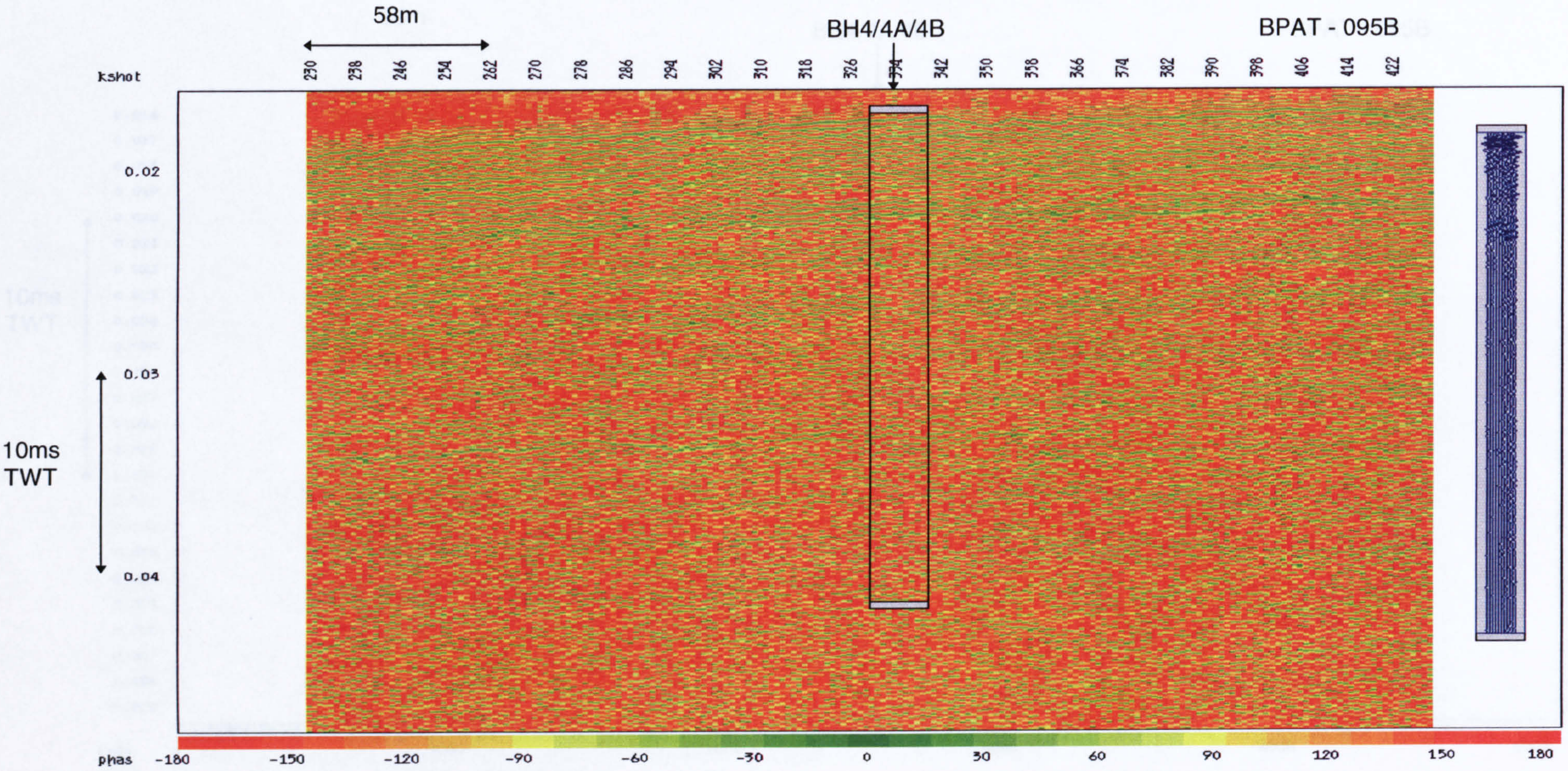

Figure 7.53. BH4/4A/4B instantaneous phase display, the box section is the wiggly trace display around the borehole location.

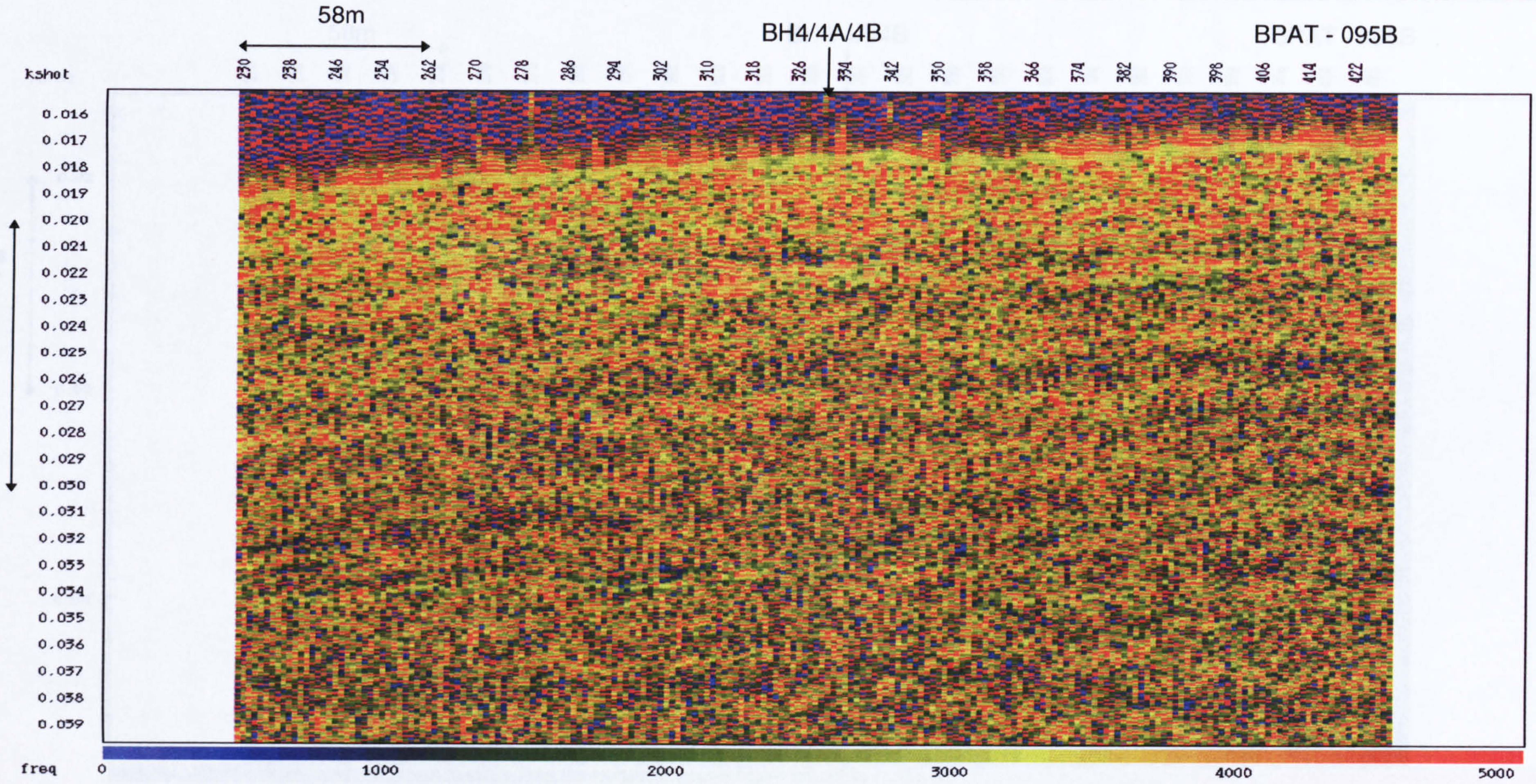

Figure 7.54. BH4/4A/4B instantaneous frequency display.

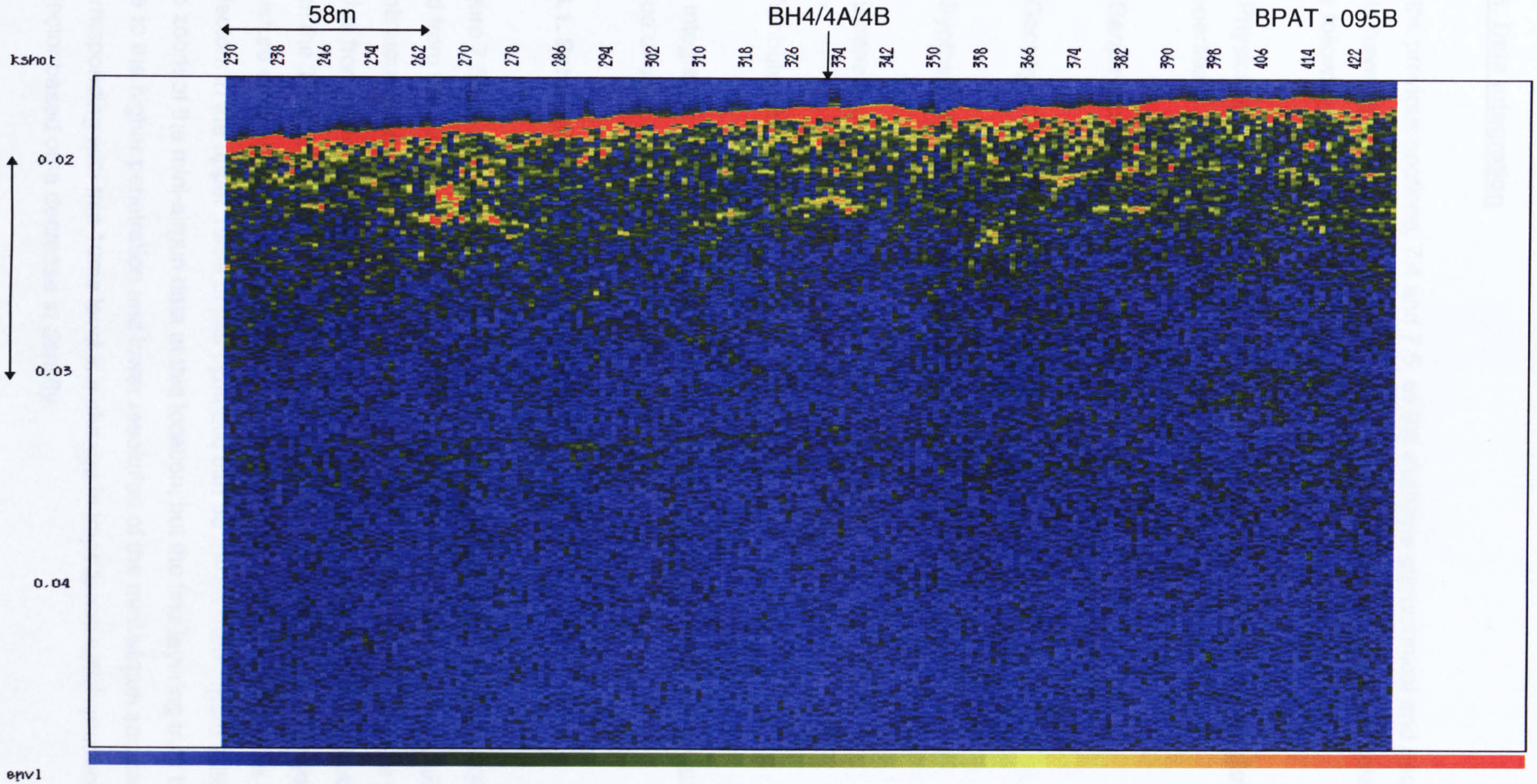

Figure 7.55. BH4/4A/4B instantaneous amplitude display.

7.6. Data integration

In the previous sections, 7.4 and 7.5, all the available geotechnical and geophysical data have been collated and presented in various forms. For each borehole location the following results have been presented:

a) Physical properties from borehole sample testing and empirically calculated properties.

b) Geophysical interpretation - deep tow boomer.

c) Geophysical interpretation - mini-airgun.

d) Synthetic seismogram - produced from a).

e) Synthetic seismogram produced from CPT data.

f) Attribute analyses.

By integrating all of these results together at each borehole location the validity and value of each method can be appraised.

7.6.1. Schiehallion - BHS3/S3A/S3B/S3C

Figure 7.56 is a representative composite of the results from BHS3/S3A/S3B/S3C and from the deep tow record the upper unit appears well layered with a fairly continuous reflector, at approximately 2.5ms below seabed, separating the layered facies from a more transparent zone below. The synthetic seismogram produced from the 'Borehole method' confirms this description, and the major changes in moisture content can be correlated with reflectors on the seismogram. The reflectors in the upper 10ms of this synthetic can be traced from Figure 7.30 which is a zoom of the mini-airgun data at this location, but the fine layering may be lost due to the higher penetration and lower resolution of the mini-airgun source. Corresponding with this 10ms level is a change in impedance which produces a reflector based on a decrease in density.

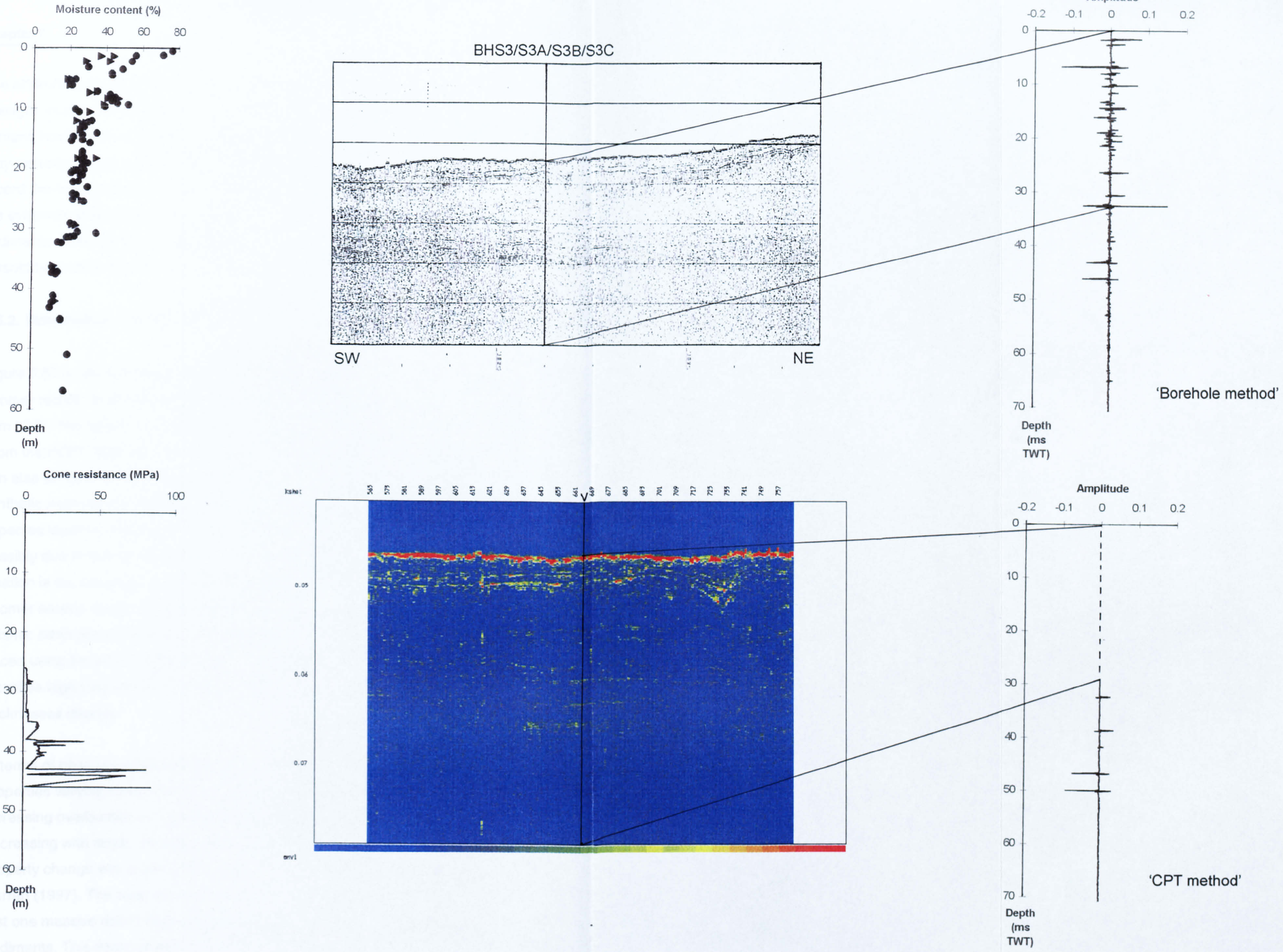

Figure 7.56. Composite of results for the BHS3/S3A/S3B/S3C location. Horizontal scale for the deep tow boomer is 1cm=98m and the vertical scale is 1cm=7.8ms TWT. The scales for the Instantaneous amplitude display are: horizontal, 1cm=46m, vertical, 1cm=4ms TWT.

The attribute analysis confirms the continuity of the reflectors based on reflection strength, phase and frequency. The upper unit has a greater higher frequency content; however in the layer below this the frequency content is more mixed, which may indicate a more chaotic mixture of sediments. From 20ms to the bottom of the record the frequencies are much lower. The seismic character of these events and the evidence above suggests a series of debris flow type events of glacigenic sediments. This inference would explain the chaotic seismic character within lensoid type clinoforms and the draping of more recent sediments.

7.6.2. Schiehallion - BHS4/S5/S6

Figure 7.57 is the representative composite for this borehole location; the deep tow boomer record for this location is different to that at BHS3/S3A/S3B/S3C which lies 6km NNE. The upper 5ms has some layering but it does not appear continuous. From the PCPT data there is an impedance change at approximately this level; this can also be seen on the synthetic produced from the borehole data. Using both synthetic methods the reflectors below this level have high amplitudes. This expected layering response is not clearly seen on the deep tow boomer record, possibly due to lack of penetration during acquisition. Further speculation at this location is the influence of grounded ice which may have produced the confused boomer section which makes sediment type differentiation very difficult. The seismic attributes identify package type features close to the seabed; these can be traced using the phase display for the continuity, and the frequency display which identifies high frequencies at the edges which may be a function of tuning as layer thicknesses change.

In terms of physical properties, none of the plots (Figures 7.14 to 7.16) show properties varying away from their general trend and as would be expected with increasing overburden in a normally consolidated sediment, i.e. moisture content decreasing with depth, density and velocity increasing with depth. This pattern of property change with depth within debris flows has been shown by Laberg and Vorren (1997). The deep tow boomer section may be interpreted as being a view of just one massive debris flow unit (Holmes, pers comms.,1999) of poorly sorted sediments. This interpretation is postulated due to the lack of correlative reflectors and the chaotic seismic character.

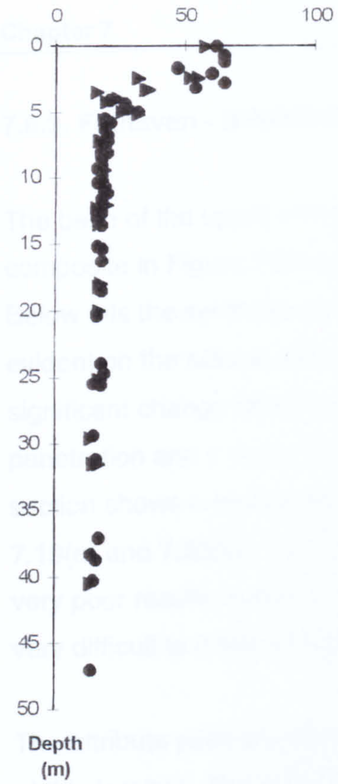

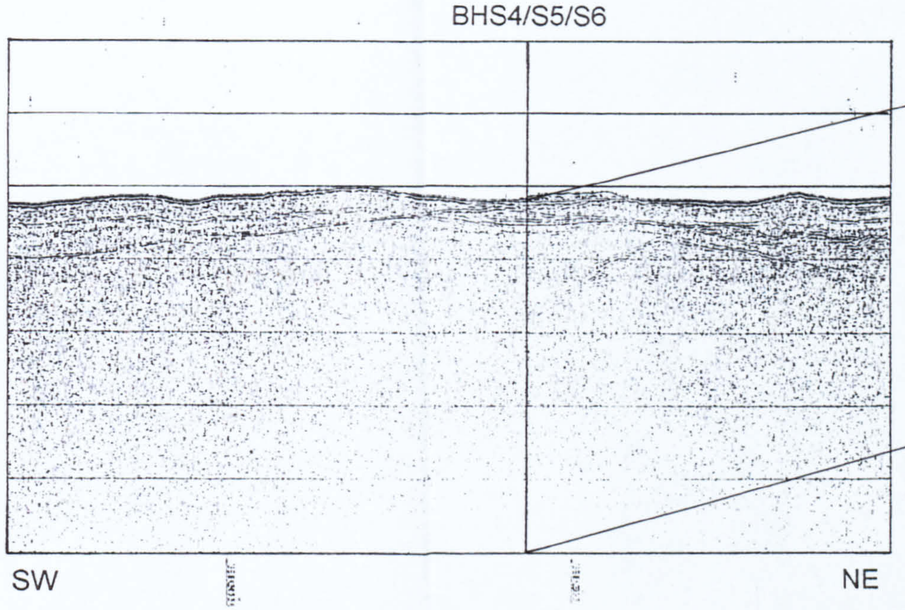

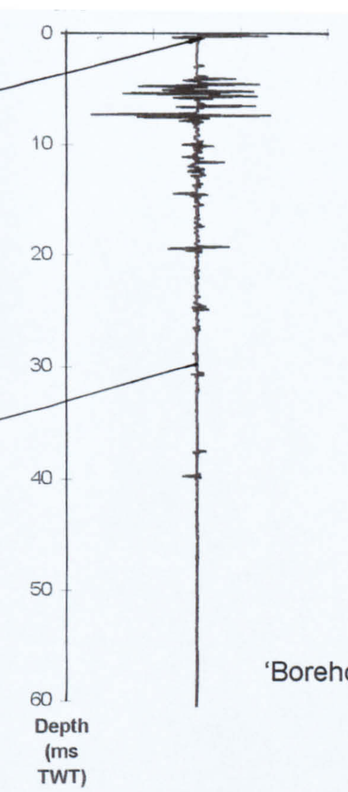

'Borehole method'

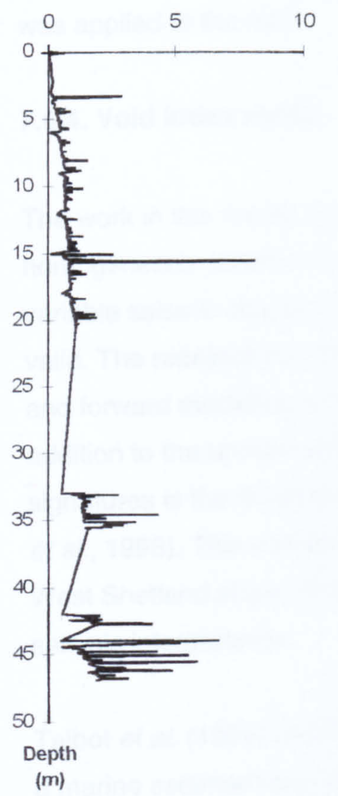

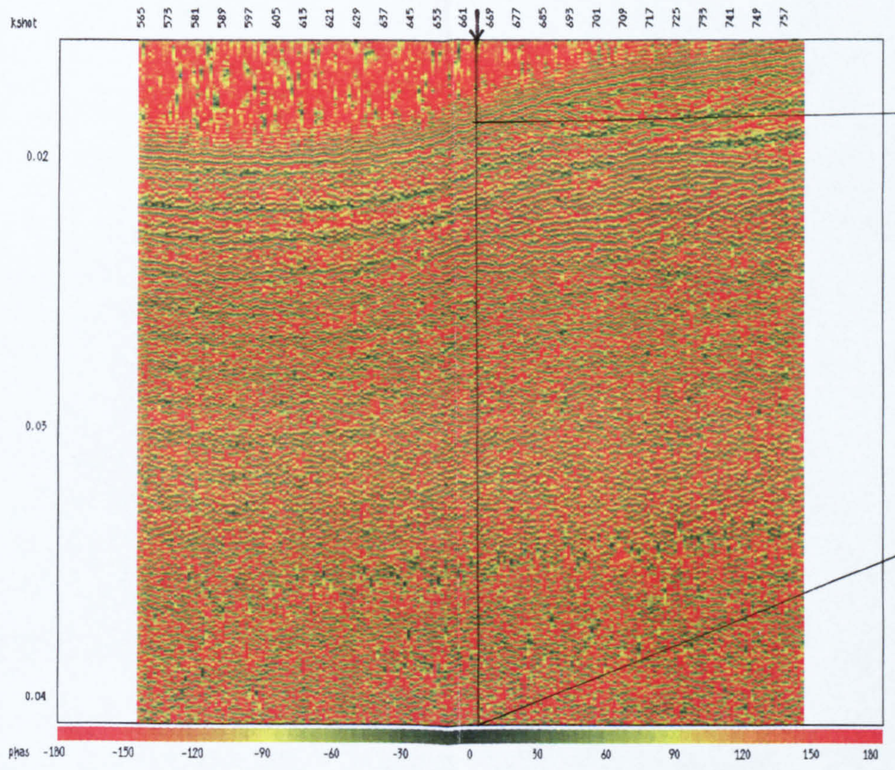

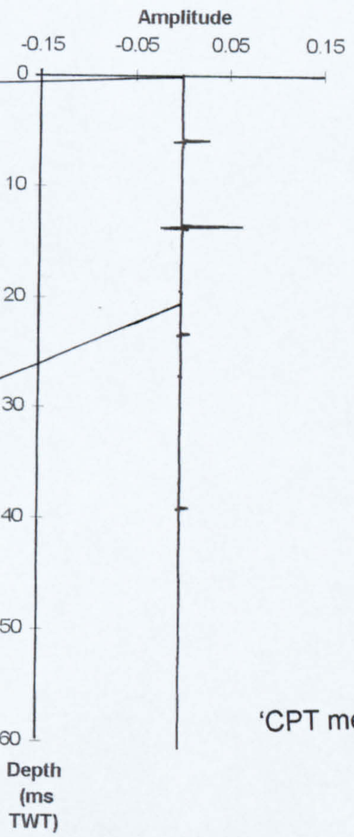

'CPT method'

Figure 7.57. Composite of results for the BHS4/S5/S6 location. Horizontal scale for the deep tow boomer is 1cm=98m and the vertical scale is 1cm=7.8ms TWT. The scales for the Instantaneous phase display are: horizontal, 1cm=46m, vertical, 1cm=2.5ms TWT.

7.6.3. Foinaven - BH4/4A/4B

The base of the upper unit from the deep tow boomer record on the representative composite in Figure 7.58 can be identified on the 'Borehole method' synthetic. Below this the synthetic gives a layered series of impedance changes which is not evident on the seismic data. On the physical property plots there is only one significant change down the profiles in the section covering the deep tow boomer penetration and it occurs at approximately 5m below seabed. However, this 5m section shows a rapidly decreasing moisture content and bulk density (Figures 7.19(a) and 7.20(a)). The 'CPT method' which was attempted at this location gave very poor results mainly due to the quality of the original CPT test data which was very difficult to interpret satisfactorily.

The attribute plots emphasise the extent of reflector continuity in the upper section at this location. The phase display also shows a strong, slightly dipping reflector 16ms below seabed which may be significant if a debris flow package interpretation was applied to the data.

7.6.4. Void index model

The work in this thesis has attempted to understand why the expectation of homogeneous seismic units indicating homogeneous physical property units, and variable seismic character indicating variable physical properties is not universally valid. The research has taken the form of cross-correlation of seismic interpretation and forward modelling techniques with geotechnical interpretation. A more recent addition to the understanding of geological processes in relation to seismic signatures is the development of the Void Index concept (Talbot *et al.*, 1994, Paul *et al.*, 1998). This concept has been applied in this project to the data from the West Shetland slope, thereby testing the applicability of this hypothesis as an aid to seismic interpretation.

Talbot *et al.* (1994) and Paul *et al.* (1998) have shown that the void index values of a marine sediment can be related to the depositional setting through an understanding of the sediment fabric. Paul *et al.* (1998) found a relationship between the sediment compression curves and the depositional environment and produced a schematic diagram of the void index model (Figure 7.59). Following this

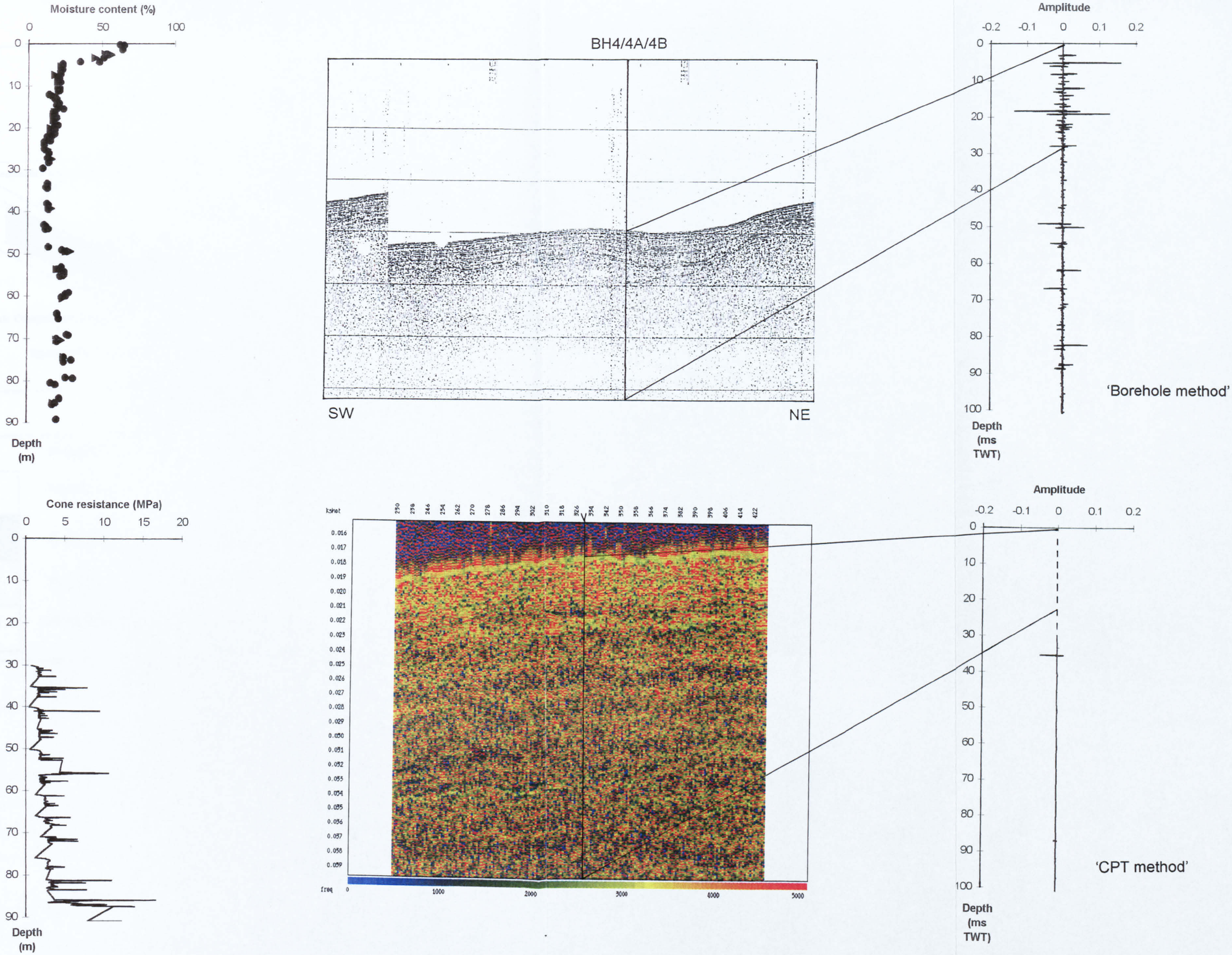

Figure 7.58. *Composite of results for the BH4/4A/4B/4C location. Horizontal scale for the deep tow boomer is 1cm=96m and the vertical scale is* 1cm=5.7ms TWT. The scales for the Instantaneous frequency display are: horizontal, 1cm=29m, vertical, 1cm=2.6ms TWT.

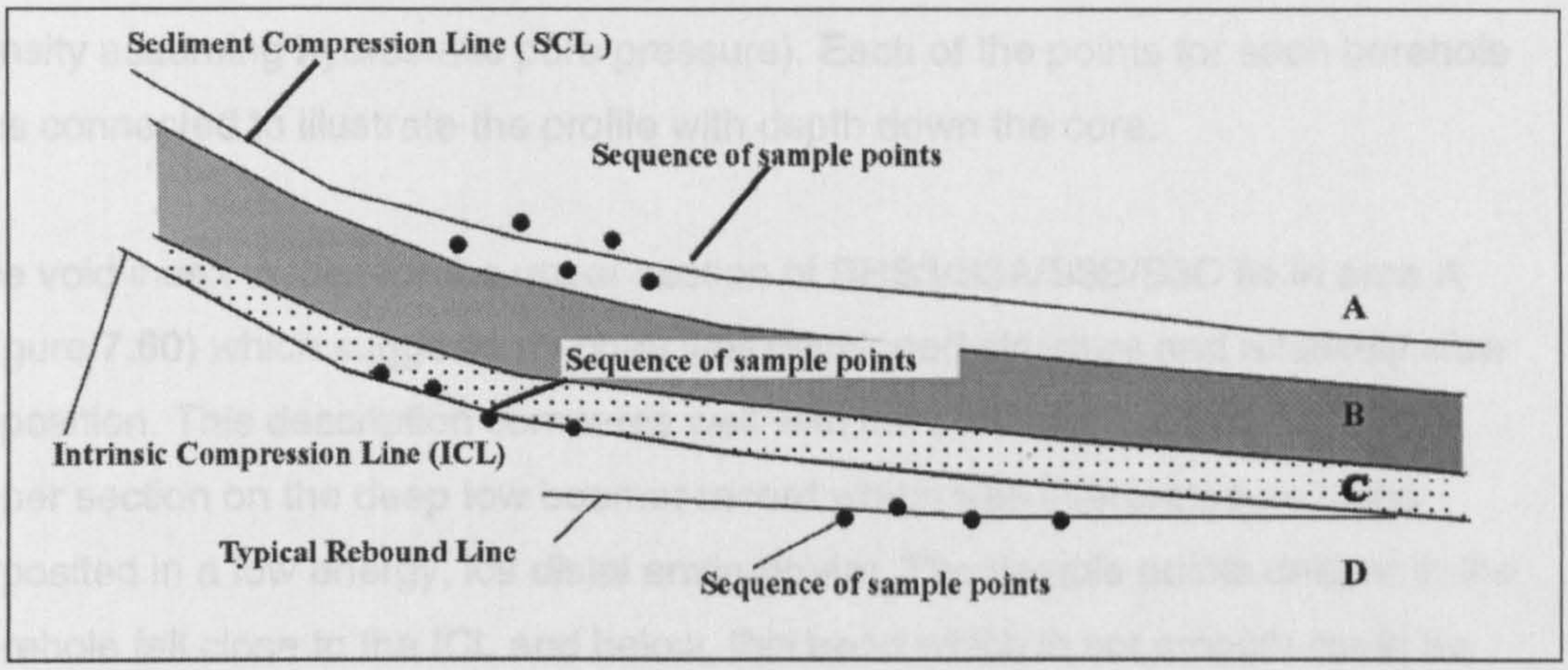

	PACKING	POSSIBLE PROCESS	ACOUSTIC FACIES
A	Structured	Hemipelgic processes/ suspension fall out	Well layered
B	Unstructured	Rapid sedimentation	Weakly layered
C	Remoulded	Mass movement	Disordered or transparent
D	Overconsolidated	Unloading	Disordered or transparent

Figure 7.59. Schematic void index diagram devised by Paul *et al.* (1998) for data from the Hebrides and West Shetland slopes.

model, the void index diagram for the boreholes on the West of Shetland slope was constructed (Figure 7.60). Void index was calculated from the sediment moisture content and liquid limit and plotted against *in situ* effective stress (calculated from density assuming hydrostatic pore pressure). Each of the points for each borehole was connected to illustrate the profile with depth down the core.

The void index values for the upper section of BHS3/S3A/S3B/S3C lie in area A (Figure 7.60) which suggests an open well developed structure and relatively slow deposition. This description compares well with the stratified appearance of the upper section on the deep tow boomer record which was interpreted as being deposited in a low energy, ice distal environment. The sample points deeper in the borehole fall close to the ICL and below, this trend which is not smooth could be indicative of different stress histories within a sediment. This is possibly related to mass movement, i.e. loading and unloading by grounded ice, or rapid deposition of large amounts of sediment. It is these depositional mechanisms which Paul *et al.* (1998) apply to sediments which plot on, or around, the ICL.

BHS4/S5/S6 has no well layered upper section and the sample points lie around the ICL, as discussed above these sediments may have a mass movement, more chaotically mixed origin. However, the trend of points is mainly in area D (Figure 7.60) which suggests overconsolidation; this overconsolidation indicates that the sediment origin may have been ice loaded at some stage before moving downslope. At the bottom end of the borehole the sample points are closer to the ICL again, which suggests a mass flow origin.

BH4/4A/4B/4C has a very open upper section, the trend in sample points is then very erratic down most of the borehole. At the base of the borehole a very overconsolidated zone with points well below the ICL is followed by the bottom zone with sample points spread between the SCL and ICL suggesting a variable consolidation history.

BH6 also displays a varying trend and the sample points lie between areas C and D. The points generally fall close to the ICL with only a couple of sample points showing overconsolidation. This suggests the mass flow explanation to be most likely for the sediments recovered from this borehole.

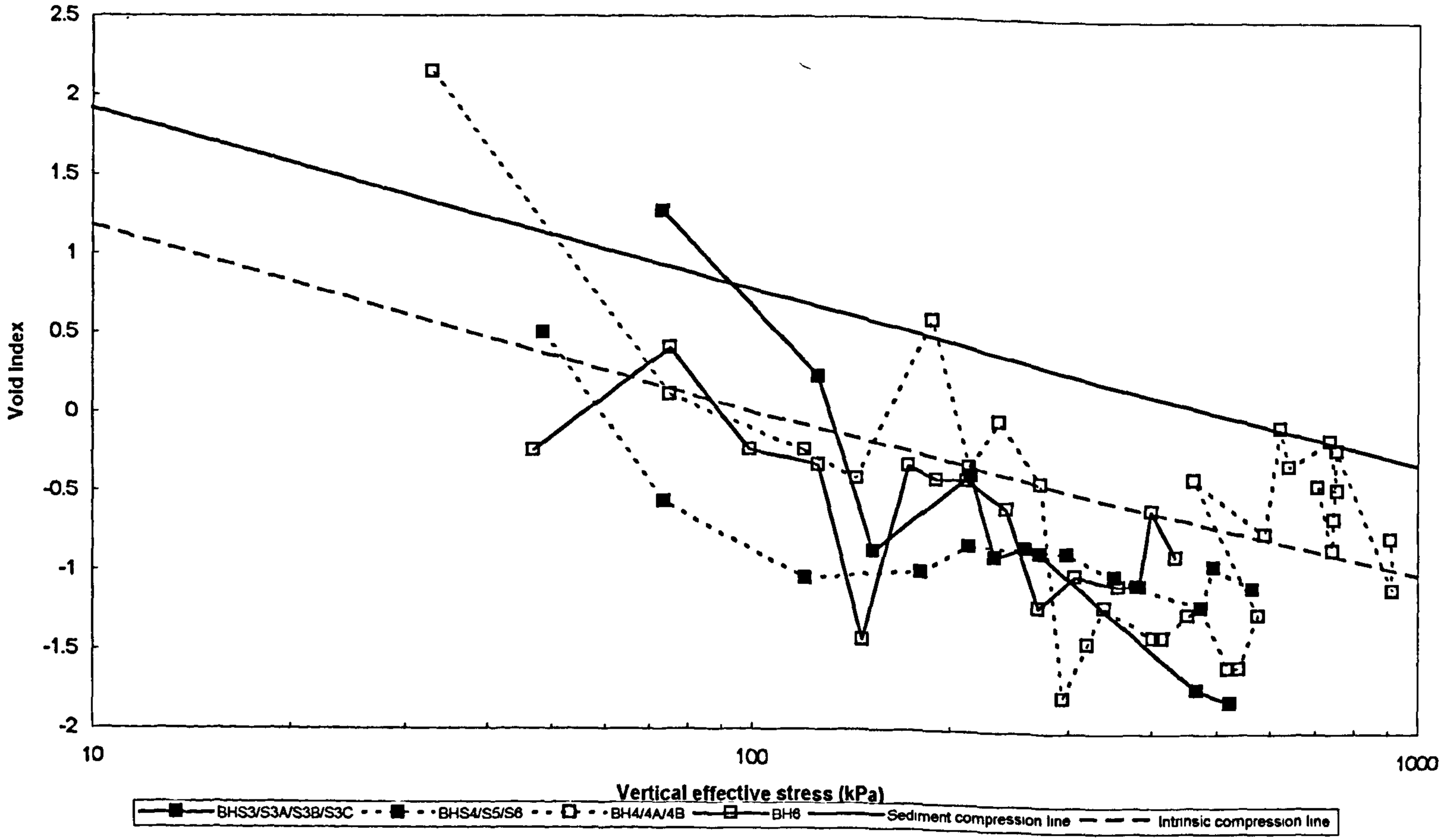

Figure 7.60. Void index model for the West Shetland slope.

7.7. Lateral variability

The modelling and analysis methods presented in this project have concentrated on specific locations. The applicability of these methods away from these locations, which is the ultimate purpose of their use, has not yet been investigated. This part of the study aims to address questions of lateral variability by testing the lateral variation of the seismic data using forward models produced by the 'CPT' and 'Borehole methods' and by attribute analysis.

Within the Foinaven area two locations were chosen, one of which is a borehole with a CPT alongside (BH6 and PCPT13), and the other a separate CPT location (PCPT 6). These locations were chosen to enable the production of synthetic seismograms by both methods at one location, and to allow comparison of the results laterally with a PCPT(6) location which lies 3.3km to the east where there is no geotechnical borehole control.

Figure 7.61 is a composite which displays the synthetic seismograms generated for BH6, PCPT13 and PCPT6 and the original seismic data. The seismic data in Figure 7.61 have had an automatic gain applied. The 'Borehole method' in Figure 7.61(a) produces a more detailed image as the reflectivity log was based on all the geotechnical sampling points. The 'CPT method' seismograms in Figure 7.61(b) and (d) identify the major lithological boundaries.

The seismic data in Figure 7.61(c) show a well-layered upper section which is draped (below 5ms) over the underlying feature, the base of which is not identifiable or not present in the section. Section 7.4.2.4. interpreted the feature as a mass flow deposit. Figure 7.61(e) shows a very similar picture to Figure 7.61(c) with a more continuously layered upper section draped over the lower section where the reflectors are broken and the geometry appears to be consistent with a mass flow/ debris flow type feature.

Figure 7.62(a) shows an envelope display around the BH6/PCPT13 location. The highest amplitude reflector is the seabed which is also seen on the synthetic seismograms. However, there are smaller reflectors immediately below the seabed which contain approximately two-thirds of the seabed amplitude. This relatively lower amplitude reflector also occurs at 5ms below seabed and appears to be

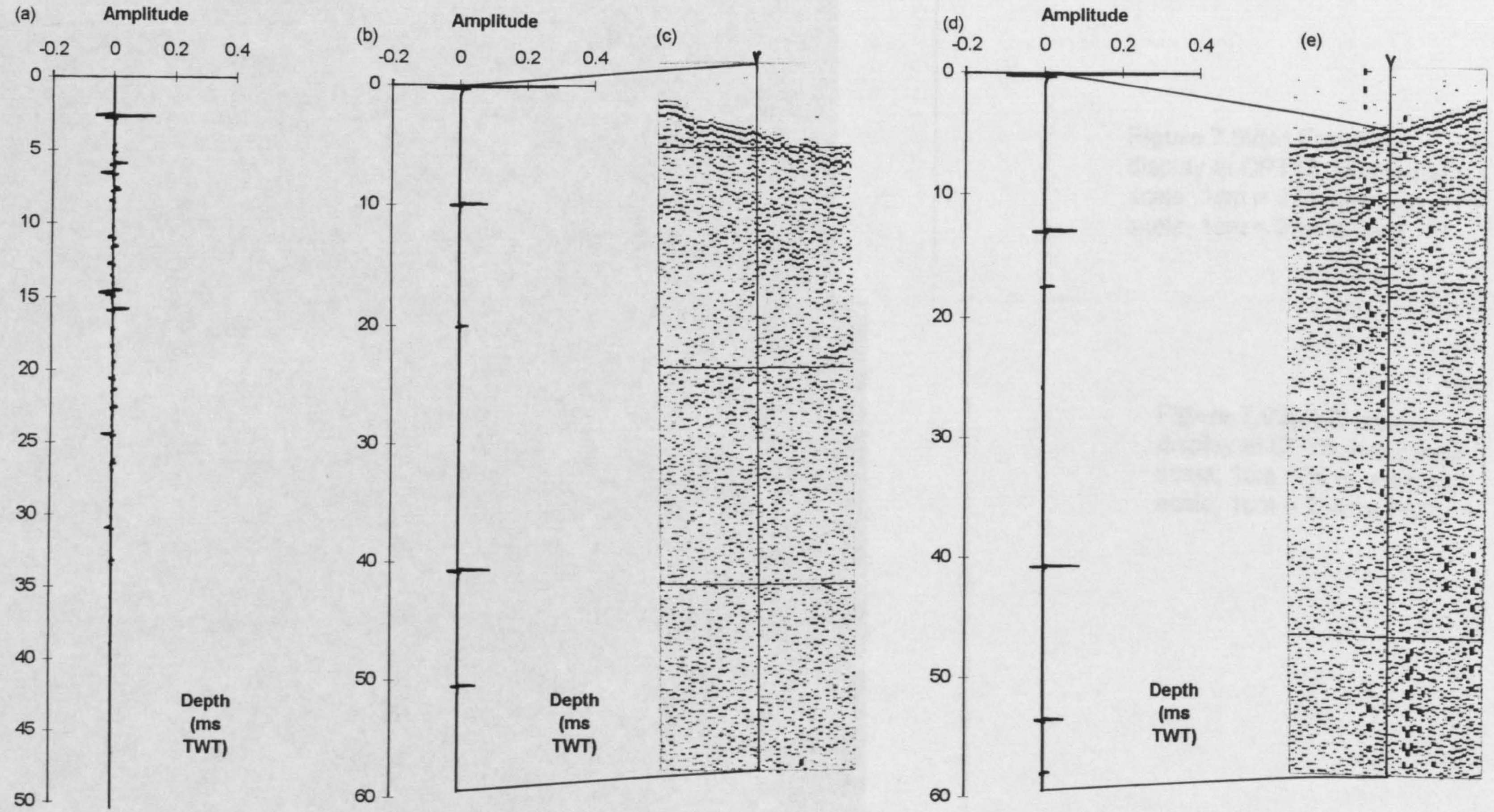

Figure 7.61. Geotechnical sampling locations and associated seismic profiles. (a) BH6, seabed at 0ms TWT (b) PCPT13, seabed at 0ms TWT. (c) Boomer profile at PCPT13, vertical scale; 1cm = 2.3ms TWT. (d) PCPT6, seabed at 0ms TWT. (e) Boomer profile at PCPT6, vertical scale; 1cm = 2.3ms TWT.

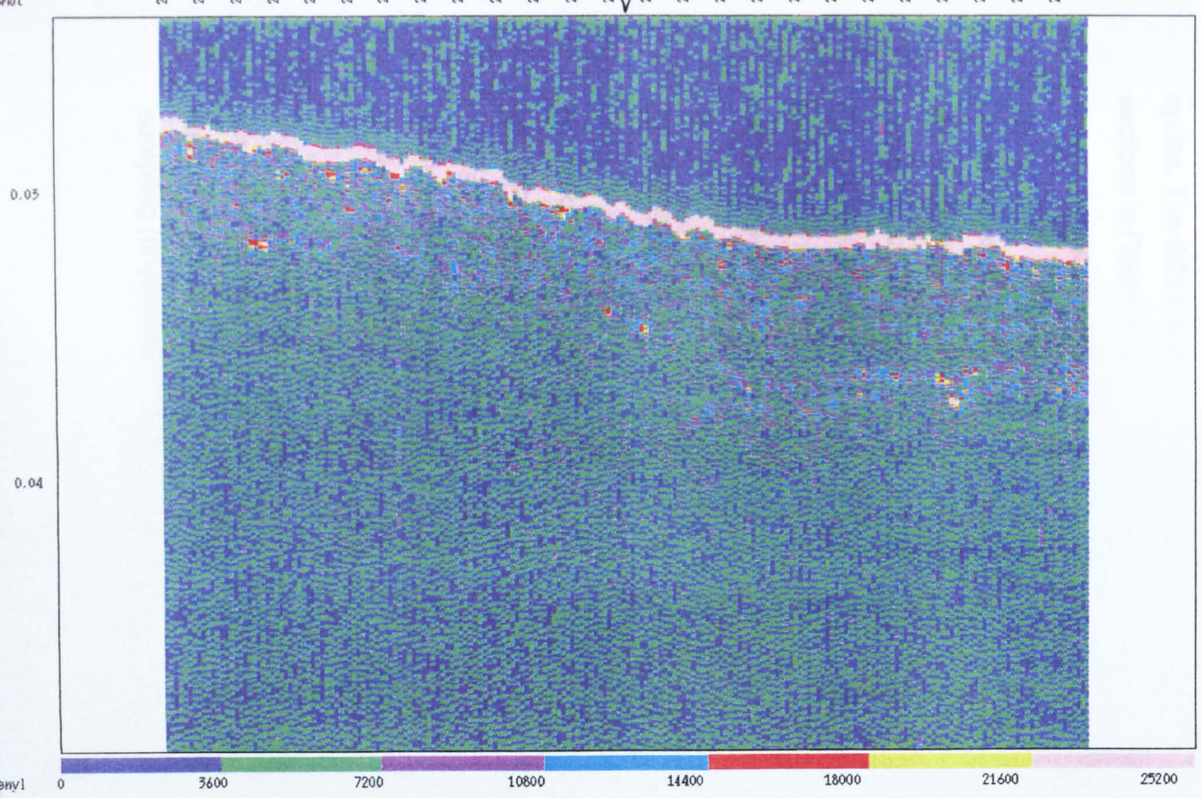

Figure 7.62(a) Envelope display at CPT13, horizontal scale; 1cm = 27m, vertical scale; 1cm = 2.4ms TWT.

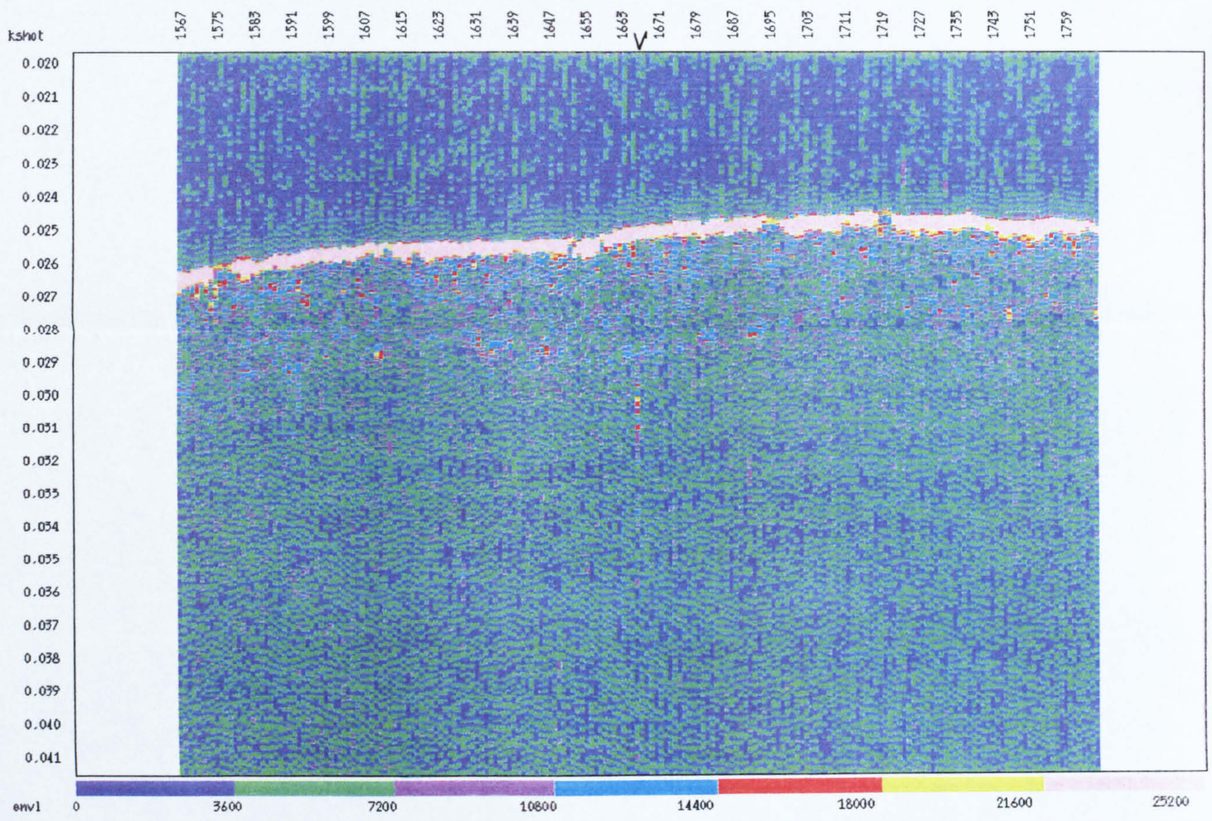

Figure 7.62(b) Envelope display midway bewteen CPT13 and CPT6, horizontal scale; 1cm = 27m, vertical scale; 1cm = 2.1ms TWT.

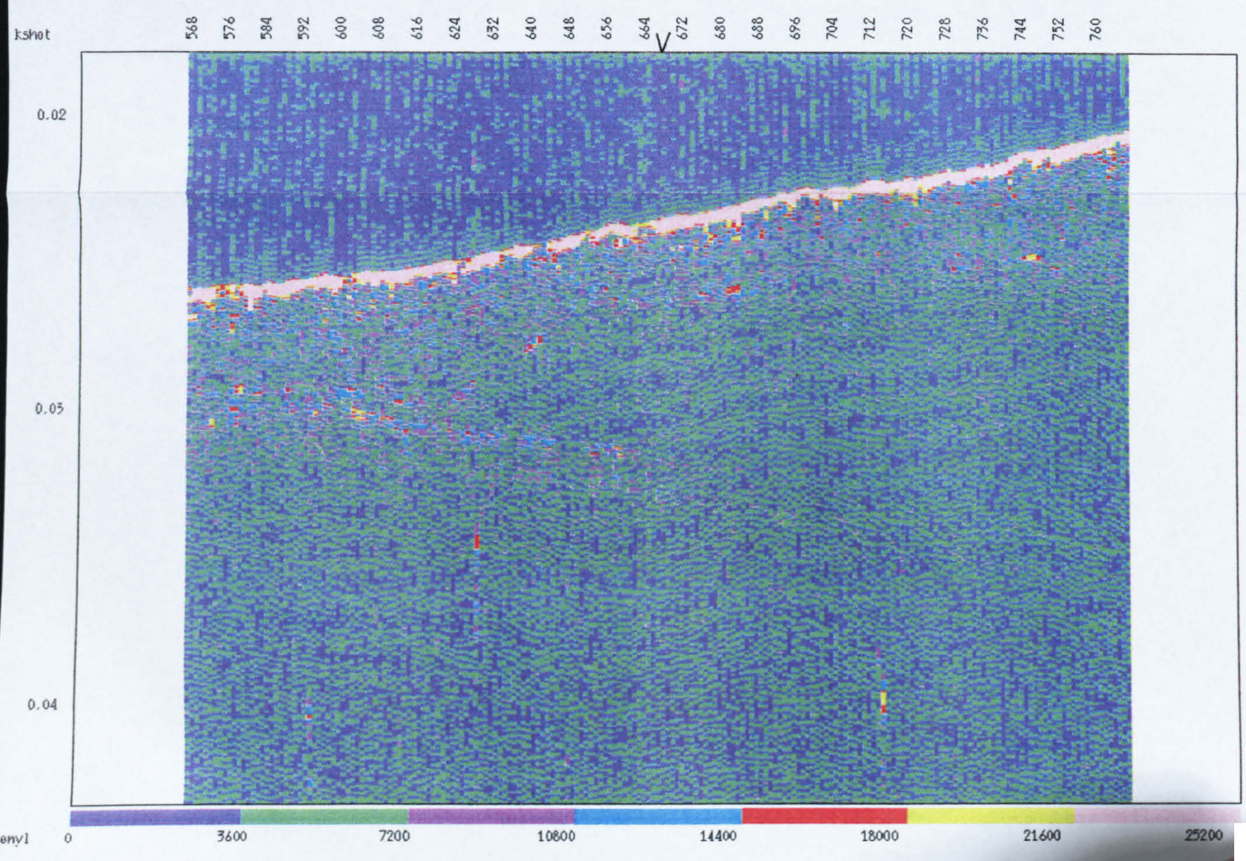

Figure 7.62(c) Envelope display at CPT6, horizontal scale; 1cm =26 m, vertical scale; 1cm = 2.4ms TWT.

consistent with the base of the upper 5ms, higher amplitude. This upper section can be seen on the borehole generated seismogram but not on the CPT generated synthetic. This may be due to the coarse sampling of the CPT profile; the major lithology graded from very soft clay through to soft and soft to firm clay.

The CPT profile in Figure 7.61(d) is similar to the previous CPT seismogram (Figure 7.61(a)) except in the depth of reflectors below seabed. The envelope display in Figure 7.62(a) shows a series of high amplitude reflectors concentrated on what could be the edge of a debris flow package. Figure 7.62(b) identifies a more broken seabed in terms of amplitude. At this point on both displays there are very few high amplitude reflectors with the overall amplitude decreasing significantly which may be the lack of penetration. In Figure 7.62(c) the seabed amplitudes are more variable with amplitudes dropping to half the maximum amplitude in almost regular cycles. The difference in seabed character is less well represented on the paper sections in Figure 7.61(c) and (e) where the type of display makes it more difficult to see changes in amplitude.

The ability, in this case, to separate amplitude variations is improved through the use of envelope displays and colour blocking. Knowledge of the geotechnical properties at BH6 would allow an estimation of the properties at PCPT6 based on the synthetic seismograms at both locations, and in particular, the borehole method seismogram can identify more detailed reflecting surfaces which may contribute to composite reflectors seen on the seismic data.

7.8. Summary

The results presented above illustrate the use of data integration, both geotechnical and geophysical, to characterise a location. In this case study the results were mainly concentrated at borehole locations for calibration and for the modelling. For an integrated interpretation, the techniques used in the case study have proved to be very applicable.

This case study has shown that the use of these types of forward models for high resolution seismic data interpretation is valid despite the paucity of geotechnical sample points. A feature of the geotechnical data used in this study was the coarse sampling (physically) of the boreholes. This meant that the synthetic seismograms

produced from the 'Borehole method' could be heavily aliased; this was particularly significant close to the seabed. This aliasing could also have been compounded by the block averaging of the reflectivity log for inputting into the synthetic seismogram program. However, when comparing the 'CPT and Borehole methods', reflectors could be correlated on both of the seismograms.

The 'CPT method' proved to be a reliable forward indicator of the gross lithology, but it is very dependent on the quality of the CPT. The 'CPT method' synthetic seismogram for BH4/4A/4B illustrated that very little information could be retrieved from a poor CPT, although it was still possible to gain an overview of the lithology.

The forward models have enabled a direct relationship to be constructed between the physical properties and the seismic data and this is particularly important away from the borehole locations. By using a more quantitative approach to the interpretation, and with the aid of the void index model, a more confident assessment of the depositional environment can be gained. The forward models allow the amplitude to be quantified in terms of physical properties which is difficult to achieve based on seismic data alone. The seismic data provide the geometry and the seismic character of the environment, and the geotechnical logging provides the physical property information. However, it is the use of forward models which, in this study, has provided the links for the integration.

These points will be discussed further in Chapter 8.

CHAPTER 8

DISCUSSION

8.1. Introduction

The results presented in Chapters 5, 6 and 7 have shown that a forward modelling approach is viable within the realms of high resolution seismic data interpretation and integration given the aims of this particular project. The methods presented in this thesis form a proposed integrated approach to assessing the seismic response seen on high resolution reflection data.

Previous work which has concentrated on qualitatively comparing physical groundtruth data with seismic records, has noted that care should be taken when assuming that a change in physical properties indicates a change in seismic facies and vice versa. Within this research three approaches have been attempted to assess the influences of physical properties on the seismic response: modelling from borehole and PCPT data, seismic facies analysis and seismic attribute analysis.

8.2. Borehole and CPT Modelling

8.2.1. The synthetic seismogram

The synthetic seismogram algorithm used within this research is for a 1-D, normal incidence scenario. The idea of forward quantitative assessment of the seismic response for high resolution seismic data based on physical properties has not previously been well documented. However, relatively recently the work of Esker *et al.* (1996) concentrated on the estimation of impedance from median grain size using empirical correlations as a means of synthetic seismogram generation. Within the current research, reported in this thesis, a simplified approach to synthetic generation was deemed necessary to build up a picture of the seismic response variables and the effects of the various physical properties hence the choice of the 1-D normal incidence program.

Much of the currently published work on physical properties and related seismic response focuses on the inverse method, i.e. extracting an impedance profile from seismic data. This approach has the advantage that it begins with the actual seismic record. However there are an equal, if not greater number of difficulties involved with this method as with forward modelling, such as the requirement for accurate recovered amplitudes and noise free data.

8.2.1.1. Assumptions

The synthetic program used in this study accounts for multiple energy, including peg-legs, and transmission losses. However, the program does not inherently account for spherical divergence or attenuation. Anstey (1960) has shown that a certain amount of attenuation can be accounted for through multiple energy and transmission losses. Therefore, it can be assumed that the synthetic seismogram program used in this study will produce some attenuation loss. The main seismic sources used throughout this study were boomers, and Verbeek and McGee (1995) have found that the boomer sources have non-spherical radiation patterns dependent on frequency. In addition, the boomer source used in Chapter 7 was deep towed which may reduce the affects of spherical spreading in the water column. However, Missiaen *et al.* (1996) used a boomer source and assumed that, as the acquisition spread was near normal incidence, then recorded data would have come from the main lobe of the radiation pattern. It was observed that, at moderate frequencies, this radiation pattern has in fact been seen to be spherical. Therefore it would have been valid to correct for spherical divergence. This divergence was shown to be the predominant cause of signal decay at the frequencies of interest and depths studied within this project. There are however, drawbacks to making corrections for divergence which are pertinent to this study. It is possible that any deeper reflections observed on an uncorrected seismogram could be lost by correcting for divergence. This may be significant in terms of subtle changes in physical properties, and therefore by not correcting there is a potentially inherent gain control. However, by not making divergence corrections, the correct absolute amplitude values will be affected as the interference calculations will not account for the divergence losses. Hron and Covey (1983) realise the use of uncorrected seismograms in the study of the subsurface. They conclude that it is mainly studies involving research on more than one type of wave which will be affected by lack of correction.

No attenuation measurements were available for the geotechnical dataset. Authors such as Missiaen *et al.* (1996), working at similar magnitudes of scale, have however assumed that absorption is negligible. Measurements of attenuation exist throughout the literature and Hamilton (1980) concludes that the differences in attenuation measured at the seabed and in the first tens of metres below seabed is negligible. Therefore, if attenuation values had been taken from studies conducted close to seabed, which is generally the case in this field of research, then it would have been valid to extrapolate over the depth of interest in this project. Missiaen *et al.* (1996) also made the assumption that the subseabed interfaces were smooth and therefore no correction for backscatter was required. This general assumption could also be applied to the environments investigated in this project.

A major factor in correcting seismograms for signal loss is the type of seismic data which the synthetic seismogram is being compared alongside. In general, the data will have gain functions applied to compensate for signal decay, and therefore care is needed if any corrections are to be made to the synthetic. The test of signal decay due to spherical divergence and absorption in Chapter 5 made a number of assumptions which have to be addressed. The attenuation coefficient used for the calculations (0.15dB/λ) was a constant over all depths and frequencies, and as Hamilton (1972) has shown, the attenuation coefficient will vary depending on the sediment type, with grain size and porosity being major influences. This variation may be even greater where overconsolidated, glacial sediments are encountered, but for the purposes of this project it is a best estimate. The spherical divergence estimate of loss with depth was based on time only and made no account for velocity; this may have the effect of altering the gradient of decay and the wavelet shape. Therefore, any corrections which are made using these assumptions are, in themselves, tentative or a best estimate as there may be no other information available.

Discussed above are the two conspicuous effects which are not automatically included in the normal incidence synthetic seismogram generated in this study. The synthetic seismogram is deemed adequate for the purposes of this project, although it is clear that if this work was advanced it could be appropriate to develop a more sophisticated synthetic seismogram procedure. Two-dimensional models are not limited to normal incidence and can take into account far more variables

such as refraction, the effects of amplitude, waveshape due to offset and interface mode conversion.

8.2.1.2. Synthetic seismogram variables

Concurrent with the assumptions discussed above are other aspects of the synthetic seismogram procedure which have to be elucidated. A reliable source wavelet is a crucial part of the convolution process and, as is often the case, it can be difficult to find a stable, digitally recorded source signature. The boomer source is often chosen as a representative source signature due to its relatively high frequencies, repeatability and sharp wavelet shape. However, within Chapters 6 and 7 of this study this choice of source was predetermined as it was a boomer source which was used to acquire the seismic data. The deep tow boomer system has an internal hydrophone which was used to record the seismic data, and the reflected data were assumed to have a very low emergence angle (i.e. close to 0). The acquisition was therefore considered to be of normal incidence and the boomer produced a good, identifiable waveshape.

An issue throughout the research was sampling frequency. A sampling frequency of 20kHz was chosen throughout. The seismic data in Chapter 7 were tested over a range of sampling frequencies and 20kHz proved to be the highest sample rate which would give a representative record length. There is a trade-off within the ELICS digital acquisition system between sampling frequency and record length. The 20kHz frequency also enabled ease of calculation for hand digitising and a realistic frequency when comparing with commercial digital systems, although it was shown that by using a lower sampling frequency the wavelet shape changed. However, with more widespread use of digital acquisition systems, commercial surveys are being recorded at higher frequencies although there still remains a trade off between storage and sampling interval to be considered. The boomer source signature used in Chapter 7 was digitised from paper; although this was adequate, it would have been preferable to have had digitally recorded signatures. Unfortunately the quality of the digitally recorded analogue data did not allow a reliable representation of the source signature.

The addition of noise onto the seismogram was a test into the effects of noise on amplitude. As commented by Walden and White (1984), an assessment of noise on

the trace can improve the accuracy of a synthetic seismogram. The resulting synthetic showed the effects on the amplitude at this 10% scale to be negligible; as a result noise was ultimately left off the synthetics produced after this test. However, not all noise is at the 10% level, each dataset was considered separately and an assessment of the signal-to-noise ratio was made for each location. All the seismic data used in this research were single channel therefore there was no possibility of improving the signal-to-noise ratio by stacking acquisition channels. However, by using the digital acquisition system it was possible to add up to 3 adjacent traces - trace averaging - which did improve the ratio marginally.

8.2.2. Borehole method

Synthetic seismograms are traditionally generated from well logs. Unfortunately well logging in commercial offshore investigations often does not commence until at least 100m below seabed, if not deeper. As a result any modelling of high resolution seismic data cannot rely on these logs being available.

Due to gaps in the dataset used to test the validity of the proposed new methodologies, empirical inter-relationships were used to calculate those properties which were missing. In this case, the relationships presented by Hamilton and Bachman (1982), which were shown to be as robust as any other commonly used regression equations found in the literature, were applied to calculate '*in situ*' velocities. In keeping with the literature, density and consequently porosity, both appeared to be a reliable indicator of changes in impedance (Mayer, 1980, Paul and Jobson, 1987).

It must be noted that all the published empirical relationships cited in this research generally were based on north west Atlantic and Pacific sediments. The maximum and minimum physical property limits for density, as defined by Hamilton and Bachman (1982), were marginally exceeded by the post-glacial and glacigenic sediments on the UK continental margin. These limits were taken to be representative of the current research geological environment as no other information on this was available. Therefore, using data which exceeded these limits was considered acceptable, with caution, in the context of this study due to the lack of other available data. The optimum method would be to create location specific regression equations for predicting the acoustic properties of a sediment.

However, as the data from the Hebrides Slope has shown, it is possible to predict velocity from density using the inter-relationships of Hamilton and Bachman (1982). These predictions did not hold for the other predictor properties which may be a function of the environment, although Orsi and Dunn (1991) confirmed the validity of using the empirical inter-relationships of Hamilton and Bachman (1982) in glacial sediments and stated the major difference in properties was a more varied mineralogy which would be expected in glacial sediments.

One of the major drawbacks of using results of tests on borehole samples is the variability in vertical sampling frequency. This is an issue which does not arise with well logs as they conventionally produce a continuous log of subsurface variability. The synthetic seismogram produced from borehole sample data will be a function of the particular chosen sampling frequency, particularly if the borehole is under-sampled in relation to the vertical resolution of the seismic source. As resolution is a function of the source wavelet length and the bandwidth, in this type of study the geotechnical sampling would be dictated by the geophysical capability for direct comparison. The added issue is in areas of deep water where long travel paths in the water column dictate the type of high resolution geophysical equipment and the shot interval. The vertical resolution of the boomer wavelet used in Chapter 7 is approximately 0.25m, however this will vary with frequency which in turn will be a function of subseabed depth. Therefore, a geotechnical sampling frequency smaller than 0.25m would be preferable. This will become critical particularly where a sediment has a series of thin layers. The interference pattern on the seismogram may be altered if the lithological layers have not been discriminated due to aliasing as a function of geotechnical sampling frequency. In the context of this study this aliasing could be a crucial factor when comparing a synthetic with actual seismic data. Optimum sampling frequency, for producing physical property profiles for the purposes of this project, is considered to be at 5-10cm intervals which would be well within the boomer wavelet for aliasing not to occur. This sample interval could also detect layers which may give rise to composite reflectors on the seismic data which may not be explainable based on seismic data alone. It would also be useful to filter the geophysical to match the geotechnical sampling frequency, but this would be dependent on the geotechnical sampling being regular.

The empirical inter-relationships used in this study have been produced from and are designed for surficial, Quaternary sediments. Within this project these

relationships have been applied to sediments at depth and appeared to give acceptable results. Ideally, if the data were available, empirical relationships could be established on a site specific basis. However, the inter-relationships of Hamilton and Bachman (1982) and others such as Richardson and Briggs could be extended to include a broader band of physical property limits.

The dataset from the Hebrides slope illustrated one of the cases identified by Stoker *et al.* (1993b) where the homogeneous sediment produces draped, layered seismic facies units. Chapter 5 illustrated this effect in the reflectivity log where reflectors were produced in apparently homogeneous glaciomarine sediments. This dataset highlighted the advantages of high frequency geotechnical sampling (5cm intervals) in an attempt to improve confidence in the lithological interpretation and the affect of lithology on the seismic response.

8.2.3. CPT method

Cone penetration classification systems do exist as mentioned in Chapter 6 and work such as that by Nauroy *et al.* (1998) is currently being published on the inter-relationships between velocity, acoustic impedance and cone resistance.

Nauroy *et al.* (1998) have established correlations between cone resistance, V_p and impedance in stiff carbonate silts (unknown carbonate %), offshore Monaco, through integration and inversion of seismic data with geotechnical data. Their work, as with the research in this thesis and in particular in relation to developing revised methods of data analysis, is based on the improvement of the integration of high resolution seismic and geotechnical data. The use of CPT data alongside seismics has proved useful both in this project and as shown by Butcher (1997) to model major lithology. However, both in the case of Nauroy *et al.* (1998) and within this research project, assumptions have to be made when manipulating CPT results for integration with seismic data.

The CPT based method developed in this study focuses on the use of a published classification chart as a basis for digitising and estimating sediment type. This is a very general, global chart where the lithological divisions are not fully defined, i.e. they do not have a definitive end point on the chart. It is therefore imperative that the assumptions are carefully considered when applying the program. However, the

results have shown that the classification provides a reasonable approximation in terms of estimating soil type, i.e. there is correlation between the program results and the borehole sample test results such as in Figure 6.16. Ideally the chart should be location specific with an adequate spread of CPTs although this density will depend on lateral variability within the area of investigation. The divisions on the chart need clear definition, although this may not be the optimum visual representation and should only be treated as a simple graphical view. The termination points and equations defining the division curves for programming are therefore very subjective; this subjectivity is much in evidence during this procedure.

The classification plots produced by the program have had no editing other than the approximations used to digitise the chart. The tentative process of assigning impedance values (see Chapter 7) creates a slightly circuitous process when borehole sample test results are used, as the classification output is compared to the borehole log and the impedances are iteratively calculated from the sample testing results. At this stage the classification plot is block-averaged to allow input into the synthetic seismogram program and to reduce the block size for storage. This will have the effect of potentially aliasing the final synthetic trace, but iteration is also possible at this stage for seismic comparison. The use of synthetic seismograms as the end product will bring in the assumptions discussed in Section 8.2.1.1.

The 'CPT method' is based around lithology and detecting, in the first instance, vertical lithological changes, and the synthetic seismogram is a representation by amplitude of impedance contrasts based on lithological variations. This method is appropriate for relating the seismic response to the lithology, but for further interpretation, seismic stratigraphy is based on the fact that impedance contrasts which can be traced laterally are based on chronostratigraphic bedding surfaces and not lateral facies change. Therefore, the lateral variability assessment in Chapter 7 illustrated the ability to relate the synthetic seismograms to the reflectors on seismic data. This enabled an assessment to be made of the physical properties within the seismic facies at a point laterally away from the borehole through the use of complex attributes based on amplitude. This is an important exercise for estimating a depositional environment through integration of geotechnical and geophysical data.

Reference is made above to correlations between CPT data and other sediment physical properties. This has tentatively been attempted in this study and produces reasonable approximations and is discussed further in the next section. In order to calculate further parameters, such as accurate undrained shear strength, detailed information on the CPT parameters is required such as cone factor and cone area ratio. Cone factor is also used to define net cone resistance which is a corrected cone resistance and may be used in preference to the measured cone resistance. Uncorrected cone resistance was used in this study as the precise information required for correction was not available. It is at this point in both methods that the empirical relationships of Hamilton and Bachman (1982) and Bachman (1985) can be used to predict a velocity and an impedance. The dangers are unknown errors which may be compounded; however this is inherent where exact measurements and their errors are not used and approximations and assumptions made. This testing was not done as both methods involve assumptions due to the lack of control on the dataset. Nevertheless the results confirm that a tentative correlation is possible as long as the user is aware of the limitations.

The empirical inter-relationships derived in Chapter 6 between cone resistance, velocity and acoustic impedance have produced a very tentative correlation. However, when the inter-relationships were tested on PCPT11 in Chapter 7 the predictions were not valid. Therefore, any assessment of the accuracy of the parameters and their affects on the resultant synthetic seismograms was not considered valid based on such tentative relationships.

8.3. Interpretation and integration of geophysical and geotechnical data

The Borehole and CPT methods discussed above have been tested alongside standard methods of interpretation for a site investigation where high resolution seismic and geotechnical data were collected.

As mentioned previously, a significant point to be made regarding the case study in the Chapter 7 dataset is that the lithology of the area is predominantly glacigenic. This creates issues in terms of the use of established empirical relationships as glacially derived sediments tend to fall outside the parameter limits as defined by, in this case, Hamilton and Bachman (1982). However, as it is an approximation which

is required and not definitive values, this approach is deemed acceptable at this level.

8.3.1. Geotechnical interpretation

The geotechnical data have identified, over both the Foinaven and Schiehallion areas (Figure 7.1), two predominant sediment types. The upper section, which consists of very soft slightly sandy clays, has high moisture contents and the sediments are probably normally consolidated. The lower section comprises very soft to stiff clay with interbedded layers of sand and possibly gravels. This unit has much lower moisture contents and may be overconsolidated. In a geological context the units can be described stratigraphically as the MacAulay and Morrison sequence respectively.

Following the diagnostic method of Baltzer *et al.* (1994) of 'geotechnical signatures', plots of cone resistance and pore pressure indicate the likely origin of these sediments as being debris flows. The profiles have relatively low gradients and the classification chart identifies low input values due to the disorganised structure of the sediment. The CPT results identify layers which may correspond to sands and gravels within the lower unit.

8.3.2. Geophysical interpretation

The deep tow boomer data reflection sequences, and in particular the sequence crossing BHS3/S3A/S3B/S3C, BH4/4A/4B and BH6 have been interpreted as two units. The upper unit probably belongs to the MacAulay sequence and is acoustically well layered and appears to be draped over the lower unit. This draping unit could also be affected by bottom current reworking (Stoker *et al.*, 1993a). The sequence is possibly overlain by a very thin layer of well sorted Holocene sands. However, strong currents will sweep away the finer fraction and the seabed may consist of a gravel armour possibly with deep water coral mixed in although this is so far unsubstantiated (Holmes, pers. comm., 1999). At the BHS4/S5/S6 location the MacAulay sequence appeared to be absent (Hamilton, pers. comm., 1996).

The lower unit is part of the Morrison sequence and has the structure of a debris flow unit, the structureless lensoid type feature being resedimented glacigenic

material and the acoustically well layered deposits are periglacial current reworked sediments (Stoker *et al.*, 1993a, Akhurst, 1989).

8.3.3. Integration

The integration of all the datasets reveals a relatively thorough picture of the section of interest below the seabed. The application of seismic attributes has been valuable in aiding the interpretation of reflector continuity which is particularly advantageous for distinguishing mass flow events. The use of complex attributes was shown to be of particular advantage when extrapolating away from the borehole location. Figure 7.62 displayed the quantitative variation of amplitude laterally which is more difficult to ascertain from a wiggly trace, equalised amplitude display. The attribute displays provide no new information on the data but are able to elucidate previously masked features.

The synthetic seismograms agreed reasonably well when compared to the seismic data, however it is crucial to bear in mind the apparent reflector spacing is a function of borehole sampling frequency where the seismogram has been generated from the borehole results. The situation should be relatively more continuous for the PCPT derived synthetic, but the seismogram is controlled by subjective block averaging before convolution.

The void index model has shown that the relationship between a sediment's compression curve and its mode of deposition is valid for the boreholes from the West Shetland slope. Good correlation was found between the deep tow boomer and the void index results in terms of seismic character and position on the model. The well layered sections on the deep tow boomer related to points close to the SCL, and the more transparent facies related to sample points close to the ICL.

8.4. Data appraisal

One of the major aspects of this research is that it makes use of a dataset collected for an alternative purpose, in this case a site investigation. The data are therefore not specific to this type of research work. This immediately introduces a series of considerations for the resultant research.

As introduced in Chapter 7, the geophysical data were collected as part of a very large 'broadbrush' survey, which was carried out over three years covering part of the West of Shetland outer shelf and slope. They were acquired to provide shallow sediment information over the Foinaven and Schiehallion reservoir areas. Commercial acquisition in this type of oceanographic regime, i.e. deep, exposed water with deepwater currents, was relatively new on the UK continental margin at the time of acquisition. As a result the acquisition parameters were continuously modified as the survey progressed which detracted from the data quality.

The geotechnical data acquisition was carried out a year later once the geophysical data had been analysed alongside ongoing drilling programmes. The geotechnical measurements were made for engineering purposes to assess the seabed and subsurface for foundation conditions.

Large resources would be needed to carry out further, possibly more detailed, geophysical investigations, and therefore, attempts to analyse the geophysical and geotechnical data in the manner of this research project, were seen as providing potential benefits to future commercial data acquisition and interpretation.

8.4.1. Drawbacks of using third party data

One of the major, and in some cases most critical, factors in the collection and application of geophysical and geotechnical data offshore is positioning.

8.4.1.1. Geotechnical data

The main disadvantage in using this particular geotechnical dataset for the project was the coarseness of the borehole sampling. For the original purposes of the survey, however, it would have been extremely costly, time consuming and potentially unnecessary to sample more frequently. The measurements were generally made every 0.5m and to ≥1.0m depending on a combination of sample recovery and measurement type.

8.4.1.2. Geophysical data

Water depth over the survey area is between 400m and 600m, and therefore a slower firing rate was required to sample the area of interest. The boomer fired between 0.9s and 1s as opposed to 0.25s, a more standard firing interval for this type of source used for high resolution studies. This sample interval was chosen to allow phasing with another acquisition system and to accommodate the large water depth. Verbeek and McGee (1995) illustrated the advantages of acquiring very highly sampled data but also highlighted the drawbacks of producing vast amounts of data in terms of storage and handling.

The most obvious drawback with the geophysical dataset was that some of the lines, shot over the geotechnical locations, had not been acquired digitally. This highlighted problems resulting from the lack of control in the dataset at the data acquisition stage.

8.5. Summary

The project has illustrated the benefits of attempting to use a fully integrated geotechnical and geophysical dataset for site investigation interpretation. The thesis has gone some way towards attempting to improve the calibration between groundtruth data and high resolution seismic data. The forward modelling approach enables an assessment of the seismic response and the factors which influence it. The seismic data can be more fully understood by using complex seismic attributes. These attributes can be linked into to the forward modelling process quantitatively and this can aid in the interpretation of the lateral variability of lithofacies. This assessment and understanding of sediment lateral variability is particularly crucial for glacially influenced sediments where there may be rapid changes in facies over relatively short distances both over the shelf to basin floor.

Empirical inter-relationships can be used with caution in glacial sediments; however their applicability to all environments would ideally be assessed on a site by site basis. Inter-relationships are more difficult to produce for relating CPT data on a one site basis alone and with no fundamental, global relationships already in place.

CHAPTER 9

CONCLUSIONS

9.1. Introduction

This research project has attempted to relate the physical properties of a marine sediment to its seismo-acoustic response, with the aim of improving high resolution seismic interpretation. This thesis tests the application of a more integrated approach to the interpretation and investigates modelling of the groundtruth data and the use of seismic attributes. The improved interpretation has been particularly aimed towards a glacigenic, deep water continental margin environment. The achievement of these aims has been through the use of forward modelling techniques alongside seismo-stratigraphic interpretation methods. The conclusions, therefore, have been divided into two sections; modelling and integration.

9.2. Borehole and CPT modelling

The main conclusion from the modelling work has been that the model is only ever as good as the inputs, although it is an obvious conclusion that the two methods produced results which could be correlated.

9.2.1. 'Borehole method'

1. Overall this method has been shown to be a useful approach for an integrated interpretation of groundtruth and seismic data.

2. The drawback in this method however was the coarse subsampling of the borehole samples as highlighted in Chapter 7. This may have been significant close to seabed within the resolution of the deep tow boomer. Esker *et al.* (1996) found that by sampling every 10-20cm then it was possible to produce a synthetic record which illuminated features which may be otherwise masked by the acquisition and processing set-up. This potential aliasing was difficult to assess on this dataset. Chapter 5 indicated that a more detailed geotechnical sampling programme produced better subsurface definition.

3. The synthetic seismogram approach chosen for the study was adequate but to pursue this approach a more flexible system would be preferred. This would involve improved automation of the process from the input of the physical properties to the output of the synthetic seismogram. Ultimately the construction of the synthetic seismogram will be dictated by the seismic data it is designed to model.

4. The use of the empirical inter-relationships was shown to be a very valid approach and when tested, density was able to be confidently used as a predictor in glacigenic sediments. The use of porosity and mean grain size with the relationships of Hamilton and Bachman (1982) were less reliable in that they predicted velocities outside the expected range.

5. The method of block-averaging of the impedance profile has a profound effect on the final synthetic seismogram. This has to be a careful process although, ultimately, it is inevitably subjective. This averaging process is dictated by the geotechnical sampling frequency and the seismogram method.

9.2.2. 'CPT method'

1. The generalised global classification chart has been shown to be applicable to UK continental margin glacially influenced sediments both in shallow and deep water. However, the optimum approach would be to construct site specific charts.

2. Two inter-relationships have been derived which relate the cone resistance to velocity and impedance:

$V_p = 11q_c + 1727$ $(r^2 = 0.5)$

$Z = 55_c + 3267$ $(r^2 = 0.5)$

However, when these relationships were tested at another location it was concluded from the results that the relationships were not applicable away from the original site. Therefore more work is needed to establish globally applicable inter-relationships which relate cone resistance with the acoustic properties of velocity and impedance.

3. Block-averaging is also used in the 'CPT method'. The advantage of the CPT test data is that they give a continuous measurement and therefore there is less reliance on the initial sampling frequency being non-aliasing. However, this method only produced an indication of major lithological units. It was shown to be the pore pressure measurements which were able to delineate more discrete layers.

9.3. Geophysical and geotechnical integration

1. The reflectors on the synthetic seismograms using the 'Borehole method' and the 'CPT method', in some instances, could be correlated and traced on the boomer records. The direct comparison of the two methods highlighted the discrepancies and subjectivity in geotechnical sampling frequency and block-averaging, and the difficulties involved with incomplete datasets and deep subseabed geotechnical penetration in large water depths.

2. The seismic attributes delineate the mass flow packages and, in some cases, add more detail than the analogue boomer record. This was particularly evident where the instantaneous amplitude was combined with the forward models. Physical properties could be inferred at a lateral distance away from the borehole based on amplitude variations.

3. The void index model accurately predicts the potential depositional environments of the sediments at each of the boreholes.

4. The geotechnical approach to the seismic data provides a very solid basis for the interpretation and an understanding of the geological environment.

9.4. Recommendations for future research

The most obvious recommendations for future work would be to acquire a highly sampled geophysical (48kHz interval) and particularly geotechnical dataset (5cm interval) over an area in a deep-water, glacially influenced, continental margin environment. This would allow an in-depth spatial validation of the empirical inter-relationships which are used to produce the forward models. This would also allow a very resolute site specific dataset to be constructed. This would be particularly crucial for the approach used in the 'CPT method' where, ideally, a site specific

classification chart would be preferable. To be able to relate CPT test results with highly sampled physical property data would allow a rigorous assessment of the 'CPT method' produced in this thesis. This assessment would also dictate the feasibility of developing the CPT method program further to in some way incorporate other properties alongside cone resistance and sleeve friction for classifying sediments and relating these to the seismic response.

The method developed within this project is purely by forward modelling and in particular the use of acoustic impedance values derived from physical properties. This approach provides a quantitative assessment of the acoustic impedance at a single location. The next step for this method of analysis would be to attempt an inversion of the seismo-acoustic data. The inversion would provide the acoustic impedance derived from the actual seismic data. This would be a test of the validity of the forward approach and its applicability to improving an interpretation.

A further step of this research would be to apply the inversion results along a seismic line, i.e. moving away from the borehole or CPT location. In essence this would be the first part of trying to develop a seismic facies/pattern recognition system. Using the results from this dataset an initial approach could be to use the mass flow/debris flow lenses as the first pattern type. A profile of this type of feature could be built which incorporated the physical properties, seismic response and instantaneous attribute responses, such as frequency and amplitude.

The combination of the forward modelling, inversion and CPT data could go some way towards producing empirical inter-relationships for glacigenic sediments.

Ultimately the project approach could be developed to output the results as 3D models. On a simple basis this could be performed through the application of gridding and contouring of 1D models which have been extrapolated through the use of character recognition. The sampling locations would act as calibration points for the physical properties. All of the results from these types of analyses could be combined at a site and referenced by a Geographic Information System (GIS), which in 3D mode could incorporate 3D interpretation visualisation.

CHAPTER 10

REFERENCES

Akhurst, M. C. (1989). Sedimentology and biostratigraphy of late Quaternary deep-water, fine grained sediments from the Faeroe-Shetland Channel: a preliminary report. British Geological Survey Technical Report, WB/89/24.

Almagor, G. (1978). Geotechnical properties of the sediments of the continental margin of Israel. Journal of Sedimentary Petrology, 48, 1267-1274.

Anstey, N. A. (1960). Attacking the problems of the synthetic seismogram. Geophysical Prospecting, 8(2), 242-259.

Anstey, N. A. (1991). Velocity in thin section. First Break, 9(10), 449-457.

Atkinson, J. (1993). An introduction to the mechanism of soils and foundations. McGraw-Hill International Ltd., pp. 337.

Attewell, P. B. & Ramana, Y. V. (1966) Wave attenuation and internal friction as functions of frequency in rocks. Geophysics, 31(6), 1049-1056.

Bachman, R. T. (1985). Acoustic and physical property relationships in marine sediment. Journal of the Acoustical Society of America, 78(2), 616-621.

Badiey, M., Cheng, A. H.-D., & Yongke, M. (1998). From geology to geoacoustics - evaluation of Biot-Stoll sound speed and attenuation for shallow water acoustics. Journal of the Acoustical Society of America, 103(1), 309-320.

Baltzer, A., Cochonat, P., & Piper, D. J. W. (1994). *In situ* geotechnical characterisation of sediments on the Nova Scotian Slope, eastern Canadian continental margin. Marine Geology, 120, 291-308.

Berteussen, K. A., & Ursin, B. (1983). Approximate computation of the acoustic impedance from seismic data. Geophysics, 48(10), 1351-1358.

Bertram, G. T. (1995). Sequence stratigraphy - a summary of the technique. Stratigraphic Research International (UK), 12.

Biot, M. A. (1956a). Theory of propagation of elastic waves in a fluid-saturated porous solid. Higher frequency range. Journal of the Acoustical Society of America, 28(2), 179-191.

Biot, M. A. (1956b). Theory of propagation of elastic waves in a fluid-saturated porous solid. Low frequency range. Journal of the Acoustical Society of America, 28(2), 168-178.

Biot, M. A. (1962). Generalised theory of acoustic propagation in porous dissipative media. Journal of the Acoustical Society of America, 34(9), 1254-1264.

Boulton, G. S., & Paul, M. A. (1976). The influence of genetic processes on some geotechnical properties of glacial tills. Quarterly Journal of Engineering Geology, 9, 159-194.

Boulton, G. S., Peacock, J. D., & Sutherland, D. G. (1991). Quaternary. In G. Y. Craig (Eds.), Geology of Scotland Bath: Geological Society of London, 503-537.

Bowles, J. E. (1984). Physical and geotechnical properties of soils. London: McGraw-Hill, pp. 578.

Breitzke, M., Grobe, H., Kuhn, G., & Muller, P. (1996). Full waveform ultrasonic transmission seismograms: A fast new method for the determination of physical and sedimentological parameters of marine sediment cores. Journal of Geophysical Research, 101(B10), 22123-22141.

Buchan, S., McCann, D. M., & Taylor-Smith, D. (1972). Relations between the acoustic and geotechnical properties of marine sediments. Quarterly Journal of Engineering Geology, 5, 265-284.

Buckingham, M. J. (1997). Theory of acoustic attenuation, dispersion and pulse propagation in unconsolidated granular materials including marine sediments. Journal of the Acoustical Society of America, 102, 5(1), 2579-2596.

Buckingham, M. J. (1998). Theory of compressional and shear waves in fluidlike marine sediments. Journal of the Acoustical Society of America, 103(1), 288-299.

Burland, J. B. (1990). On the compressibility and shear strength of natural clays. Geotechnique, 40(3), 329-378.

Butcher, J. A. (1997). Seismic stratigraphy of shallow water Quaternary sediments around the U.K. PhD thesis, University of Wales.

Carrion, P. M., & Patton, W. A. (1983). Criteria for the resolution and reconstruction of acoustic impedance. Journal of Geophysical Research, 88(B12), 10349-10358.

Cernica, J. N. (1995). Geotechnical engineering soil mechanics. Chichester New York: John Wiley and Sons Inc., pp. 453.

Claerbout, J. F. (1968). Synthesis of a layered medium from its acoustic transmission response. Geophysics, 33(2), 264-269.

Conway, A. M., & Hill, A. W. (1994). Signal enhancement of single channel high resolution airgun data for use in deep water drilling hazards surveys. In EAEG 56th Meeting and Technical exhibition. Vienna, Austria.

Damuth, J. E., & Olsen, H. C. (1993). Preliminary observations of Neogene-Quaternary depositional processes in the Faeroe-Shetland Channel revealed by high-resolution seismic facies analysis. In J. R. Parker (Ed.), Petroleum Geology of Northwest Europe. The Geological Society, 1035-1045.

Davis, A. M. (1999). Personal communication.

Earle, M. M. (1989). Structural and stratigraphic evolution of the Faeroe-Shetland Channel and Northern Rockall Trough. AAPG Memoir, 46, 461-469.

Esker, D., Sheridan, R. E., Ashley, G. M., Waldner, J. S., & Hall, D. W. (1996). Synthetic seismograms from vibracores: A case study in correlating the late Quaternary seismic stratigraphy of the New Jersey inner continental shelf. Journal of Sedimentary Research, 66(6), 1156-1168.

Eyles, C. H., Eyles, N., & Miall, A. D. (1985). Models of glaciomarine sedimentation and their application to the interpretation of ancient glacial sequences. Palaeogeography, Palaeoclimatology, Palaeoecology, 51, 15-84.

Eyles, N., Eyles, C. H., & Miall, A. D. (1983). Lithofacies types and vertical profile models; an alternative approach to the description and environmental interpretation of glacial diamict and diamictite sequences. Sedimentology, 30, 393-410.

Faust, L. Y. (1951). Seismic velocity as a function of depth and geologic time. Geophysics, 16, 192-206.

Fowler, J. & Cohen, L. (1990). Practical statistics for field biology. Chichester: John Wiley & Sons, pp. 227.

Fuchs, K., & Muller, G. (1971). Computation of synthetic seismograms with the reflectivity method and comparison with observations. Geophysical Journal of the Royal Astronomical Society, 23, 417-433.

Fugro Ltd. (1994). Cyclic soil parameters - Schiehallion, Blocks 214/19 and 20, 205/16/17/21 - AFP Phase 2 No. 55067-5. Fugro Ltd.

Fugro-Geoteam Ltd. (1997). A.L.E. Pipeline route survey for Total Oil Marine PLC (Unpublished, No. M2025).

Fyfe, J. A. (1985). DEVIL'S HOLE, 56°N - 00°, 1:250 000 map series. Quaternary Geology. British Geological Survey.

Ganley, D. C. (1981). A method for calculating synthetic seismograms which include the effects of absorption and dispersion. Geophysics, 46(8), 1100-1107.

Gardner, G. H. F., Gardner, L. W., & Gregory, A. R. (1974). Formation velocity and density - the diagnostic basics for stratigraphic traps. Geophysics, 39(6), 770-780.

Gassmann, F. (1951). Elastic waves through a packing of spheres. Geophysics, 16, 673-685.

Geertsma, J., & Smit, D. C. (1961). Some aspects of elastic wave propagation in fluid-saturated porous solids. Geophysics, 26(2), 169-181.

Hall, A. M. (1991). Pre-Quaternary landscape evolution in the Scottish Highlands. Transactions of the Royal Society of Edinburgh: Earth Sciences, 82, 1-26.

Hamilton, E. L. (1970a). Reflection coefficients and bottom losses at normal incidence computed from Pacific sediment properties. Geophysics, 35(6), 995-1004.

Hamilton, E. L. (1970b). Sound velocity and related properties of marine sediments, North Pacific. Journal of Geophysical Research, 75(23), 4423-4446.

Hamilton, E. L. (1971a). Elastic properties of marine sediments. Journal of Geophysical Research, 76(2), 579-603.

Hamilton, E. L. (1971b). Prediction of *in situ* acoustic and elastic properties of marine sediments. Geophysics, 36(2), 266-284.

Hamilton, E. L. (1972). Compressional wave attenuation in marine sediments. Geophysics, 37(4), 620-646.

Hamilton, E. L. (1978). Sound velocity-density reflections in sea-floor sediments and rocks. Journal of the Acoustical Society of America, 63(2), 366-377.

Hamilton, E. L. (1979). Sound velocity gradients in marine sediments. Journal of the Acoustical Society of America, 65(4).

Hamilton, E. L. (1980). Geoacoustic modelling of the sea floor. Journal of the Acoustical Society of America, 68(5), 1313-1340.

Hamilton, E. L., & Bachman, R. T. (1982). Sound velocity and related properties of marine sediments. Journal of the Acoustical Society of America, 72(6), 1891-1904.

Hamilton, I. W. (1996). Geophysical investigation of Foinaven/Schiehallion. In Towards 2000, Metres or Millennium - Deepwater Site Investigation. London.

Hamilton, I. W. (1996). Personal communication.

Hamilton, E. L., Shumway, G., Menard, H. W., & Shipek, C. J. (1956). Acoustic and other physical properties of shallow-water sediments off San Diego. Journal of the Acoustical Society of America, 28(1), 1-15.

Hampson, K., & Power, P. (1996). Geotechnical investigations for the Foinaven and Schiehallion developments, West of Shetland. In SUT-Towards 2000 Metres or Millennium. London.

Haszeldine, R. S. (1984). Carboniferous North Atlantic paleogeography: stratigraphic evidence for rifting, not megashear or subduction. Geological Magazine, 121(5), 443-463.

Haynes, R. (1996). UWB Eckernförde sub-bottom profiling and acoustic sediment classification experiments. Internal document, UWB.

Haynes, R., Bennell, J. D., Davis, A. M., & Reynolds, J. M. (1993a). Advantages offered by the routine acquisition of digital high-resolution subbottom profiling data. Proceedings of the Institute of Acoustics, 15(2), 165-172.

Haynes, R., Davis, A. M., Reynolds, J. M., & Taylor, D. I. (1993b). The extraction of geotechnical information from high-resolution seismic reflection data. In D. A. Ardus, D. Clare, A. Hill, R. Hobbs, R. J. Jardine, & J. M. Squire (Ed.), Offshore site investigation and foundation behaviour, 28. London: Kluwer Academic Publishers, 215-228.

Hepton, P. (1989). Shear wave velocity measurements during penetration testing. PhD thesis, University of Wales.

Hill, M. N. (1952). Seismic refraction shooting in an area of the eastern Atlantic. Philosophical Transactions of the Royal Society of London, 244(Series A), 561-594.

Holmes, R. (1999). Personal communication.

Holmes, R., Ruckley, N., Graham, C. & Bone, B. (1991). FOULA, 60°N - 04°W, 1:250 000 map series. Quaternary Geology. British Geological Survey.

Horn, D. R., Horn, B. M., & Delach, M. N. (1968). Correlation between acoustical and other physical properties of deep-sea cores. Journal of Geophysical Research, 73, 1939-1957.

Hron, F., & Covey, J. D. (1983). Wavefront divergence, multiples and converted waves in synthetic seismograms. Geophysical Prospecting, 31, 436-456.

Huws, D. G. (1993). Measuring and modelling the *in situ* physical properties of marine sediments. PhD thesis, University of Wales.

Jackson, D. I., Jackson, A. A., Evans, D., Wingfield, R. T. R., Barnes, R. P., & Arthur, M. J. (1995). The geology of Irish Sea. London: HMSO, pp. 123.

Jannssen, D., Voss, J., & Theilen, F. (1985). Comparison of methods to determine Q in shallow marine sediments from vertical reflection seismograms. Geophysical Prospecting, 33, 479-497.

Josenhaus, H. W., & Fader, G. B. J. 1989. A comparison of models of glacial sedimentation along the eastern Canadian margin. Marine Geology, 85, 273-300.

Kearey, P., & Brooks, M. (1991). An introduction to geophysical exploration (2nd Ed.). London: Blackwell Scientific Publications, pp. 254.

Kenyon, N. H. (1986). Evidence from bedforms for a strong poleward current along the upper continental slope of Northwest Europe. Marine Geology, 72, 187-198.

Kibblewhite, A. C. (1989). Attenuation of sound in marine sediments: A review into emphasis on new low-frequency data. Journal of the Acoustical Society of America, 86(2), 716-738.

Laberg, J. S., & Vorren, T. O. (1997). Debris flow deposits on a glacier-fed submarine fan off the Western Barents Sea continental shelf. In Davies, T. A., Bell, T., Cooper, A. K., Josenhans, H., Polyak, L., Solheim, A., Stoker, M. S. & Stravers, J. A. (Eds.), Glaciated continental margins: An atlas of acoustic images. London: Chapman & Hall, 122-123.

Lunne, T., & Powell, J. J. M. (1993). Recent developments in *in situ* testing in offshore soil investigations. In D. A. Ardus, D. Clare, A. Hill, R. Hobbs, R. J. Jardine, & J. M. Squire (Ed.), Offshore site investigation and foundation behaviour, 28. London: Kluwer Academic Publishers, 147-180.

Mayer, L. A. (1980). Deep-sea carbonates: physical property relationships and the origin of high-frequency acoustic reflectors. Marine Geology, 38, 165-183.

McCann, C., & McCann, D. M. (1969). The attenuation of compressional waves in marine sediments. Geophysics, 34, 882-892.

McCann, C., & McCann, D. M. (1985). A theory of compressional wave attenuation in non-cohesive sediments. Geophysics, 50(8), 1311-1317.

McGee, T. M. (1991). Modelling 1D wave propagation in a system of absorbing layers. Geophysical Prospecting, 39, 29-49.

McGee, T. M. (1995). High-resolution marine reflection profiling for engineering and environmental purposes. Part A : Acquiring analogue seismic signals. Journal of Applied Geophysics, 33, 271-285.

McQuillin, R., Bacon, M., & Barclay, W. (1986). An introduction to seismic interpretation (2nd Ed.). London: Graham & Trotman Ltd., pp. 287.

Meadows, N. S., Macchi, L,, Cubitt, J. M. & Johnson, B. (1987). Sedimentology and reservoir potential in the west of Shetland, UK, exploration area. In Brooks, J. & Glennie, K. (Eds): Petroleum Geology of NW Europe. London: Graham & Trotman Ltd., 723-736.

Meigh, A. C. (1987). Cone penetration testing: methods and interpretation No. Construction Industry Research and Information Association, pp. 141.

Miller, K. G., & Tucholke, B. E. (1983). Development of Cenozoic abyssal circulation south of the Greenland-Scotland Ridge. In M. H. P. e. a. Bott (Eds.), Structure and development of the Greenland-Scotland Ridge, 549-589.

Missiaen, T., McGee, T., Pearks, D., Ollier, G., & Thielen, F. (1996). An interdisciplinary approach to the evaluation of physical parameters of shallow marine sediments. In M. De Batist & P. Jacobs (Eds.), Geology of Siliciclastic Shelf Seas, Geological Society Special Publication. London: The Geological Society, 299-322.

Mitchum Jr., R. M., & Vail, P. R. (1977). Seismic stratigraphy and global changes in sea level, part 7: seismic stratigraphic interpretation procedure. AAPG Memoir, 26, 135-143.

Mitchum, Jr., R. M., Vail, P. R., & Sangree, J. B. (1977). Seismic stratigraphy and global changes of sea level, part 6: stratigraphic interpretation of seismic reflection patterns in depositional sequences. AAPG Memoir, 26, 117-133.

Moran, K., Hill, P. R., & Blasco, S. M. (1989). Interpretation of piezocone penetrometer profiles in sediment from the MacKenzie Trough, Canadian Beaufort Sea. Journal of Sedimentary Petrology, 59(1), 88-97.

Muthukrishniah, K., Reji, Z., Murthy, G. R. K., & Nair, P. V. (1995). Relationship between geophysical and geotechnical properties of marine sediments using Biot-Stoll model. Marine Georesources and Geotechnology, 13(3), 243-261.

Myers, K. J., & Milton, N. J. (1996). Concepts and principles of sequence stratigraphy. In D. Emery & K. J. Myers (Eds). Sequence stratigraphy. Oxford: Blackwell Science, 11-41.

Nafe, J. E., & Drake, C. L. (1957). Variation with depth in shallow and deep water marine sediments of porosity, density and the velocities of compressional and shear waves. Geophysics, 22(3), 523-552.

Nauroy, J.-F., Dubois, J.-C., Colliat, J.-L., Kervadec, J.-P., & Meunier, J. (1998). The Geosis method of integrating VHR seismic and geotechnical data in offshore site investigations. In D. Ardus, R. Hobbs, M. Horsnell, R. Jardine, D. Long, & J. Sommerville (Ed.), Offshore site investigation and foundation behaviour - New frontiers. London: SUT, 175-198.

Nobes, D. C. (1989). A test of a simple model of the acoustic velocity in marine sediments. Journal of the Acoustical Society of America, 86(1), 290-294.

O'Doherty, R. F., & Anstey, N. A. (1971). Reflections on amplitudes. Geophysical Prospecting, 19(3), 430-458.

Oldenburg, D. W., Scheuer, T., & Levy, S. (1983). Recovery of the acoustic impedance from reflection seismograms. Geophysics, 48(10), 1318-1337.

Olsen, R. S., & Malone, P. G. (1988). Soil classification and site characterisation using the cone penetrometer test. In D. Ruiter (Eds.), Penetration testing. Rotterdam: Balkema, 887-893.

Orsi, T. H., & Dunn, D. A. (1991). Correlations between sound velocity and related properties of glacio-marine sediments: Barents Sea. Geo-Marine Letters, 11, 79-83.

Panda, S., LeBlanc, L. R., & Schock, S. G. (1994). Sediment classification based on impedance and attenuation estimation. Journal of the Acoustical Society of America, 96(1), 3022-3035.

Paul, M. A. (1996). Personal communication.

Paul, M. A., & Jobson, L. M. (1987). On the acoustic and geotechnical properties of soft sediments from the Witch Ground Basin, central North Sea (Report of the MTD Ltd. Research Grant No. GR/C/71385). Heriot-Watt University.

Paul, M. A., Talbot, L. A., & Stoker, M. S. (1993). Geotechnical properties of sediments from the continental slope northwest of the British Isles. In D. A. Ardus, D. Clare, A. Hill, R. Hobbs, R. J. Jardine, & J. M. Squire (Ed.), Offshore site investigation and foundation behaviour, 28. London: Kluwer Academic Publishers, 77-106.

Paul, M. A., Talbot, L. A., & Stoker, M. S. (1998). Shallow geotechnical profiles, acoustic character and depositional history in glacially influenced sediments from the Hebrides and West Shetland Slopes. In M. S. Stoker, E. D, & A. Cramp (Eds.), Geological Processes on Continental Margins: Sedimentation, Mass-Wasting and Stability. London: Geological Society Special Publication, 117-131.

Peterson, R. A., Fillippone, W. R., & Coker, F. B. (1955). The synthesis of seismograms from well log data. Geophysics, 20(3), 516-538.

Posamentier, H. W., Jervey, M. T., & Vail, P. R. (1988). Eustatic controls on clastic deposition. In Sea level Changes: An integrated approach, Wilgus, C. K. *et*

al., (Eds.). Society of Economic Palaeontologists and Mineralogists Special Publication 42, 54-109.

Power, P., & Barwise, A. (1996). Deepwater PCPT's for drilling rig sites. In SUT conference, Towards 2000 metres or Millennium. London.

Power, P. T., & Aldridge, T. R. (1997). Over the edge. Ground Engineering, October 1997, 22-24.

Richardson, M. D., & Briggs, K. B. (1993). On the use of acoustic impedance values to determine sediment properties. Proceedings of the Institute of Acoustics, 15(2), 15-24.

Roberts, D. G., Bott, M. H. P., & Uruski, C. (1983). Structure and origin of the Wyville-Thomson Ridge. In M. H. P. Bott, S. Saxov, M. Talwani, & J. Thiede (Eds.), Structure and Development of the Greenland-Scotland Ridge - new methods and concepts New York: Plenum Press, 133-158.

Robertson, J. D., & Nogami, H. H. (1984). Complex seismic trace analysis of thin beds. Geophysics, 49(4), 344-352.

Robertson, P. K. (1990). Soil classification using the cone penetration test. Canadian Geotechnical Journal, 27, 151-158.

Robertson, P. K., & Campanella, R. G. (1983a) Interpretation of cone penetration tests. Part 1: Sand. Canadian Geotechnical Journal, 20, 718-733.

Robertson, P. K., & Campanella, R. G. (1983b) Interpretation of cone penetration tests. Part 2: Clay. Canadian Geotechnical Journal, 20, 734-745.

Sangree, J. B., & Widmier, J. M. (1979). Interpretation of depositional facies from seismic data. Geophysics, 44(2), 131-160.

Saunders, P. M. (1990). Cold outflow from the Faeroe Bank Channel. Journal of Physical Oceanography, 20, 29-43.

Sawyer, W. B., B, R., & Bennett, R. H. (1997). Geotechnical property variability of continental margin sediments: high-resolution vertical and lateral data from the northern California slope. Marine Georesources and Geotechnology, 15, 283-304.

Schmertmann, J. H. (1978). Guidelines for CPT performance and design. US Department of Transport, Federal Highways Administration Offices of Research and Development, Washington (DC), Report No. FHWA-TS-78-209, pp. 145.

Schnack-Friedrichsen, A. (1997) 1-D modelling of the seismic signature relating to the upper boundary of the Danian Limestone in the Danish North Sea. MSc thesis, University of Wales.

Schreiber, B. C. (1968). Sound velocity in deep sea sediments. Journal of Geophysical Research, 73(4), 1259-1268.

Schultheiss, P. J. (1983). The influence of packing structure on seismic wave velocities in sediments (Marine Geological Report No. 83/1). University College of North Wales, Bangor.

Scrutton, R. A. (1986). The geology, crustal structure and evolution of the Rockall Trough and the Faeroe-Shetland Channel. Proceedings of the Royal Society of Edinburgh, 88B, 7-26.

Sheriff, R. E. (1975). Factors affecting seismic amplitudes. Geophysical Prospecting, 23, 125-138.

Sheriff, R. E. (1977). Limitations on resolution of seismic reflections and geologic detail derivable from them. AAPG Memoir, 26, 3-14.

Sheriff, R. E. (1980). Seismic Stratigraphy. Boston: International Human Resources Development Corporation, pp. 227.

Sheriff, R. E., & Geldart, L. P. (1995). Exploration Seismology (2nd ed.). Cambridge: Cambridge University Press, pp. 592.

Sinvhal, A., & Sinvhal, H. (1992). Seismic Modelling and Pattern Recognition in Oil Exploration. Boston: Kluwer Academic Publishers, pp. 178.

Smith, G. N. (1990). Elements of soil mechanics (6th Ed.). Oxford: BSP Professional Books, pp. 509.

Spencer, A. M., & Eldholm, O. (1993). Atlantic margin exploration Cretaceous-Tertiary evolution, basin development and petroleum geology. Introduction and review. In J. R. Parker (Ed.), Petroleum Geology of northwest Europe: Proceedings of the 4th Conference. The Geological Society.

Stewart, F. S., & Stoker, M. S. (1990). Problems associated with seismic facies analysis of diamicton-dominated, shelf glacigenic sequences. Geo-Marine Letters, 10, 151-156.

Stoker, M.S. (1988). Pleistocene ice-proximal glaciomarine sediments in boreholes from the Hebrides Shelf and Wyville-Thomson Ridge, NW UK Continental Shelf. Scottish Journal of Geology, 24(3), 249-262.

Stoker, M. S. (1990a). Glacially influenced sedimentation on the Hebridean slope, northwestern United Kingdom continental margin. In J. A. Dowdeswell & J. D. Scourse (Eds.), Glaciomarine Environments: processes and sediments. Geological Society Special Publication No. 53, 349-362.

Stoker, M. S. (1995). The influence of glacigenic sedimentation on slope-apron development on the continental margin off north-west Britain. In R. A. Scrutton, G. B. Shimmield, M. S. Stoker, & A. W. Tudhope (Eds.), Tectonics, sedimentation and palaeoceanography of North Atlantic margins. Geological Society Special Publication No. 90, 159-177.

Stoker, M. S., Harland, R., & Graham, D. K. (1991). Glacially influenced basin plain sedimentation in the southern Faeroe-Shetland Channel, northwest United Kingdom continental margin. Marine Geology, 100, 185-199.

Stoker, M. S., Hitchen, K., & Graham, C. C. (1993a). The geology of the Hebrides and West Shetland Shelves and adjacent deepwater areas. London: HMSO, pp. 149.

Stoker, M. S., & Holmes, R. (1991). Submarine end moraines as indicators of Pleistocene ice limits off northwest Britain. Journal of the Geological Society of London, 148, 431-434.

Stoker, M. S., Leslie, A. B., Scott, W. D., Briden, J. C., Hine, N. M., Harland, R., Wilkinson, I. P., Evans, D., & Ardus, D. A. (1994). A record of Late Cenozoic stratigraphy, sedimentation and climate change. Journal of the Geological Society of London, 151(2), 1-15.

Stoker, M. S., Stewart, F. S., Paul, M. A., & Long, D. (1993b). Problems associated with seismic facies analysis of Quaternary sediments on the northern UK continental margin. In D. A. Ardus, D. Clare, A. Hill, R. Hobbs, R. J. Jardine, & J. M. Squire (Ed.), Offshore site investigation and foundation behaviour, 28. London: Kluwer Academic, 239-262.

Stoll, R. D. (1977). Acoustic waves in ocean sediments. Geophysics, 42(4), 715-725.

Stoll, R. D. (1986). Acoustic waves in marine sediments. In T. Akal & J. M. Berkson (Eds.), Ocean Seismo-Acoustics. New York: Plenum Press, 417-434.

Stoll, R. D. (1989). Sediment Acoustics. Berlin: Springer-Verlag, pp. 155.

Syvitski, J. P. M. (1991). Towards an understanding of sediment deposition on glaciated continental shelves. Continental Shelf Research, 11(8-10), 897-937.

Talbot, L. A., Paul, M. A., & Stoker, M. S. (1994). Geotechnical and acoustic characteristics of Plio-Pleistocene sediments from the Hebrides Slope. Geo-Marine Letters, 14, 244-251.

Taner, M. T., Koehler, F., & Sheriff, R. E. (1979). Complex trace analysis. Geophysics, 44, 1041-1063.

Taner, M. T., & Sheriff, R. E. (1977). Application of amplitude, frequency and other attributes to stratigraphic and hydrocarbon determination. AAPG Memoir, 26, 301-328.

Tankard, A. J., & Balkwill, H. R. (1988). Extensional tectonics and stratigraphy of the North Atlantic margins: Introduction. AAPG Memoir, 46, 1-4.

Telford, W. M., Geldart, L. P., Sheriff, R. E., & Keys, D. A. (1976). Applied Geophysics. Cambridge: Cambridge University Press, pp. 770.

Thorne, J. A. (1992). An analysis of the implicit assumptions of the methodology of seismic sequence stratigraphy. In J. S. Watkins, F. Zhiqiang, & K. J. McMillen (Eds.), AAPG Memoir 53 Tulsa, USA: AAPG, 375-394.

Thybo, H. (1989). Wrap-around removal from one-dimensional synthetic seismograms. Geophysics, 54(7), 911-915.

Toksoz, M. N., Johnston, D. H., & Timur, A. (1979). Attenuation of seismic waves in dry and saturated rocks : 1. Laboratory measurements. Geophysics, 44(4), 681-690.

Trabant, P. K. (1984). Applied high-resolution geophysical methods: offshore geoengineering hazards. Boston: International Human Resources Development Corp., pp. 265.

Treitel, S., & Robinson, E. A. (1966). Seismic wave propagation in layered media in terms of communication. Geophysics, 31, 17-32.

Trorey, A. W. (1962). Theoretical seismograms with frequency and depth dependent absorption. Geophysics, 27, 766-785.

Turgut, A., & Yamamoto, T. (1988). Synthetic seismograms for marine sediments and determination of porosity and permeability. Geophysics, 53(8), 1056-1067.

Turner, J. D., & Scrutton, R. A. (1993). Subsidence patterns in western margin basins; evidence from the Faeroe-Shetland Basin. In J. R. Parker (Ed.), Petroleum Geology of northwest Europe: Proceedings of the 4th Conference. London: The Geological Society, 975-983.

UKOOA (1996). Guidelines for the conduct of mobile drilling rig site survey. Volume 2.

Urick, R. J. (1947). A sound velocity method for determining the compressibility of finely divided substances. Journal of Applied Physics, 18, 983-987.

Vail, P. R. (1987). Seismic stratigraphy interpretation using sequence stratigraphy, Part 1: Seismic stratigraphy interpretation procedure. In A. W. Bally (Ed.). Atlas of seismic stratigraphy, Volume 1. AAPG, Studies in geology, 27, 1-10.

Vail, P. R., Mitchum Jr., R. M., Todd, R. G., Widmier, J. M., Thompson, S., Sangree, J. B., Bubb, J. N., & Hatlied, W. G. (1977a). Seismic stratigraphy and global changes of sea-level. AAPG Memoir, 26, 49-51.

Vail, P. R., Mitchum, Jr., R. M. & Thompson, S. (1977b). Relative changes of sea level from coastal onlap. AAPG Memoir, 26, 63-81.

Verbeek, N. H., & McGee, T. M. (1995). Characteristics of high-resolution marine reflection profiling sources. Journal of Applied Geophysics, 33, 251-269.

Walden, A. T., & White, R. E. (1984). On errors of fit and accuracy in matching synthetic seismograms and seismic traces. Geophysical Prospecting, 32, 871-891.

White, R. E. (1991). Properties of instantaneous seismic attributes. The Leading Edge, July 1991, 26-32.

Whitten, D. G. A., & Brooks, J. R. V. (1972). Dictionary of Geology. London: Penguin Books, pp. 495.

Widess, M. B. (1973). How thin is a thin bed. Geophysics, 38(6), 1176-1180.

Wilkens, R. H., & Richardson, M.D. (1998). The influence of gas bubbles on sediment acoustic properties: in situ, laboratory, and theoretical results from Eckernförde Bay, Baltic sea. Continental Shelf Research, 18, 1859-1892.

Williams, G. P. (1983). Improper use of regression equations in earth sciences. Geology, 1(4), 195-197.

Wingfield, R. T. R. (1984). LIVERPOOL BAY, 53°N - 04°W, 1:250 000 map series. Seabed Sediments and Quaternary Geology. British Geological Survey.

Wood, A. B. (1955). A textbook of sound (3rd Ed.). London: G. Bell and sons Ltd., pp. 610.

Wuenschel, P. C. (1960). Seismogram synthesis including multiples and transmission coefficients. Geophysics, 25(1), 106-129.

Wyllie, M. R. J., Gregory, A. R., & Gardner, L. W. (1956). Elastic wave velocities in heterogeneous and porous media. Geophysics, 21(1), 41-70.

Zhang, Z., & Tumay, M. T. (1996). Simplification of soil classification charts derived from the Cone Penetration Test. Geotechnical Testing Journal, 19(2), 203-216.

Ziolkowski, A. (1991). Why don't we measure seismic signatures. Geophysics, 56(2), 190-201.

APPENDIX A - TENLAYERS PROGRAM

```
c234567
c     This program is for inputting data, calling TENLAYERS and writing
c     floating point output to a file.

      program filelayers
      dimension LT(10),R(10),Q(9999),cq(9999)
      character*80 fileout,ofile2
      write(6,1000)
1000  format(" No. of layers between the halfspaces? (max.=10) ",$)
      read (5,*) NL
      write(6,1010)
1010  format(" Value of 0-th reflection coefficient? ",$)
      read (5,*) R0
      do 10 i=1,NL
        write (6,1020) i
1020    format(" Two-way thickness of layer ",i2,"? ",$)
        read (5,*) LT(i)
        write (6,1030) i
1030    format(" Value of ",i2,"-th reflection coefficient? ",$)
  10    read (5,*) R(i)
      write(6,1040)
1040  format(" No. of output points desired? (max.=9999) ",$)
      read(5,*) NO
  300 write(6,3060)
3010  format(a80)
3020  format(" invalid file name, leading character cannot be blank")
3030  format (" IOSTAT error",i4," in opening file ",a80)
3040  format(" see Appendix F of Fortran Manual")
3050  format(" can't find file ",a80)
3060  format(" give name of output file: ",$)
3070  format(" error ",i4," in writing data point ",i4)
      read(5,3010) fileout
      if(fileout(1:1).ne." ") goto 320
      write(6,3020)
      goto 300
  320 open(30,file=fileout,status="new",form="formatted",
     *err=330,iostat=ios)
      goto 340
  330 write(6,3030) ios,fileout
      if(ios.ne.118) write(6,3040)
      if(ios.eq.118) write(6,3050) fileout
      stop(" aborted because of output file name")
  340   idtype=1
      xmin=0.
      xstep=1.
      write(30,4055,err=345,iostat=ios) idtype,xmin,xstep,NO
4055  format(i1,2X,f8.6,1X,f8.6,1X,i4)
      write(6,4056) idtype,xmin,xstep,NO
4056  format(" output: idtype = ",i1,", xmin = ",f8.6,", xstep = ",f8.6,
     c" NO =",i4)
      goto 347
  345   write(6,4070) ios
4070  format(" error ",i4," in writing output file header")
      goto 370
```

```
347 call TENLAYERS(NL,R0,LT,R,NO,Q)
        call convolv2(q,no,cq,ncq)
    do 360 i=1,NO
      write(30,*,err=350,iostat=ios) Q(i)
      goto 360
350    write(6,3070) ios,i
360 continue

        print*,' give me the CONVOLUTION output file name'
        read(*,'(a)')ofile2
        open(60,file=ofile2,status='unknown')
        do i=1,ncq
         write(60,*)cq(i)
        enddo

 370 close(30)
     continue
     end


c     Subroutine TENLAYERS calculates the impulse response of a plane
c     wave normally incident to a system of parallel layers situated
c     between two halfspaces.  The interfaces of the system are numbered
c     in the direction of propagation, the first encountered being the
c     zero-th interface located between a halfspace and the first layer.
c     The reference point is within the first layer immediately beyond
c     the zero-th interface.  As presently dimensioned, a maximum of ten
c     layers may be input.  The thickness of each layer is input as an
c     integral multiple of some unit thickness which scales the system.
c     The reflection coefficient of each interface is input as a real
c     number of magnitude unity or less.  A positive coefficient implies
c     that acoustic impedance increases in the direction of propagation.
c     The output is a specified number of points which comprise the
c     leading terms of an infinite series.  As presently dimensioned,
c     a maximum of 1024 points may be output.  Absorption is not taken
c     into account.  The input parameters are:
c          NL = number of layers between the halfspaces (1-10),
c          R0 = reflection coefficient of the zero-th interface,
c       LT(I) = two-way thickness of I-th layer,
c        R(I) = reflection coefficient of the I-th interface,
c          NO = number of amplitudes output (1-9999),
c       Q(NO) = array into which output is placed.

SUBROUTINE TENLAYERS(NL,R0,LT,R,NO,Q)
DIMENSION LT(1),R(1),Q(1)
DIMENSION E(10,9999),F(10,9999),G(10,9999),H(10,9999),DRF(9999)
IF (NL.LT.1) THEN
  WRITE(6,*)"less than one layer input"
  GO TO 100
ELSE IF (NL.GT.10) THEN
  WRITE(6,*)"more than 10 layers input"
  GO TO 100
ELSE IF (NO.LT.1) THEN
  WRITE(6,*)"less than one output amplitude requested"
```

```
   GO TO 100
ELSE IF (NO.GT.9999) THEN
   WRITE(6,*)"more than 9999 output amplitudes requested"
   GO TO 100
ELSE IF (R0**2.GT.1.0) THEN
   WRITE(6,*)"unity exceeded for reflection coefficient R0"
   GO TO 100
END IF
DO 1 I=1,NL
   IF(R(I)**2.GT.1.0) THEN
      WRITE(6,*)"unity exceeded for reflection coefficient R",I
      GO TO 100
      ELSE
      END IF
 1 CONTINUE
   IO=1+LT(1)
   DO 10 J=1,IO
      E(1,J)=0.0
      F(1,J)=0.0
      G(1,J)=0.0
      H(1,J)=0.0
10 CONTINUE
   E(1,1)=1.0
   F(1,1)=R(1)
   G(1,IO)=R(1)
   H(1,IO)=1.0
   IF(NL.EQ.1) GO TO 40
   DO 35 I=2,NL
      JSUB=MIN0(IO,LT(I))
      DO 20 J=1,JSUB
         E(I,J)=E(I-1,J)
         F(I,J)=R(I)*E(I-1,J)
         G(I,J)=G(I-1,J)
         H(I,J)=R(I)*G(I-1,J)
20    JJ=J
      IF(LT(I).LE.IO) GO TO 30
      DO 25 J=IO+1,LT(I)
         E(I,J)=E(I-1,J)
         F(I,J)=R(I)*E(I-1,J)
         G(I,J)=G(I-1,J)
         H(I,J)=R(I)*G(I-1,J)
25    JJ=J
30    IO=IO+LT(I)
      DO 35 J=JJ+1,IO
         E(I,J)=E(I-1,J)+R(I)*F(I-1,J-LT(I))
         F(I,J)=R(I)*E(I-1,J)+F(I-1,J-LT(I))
         G(I,J)=G(I-1,J)+R(I)*H(I-1,J-LT(I))
         H(I,J)=R(I)*G(I-1,J)+H(I-1,J-LT(I))
   35 CONTINUE
   40 DO 45 J=1,IO
      DRF(J)=E(NL,J)+R0*G(NL,J)
c     WRITE(6,1000) NL,J,E(NL,J),F(NL,J),G(NL,J),H(NL,J),DRF(J)
 1000 FORMAT("NL=",i2,", J=",i4," E=",f10.7," F=",f10.7," G=",f10.7,
     c" H=",f10.7," DRF=",f10.7,$)
```

```
45 CONTINUE
  DO 50 I=1,NO
50    Q(I)=0.0
        ISUB=MIN0(IO,NO)
  DO 55 I=1,ISUB
55    Q(I)=G(NL,I)
  DO 60 I=1,NO
    IF (I.EQ.NO) GO TO 100
    K=I
    DO 60 J=1,ISUB
    K=K+1
 60    Q(K)=Q(K)-Q(I)*(E(NL,J+1)+R0*G(NL,J+1))
100 CONTINUE
   RETURN
   END


        subroutine convolv2(rfln,nrfln,syn,nconv)

C process to read in disk files, do the convolution and write out to a file
c for graphical input elsewhere
c declare the arrays
        dimension rfln(1),source(300),syn(1)
        character*40 fil
c Ask for source file

        print*,' Give me the SOURCE file name'
        read(*,'(a)')fil

c open the files to input for the convolution

        OPEN(50,file= fil,status='old')
        do i=1,300
          read(50,*,end=101)source(i)
        enddo
101     nsour=i-1
        do i=1,nrfln
          do j=1,nsour
         syn(j + i-1) = (rfln(i) * source(j)) + syn(j + i-1)
        enddo
         enddo

c print output on the screen
        nconv=nrfln+nsou-1
        do i=1,nconv
           PRINT*, syn(i)
        enddo
        close(50)
        return
                                                    end
```

APPENDIX B - CPT CLASSIFICATION PROGRAM

```
/*
**  Program to interpret Cone Penetration Test (CPT) output.
*/
#include <stdio.h>
#include <math.h>

#define INPUT_FILE   "input.dat"
#define OUTPUT_FILE  "output.dat"
#define DEBUG_FILE   "debug.dat"

#define MAX_INPUT_VALUES    10000
#define NUM_CLASSIFICATIONS  14

int   get_classification(float x, float y);
float get_impedance(int classification);

/* cpt equations and intersection points - calculated from
   Robertson and Campanella interpretation chart (Fugro supplied).
    y1 and y2 are linear.
*/

float  y3(float x);
float  y4(float x);
float  y5(float x);
float  y6(float x);
float  y7(float x);
float  y8(float x);
float  y9(float x);
float y10(float x);
float y11(float x);
float y12(float x);
float y13(float x);

void main(void)
{
    FILE*  in;
    FILE*  out;
    FILE*  debug;

    int i;
    float k,j;

    int   num_data_points;

    float  Rf[MAX_INPUT_VALUES];
    float   d[MAX_INPUT_VALUES];
    float  qc[MAX_INPUT_VALUES];
    float  fs[MAX_INPUT_VALUES];

    int    nr;
    float   z;

/* Try open all these files now so we don't come a cropper
   later...
```

```
*/
if(!(in = fopen(INPUT_FILE, "r"))){
    fprintf(stderr, "Couldn't open input file: <%s>.\n", INPUT_FILE);
    exit(1);
}

if(!(out = fopen(OUTPUT_FILE, "w+"))){
    fprintf(stderr, "Couldn't open output file: <%s>.\n", OUTPUT_FILE);
    exit(1);
}

#if defined(DEBUG)
    if(!(debug = fopen(DEBUG_FILE, "w+"))){
        fprintf(stderr, "Couldn't open debug file: <%s>.\n", DEBUG_FILE);
        exit(1);
    }
#endif

    /* Read in the input data */
    for(i = 0; i < MAX_INPUT_VALUES; i++){
        if(fscanf(in,"%f %f %f %f %f", &d[i], &qc[i], &fs[i], &k, &k) == EOF){
            break;
        } else {
            Rf[i] = (fs[i]/qc[i])*100;
        }
    }

    num_data_points = i;

#if defined(DEBUG)
    fprintf(stdout, "Number of data points <%d>\n", num_data_points);
#endif

#if defined(DEBUG)
    for(j = 4.7; j < 6.75; j = j + 0.1){
        fprintf(stdout, "Y5(%f) : %f\n", j, y5(j));
    }
#endif

    /* Go through all the data points and see what area of the
    **  classification chart the points lie. Then for each point, convert
    ** the classification (nr) to an equivalent impedance (z) and write
    ** out a table of depth (d(i)) versus z in the output file.  file.
    */
    for(i = 0; i < num_data_points; i++){
        nr = get_classification(Rf[i], qc[i]);
        z  = get_impedance(nr);
        fprintf(out, "%f %f %f %d %f\n", d[i], Rf[i], qc[i], nr, z);
    }

    fprintf(stdout, "Processed <%d> data points, output written to <%s>.\n",
            num_data_points, OUTPUT_FILE);
    exit(0);
}
```

```
int get_classification(float x, float y)
{

/* Intersection data for the equations y3->y12.  x3_x12 is the X
   co-ord of the point where eqn y3 intersects y12. These values
   tell us between which points it is valid to apply the equations.
*/

#define max_y    100.0
#define min_y    0.0
#define max_x    8.0
#define min_x    0.0
#define x1       0.5
#define x2       1.5
#define x3_x12   2.1
#define x3_x13   3.6
#define x4_x7    2.5
#define x4_x8    2.9
#define x4_x9    3.35
#define x4_x10   3.7
#define x4_x11   4.15
#define x4_x13   5.0
#define x5_0     4.7
#define x5_x7    4.85
#define x5_x8    5.15
#define x5_x9    5.5
#define x5_x10   5.95
#define x5_x11   6.45
#define x5_x13   6.75
#define x6_0     5.85
#define x6_x13   7.15
#define x7_x12   2.45
#define x12_0    2.5

#define y6_y13   1.85

    /* Check for Area A */
    if((x <= x1) && (x > min_x) && (y >= y12(x)) && (y < max_y)){
        return 1;
    }
    /* Check for Area B */
    if((x <= x2) && (x > x1) && (y >= y12(x)) && (y < max_y)){
    return 2;
}
/* Check for Area C */
if((x > x2) && (x <= x3_x13)) {
    if(((x <= x3_x12) && (y < y13(x)) && (y >= y12(x))) ||
       ((x >  x3_x12) && (y < y13(x)) && (y >= y3(x)))){
        return 3;
    }
}
/* Check for Area D */
if((x <= x4_x13) && (x > x3_x12)) {
    if(((x <= x7_x12) && (y >= y12(x)) && (y < y3(x))) ||
```

```
      ((x > x7_x12)  && (x <= x4_x7) && (y >= y7(x)) && (y < y3(x)))  ||
      ((x > x4_x7)  && (x <= x3_x13)  && (y >= y4(x)) && (y < y3(x))) ||
      ((x > x3_x13)   && (y >= y4(x))  && (y < y13(x)))){
       return 4;
    }
}
/* Check for Area E */
if(( x > min_x) && (x <= x12_0) && (y >= min_y) && (y < y12(x))){
    return 5;
}
/* Check for Area F */
if((x > x7_x12) && (x <= x5_x7) && (y >= min_y)){
    if(((x <= x12_0) && (y >= y12(x)) && (y < y7(x))) ||
      ((x > x12_0)  && (x <= x5_0)   && (y < y7(x))) ||
      ((x > x5_0)   && (y >= y5(x))  && (y < y7(x)))){
       return 6;
    }
}
/* Check for Area G */
if((x > x4_x7) && (x <= x5_x8)){
    if(((x > x4_x7) && (x <= x4_x8) && (y >= y7(x)) && (y < y4(x))) ||
      ((x > x4_x8) && (x <= x5_x7) && (y >= y7(x)) && (y < y8(x))) ||
      ((x > x5_x7) && (y >= y5(x)) && (y < y8(x)))){
       return 7;
    }
}
/* Check for Area H*/
if((x > x4_x8) && (x <= x5_x9)){
    if(((x > x4_x8) && (x <= x4_x9) && (y >= y8(x)) && (y < y4(x))) ||
      ((x > x4_x9) && (x <= x5_x8) && (y >= y8(x)) && (y < y9(x))) ||
      ((x > x5_x8) && (y >= y5(x)) && (y < y9(x)))){
       return 8;
    }
}
/* Check for Area I */
if((x > x4_x9) && (x <= x5_x10)){
    if(((x > x4_x9)  && (x <= x4_x10) && (y >= y9(x)) && (y < y4(x)))  ||
      ((x > x4_x10) && (x <= x5_x9)  && (y >= y9(x)) && (y < y10(x))) ||
      ((x > x5_x9)  && (y >= y5(x))  && (y < y10(x)))){
       return 9;
    }
}
/* Check for Area J */
if((x > x4_x10) && (x <= x5_x11)){
    if(((x > x4_x10) && (x <= x4_x11) && (y >= y10(x)) && (y < y4(x)))  ||
      ((x > x4_x11) && (x <= x5_x10) && (y >= y10(x)) && (y < y11(x))) ||
      ((x > x5_x10) && (y >= y5(x))  && (y < y11(x)))){
       return 10;
    }
}
/* Check for Area K */
if((x > x4_x11) && (x <= x5_x13)){
    if(((x > x4_x11) && (x <= x4_x13) && (y >= y11(x)) && (y < y4(x)))  ||
      ((x > x4_x13) && (x <= x5_x11) && (y >= y11(x)) && (y < y13(x))) ||
```

```
        ((x > x5_x11) && (y >= y5(x))  && (y < y13(x)))){
         return 11;
      }
   }
   /* Check for Area L */
   if((x > x5_0) && (x <= x6_x13) && (y >= min_y)){
      if(((x <= x6_0) && (y < y5(x)))                                    ||
        ((x > x6_0)  && (x <= x5_x13) && (y >= y6(x)) && (y < y5(x))) ||
        ((x > x5_x13) && (y < y13(x)) && (y >= y6(x)))){
         return 12;
      }
   }
   /* Check for Area M */
   if((x > x6_0) && (x <= max_x) && (y >= 0)){
      if(((x <= x6_x13) && (y < y6(x))) ||
        ((x > x6_x13)  && (y < y6_y13))){
         return 13;
      }
   }
   /* Check for Area N (unclassified) */
   if((x > x2) && (x <= max_x) && (y < max_y)){
      if(((x <= x6_x13) && (y >= y13(x))) ||
        ((x > x6_x13) && (y >= y6_y13))){
         return 14;
      }
   }
   return -1;
}

float get_impedance(int classification)
{
   /*
     !!!!!!!!Need to fill in proper impedance values here!!!!!!
   */
   float Z[NUM_CLASSIFICATIONS] = {1,2,3,4,5,6,7,8,9,10,11,12,13,14};

   classification--;

   if((classification >= 0) && (classification < NUM_CLASSIFICATIONS)){
      return Z[classification];
   } else {
      return -1;
   }
}



float y3(float x)
{
   return (12.011*pow(x,4)-112.42*pow(x,3)+400.94*pow(x,2)-640.03*x+384.1);
}

float y4(float x)
{
```

```
    return (1.0684*pow(x,4)-14.832*pow(x,3)+78.966*pow(x,2)-187.25*x+165.7);
}

float y5(float x)
{
    return (0.8849*pow(x,2)-7.802*x+17.33);
}

float y6(float x)
{
    return (1.3939*pow(x,2)-16.312*x+48.041);
}

float y7(float x)
{
    return (-0.01*pow(x,2)+0.07*x+0.28);
}

float y8(float x)
{
    return (-0.02*pow(x,2)+0.13*x+0.5);
}

float y9(float x)
{
    return (0.025*pow(x,3)-0.321*pow(x,2)+1.2513*x+0.0763);
}

float y10(float x)
{
    return (-0.025*pow(x,2)+0.075*x+2.5);
}

float y11(float x)
{
    return (-0.25*pow(x,2)+1.95*x+1.4);
}

float y12(float x)
{
    return (-0.3988*pow(x,4)+1.87*pow(x,3)-2.8611*pow(x,2)+1.0224*x+1.7988);
}

float y13(float  x)
{
     return (-0.6156*pow(x,4)+11.863*pow(x,3)-77.569*pow(x,2)+177.43*x-28.54);}
```